Deltares

Enabling Delta Life

Validation of dune impact models using European field data

Deliverable 4.1 and 4.2 (combined): validation of XBeach and off-the-shelf models

micore

Title
Validation of dune impact models using European field data

Client	Project	Reference	Pages
European Union - Framework Programme 7	1002266-000	1002266-000-ZKS-0001-	171 of 222

Keywords
Dune erosion, dune overwash, morphological modelling, XBeach, field measuremens, Europe, coastal risk

Summary
The objective of the modelling effort within MICORE is to use, validate and extend an open-source coastal erosion model called XBeach (Roelvink, et al. 2009) for various European coastal sites and compare its outputs with off-the-shelf packages such as LITPROF, SMC, SBeach, IO-BAS and Durosta, which are now locally used. The coastal sites where field data was collected include Lido di Dante-Lido di Classe, Ravenna (Italy), Praia de Faro (Portugal), Urban beaches of Cadiz Bay (Spain), Lido of Sete to Marseillan Beach (France), The Dee Estuary (United Kingdom), Egmond Beach (The Netherlands), Mariakerke Beach (Belgium), Dziwnow Spit (Poland) and Kamchia-Shkorpilovtsi Beach (Bulgaria). Each field site has a unique bathymetry/topography and/or wave/tidal climate and will contribute to and test the modelled physics under a wide range of environmental conditions. We found that for some sites the XBeach model performed well (Belgium and the UK). For some sites satisfactory results were obtained (Italy, Portugal, Spain), especially when a 2D model was used (Bulgaria). The model results all showed that berm erosion was overpredicted by XBeach. Poorer results were obtained for the Polish and the French case. For the latter only bar migration was measured for which the model is not originally developed.

References
European Community's Seventh Framework Programme under grant agreement n° 202798 (MICORE Project), under Deltares project number 1002266.

Version	Date	Author	Initials	Review	Initials	Approval	Initials
1.0	15 Feb 2011	J. van Thiel de Vries		J.A. Roelvink		T. Schilperoort	
		A.R. van Dongeren					

State
final

Contents

List of Tables i
List of Figures iii

1 Introduction 1
1.1 General Aims of the Project 1
1.2 Specific aims of WP 4 2
1.2.1 Objectives 2
1.2.2 Background 3
1.2.3 Phases of the WP4 4
1.2.4 Deliverables of activities (WP4) 6
1.3 Contributing partners 6
1.4 Summary and main results of the validation study 7
1.4.1 Introduction 7
1.4.2 Study sites and measured data 7
1.4.3 Modelling 8
1.4.4 Results 9

2 Lido di Dante, Italy 13
2.1 Objectives 13
2.2 Site and climatology 13
2.2.1 Description of area 13
2.2.2 Storms considered 14
2.2.3 Measurements 15
2.3 Model results 18
2.3.1 Simulation results with Off-the shelf Model 18
2.3.2 Simulation results with XBeach model 19
2.4 Synthesis 25
2.5 Conclusions 25

3 Praia de Faro, Portugal 27
3.1 Objectives 27
3.2 Site and climatology 27
3.3 Methodology 28
3.3.1 Hydrodynamic data 28
3.3.2 Wave modelling results 29
3.3.3 Topo-bathymetric data 30
3.3.4 XBeach modelling 30
3.4 Model results 32
3.4.1 Simulation results with Off-the shelf Model 32
3.4.2 Simulation results with XBeach model 32
3.5 Summary and Conclusions 36

4 Cadiz Urban Beach, Spain 37
4.1 Objectives 37
4.2 Site and climatology 37
4.2.1 Description of area 37
4.2.2 Storms considered 39

4.2.3 Measurements 40
4.3 Model results 41
4.3.1 Simulation results with Off-the shelf Model 41
4.3.2 Simulation results with XBeach model 41
4.4 Synthesis 44
4.5 Conclusions 44

5 Lido di Sète 47
5.1 Objectives 47
5.2 Site and climatology 47
5.2.1 Description of area 47
5.2.2 Climatology 48
5.2.3 Storms considered 49
5.2.4 Measurements 50
5.3 Model results 50
5.3.1 Simulation results with Off-the shelf Model 50
5.3.2 Simulation results with XBeach model 56
5.4 Conclusion 58

6 Mariakerke and Ostend Beach, Belgium 59
6.1 Objectives 59
6.2 Site and climatology 59
6.2.1 Description of area 59
6.2.2 Storms considered 66
6.2.3 Measurements 74
6.3 Model results 76
6.3.1 Simulation results with Off-the shelf Model 76
6.3.2 Simulation results with XBeach model 80
6.4 Synthesis 87
6.5 Conclusions 95

7 Sefton Coast, England 97
7.1 Objectives 97
7.2 Site and climatology 98
7.2.1 Description of area 98
7.2.2 Climatology 100
7.2.3 Storms considered 101
7.3 Model results 105
7.3.1 1D (beach profile) modelling 105
7.3.2 2D selected key area modelling 110
7.3.3 2D wide area modelling 115
7.3.4 Coastal flooding model 119
7.4 Summary and conclusions 121

8 Dziwnow Spit, Poland 125
8.1 Objectives 125
8.2 Site and climatology 125
8.2.1 Description of area 125
8.2.2 Storms considered 130
8.2.3 Measurements 131
8.3 Model results 136

8.3.1 Simulation results with XBeach model 136
8.4 Synthesis 140
8.5 Conclusions 141

9 Kamchia Shkorpilovtsi Beach, Bulgaria 143
9.1 Objectives 143
9.2 Site and climatology 143
9.2.1 Description of area 143
9.2.2 Storms considered 145
9.2.3 Measurements 151
9.3 Model results 157
9.3.1 Simulation results with off-the-shelf model 157
9.3.2 Simulation results with XBeach model 159
9.4 Synthesis 164
9.5 Conclusions 166

10 Testbed, the Netherlands 167
10.1 Objectives 167

11 References 169

Appendices

A SWAN A-1
A.1 Originator A-1
A.2 Website/reference A-1
A.3 Description A-1
A.4 Governing equations A-2
A.4.1 Wind input A-2
A.4.2 Four-wave interactions A-2
A.4.3 Whitecapping A-3

B STWAVE B-1
B.1 Originator B-1
B.2 References / Websites B-1
B.3 Short Description: B-1

C LITPROF C-1
C.1 Originator C-1
C.2 References / Websites C-1
C.3 Short Description: C-1

D TRANSED D-1
D.1 Originator D-1
D.2 References / Websites D-1
D.3 Short Description: D-1

E XBeach E-1
E.1 Originator E-1
E.2 Website E-1

E.3 Description E-1

F SMC-model F-1
F.1 Originator F-1
F.2 Website F-1
F.3 Short Description F-1
F.3.1 Hydrodynamic Model F-2
F.3.2 Wave Dissipation Model F-2
F.3.3 Return Current Model F-3
F.3.4 Sediment Transport Model F-3
F.3.5 Transport in the swash zone F-3
F.3.6 References F-4

G SBEACH G-1
G.1 Originator G-1
G.2 Website G-1
G.3 Short description G-1

H MARS H-1
H.1 Originator H-1
H.2 Website H-1
H.3 Short description H-1
H.4 References: H-2

I Durosta I-1
I.1 Originator I-1
I.2 Website I-1
I.3 Short description I-1

J Storms along the Sefton Coast J-1
J.1 Introduction. J-1
J.2 Extreme conditions J-2
J.2.1 Wave conditions J-2
J.2.2 Surge conditions J-3
J.2.3 Tidal conditions J-3
J.2.4 Tidal conditions J-4
J.3 Historical events J-8
J.4 References J-9

K The Liverpool Bay Model K-1
K.1 Model description K-1
K.1.1 Wetting and drying using TVD volume fluxes K-2
K.1.2 Bathymetry and boundary conditions K-3
K.1.3 Model open boundary conditions K-3
K.1.4 Model bathymetry K-4
K.2 Comparisons with observations K-4
K.2.1 Sea surface currents K-5
K.2.2 Stratification K-5
K.2.3 Surge modelling K-6
K.3 References K-7

L Testbed report **L-1**

List of Tables

Table 1.1 Project partners (beneficiaries) 6

Table 2.1 Statistics of profile configurations and storm response for the two storms and four profile locations modelled. Shoreline retreat is defined by the change in the 0.5 m contour line and the intertidal slope between the ±0.3 m contours. 17

Table 2.2 Brier Skill Score results for SBEACH model runs using default settings as well as adjusting the transport rate coefficient K and the maximum slope prior to avalanching. Values in brackets indicate the BSS above MSL only. Bold values indicate the optimum settings selected. 19

Table 2.3 Brier Skill Score results for XBeach model runs for the two storm events using various combinations of parameter settings. Values in brackets indicate the BSS above MSL. Bold values indicate the optimum settings selected. 22

Table 3.1 Information on wave, tides and surge levels data sources 29

Table 3.2 Values of important XBeach parameters considered for the February 2009 storms. Note that all possible combinations of the mentioned values were considered 31

Table 4.1 Values of the most important parameters used for the test-case of Cadiz. 42

Table 5.1 Summary of Storm characteristics 50

Table 6.1 Specifications directional wave rider buoy Ostend Noodstrand. 67

Table 6.2 Timetable monitoring program. 74

Table 6.3 Available hydrodynamic parameters from the Flemish banks Monitoring Network. 75

Table 6.4 Brier Skill Scores for the XBeach and Durosta model predictions for the November 2007 storm on Ostend beach. 88

Table 7.1 Characteristics of events causing significant erosion or flooding impact: (1) 22 January to 8 February 2002; (2) 21 December 2004 to 24 January 2005; (3) 18 August to 22 September 2005; (4) 22 September to 12 October 2006; (5) 10 July to 06 August 2007; and (6) 03 March to 19 March 2008. 109

Table 7.2 Measures of XBeach model performance for events listed in Table 7.1. 110

Table 8.1 Cross-shore granulometric characteristic of the beach (sample 1 - dune foot, sample 6 – near water line). 126

Table 8.2 Basic characteristic of WAM model applied over the Baltic Sea (Cieślikiewicz, Paplińska-Swerpel, 2008). 135

Table 8.3 Locations of directional waverider buoy stations and periods of measurements (Cieślikiewicz, Paplińska-Swerpel, 2008). 136

Table 8.4 Values of parameters used for model simulations. 137

Table 9.1 Overview of morphological changes caused by the examined storms 146

Table 9.2 Statistics for the storm February 2009 146

Table 9.3 Statistics for the storm April 2009 147

Table 9.4	Statistics for the storm November 2009	148
Table 9.5	Statistics for the storm December 2009	149
Table 9.6	Statistics for the storm March 2010	150
Table 9.7	Brier skill score for IO-BASMM	157
Table 9.8	Brier skill score for 1D XBeach	161
Table 9.9	Brier skill score for 2D XBeach	164
Table F.1	Default values for the parameters of the different dissipation models	F-3

List of Figures

Figure 1.1 The MICORE study sites in the European Union. 8

Figure 2.1 Map of the Lido di Dante-Lido di Classe site, on the Adriatic Sea in Northern Italy. 14

Figure 2.2 Characteristics of the two storms used for model calibration: significant wave height (Hs), peak period (Tp), direction (Dir) and water level (WL). 15

Figure 2.3 Location of the five profile lines (Profiles MN15, MN10, MS17, MS22 and MS38) selected for 1DH modelling at the Lido di Dante – Lido di Classe site. The red box represents the model domain for 2DH modelling 16

Figure 2.4 Results of SBEACH and XBeach modelling of the 1-3 December 2008 storm event for profiles MS22, MS17, MN10 and MN15. Pre-storm measurements are represented by solid black lines whereas post-stom measurements by dashed black lines. 20

Figure 2.5 Results of SBEACH and XBeach modelling of the 9-10 March 2010 storm event for profiles MS22, MS17, MN10 and MN15. Pre-storm measurements are represented by solid black lines whereas post-stom measurements by dashed black lines. 21

Figure 2.6 a) Two-dimensional model setup for Lido di Classe, where a series of emerged offshore breakwater structures are present, b) Water level comparison between 1DH and 2DH XBeach simulations at a single time-step for the December 2008 storm 24

Figure 3.1 Map of South Portugal showing the study area, the Portuguese Hydrographic Institute buoy and the Huelva tidal gauge locations (a). Ancão Peninsula including Faro beach, showing the topographic survey transects and the location of the Infinity pressure transducer (b). 27

Figure 3.2 Validation of wave propagation model results showing Hs values modelled with SWAN (red) and Infinity PT data (blue). 30

Figure 3.3 Wave conditions during the February 2009 storm event. From top to bottom: Water level, Significant wave height, Peak period, Peak direction. Black vertical lines denote the timing of pre- and post-storm topo-bathymetric surveys. 31

Figure 3.4 The December 2009-January 2010 storms. From top to bottom: Water level; Significant wave height, Peak period and Peak direction. Black vertical lines denote the timing of pre- and post-storm bathymetric surveys and numbers the period considered for XBeach testing. 32

Figure 3.5 Beach profile envelopes (x, y dimensions in m; results from Event I-2) showing XBeach sensitivity to the tested parameters. Parameter name indicated in bottom right of each subplot. Mean Sea level MSL=2 m. 33

Figure 3.6 Summary of XBeach calibration efforts and impact of the facua, wetslope, lws, form, wci, gwf, turb, nspr parameters on performance. a): Best (maximum) Brier Skill Scores (BSS) of the tests grouped by parameter value (indicated by red numbers). Low y-axis is set to -1 for better display b): Average BSS value per groups of runs December 2009 Storms tests. 34

Figure 3.7 Histograms of Brier Skill Scores (BSS) of all the tested model set-ups per event. 34

Figure 3.8 Beach profiles (x, y dimensions in m) showing the best cases of XBeach and LITPROF simulations for the 5 different transects. Brier Skill Scores are indicated in the legend along with the initial and final profiles. 35

Figure 4.1 Location map of the study area (left) and aerial-photo of the study area of Cadiz(Spain)with overlaying topo-bathymetric modelling profiles. 38

Figure 4.2 Oceanographic conditions during the calibration storm event in the area of Cadiz (light shaded area): (a) Total sea level variation in the area measured by the tidal gauge of the port of Cadiz; (b) Significant wave height (Hs) and (c) Spectral peak wave period (Tp) measured by the coast buoy.Dark shaded area represent actual simulation period. For measurement locations see Figure 4.1. 39

Figure 4.3 Pre- (left) and pos-storm (center) topographic surveys in the city of Cadiz together with the erosion-accretion map (right). All variables are in meter. 40

Figure 4.4 Comparison of the initial bathymetry for the three profiles in the area of Cadiz. North profile (blue) is in real depth values and the central (red) and south (green) profiles are displaced vertically by -5m and -10m respectively. 41

Figure 4.5 Initial (dashed black), final (black) and XBEACH (red) and off-the-shelf (blue) results for the North profile of the Cadiz test case. 42

Figure 4.6 Initial (dashed black), final (black) and XBEACH (red) and off-the-shelf (blue) results for the Central profile of the Cadiz test case 43

Figure 4.7 Initial (dashed black), final (black) and XBEACH (red) and off-the-shelf (blue) results for the South profile of the Cadiz test case. 44

Figure 5.1 Site location in France. 47

Figure 5.2 Bathymetry of the study site the November 12th 2008. 48

Figure 5.3 Significant wave height at the Sète offshore buoy 49

Figure 5.4 Observed sea-level at the Sète harbour 49

Figure 5.5 Calculation domain of SWAN. The Sète buoy is located in the lower right corner of the figure. The MARSOUIN domain is represented by the red rectangle 51

Figure 5.6 Calculation domain of the south zone for MARSOUIN simulation 52

Figure 5.7 Calculation domain used for the hydrodynamics / morphodynamics in the north zone. The longshore extension is 1400 m. This domain is representative of the pre-storm configuration. 52

Figure 5.8 Current velocities during the apex of the storm : frontal wave forcing (December the 26th at 4pm) 53

Figure 5.9 Current velocity during the second phase of the storm : oblique wave forcing (December the 31th at 7pm) 54

Figure 5.10 Computed morphological response of the bar system modelled by MARSOUIN during the two phases of the storm 54

Figure 5.11 Computed morphological response of the bar system modelled by MARSOUIN during the two phases of the storm 55

Figure 5.12 Beach profile. South Site. The 06/01/2009. Facua parameter = 0.2 / morfac=20 57

Figure 5.13 Beach profile. South Site. The 06/01/2009. Facua parameter = 0.3 / morfac=30 58

Figure 6.1 Location of project area (source: Flemish Coastal Division). The orange part in the inset is the land area below MHW. 60

Figure 6.2 Overview of fixed and dynamic coastal defence techniques along the Belgian coast (www.kustatlas.be). 61

Figure 6.3 Mariakerke coastal zone, the study area is located between section 96 and 108 63

Figure 6.4 Dyke, promenade and beach at Mariakerke. Note the apartment buildings on the dyke 63

Figure 6.5 Typical beach profile at Mariakerke. 64

Figure 6.6 Comparison erosion/sedimentation trends wet and dry beach for 1998-1999-2007 64

Figure 6.7 Beach scarp erosion (storm with 1/10 yr retour period) 65

Figure 6.8 Dyke and beach at Ostend centrum. 65

Figure 6.9 Measured water level at Ostend during the storm of November 2007. 67

Figure 6.10 Measured significant wave height and peak wave period at Ostend during the storm of November 2007. 68

Figure 6.11 Survey October (c46c47) – measurement points 69

Figure 6.12 Survey October (c46c47) – contours 69

Figure 6.13 Survey November (c48c49) – location measurement points. 70

Figure 6.14 Survey November (c48c49) – contours. 70

Figure 6.15 Division into coastal sections. 71

Figure 6.16 Profile measurement before and after November 2007 storm in section 113a. 71

Figure 6.17 Profile measurement before and after November 2007 storm in section 114a. 72

Figure 6.18 Profile measurement before and after November 2007 storm in section 115a. 72

Figure 6.19 Profile measurement before and after November 2007 storm in section 116a. 73

Figure 6.20 Profile measurement before and after November 2007 storm in section 117a. 73

Figure 6.21 Flemish Banks Monitoring Network. 76

Figure 6.22 Comparison Durosta model result with measurements for section 113a. 77

Figure 6.23 Comparison Durosta model result with measurements for section 114a. 78

Figure 6.24 Comparison Durosta model result with measurements for section 115a. 78

Figure 6.25 Comparison Durosta model result with measurements for section 116a. 79

Figure 6.26 Comparison Durosta model result with measurements for section 117a. 79

Figure 6.27 Figure 7 1: grid of the 1D XBeach model. 80

Figure 6.28 Comparison XBeach model results with measurements for section 113a. 81

Figure 6.29 Comparison XBeach model results with measurements for section 114a. 81
Figure 6.30 Comparison XBeach model results with measurements for section 115a. 82
Figure 6.31 Comparison XBeach model results with measurements for section 116a. 82
Figure 6.32 Comparison XBeach model results with measurements for section 117a. 83
Figure 6.33 Original bathymetry (heights in m TAW) 84
Figure 6.34 Grid 2D XBeach model test3b (color scale = height in m TAW) 84
Figure 6.35 Comparison XBeach model results (best settings) with measurements for section 113a. 85
Figure 6.36 Comparison XBeach model results (best settings) with measurements for section 114a. 85
Figure 6.37 Comparison XBeach model results (best settings) with measurements for section 115a. 86
Figure 6.38 Comparison XBeach model results (best settings) with measurements for section 116a. 86
Figure 6.39 Comparison XBeach model results (best settings) with measurements for section 117a. 87
Figure 6.40 XBeach & Durosta model results with measurements for section 113a. 88
Figure 6.41 XBeach & Durosta model results with measurements for section 114a. 89
Figure 6.42 XBeach & Durosta model results with measurements for section 115a. 89
Figure 6.43 XBeach & Durosta model results with measurements for section 116a. 90
Figure 6.44 XBeach & Durosta model results with measurements for section 117a. 90
Figure 6.45: Erosion (blue) – sedimentation (red) pattern caused by the November 2007 storm event (color scale = height in m). 91
Figure 6.46 1000-years storm: water level (tide + storm surge) 92
Figure 6.47 1000-years storm: significant wave height Hs and peak wave period Tp. 92
Figure 6.48 Comparison of predicted beach erosion with XBeach and Durosta for section 113. 93
Figure 6.49 Comparison of predicted beach erosion with XBeach and Durosta for section 114. 93
Figure 6.50 Comparison of predicted beach erosion with XBeach and Durosta for section 115. 94
Figure 6.51 Comparison of predicted beach erosion with XBeach and Durosta for section 116. 94
Figure 6.52 Comparison of predicted beach erosion with XBeach and Durosta for section 117. 95
Figure 7.1 Sefton Coast is located in Northwest England (insert) and presents 16 km of undefended coastlines (aerial photograph taken in 2005). The lines indicate shoreline transects used to determine rates of dune and shoreline recession. Coordinates in British National Grid (m). The photographs show four different coastal locations. 99

Figure 7.2 Predicted surface pressure chart for 09h00GMT 31 March 2010 (source: Weatheronline.co.uk). 102

Figure 7.3 Predicted average surface wind speeds for 09h00GMT 31 March 2010 (source: Weatheronline.co.uk). Note the strong NW winds in the Irish Sea region affecting the Sefton coastline. 102

Figure 7.4 Predicted maximum wind gusts for 09h00GMT 31 March 2010 (source: Weatheronline.co.uk). Note: most of the western side of the UK is affected by strong winds. 103

Figure 7.5 Meteorological conditions measured at Hilbre Island weather station prior to, during and after the 31 March 2010 storm, Sefton coast, NW UK showing atmospheric pressure, average wind speed, maximum gust speed and wind direction. 103

Figure 7.6 Measured wave conditions at 53°32'.06N and 003°21'.16W in 22m of water prior to, during and after the 31 March 2010 storm, Sefton coast, NW UK showing significant wave height (Hm0), peak wave period (Tp), zero up crossing wave period (Tz), peak wave direction (P dir) and directional wave spreading (Dir spread). 104

Figure 7.7 Tidal elevations: predicted at Liverpool; measured at Liverpool Gladstone Dock; measured at Heysham; and the difference between Liverpool and Heysham records. The black line indicates the period when the low pressure tracked eastwards across the Irish sea and the red line denotes the period when average wind speed was c. 20m/s (i.e. the height of the storm). 104

Figure 7.8 Measured and enhanced wave and tidal conditions (ODN) used to force the 1D XBeach simulations of the 31 March 2010 storm event. 106

Figure 7.9 DTM of the Formby Point XBeach modelling domain comprising combined topographic lidar survey data (2008), UoP DGPS beach survey (2008) and POL Liverpool Bay bathymetry. Also shown by red lines are the SMBC beach profiles lines P11, P12, P14, P15, P17 and P18 selected for 1D XBeach storm impact modelling. 106

Figure 7.10 Aerial photographs showing the location of the three extreme event scenario simulations at Formby Point and the north and south of Formby Point . Photos. From Sefton Metropolitan Borough Council, 2008. 107

Figure 7.11a. XBeach model results using **measured** hydrodynamic conditions (Figure 7.10) for the upper parts of SMBC beach profiles lines P14, P15, P17 and P18. The dashed black lines show the measured profile before the storm, the solid black lines shows the measured profile after the storm and the red line shows the profiles predicted by XBeach after simulation of the March 31 2010 storm. 108

Figure 7.12 Extreme event simulation in 2D (with enhancements) around P17 (Figure 7.8) showing inundation of a dune blowout region. The numbers above each plot indicate elapsed time from the start of the model run (s). 111

Figure 7.13a Extreme event simulation in 2D (with enhancements) around P14 (Figure 7.10) showing dune inundation and erosion. The numbers above each plot indicate elapsed time from the start of the model run (s). 113

Figure 7.14a. 2D Extreme event simulation to the south of Formby Point showing inundation of regions behind the dunes and erosion. The numbers above each plot indicate elapsed time from the start of the model run (s). 114

Figure 7.15a Pre-storm bathymetry and topography (from lidar) used in the 2D wide-area simulation of the Sefton coastline for the March 2010 storm. 116

Figure 7.16 Measured changes in beach topography between 28/3/2010 and 5/4/2010 showing the unusual accretion feature close to Formby Point (upper panel) and measured and predicted (XBeach) alongshore changes in beach volume during the same period (lower panel). 118

Figure 7.17 Oblique aerial photograph of the River Alt north of Hightown at low water (left panel); and GoogleEarth image of the River Alt showing the extent of the XBeach flooding model and the course of the river. Note the proximity of light industry and residential areas. 119

Figure 7.18a. 2D simulation of an enhanced storm impact on the River Alt, north from Hightown showing stages in coastal flooding attributable to high tidal levels and flood fluvial discharge. The numbers above each plot indicate elapsed time from the start of the model run (hours). 120

Figure 8.1 Dziwnow Spit from the air. 125

Figure 8.2 Diagram of the coastal protections methods development (Dudzińska-Nowak, 2006). 127

Figure 8.3 Coast line changes on the investigated area in time period 1938-1996 on a base air photographs (red areas – erosion, yellow areas - accumulation) (Dudzińska-Nowak, 2006). 127

Figure 8.4 Diagram of the 25 years coastal changes prediction – optimistic scenario (Furmańczyk, Dudzińska-Nowak, 2008). 128

Figure 8.5 Diagram of the 25 years coastal changes prediction – pessimistic scenario (Furmańczyk, Dudzińska-Nowak, 2008). 128

Figure 8.6 Wind rose for the Pomeranian Bay coast (Zeidler et al. 1995). 129

Figure 8.7 Wave rose for the Pomeranian Bay coast: (1) 0<H<25cm; (2) 26<H<50cm; (3) 51<H<100cm, (4) H>101 cm (Zeidler et al. 1995). 130

Figure 8.8 Time-series of mean sea level since 1st January 2008 to 1st April 2010. Green line show mean sea level in the Polish coast; red rectangle show storm surge during selected storm (data from MO tide gauge). 130

Figure 8.9 Time-series of significant wave height (Hs), wave period (Tp), wave direction (Wave Dir) and mean sea level (MSL) during extreme storm (data from WAM model and MO tide gauge).. 131

Figure 8.10 Localization of measurements and control areas. 131

Figure 8.11 Dates of pre- and post-storm measurements carried out between August and November 2009 used to model calibration. 132

Figure 8.12 3D models comparison created on the base of pre- and post-storm RTK GPS measurements (area no.1). 132

Figure 8.13 3D models comparison created on the base of pre- and post-storm RTK GPS measurements (area no.2). 133

Figure 9.1 Study site location. Deployment of measuring equipment is indicated as follows: ⟠ - position of meteorological station and radar sea level gauge; ♦ - location of the ADCP. Topo-bathymetric profiles are drawn with straight black lines. Typical

cross-shore beach profiles are shown: Profile 3 in the north part is uni-sloped with dune crest at 4.0m and Profile 8 in the south part is bi-sloped. 144

Figure 9.2 Summary of all types of measurements performed and wave history during two measuring seasons. 145

Figure 9.3 Time series of significant wave height Hs, mean wave period Tm, and mean wave direction for the storm February 2009. 146

Figure 9.4 Pre-storm and post-storm profiles along the scientific pier for storm February 2009 147

Figure 9.5 Time series of significant wave height Hs, mean wave period Tm, and mean wave direction for the storm April 2009. 147

Figure 9.6 Pre-storm and post-storm profiles along the scientific pier for storm April 2009 148

Figure 9.7 Time series of significant wave height Hs, peak wave period Tp, and mean wave direction for the storm November 2009 148

Figure 9.8 Pre-storm and post-storm profiles along the scientific pier for storm November 2009 149

Figure 9.9 Time series of significant wave height Hs, peak wave period Tp, and mean wave direction for the storm December 2009 149

Figure 9.10 Pre-storm and post-storm profiles along the scientific pier for storm December 2009 150

Figure 9.11 Time series of significant wave height Hs, peak wave period Tp, and mean wave direction for the storm March 2010 150

Figure 9.12 Pre-storm and post-storm profiles along the scientific pier for storm March 2010 151

Figure 9.13 Sea level measured at Shkorpilovtsi study site combined with wave and wind parameters during the storm in March 2010 152

Figure 9.14 Map of pre-storm bathymetry for 2D modelling and location of transects used for 1D modelling. 153

Figure 9.15 Map of post-storm bathymetry for 2D modelling and location of transects used for 1D modelling 154

Figure 9.16 Pre-storm and post-storm profiles along the Profile 4, shown in Figure 9.14 and Figure 9.15 for storm March 2010 155

Figure 9.17 Pre-storm and post-storm profiles along the Profile 18, shown in Figures 14 and 15 for storm March 2010 156

Figure 9.18 Pre-storm and post-storm profiles along the Profile 20, shown in Figure 9.14 and Figure 9.15 for storm March 2010 156

Figure 9.19 Model results of IO-BASMM for the Profile 4 158

Figure 9.20 Model results of IO-BASMM for the Profile 18 158

Figure 9.21 Model results of IO-BASMM for the Profile 20 159

Figure 9.22 Model results of XBeach for the Profile 4 160

Figure 9.23 Model results of XBeach for the Profile 18 160

Figure 9.24 Model results of XBeach for the Profile 20 161
Figure 9.25 Measured deformations (left panel), calculated deformations (right panel) 162
Figure 9.26 Model results of 2D XBeach simulation sliced at Profile 4 163
Figure 9.27 Model results of 2D XBeach simulation sliced at Profile 18 163
Figure 9.28 Model results of 2D XBeach simulation sliced at Profile 20 164

Figure H.1 Illustration of the use of nested grids. Calculation domain used for the “Pertuis Charentais” area (France). H-2

1 Introduction

1.1 General Aims of the Project

The European funded project MICORE - Morphological Impacts and COastal Risks induced by Extreme storm events – has as the main objective to develop and demonstrate on-line tools for reliable predictions of the morphological impact of marine storm events in support of civil protection mitigation strategies. Severe storms have historically affected European coastlines and the impact of each storm has been evaluated in different ways in different countries. The project is specifically targeted to contribute to the development of a probabilistic mapping of the morphological impact of marine storms and to the production of early warning and information systems to support long-term disaster reduction.

The project is organized in seven so-called Work Packages, which in summary reads as follows:

1 Work package 1

To undertake a review of historical marine storms that had a significant impact on a representative number of sensitive European regional coastlines. The diverse range of coastal regions of the European Union is selected according to wave exposure, tidal regime and socio-economical pressures. They include outmost regions of the European Union at the border with surrounding states (e.g. the area of the Gibraltar Strait, the Baltic and Black Sea), as well as coastlines bordering open ocean and semi-enclosed shelf seas.

2 Work package 2

To collate data related to occurrence of significative extreme events and socio-economic impacts in a database. Parameters will include:

- characteristics of the storms: wind and wave measurements, wave hindcasts, tide measurements, surge computations;
- morphological impacts including pre- and post-storm beach profiles, presence of dune overwashing/overtopping, damage to coastal structures;
- socio-economic impact including cost of reconstruction, loss of lives and property, dune reconstruction and beach replenishment;
- civil protection schemes, implementation of warning systems and preparation of hazard and vulnerability maps;
- competent authorities and statutory bodies and voluntary organisations for warnings

3 Work package 3

To undertake monitoring of nine European case study sites for a period of 1 year with the following aims:

- to collect new data sets of bathymetry and topography using state-of-the-art technology (Lidar, ARGUS, Radar, DGPS); to simultaneously measure the forcing agents (wind and waves, tides, surges) that trigger the events;
- to map the impact of the storms on living and non-living resources using portable GIS methods.

4 Work package 4

To test and develop reliable methods for numerical modelling of storm-induced morphological changes for the following purposes:

- to test the predictive capability of wave and surge hindcast models routinely used by end users in each region of interest;
- to link morphological models with wave hindcast models;
- to evaluate the accuracy of off-the-shelf morphological models for prediction of extreme erosion hot-spots;
- to test and develop a new open-source morphological model for the prediction of storm impacts.

5 Work package 5

To set-up real-time warning systems and to implement their use within Civil Protection agencies with the aim of:

- linking morphological models with wave hindcast models;
- preparing early warning protocols;
- developing an expert system in support of long-term disaster reduction including timely disaster relief operations.

6 Work package 6

To disseminate results to end users at national, European and International levels through:

- a series of non-technical workshops;
- production of a multi-language report;
- production of storm impact video-clips;
- implementation of an interactive website with Web-GIS technology.

7 Overall project management.

1.2 Specific aims of WP 4

1.2.1 Objectives

The objective of this work package is to use, validate and extend the free-ware XBeach model for various European coastal hazard situations and to compare its outputs with off-the-shelf packages. The end goal is to incorporate jointly-developed (between partners) algorithms into one shared operational forecast/predictive model able to predict coastal hazards occurring on a time-scale of storm durations (days). Dune breach, dune erosion, wave run-up and overtopping will be predicted for storm and extreme meteorological conditions for a wide variety of coasts. The model could thus be used for the design of preventive measures, either coastal defences, mitigation or evacuation schemes.

The specific objectives per task are as follows.

1. Existing Data and Models
- Definition of models and test cases (from data in WP2).
- Set-up of test case modelling studies.
- Calibrate, validate and test off-the-shelf models prediction capabilities.

2. XBeach model
- Distribute the XBeach model to partners.
- Improve the resolution of bathymetry using Argus video and/or x-band radar data (where available).
- Calibrate, validate and verify the XBeach prediction capability for test cases defined in Task1.
- Develop functionality and routines for impact assessment.
- Incorporate XBeach into UCIT.

3. Connection with socio-economic impact
- Connect off-the-shelf and XBeach models with socio-economic impacts via Storm Impact Indicators (SIIs) in a GIS platform from where risk maps and associated socio-economic impacts can be derived for a range of storm/flood conditions

1.2.2 Background

A major aim is to test new and off-the-shelf models able to predict coastal changes after major storms. In WP4 routine models already used at each site will be tested with old and new datasets, while a new open-source model will be calibrated to give new means of predicting storm effects. A new model (XBeach) will be used to predict coastal changes generated by high energy events. XBeach is open-source and thus allows all the partners to modify the codes in order to calibrate it. The model will be a useful means for European countries to produce predictions of storm impacts on beaches considering all the information available. The new model will be relevant to many different conditions among European coastlines, so that it will be suitable for countries facing the Atlantic Ocean as well as for countries facing the Mediterranean Sea or the Black Sea. XBeach will be used together with information regarding the socio-economic impact of storms so that a complete set of data will be obtained to produce risk maps (WP5). The outputs from the connection between the model and the socio-economic impact will be used to develop Storm Impact Indicators (SIIs) that will be defined considering the impact of future storm scenarios, based on historical storm information (WP1) and new data collected within the MICORE Project (WP3), both morphological and hydrodynamics. The Indicators will be related with the possible damage to natural and/or human properties, to the magnitudes (small, medium or high damage or complete destruction) and to the longshore and cross-shore spatial impact of the events. An Impact Threshold will be defined in order to know which are and will be the hydrodynamic and morphological conditions that lead to a coastal disaster or to damage to coastal structures and sensitive ecological environments like dunes and salt marshes. SIIs' thresholds will become important criteria to create risk maps with different risk levels according to oceanographic predictions.

XBeach is a freeware numerical model which is developed by Delft partners (UNESCO-IHE, Deltares and TU Delft) under continuing funding by the US Army Corps of Engineers for the application to U.S. sandy coastlines under hurricane conditions. This model solves the nonlinear shallow water equations for water surface elevations and the energy equations for short wave transformation in a coastal region of a few kilometres alongshore by one kilometre

cross-shore. The hydrodynamic equations are coupled with sediment transport equations, both in the subtidal area and on the shore- and dune face, so that coastal and dune erosion and dune overwash processes as well as wave run-up and overtopping can be modelled. The input required is the bathymetry/topography, the offshore wave conditions (integral wave parameters) and surge levels (to be supplied by WP 2). The model then computes the wave transformations, time-varying set up, swash, wave-driven currents and sediment transport. This model is well suited for the study of coastal hazards for a wide variety of European coasts after extension and validation proposed in this project.

1.2.3 Phases of the WP4

1.2.3.1 Task 1: Testing of off-the-shelf models

Phase 1.1: Definition

Months 1-2: In the first phase the WP leader will draft a memo with an overview of the available (i.e. proposed by the partners) off-the-shelf models and make a proposal for the data sets (lab and field data) which should be used for evaluation. This memo will be circulated among partners for review and comments, after receipt of which the WP leader will produce a final draft.

Month 6: First meeting with partners in WP4 to discuss and finalize the memo. The product is a final memo describing the models and the data sets.

Phase 1.2: Intake of data

Months 3-18: Intake of data sets for validation. These data sets will be delivered by partners and stored by WP leader in the data base developed in WP2, and may include the data collected under WP1/3 (field cases) but also laboratory cases. The data will be available for partners for testing their selected off-the-shelf model. The product is a digital database of field (WP2) and lab cases.

Phase 1.3: Testing of models

Month 3-24: Testing, calibration and validation of off-the-shelf models by partners. The product is an integrated report based on the assessment reports from each partner including a critical review on the basis of which either model can be improved. The integration will be done by the WP leader.

1.2.3.2 Task 2 XBeach model

Phase 2.1: Distribution

Month 6: The XBeach model (see Background above) will be distributed to partners under a GNU Lesser license (Free of charge). The distribution will be accompanied by a training session. After the project end, extension of license for project participants will be negotiated. Training by the WP leader in the use of XBeach will be given at Delft concurrent with the meeting described in Phase 1.1.

Phase 2.2: Improvement of bathymetry

Months 6-14, ongoing to Month 30: Improvement of resolution of bathymetry using Argus video or x-band radar data. This can be done using the Beach Wizard system, which will be provided free to interested partners for the duration of the project. The system needs an Argus video station or x-band radar station. We foresee application to video-outfitted sites at Egmond Beach (Netherlands), Lido di Dante (Italy), Lido di Sète (France), Ria Formosa (Portugal) and to the x-band radar station on the Dee Estuary (UK). For this purpose, the Beach Wizard system will be integrated with XBeach by the WP leader before the distribution. The distribution will be accompanied by training at Delft in the use of the system including video/radar data preparation.

Phase 2.3: Validation of model

Months 7-30: Testing, calibration and validation of XBeach by partners on the basis of available field and lab data. The product is an integrated report based on the assessment reports from each partner including a critical review on the basis of which either model can be improved. The integration will be done by the WP leader.

Phase 2.4: Development of functionalities

Months 7-30: In this phase we will develop extensions to XBeach in conjunction with partners and in order to:

- Include typical (relevant for European coasts) structures such as seawalls, offshore breakwaters and groins, and sediment transport formulations for shingle and pebble beaches.·
- Coupling of XBeach with larger-scale (coastal sea scale of order 100 kilometres) wave and surge models in order to have the latter two provide offshore boundary conditions for XBeach.
- Development of routines for impact assessments (to generate information for WP5)

Phase 2.5: Incorporation of XBeach into UCIT

Months 24-30, starting earlier if possible: Incorporation of XBeach into the UCIT model/data toolkit which will allow users to quickly make predictive evaluations using relevant measured (WP2 product) or Beach Wizard-generated (from Argus/radar WP3) bathymetries.Meetings on Task 2 will be held in Months 18 and 24, coinciding with the general project meetings.

1.2.3.3 Task 3: Connection with socio-economic impact

Months 24-30: To connect off-the-shelf models and XBeach model with the socio-economic impact via Storm Impact Indicators (SIIs). The main focus of WP 4 is to assess the natural hazards (erosion, flooding etc.) to coastal areas. The socio economic impact will mainly be focused on the translation of hazards into risks. The translation of hazards to risks is performed by WP5. The work in WP4 under this heading is to develop routines that extract from the database and model results the information required by WP5. The project will conclude with a final meeting, coinciding with the general final project meeting, and a final report (Month 36).

1.2.4 Deliverables of activities (WP4)

The deliverables of WP4 are:
- D 4.1: Calibration and validation of off-the-shelf models (Delivery date: month 24)
- D 4.2: Calibration and validation of XBeach (Delivery date: month 30)

This report is a combined deliverable D4.1 and D4.2.

- D 4.3: New algorithms for storm impact prediction (Delivery date: month 30)
- D 4.4: Definition of SIIs (Delivery date: month 30)
- D 4.5: Connection of models with socio-economic impact (Delivery date: month 30)

1.3 Contributing partners

The following table lists the partners (beneficiaries). Note that not all partners participate in this WP4 and that some have combined efforts.

Table 1.1 Project partners (beneficiaries)

Beneficiary Number *	Beneficiary name	Beneficiary short name	Country	WP4 partner
1 (coordinator)	University of Ferrara	UniFe	Italy	Yes
2	Hydro-Meteorological and Climatological Service of the Emilia Romagna Region, Italy (ARPA)	ARPA	Italy	Yes with 1)
3	Geological Survey of the Emilia-Romagna Region	SGSS	Italy	No
4	University of Algarve	UALG	Portugal	Yes
5	University of Lisbon - Fundação da Faculdade de Ciências da Universidade de Lisboa	FFCUL	Portugal	Yes, with 4)
6	University of Cadiz	UCA	Spain	Yes
7	BRGM-French Geological Survey - Regional Geological Survey of Languedoc-Roussillon Montpellier	BRGM	France	Yes
8	International Marine Dredging Consultants	IMDC	Belgium	Yes
9	University of Plymouth	UoP	UK	Yes, until Month 30 and with 14)

10	University of Szczecin	USZ	Poland	Yes
11	Institute of Oceanology, Bulgarian Academy of Sciences	IO-BAS	Bulgaria	Yes
12	Stichting Deltares	WLD	The Netherlands	Yes
13	Technical University of Delft	TUD	The Netherlands	Yes, with 12)
14	Proudman Oceanographic Laboratory	POL	UK	Yes
15	University Pablo de Olavide	UPO	Spain	No
16	Consorzio Ferrara Ricerche	CFR	Italy	No

1.4 Summary and main results of the validation study

1.4.1 Introduction

The European funded project MICORE - Morphological Impacts and COastal Risks induced by Extreme storm events – has as the main objective to develop and demonstrate on-line tools for reliable predictions of the morphological impact of marine storm events in support of civil protection mitigation strategies. Severe storms have historically affected European coastlines and the impact of each storm has been evaluated in different ways in different countries. The project is specifically targeted to contribute to the development of a common probabilistic mapping of the morphological impact of marine storms and to the production of early warning and information systems to support long-term disaster reduction.

The first step in the modelling effort is to compare the results of a newly-developed coastal response model called XBeach (Roelvink et al, 2009) with existing off-the-shelf models, using data gathered at nine different sites in the EU.

1.4.2 Study sites and measured data

The objective of modelling effort within MICORE is to use, validate and extend a open-source coastal erosion model called XBeach (Roelvink, et al. 2009) for various European coastal sites and to compare its outputs with off-the-shelf packages such as LITPROF, SMC, SBeach, IO-BAS and Durosta which are now locally used.

The coastal sites where field data was collected are shown in Figure 1.1 and include Lido di Dante-Lido di Classe, Ravenna (Italy), Praia de Faro (Portugal), Urban beaches of Cadiz Bay (Spain), Lido of Sete to Marseillan Beach (France), The Dee Estuary (United Kingdom), Egmond Beach (The Netherlands), Mariakerke Beach (Belgium), Dziwnow Spit (Poland) and Kamchia-Shkorpilovtsi Beach (Bulgaria). Each field site has a unique bathymetry/topography and/or wave/tidal climate and will contribute to and test the modelled physics under a wide range of environmental conditions. The sites are all described in the following chapters.

Field data collection was initiated in the Fall of 2008 and concluded in 2010. These are reported under Work Package 3. Unfortunately, no major storms have been recorded in Northern Europe but some have occurred in the Mediterranean Sea. For this reason the testing of the model at the Belgian and British sites was done using historical storm data, while the Dutch field campaign was replaced with a model assessment using extensive laboratory and extra-European field data.

The measured data includes water levels (tide and surge), wave heights (offshore and nearshore) and pre- and post-storm morphology, with which it is possible to evaluate the performance of several cross-shore profile models.

Figure 1.1 The MICORE study sites in the European Union.

1.4.3 Modelling

1.4.3.1 Off-the-shelf models

The coastal response is evaluated by a number of existing 1-D coastal profile models. These models include LITPROF (Broker et al, 1991; Elfrink et al., 2000; DHI, 2009), SMC (U. Cantabria, 2009), SBeach (Larson and Kraus, 1989; Larson et al., 1990; Larson et al., 2004), the IO-BAS model (Trifonova, 2007) and Durosta (Steetzel, 1993). These models are limited by the inherent assumption of longshore uniformity in forcing and bed profile. Longshore dynamics caused by changes in dune height, shoreline angle and wave conditions can only be parametrically incorporated in cross-shore profile models. Field studies have shown that overwash is highly influenced by spatial variations in forcing and dune strength (Morton and

Sallenger, 2003). Also, time-dependency of the wave forcing is only accounted for in a parametric way. It is obvious that this is important since time-varying forcing generates infragravity waves which are important in the swash zone. Therefore it would appear important for any model to incorporate longshore variation and IG wave motion in order to successfully simulate dune erosion and overwash in a broad range of cases. This is the reason why a new two-dimensional and time-dependent model, called XBeach, is an important innovation in this field of coastal research.

1.4.3.2 XBeach model

XBeach is a time-dependent 2D horizontal morphological model which concurrently solves the time-dependent short wave action balance, the roller energy equations, the nonlinear shallow water equations of mass and momentum, sediment transport formulations and bed update on the scale of wave groups. We refer to Roelvink et al. (2009) for details on the model description.

With respect to the wave action and roller equations, the directional distribution of the wave action density is taken into account in the model. The frequency domain is reduced to a single representative peak frequency, assuming a narrow banded incident spectrum. The wave action and roller energy are used to compute radiation stress (gradients) which are on the right-hand side of the nonlinear shallow water equations. Using these formulations it is possible to generate directionally-spread infragravity waves and time-varying currents. To include short wave-induced mass fluxes and return flows in shallow water, XBeach uses the Generalized Lagrangian Mean formulation (Andrews and McIntyre, 1978).

Sediment transport rates are calculated using an advection-diffusion equation (Galapatti and Vreugdenhil, 1985). The equilibrium concentration source-sink term is calculated using the Soulsby-Van Rijn formulation (Soulsby, 1997).

The XBeach model can be applied to areas extending several kilometers in the longshore and about a kilometer (several surfzone widths) in the cross-shore. This limited extent implies that it needs boundary conditions of tidal- and wind/pressure-driven water levels, deeper-water (outside the surfzone) wave boundary conditions and bathymetry. The wave boundary conditions can be applied as time series of the instantaneous wave height including wave grouping, or alternatively, the time-steady wave forcing can be used (which may still result in unsteady currents and surface elevation).

1.4.4 Results

In this section the results are collated from the conclusions which are detailed below. For the case of **Lido di Dante, Italy**, which has a mixture of pristine and urbanized beaches, the modelling effort showed that XBeach performs better than SBeach in terms of the Brier Skill Score, particularly in its ability to simulate frontal dune erosion with reasonable degree of skill. Optimal results are obtained by using a slightly modified parameter set from default values. Model testing in the section of the study site with offshore breakwater structures highlights the necessity to run two-dimensional model simulations for these cases. This is because of the inability of water to return seaward in one-dimensional simulations, resulting in unreasonable water level increases behind the structures. This problem is shown to be overcome in 2DH mode.

At **Praia de Faro, Portugal** beach profile response to storm conditions at 3 beach transects at the reflective Faro Beach, were used for extensive testing/calibration of XBeach. Sensitivity runs showed that alongshore profile morphology variations even for the same site, may require different calibration settings in order to achieve optimal performance. The main discrepancies compared to the field measurements were related to the overestimation of berm erosion and the intense avalanching/beach scarp formation; which are rare at the study site. Moreover, the simulations resulted in morphological change along a narrower profile section than observed; and did not predict offshore bar formation.

The study highlights that predicting beach profile morphodynamic response during storm events at steep reflective beaches with XBeach is demanding. However, results were satisfactory after calibration and resulted in BSS of the range 0.2-0.7. The estimated BSS values are significantly superior compared to the ones of the LITPROF optimal cases.

At **Cadiz Urban Beaches in Spain,** the three profiles produced valid results for both the XBEACH and the off-the-shelf Petra model. The North and Central profile performed better while the South profile showed significant higher berm erosion. BSS values were better for the off-the-shelf model but that was mainly because of the reduced berm erosion since over the rest of the intertidal area the two models produced equal results. The elevations of the erosion over the upper part of the beach in the XBEACH simulation are in agreement with field values of run-up (Stockdon et al., 2006). Hence, the increased sediment transport over this part of the profile it is not due to the overestimation of the hydrodynamic processes but more due to overestimation of the complex sediment transport processes over the swash zone. This sediment transport processes, that will be important in the simulation of higher energy events, are absent from the SMC (PETRA) model. The absence of the long waves run up and sediment transport in the SMC (PETRA) resulted in an advantage of the model over the simulation of the mild storm conditions used in the present case but it will probably be inadequate for higher storm events.

At **Lido di Sète, France**, the reference event was a mild storm which occurred on December 26th 2008. Two models, Marsouin and XBeach, were tested in different configurations. From the results, it was concluded that morphological responses obtained by the models does not correspond very well to field measurements. According to Marsouin, many processes are not taken into account, specifically cross-shore processes, defined by wave asymmetry, and infragravity dynamics. The first one is probably in charge of the inner bar offshore migration that is why we do not observe this movement on the Marsouin's result. Knowing that Marsouin is not able to calculate run-up values, it cannot reproduce the sand deposit on the beach. With regard to XBeach, results do not match with field measurements because the modelled event pertains to bar migration in a mild storm, for which XBeach is not intended.

At **Ostende Beach and Mariakerke Beach, Belgium**, the 1D version of the XBeach model shows good performance: the erosion profile near and above the water level is well reproduced. In general the performance of XBeach is at least as good as Durosta for beach erosion where no "hard structure" (e.g. dykes) are involved. Brier skill scores of on average 0.45 are found for Durosta, while about 0.53 is found for XBeach. The 2D XBeach model gives slightly better results, especially in sections in areas where both the dike and the beach in front are curved, which causes higher gradients in the sediment transport. This clearly illustrates a case where the use of a 2D model instead of a 1D model is preferable.

The models were also applied to a hypothetical 1/1000 year event. Quite some difference are noticed between Durosta and XBeach, the most important being the smaller amount of erosion found with XBeach close to the dyke. Since no reflection of short waves is included in the model, the scour (hole) near the dyke will probably be underestimated. This is clearly a point where improvement can be made.

At the **Sefton Coast, UK,** the 31 March 2010 storm allowed the calibration of the XBeach model using “factory settings” as much as possible. Post-storm morphology, quantified using the dune toe survey data to define the dune recession, indicates that XBeach predictions of erosion are approximately correct. It is now considered that the XBeach model setup for the UK site is completed and provides a good and reliable indication of storm impact on the dune frontage.

Test were undertaken to assess if multiple 1D or a single 2D XBeach model is required to accurately describe the observed spatial differences in coastal responses to a storm. With the recent addition of a modelling option to add oblique wave to 1D models, the alongshore current is simulated, resulting in more effective removal of eroded sediment in the alongshore direction. In the simulations reported here, this gave better agreement between measured and predicted post-storm profiles (increase in Brier skills score of c. 10%). Results also matched more closely those obtained using the 2D version of the model. 1D model runs are quicker to perform making multiple test practicable and allowing sensitivity analyses of model outcomes to be undertaken.

The optimised XBeach model has been applied to a number of historical storms in the period 2002 to 2008, and in all cases XBeach reproduced the morphological change with moderate skill. These results demonstrate that XBeach has a good ability to assess the impact of storms in the future and may even have utility when predicting how a given coastline may respond to elevated sea levels and more severe storms.

The River Alt study presents a situation that is not uncommon in the UK, and one that provides an efficient flood route for salt water intrusions into inland areas. In cases where coastal dunes are less well-developed than for the case examined here, storm damage and breaching could greatly enhance inundation of similar fluvial systems by the sea, and lead to unexpected flooding to inland areas. It is believed that although other flood models with flexible mesh gridding systems provide a better means of simulating situations like the River Alt (e.g. MIKE), they are unable to reproduce well coastal processes that might act to compromise defences. In this respect the use of XBeach may provide an early warning of such events and thus provide an opportunity to devise suitable mitigation.

Three profiles located in the investigated area of **Dziwnow Spit, Poland** were used to test the XBeach model. Simulation results for profiles located in an area where natural process are not disturbed by the presence of structures (profile 386.5 and 386) showed higher BSS values than profile 391 which is situated close to the jetty. The results show a good reproduction of beach and dune erosion while the underwater part of the profiles, especially where a bar system is present, are too smooth. The deviations resulted in a maximum Brier Skill Score of 0.39.

At **Kamchia-Shkorpilovtsi Beach, in Bulgaria**, a comparison between two 1D models (IO-BASMM and 1D XBeach) shows that neither of them give satisfactory results at the sub-aerial beach. XBeach overestimates berm erosion in all cases, while IO-BASMM does the contrary except for the simulation over Profile 18 (Figure 9.20). In the profile portion between shoreline and trough, where erosion takes place during storm, IO-BASMM predicts small erosion (i.e. underestimates erosion), while XBeach predicts deposition.

The model performance results in either negative or very low BSS values for both models. Inspection of the pre- and post-storm bathymetries revealed that two-dimensional processes are likely to be important, and that 1D cross-shore profile models cannot expect to give good results (unless heavily tuned). The 2D XBeach implementation shows considerably better prediction of berm erosion, although the case is not the same with respect to the bar. Moreover, calculated maximum run-up represents very well observed post-storm state of the sub-aerial beach and almost coincides with measured impact.

2 Lido di Dante, Italy

Mitch Harley, Clara Armaroli and Paolo Ciavola, U. Ferrara, Italy.

2.1 Objectives

For the Italian study site, the modelling objectives are to simulate within a reasonable degree of accuracy the marine storm response at both the natural and protected sections of coastline that characterise this region. For the natural sections the modelling is focused on dune behaviour, in particular the amount of dune erosion caused by a storm and whether or not overtopping/flooding of the backshore occurs. Urbanised sections meanwhile are most often protected by a series of offshore breakwaters and the model needs to be assessed as to how well it operates under such configurations. Specifically the model behaviour with regards to wave transmission over the breakwaters and erosion/flooding of urban areas behind the structures needs to be evaluated.

Another modelling objective for this site is concerning coastal management. As an additional protection measure, artificial dunes are constructed before each winter to protect urban areas from marine storms. While this is currently done using the on-site experience of the operator, modelling can be used to optimise the placement and configuration of these dunes.

2.2 Site and climatology

2.2.1 Description of area

The study site is the Lido di Dante-Lido di Classe area – an 8 km stretch of sandy beaches along the Emilia-Romagna coastline in northern Italy and facing the Adriatic Sea (Figure 2.1). The site is a mixture of urbanised (approximately 40% of the total area) and relatively pristine (approximately 60%) coastal environments. The seaside towns of Lido di Dante and Lido di Classe are located at the site's northern and southern boundaries respectively. Offshore from these towns are a series of shore-parallel emerged and submerged breakwaters that offer some protection during energetic conditions. Between the towns is a natural park consisting of natural vegetated dunes and no coastal protection. Three river mouths are located at the site: one at Lido di Dante (Fiumi Uniti); one at Lido di Classe (Fiume Savio); and one bisecting the natural park in the centre of the study site (Torrente Bevano).

The submerged beach is generally composed of fine sand, while the beachface is made up of fine to medium sands (D50 ≈ 0.02 mm). The intertidal beach slope varies significantly along the 8 km of coastline, from mild (2.5%) to steep (14%). Steep values are representative of areas adjacent to coastal defence structures (i.e. groins) while the area inside the natural park generally consists of lower gradients. The mean submerged beach slope is 3%. According to the morphodynamic classification of Wright and Short (1984), the beaches are considered as having intermediate beach states. Low tide terraces are often observed both in the protected and natural areas. Submerged longshore bars meanwhile are only present in the areas outside of offshore structures.

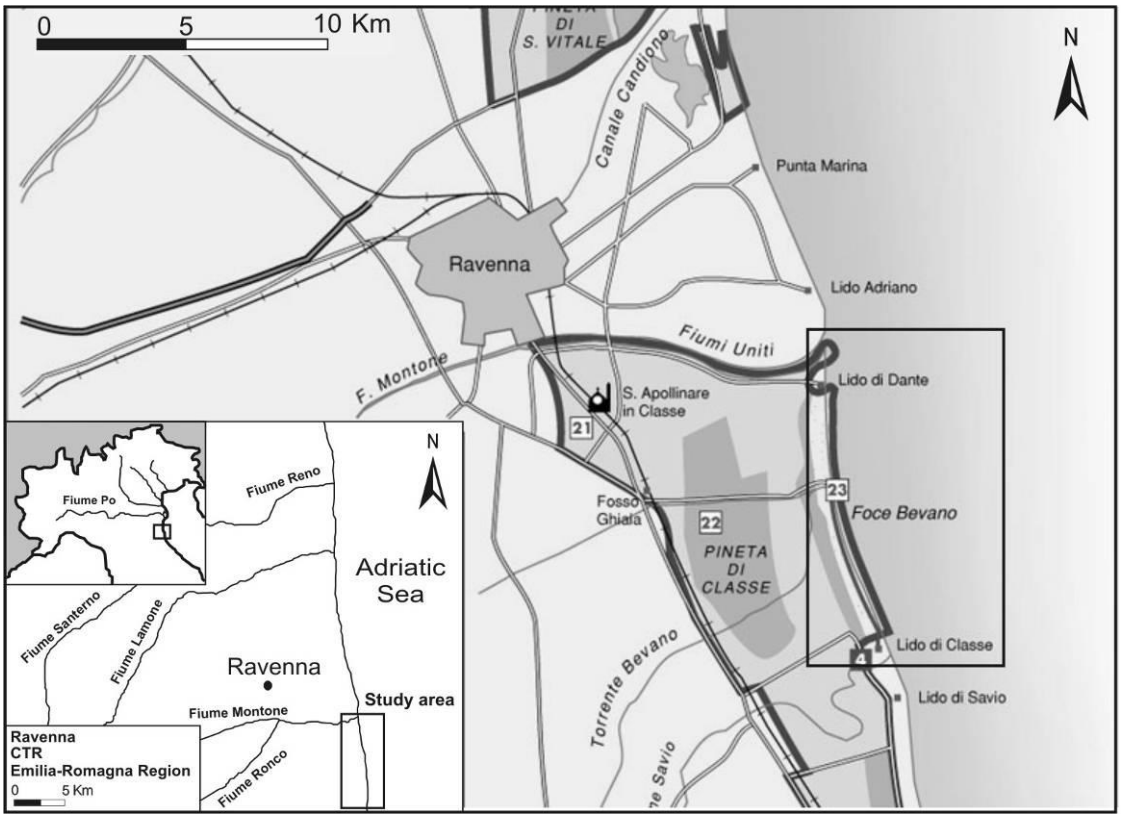

Figure 2.1 Map of the Lido di Dante-Lido di Classe site, on the Adriatic Sea in Northern Italy.

The wave climate of this region is generally small, with 91% of significant wave heights below 1.25 m. The prevalent wave direction is from the east, while the most intense storms are from the ENE (known as the “Bora wind”). The Bora wind is a strong, cold, gusty wind that blows intermittently but mainly during the winter months. It not only has a strong influence on the wave climate of this region, but of the general circulation patterns of the entire Adriatic Sea. South-easterly waves meanwhile are much less significant, since SE winds are sheltered to some degree by the Conero Headland approximately 120 km south of the site.

In regards to water level variations, the area is microtidal with a mean neap tidal range of 30-40 cm and a mean spring tidal range of 80-90 cm. The tidal signal has both diurnal and semidiurnal components. Tidal anomalies of up to double the maximum tidal elevation can occur as a result of surge. This is particularly the case during SE wind conditions, where the fetch across the Adriatic Sea is greatest.

2.2.2 Storms considered

Within the 2008-2010 monitoring period, two storms were selected for calibration of the off-the-shelf and XBeach (see Appendix E) models. The characteristics of these two storms are presented in Figure 2.2.

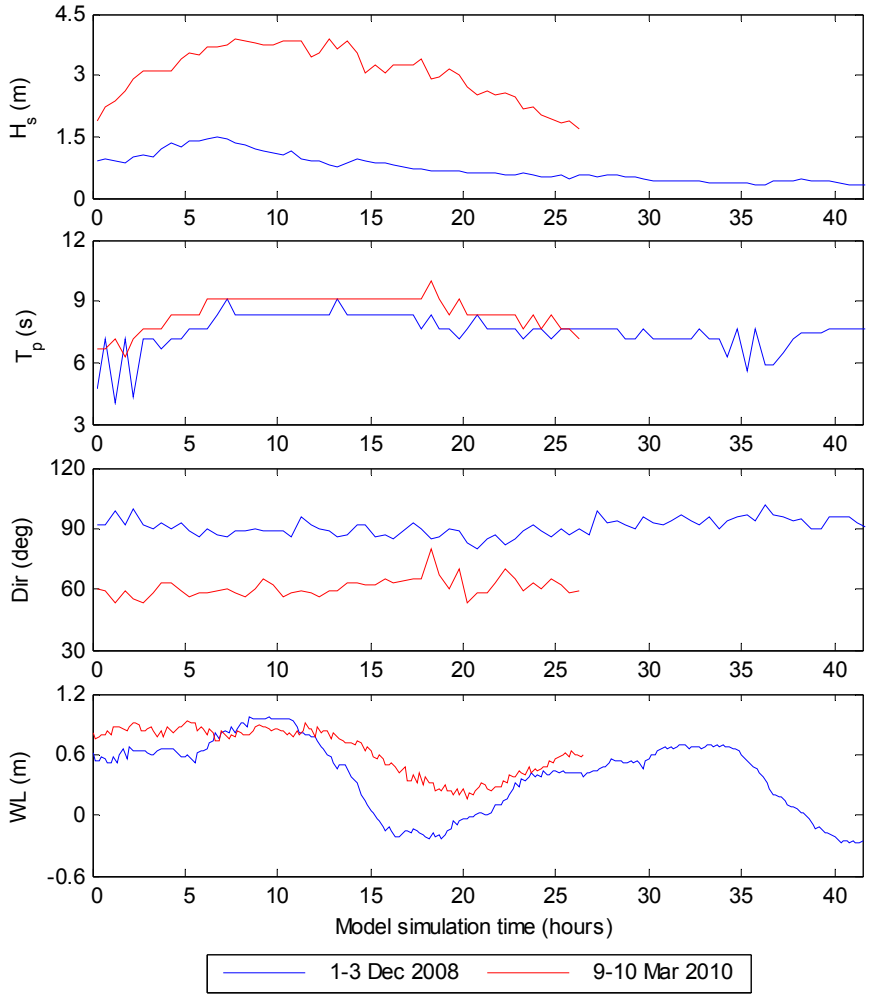

Figure 2.2 Characteristics of the two storms used for model calibration: significant wave height (Hs), peak period (Tp), direction (Dir) and water level (WL).

The first storm occurred between 1-3 December 2008 and is characterised by small waves (peak Hs = 1.47 m) but very high water levels (peak WL = 0.92 m). The direction of this storm was from the east with wave periods around 8 seconds.

The second storm occurred between 9-10 March 2010 and represents a combination of both very large waves (peak Hs = 3.91m, roughly equivalent to a 1-in-5 year return interval) and high water levels (peak WL = 0.93 m). The direction of this storm was from the ENE, with slightly longer wave periods (around 9 seconds).

2.2.3 Measurements

2.2.3.1 Hydrodynamic measurements

Wave data was taken from the wave buoy located approximately 20 km south of the site and 5.5 km offshore from the town of Cesenatico (44.2155°N, 12.4766°E). This buoy is located in approximately 10 m water depth. Tide data was obtained from a tide gauge located approximately 10 km to the north of the site at Porto Corsini, Ravenna.

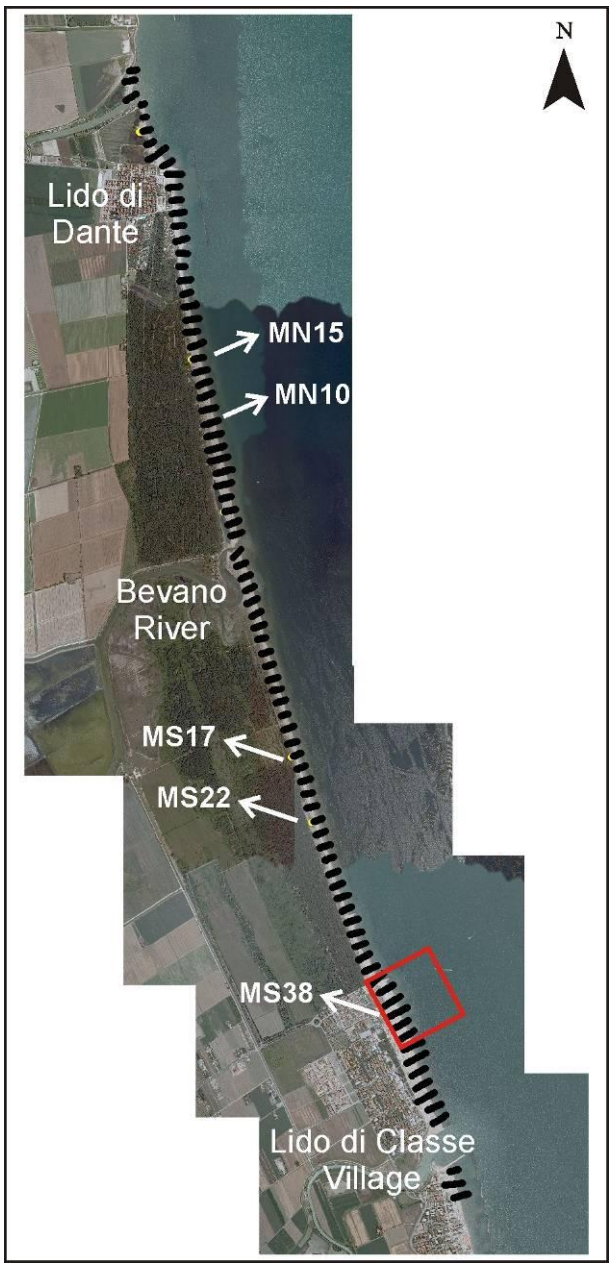

Figure 2.3 Location of the five profile lines (Profiles MN15, MN10, MS17, MS22 and MS38) selected for 1DH modelling at the Lido di Dante – Lido di Classe site. The red box represents the model domain for 2DH modelling

2.2.3.2 Morphological measurements

Topographic measurements were undertaken by measuring cross-shore profile lines 100 m apart using RTK-GPS. Bathymetric measurements of the same profile lines were meanwhile undertaken using a single-beam echo sounder. A single topographic LIDAR survey was performed on 10 March 2009 to complement a bathymetric LIDAR survey of the study site in early June 2006. A more detailed discussion about morphological measurements is presented in report D1.3.

From this dataset of the entire study site, five profile lines were initially selected for one-dimensional depth-averaged (1DH) modelling of the two storm events. These profile lines are indicated in Figure 2.3. Four of the profile lines are located in the natural area, with two (Profiles MN10 and MN15) to the north of the Bevano river mouth and two (Profiles MS17 and MS22) to the south. The fifth profile line (Profile MS38) is located in the town of Lido di Classe and disects one of the offshore breakwater structures there. For reasons discussed below however, 1DH modelling of this profile line was found to be inadequate and warranted running two-dimensional depth-averaged (2DH) model simulations in this region with offshore structures instead. Hence 1DH model calibration was restricted to the four profiles in the natural area.

A combination of morphological data was used to create complete cross-shore profile lines for input into the models. For the December 2008 storm, pre-storm morphology was obtained from a topographic and bathymetric survey conducted between 29 September and 1 October 2008. Topographic, but not bathymetric, measurements conducted between 9-12 February 2009 were used for the post-storm measurements. For the March 2010 storm, pre-storm morphology was derived from a topographic survey undertaken in February 2010 and a bathymetric survey undertaken in September 2009. Topographic, but not bathymetric, measurements were performed one week after this storm (between 16-19 March) and used for the post-storm measurements.

Statistics of the initial profile configurations of these four profile lines as well as the beach response (shoreline retreat and volume lost above MSL) are listed in Table 2.1. As can be seen from these statistics, minor sand volume loss of up to a maximum of 13.2 m^3/m above MSL is observed for these two storms. Shoreline retreat of up to 8.7 m is also observed, although profile MN15 actually indicates minor shoreline accretion. This is due to eroding sand from the upper dune profile depositing on the lower profile.

Table 2.1 Statistics of profile configurations and storm response for the two storms and four profile locations modelled. Shoreline retreat is defined by the change in the 0.5 m contour line and the intertidal slope between the ±0.3 m contours.

Profile	December 2008 Storm				March 2010 Storm			
Statistic	**MS22**	**MS17**	**MN10**	**MN15**	**MS22**	**MS17**	**MN10**	**MN15**
Dune crest height (m)	2.7	3.4	4.2	3.3	2.8	3.4	4.0	2.7
Initial intertidal beach slope	0.04	0.04	0.07	0.14	0.03	0.02	0.06	0.08
Final intertidal beach slope	0.06	0.04	0.02	0.03	0.02	0.01	0.04	0.01
Shoreline retreat (m)	8.7	0.5	6.6	2.6	4.6	7.9	3.9	-1.3
Volume lost above MSL (m3/m)	13.2	4.0	12.4	6.1	8.3	12.6	11.6	3.7

2.3 Model results

2.3.1 Simulation results with Off-the shelf Model

The off-the-shelf model used for the Italian site is SBEACH (see Appendix G), a component of the Coastal Engineering Design and Analysis System (CEDAS Version 3.04). A complete description of the SBEACH model is provided in the Appendix G.

Model calibration was performed on the four profile lines for the two storm events discussed above. Initially SBEACH was run using default settings, with modifications made only for site-specific parameters. These settings are summarised as:

- constant grid (grid width = 1 m for December 2008 storm, 2 m for March 2010 storm)
- landward surf zone depth = 1 m
- effective grain size = 0.2 mm
- max. slope prior to avalanching = 45°
- transport rate coefficient K = 1.75 x 10^{-6} m^4/N
- overwash transport parameter = 0.005
- coefficient for slope-dependent term = 0.002
- transport rate decay coefficient multiplier = 0.5
- water temperature = 15°C
- wave height randomization = on

Each model run was compared to post-storm measurements to calculate the Brier Skill Score (BSS). These BSS results are listed in Table 2.2. Considering default settings for the December 2008 storm, BSS values are slightly positive for three of the four profile lines (average BSS = 0.04). For the March 2010 storm meanwhile all BSS values are negative. These negative values are the result of SBEACH overestimating the erosion resulting from this storm. This is particularly the case for profile MN15, where the model simulates a complete destruction of the dune. The average BSS for three of the four profiles (neglecting profile MN15 to avoid biasing of this result) is -2.15.

As well as default settings, the performance of SBEACH was tested by individually modifying two SBEACH tuning parameters – the transport rate coefficient K and the maximum slope prior to avalanching. From its default value of 1.75 x 10^{-6} m^4/N, K values of 2.5 x 10^{-6} m^4/N (the maximum value suggested in the SBEACH manual) and the equivalent decrease of 1.0 x 10^{-6} m^4/N were assessed. Likewise the model was run using avalanching slopes of 25° and 60° (default value = 45°).

In general, modifying these two tuning parameters was found to make only minor differences on SBEACH model performance. The optimal parameter settings in terms of the BSS was found to be using a K value of 2.5 x 10^{-6} m^4/N. In this case there is a slight improvement in the BSS for the December 2008 storm (average BSS = 0.06). The average BSS for three of the four profiles of the March 2010 storm also increases to -1.11, albeit still negative.

Figures 2.4 and 2.5 display the results of SBEACH modelling using this optimised setting of K = 2.5 x 10^{-6} m^4/N for the December 2008 and March 2010 storms respectively. As can be seen in these figures, SBEACH simulations show an underestimation of erosion for the December 2008 storm, with no change in the upper dune profile and only minor erosion of the lower profile. For the March 2010 storm however the SBEACH simulations indicate an overestimation of erosion of the profile above MSL, particularly with the complete destruction of the dune at Profile MN15.

Table 2.2 Brier Skill Score results for SBEACH model runs using default settings as well as adjusting the transport rate coefficient K and the maximum slope prior to avalanching. Values in brackets indicate the BSS above MSL only. Bold values indicate the optimum settings selected.

Storm	Parameter set	MS22	MS17	MN10	MN15	Average
December 2008	Default	0.16 (0.05)	-0.07 (0.01)	0.04 (0.12)	0.02 (-0.16)	0.04 (0.01)
	K = 1.0e-6	0.13 (0.03)	-0.12 (-0.01)	0.04 (0.10)	-0.03 (0.00)	0.01 (0.03)
	K = 2.5e-6	***0.18 (0.05)***	***-0.05 (0.00)***	***0.04 (0.12)***	***0.05 (-0.36)***	***0.06 (-0.05)***
	slope = 25°	0.16 (0.05)	-0.22 (-0.36)	0.03 (0.11)	0.01 (-0.25)	-0.01 (-0.11)
	slope = 60°	0.16 (0.05)	0.01 (-0.08)	0.04 (0.12)	0.02 (-0.16)	0.06 (-0.02)
March 2010	Default	-1.52 (-1.31)	-2.92 (-3.12)*	-2.02 (-2.01)	-0.91 (-13.23)*	-2.15** (-2.15**)
	K = 1.0e-6	-2.53 (-2.26)	-0.21 (-0.17)	-1.79 (-1.86)	-1.18 (-15.48)*	-1.51** (-1.43**)
	K = 2.5e-6	***-1.05 (-0.89)***	***-0.01 (0.15)***	***-2.26 (-2.34)***	***-0.82 (-12.39)****	***-1.11** (-1.03**)***
	slope = 25°	-1.52 (-1.31)	-2.93 (-3.13)*	-2.00 (-2.07)	-0.91 (-13.23)*	-2.17** (-2.17**)
	slope = 60°	-1.52 (-1.31)	-2.92 (-3.12)*	-2.02 (-2.17)	-0.91 (-13.23)*	-2.15** (-2.20**)

* Complete dune erosion observed

** Profile MN15 excluded from averaging to avoid biasing

2.3.2 Simulation results with XBeach model

2.3.2.1 1DH simulations

All XBeach simulations were undertaken using Version 18 release date 14/07/2010. As with the off-the-shelf model, 1DH XBeach simulations were initially performed using default settings and only adjusting for site-specific parameters, summarised as:

- variable cross-shore grid (minimum grid size = 1 m)
- D50 = 0.2 mm, D90 = 0.3 mm
- morfac = 10
- instat = 41 (gamma = 3.3, spreading = 5°)

BSS values using these default settings at each of the four profile locations and for both of the storm events are listed in Table 2.3. These results indicate that XBeach simulations using default settings for the December 2008 storm perform reasonably well, with a maximum BSS values of 0.77 at Profile MN10 and an average BSS for all four profiles of 0.45. For the March 2010 storm meanwhile, the BSS values are all negative and, as was the case for the SBEACH simulations, Profile MN15 is completely eroded. The average BSS for the three remaining profiles is -4.02.

A total of fourteen combinations of XBeach parameter settings were tested for each profile and storm event. These combinations were obtained by increasing and decreasing certain individual parameters from two different parameter sets – the default settings described above and a second experimental parameter set (hereafter called Parameter Set 1) suggested by model developers. The individual parameters modified were the critical avalanching slope above water (dryslp), the critical avalanching slope below water (wetslp) and the maximum allowed wave height over water depth (gammax).

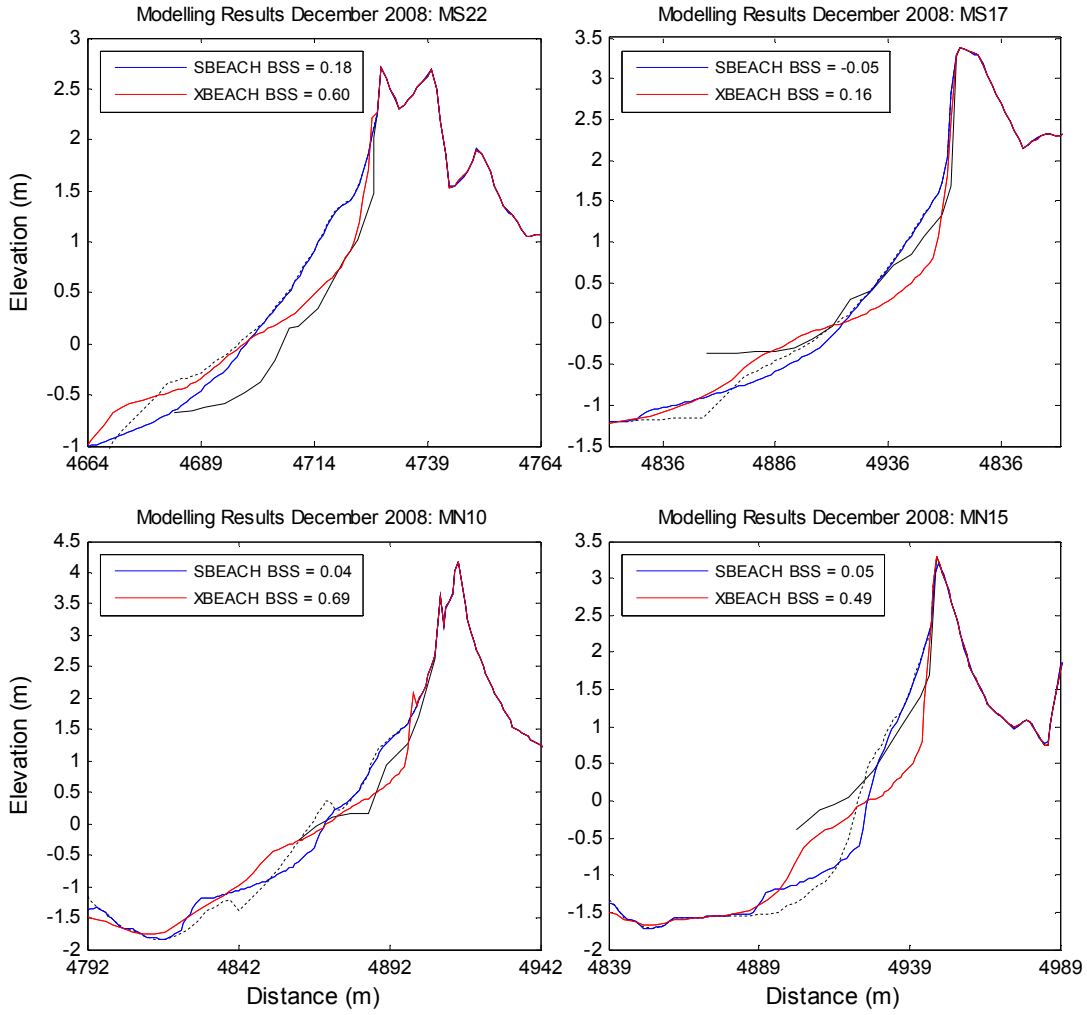

Figure 2.4 Results of SBEACH and XBeach modelling of the 1-3 December 2008 storm event for profiles MS22, MS17, MN10 and MN15. Pre-storm measurements are represented by solid black lines whereas post-stom measurements by dashed black lines.

Parameter Set 1 is defined by the following adjustments from the default settings:

- maximum Courant number CFL = 0.8
- threshold water depth for concentration and return flow hmin = 0.01
- threshold for drying and flooding = 0.01
- nuhfac = 1

Comparing BSS results from the two parameter sets with no adjustments to dryslp, wetslp or gammax indicates that using Parameter Set 1 results in minor improvements in model performance compared to default settings. The average BSS values using Parameter Set 1 for the December 2008 storm is 0.53, as opposed to 0.45 for the default settings. The average BSS is however still negative for the March 2010 storm (average BSS = -2.56) and once again the dune at Profile MN15 is destroyed.

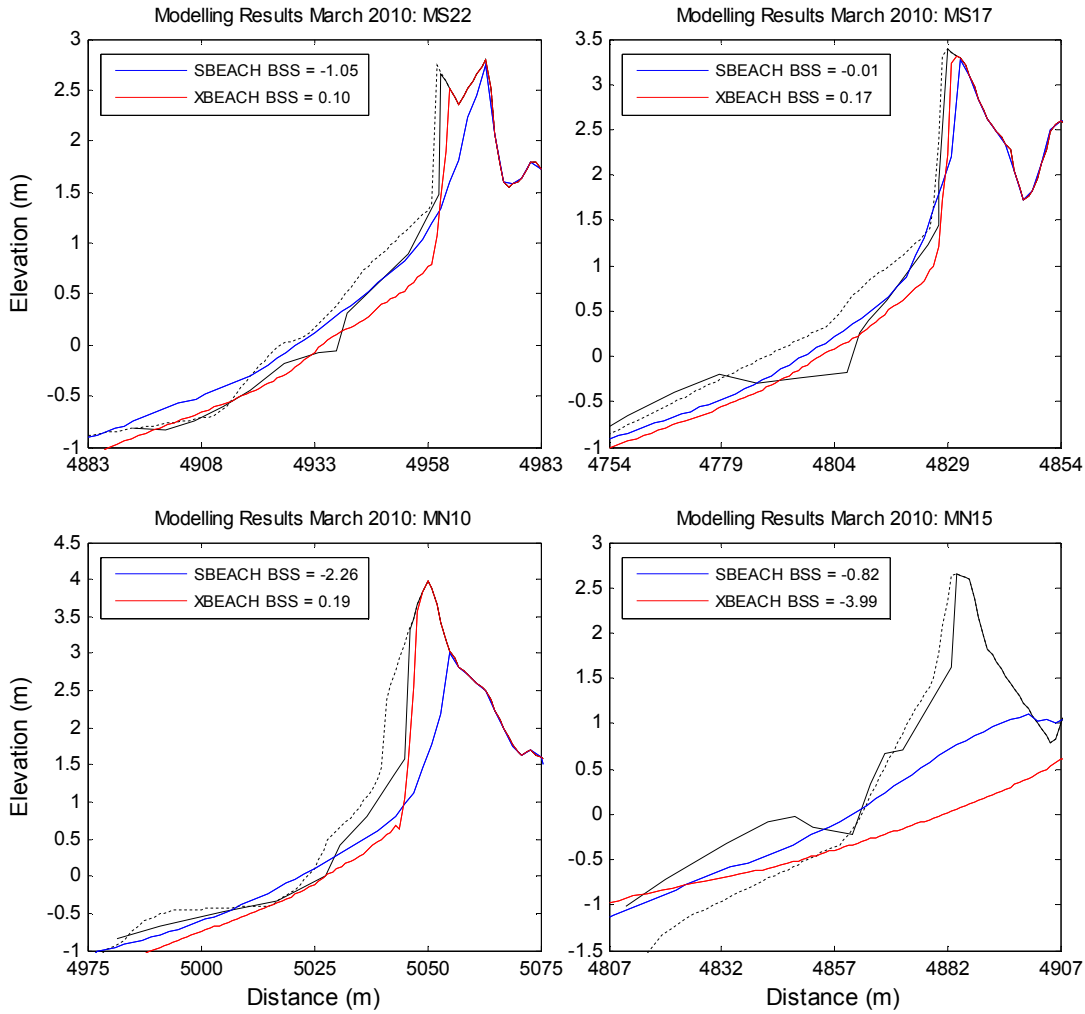

Figure 2.5 Results of SBEACH and XBeach modelling of the 9-10 March 2010 storm event for profiles MS22, MS17, MN10 and MN15. Pre-storm measurements are represented by solid black lines whereas post-storm measurements by dashed black lines.

Considering all fourteen different combinations tested, the optimal settings with regards to the BSS over both storm events was found using Parameter Set 1 and increasing wetslp to 0.5 (from a default value of 0.3). In this case the average BSS across four profiles for the December 2008 event is 0.49. Importantly, while this combination still predicts the dune of Profile MN15 being completely eroded for the March 2010, it is the only one of the fourteen where the BSS for the other three profile lines for the March storm are positive (average BSS = 0.15).

Plots of the model performance for the December 2008 and March 2010 storms using these optimised parameter settings are shown in Figures 2.4 and 2.5 respectively. These figures indicate that the model in general replicates frontal dune erosion with reasonable accuracy in each of the two storm events. The model does however appear to overestimate erosion of the lower subaerial beach, most noticeably between the MSL and +1m contour lines.

Table 2.3 Brier Skill Score results for XBeach model runs for the two storm events using various combinations of parameter settings. Values in brackets indicate the BSS above MSL. Bold values indicate the optimum settings selected.

Storm	Parameter set	Alteration	MS22	MS17	MN10	MN15	Average
December 2008	Default	None	0.56 (0.73)	-0.06 (-1.16)	0.77 (0.78)	0.54 (-1.91)	0.45 (-0.39)
		dryslp = 0.5	0.51 (0.80)	0.02 (-0.93)	0.79 (0.79)	0.50 (-2.23)	0.46 (-0.39)
		dryslp = 2	0.43 (0.59)	0.19 (-0.60)	0.79 (0.79)	0.59 (-1.54)	0.50 (-0.19)
		wetslp = 0.1	-0.86 (-0.86)	-2.55 (-6.90)	-0.12 (-0.10)	-2.54 (-23.88)*	-1.52 (-7.94)
		wetslp = 0.5	0.53 (0.72)	0.16 (-0.62)	0.75 (0.75)	0.47 (-2.00)	0.48 (-0.29)
		gammax = 0.5	0.37 (0.40)	-0.41 (0.03)	0.57 (0.57)	-0.03 (0.17)	0.13 (0.29)
		gammax = 5	-1.49 (-1.28)	-4.29 (-10.77)	-2.02 (-2.00)	-2.27 (-21.93)*	-2.52 (-9.00)
	Parameter Set 1	None	0.58 (0.81)	0.29 (-0.16)	0.73 (0.73)	0.52 (-1.95)	0.53 (-0.14)
		dryslp = 0.5	0.60 (0.78)	0.23 (-0.38)	0.78 (0.78)	0.49 (-2.31)	0.53 (-0.28)
		dryslp = 2	0.57 (0.77)	0.12 (-0.74)	0.75 (0.75)	0.39 (-2.89)	0.46 (-0.53)
		wetslp = 0.1	-0.44 (-0.39)	-1.93 (-5.85)	0.77 (0.79)	-2.34 (-22.67)*	-0.99 (-7.03)
		wetslp = 0.5	***0.60 (0.70)***	***0.16 (-0.35)***	***0.69 (0.69)***	***0.49 (-1.86)***	***0.49 (-0.21)***
		gammax = 0.5	0.25 (0.20)	-0.44 (0.00)	0.34 (0.34)	-0.03 (0.17)	0.03 (0.18)
		gammax = 5	-1.49 (-1.28)	-4.29 (-10.77)	-1.56 (-1.51)	-2.27 (-21.93)*	-2.40 (-8.89)
March 2010	Default	None	-4.20 (-4.47)	-3.63 (-3.87)	-4.24 (-4.41)	-4.89 (-43.40)*	-4.02 (-4.25)
		dryslp = 0.5	-20.67 (-21.56)*	-2.84 (-3.09)	-4.26 (-4.38)	-4.55 (-40.90)*	-9.26 (-9.68)
		dryslp = 2	-3.96 (-3.95)	-2.52 (-2.55)	-5.02 (-5.20)	-5.28 (-46.77)*	-3.83 (-3.90)
		wetslp = 0.1	-21.13 (-22.58)*	-9.12 (-9.76)	-17.62 (-17.84)*	-4.00 (-36.37)*	-15.96 (-16.70)
		wetslp = 0.5	0.45 (0.44)	0.07 (0.28)	-1.00 (-1.02)	-4.88 (-43.46)*	-0.16 (-0.10)
		gammax = 0.5	-1.42 (-1.47)	-2.32 (-2.46)	-3.07 (-3.01)	-4.38 (-39.13)*	-2.27 (-2.31)

		gammax = 5	-18.72 (-19.50)*	-17.64 (-18.73)*	-16.87 (-17.15)*	-4.59 (-41.27)*	-17.74 (-18.46)
	Parameter Set 1	none	-3.30 (-3.38)	-0.55 (-0.40)	-3.84 (-3.99)	-4.61 (-41.15)*	-2.56** (-2.59**)
		dryslp = 0.5	-2.72 (-2.90)	-0.33 (-0.29)	-4.70 (-4.90)	-4.47 (-39.20)*	-2.57** (-2.70**)
		dryslp = 2	-4.39 (-4.59)	-1.51 (-1.38)	-3.47 (-3.61)	-3.84 (-35.63)*	-3.12** (-3.19**)
		wetslp = 0.1	-17.93 (-18.48)*	-9.83 (-10.49)	-14.72 (-14.83)*	-4.64 (-41.79)*	-14.16** (-14.60**)
		wetslp = 0.5	***0.10 (0.06)***	***0.17 (0.56)***	***0.19 (0.32)***	***-3.99 (-34.96)****	***0.15** (0.31**)***
		gammax = 0.5	0.43 (0.52)	-0.68 (0.45)	-0.53 (-0.35)	-0.73 (-3.23)	-0.26** (0.21**)
		gammax = 5	0.28 (0.34)	-15.95 (-16.65)*	-17.15 (-17.03)*	-5.48 (-48.09)*	-10.94** (-11-11**)

* Complete dune destruction observed

** Profile MN15 excluded from averaging to avoid biasing

2.3.2.2 2DH simulations

1DH XBeach simulations were also performed on Profile MS38, the profile containing an offshore breakwater structure. However from initial testing of this profile line it became readily apparent that 1DH simulations are not suitable for this section of the coast where offshore breakwaters are present. This is because model simulations indicated waves breaking on the structure causing a large degree of wave setup behind the structure. Because the structure is considered non-porous in the model, there is no means in a 1DH simulation by which this water can return seawards. Such a scenario subsequently results in an unreasonable and sharp increase in water level in the order of 1-2 m landward of the structure (see Figure 2.6b).

To better simulate these processes, a two-dimensional depth-averaged (2DH) model was established for a 450 m alongshore section of Lido di Classe (Figure 2.6a). This section contains three of the ten emerged (breakwater height ≈ 0.6 m) offshore breakwaters with gaps between each. Three-dimensional topographic data for this model was obtained from the MICORE topographic LIDAR survey in March 2009, whereas bathymetric data was taken from the earlier 2006 bathymetric LIDAR survey.

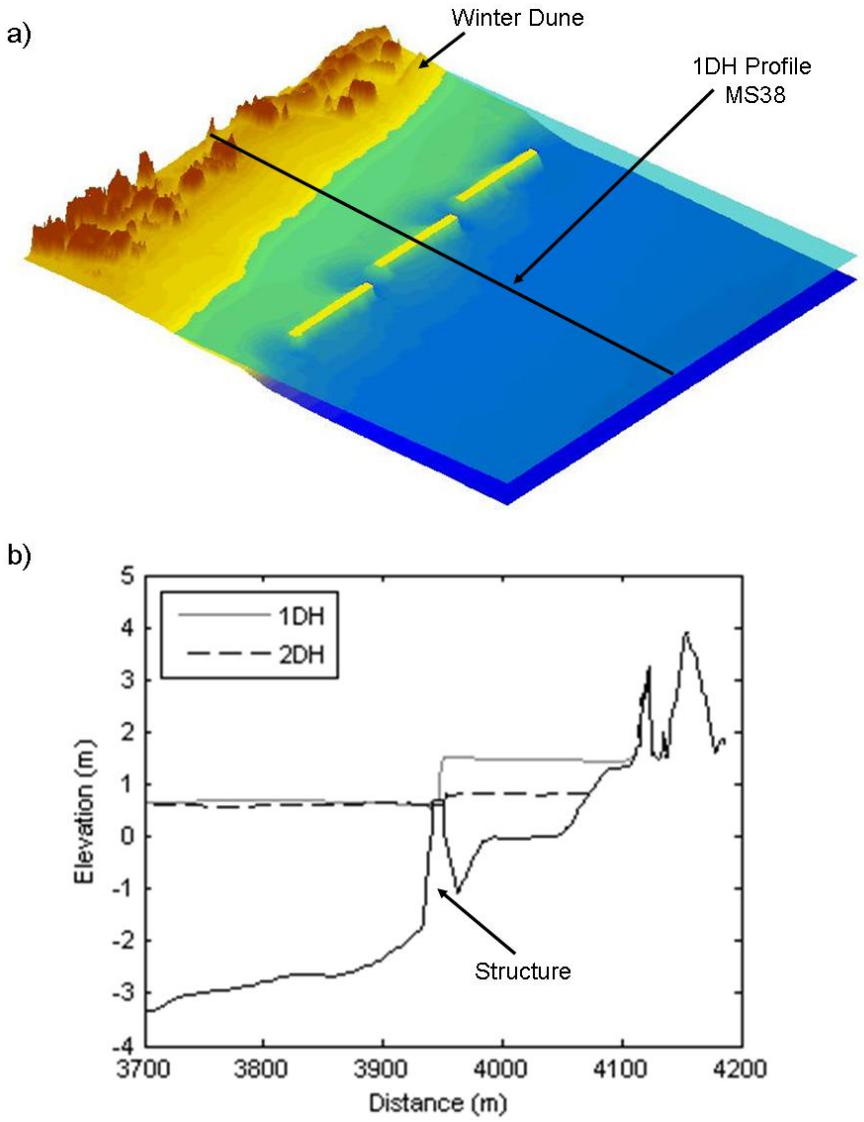

Figure 2.6 a) Two-dimensional model setup for Lido di Classe, where a series of emerged offshore breakwater structures are present, b) Water level comparison between 1DH and 2DH XBeach simulations at a single time-step for the December 2008 storm

A single model run on this 2DH configuration was undertaken for the December 2008 storm using Parameter Set 1 (detailed above). Because the section inside the offshore breakwater in this model configuration is now connected with the open sea, water can return seaward through the gaps in the offshore structures. As shown in Figure 2.6b, which compares the cross-shore water level variability for the 1DH and 2DH simulation at the same model time step, the wave setup landward of the breakwater is significantly reduced in the 2DH simulation.

This 2DH simulation also indicates the potential for optimising configurations of the winter dune, a future modelling objective at the Italian site. The topographic LIDAR survey used in the model contains a winter dune at its northern boundary (see Figure 2.6a) that was constructed to protect one of the buildings at risk. Observations of this simulation indicate that this artificial dune helps to prevent flooding of the building during the very high water levels associated with this storm.

2.4 Synthesis

Extensive model testing has been undertaken at the Italian site using SBEACH as the off-the-shelf model and XBeach for two different storm events – one storm where there are very high water levels but very small waves and another where there is a combination of both high waves and water levels. Considering the Brier Skill Score as a measure of model performance, an optimal set of parameters has been determined for each of the two models. In all but one of the eight cases tested (Profile MN15 for the March 2010 storm), the BSS is noticeably better for the XBeach model than for SBEACH. This is likely due to the fact that XBeach takes into account long wave variability, which is an important process determining dune erosion and is not considered in SBEACH.

For Profile MN15 of the March 2010 storm, both SBEACH and XBeach predicted a complete destruction of the dune where post-storm measurements indicate that only very minor (< 5 m^3/m) dune erosion in fact occurred. This complete dune destruction is a result of the models simulating overtopping of the dune. The reason why the models simulate dune overtopping for this profile line and not the others is most likely related to its steeper beach face and its lack of any prominent offshore sand bar. This means that there is a much narrower surf zone where wave energy is dissipated, so that waves continue up the beach and overtop the dune. Because the dunes of this coastline are low and small and are backed by an extensive low-lying area, it makes the modelling particularly sensitive to overtopping. Hence a slight overestimation of wave energy and run-up can result in overtopping and hence the significant morphological changes observed at Profile MN15. An important process that is currently not considered in the models is dune vegetation that is present across the natural study area. This vegetation acts to stabilise the dunes during storms to prevent such erosion.

All model testing has been calibrated against the Brier Skill Score, which considers the variability in pre and post-storm measurements compared to that predicted by the model. However a limitation of this model testing is the amount of time between the storm passing and post-storm measurements being taken. In the case of the December 2008 storm in particular, another minor storm event occurred on the 25 December 2008 before the February 2009 measurements and was not considered in the modelling. Nevertheless, the XBeach model under all parameter settings had a tendency to overestimate erosion over this period rather than underestimate it (as should be the case if this storm caused did in fact cause any noticeable erosion). The optimum parameter settings was the one that minimised this erosion overestimation.

2.5 Conclusions

This study has revealed many insights into storm erosion modelling at the Italian site. The first point is that comparisons between the XBeach and SBEACH models for the storms considered indicate that XBeach performs better in terms of the Brier Skill Score, particularly in its ability to simulate frontal dune erosion with reasonable degree of skill. Optimum results are obtained by using a slightly modified parameter set from default values, most notably increasing the critical avalanching slope below water (wetslp) from its default value of 0.3 to a value of 0.5.

The second point is that the small and low dunes in the natural section of the study site means that the modelling is susceptible to predicting overtopping and complete destruction of the dunes, as was observed in one of the four profiles tested. This means that model predictions of dune overtopping and complete dune erosion at this site need to be considered with care.

Finally, model testing in the section of the study site with offshore breakwater structures highlights the necessity to run two-dimensional model simulations for these cases. This is because of the inability of water to return seaward in one-dimensional simulations, resulting in unreasonable water level increases behind the structures. This problem is shown to be overcome in 2DH mode.

3 Praia de Faro, Portugal

Michalis Vousdoukas and Oscar Ferreira, U. Algarve, Portugal.

3.1 Objectives

The study objective is to evaluate storm-induced erosion at the Ancão Peninsula. Tests were performed against monitored data and the model will be used both for almost real-time forecast and to determine consequences of storms with an associated return period.

3.2 Site and climatology

Faro Beach is located in the meso-tidal, NW–SE oriented sandy Ancão Peninsula (South Portugal, Figure 3.1). Tides in the area are semi-diurnal, with average ranges of 2.8 m for spring-tides and 1.3 m during neap tides, although a maximum range of 3.5 m can be reached. The offshore wave climate is moderate to high, with an average annual significant offshore wave height H_s=0.92 m and average peak wave period T_p=8.2 s (Ferreira, Vousdoukas and Ciavola, 2009 and references therein). Waves are mostly west-southwest (occurrence ~71%), while shorter period SE waves by regional winds are also frequent (23%) (Ferreira, Vousdoukas and Ciavola, 2009 and references therein). Storm events in the region are considered when the significant offshore wave height exceeds 3 m and typically correspond to less than 1% of the offshore wave climate.

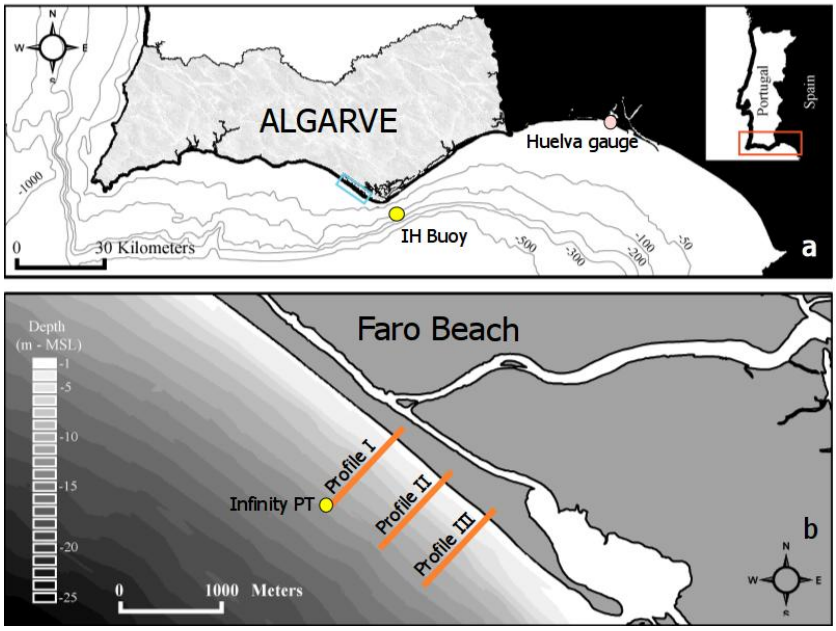

Figure 3.1 Map of South Portugal showing the study area, the Portuguese Hydrographic Institute buoy and the Huelva tidal gauge locations (a). Ancão Peninsula including Faro beach, showing the topographic survey transects and the location of the Infinity pressure transducer (b).

The main sedimentary source for Ancão Peninsula is the eastward-directed longshore drift, nourished by updrift cliff erosion (Dias, 1986). Ancão Peninsula shoreline trend changed from a generic accretion or dynamic equilibrium condition in 1945/1976 to a state where accretion dominates at the eastern part and erosion prevails at the western sector (Ferreira et al., 2006). The shoreline retreat at the western Ancão Peninsula is associated to the eastern displacement of an erosive process started on the 1970s with the construction of the Vilamoura Marina jetties (Correia et al., 1996), 10 km to the west of the Ancão Peninsula. The western part is characterised by stable foredune with blowouts (Dias, 1988) and dune bluffs, but the eastern part is more dynamic with lower incipient foredunes.

At the landward side of the barrier, a sandy beach exists in an environment dominated by the tidal currents and minor fetch-limited waves (Carrasco et al., 2008). At the seaward side, the oceanic beach has a sub-aerial width of about 60-80 m, average beach face slope of 0.1, and average nearshore slope of 0.01.

Closure depth in this area has been determined by several authors, with the more recent estimates pointing to 10 m below MSL (Dolbeth et al., 2007). The beach can be classified as 'Low Tide Terrace + Rip', with a reflective to intermediate behavior (Martins et al., 1996).

Beach sediments are usually coarse sands. Fine to very fine sands were observed near the shore down to 4 m depth, however in deeper areas >6-7m, there were coarser sands down to 20 m depth (Dolbeth et al., 2007).

Ancão Peninsula has alongshore differences in urban development. The central sector is urbanised (locally called Praia de Faro) and therefore sediment dynamics are conditioned by human actions. The urban area is densely occupied and buildings are mostly fishermen family houses, vacation houses and touristic infrastructure. Beach accessibility is relatively good, with a road access by bridge, some car parking along the urban area and also public transportation from the mainland city. The buildings, parking and roads have almost completely overtaken the natural dunes in this part of Ancão Peninsula. To the east of Faro beach settlement, Ancão Peninsula has a low-density population consisting mainly of fishermen, most of whom inhabit the lagoon margin. The western part is mostly uninhabited except for a few beach facilities and walking paths.

3.3 Methodology

3.3.1 Hydrodynamic data

Wave and tide data are available from 3 sources: Portuguese Hydrographic Institute (from now on referred as IH), Puertos del Estado (Spanish Port Authorities), and from an Infinity PT deployed 1 km offshore of Faro beach, at depth ~15 m (see Figure 3.1). No surge model is available for Faro Beach and a surge height estimated according to previous studies is considered (Gama et al., 1994).

Table 3.1 Information on wave, tides and surge levels data sources

Source / Data	Location	Monitoring periods
www.hidrografico.pt — Directional wave data	At 93 m depth offshore Cape Sta Maria (c. 10 km off Faro beach)	Continuous (with occasional data gaps)
www.puertos.es — Tide/surge level	Huelva	Continuous
www.igeo.pt — Tide/surge level	Lagos harbor	After 15/4/2009
Infinity PT — Non-directional wave data, tide/surge level	At ≈ 15 m depth offshore Faro beach	16/3/2009-16/05/2009 18/09/2009-20/01/2010

The Infinity PT is the most reliable source for wave and tide data, with the only drawback that it doesn't provide information on wave direction. When Infinity data are not available - as in the case of the February 2009 storms - the Huelva tide and IH wave data are being used. The instrument monitored successfully the Winter 2009-2010 events and that data has been used for the XBeach runs (see Appendix E) discussed here.

The IH buoy was found to record systematically higher Hs values compared to the Infinity PT, making joint use of both sources more difficult. That could be due to the fact that the buoy, located 10 km southeast of Faro beach, is affected by some wave sectors that do not reach the Faro beach (i.e. WNW) or arrive at the shore after significant refraction.

3.3.2 Wave modelling results

To achieve continuous availability of off-shore wave data (including wave direction) a wave models chain was calibrated, consisting of one-way-nested (offshore to onshore) spectral wave models, starting from a large-scale model covering the whole North-Atlantic and ending with a fine resolution model at the study site.

The North Atlantic WaveWatch III model of Dodet et al. (2010) was used to generate hourly spectral outputs at the external boundary of a finer grid covering the Gulf of Cadiz. This well-validated model is fed with 6-h wind fields from the NCEP/NCAR Reanalysis wind fields (Kalnay et al., 1996) available with a global Gaussian Longitude-Latitude T62 resolution (~210 km). The model spatial grid covers the North Atlantic Ocean, from 80.0ºW to 0.0ºW in longitude and 0.0ºN to 70.0ºN in latitude, with 0.5º resolution.

The intermediate Wavewatch III Gulf of Cadiz model has a 0.05º resolution and extends from 10.0ºW to 6.0ºW in longitude and from 34.0ºN to 39.0ºN in latitude. The spectral grid and the wind forcing is the same than those used for the North Atlantic model. Hourly spectral outputs were generated to force the local SWAN model (Appendix A).

The local Faro Beach SWAN model has been preferred to Wavewatch III in order to simulate the wave propagation close to the coast. Indeed the former model represents more accurately the nearshore physical processes in comparison to the latter, and is thus more adapted for nearshore wave propagation. The model grid has a 500m resolution and covers a rectangle of 40 x 20 km situated offshore Praia do Faro. Hourly time-series of mean wave parameters (H_s, T_p, T_m, M_{wd}) were generated in order to validate model results against measured data and to force the XBeach model when the results are satisfactory.

Validation of model results took place through comparisons between wave height time-series measured by the Infinity PT and outputs from the SWAN model. The statistical errors calculated for the period March 2009 – February 2010 (bias = -8 cm, RMSE = 21cm and NRMSE = 26.7 %) showed that our modelling strategy enables to reproduce rather well the wave height conditions. For the same period, when considering only wave heights greater than 1m, the NRMSE decreases to 18.4%, which is considered sufficiently accurate for the scope of the present use.

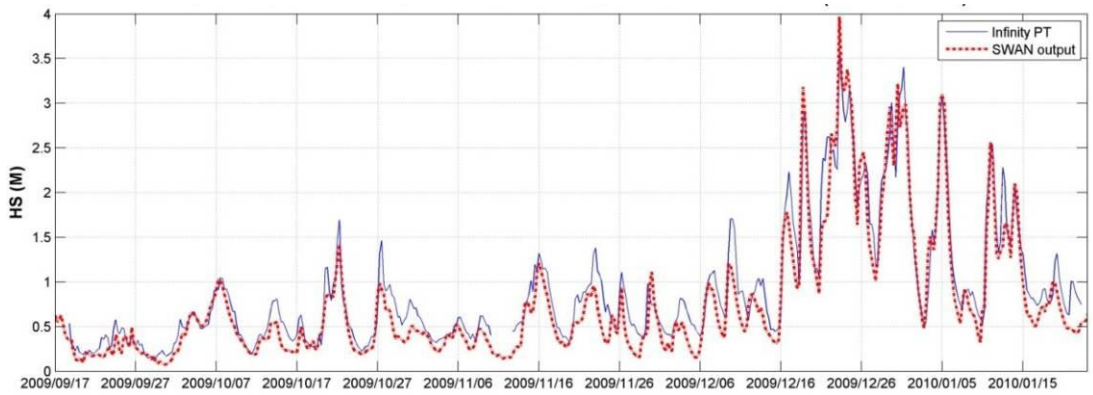

Figure 3.2 Validation of wave propagation model results showing Hs values modelled with SWAN (red) and Infinity PT data (blue).

3.3.3 Topo-bathymetric data

Topographic data were collected through RTK-DGPS surveys (estimated accuracy around ~5 cm) and bathymetric profiles were acquired using 2 RTK GPSs and an echo-sounder; with estimated accuracy around ~1 m for horizontal positioning and ~20 cm for vertical leveling. Pre- and post- storm topo-bathymetric data were collected along 3 cross-shore transects distributed along the Faro Beach coastline (Figure 3.1b).

3.3.4 XBeach modelling

During an extensive topographic monitoring period (September 2008-February 2010) the morphological impact of two significant storm events was recorded. The first event took place between 31/1/2009 and 3/2/2009 and for the ~24 hours of its peak (coinciding with spring tide), the beach was exposed to WSW waves, with the maximum significant wave height reaching ~5 m and the peak period ~15 s (Figure 3.3). Pre- and post storm topographic and bathymetric data collected along 2 transects (II, III, see Figure 3.1b) are considered for the present study.

The second event was a group of several individual WSW storms taking place from 18/12/2009 until 5/1/2010. Significant wave height reached almost 4 m and peak period 15 sec, and such conditions coincided with both spring and neap tides (Figure 3.4). Morphological response was monitored along transect I (Figure 3.1b), with almost daily topographic and pre- and post storm bathymetric surveys. In the present study three events of storm-induced beach erosion are considered for XBeach calibration in the present contribution (see numbering 1-3 in Figure 3.4).

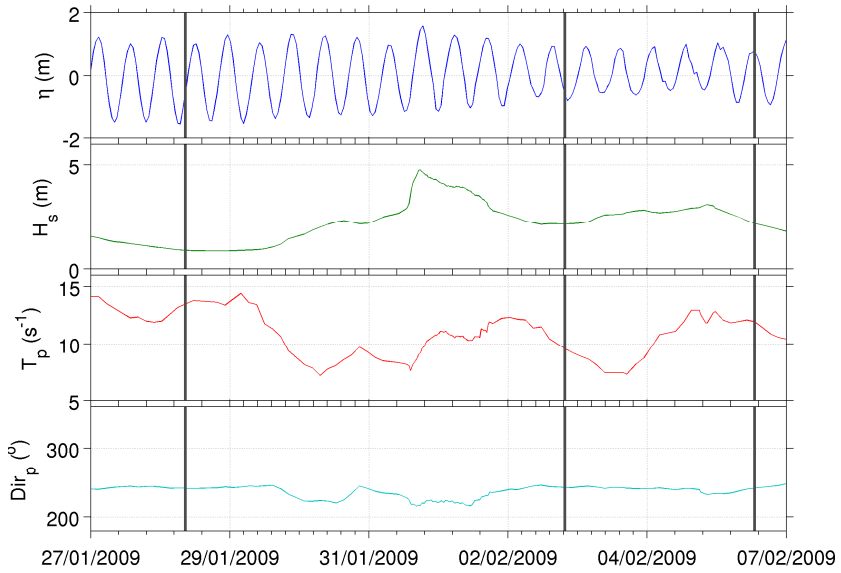

Figure 3.3 Wave conditions during the February 2009 storm event. From top to bottom: Water level, Significant wave height, Peak period, Peak direction. Black vertical lines denote the timing of pre- and post-storm topo-bathymetric surveys.

Extensive XBeach testing took place considering model set-ups combining different values of the following parameters (see also Roelvink *et al.*, 2009): *facua, wetslope, lws, form, wci, gwf, turb, nspr, morfac* (more information on Table 3.2). All combinations resulted in 768 run cases per storm event and were all tested for the 5 separate events which involved the main types of beach profile morphologies found at the study area: from *reflective* to *low-tide terrace* (profiles I to III). Morphological time run durations was 12-18 hours depending on the case and wave boundary conditions were implemented as time series of sea states (instat=41). XBeach modelling results were evaluated on the grounds of Brier Skill Score values (BSS), estimated considering the profile section -2 m>z>6 m (relative to MSL). All runs took place using model revision 1241.

Table 3.2 Values of important XBeach parameters considered for the February 2009 storms. Note that all possible combinations of the mentioned values were considered

Parameter	Values	Parameter	Values
facua	0.1, 0.3	turb	0, 1, 2
wetslope	0.2, 0.4	nspr	0, 1
lws	0, 1	gwf	0 1
form	1, 2	morfac	5, 10
wci	0, 1	d_{50}	0.5 mm

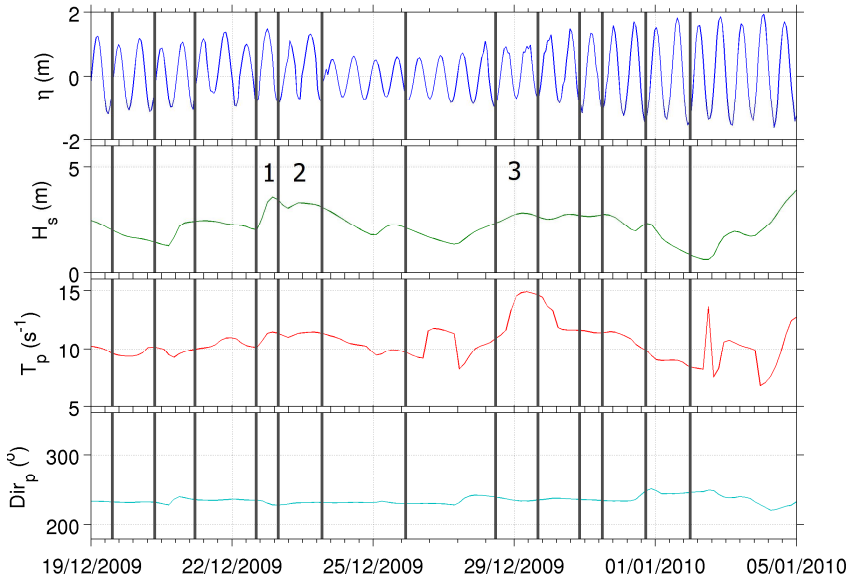

Figure 3.4 The December 2009-January 2010 storms. From top to bottom: Water level; Significant wave height, Peak period and Peak direction. Black vertical lines denote the timing of pre- and post-storm bathymetric surveys and numbers the period considered for XBeach testing.

3.4 Model results

3.4.1 Simulation results with Off-the shelf Model

The off-the-shelf model used for Faro Beach was LITPROF (see Appendix C) and is compared on the grounds of simulation results from the February 2008 storm on Profiles A to E. LITPROF was rigorously calibrated/tested using a single test case profile located at the study site considering different wave theories, as well as mean grain size, grain size distribution spreading δ and bed roughness k values, while both academic and commercial licences of the model were used. For the 5 tested cases, LITPROF produced Brier Skill Scores ranging from -0.32 to 0.32 and the performance was overall inferior compared to the one of XBeach.

3.4.2 Simulation results with XBeach model

Model sensitivity tests in 768 x 5 runs showed that the model's performance varied with changes of the input parameters, as well as with the beach morphology. A general remark on the XBeach simulated profiles is that they tend to overestimate berm erosion and to predict avalanching, generating scarps on the upper profile. This is a significant deviation from field observations; which did not demonstrate the presence of scarp features. An example of the model's sensitivity to variations of the calibration parameters is given in Figure 3.6 (event I-2). The parameters *facua, wetslope, form* and *lws* appear to have a direct impact on the predicted berm erosion and the amount of sediment transported off-shore. This can be discerned from the 'grouping' of the XBeach generated profiles per parameter values (Figure 3.6).

BSS values from all model sensitivity tests are summarized in Figure 3.6, showing the maximum and mean BSS values from all runs, grouped according to the parameter value used (see also Figure 3.6).

The range of the BSS was from -16.75 to 0.7 and most of the tested cases resulted in negative values, as also indicated by the mean BSS (Figure 3.6b). The model was found to be more sensitive to the *form* parameter, defining the sediment transport equation used. Setting *form*=2 (Van Rijn-Reniers-Van Thiel formula) resulting in significantly improved performance (Figure 3.6).

While the maximum BSS values (Figure 3.6a) indicate the best obtained result, differences between the average BSS's (Figure 3.6b) show the sensitivity of the model to each parameter and the robustness for each value. The best performance was obtained by de-activating long wave stirring, wave current interaction and short wave turbulence (*lws*=0, *wci*=0, *turb*=0, respectively); keeping directional spreading of long waves and groundwater flow on (*nspr*=1, *gwf*=1, respectively); and using the lower *morfac*, *facua* and *wetslope* parameters (in that case *morfac*=5, *facua*=0.1 and *wetslope*=0.2, respectively).

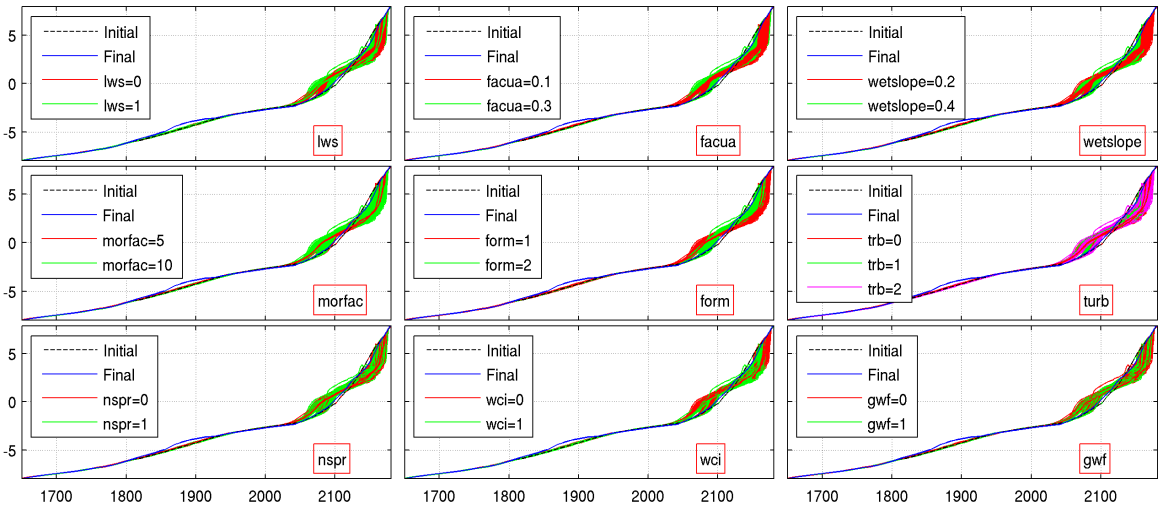

Figure 3.5 Beach profile envelopes (x, y dimensions in m; results from Event I-2) showing XBeach sensitivity to the tested parameters. Parameter name indicated in bottom right of each subplot. Mean Sea level MSL=2 m.

The average BSS values indicate the sensitivity of the model to specific parameters and the tests showed that *turb, nspr, wci* and *gwf* are the ones that affect less the simulated morphological response (Figure 3.6b). On the other hand, it is interesting that for *lws, facua* and *wetslp,* the trends of the mean and maximum BSS values are different, which implies that the set-up that provides the optimal result (higher BSS for lower parameter values, see Figure 3.6a) is not the one that guarantees robust model performance when the other parameter values change (higher BSS for higher parameter values, see Figure 3.6b). The above is related also to the fact that XBeach performed better with higher *facua* and *wetslope* values at the reflective parts of Faro Beach (Profile I) and with lower values at the less steep ones (Profiles II and especially III). This is a limitation and implies certain compromise in performance if a calibration for the entire study area is desired.

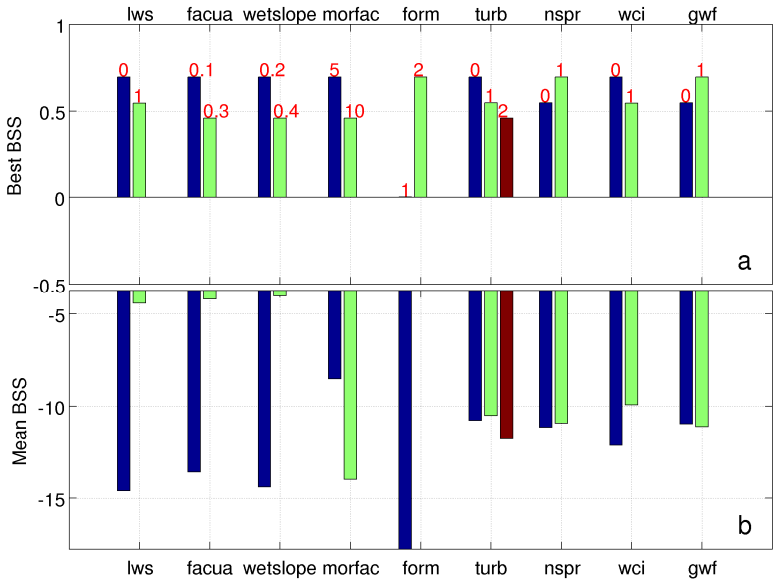

Figure 3.6 Summary of XBeach calibration efforts and impact of the facua, wetslope, lws, form, wci, gwf, turb, nspr parameters on performance. a): Best (maximum) Brier Skill Scores (BSS) of the tests grouped by parameter value (indicated by red numbers). Low y-axis is set to -1 for better display b): Average BSS value per groups of runs December 2009 Storms tests.

As a general observation, the model appears to be more sensitive to calibration changes when tested at the steeper profile (I), with the exception of event I-3 for which the BSS distribution is skewed towards positive values (Figure 3.8). For cases I-1, I-2 and II, it can be seen that the percentage of runs with BSS>0 for the whole ensemble is very small. This implies that the model either tends to predict a specific type of beach profile response, like the one observed in cases I-3 and III, or it is more robust for mildly sloping beaches.

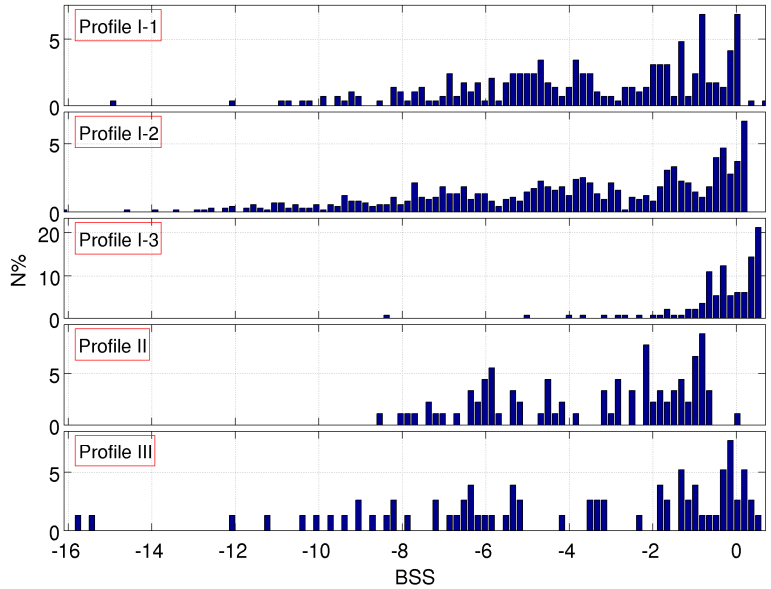

Figure 3.7 Histograms of Brier Skill Scores (BSS) of all the tested model set-ups per event.

The best simulation results for each modelled profile is shown in Figure 3.8. In most cases XBeach simulations predict satisfactorily berm erosion (Transects I-2, II, III), while in others, predicted upper profile erosion falls behind (II) or exceeds the one observed (I-1). The model appears to predict accurately the landward limit of erosion and the profile pivoting point and the simulated morphological response is realistic, with the only discrepancy being the tendency to sometimes generate steep scarps on the upper beachface (I-1). Brier Skill Scores for these optimal runs range from 0.27 to 0.7, while in some tested cases the volume of sand on the topographic measurements is not maintained (e.g. I-1, I-2, II), a fact which limits the maximum possible BSS. The observed volume differences can be related to longshore sediment transport which tends to be towards south east during storms. Interventions during storm conditions by the local authorities are also likely along profiles I, II; such as addition or re-distribution of sediment along the upper profile. Both factors cannot be resolved by a beach profile model and are likely to introduce artifacts to the present field observations by affecting profile shape and sediment budget. However, such interventions were not observed during the studied storms and most likely were of small scale or taking place in other locations of Faro Beach.

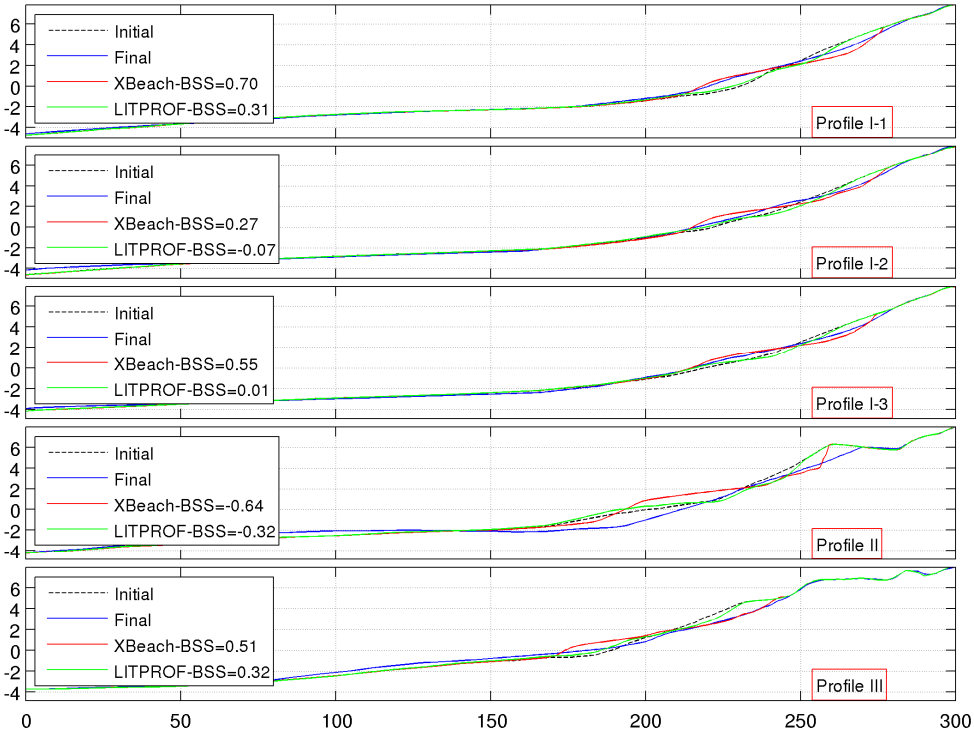

Figure 3.8 Beach profiles (x, y dimensions in m) showing the best cases of XBeach and LITPROF simulations for the 5 different transects. Brier Skill Scores are indicated in the legend along with the initial and final profiles.

Another deviation of the simulated profiles from the field observations is the presence of a narrower profile section with morphological change (Figure 3.8). In the XBeach simulations erosion/deposition is observed along the profile section -2 m<x<6 m (MSL=2 m), while the bathymetric data, show variations also along the deeper parts of the beach. It is true that topographic measurements are more accurate and are more rapidly updated than bathymetric ones, since in the present case bathymetric data were only obtained few days after the storm, immediately after navigation was allowed by the wave conditions.

However, the discrepancies along the submerged profile sections are significant, and cannot be attributed only to data collection artifacts. Especially in Profiles I-2, II, III offshore bars appear to have formed after the event at distances x=0, 70, 120 m, respectively for each case. However those profile sections remain intact during the simulations and morphological change is restricted to the berm and the beach-face.

The impact of the December 2009 storms was monitored by almost daily topographic surveys along a beach section ~100 m wide alongshore, found at the reflective central part of Faro beach (Profile I, see Figure 1). The storm group was formed by 5 individual storm events (see Figure 3.4) and the intensive surveying scheme allowed tracking morphological change during the whole duration and several pre- and post-storm profiles were collected for XBeach testing. However only three individual events were used in the present contribution, since the simulated response for storm group was unrealistic and resulted in increased cumulative erosion. While field measurements showed that the upper profile change gradually decelerated, as Faro Beach appeared to reach a state of morphological equilibrium (see also Vousdoukas, Almeida and Ferreira, 2010 submitted), XBeach simulations predicted increased berm erosion for each consequent storm. On the other hand, predicting the morphological impact of consequent storms (groups) remains an open topic of research (e.g. Ferreira, 2005) and is beyond the capabilities of current state-of-the-art beach profile evolution models.

3.5 Summary and Conclusions

Measurements of beach profile response to storm conditions, at 3 beach transects at the reflective Faro Beach, were used for extensive testing/calibration of XBeach (revision 1241). Sets of runs for 768 different set-ups for 5 storm events, showed that alongshore profile morphology variations even for the same site, may require different calibration settings in order to achieve optimal performance. XBeach performed better with higher *facua* and *wetslope* values at the reflective parts of the study area and with lower values at the less steep ones.

Model sensitivity to calibration settings appeared to increase with beach slope; while the majority of the tested set-ups resulted in negative Brier Skill Scores (BSS). The main discrepancies compared to the field measurements were related to the overestimation of berm erosion and the intense avalanching/beach scarp formation; which are rare at the study site. Moreover, the simulations resulted in morphological change along a narrower profile section than observed; and did not predict offshore bar formation.

The study highlights that predicting beach profile morphodynamic response during storm events at steep reflective beaches with XBeach may be more demanding. However, results can be satisfactory after proper calibration and for the present study, the optimal cases resulted in BSS of the range 0.2-0.7. The estimated BSS values are significantly superior compared to the ones of the LITPROF optimal cases.

The best performance for the analyzed reflective beach was obtained by de-activating long wave stirring, wave-current interaction and short wave turbulence (*lws*=0, *wci*=0, *turb*=0, respectively); keeping directional spreading of long waves and groundwater flow on (*nspr*=1, *gwf*=1, respectively); and using the lower *morfac*, *facua* and *wetslope* parameters (at the present case *morfac*=5, *facua*=0.1 and *wetslope*=0.2, respectively). The tests also showed that *turb, nspr, wci* and *gwf* are the parameters that affect less the simulated morphological response, while setting *lws*=1 and using higher *facua* and *wetslope* (0.3 and 0.4, respectively), improved robustness among the tested cases.

4 Cadiz Urban Beach, Spain

Theocharis A. Plomaritis, Javier Benevente and Tomas Fernandez-Montblanc, U. Cadiz, Spain

4.1 Objectives

The modelling objectives in the area if Cadiz are to simulate the effect of different storm events on the natural and urbanized beach settings, in order to predict coastal retreat rate due to storms. If possible, another objective will be the prediction of the maximum flood height and study the role of different geological constraints; such as offshore rocky outcrops and underlying impermeable layers, on the beach response.

4.2 Site and climatology

4.2.1 Description of area

The field site is located around Cadiz town, in south-western Spain, facing the Atlantic Ocean (Figure 4.1) The study area is a meso-tidal coast with a mean tidal range of 3.2 m and 1.1 m during springs and neaps tides, respectively. Dominant winds blow from ESE (19.6% of annual occurrence) and WNW (12.8%), which together with coastline orientation makes sea and swell waves approach generally from the third and fourth quadrants. According to this, prevailing longshore drift is directed south-eastwards. Significant wave height is usually lower than 1 m, with waves over 4 m high being uncommon and occurring only during the most important storms, which usually take place between November and March and approach from the third quadrant. In fact, waves greater than 1.5 m are considered storm waves, so the area can be classified as a low-energy one.

Concerning the geological setting, the investigated area is located in the southern part of Cadiz Bay. It belongs to the end of the Guadalquivir Neogene depression, characterized by soft, sub-horizontal sedimentary deposits which give rise to a linear NNW-SSE oriented, low-lying coastline. The most important river courses in this area are the Guadalquivir and Guadalete rivers, which flow north of the study site.

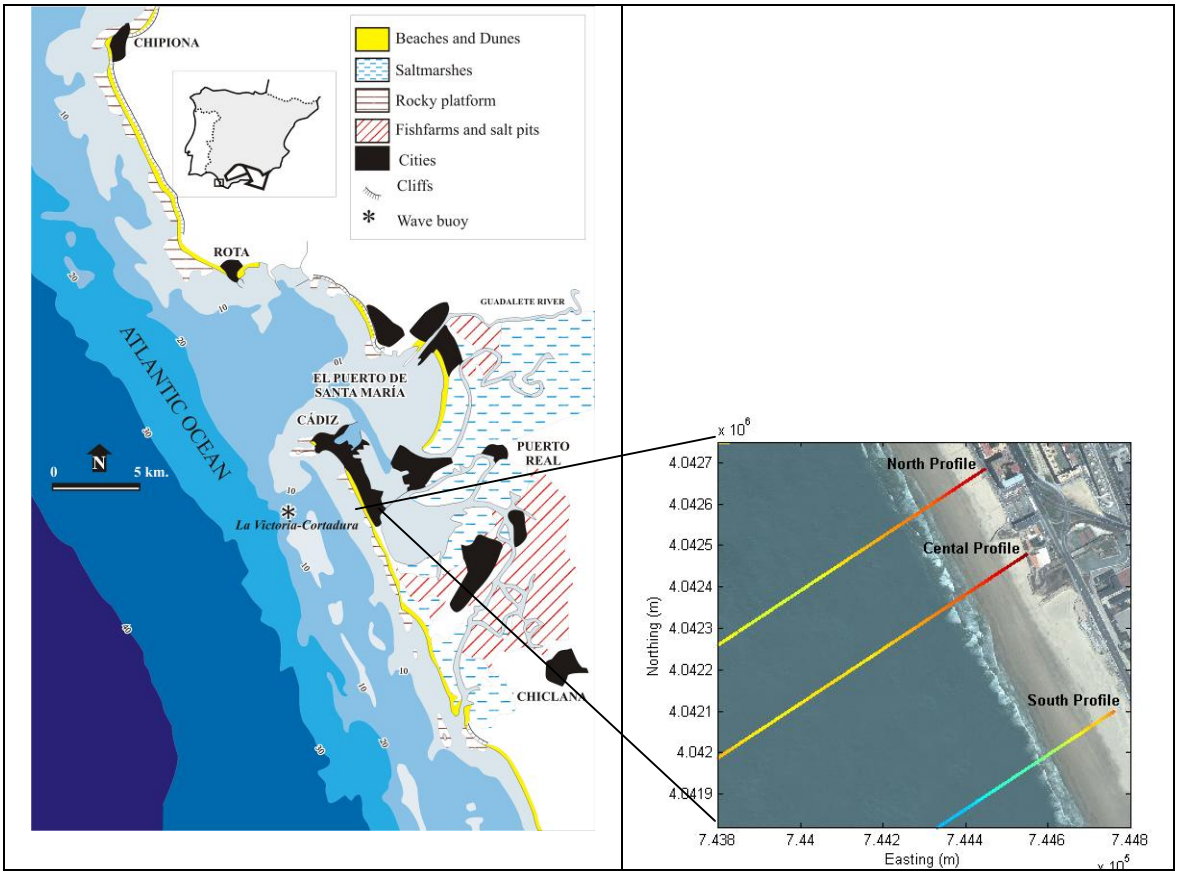

Figure 4.1 Location map of the study area (left) and aerial-photo of the study area of Cadiz(Spain)with overlaying topo-bathymetric modelling profiles.

From a geomorphological point of view, the study area is composed by the joining of two elongated sandy bodies forming a barrier. To the north, the beach of Cortadura is located on a tail-shaped tombolo which links the rocky outcrops of Cadiz and San Fernando; to the South, the beach of Camposoto is situated in the northern sector of Sancti Petri sand spit (Figure 4.1). Bathymetric contours in the study site are in general parallel to the coastline and the nearshore zone shows a gentle slope, interrupted by several shoreline-parallel rocky outcrops. The morphological characteristics of these outcrops (height, length, and distance from the coast) are controlling the amount of energy that can propagate towards different sectors of the Cadiz coast.

In more detail, La Victoria-Cortadura is an urban beach located in Cadiz city. It is a sandy beach around 3500 m long, backed by a seafront on its major part and, on its southernmost sector, by foredunes and a low, mostly non-vegetated dune ridge artificially stabilised by fences. The beach is especially crowded during the summer period, and beach facilities can be found at one location. It is an intermediate-dissipative beach composed by medium to fine quartz-rich sands (D_{50}=200μm). Wide, flat bars are often observed on the foreshore. The beach is characterized by a wide surf zone with prevailing spilling breakers.

4.2.2 Storms considered

The storm event that was selected for calibration is a moderate storm event with a return period of about 1 year and took place on the 30thOctober 2008 and lasted for 48 hours. A summary of the hydrodynamic conditions during this event are presented in Figure 4.2 together with the pre- and post storm conditions. The maximum significant wave (H_s) height during the peak of the event was 3.7m with a spectral period (T_p) of 8.7sec (Figure 4.2b and c). The total duration of the storm was 46 hours (light grey shaded area). The tidal conditions over that period were from springs to neaps with an average tidal range of 2.27m (Figure 4.2a). The reasons for the selection of this event as a calibration case were both scientific and logistical: (i) this particular event is a typical storm event for the area and also was the first storm of the season that resulted in a significant morphological change; the erosion of the berm and the transition of the beach profile from summer to winter. (ii) In logistic terms, a dilated beach topography and bathymetry was obtained a few days before the event and a second topographic survey was undertaken immediately after the event. These measurements provide a sound initial bathymetry for the model and a good ground-truthing for the model evaluation respectively. Furthermore, the duration of the storm is relatively short and gives flexibility in the calibration process.

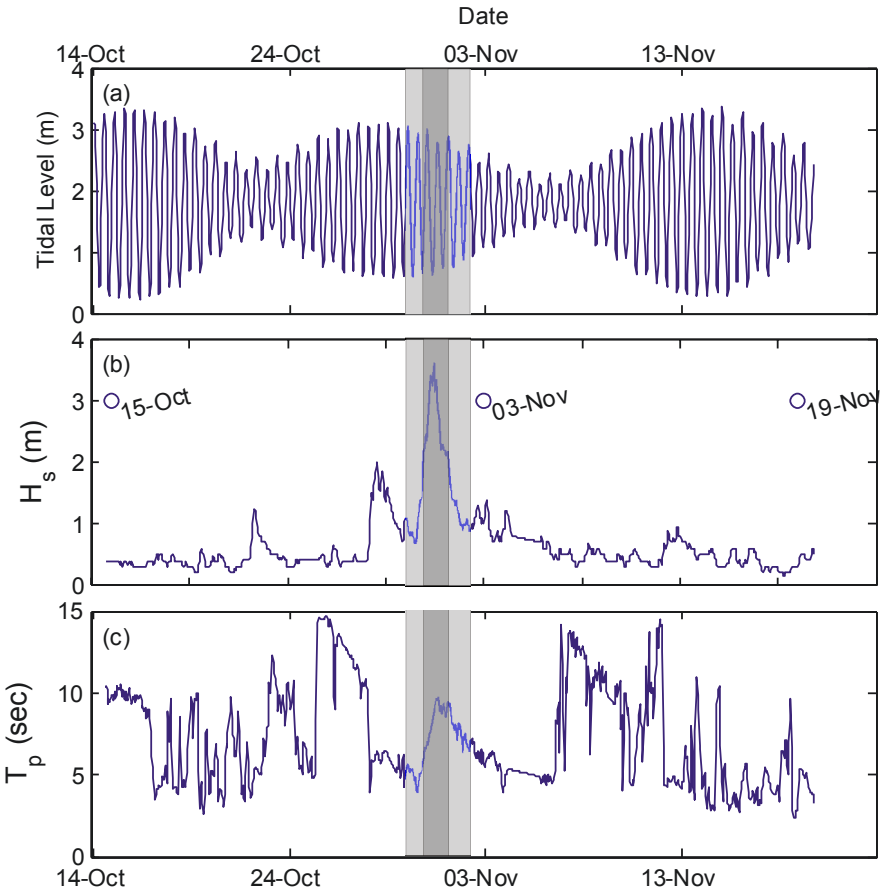

Figure 4.2 Oceanographic conditions during the calibration storm event in the area of Cadiz (light shaded area): (a) Total sea level variation in the area measured by the tidal gauge of the port of Cadiz; (b) Significant wave height (Hs) and (c) Spectral peak wave period (Tp) measured by the coast buoy.Dark shaded area represent actual simulation period. For measurement locations see Figure 4.1.

4.2.3 Measurements

Regarding hydrodynamic forcing records, in the surroundings of the study area there is a wave buoy belonging to the National Port Authority, located at a depth of 21 m offshore Cadiz city at the coordinates 36º 29.97' N / 6º 20.03' W (). It is a directional Triaxys buoy that has been into operation since 2001, currently providing hourly measurements of significant wave height (H_s), peak period (T_p), mean period (T_m) and mean wave direction (Dir_m).

Tide and sea level variation data are measured by the tide gauge in the port of Cadiz (Figure 4.1) operated by the Spanish Oceanography Institute. The tide gauge provides current records of sea level height every 5 minutes (the above data are been downloaded automatically on a daily basis).

Topographic measurements are been undertaken regularly on a monthly basis under normal conditions. Additional topographies are made before and after each storm based on weather prediction. The pre-storm and post-storm topography, together with an erosion accretion map for the storm described above are presented in Figure 4.3. It had to be noted the different erosion patterns over the north and south part of the study area. Higher erosion values over the berm are present over the north part with a pivoting point within the intertidal zone. Over the south part erosion is spread over the whole intertidal area (Figure 4.3 right). This difference is probably due to the more dissipative foreshore profile of the south part of the study area. Data are collected with the use of an RTK-GPS.

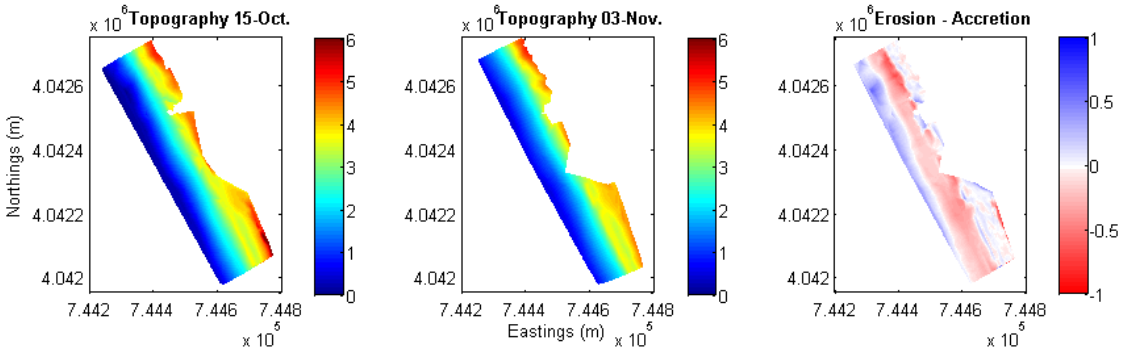

Figure 4.3 Pre- (left) and pos-storm (center) topographic surveys in the city of Cadiz together with the erosion-accretion map (right). All variables are in meter.

In order to capture the differences over the study area and to maximize the efficiency of the calibration process three profiles were selected along the area. The location of the profiles are shown in Figure 4.1 and the topo-bathymetric differences in Figure 4.4. The North profile is characterizes by the foreshore slope of 0.04 and an offshore reef that reaches depth of 5 metres. The central profile has a foreshore slope of 0.035 and a flatter offshore reef (max depth 10m); however, this profile present a narrower, but more nearshore reef at a distance of 4km from the offshore limit. Finally the south profile has the most dissipative foreshore slope (0.030) and less pronounced reefs.

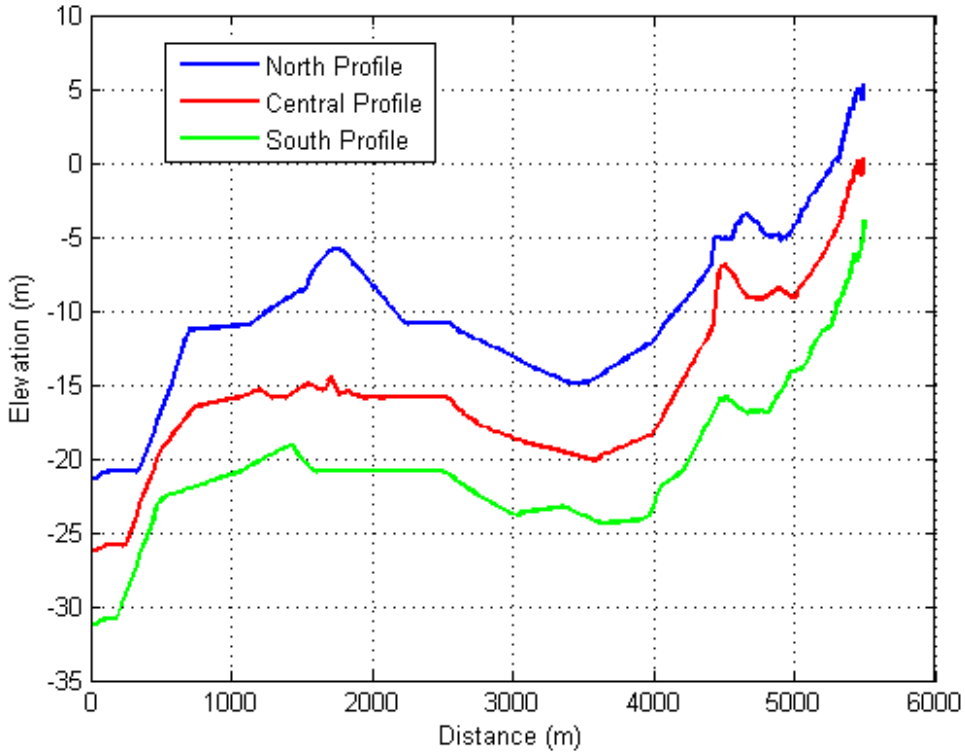

Figure 4.4 Comparison of the initial bathymetry for the three profiles in the area of Cadiz. North profile (blue) is in real depth values and the central (red) and south (green) profiles are displaced vertically by -5m and -10m respectively.

4.3 Model results

4.3.1 Simulation results with Off-the shelf Model

The off-the-shelf model SMC (see Appendix F), developed by the University of Cantabria, was used to used to predict the morphological changes of the storm described above. In particular the MOPLA module was used for the wave propagation to the coast and the 1D morphological model PETRA was used to predict the profile evolution (for details see Appendix F) . The results obtained from PETRA are presented together with the XBEACH results. The simulations were undertaken using default parameters. The model results are in general good agreement with the observed final profile. Erosion of the berm was predicted and beach pivoting around mean see level (1.9m above hydrographic zero) Some discrepancies are present over the upper intertidal zone where as a result of the berm erosion a scarp its formed close to the point of maximum run-up. Over the rest of the profile the beach slope and elevations is been predicted correctly with small diversions from the measured final profile.

4.3.2 Simulation results with XBeach model

XBEACH simulations were performed for all profiles using the same parameters. In general, default parameters were used apart from the wave breaking parameter gamma that was calculated on the bases of field measurement. The most important parameters used are presented in Table 4.1.

Table 4.1 Values of the most important parameters used for the test-case of Cadiz.

gamma	0.44
C	60
D_{50}	0.200mm
facua	0.1
form	vanthiel_vanrijn
Instat	41

The XBEACH and CMS simulations for the North profile are presented in Figure 4.5. The two models, despite the fact that they simulate different physical processes both produce a relative good final profile.The intertidal beach slope, the bed elevation and the pivoting point are in very good agreement with the measurements. Differences are more pronounced over the berm area. Here the two models show a different response. XBEACH is over predicting the berm erosion and the wave run up while the off-the-shelf model results to a profile much closer to the measured data but with a pronounced scarp that it is not present in the measurements. Over the simulation time the maximum offshore water elevation measured in the beach was 3.55m above the hydrographic zero. The Briel Skill Scores (BSS) for both models where high with0.69 for XBEACH and 0.92 for SMC (PETRA).

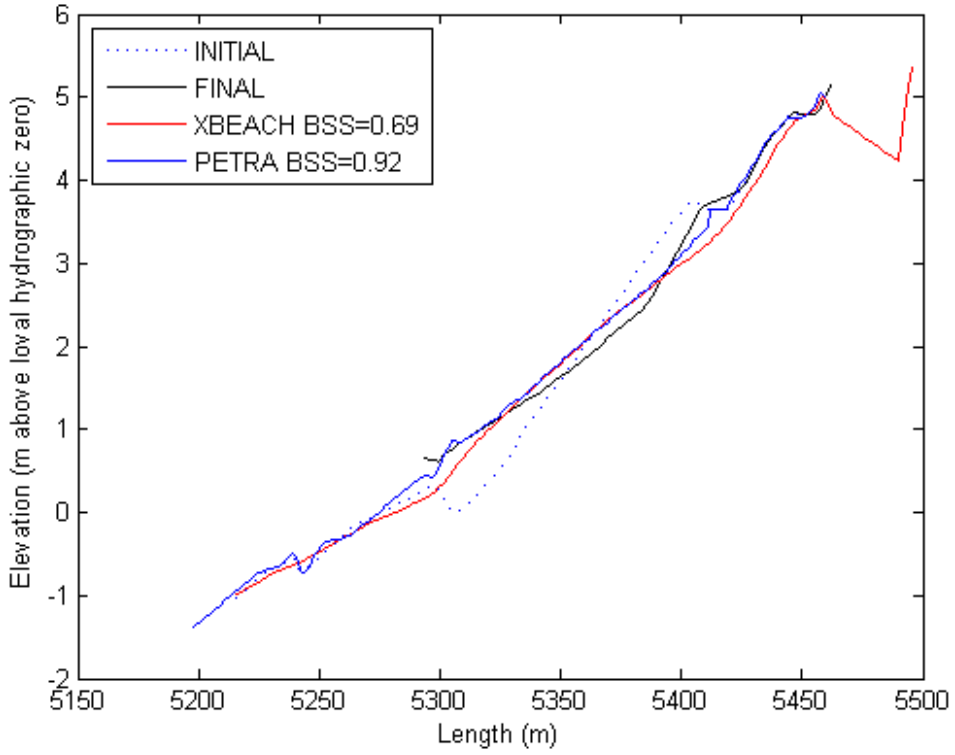

Figure 4.5 Initial (dashed black), final (black) and XBEACH (red) and off-the-shelf (blue) results for the North profile of the Cadiz test case.

Over the Central profile the response of the two models was similar (Figure 4.6) despite the fact that the total volume of sediment displacement was reduced by 40%. The correct response of the two models is probably due to the good representation of the offshore bathymetric changes that led to correct wave transformation over intermediate depths and surf zone.

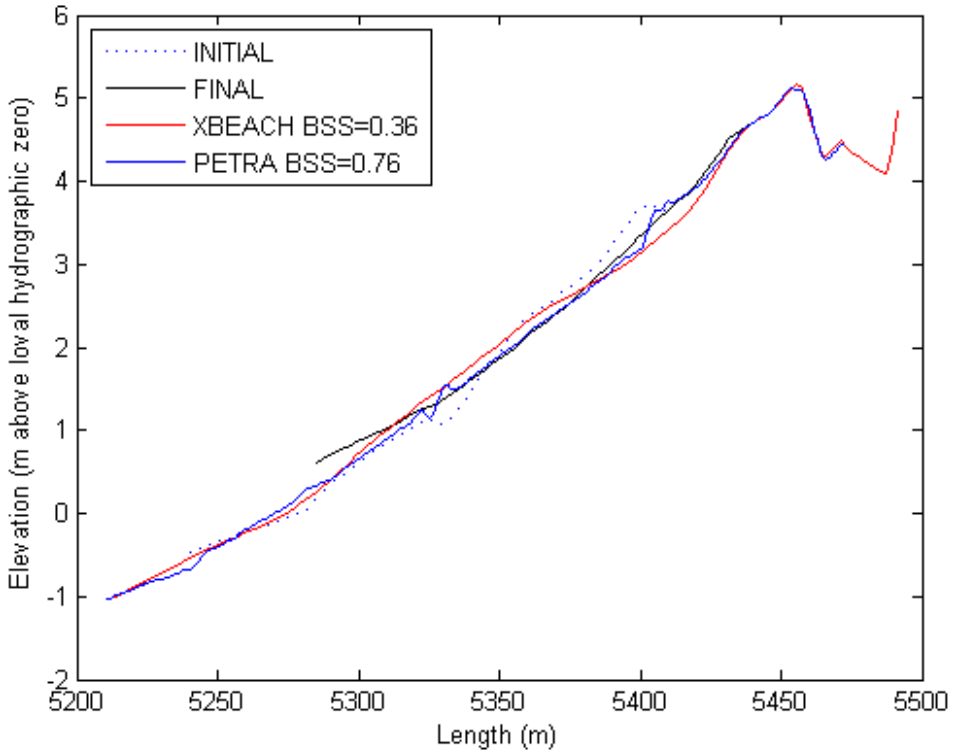

Figure 4.6 Initial (dashed black), final (black) and XBEACH (red) and off-the-shelf (blue) results for the Central profile of the Cadiz test case

Significant overestimation of the berm erosion is produced by both models over the South profile (Figure 4.7). It is characteristic that although the sea level height at the offshore boundary, during the modelled event, reached maximum values of 3.55m above hydrographic zero the measured erosion values start at a height of around 3.2m suggesting significant loss of energy of the long wave bore in the swash zone. Despite the above result the intertidal slope was predicted correctly by both models. The BSS computed were low due to the overestimation of the berm erosion.

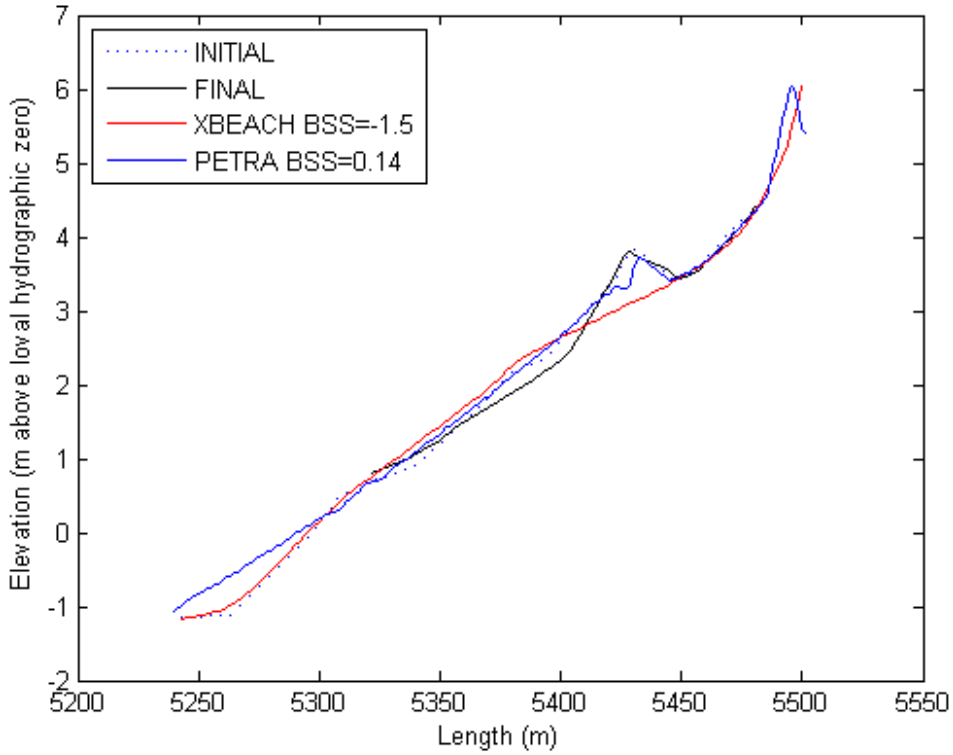

Figure 4.7 Initial (dashed black), final (black) and XBEACH (red) and off-the-shelf (blue) results for the South profile of the Cadiz test case.

4.4 Synthesis

XBEACH produced improved result in comparison with the previous version and this was mainly due to the implementation of the van Thiel-van Rijn sediment transport and waveform. On the other hand SMC (PETRA) is a closed model with limited flexibility, since there are not many calibration parameters apart from the in situ sediment properties. The breaking and sediment transport formulae can be changed in the SMC (PETRA) but variation of their parameters is not possible. The absence of the long waves run up and sediment transport in the SMC (PETRA) resulted in an advantage of the model over the simulation of the mild storm conditions used in the present case but it will probably be inadequate for higher storm events. A possible explanation for the overestimation of the swash transports could be the fact that XBeach runs were carried out in purely cross-shore mode, thereby neglecting the effects of wave directional spreading (which tends to reduce the infragravity waves) and refraction; see also Chapter 9.

4.5 Conclusions

The summary of the results of the three profile tested over the study area of Cadiz produced valid results for both the XBEACH and the off-the-shelf model. The North and Central profile performed better while the South profile showed significant higher berm erosion. BSS values were better for the off-the-shelf model but that was mainly because of the reduced berm erosion since over the rest of the intertidal area the two models produced equal results.

The elevations of the erosion over the upper part of the beach in the XBEACH simulation are in agreement with field values of run-up (Stockdon et al., 2006). Hence, the increased sediment transport over this part of the profile it is not due to the overestimation of the hydrodynamic processes but more due to overestimation of the complex sediment transport processes over the swash zone. This sediment transport processes, that will be important in the simulation of higher energy events, are absent from the SMC (PETRA) model.

5 Lido di Sète

Rémi Belon, Jérôme Thiebot, Déborah Idier, Yann Balouin and Mathieu Gervais, BGRM, France.

5.1 Objectives

The purpose is to compare results of two models - Marsouin (see Appendix H) and XBeach (see Appendix E) - against monitored data during storm events on the Lido of Sète.

The models could be used to evaluate impacts of storms on the morphology and they could be integrated in a real-time forecast system which will be developed thereafter.

5.2 Site and climatology

5.2.1 Description of area

Figure 5.1 Site location in France.

The study area is located on the lido of Sète in France at the Mediterranean coast (see Figure 5.1). Two sites are studied (Figure 5.2):

- One cross-shore profile at the South.
- One 2D area at the North.

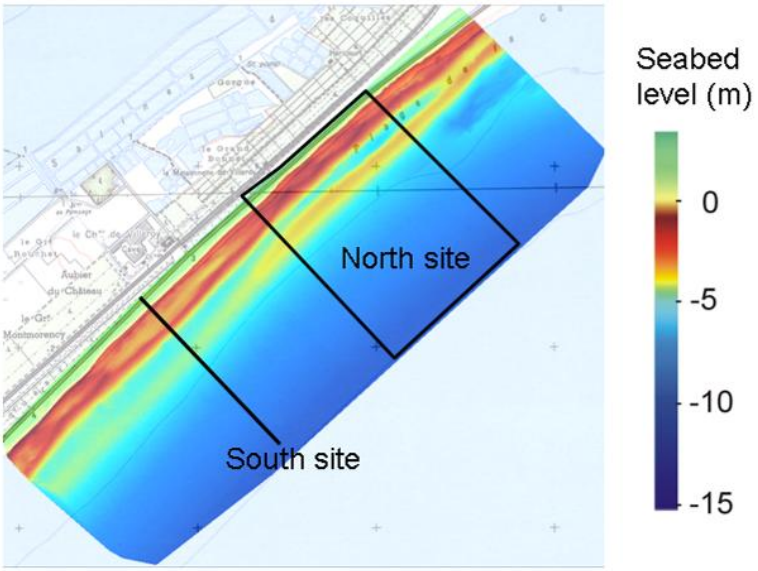

Figure 5.2 Bathymetry of the study site the November 12th 2008.

5.2.2 Climatology

The Lido of Sète is a typical Mediterranean sedimentary coastal system trapped between the rocky coast of the Mont Saint Clair at Sète, and the volcanic cliffs of the Cap d'Agde.

The beach is narrow, composed of sand with a mean grain size between 125 and 320µm. The dune system is very narrow, covered by wooden stacks. It was built artificially during the retreat of the national road that was initially fronting the beach. The nearshore zone is characterized by the presence of a set of longshore bars. Crescentic patterns with different wavelengths are observed. In the studied area, two nearshore bars are present. The external system is a crescentic bar system with an important wave length (around 2 km), while the internal bar presents an important alongshore variability. In the northern part of the area, well-developed crescentic bars can be observed (wave length ~400m), while in the southern area, the wavelength is much more important, and the bar can assumed as linear. The cross-shore migration of the bars is closely related to a sequential dynamics, by a succession of deposits over the bar slopes (Akouango, 1997). The dynamics of the bars alternates and oscillates around a mean position and net offshore movement (NOM).

Exchanges with the adjacent sandy coastlines are very low and this area can be considered as an independent coastal sedimentary cell. Coastal dynamics in the sedimentary cell is governed by two main factors: the wave action and the wind.

The most important wind directions are NNW, Tramontane winds (36%). NE and SE winds blow 15% of the time. The mean aeolian transport at the site of Sète (BCEOM, 2000) is about 250m3/m/yr. This estimation is based upon observations made between 1978 and 1983. Thus, the morphological behavior of the system is based upon two dynamic factors: the south-eastern storms and the land winds. The first pushes the sediments hold in the submerged system onto the backshore (or conversely, depending on the capacity of energy absorption of the beach), and the second returns the sediments to the beach, hence restoring the shoreline.

The Mediterranean Sea is a micro-tidal system with tidal amplitude of 0.10m during neap tide and 0.46 m during the highest spring tide. The data from tide gauges and satellite observations show that the mean sea level raised 15 cm since the beginning of the 20th century, at a mean speed of 1.5 mm/yr. Wave climate is of low energy with a mean significant wave height of 0.8 m. 80% of the significant wave height is less than 1 m. However, storm events can have a significant impact on the coastline and are associated with SE waves having a significant wave height that sometimes reaches 8 m. Energetic SE events (Hs ~ 4m) usually occur during the period from November to March. Storm surge can easily reach 1 m, and when Hs is over 4 m, the beach is usually submerged.

The beach is eroding with a shoreline retreat that was around 1 m/y during the last 50 years. However, during storms, shoreline retreat can reach more than 10 m. The main storm observed storm responses are beach erosion, dune erosion and dune overtopping.

5.2.3 Storms considered

From November 2008 to March 2009, the strongest wave height occurs on December 26th 2008, with a significant wave height reaching 4 m offshore of the lido of Sète (Figure 5.3). The mean water level (observed in the port of Sète) was around 40 cm/MSL, and the storm surge was around 25 cm (Figure 5.4).

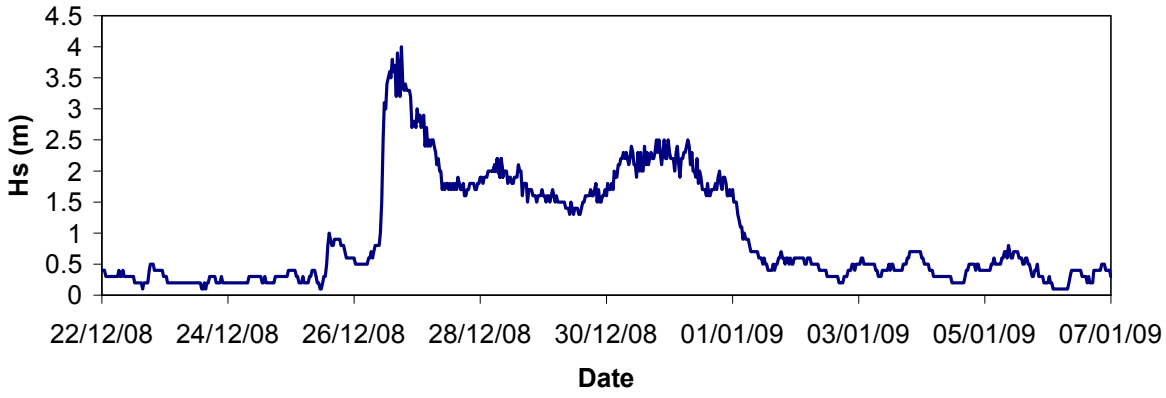

Figure 5.3 Significant wave height at the Sète offshore buoy

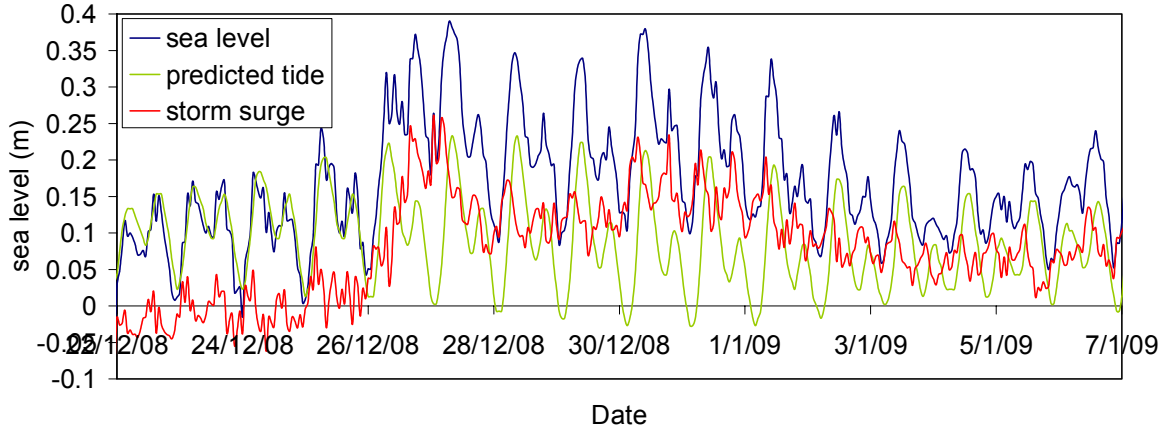

Figure 5.4 Observed sea-level at the Sète harbour

This storm was one of the most energetic and its characteristics can be summarized as:

Table 5.1 Summary of Storm characteristics

Peak Storm date	Hs max	Ts at Hs max	direction when Hs max	Incidence	Sea level when Hs max	duration	Energy
date	*m*	*S*	*°N*	°	*m*	*h*	*MW*
26/12/08 18h	3.99	10	121.12	-17	0.65	140	8.014

5.2.4 Measurements

5.2.4.1 Bathymetric and topographic measurements

In order to analyse and reproduce storm impacts on the morphology, we conducted bathymetric and topographic measurements before and after storms. An initial complete topo-bathymetry was obtained in November 2008 (75 profiles with 50 m spacing).

Just before the storm, a small survey was undertaken in the selected areas: in the southern zone with a linear bar system, and the northern zone with crescentic bars. In the south, we had two profiles measured on December 22th, 2008 and four profiles measured on January 6th, 2009. In the north, we have two profiles measured on December 22th, 2008 and eleven profiles measured on January 6th, 2009.

5.2.4.2 Wind

We have recovered wind data (velocity fields and pressure fields) from satellite measurements of seawind every 6 hours. Moreover, local wind measurements were downloaded from internet (http://www.meteociel.fr/).

5.2.4.3 Waves

In order to estimate the wave characteristics at the boundaries of the morphodynamic model, the waves measured at the Sète buoy are propagated from the offshore till 900 m from the coast, using the SWAN code (Booij et al., 1999, see Appendix A).

5.2.4.4 Sea-level

The sea-level data measured at the Sète harbour, located just at the north of the study site are used (Figure 5.4, blue line). The tide elevation simulation was obtained from the SHOM (Service Hydrographique de la Marine).

5.3 Model results

5.3.1 Simulation results with Off-the shelf Model

The MARSOUIN code contains the physics to simulate some of the 2DH hydrodynamical processes that occur in the surf zone. It calculates the wave characteristics, the wave set-up and the wave and depth – averaged currents. Concerning the morphodynamics, the

MARSOUIN code is dedicated to simulate the dynamics of sandbar systems from the coupling between bed evolution and hydrodynamic forcing (wave, current and sea level), that is to say self-organization.

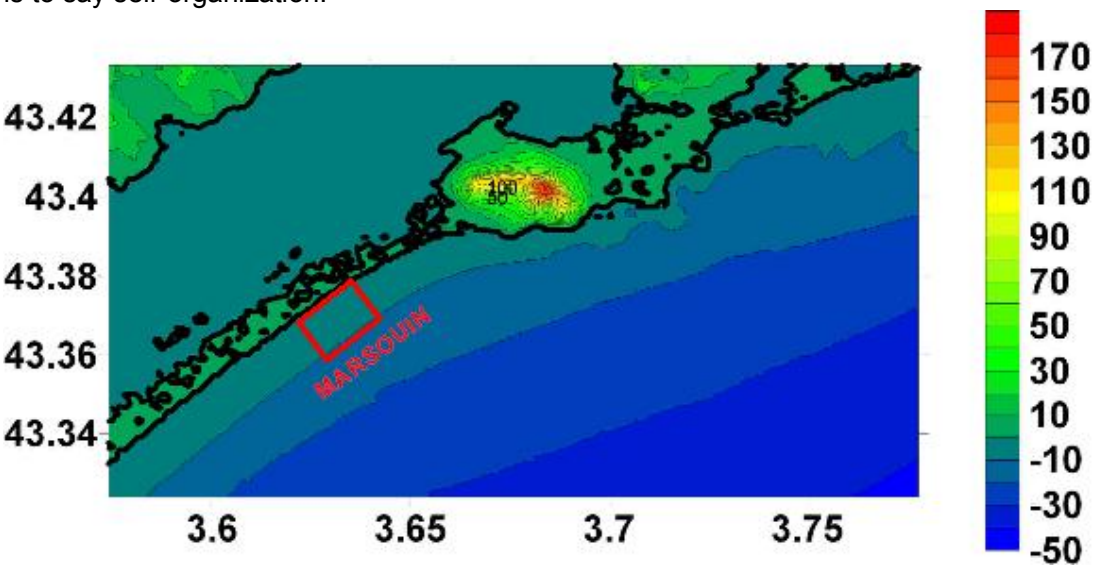

Figure 5.5 Calculation domain of SWAN. The Sète buoy is located in the lower right corner of the figure. The MARSOUIN domain is represented by the red rectangle

The major limitation concerning the morphodynamics is that wave asymmetry is not yet implemented. As a consequence, the cross-shore migration of sandbars can not be simulated properly. Moreover, the infragravity wave dynamics is not taken into account in MARSOUIN. Therefore, the swash zone morphodynamics can not be modelled satisfactorily.

The sandbars in the south zone (Figure 5.6) are quasi rectilinear and remain parallel to the shore during the 2008-2009 field campaign. The most significant changes occurred in the cross-shore direction (cross-shore migration) which cannot be properly modelled using MARSOUIN (partly, because wave asymmetry is not implemented). As a consequence the south zone data is used for the hydrodynamics validation only (not for the morphodynamics).

The north zone is characterized by the presence of sedimentary patterns having a 3D shape: rip channels, crescentic bars. The presence of non-uniformities alongshore suggests that 2DH processes play a significant role in the surf zone dynamics. Among those processes, we can foresee that the appearance of rhythmic sedimentary patterns from self-organisation will cause the formation of 2DH recirculation cells, the appearance of rip currents, and the presence of wave energy focalisation zones alongshore. Regarding the physics contained in MARSOUIN, those 2DH processes can be modelled, the north zone is therefore chosen to model both the hydrodynamics and the morphodynamics.

5.3.1.1 *Bathymetry and spatial discretisation*

The bathymetric profiles measured on January 6th, 2009 have been used to build the computation domain used for the hydrodynamic modelling of the southern zone. Only a narrow zone is covered by the measurements (approximately 200 m in the longshore direction). This zone has been extended alongshore so that lateral periodic boundary conditions could be applied in MARSOUIN. The extension has been chosen large enough to avoid shading effect concerning the wave propagation.

The computation grid for the south zone measures 700 m and 1060 m in the longshore and cross-shore direction respectively. The grid spacing (uniform) is 10 m is both directions.

For the northern zone (Figure 5.7), the pre-storm configuration of the bathymetry has been built using the bathymetric data measured on November the 18^{h} - 20th, in 2008 (only few morphological changes have been observed between November the 18 - 20th and the beginning of the storm (December the 26th). The available data cover a zone with a longshore extension of approximately 700 m. With the extension alongshore (to avoid shading effect and to allow the use of periodic conditions), the calculation domain for the north zone measures 1400 m and 1100 m in the longshore and cross-shore direction respectively.

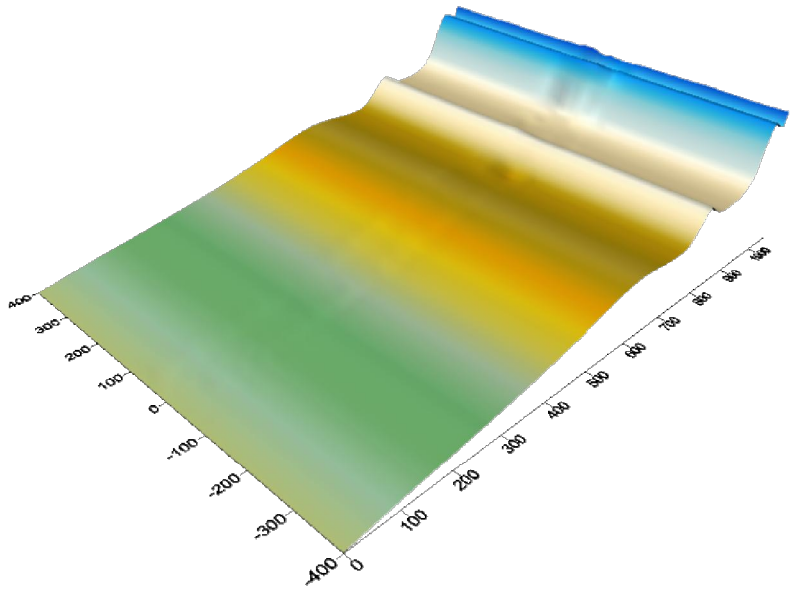

Figure 5.6 Calculation domain of the south zone for MARSOUIN simulation

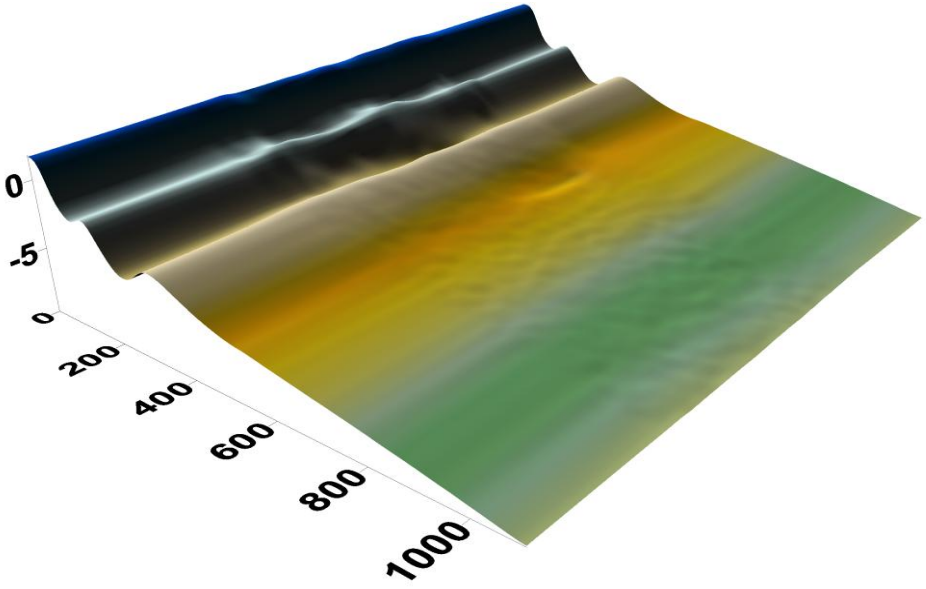

Figure 5.7 Calculation domain used for the hydrodynamics / morphodynamics in the north zone. The longshore extension is 1400 m. This domain is representative of the pre-storm configuration.

5.3.1.2 Forcing conditions: Waves and sea level

The wave characteristics at the offshore and lateral boundaries of the MARSOUIN model are estimated using the results of a SWAN computation. The SWAN calculation domain is illustrated in Figure 5.5 The waves characteristics measured at the Sète buoy have been applied at the boundaries of the SWAN model.

The sea-level data measured in the harbour of Sète are used for the calculation (Figure 5.4, blue line). This data takes into account both tide and surge effects.

5.3.1.3 Hydrodynamics validation

No hydrodynamic data are available yet for the winter 2008-2009 campaign that is why the validation is qualitative only.

The results presented hereafter concern the hydrodynamics of the northern zone. Except the case of small wave (Hs < 1-2 m) for which current velocities are not significant over the sandbars, two different hydrodynamic configurations have been encountered during the storm. The current field for the first configuration is illustrated in Figure 5.8. It is observed when the waves are frontal during the first part of the storm. The results of MARSOUIN indicate that this situation favours the appearance of recirculation cells.

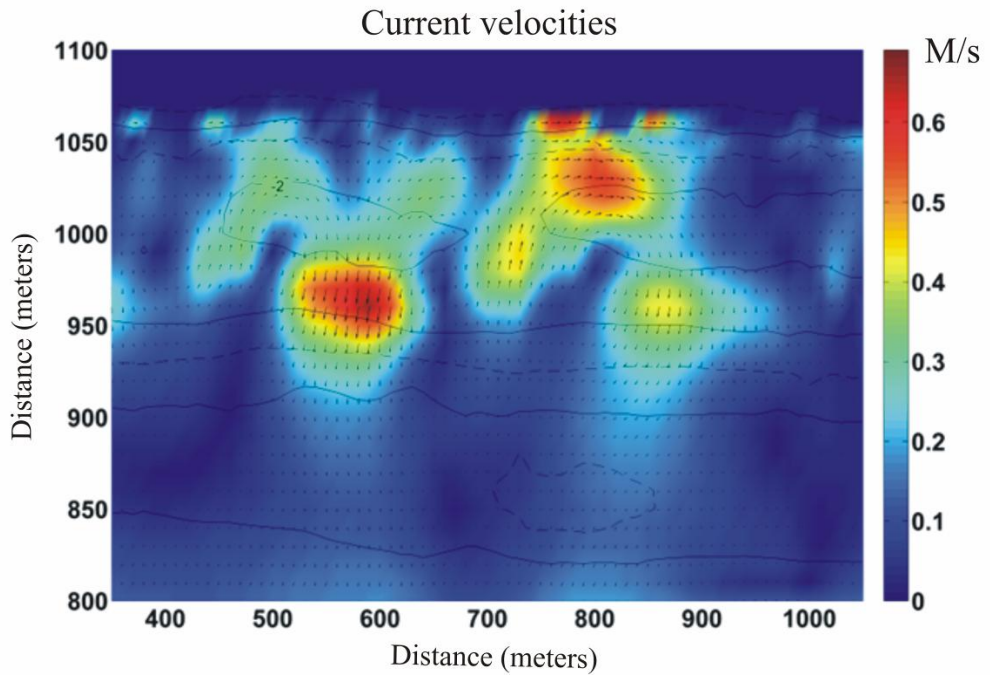

Figure 5.8 Current velocities during the apex of the storm : frontal wave forcing (December the 26th at 4pm)

The second configuration corresponds to the second part of the storm (December the 28th – January the 1st). During this period, the waves come from the South (oblique wave forcing). The current field is illustrated in Figure 5.9. They are still recirculation cells but the latter are much elongated than in the first part of the storm because the wave obliquity induce a significant longshore current (from the SO).

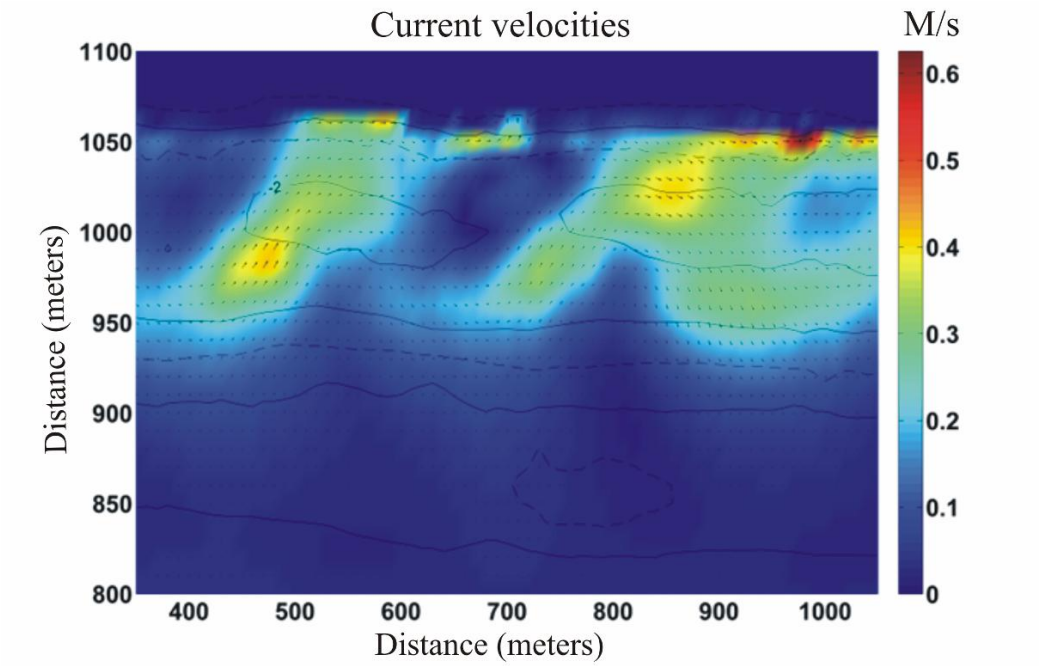

Figure 5.9 Current velocity during the second phase of the storm : oblique wave forcing (December the 31th at 7pm)

5.3.1.4 Morphodynamics validation

For the morphodynamics modelling, the northern zone is used. The results are illustrated in Figure 5.10. Erosion – accretion reach more than 0.5 m along the inner bar while the other part of the surf zone remain stable.

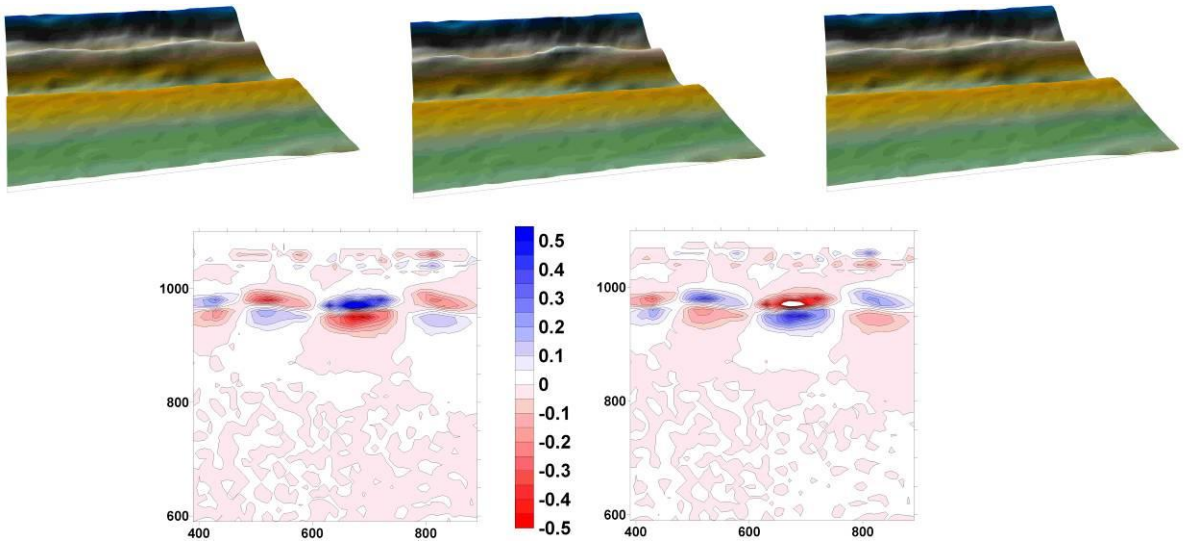

Figure 5.10 Computed morphological response of the bar system modelled by MARSOUIN during the two phases of the storm

Three phases can be distinguished in terms of morphodynamics (Figure 5.10):

- The first one is the period before the storm. As waves remains small during this period, no significant morphological changes have been modelled. This is consistent with

measurements: no significant changes between the profiles measured on December the 22th and on November the 18-20th.

- The second one is the first part of the storm when the waves are frontal (December the 26-27th). Significant changes have been modelled by MARSOUIN during this phase especially along the inner bar. The shoals present before the storm has been submitted to accretion whereas erosion occur in the trough (i.e. the 3D aspect of the inner bar increases). It seems that the pre-storm bathymetry has initiated the appearance of recirculation cells with current directed offshore over the trough and onshore over the shoals (Figure 5.8).
- The third one occurs after the apex of the storm. The morphological evolutions are opposite to the one observed during the second phase. Inner bar shoals are eroded while accretion occurs in the trough (i.e. the 3D aspect of the inner bar decreases). The difference in the morphological response during the second and the third phase can certainly be related to the fact the longshore current has been reinforced by the increase in wave angle offshore. Moreover, the breaking zone has moved onshore because the wave height decreases.

The comparison with the post-storm measured bathymetry reveals that (Figure 5.11) MARSOUIN fails at modelling the morphological response of the bar system during this storm. Some processes are missing in the model. The bad results can probably be imputed to the fact that cross-shore processes are crudely simulated yet (wave asymmetry is lacking). The fact that infra-gravity wave dynamics are not considered should also be partly responsible for the bad results.

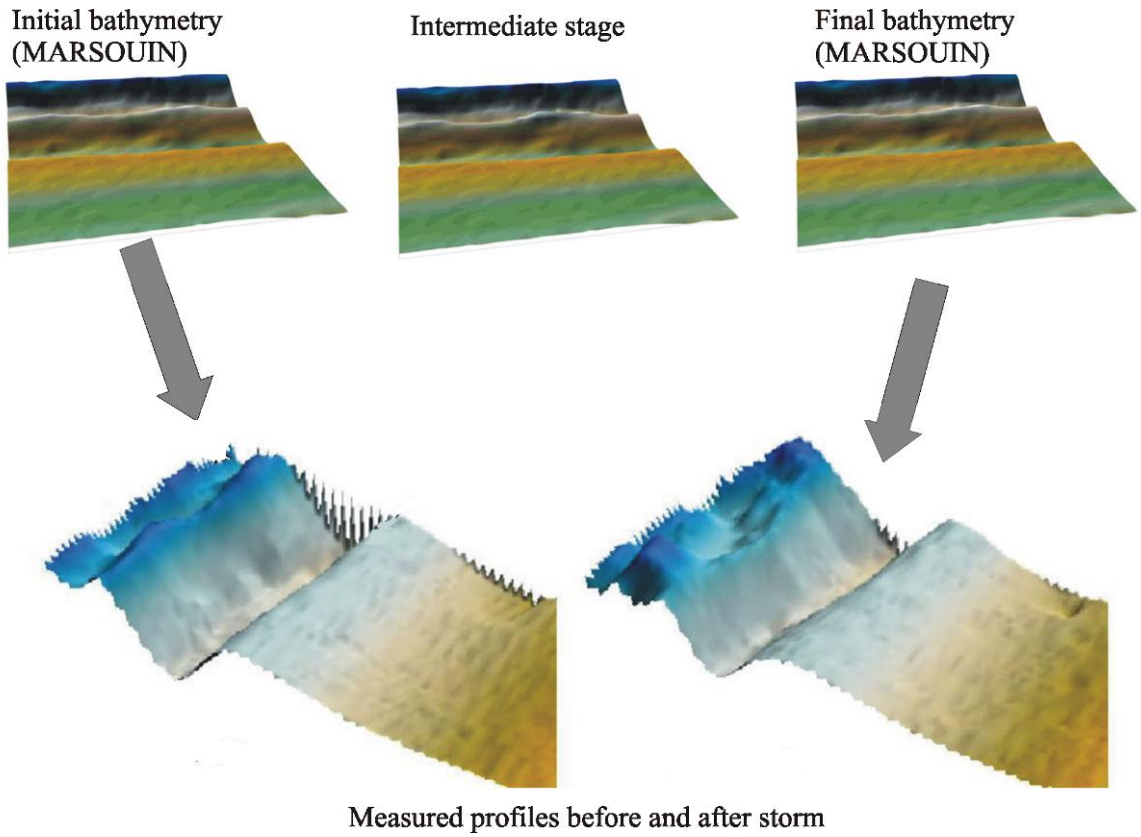

Figure 5.11 Computed morphological response of the bar system modelled by MARSOUIN during the two phases of the storm

Finally, additional tests are required to identify the missing process. The comparison with the results of XBeach (either at the southern or northern zone) will certainly be useful in this perspective.

5.3.2 Simulation results with XBeach model

The results presented here are obtained for a computation starting the 22/12/2008 and ending the 06/01/2009, and for the South Area.

5.3.2.1 Bathymetry and spatial discretisation

For the present computation, a longshore uniform bathymetry is used, corresponding to the Southern part of the study area (Figure 5.2). A variable grid size is used, from dx=2m (from the coast to the external bar), to 10 m at the offshore boundary. dy =10 m.

5.3.2.2 Forcing conditions: Waves and sea level

The wave conditions are imposed at 900m offshore (results from SWAN computations). The significant wave height, the mean direction and the peak period obtained using SWAN are used and a Jonswap spectrum is applied.

The sea-level data observed at the Sète harbour are used (Figure 5.4, blue line).

5.3.2.3 Model Parameters

Regarding the numerical parameters, the most sensitive parameters seem to be *facua* (this parameter takes into account the wave asymmetry and wave skewness in the sediment transport) and *morfac,* which is the morphological acceleration factor.
For a simulation of 6 minutes with morfac equal to 10, you effectively simulate the morphological evolution over one hour.

5.3.2.4 Results

- Morfac=20 and facua=0.2 (morfacopt=1)

Unlike the results obtained with the previous XBeach version, using the same parameters we obtained responses totally different. Indeed, with the new version, we observe a narrowing of the beach with a sand deposit in the pit (Figure 5.12). The erosion of the inner bar is also accentuated whereas in reality, we just observe an offshore migration.

For this computation, the Brier Skill Score (BSS) value is equal to -0.6353 which is the worst score realised.

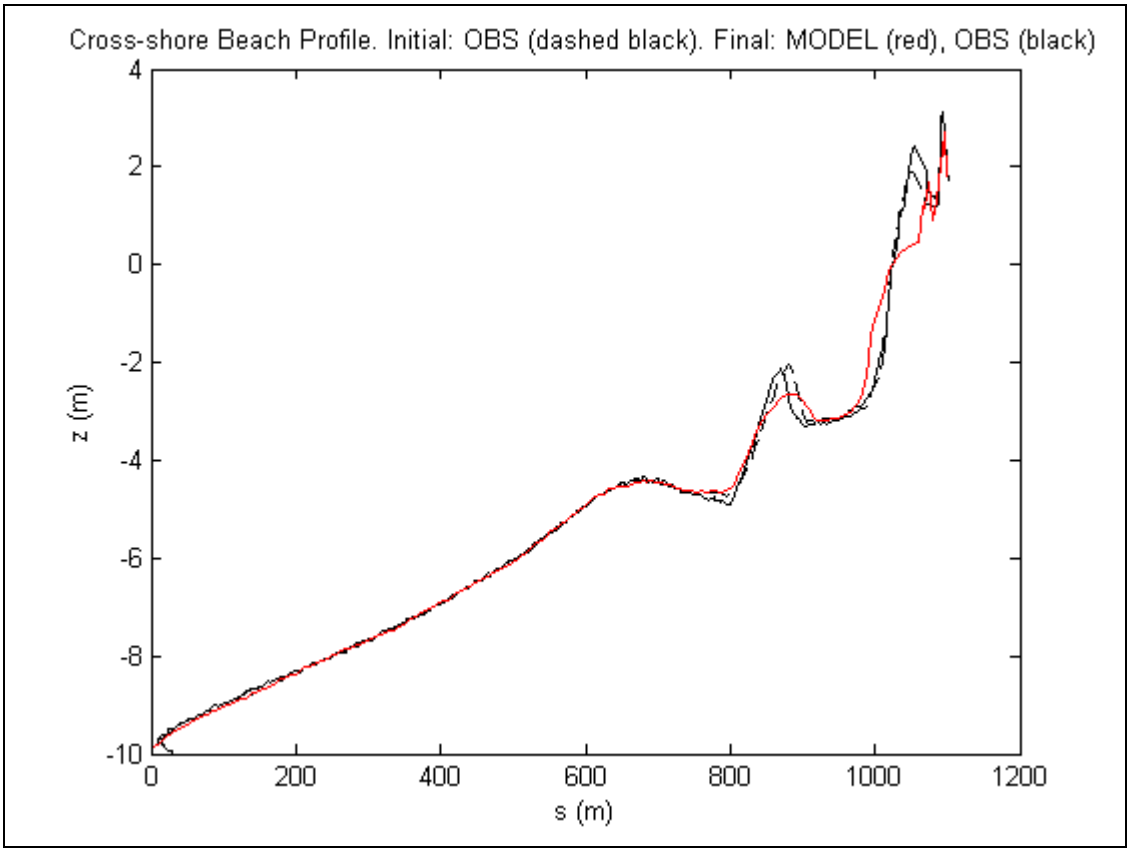

Figure 5.12 Beach profile. South Site. The 06/01/2009. Facua parameter = 0.2 / morfac=20

- Morfac=30 and facua=0.3 (morfacopt=1)

These results (Figure 5.13) are quite similar to those obtained with the previous XBeach version. However, in this case, the Brier Skill Score (BSS) value is equal to 0.0125 which is the better score realised.

We still observe the erosion of the inner bar and the deposit of sand on the beach is not represented.

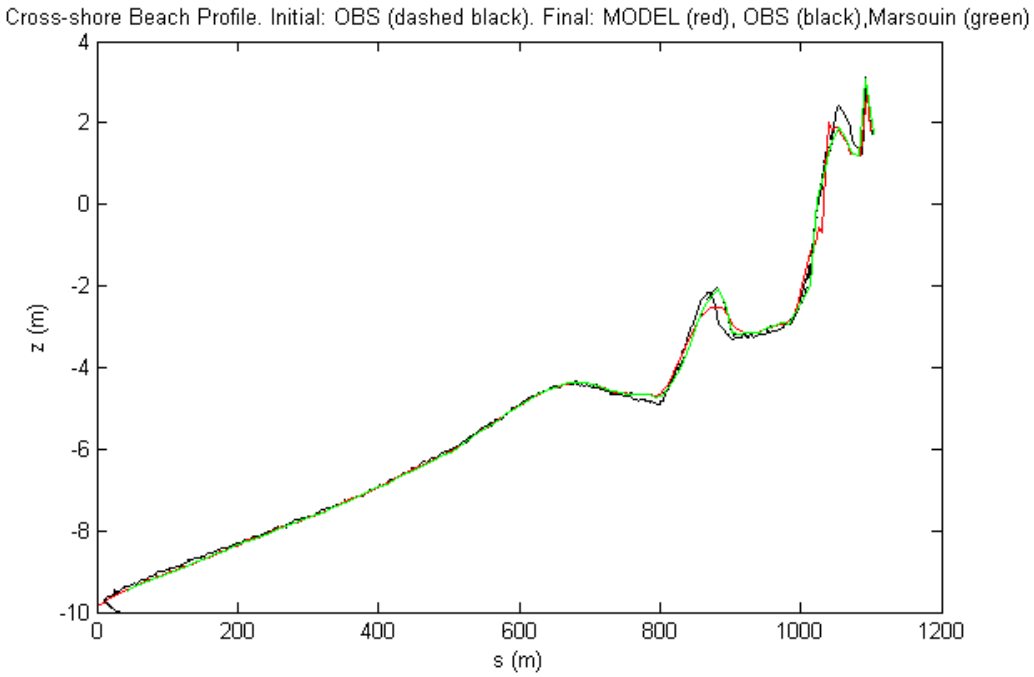

Figure 5.13 Beach profile. South Site. The 06/01/2009. Facua parameter = 0.3 / morfac=30

5.4 Conclusion

The reference event was the storm which occurred on December 26th 2008. We have simulated this storm with two models, Marsouin and XBeach, in different configurations. From the results, we can say that morphological responses obtained by the models does not correspond very well to field measurements.

According to Marsouin, many processes are not taken into account, specifically cross-shore processes, defined by wave asymmetry, and infragravity dynamics. The first one is probably in charge of the inner bar offshore migration that is why we do not observe this movement on the Marsouin's result. Knowing that Marsouin is not able to calculate run-up values, it cannot reproduce the sand deposit on the beach.

With regard to XBeach, results do not match with field measurements because the modelled event pertains to bar migration in a mild storm, for which XBeach is not intended. Different test cases have been done without obtaining more realistic results, reducing period of simulation, modifying parameter values, using a profile with variable gridsize.

6 Mariakerke and Ostend Beach, Belgium

Annelies Bolle and Piet Haerens, IMDC, Belgium

6.1 Objectives

The objectives of IMDC with regard to the modelling effort are to test and calibrate the XBeach model, in order to improve the beach erosion predictions. Beach erosion is currently estimated with Durosta (see Appendix I) and is an important element in the evaluation and design of the coastal defences.

For most coastal towns and cities along the Belgian coast, the coastal defence consists of the combination of a dyke with a beach in front. During storm, the overtopping discharge over the dyke needs to be known, to determine whether the safety of inhabited properties behind the dyke and in the hinterland can be guaranteed. The beach profile in front of the dyke determines to a high extent this overtopping discharges.

The measurement campaign for the MICORE project is performed on Mariakerke Beach. The hydrodynamic measurements (waves, currents & turbidity) have been analysed in search of a relation between hydrodynamic conditions and morphological changes during “normal” conditions. This analysis is described in the data analysis report (IMDC, 2010) and the main outcomes were:

- Severe storm did not occur within the measurement period, so no significant storm impacts have been monitored in Mariakerke.
- During “normal” conditions, an influence of the wind has been detected in the upper layers.of the water column However, since XBeach is a 2D model, these processes cannot be modelled.
- Moreover, a historical dataset is available for the beach of Ostend, just East of Mariakerke. The coastal defence is comparable: a dyke with in front an (artificial) beach. For the storm of 7 to 9 November 2007, topographic and bathymetric measurements are available just before and after the storm, as well as the time series of hydrodynamic conditions during this storm event (see Section 6.2.2).

Based on these findings we decided to focus the XBeach modelling on Ostend, a site nearby, where a historical dataset will be applied to calibrate and test XBeach for storm impact on the beach.

6.2 Site and climatology

6.2.1 Description of area

6.2.1.1 Belgian Coast

The Belgian coast is situated at the southern part of the North Sea and is 65 km long (Figure 6.1). It is part of the sandy and rectilinear Southern North Sea Coastline that stretches from Cap Blanc Nez (north of France) in the west to the Scheldt Estuary (the Netherlands) in the East.

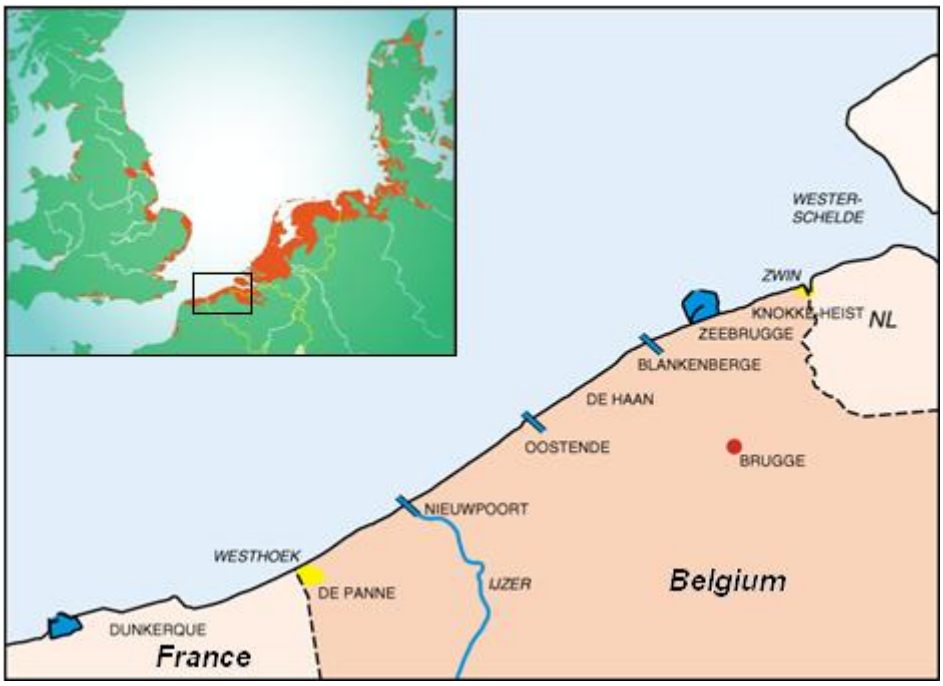

Figure 6.1 Location of project area (source: Flemish Coastal Division). The orange part in the inset is the land area below MHW.

The Belgian coast has a bi-diurnal tide with a small asymmetry and an average tidal range of 4m. The tidal wave moves along the coast from west to east. The tidal range decreases in the same direction by ± 0.5 m. Spring tides occur twice a month when the tidal variation has reached its maximum (± 5 m), while for neap tides occur the tidal range reaches its minimum, i.e. ± 3 m. The tidal curve has an asymmetric shape because the low tide lasts half an hour longer than the high tide. Meteorological circumstances can significantly influence the curve as well. Long-lasting intense winds may influence the water level, resulting in extremely low or high water levels. This important tidal range is linked to quite significant tidal currents, which exceeds generally 1.5 knots in the near shore areas. Because of the shallow seas and the short fetch, waves are typically short crested at the Belgian coast.

The wave climate along the coast is mainly determined by meteorological circumstances, predominantly westerly winds, and by the shallow depth of the North Sea. Under normal circumstances the wave along the coast is lower than 1 meter. During (heavy) storms wave heights of over 5 meters can occur. The wave period is 3 to 4 seconds under calm weather conditions, but during storms it can reach 10 to 15 seconds (IMDC, 2005).

The Belgian coast is protected by a dynamic coastal defence as well as fixed coastal structures. The dynamic defence consists of dunes, sandbanks and beaches as elements of a natural system that protects the coastline from the forces of the sea. This protective belt is a few hundred meters to several kilometres wide and locally up to 30 meters high. In some places, the coastline is reinforced by rigid coastal defence structures. Typically fixed coastal structures used in Belgium are groins, seawalls, beach groins, breakwaters, etc. An overview of the coastal defence along the Belgian coast is shown on Figure 6.2. There are 4 harbours/tidal inlets at Nieuwpoort, Ostend, Blankenberge and Zeebrugge and the Zwin (tidal inlet) (see Figure 6.1).

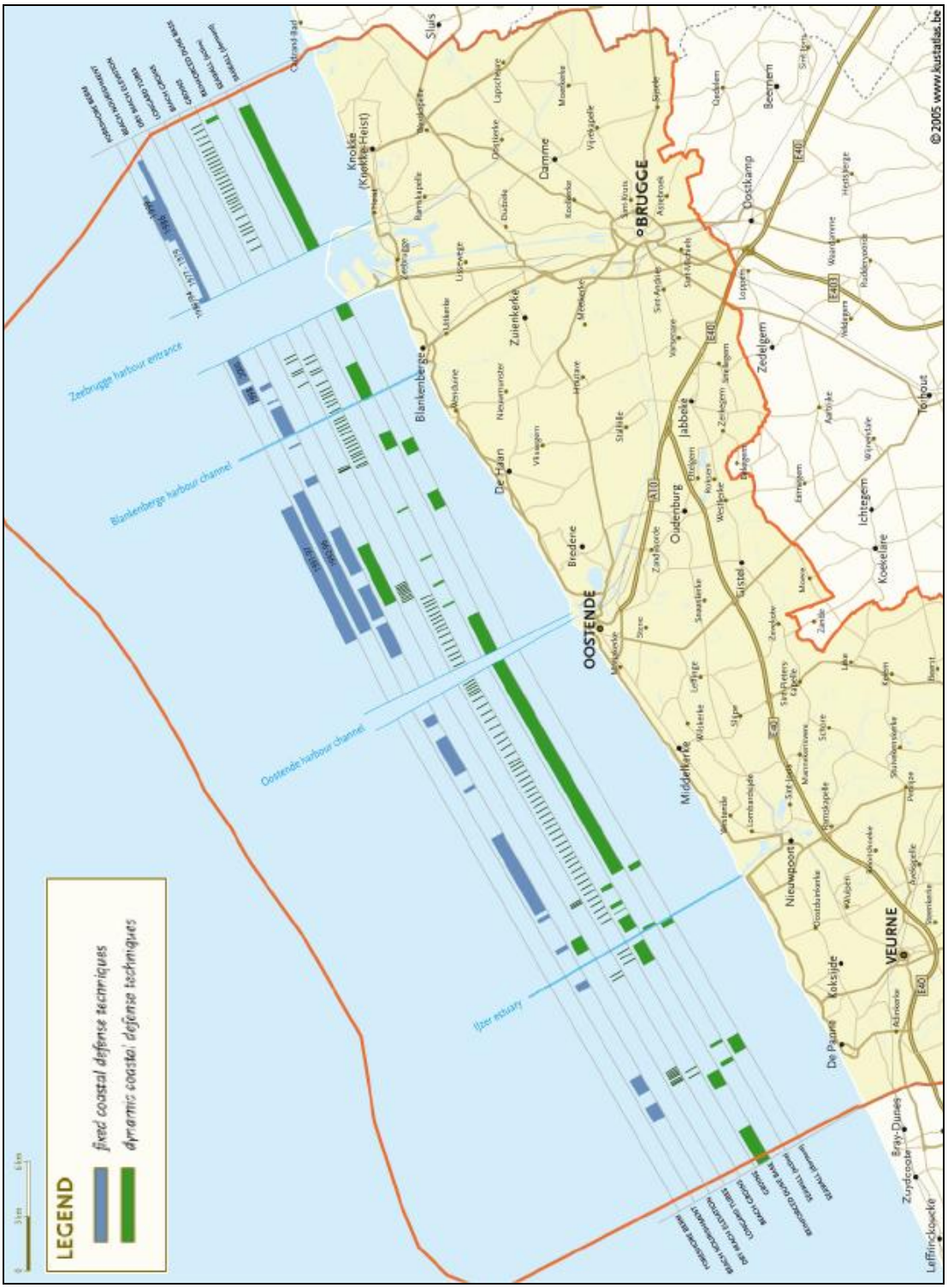

Figure 6.2 Overview of fixed and dynamic coastal defence techniques along the Belgian coast (www.kustatlas.be).

Net alongshore transport is predominantly in north-easterly direction. Close to the coast there is a southeast-oriented residual sediment transport parallel to the coast and flood dominant, with volumes between 0.6 and 5 tonnes/m/day. In the open sea (north of the sandbanks) sediment transport is southwest oriented. (Lanckneus, 2002)

About 20 % of the coastline shows accumulation, 40 % is under erosion and the remaining part is relatively stable (Kustatlas, 2008). However, natural processes or human interference can reinforce, weaken or even completely reverse this situation very quickly. Moreover, the coastal system is always subject to temporary variations caused by hydro-meteorological circumstances, and it inevitably undergoes change over a longer period of time.

The population density along the coast is high, especially during the tourist season. Over long stretches of the coast apartment buildings are constructed on the dyke, with only limited distance between the buildings and the beach.

Protecting the coastline is essential as both the coast and the polders behind it (which are at risk of being flooded at high tide) are of great economic, recreational and ecological value.

6.2.1.2 Mariakerke

Mariakerke is located almost in the middle of the Belgian coast, just westwards of Ostend. At this location there is a dyke, with in front a beach. The dissipative beach is characterised by a low beach gradient, a surf zone with the presence of numerous spilling lines of breakers and by fine to medium sandy sediments. The average tidal range at Mariakerke is 3.88 m, which makes it a macro-tidal beach.

Figure 6.4 gives an overview of the area. As can be seen in the aerial picture, the study area is densely populated, with apartment buildings on the dyke (see Figure 6.4). Only small sections consist of dune area. From profile 96 to profile 108 a sea dyke can be found, residential areas are in sections 98-100, and 103-108 (IMDC, 2004). This is an example of an urban beach with a high touristic value. The coastal defence (dyke + beach) is designed to give protection for a T100 storm event (return period 100 years).

Since 1993 maintenance beach nourishments are carried out, with an average volume of 26.000 m³/year for the entire area. Recently bigger volumes have been nourished to guarantee the minimum protection level (autumn 2005: 141.200 m³, autumn 2006: 97.700 m³). The most recent nourishment was carried out in 2007-2008: 186.000m³.

Figure 6.3 Mariakerke coastal zone, the study area is located between section 96 and 108

Figure 6.4 Dyke, promenade and beach at Mariakerke. Note the apartment buildings on the dyke

The beach profile at Mariakerke is characterised by a sea dyke (with height varying between +8m TAW and + 9.70m TAW), a dry beach and a bar-through system, illustrated on Figure 6.5.

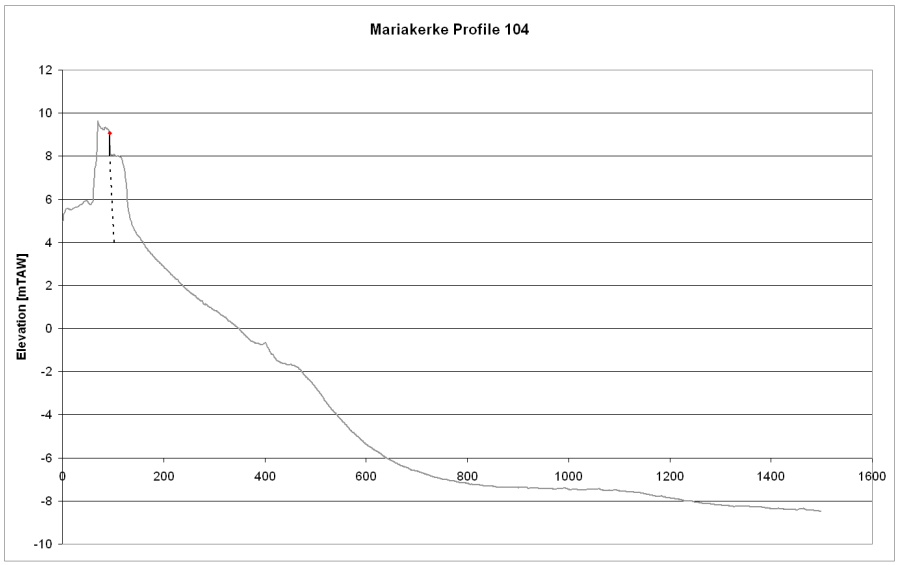

Figure 6.5 Typical beach profile at Mariakerke.

Figure 6.6 shows the erosion / sedimentation trends for the wet and dry beach, calculated over the 10-20 previous years, for 1998, 1999 and 2007 (AWK, 1998 & 1999; Houthuys, 2008). As can be seen in the figures, the beach volume is relatively stable over the area, and the trends do not change significantly over the years.

Storm events however, can cause severe erosion. For example beach scarps can be formed during a storm, as shown on Figure 6.7.

Figure 6.6 Comparison erosion/sedimentation trends wet and dry beach for 1998-1999-2007

Figure 6.7 Beach scarp erosion (storm with 1/10 yr retour period)

6.2.1.3 Ostend

Because the past winter only moderate storms occurred along the Belgian coastline, it was decided to use the available data-set of the Ostend beach (adjacent to Mariakerke) to test the XBeach capacities. The Ostend beach (Figure 6.8), located almost in the middle of the Belgian coast, is a dissipative beach, characterised by a low beach gradient, a surf zone with the presence of numerous spilling lines of breakers and by fine to medium sandy sediments (D50=0.214 mm). The study area is densely populated with apartment buildings on the dyke and a promenade protected by a seawall without naturally-developed dunes. The coastal defence is designed for to give protection for a T100 storm event (return period of 100 years).

Figure 6.8 Dyke and beach at Ostend centrum.

6.2.2 Storms considered

Since our main interest is to improve the beach erosion predictions during storm events, a historical data set for Ostend beach has been used for the calibration of the models. For the storm of 8 to 10 November 2007 water levels and wave parameters have been measured throughout the storm. The bathymetry and beach topography have been measured before and after the storm.

6.2.2.1 Storm Development

Between 08/11/2007 0000Z and 1800Z an active depression moves from just southeast of Iceland towards Norway and settles afterwards in south Scandinavia. On the back of this depression, strong northerly wind fields develop and spread over the Norwegian Sea and the North Sea. This situation causes high water levels and waves along the North Sea Coasts (Versluys, 2007).

Thursday 8 November is three days before spring tide. The presence of a strong North – to North-Westerly wind field from the Greenland sea to all over the North Sea causes during the night of Thursday 8 to Friday 9 November for a surge of 1.45m, which results in a high water of +5.93m TAW. On the following low water of Friday morning, the surge is 2.08m so the low water level sticks to +2.57m TAW. The high water of Friday noon has still a surge of 1.27m, resulting in a high water level of +5.75m TAW. Due to the backing and decreasing of the wind, the next high water the surge is only 0.19m.

Due to the increasing and veering of the wind during the passage of the front on Thursday 8 November 1800Z, the waves at full sea increase spectacularly, reaching a significant wave height of 4.5 to 5.0m (with peaks around 8 to 9m) on Friday morning 9 November. From Friday noon, the waves decrease gradually, but keep fluctuating till Saturday noon around 3m (with peaks up to 5.5m).

A bit more towards the coast, the waves increase Thursday evening 8 November up to 2.5 – 3.2m (with peaks up to 6m). From Friday noon the waves decrease gradually, but fluctuate around 2m (with peaks from 3.5 to 4m).

Nearby the coast (Ostend) the significant wave height was all the time slightly higher compared to a bit further offshore. For Ostend the highest observed significant wave height is 3.7m. During the period July 2002 till April 2006, the significant wave height of 3.5m was exceeded only in 0.01% of the cases.

6.2.2.2 Hydrodynamic Data

Within the framework “Structural repair of the coastal defences in Ostend and the improvement of the harbour entrance” a directional waverider buoy was deployed near Ostend Noodstrand (Table 6.1). The time series originating from this buoy have been used.

Table 6.1 Specifications directional wave rider buoy Ostend Noodstrand.

Type	X coordinate [WGS84]	Y coordinate [WGS84]	Local water depth [m TAW]	Measurement frequency	measurement period	available parameters
Directional Waverider	493612.41	5676314.44	6.1	30 min	07/11/2007-12/11/2007	Hm0, Hm1 GTZ, RLF, RHF

The peak wave period is not directly available from the measurements. The peak period is taken equal to 1.3 * the average wave period (T_Z). The water level is measured at the tide gauge is Ostend harbour. The time series contains the average water level over a period of 5 minutes, with a measurement frequency of 5 minutes.

Figure 6.9 and Figure 6.10 show the relevant measured hydrodynamic data during the storm event of 8 to 10 November 2007. The water level shows a clear setup (1 to 2m) in the first 20 hours, reaching a level of about 6m TAW at high water. TAW is about mean sea level (MSL). At the same time the significant wave height at the “Oostende Noodstrand” buoy (near-shore at -6m TAW) is 3 to 3.5m and the peak wave period is around 8s. The wave direction is almost perpendicular to the coast. In the models, the entire 48 hours have been simulated.

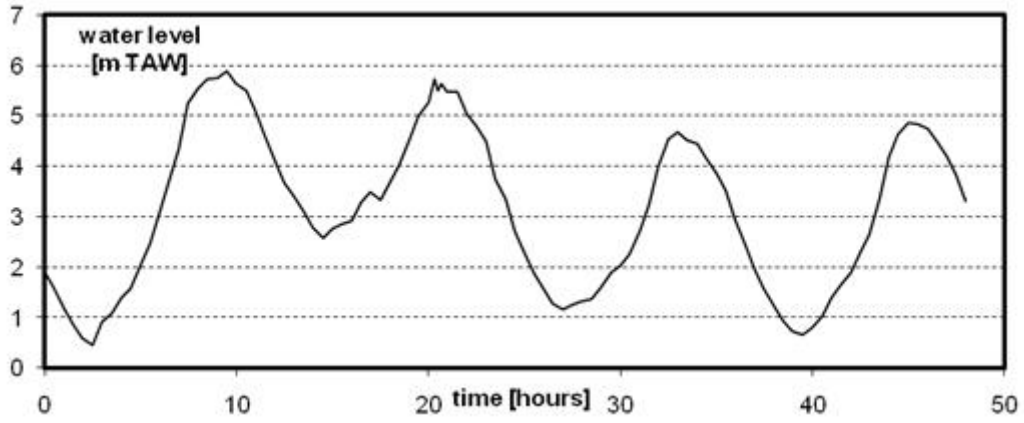

Figure 6.9 Measured water level at Ostend during the storm of November 2007.

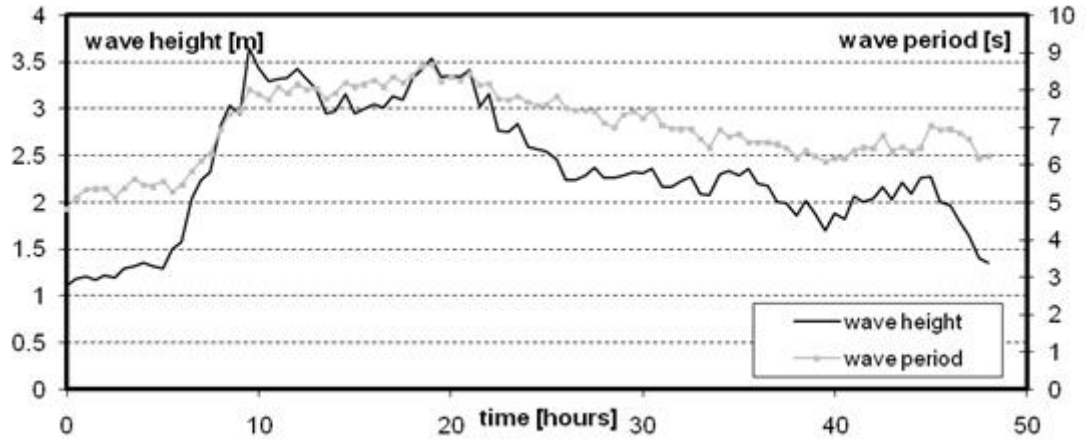

Figure 6.10 Measured significant wave height and peak wave period at Ostend during the storm of November 2007.

6.2.2.3 Bathymetry, topography & grain size

The grain sizes of the beach are considered to be uniform within one coastal section. The measurements after the second beach nourishment are used. This resulted in a D_{50} of 0.214mm for the beach in sections 113 to 117.

Measurements of bathymetry and beach topography were carried out before and after the storm. The following two datasets will be used:

- c46c47 (October 2007; outsurvey from the beach nourishment)
- c48c49 (survey after the storm of 8 to 9 November 2007)

Since the resolution of the data is strongly different for the two measurements, it was decided to use the data from the individually measured cross-shore profiles, instead of defining profiles from an interpolated DTM. Two profiles were measured in sections 114 to 116, only one profile in section 113. Figure 6.11 and Figure 6.13 show the available measurements of both datasets. The contours are shown on Figure 6.12 and Figure 6.14.

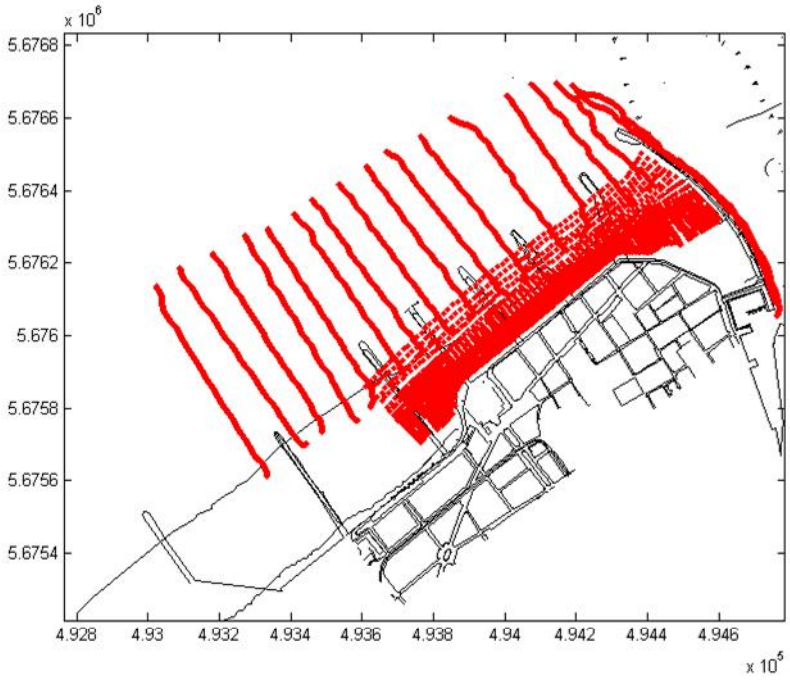

Figure 6.11 Survey October (c46c47) – measurement points

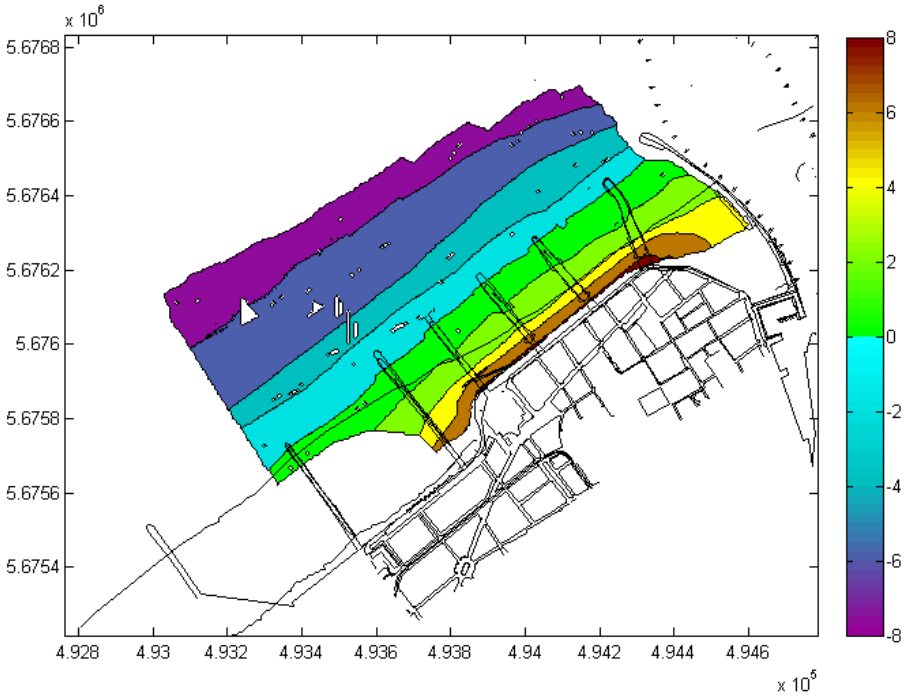

Figure 6.12 Survey October (c46c47) – contours

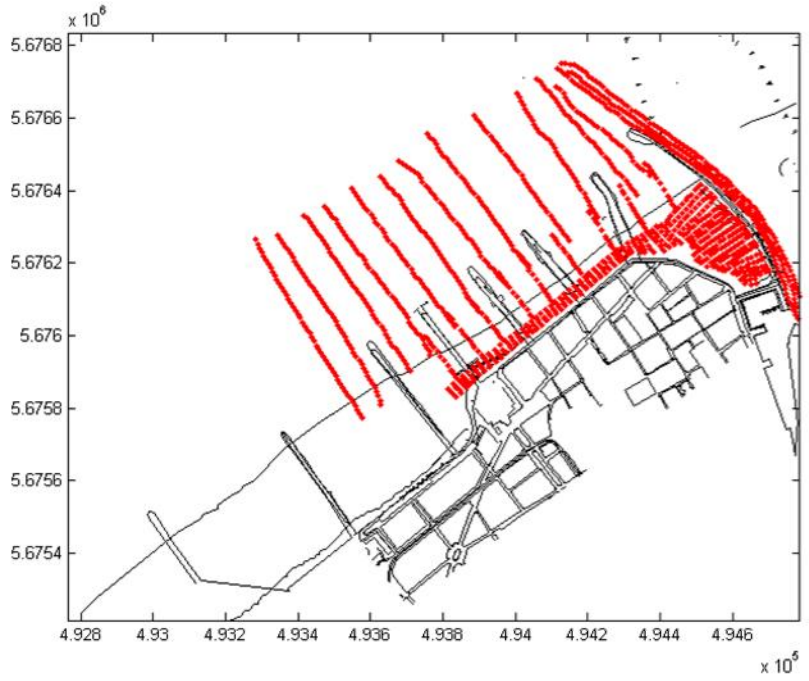

Figure 6.13 Survey November (c48c49) – location measurement points.

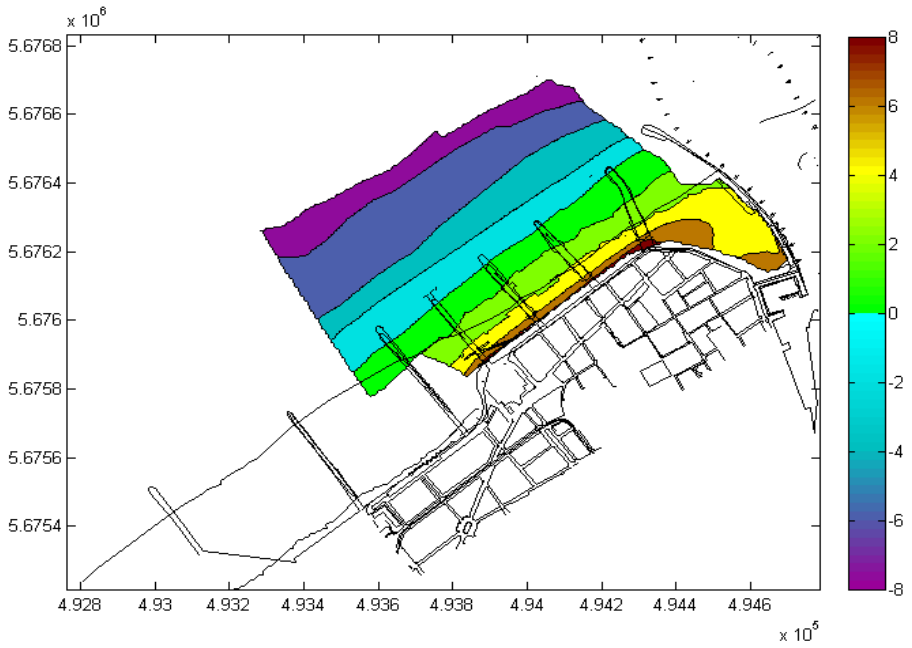

Figure 6.14 Survey November (c48c49) – contours.

From these datasets, profiles before and after the storm have been compared. Hereafter, a comparison of the beach profile before and after the storm is shown on Figure 6.16 to Figure 6.20. The location of the coastal sections is indicated on Figure 6.15.

The effect of the storm is clearly visible on all profiles. The berm of the beach above +4m TAW has been eroded over several meters, all along the coast of Ostend centre.

The erosion is also more important in sections 113 and 117, than in sections 114, 115 and 116. This is possible due to 2D effects: in these two sections, the dyke and the beach in front is curved.

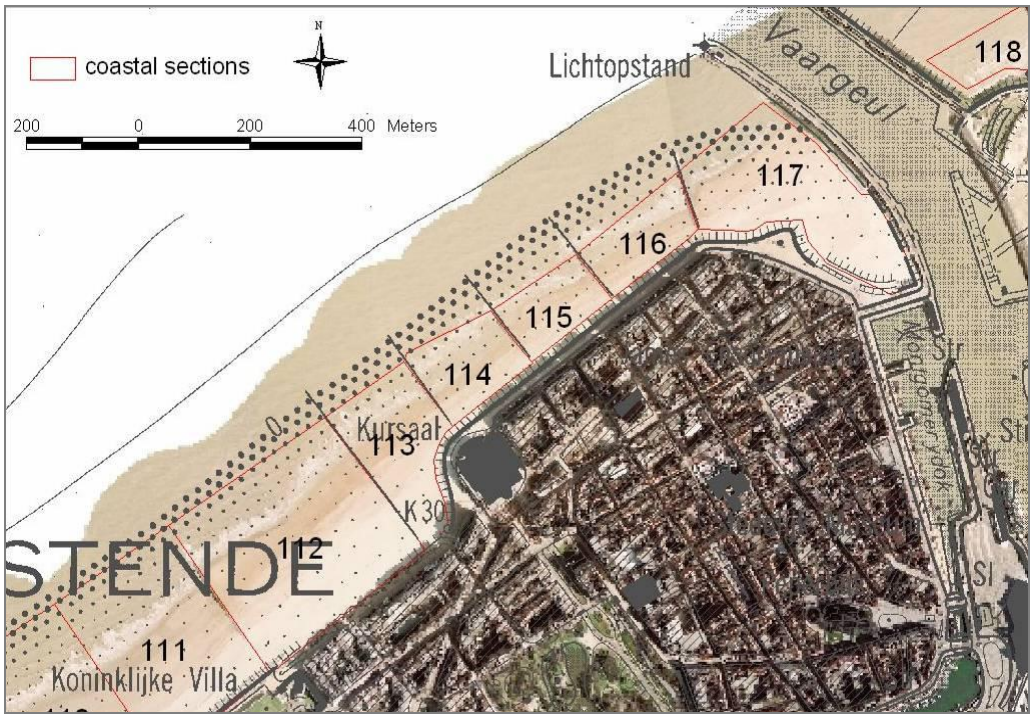

Figure 6.15 Division into coastal sections.

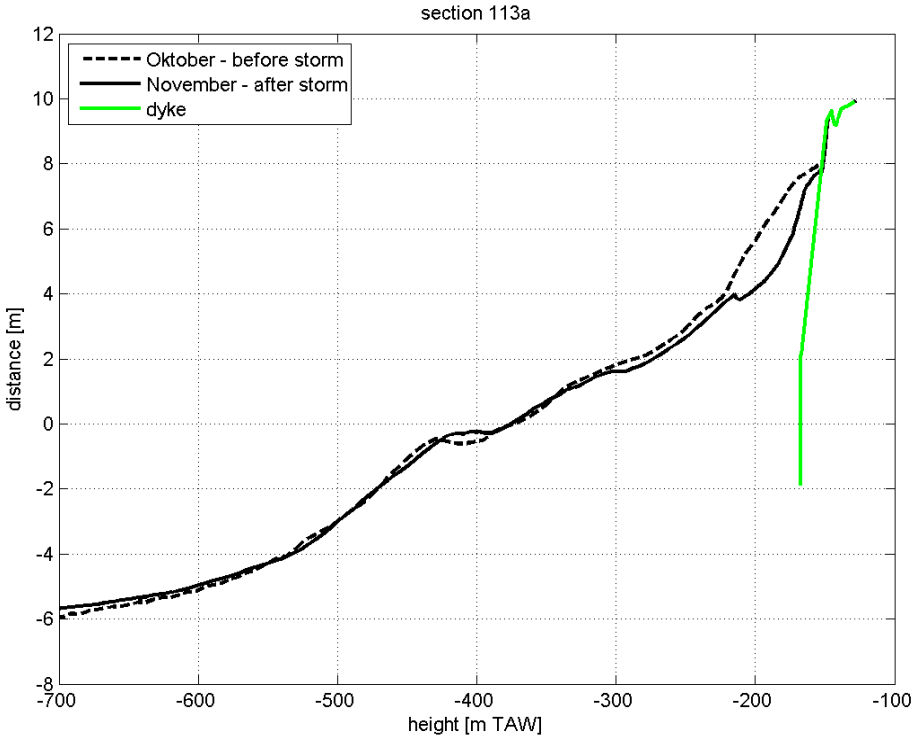

Figure 6.16 Profile measurement before and after November 2007 storm in section 113a.

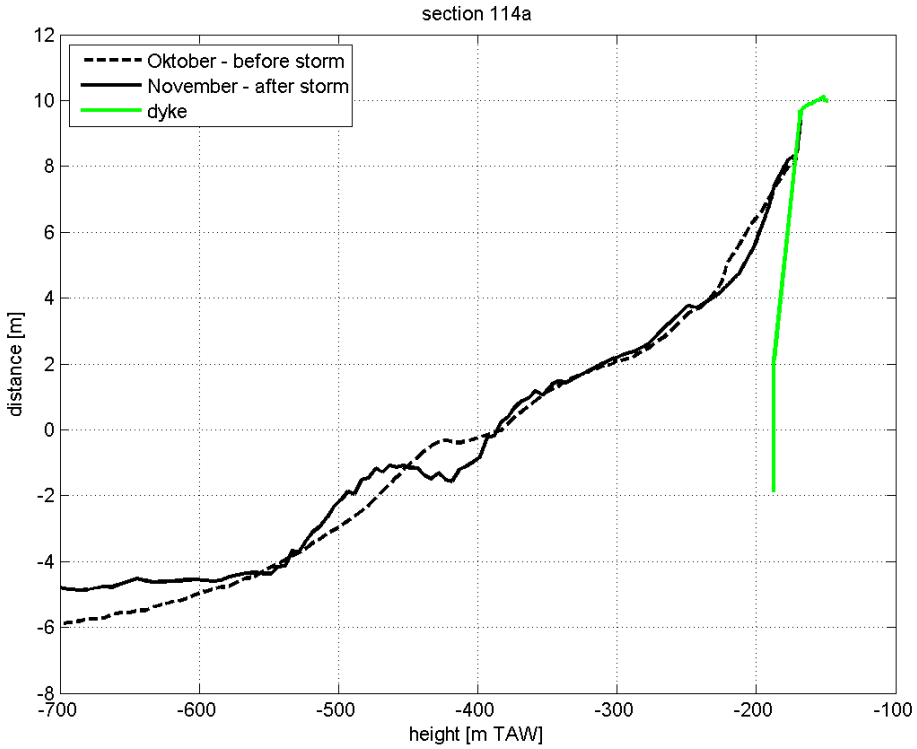

Figure 6.17 Profile measurement before and after November 2007 storm in section 114a.

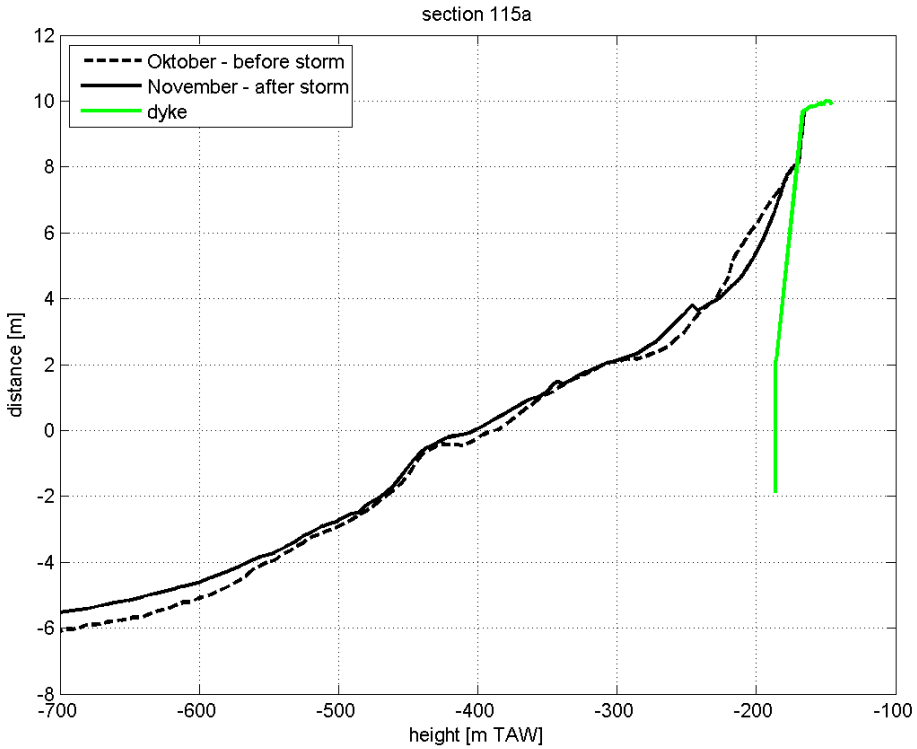

Figure 6.18 Profile measurement before and after November 2007 storm in section 115a.

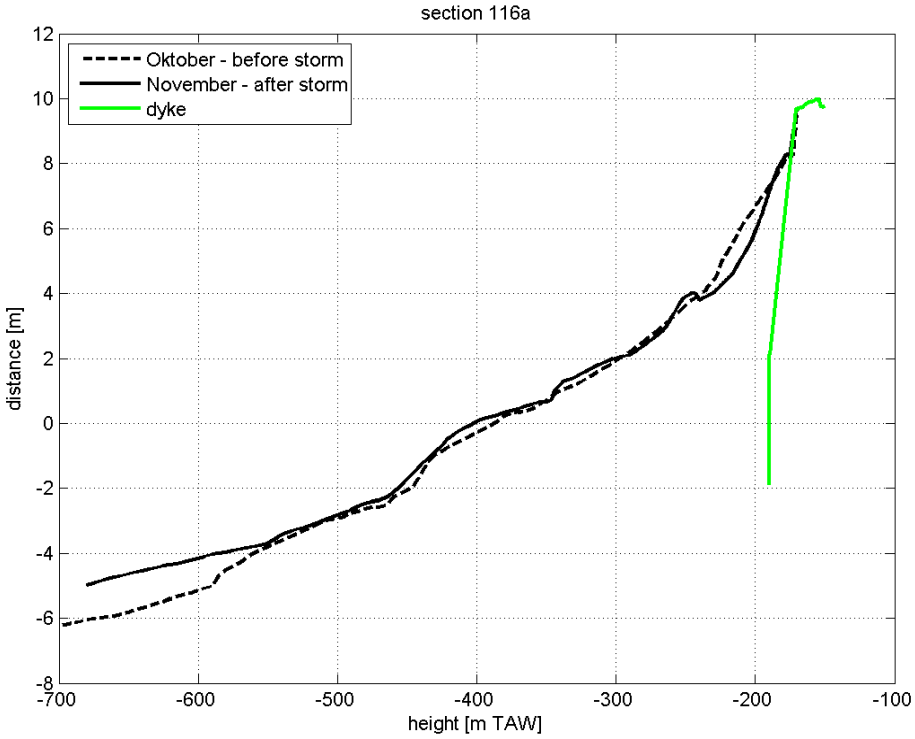

Figure 6.19 Profile measurement before and after November 2007 storm in section 116a.

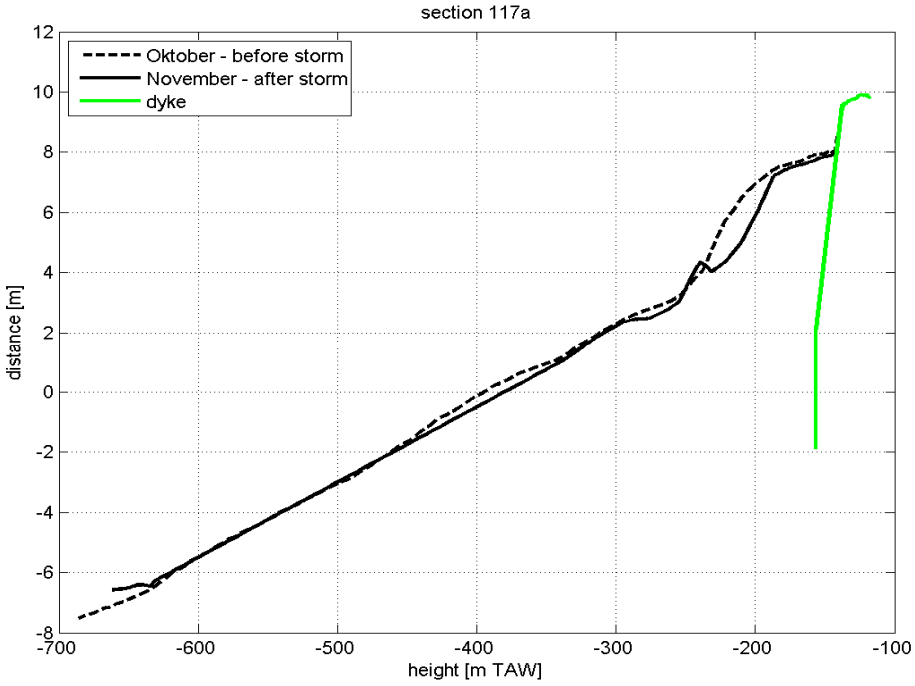

Figure 6.20 Profile measurement before and after November 2007 storm in section 117a.

6.2.3 Measurements

6.2.3.1 Mariakerke

Site monitoring at Mariakerke is focused on the measurements of hydrodynamic conditions on the one hand and morphological changes on the other hand. This paragraph describes the specific monitoring program at Mariakerke for both types of measurements. The timetable of the site monitoring campaign (topography, bathymetry & grain size) is given in Table 6.2. For a more detailed description, the report of WP3 should be consulted.

Morphological site conditions are not continuously measured, but on frequent basis. Starting with a reference measurement, during the first winter months measurements are performed after each significant storm or every two months. During the summer months no measurement are undertaken, and at the end of the summer of 2009 a new reference measurement is done. From September 2009 until April 2010 measurement efforts are focused on storm events only. During the 1.5-year monitoring period seven morphological measurement campaigns are organized. The timetable is shown in Table 6.2, including the exact dates of the measurements

Most of the hydrodynamic conditions are measured in a continuous mode. In addition to this a near-shore detailed hydrodynamic monitoring campaign is organized between December 2008 and April 2009.

Table 6.2 Timetable monitoring program.

Overview WP3 - Information based on Table 1.4 (DoW pg. 27)

WP3 - ITEMS	Oct-08	Nov-08	Dec-08	Jan-09	Feb-09	Mar-09	Apr-09	May-09	Jun-09	Jul-09	Aug-09	Sep-09	Oct-09	Nov-09	Dec-09	Jan-10	Feb-10	Mar-10	Apr-10	May-10	Sep-10
	5	6	7	8	9	10	11	12	13	14	15	16	17	18	19	20	21	22	23	24	
WP3 - Storm Specific monitoring				According DoW : 6 to 18																	
Long term monitoring																					
Topography	17/10/2008	26/11/2008	17/12/2008		12/02/2009		28/04/2009					10/09/2009					-	05/03/2010	30/04/2010		13/09/2010
Bathymetry	17/10/2008	-	17/12/2008		13/02/2009		14/04/2009					23/09/2009					24/02/2010	10/03/2010	29/04/2010		28/09/2010
Lidar												22/09/2009									
Sediment sampling	23/10/2008	-	15/12/2008		13/02/2009		-					21/09/2009					-	-	29/04/2010		-
Hydrodynamics																					
Hydrodynamic campaign																					
Offshore waves	By wave rider bouy at Akkaert (22m depth)																				
Nearshore waves	By wave rider bouy at Oostende Noodstrand (6m depth)																				
Tide	By tidal gauge in Ostend																				
Wind	By wind measurements at Westhinder (offshore)																				
Measurment nº	t0	t1	t2		t3		t4					t5					t6	t7	t8		t9

According DoW
Extention of duration of measurement campaign
Executed measurments

6.2.3.2 Methods: Beach Morphology

Bathymetric and topographic measurement campaigns are performed to register on a regular basis the morphological characteristics of the beach. In addition to these two techniques the results of LIDAR flight topography are available and the grain size distribution of the beach sediment is analysed.

Topographic surveys are performed to map the sub-aerial part of the beach, while bathymetric surveys are used to map the surf zone by means of single- and multi-beam measurements. The latter shall be used for the characterisation of submerged features like near-shore bars. Sufficient overlap of bathymetric and topographic measurements is needed to create continuous cross-shore profiles and a detailed digital terrain model.
Surface sediment sampling is performed on the beach and offshore. These samples are taken on the same cross-shore profiles as used for the topographic and bathymetric surveys.

It is foreseen that specific storm related data should be collected including:

- Morphologic evolution and identification of features generated by storms (e.g.. beach scarps);
- The maximum water level reached during the storm and mapping of eventual inundation areas.
- Post-storm campaigns can address the morphologic evolution and the beach recovery processes.

6.2.3.3 *Methods: Hydrodynamic site conditions*

The Monitoring Network of the Flemish Government (which is end-user of MICORE) provides most of the measurements of the hydrodynamic conditions for the study site. The Flemish Banks Monitoring Network consists of a marine monitoring network, weather forecasting centres on the shore and a computer network in Ostend (see Figure 6.21).

The marine network is made up of measuring masts and buoys, equipped with hydro-meteorological sensors. The data centre gathers, processes and exchanges operational data with international monitoring networks, research institutes and universities.
The Flemish Banks Monitoring Network provides data on the Belgian Continental Shelf of wave height, wave direction, wave period, wave energy, tide, wind speed, wind direction at several locations, see Table 6.3. For the Mariakerke test case site a selection of the available measurements is made.

Table 6.3 Available hydrodynamic parameters from the Flemish banks Monitoring Network.

Location	Wave height	Wave period	Wave direction	Wave energy	Tide	Wind speed	Wind direction
A2 Boei	X	X		X	X		
Appelzak					X		
Bol van Heist	X	X	X	X	X		
Bol van Knokke	X	X	X	X	X		
Kwintebank	X	X					
Nieuwpoort					X		
Oostende	X	X		X	X		
Oostende Noodstrand	X	X					
Scheur Wielingen	X	X			X		
Thorntonbank Zuid	X	X					
Trapegeer	X	X					
Wandelaar					X	X	X
Westhinder	X	X	X	X	X	X	X
Zeebrugge I						X	X
Zeebrugge II					X		
Zeebrugge III						X	X
ZW-Akkaert	X	X		X			

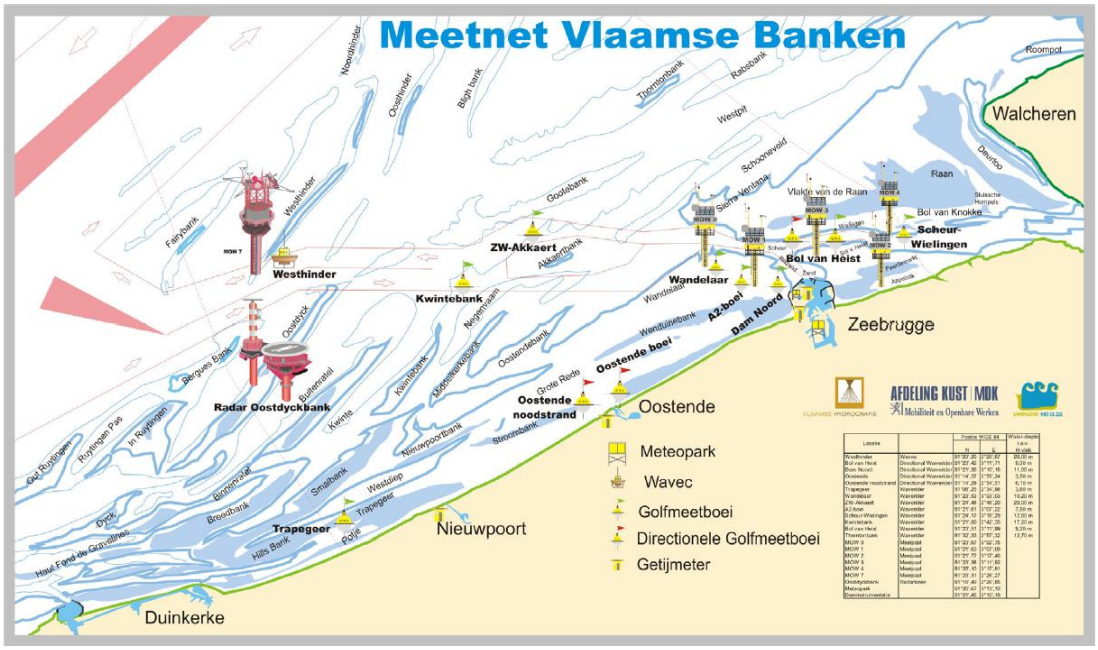

Figure 6.21 Flemish Banks Monitoring Network.

Within the Monitoring Network the offshore devices at Westhinder provide the necessary wind data (velocity and direction). ZW Akkaert and Westhinder provide offshore wave data (significant wave height, period, energy and direction), while near-shore wave data (significant wave height, period, energy and direction) is obtained from the Oostende Noodstrand buoy. The equipment at Westhinder and in the port of Ostend is used for registration of the water level (m TAW).

In addition to the available data from the Flemish Banks Monitoring Network, an site specific hydrodynamic survey is performed on Mariakerke beach. This campaign includes the registration of turbidity, currents, water levels and wave climate at different locations in the cross-shore beach profile.

The purpose of this measurement campaign is to investigate the cross-shore variability of the hydrodynamic parameters and to analyse the influence of storm events on these parameters.

6.3 Model results

6.3.1 Simulation results with Off-the shelf Model

Currently, beach and dune erosion at the Belgian coast is estimated with Durosta (for the model description: see appendix A). For the storm of November 2007, calculations have been performed with Durosta for Ostend beach and compared with the measurements.

Durosta has been run with default settings. Several profiles (1D) have been modelled on a grid that varies from 6m offshore to 1m near the seawall. The seawall has been included as a non-erodible element.

Figure 6.22 to Figure 6.26 show the comparison of the predictions from Durosta with the measurements. The measured and calculated profile after the storm agree quite well. The part of the profile, above the maximum water level is not eroded in the Durosta simulations.

The measurements however indicate that also a part of this beach is eroded. In Durosta a steep beach erosion front is created, somewhat steeper than is measured. This is visible in all sections. The storm produces also a bar on the 4m-contour, which is not reproduced by Durosta.

In sections 113 and 117 the erosion is underestimated with Durosta. These sections are situated at the Southwest and Northeast end of Ostend centre beach (see Figure 6.15) and are attacked more severely due to 2D effects. The gradient in the longshore transport influences the erosion on these spots. Since Durosta is a 1D model, these effects cannot be taken into account.

Durosta gives a good estimate of the erosion profile of the beach due to storm impact, as long as the beach is more or less straight. The situation in section 113 (near Ostend casino) is very specific and not representative for the entire coast. For these specific sites a 2D approach might be necessary.

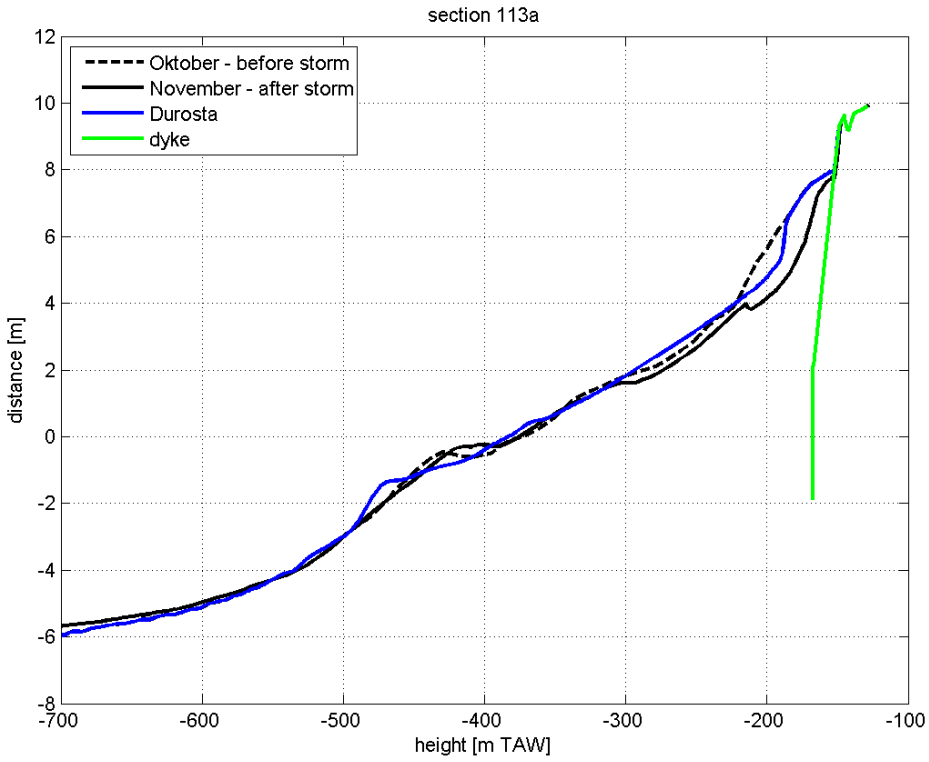

Figure 6.22 Comparison Durosta model result with measurements for section 113a.

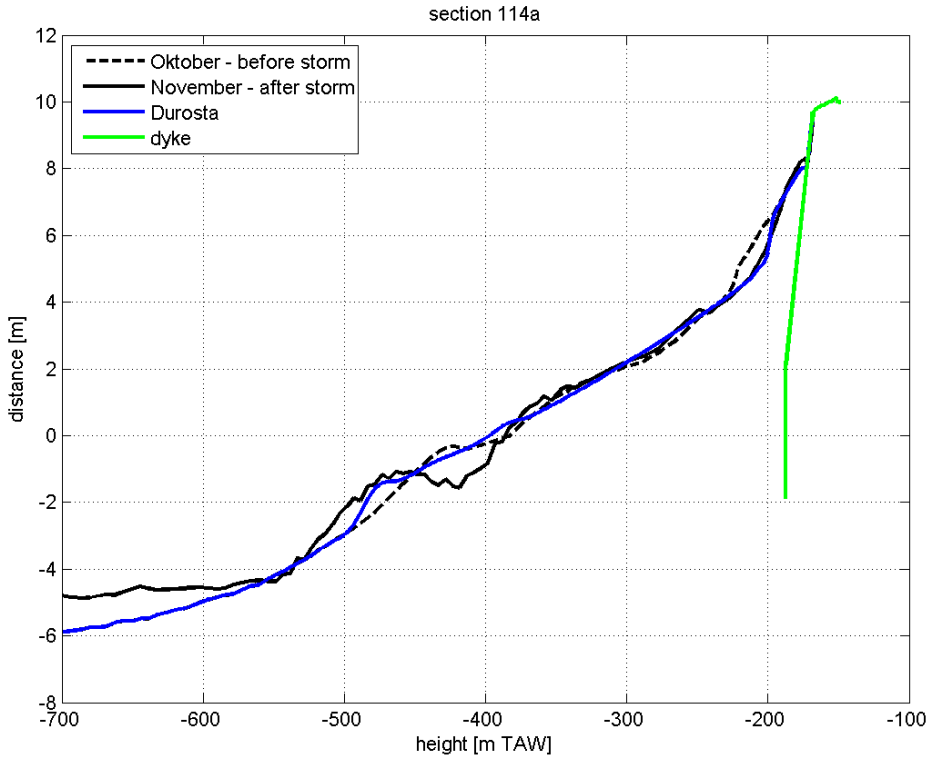

Figure 6.23 Comparison Durosta model result with measurements for section 114a.

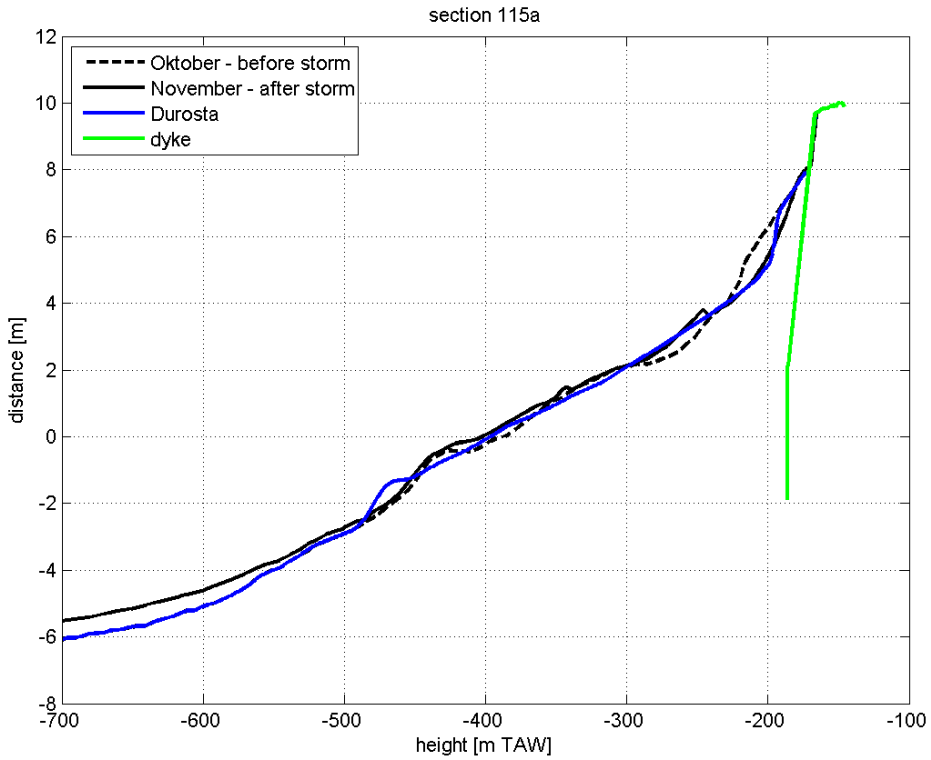

Figure 6.24 Comparison Durosta model result with measurements for section 115a.

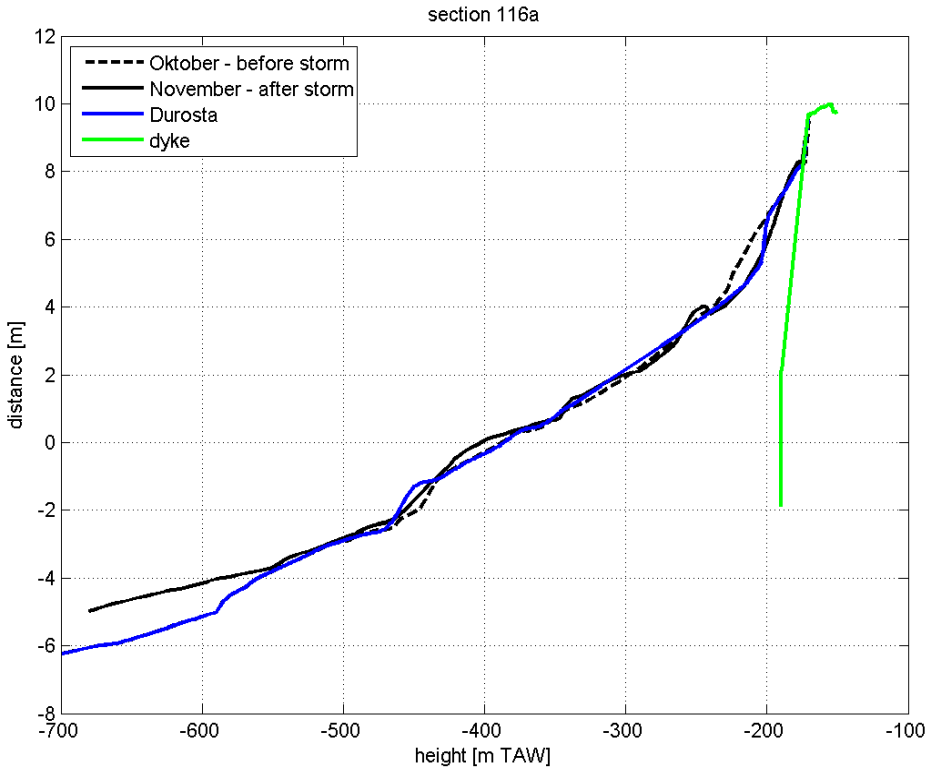

Figure 6.25 Comparison Durosta model result with measurements for section 116a.

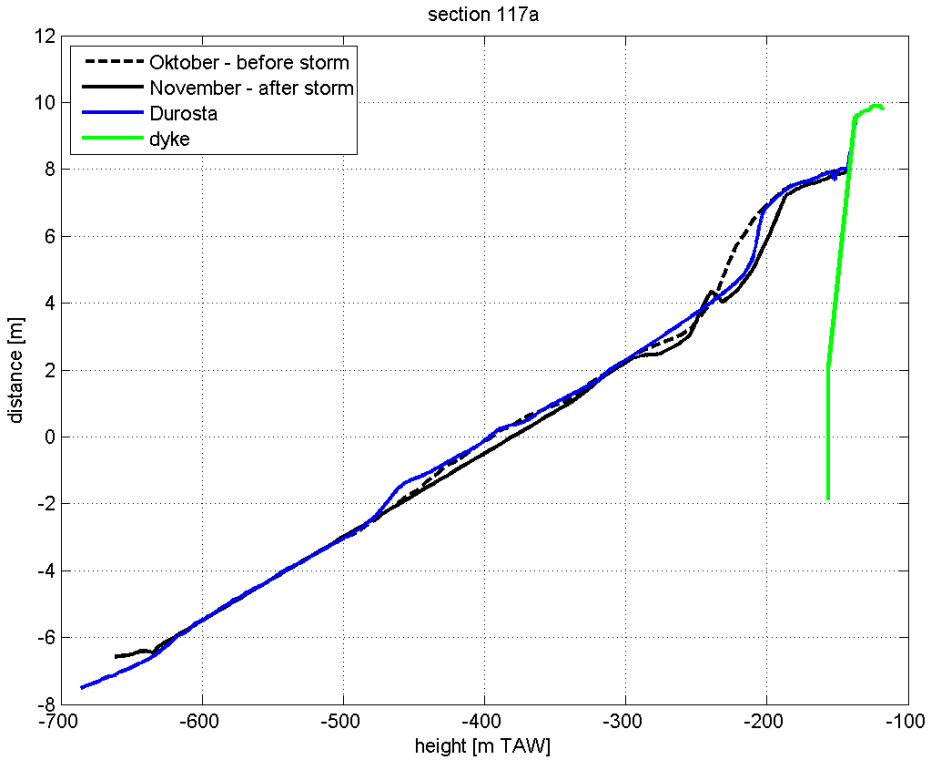

Figure 6.26 Comparison Durosta model result with measurements for section 117a.

6.3.2 Simulation results with XBeach model

6.3.2.1 1D XBeach model

To compare the performance of XBeach with Durosta, the same 1D-profiles haven been modelled for Ostend beach. The grid in XBeach has been chosen identical to that of Durosta and varies from 6m offshore to 1m near the seawall.

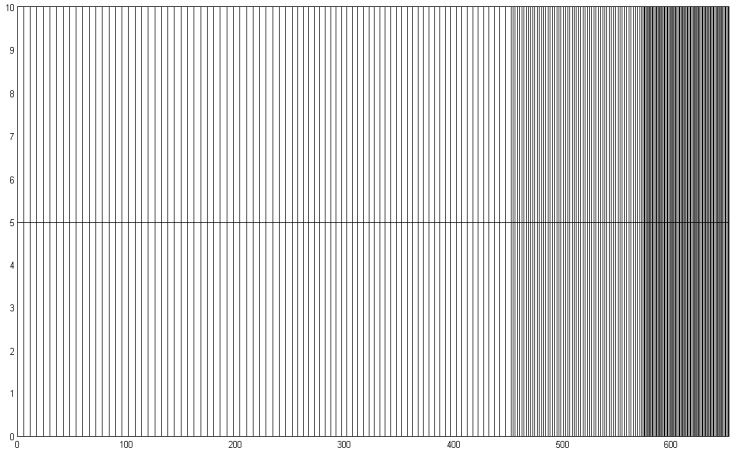

Figure 6.27 Figure 7 1: grid of the 1D XBeach model.

Figure 6.28 through Figure 6.32 show the comparison of the model results from XBeach and Durosta with the measurements. In sections 114, 115 and 116 the beach erosion front is well simulated. Also the slope of this front agrees well with the measurements. In sections 113 and 117 the beach erosion is underestimated. This is most probably due to the 2D effects which are important at these outer ends of the beach. Between the 0m and 4m TAW contour, the modelled beach is more uniform than the measurements. Small berms are not (sufficiently) modelled in XBeach.

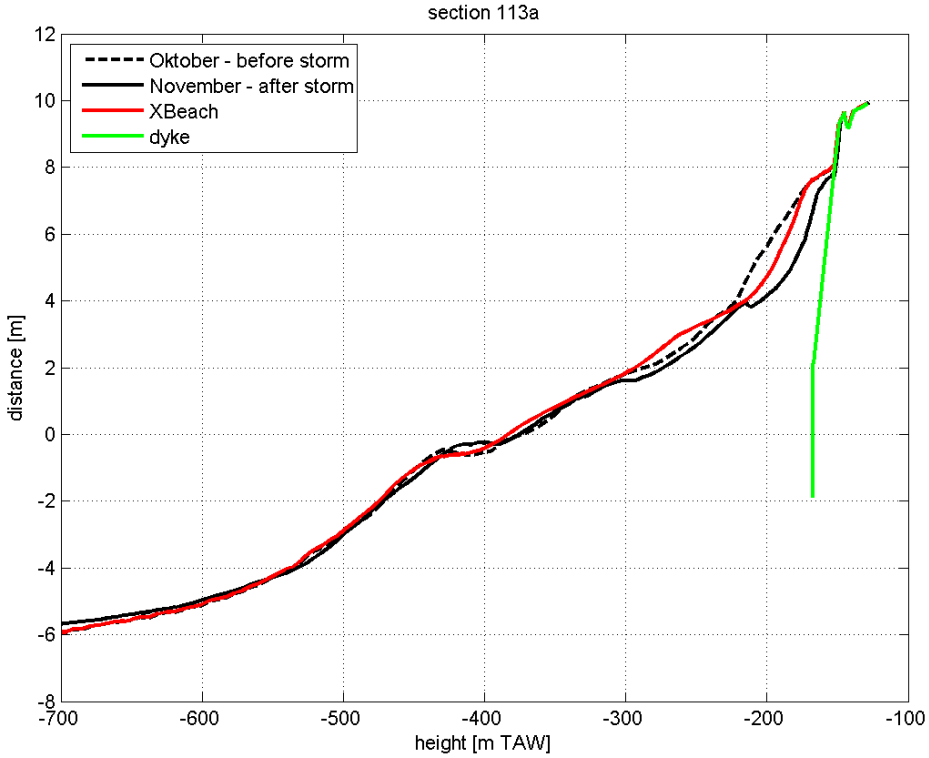

Figure 6.28 Comparison XBeach model results with measurements for section 113a.

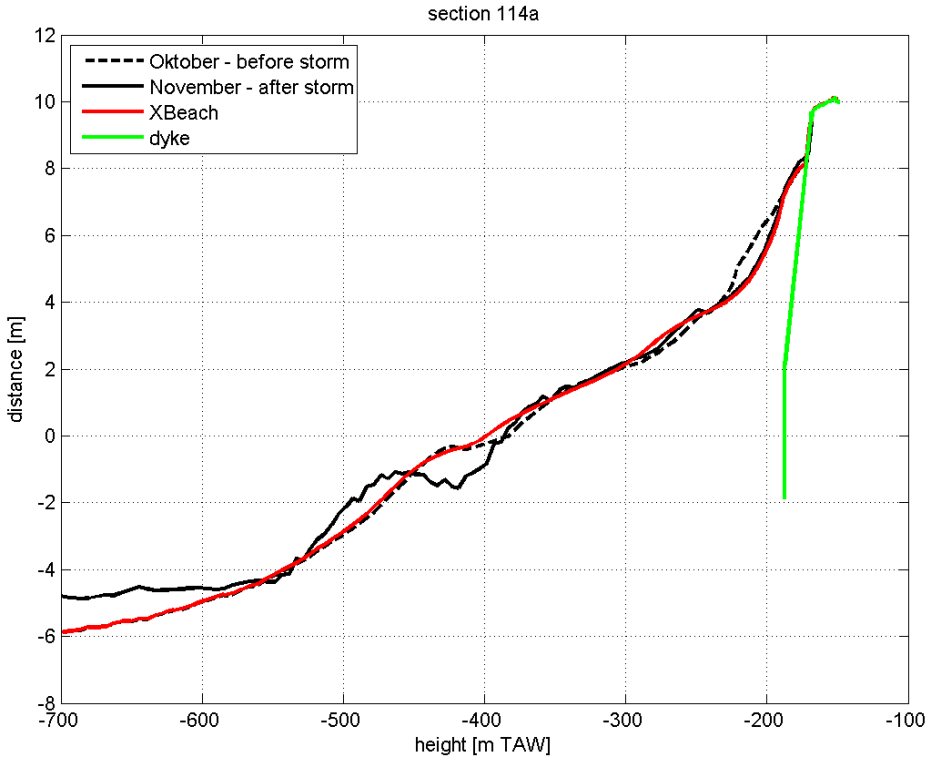

Figure 6.29 Comparison XBeach model results with measurements for section 114a.

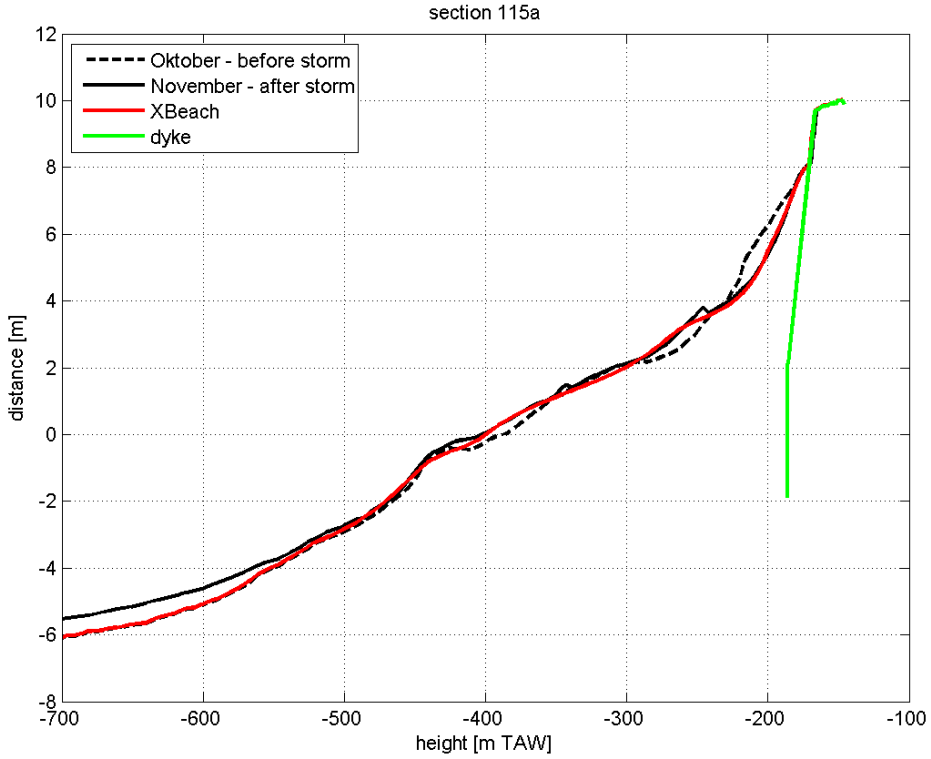

Figure 6.30 Comparison XBeach model results with measurements for section 115a.

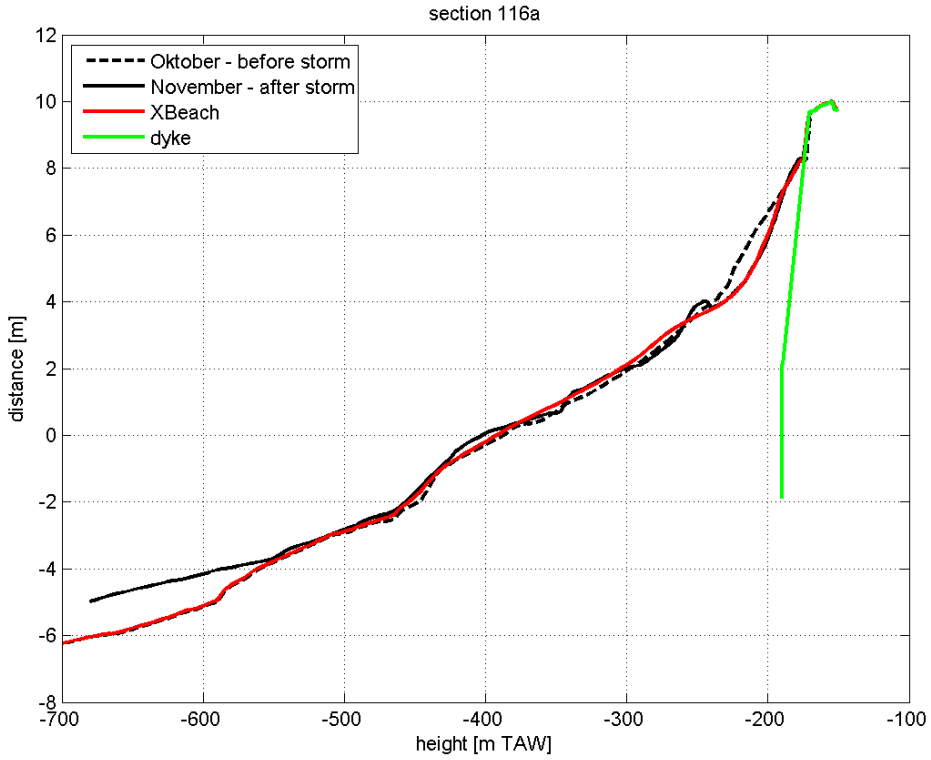

Figure 6.31 Comparison XBeach model results with measurements for section 116a.

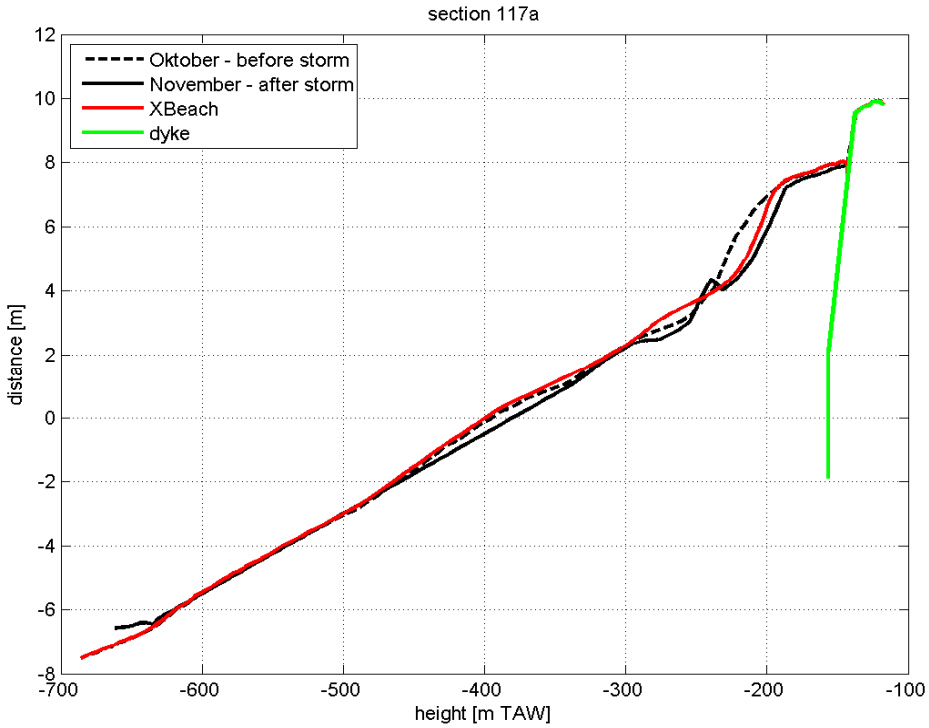

Figure 6.32 Comparison XBeach model results with measurements for section 117a.

6.3.2.2 2D XBeach model

For the 2D model, the bathymetry and topography are based on the measurments of the beach, foreshore and the dyke (same dataset as used for the 1D model, see Figure 6.33). In the areas near the borders of the model, where no data were available, the bathymetry was extended alongshore with a simiar profile, creating more uniform model boundaries. Also towards the sea, the bathymetrie was extended at a uniform depth the avoid abrupt depth changes along the seaward border. Figure 6.34 shows the non-uniform rectangular grid apllied in XBeach. The cell size decreases near and on the beach, in the shallow water.

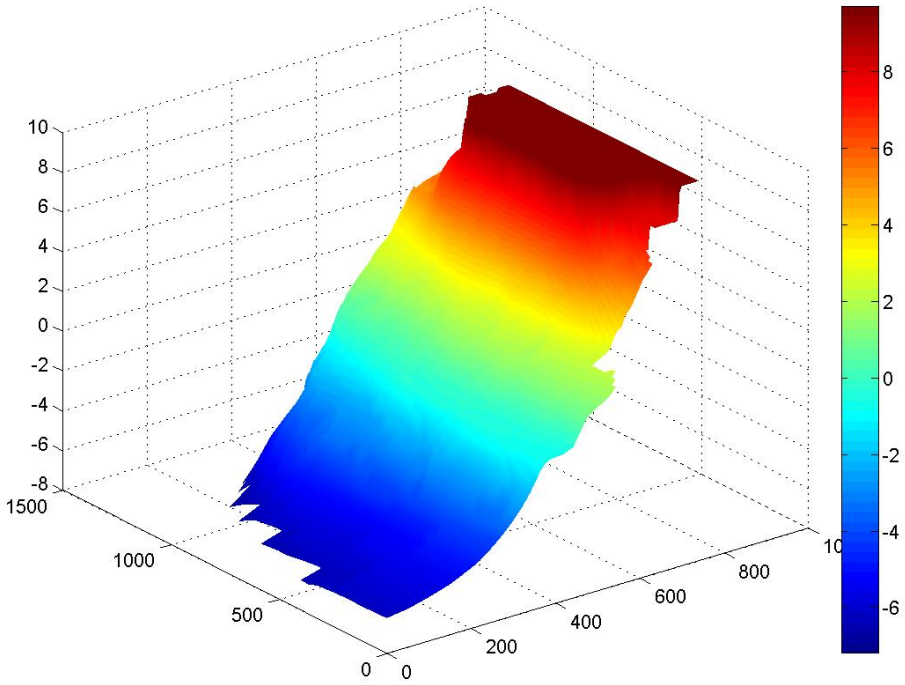

Figure 6.33 Original bathymetry (heights in m TAW)

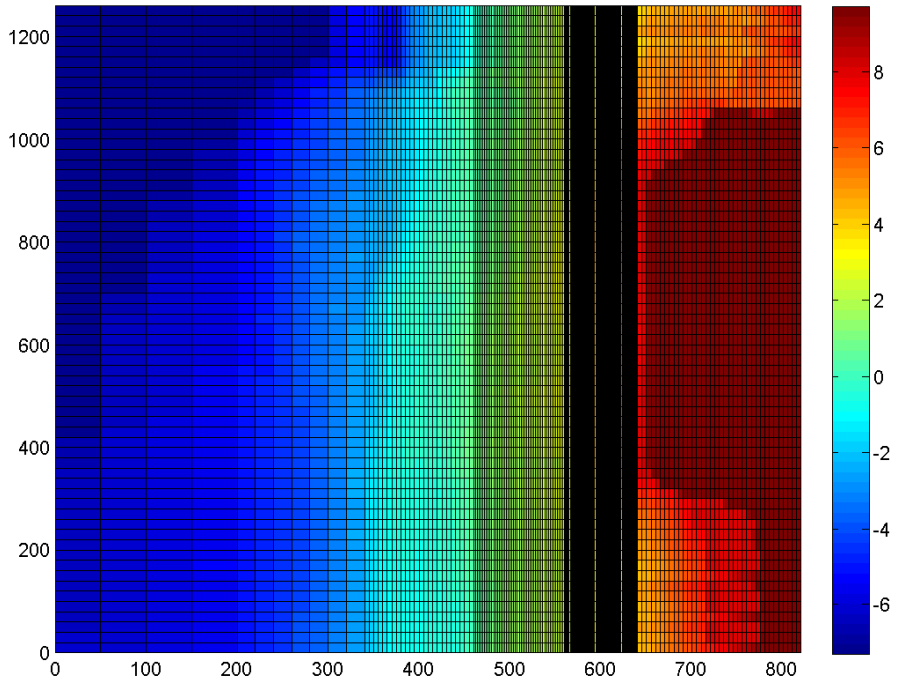

Figure 6.34 Grid 2D XBeach model test3b (color scale = height in m TAW)

The same storm event has been modelled, which allows comparison with both measurements and 1D model results (Durosta and XBeach). Figure 6.35 to Figure 6.39 show the comparison of these model results for a couple of profiles.

The 2D XBeach model gives good results, especially in sections 113 and 117 where the 1D models clearly underestimate the amount of erosion. These sections are located in areas

where both the dike and the beach in front are curved, which causes higher gradients in the sediment transport.

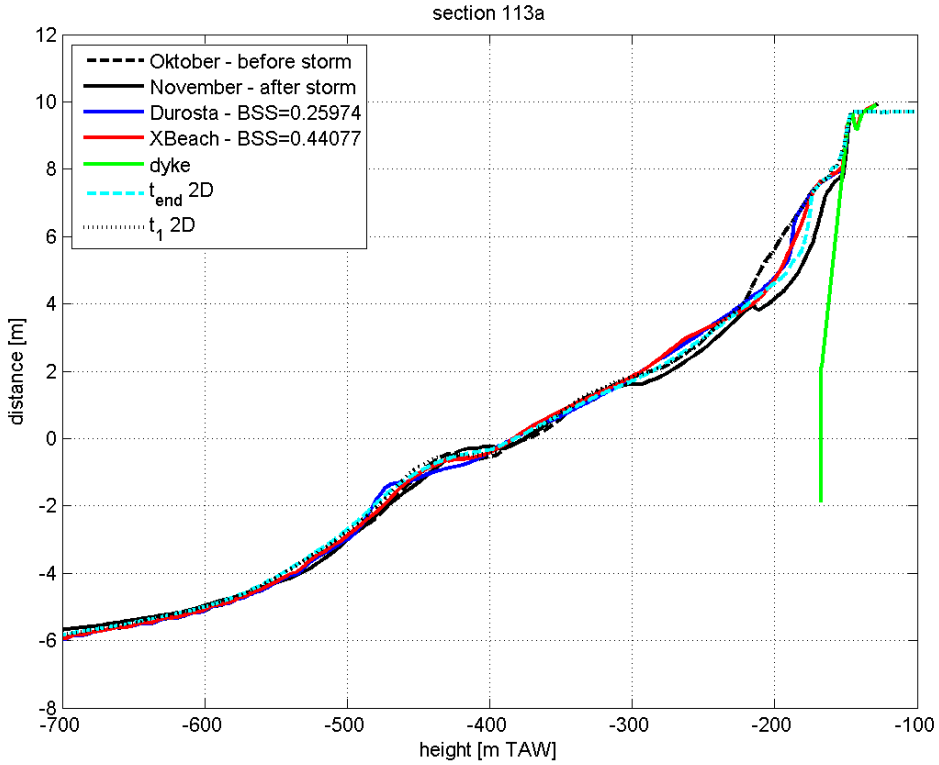

Figure 6.35 Comparison XBeach model results (best settings) with measurements for section 113a.

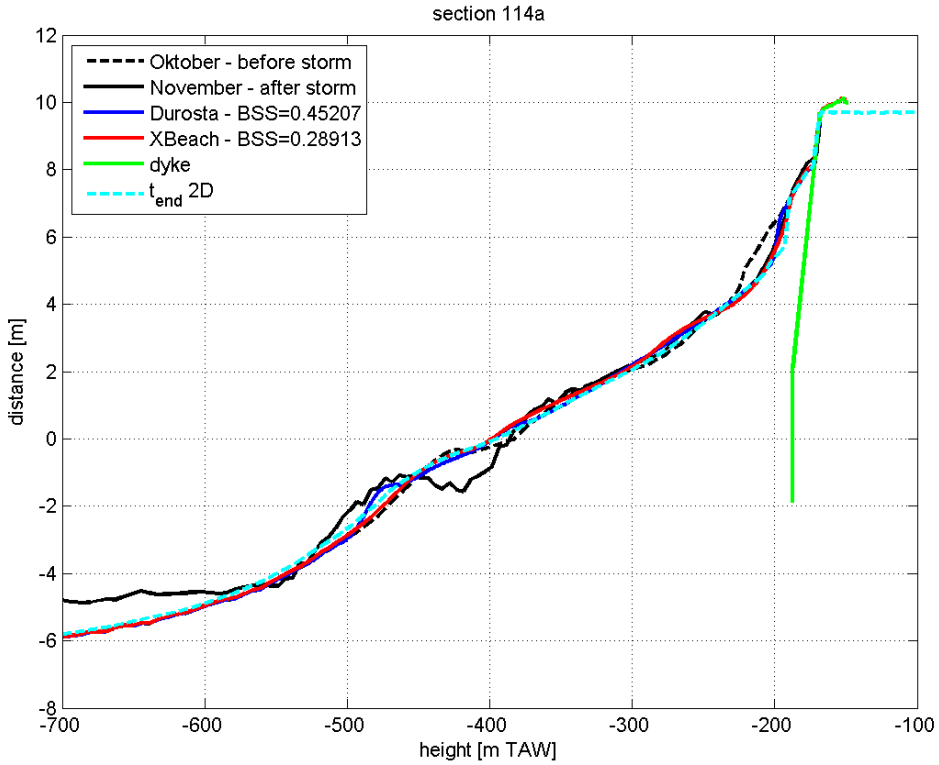

Figure 6.36 Comparison XBeach model results (best settings) with measurements for section 114a.

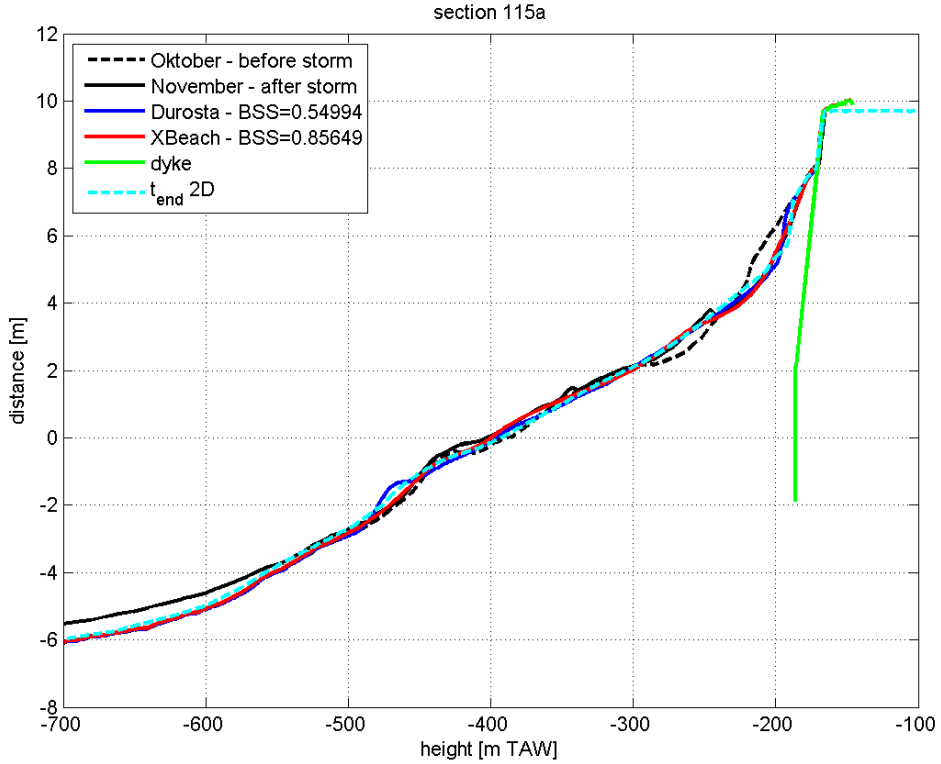

Figure 6.37 Comparison XBeach model results (best settings) with measurements for section 115a.

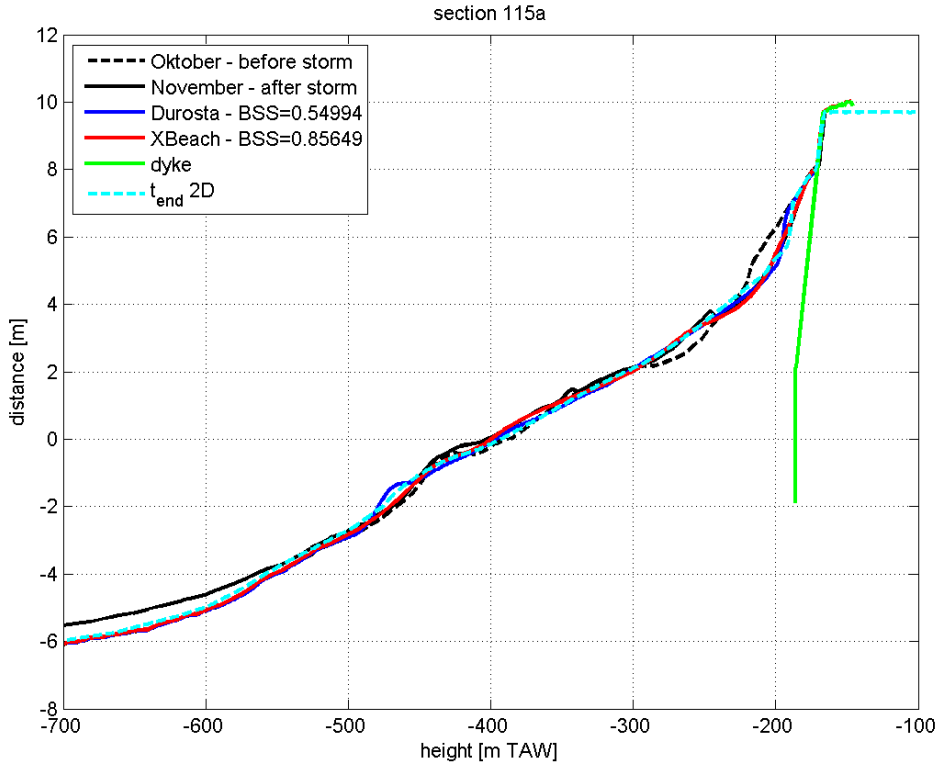

Figure 6.38 Comparison XBeach model results (best settings) with measurements for section 116a.

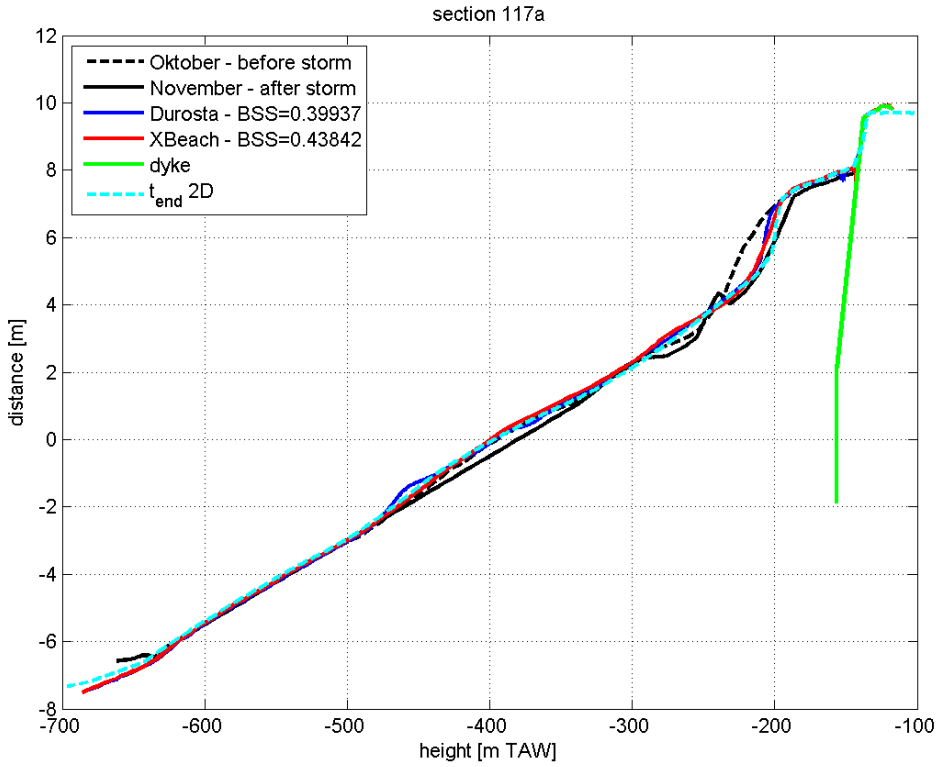

Figure 6.39 Comparison XBeach model results (best settings) with measurements for section 117a.

6.4 Synthesis

In this chapter the performance of XBeach will be compared with Durosta. Since Durosta is a 1D model, also XBeach has initially been applied in 1D mode. Later on, also the possibilities of a 2DH XBeach model were explored.

On Figure 6.40 to Figure 6.44 the model results from XBeach and Durosta are compared with the measurements for the November 2007 storm on Ostend beach. Additionally the Brier Skill Score has been determined for the profile between the dyke and -500m (as shown on the figures).

Table 6.4 gives a summary of the Brier skill Scores (BSS) for Durosta and XBeach for all the profiles. Brier skill scores of on average 0.45 are found for Durosta, while about 0.53 is found for XBeach. For 6 out of 8 profiles, XBeach obtains a better score than Durosta. In section 114 XBeach's prediction differs more from the measured profile than Durosta does. This is due to the prediction in the lower part of the profile (between -400 and -500; see Figure 6.41). In the upper part however, the beach erosion front (and the slope) is better predicted with XBeach.

Both XBeach and Durosta give a more uniform beach profile than the measurements. Small bars in the profile are hardly predicted with the models.

From this comparison it can be concluded that the 1D mode of XBeach delivers in most cases a slightly better result than Durosta. Especially the prediction of the beach erosion front is more accurate in XBeach.

Table 6.4 Brier Skill Scores for the XBeach and Durosta model predictions for the November 2007 storm on Ostend beach.

Section [number]	***Brier Skill Score (BSS)***	
	Durosta	XBeach
113a	0.3	0.4
114a	0.5	0.3
114b	0.4	0.3
115a	0.6	0.9
115b	0.5	0.7
116a	0.5	0.7
116b	0.5	0.6
117a	0.4	0.4
average	0.5	0.5

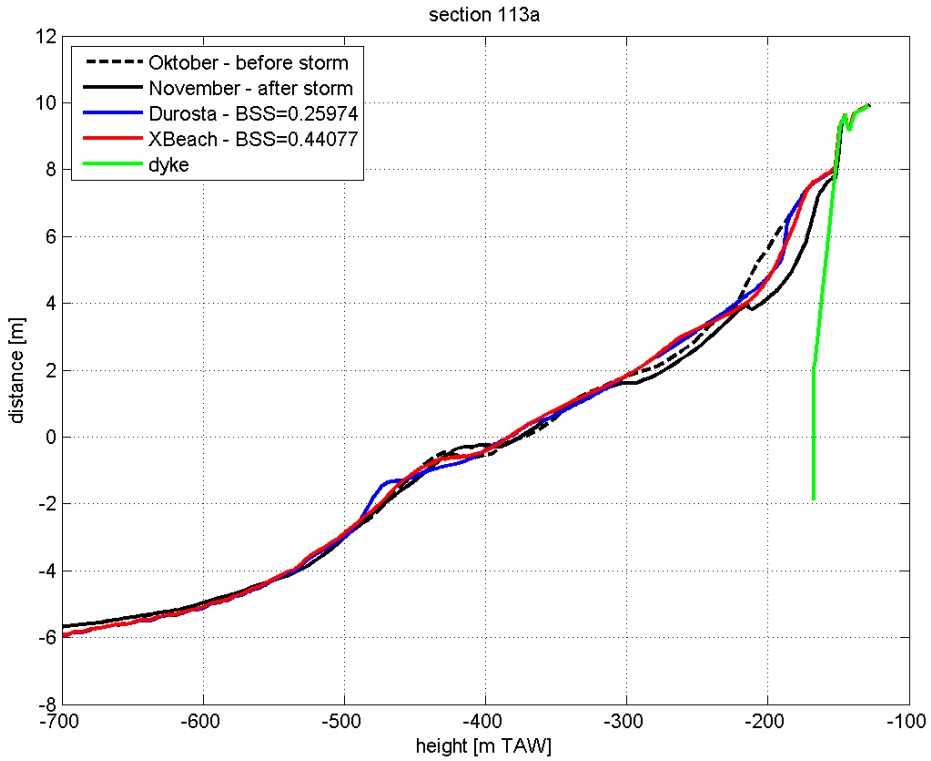

Figure 6.40 XBeach & Durosta model results with measurements for section 113a.

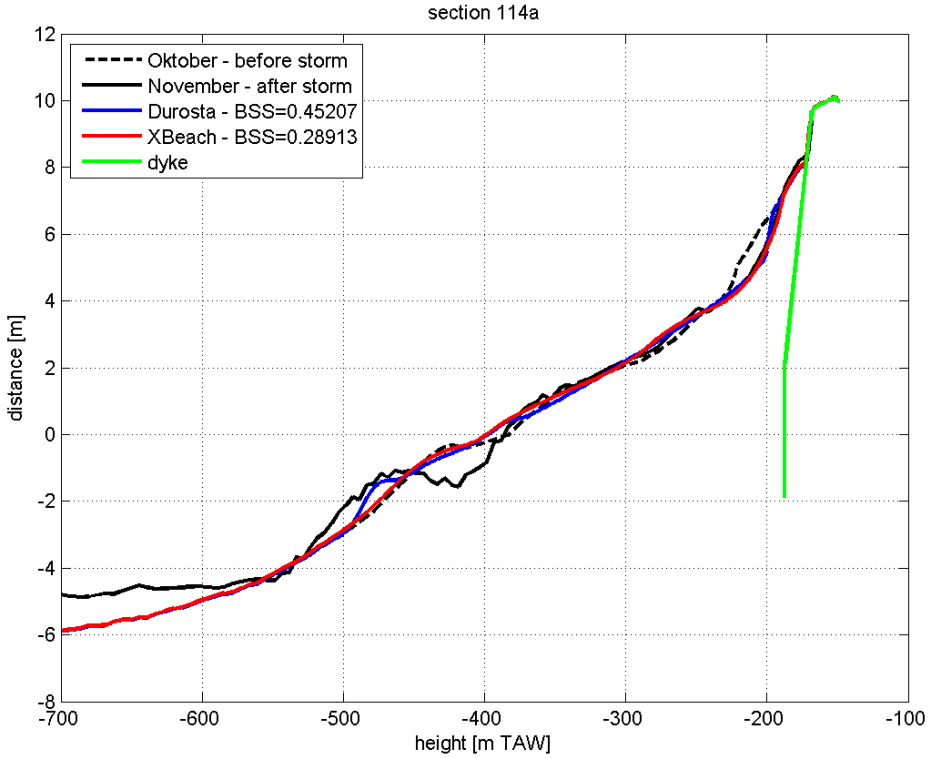

Figure 6.41 XBeach & Durosta model results with measurements for section 114a.

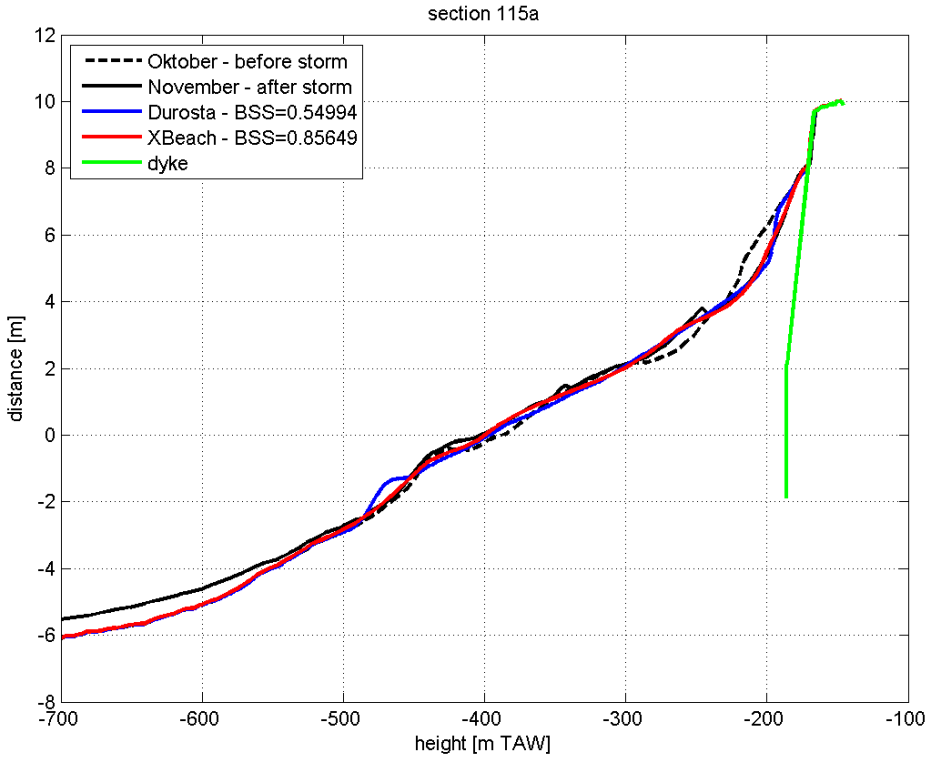

Figure 6.42 XBeach & Durosta model results with measurements for section 115a.

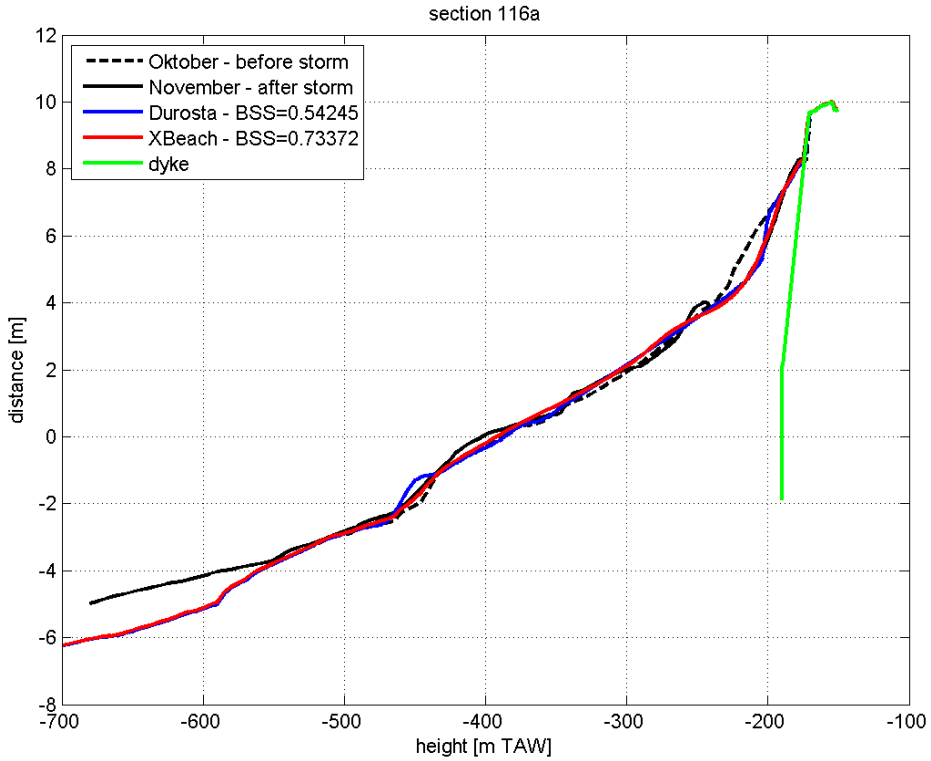

Figure 6.43 XBeach & Durosta model results with measurements for section 116a.

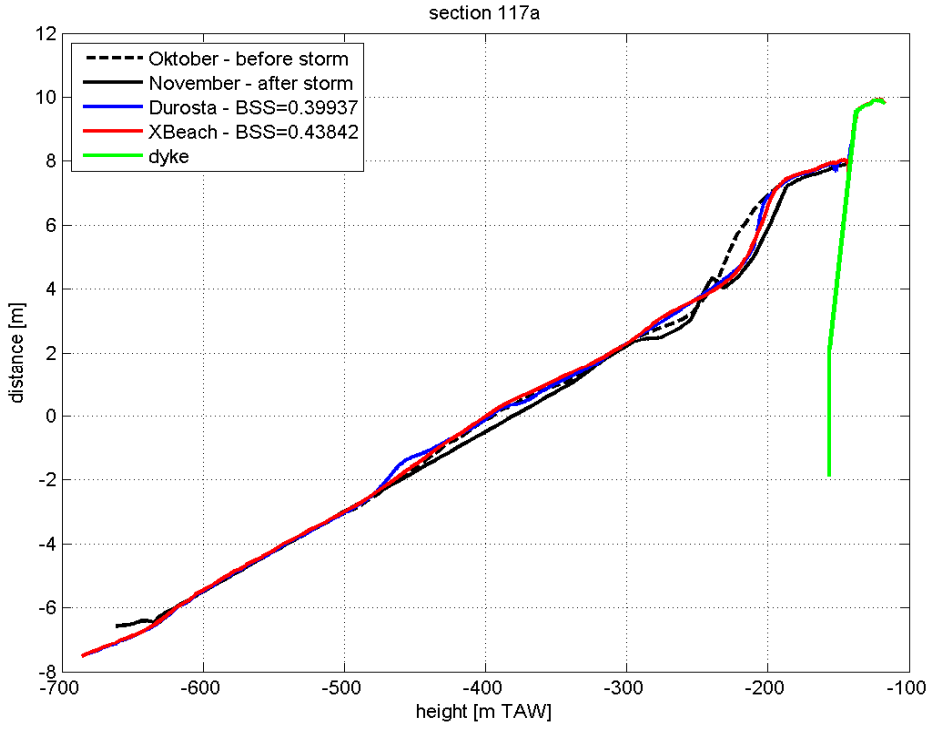

Figure 6.44 XBeach & Durosta model results with measurements for section 117a.

The 2D erosion-sedimentation pattern is shown on the map below (Figure 6.45). This illustrates that the edges of the protruding “emergency beach” are most vulnerable for erosion. At these locations the use of a 2D model instead of a 1D model is preferable (see section 113 and 117 on Figure 6.40 and Figure 6.44).

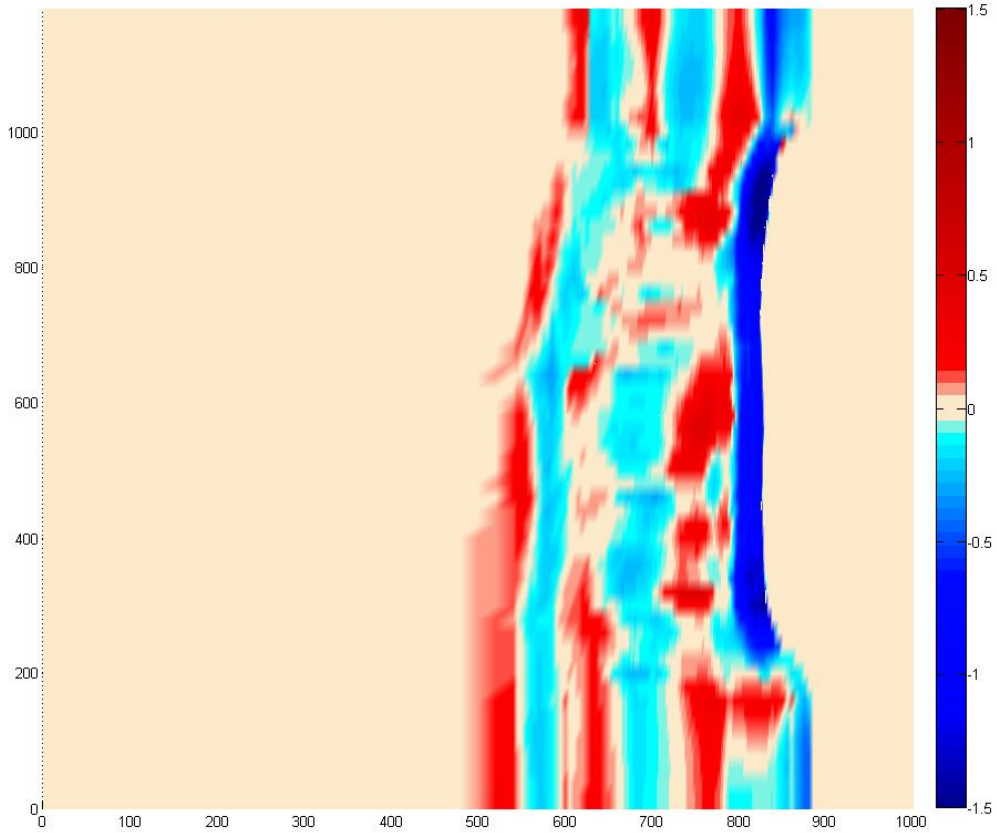

Figure 6.45: Erosion (blue) – sedimentation (red) pattern caused by the November 2007 storm event (color scale = height in m).

6.4.1.1 Estimated impact of a 1000-years storm event

For the design of new coastal protection systems, a 1 in 1000 years storm event is often considered along the Flemish coast. Traditionally predictions are made with Durosta. These calculations are now compared with XBeach. Since there are no measurements available for a 1000-years storm event, no Brier Skill Score can be calculated, nor can be decided which model is the best.

The hydrodynamic conditions for the 1000-years storm are as follows:

- A storm duration of about 46 hours.
- Water level: tide including storm surge (Figure 6.46).
- Wave characteristics vary during the storm: Hs reaches about 5.2m and Tp about 12.6s at the peak of the storm (Figure 6.47).

The beach profile is a measured profile and the grains size is taken uniform with D50 = 0.214mm.

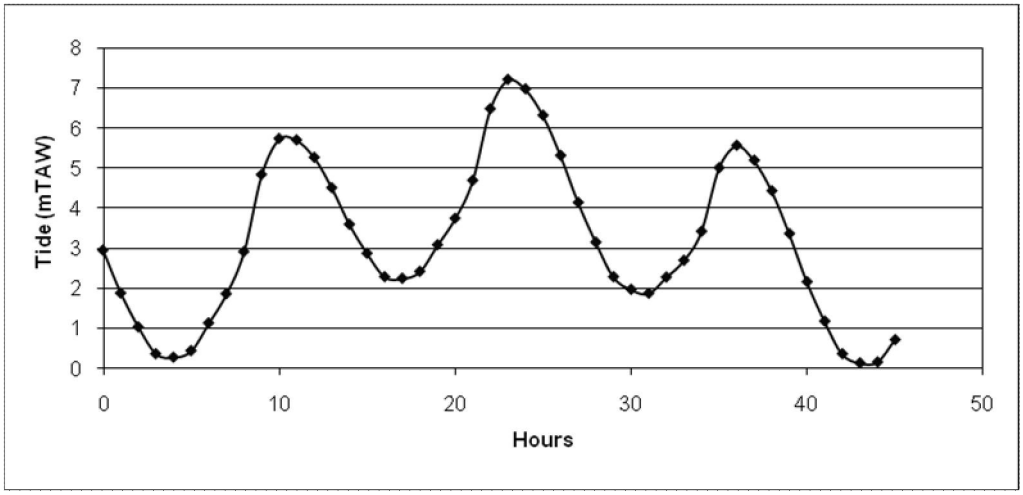

Figure 6.46 1000-years storm: water level (tide + storm surge)

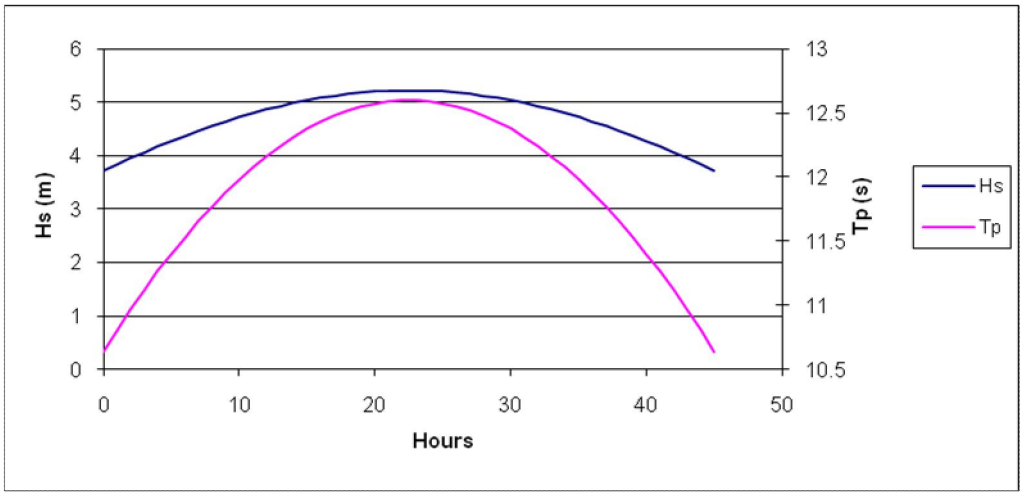

Figure 6.47 1000-years storm: significant wave height Hs and peak wave period Tp.

Figure 6.48 to Figure 6.52 compare the predicted beach profiles calculated with XBeach and Durosta. Some differences can be observed:

- The shape of the eroded profile: Durosta predicts a beach profile with a more or less uniform slope, whereas XBeach predicts a S-shaped profile.
- The erosion close to the dyke: Durosta predicts more erosion close to the dyke and even shows a kind of scour hole. XBeach shows less erosion, most possibly because the model only includes the reflection of the long waves, and not the reflection from the short waves. This can lead to an under prediction of the scour (hole) near the base of the seawall. More detailed investigations and comparison with model tests or in situ measurements should be performed to get a better understanding of this problem.
- The distance the eroded material has moved: in XBeach the sand does not move away that far and a kind of “berm” is formed. In Durosta the eroded material is deposited further seaward (between -5 and -6m TAW).
- Changes at the seaward edge: In Durosta no changes are observed at the seaward boundary. In XBeach the profile does change at the seaward boundary, which suggest that the profile length should be increased.

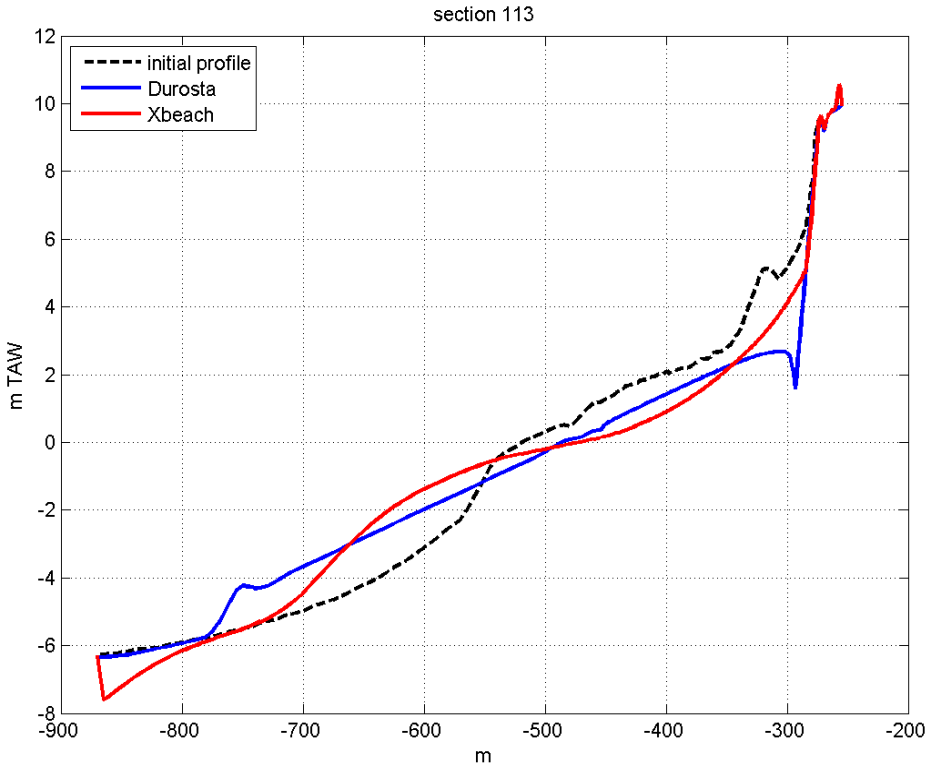

Figure 6.48 Comparison of predicted beach erosion with XBeach and Durosta for section 113.

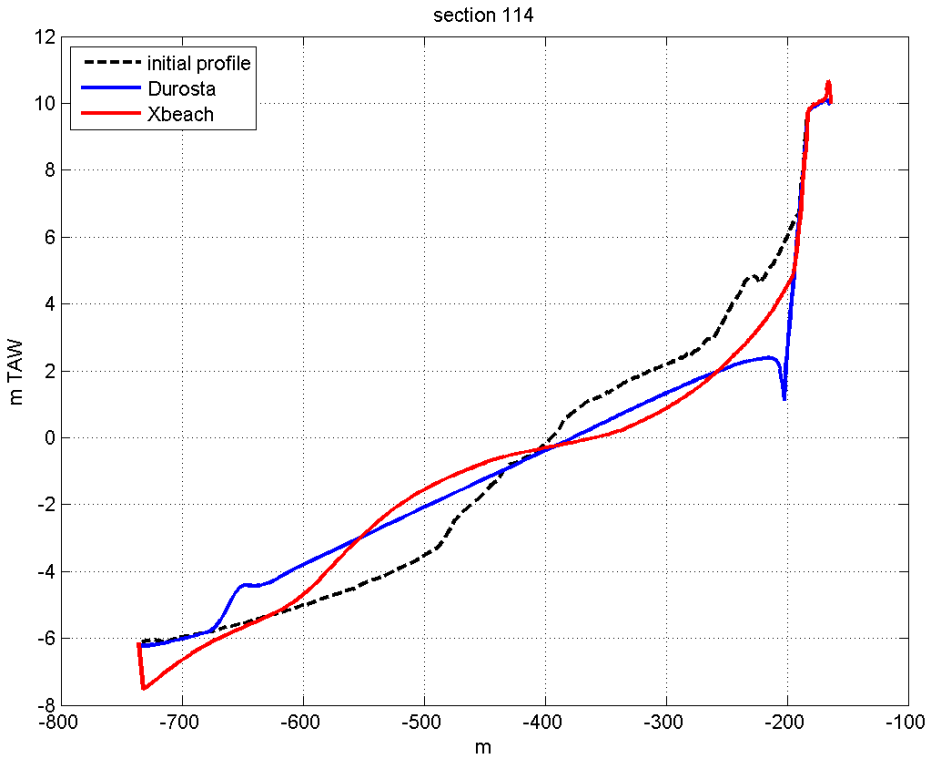

Figure 6.49 Comparison of predicted beach erosion with XBeach and Durosta for section 114.

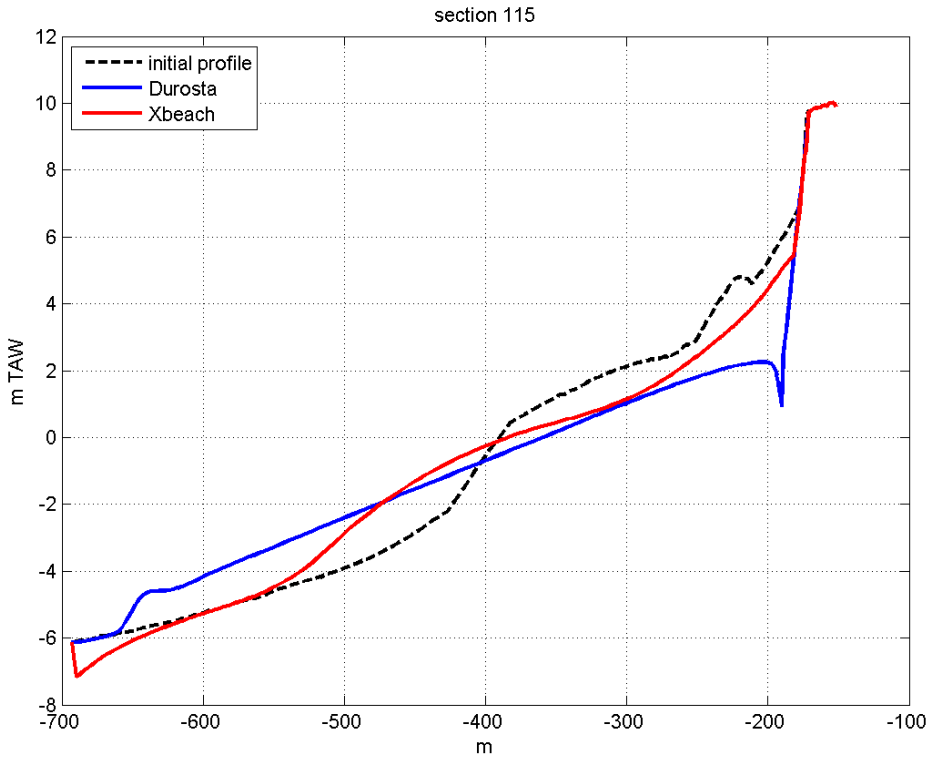

Figure 6.50 Comparison of predicted beach erosion with XBeach and Durosta for section 115.

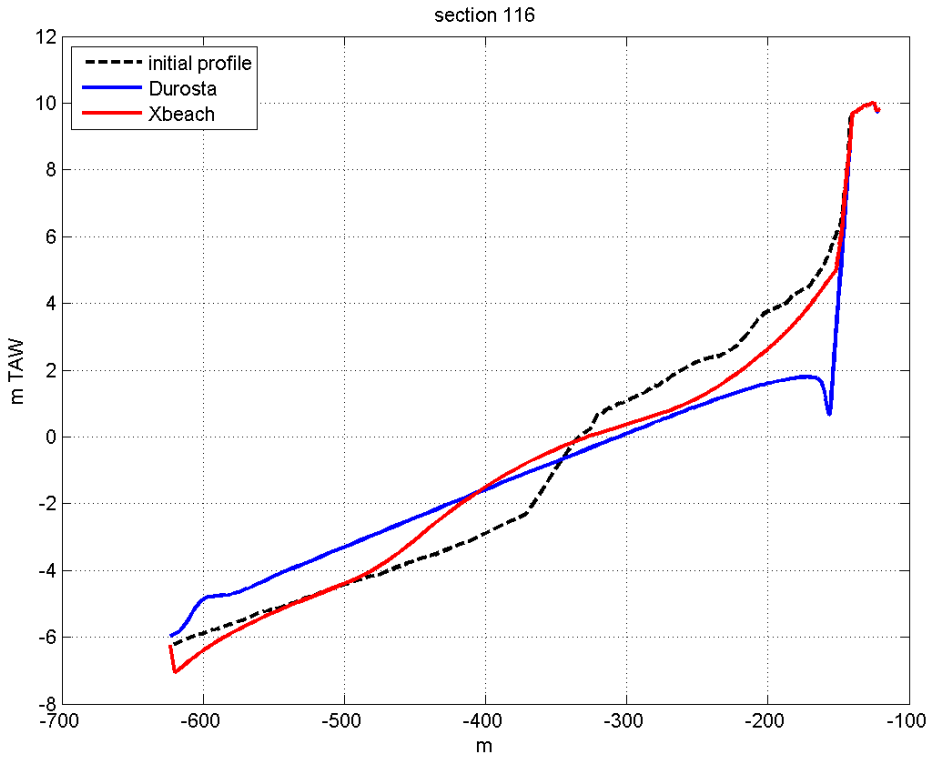

Figure 6.51 Comparison of predicted beach erosion with XBeach and Durosta for section 116.

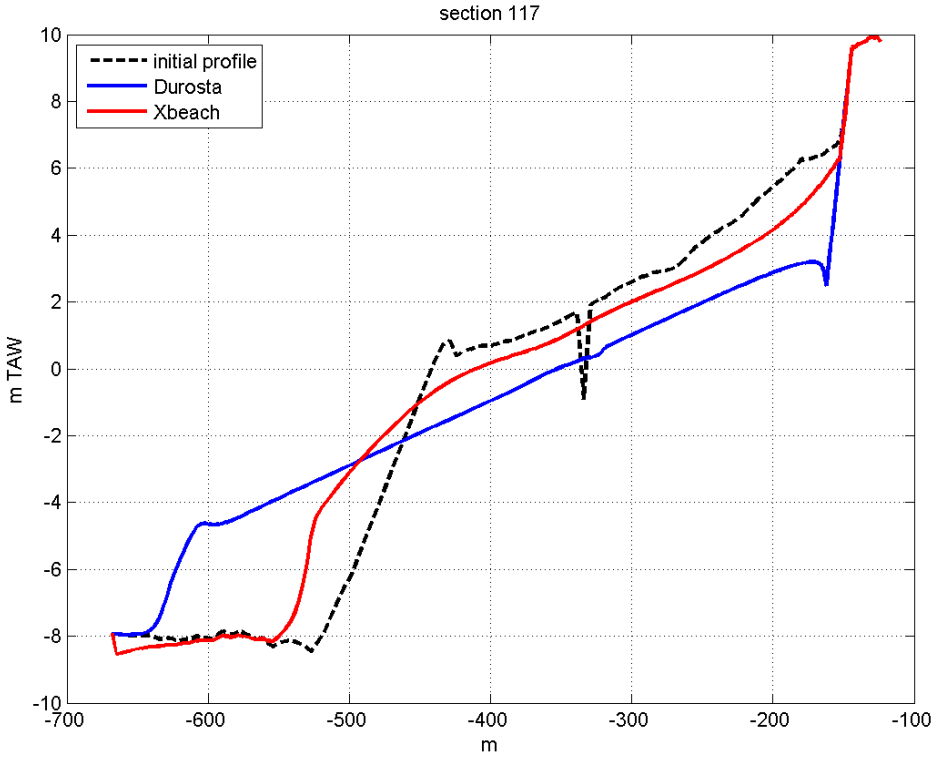

Figure 6.52 Comparison of predicted beach erosion with XBeach and Durosta for section 117.

6.5 Conclusions

The XBeach model (v18) has been applied for the prediction of the storm impact on the beach of Ostend. The hydrodynamic measurements during the storm on 7-9 November 2007, together with the bathymetric and topographic surveys before and after this storm event, allow to validate the XBeach model for this type of coast. Additionally comparison is made with the results of the Durosta model.

The 1D model results for the November 2007 storm show a good performance of the XBeach model: the erosion profile near and above the water level is well reproduced. In general the performance of XBeach is at least as good as Durosta for beach erosion where no “hard structure” (e.g. dykes) are involved. Brier skill scores of on average 0.45 are found for Durosta, while about 0.53 is found for XBeach.

The 2D XBeach model gives slightly better results, especially in sections 113 and 117 where the 1D models clearly underestimate the amount of erosion. These sections are located in areas where both the dike and the beach in front are curved, which causes higher gradients in the sediment transport. This clearly illustrates a case where the use of a 2D model instead of a 1D model is preferable.

Although no measurements are available where the erosion profiles reach the dyke, it was decided to compare the 1D results of XBeach and Durosta for a 1000-years storm event. For this kind of storm the erosion profile reaches the dyke. Quite some difference are noticed between Durosta and XBeach, the most important being the smaller amount of erosion found with XBeach close to the dyke. Since no reflection of short waves is included in the model, the scour (hole) near the dyke will probably be underestimated. This is clearly a point where improvement can be made.

7 Sefton Coast, England

Jon J. Williams (ABPMER), Jenny Brown (POL), Luciana S. Esteves (London Metropolitan Business School) and Alex Souza (POL), UK.

7.1 Objectives

The primary aim of numerical modelling undertaken by the UK team has been to simulate the morphological impact of observed storm events along the shoreline of the study site in NW UK. In common with many field location, data defining tidal/surge water levels, offshore and near-shore waves, beach sediments, bathymetry and topography are incomplete in both space and time. Thus from the outset it has been necessary in some cases to utilise existing 'shelf-scale' numerical models to define offshore boundary conditions, and to combine a wide range of data sources to obtain the most-up-to-date DTMs for modelling applications. In addition, sediments have been collected and analysed to enable physical characterisation of the beach and dune sediments, and all available metocean and shoreline evolution data from 1980 was collated to assist interpretation of past storm impacts. In order to quantify the morphological impact of a storm event occurring during the lifetime of the MICORE project, beach and dune surveys were commissioned during the period Jan 2008 to March 2010. Fortunately, a storm event occurred at the end of this period and provided an opportunity to test rigorously the performance of the XBeach model used in the present project to predict storm impacts on sandy coasts.

One aim of WP4 concerned the use of off-the-shelf models, and the subsequent comparison between results from these models, and results from XBeach. The UK team did not have access to models such as LITPROF and felt that, given the 2D nature of the observed changes in coastal morphology at the UK site, the use of SBeach (see Appendix G) would not be very helpful. However, use was made of the specialist POLCOMS-WAM-GOTM modelling system (Appendix K) to define offshore and nearshore metocean conditions pertaining during storm events. Here the focus has been on the calibration of the XBeach model to replicate as closely as possible the storm-induced morphological changes in the beach topography and dune frontage along the Sefton coastline and to then apply the model to examine how larger storms may impact in the future. This latter aim is directed at assisting new ways of providing an early warning of impending dangers posed by coastal flooding should natural or anthropogenic sea defences fail.

The primary objectives of the XBeach modelling have been to:

- tune (if necessary) the XBeach parameter setting to obtain the closest match between observed and predicted beach profile changes attributable to storms of moderate intensity;
- identify through sensitivity analyses which XBeach parameters exert the greatest influence on simulation outcomes;
- assess if multiple 1D or a single 2D XBeach model is required to accurately describe the observed spatial differences in coastal responses to a storm;
- use the optimised XBeach model to investigate beach profile responses to a number of historical storms where field validation data is more restricted;
- use scenarios to investigate the coastal response to as yet unobserved extreme event and to elevated mean sea level conditions in line with IPCC predictions; and

- examine the threat of coastal flooding in the event of an extreme event and/or dune breaching. This scenario also addresses the additional impacts of high fluvial discharge of the River Alt in the south of the study region.

In this report we focus the main attention on the only storm event to occur at the UK site since the beginning of the MICORE project, where pre- and post-storm beach and dune conditions were measured, thus providing a good test case with which to calibrate, validate and verify XBeach simulations of the storm impact on the coastline. This provides the essential evidence necessary to support other XBeach results from this site. In cases where data are absent, or when model hindcast runs have been undertaken, the NOC Liverpool Bay model (LBM, see Appendix K) has also been used to provide a resource to define offshore boundary conditions necessary to simulate historical storms.

In initial work predictions of tides/surge elevations and waves from the NOC Liverpool Bay model (see Appendix K) were used to simulate some historical storms using XBeach. Here the primary objective of the morphological modelling effort was been to reproduce the principal characteristics of observed dune erosion along the Sefton coast. Six storm periods occurring since 2001 were examined: 22/01/2002 to 08/02/2002, 21/12/2004 to 24/01/2005, 18/08/2005 to 22/09/2005, 22/09/2006 to 12/10/2006, 10/07/2007 to 06/08/2007 and 03/03/2008 to 19/03/2008 (Esteves et al., 2010). In all cases dune erosion in response to storms of around 2m to 6m was measured during post-storm dune toe surveys.

Owing to the significant risk to lives and property at the UK site, coastal flooding risk has been investigated in the third part of the modelling study using a range of extreme case scenarios for tidal/surge elevations and waves. Attention has been focussed on dune blowout regions close to Formby Point most susceptible to overwashing and breaching and to the flood plain of the River Alt located to the north of Hightown. It is noted that in the past the Hightown region has been affected by coastal flooding events with resulting damage to property and infrastructure, but without loss of life or personal injury. Present day flood defences against fluvial and coastal threats make future flood events very unlikely.

7.2 Site and climatology

7.2.1 Description of area

The Sefton coast borders the eastern Irish Sea and extends 36km northwards from the Mersey estuary to the Ribble estuary (see inset Figure1). The UK XBeach modelling studies in MICORE WP4 have focused predominantly on a 16km-long stretch of coastline around Formby Point dominated by recreational beaches and one of the largest coastal dune systems of Great Britain, which extends 4km inland and has dune heights reaching 30m (Figure1). These dunes have high recreational and conservation value and form an effective coastal flood defence for urban development, high-grade agricultural land and a significant number of conservation areas of national and international importance.

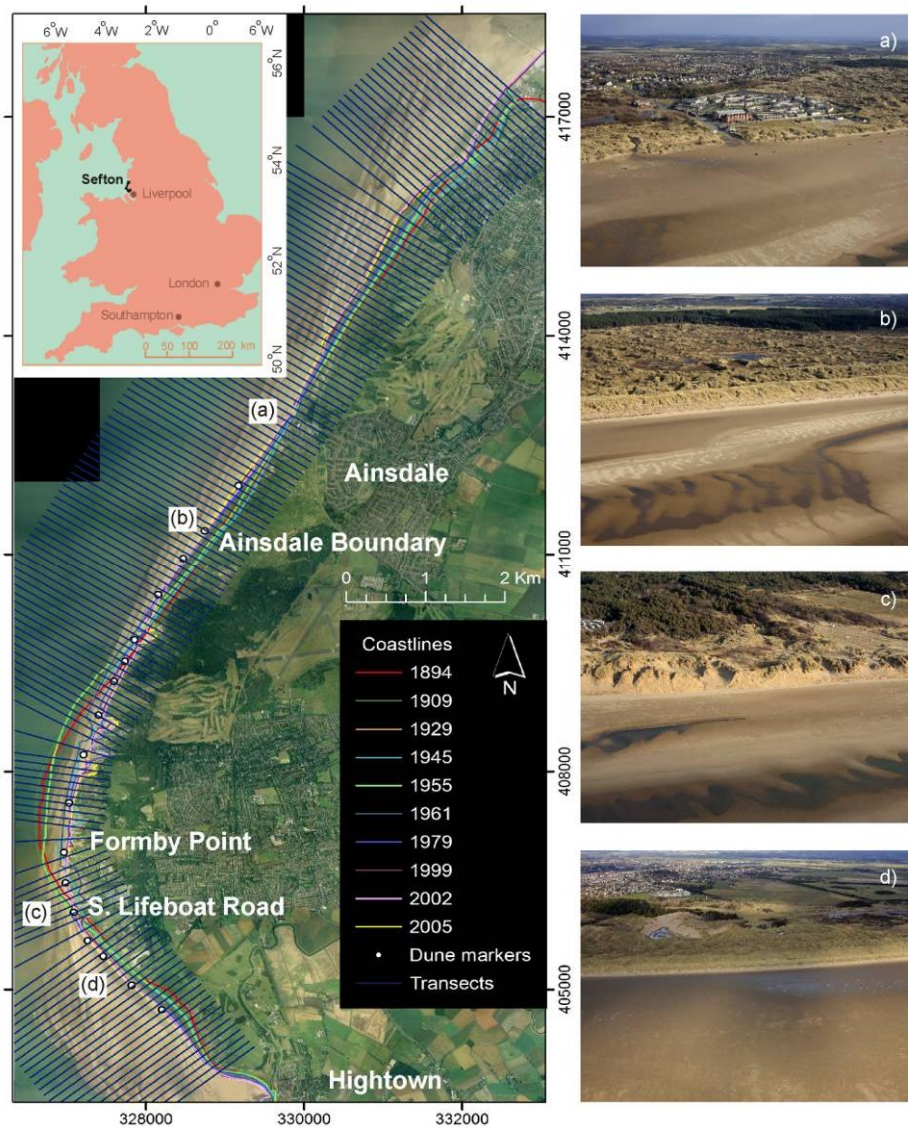

Figure 7.1 Sefton Coast is located in Northwest England (insert) and presents 16 km of undefended coastlines (aerial photograph taken in 2005). The lines indicate shoreline transects used to determine rates of dune and shoreline recession. Coordinates in British National Grid (m). The photographs show four different coastal locations.

Studies suggest that Formby Point is a divergent sediment cell boundary, and local beach/dune erosion supplies sediments to the accreting shores northward and southward (Pye and Neal, 1994; Pye and Blott, 2008; Halcrow, 2009). Dunes north of the River Alt have been eroding since 1900 (Gresswell, 1937, 1953; Parker, 1969; Pye and Neal, 1994; Pye and Blott, 2008) with rates of dune retreat reaching 5 m/year from 2001 to 2008 north of Formby Point (Esteves et al, 2009). According to Parker (1969) and Pye and Blott (2008), dune erosion due to wave action along the Sefton coast occurs when water levels at Liverpool are above 3.9m OD (8.83m Chart Datum) and becomes severe when levels exceed 5.2m OD (10.13m Chart Datum). Soaking of the dune toe and wave undercutting causes slumping of the dune face and dune retreat, (Parker, 1969; Pye and Blott, 2008). Significant erosion has also been linked to events when storm surges coincide with high wave energy (Pye and Blott, 2008; Halcrow, 2009). Liverpool Bay experiences a semi-diurnal macrotidal regime with mean spring tidal range of about 10m at the mouths of the estuaries.

Therefore, storm surges are likely to cause erosion only when they also coincide with spring high tides (Appendix J). Pye and Blott (2008) suggest that smaller storms erode only sections of the coast while erosion throughout the length of the Sefton dune frontage only occurs during the most severe storms (i.e., greater than 1 in 10 year events). Due to the protection afforded by the dune system, the Sefton coast is currently more susceptible to flooding from rivers than from coastal storms. However, the development of dune blowouts and the rapid retreat of the frontal dunes increase the risk of natural habitats and urban areas to flooding. A study to quantify thresholds for significant dune erosion along the Sefton Coast is reported by Esteves et al., (2010). Further, a helpful summary of storm conditions along the Sefton Coast is given in Appendix J. This is included here as it explains the complex interplay between the meteorological conditions, the tidal modulation of water levels, antecedent conditions and the coastal system, and shows that simple relationships between high tidal/surge levels and large waves, and the impact these have on the Sefton coastline cannot be established owing to complex hydrodynamic interactions. Only through use of the modelling approach described here to define offshore conditions can any attempt to predict shoreline impacts be made using model such as XBeach.

7.2.2 Climatology

The Sefton Coast extends approximately 36 km from the Mersey Estuary in the south and the Ribble Estuary in the north and encompasses the towns of Crosby, Aisdale and Southport. This coastline is characterised by a large, mobile dune system and the multiple sand bars that extend almost continuously from Liverpool to Southport, with a maximum inland extent of c. 4 km at Formby Point. Before 1900, dunes to the north of the River Alt experienced seawards accretion. However, around 1910 erosion began at Formby Point and along the coast between the River Alt estuary at Hightown and Blundellsands. Since that time the beach and frontal dunes have continued to erode and the limit of erosion has shifted northwards. Steady dune accretion has been observed on south side of Formby Point and between Ainsdale and Southport. Net accretion has also been dominant further south between Crosby and Seaforth.

Erosion of the Sefton coast results from a divergent sediment cell limit located at Formby Point, from where longshore currents transport sand northwards and southwards favouring accretion along adjacent shorelines. Wave erosion of the Sefton coast occurs when mean tidal levels at Liverpool are above 3.9 m OD and becomes severe when levels exceed 5.2 m OD. These conditions result in soaking of the dune toe, severe wave undercutting and resultant rapid slumping and retreat of the dune face. During stormy periods, when the levels of successive high tides may be raised by a surge component of up to 1.5 m or more, dune recession of 5 – 10 m can readily occur at Formby Point. Rates of dune erosion are estimated between 3.5 m/year and 5 m/year in the last century, although rates have varied through time (e.g. higher rates between 1958 and the early 1970's, followed by a period of slower erosion during the later 1970's and 1980's). The most severe storm surge-induced erosion on record occurred around 26 February 1990, but other significant events occurred in 1967, 1976, 1983, 1997 and 2002. A breach in the dune system, if allowed to proceed unchecked, would result in severe flooding affecting agriculture, infrastructure and developments. However, this is considered to constitute a very rare event, and emergency action could mitigate damage. It is considered that the present shoreline is not in equilibrium with current coastal processes and that further changes will occur.

Liverpool Bay in the eastern Irish Sea experiences a semi-diurnal macrotidal regime with mean spring tidal ranges around 10 m at the mouths of the estuaries. Strong tidal currents reach up to 1 m/s on spring tides. These can exceed 1.5 m/s during storms at some locations and storm surges are frequent and typically produce a positive elevation of 1 m (Jones & Davies, 1997; 1998).

Data from established tide gauge sites (http://www.pol.ac.uk/ntslf/ networks.html) show maximum positive storm surge elevations of 2.60 m at Heysham on 26 February 1990 and 2.26 m and at Liverpool on 27 October 2002. These data also show an increased frequency of extreme high tides since 1990, compared with the period 1963-1990 (cf. Woodworth & Blackman, 2002).

Estimates for maximum wave height (Hmax) for the Irish Sea range from 8 - 15 m (HRS, 1977; Devoy, 2000). The limited fetch restricts wave development while topographic and bathymetric features limit the incursion of swell from the Atlantic. Based on interpolated data for the Irish Sea, Hs50 for Liverpool is c. 8 m (Draper & Carter, 1982; UK Dept. of Energy, 1990; Draper, 1992). Refraction, reflection, shoaling and wave breaking dissipate a significant proportion of the total wave energy in the coastal zone fronting the site. Measurements of waves have been obtained since c. 2002 in the Hilbre Channel, at position 53o23.6' N, 03o14.21'W.

The majority of the study area comprises soft and granular estuary deposits of sand, silt, clay and peat. Sandstone rocks outcrop along parts of the Wirral shoreline. The British Geological Survey (BGS) hold digital maps of sea bed sediments for the UK study area (DigSBS250). These are based on sea-bed grab samples of the top 0.1m, combined with cores and dredge samples. A standard Folk (1980) triangle classification has been used based on the gravel percentage and the sand to mud ratio. Sediment studies have been commissioned by SMBC and are reported by SMBC (1981), Blott & Pye (2003) and Pye et al. (2006a, b). The Sefton Coast sediment regime is dominated by the estuaries of the Mersey and Ribble. Their meeting zone offshore has resulted in the formation of Taylor's Bank, a large intertidal sand body located offshore from Formby point. Studies of net sediment transport pathways for the region are limited both geographically and temporally (e.g. Halliwell, 1973) and are the subject of contemporary research. Natural sediment processes have been considerably influenced by the training walls constructed in the estuaries, dredging of navigation channels, land reclamation and coastal defence works. Studies of offshore/beach/dune sediment exchange processes are reported by Parker (1975), Caplin (1991), Jay (1998) and Pye (2003).

7.2.3 Storms considered

The storm used here to calibrate and verify XBeach occurred on 31 March 2010. This was the first storm at the UK site since the winter of 2008 and occurred at the end of a period of field data collection. The storm was generated as a low pressure system (980mb) tracked from west to east across the UK during 29 March 2010 to 1 April 2010, (Figure 7.2). At the peak of the storm average wind speeds in the Irish Sea reached c. 20m/s with gusts exceeding 25m/s (Figure 7.3 and 4). The wind direction was c. 310^{o}, a direction providing the largest fetch relative to the Sefton coast, (Figure 7.3). In addition to the synoptic charts shown in Figs. 2 to 4, Figure 7.5 shows meteorological conditions measured at the Hilbre Island weather station for the period 29 March 2010 to 3 April 2010.

Wave conditions measured by a directional wave buoy located at 53°32'.06N and 003°21'.16W in 22m of water prior to, during and after the 31 March 2010 storm, Sefton coast, NW UK are shown in Figure 7.6. This figure included time-series of showing significant wave height (Hm0), peak wave period (Tp), zero up crossing wave period (Tz), peak wave direction (P dir) and directional wave spreading (Dir spread). Figure 7.6 shows that Hm0 and Tp values peaked at 3.9m and 8.2s respectively with sustained Hm0 values of more than 3.5m for c. 12 hours. Historically, storms with these characteristics are not unusual, typically occurring once or twice a year. However, it is more unusual that such events are also coincident with peak Spring tide, making the present event especially interesting for the MICORE project.

Figure 7.7 shows the following tidal elevation data: a) predicted level at Liverpool (POLCOMS); measured level at Liverpool Gladstone Dock; measured level at Heysham; and the difference between Liverpool and Heysham records. In Figure 7.7, the black line indicates the period when the low pressure tracked eastwards across the Irish sea and the red line denotes the period when average wind speed was c. 20m/s (i.e. the height of the storm). The largest waves recorded were approximately coincident with high springs tides c. 10m CD at Liverpool Gladstone Dock (Figure 7.6 and 7). By the criteria outlined above the event of 31 March 2010 would therefore be expected to have a morphological impact along the Sefton coastline. In particular, tidal elevations were sufficient to soak the toe of the dunes, and expose the dunes and upper beach to wave action.

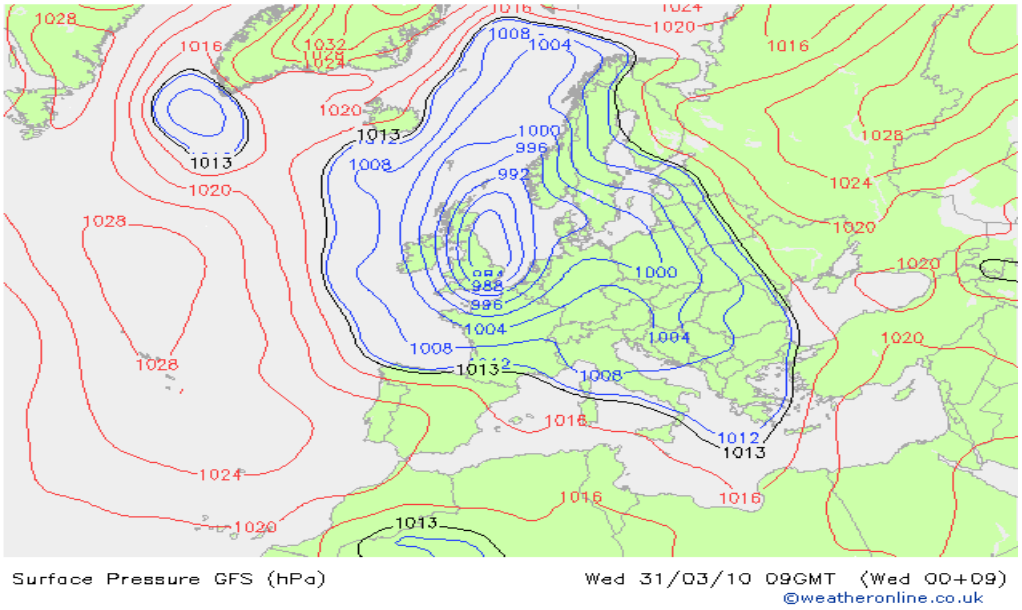

Figure 7.2 Predicted surface pressure chart for 09h00GMT 31 March 2010 (source: Weatheronline.co.uk).

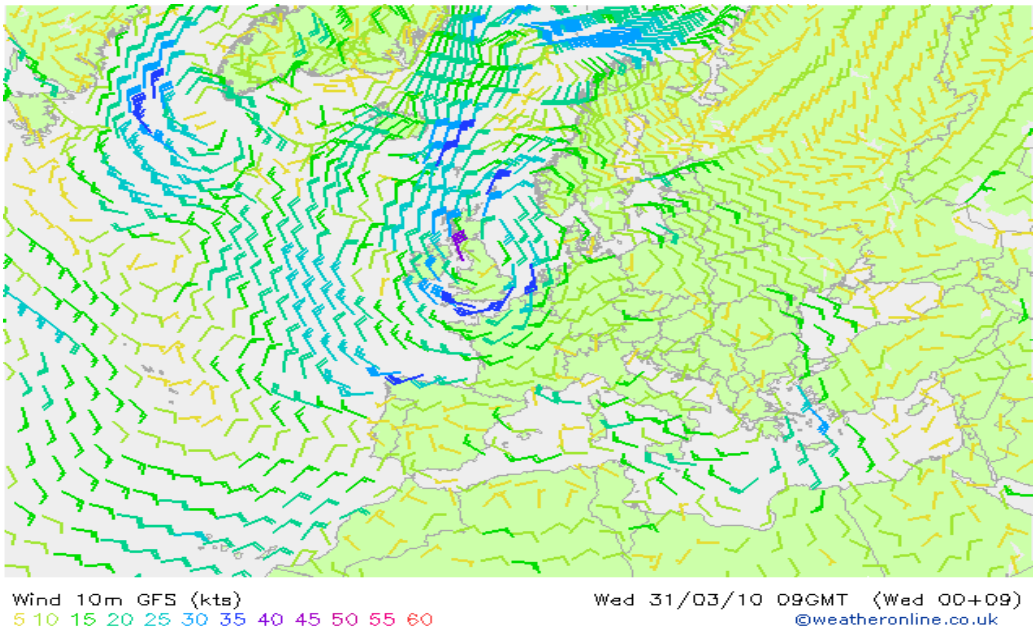

Figure 7.3 Predicted average surface wind speeds for 09h00GMT 31 March 2010 (source: Weatheronline.co.uk). Note the strong NW winds in the Irish Sea region affecting the Sefton coastline.

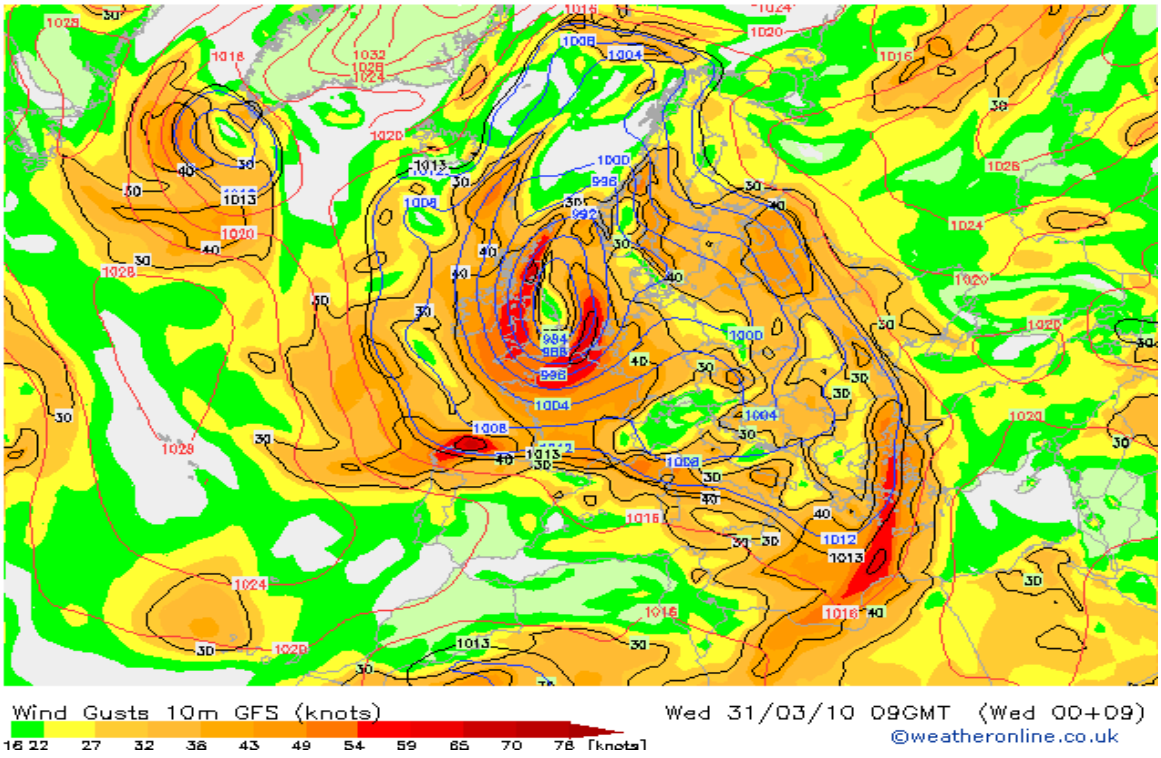

Figure 7.4 Predicted maximum wind gusts for 09h00GMT 31 March 2010 (source: Weatheronline.co.uk). Note: most of the western side of the UK is affected by strong winds.

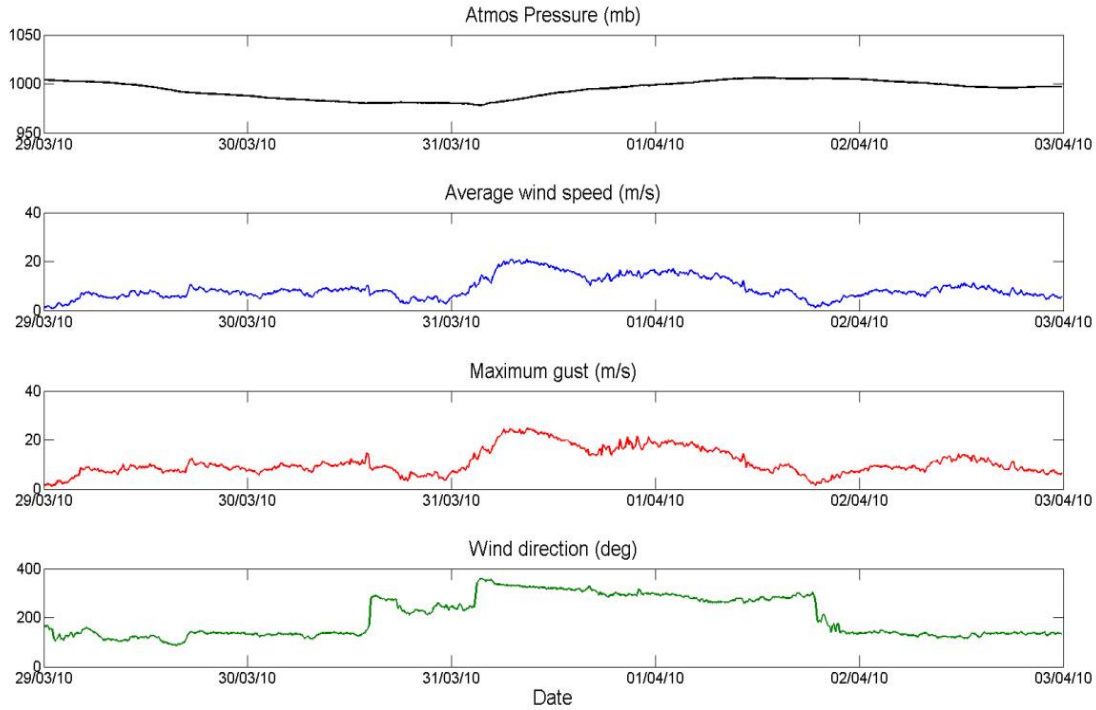

Figure 7.5 Meteorological conditions measured at Hilbre Island weather station prior to, during and after the 31 March 2010 storm, Sefton coast, NW UK showing atmospheric pressure, average wind speed, maximum gust speed and wind direction.

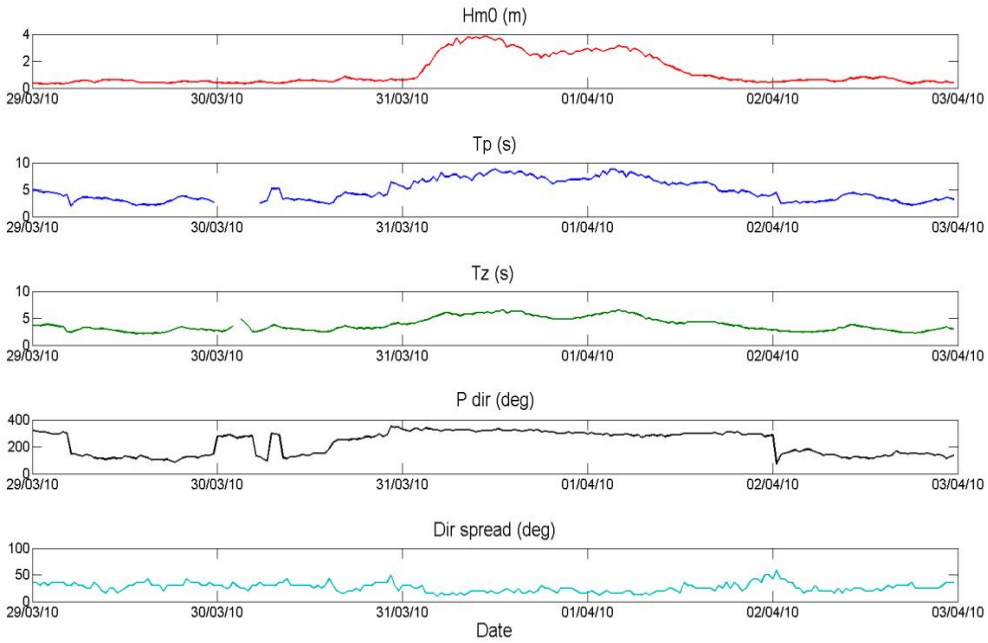

Figure 7.6 Measured wave conditions at 53°32'.06N and 003°21'.16W in 22m of water prior to, during and after the 31 March 2010 storm, Sefton coast, NW UK showing significant wave height (Hm0), peak wave period (Tp), zero up crossing wave period (Tz), peak wave direction (P dir) and directional wave spreading (Dir spread).

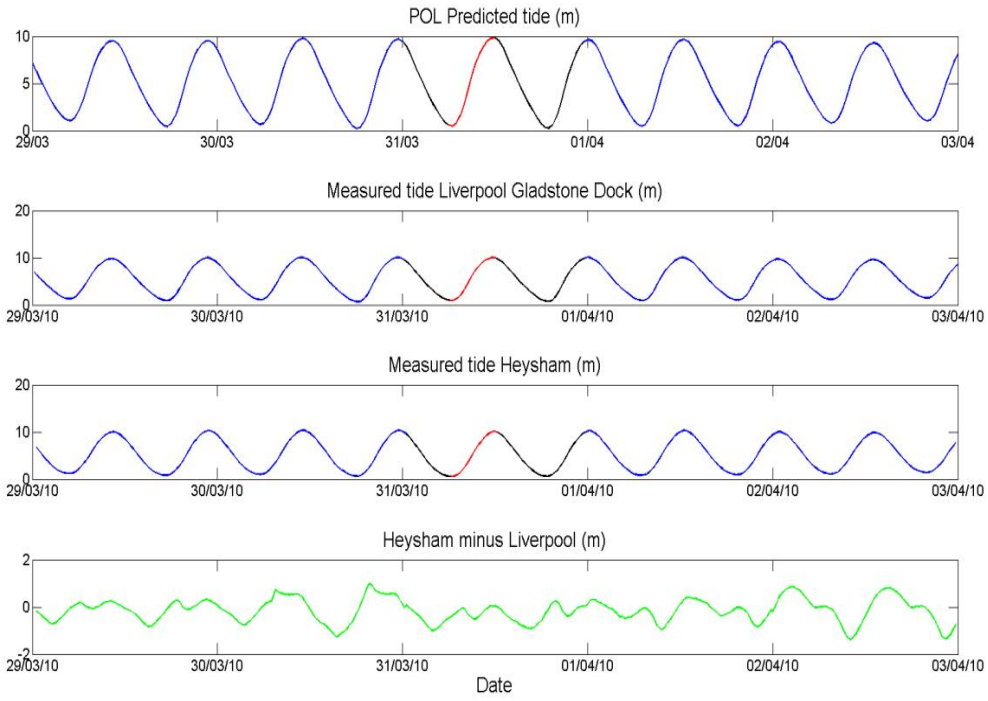

Figure 7.7 Tidal elevations: predicted at Liverpool; measured at Liverpool Gladstone Dock; measured at Heysham; and the difference between Liverpool and Heysham records. The black line indicates the period when the low pressure tracked eastwards across the Irish sea and the red line denotes the period when average wind speed was c. 20m/s (i.e. the height of the storm).

7.3 Model results

XBeach modelling has been undertaken using the Quatorze Juillet MPI version of XBeach running on dual and quad core Windows machines. It has been used principally to simulate in 1D and 2D the March 31 2010 storm described above where pre- and post-storm beach survey data are available, and where good hydrodynamic measurements characterising the metocean climate exist. In addition, the modelling work has also examine a number of test scenarios where mean sea level has been increased to account for predicted climate change, and where wave conditions have been enhanced to represent a more severe storm than the March 31 2010 event. This enhancement has been established from return frequency tables derived from Met. Office wave data and is broadly in line with the expected 1:100 year event at this location.

As stated at the outset of this report it was intended to identify through sensitivity analyses which XBeach parameters exert the greatest influence on simulation outcomes. Using 1D test cases, this was attempted with a focus on the parameters **facua** (asymmetry transport), **cf**, **wetslope**, **form** (sediment transport formula), **nuhv** (additional shear dispersion factor), **eps** (threshold depth for drying and flooding) and **morfac** (morphological factor) parameters. A large number of systematic test were undertaken in which a range of XBeach parameter settings (including some not identified above) were adjusted between their recommended minimum and maximum settings. The resulting post-storm beach profiles predicted by XBeach were compared with the measured profiles and assessed for accuracy using the Brier skills score. In summary the following observations can be reported from the results of this calibration and validation exercise for the UK site: (a) no single parameter exerted a strong influence providing the value chosen did not fall outside the guidelines recommended by Deltares; (b) changing multiple parameter to values other than 'factory' settings resulted in confusing results, where the effect of changing one parameter could be either cancelled out or enhanced by changes in another; (c) in attempts to improve model skill, any changes made to parameters must be carried out in a systematic way, and remain physically realistic.

7.3.1 1D (beach profile) modelling

Simulation of beach profile responses to the March 31 2010 storm involved the application of the XBeach model in 1D mode with oblique waves (JONSWAP spectrum). To reduce run time, and to capture the period when dune erosion was observed, the model was forced using measured wave and tidal conditions during the peak of the storm activity when measured mean water level exceeded 4m ODN, (Figure 7.8). In a second test-series, looking at the resilience of the coastal dunes and at related coastal flooding risks, enhancements were made to both the tidal/surge elevations and to the wave data to simulate a storm of higher magnitude. These enhancements were selected to simulate as closely as possible a 1:100 year event and are also illustrated in Figure 7.8.

Figure 7.9 shows a DTM of the Formby Point XBeach modelling domain comprising combined topographic lidar survey data (2008), UoP DGPS beach survey (2008) and POL Liverpool Bay bathymetry (dates variable from 2000 to 2008). Also shown in Figure 7.9 by the red lines are the SMBC beach profiles lines P11, P12, P14, P15, P17 and P18. These are established annual beach survey lines that extend in most cases from the crest of the coastal dune ridge to the spring low water line. Owing to the availability of good pre- and post-storm data, profile lines P14, P15, P17 and P18 were selected for 1D XBeach storm impact modelling. Aerial photographs taken in 2008 shown in Figure 7.10 indicate the approximate location of the four beach/dune profiles located to the North of Formby Point. These are intended only as a guide to show the main characteristics of the local coastal morphology.

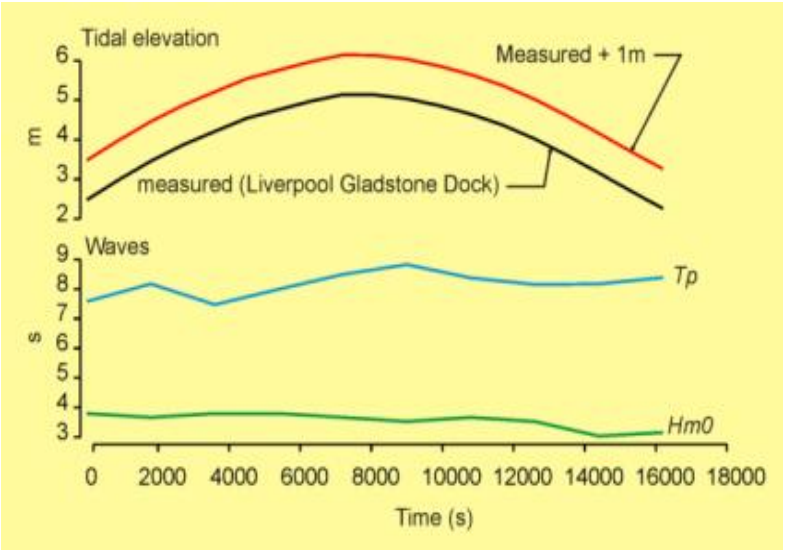

Figure 7.8 Measured and enhanced wave and tidal conditions (ODN) used to force the 1D XBeach simulations of the 31 March 2010 storm event.

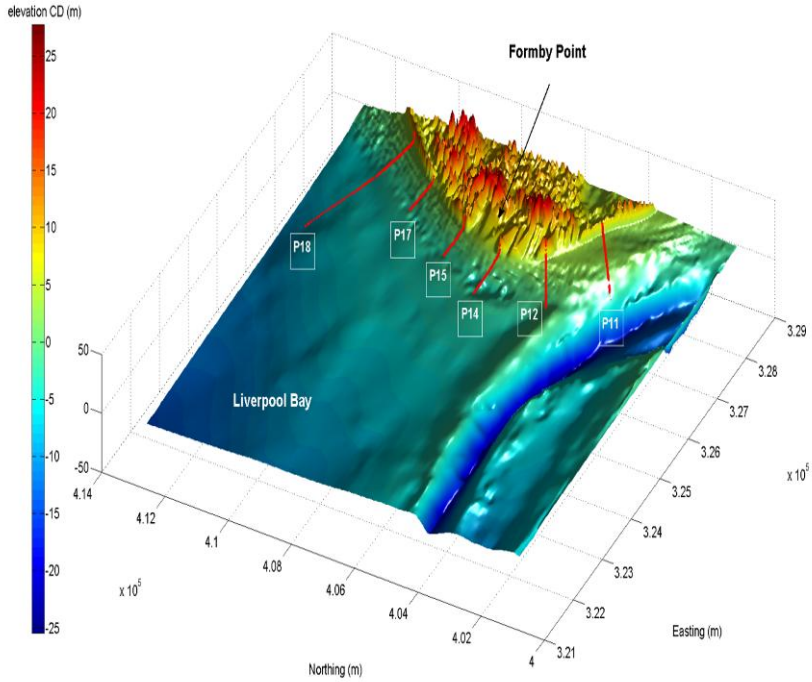

Figure 7.9 DTM of the Formby Point XBeach modelling domain comprising combined topographic lidar survey data (2008), UoP DGPS beach survey (2008) and POL Liverpool Bay bathymetry. Also shown by red lines are the SMBC beach profiles lines P11, P12, P14, P15, P17 and P18 selected for 1D XBeach storm impact modelling.

Figure 7.10 Aerial photographs showing the location of the three extreme event scenario simulations at Formby Point and the north and south of Formby Point . Photos. From Sefton Metropolitan Borough Council, 2008.

Figure 7.11a shows XBeach model results obtained using **measured** hydrodynamic conditions (Figure 7.8) for the upper parts of SMBC beach profiles lines P14, P15, P17 and P18. Here the dashed black lines show the measured profile before the storm, the solid black lines shows the measured profile after the storm and the red line shows the profiles predicted by XBeach after simulation of the March 31 2010 storm. In all cases predicted post-storm profile lines 14, 15, 17 and 18 show erosion of the dune toe and deposition of the eroded sediment in the regions in front of the dunes. Examination of XBeach output indicates that the majority of the erosion is a result of wave undercutting of the dune and slumping. This erosion process is closely similar to the process observed in the field during this storm (SMBC, pers. comm.). In general Figure 7.11a shows a dune recession c. 3m to 5m during this storm event and is typical of erosion for storms of a similar magnitude in the past. Also shown are Brier skills scores for each simulation which indicate a good agreement between measured and predicted beach profile response to the storm (cf. Van Rijn et al., 2003). Although in all cases XBeach has a slight tendency to over-estimate dune recession and accretion on the shoreface, the beach and dune profile adjustments to the storm are generally reproduced well by the model. As noted by other researchers, extension of the model run time to investigate how eroded sediment is re-distributed across the model domain failed to simulate significant accretion processes associated with the re-establishment of the berm. Although there was a re-distribution of sediments, subsequent erosion of the profile was small.

In Figure 7.11b XBeach model results using enhanced hydrodynamic conditions (Figure 7.8) are shown for the same profiles. In these cases, XBeach predicts significantly more beach and dune erosion. Although we have no means of verifying the accuracy of these predictions, they are helpful in demonstrating that the present coastline apparently remains relatively resilient even in these extreme conditions. It is also noted, however, that soaking of the dune toe is not simulated by XBeach and this process might be expected to be even more effective in the enhanced conditions and lead to more pronounced erosion than that predicted by XBeach.

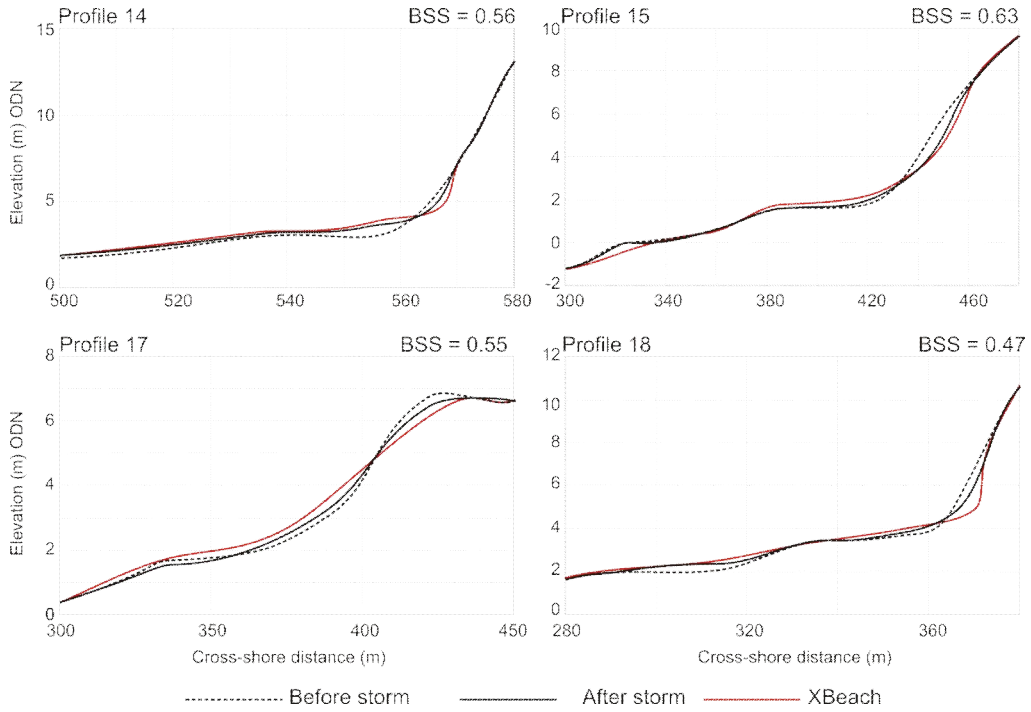

*Figure 7.11a. XBeach model results using **measured** hydrodynamic conditions (Figure 7.10) for the upper parts of SMBC beach profiles lines P14, P15, P17 and P18. The dashed black lines show the measured profile before the storm, the solid black lines shows the measured profile after the storm and the red line shows the profiles predicted by XBeach after simulation of the March 31 2010 storm.*

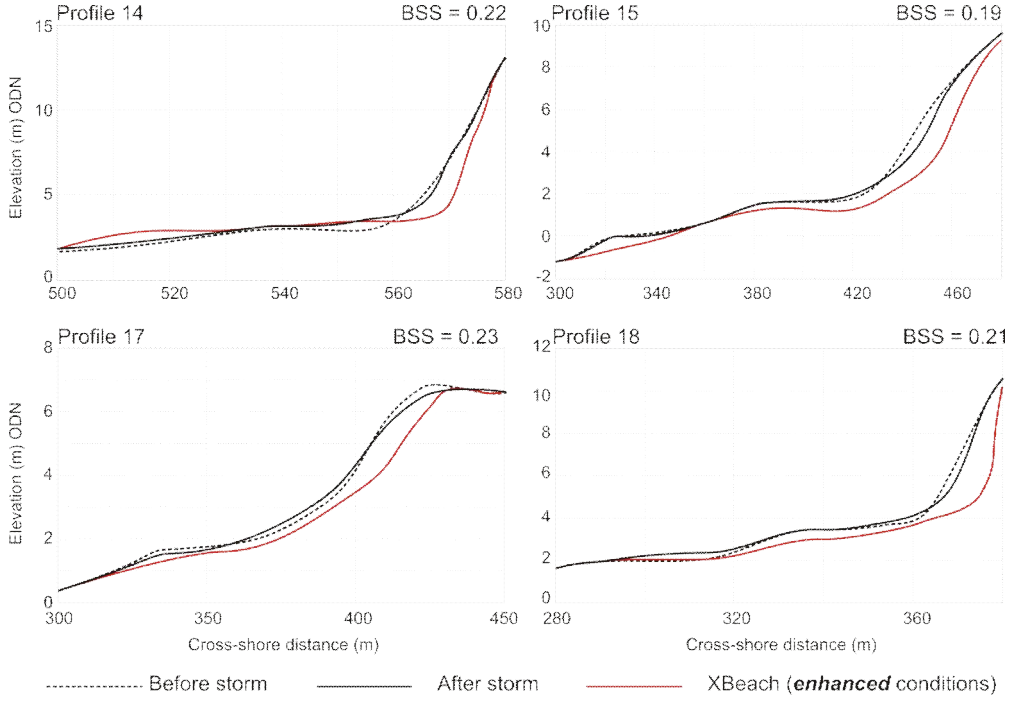

*Figure 7.11b. XBeach model results using **enhanced** hydrodynamic conditions (Figure 7.10) for the upper parts of SMBC beach profiles lines P14, P15, P17 and P18. The dashed black lines show the measured profile before the storm, the solid black lines shows the measured profile after the storm and the red line shows the profiles predicted by XBeach after simulation of the March 31 2010 storm.*

Additional 1D model runs were undertaken for events causing significant erosion or flooding impact during the period 2002 to 2008 using SMBC beach profiles lines P14, P15, P17 and P18. Unfortunately in some cases the period between measured pre-storm profiles and subsequent post-storm profiles exceeded three weeks making observed changes in all beach profiles difficult to ascribe to a given storm. Nevertheless, the available data, summarised in Table 1, provides a useful indication of typical shoreline recession derived from aerial photographs, lidar surveys and beach surveys, and thus allows a mechanism to compare the coastal impacts predicted by XBeach with those observed. It is noted that the dune retreat values in Table 1 have an error (attributable to the spatial resolution of the original data) of ±2m, or approximately 20% of the typical observed dune recession distances.

In total 6 events have been modelled using the best available information between the years 2002 and 2008 (Table 1). This includes: (a) maximum water levels (tide plus surge) measured at Heysham and Liverpool, and modelled for Formby Point (Appendix J); (b) measured maximum surge levels at Heysham and Liverpool; (c) modelled significant wave height and peak period; and (d) modelled peak wind speed, (Table 1). Although during each of these events approximately 10m of dune frontage was lost (Table 1), these losses varied considerably in the alongshore direction, with some regions loosing significantly more, or significantly less dune sediment (Esteves et al., 2009; 2010). Using the hydrodynamic data (Table 1), XBeach model simulations were run for each event. The duration of the run was confined to a single simulated tidal cycle conforming to the maximum water levels indicated in Table 1 (typical of the storms in the eastern Irish Sea) and wave conditions at the offshore boundary were assumed to be time-invariant. Modelled wind data was also input into the XBeach model. Sediment parameters were defined using data from samples collected on previous occasions in the field. In all runs, XBeach model parameters were not adjusted from the recommended settings.

Table 7.1 Characteristics of events causing significant erosion or flooding impact: (1) 22 January to 8 February 2002; (2) 21 December 2004 to 24 January 2005; (3) 18 August to 22 September 2005; (4) 22 September to 12 October 2006; (5) 10 July to 06 August 2007; and (6) 03 March to 19 March 2008.

Date	Max water level[a] (m CD)			Max surge level (m)		H_{m0} [b] (m)	Tp [b] (m)	Peak Wind speed (m/s), Liverpool Bay	Observed Coastal Impact
	Heysham	Liverpool	Formby Point[b]	Heysham	Liverpool				
1	11.35	10.68	10.7	1.28	1.13	3.0	9.2	22.0[b]	Up to 13 m of dune retreat along the entire dune frontage
2	10.85	10.40	10.0	2.08	1.75	5.4	8.9	26.9[b]	Up to 9 m of dune retreat observed along most of the dune frontage
3	10.27	10.27	9.7	0.99	1.08	1.0	8.6	18.9[b]	Up to 9 m of dune retreat observed along most of the dune frontage
4	10.70	10.55	9.9	0.36	1.01	3.3	9.1	17.7[b]	Up to 9 m of dune retreat observed along the entire dune frontage
5	9.93	9.72	9.4	0.51	0.56	1.0	9.5	15.5[b]	Up to 10 m of dune retreat observed along most of the dune frontage. Reduced erosion to the south and at Formby Point.
6	10.81	10.56	10.3	1.66	1.93	2.9	7.9	26.9[b]	Up to 14 m of dune retreat observed along the entire dune frontage.

[a] Tide plus surge; [b] Model results (see Appendix K)

Where possible, the performance of the XBeach model in predicting beach profile changes was assessed using a Brier skills score value. In cases where the interval between successive survey information was too long to be considered valid, the predicted dune recession distance was compared with the observed recession. These results are summarised in Table 2.

Considering the dune retreat first, Table 2 shows that the predicted values agree broadly with the typical observed retreat distances for the selected events. However, in all but one case, XBeach over-estimates recession by approximately 20%. Although for the reasons outlined above it is not possible to obtain Brier skill scores for all events and all profiles, Table 2 indicated that, in general, XBeach is performing moderately well in predicting the post-storm beach profiles. It must be remembered however, that there is uncertainty in the field data attributable to lag time between the storm and the beach/dune survey date. It is know, for example, that during the post-storm period sediment derived from dune slumping processes can be quite rapidly move alongshore and/or distributed across-shore to leave little evidence in the beach profiles data.

	Brier Skill score					
Date	P14	P15	P17	P18	Observed dune retreat	Predicted dune retreat
22 Jan to 8 Feb 2002	-	-	-	-	Up to 13m±2m	15m
21 Dec 2004 to 24 Jan	0.46	-	0.52	-	Up to 9m±2m	10m
18 Aug to 22 Sept 2005	0.47	0.51	0.63	-	Up to 9m±2m	14m
22 Sept to12 Oct 2006	-	0.61	0.44	0.34	Up to 9m±2m	6m
10 July to 06 Aug 2007	0.55	0.64	0.48	0.59	Up to 10m±2m	12m
03 Mar to19 Mar 2008	-	-	-	0.43	Up to 14m±2m	18m

Table 7.2 Measures of XBeach model performance for events listed in Table 7.1.

The results presented thus far have demonstrated that XBeach has reasonable skill in predicting the beach profile response to the range of storm events examined. Further, it is able to reproduce well the dune erosion occurring at times of extreme high water (i.e. > 10.2m ODN at Liverpool). Closer examination of the time evolution of the XBeach simulations shows that the dune failure mechanism in the model is related to wave undercutting and slope avalanching. This is considered to be a good representation of the actual physical processes in the field.

7.3.2 2D selected key area modelling

The 2D XBeach models presented here utilised a variable grid configuration to allow faster run times and higher resolution of the upper beach and dune topography (typically 1.5 m resolution). Further offshore, where gradients are small, grid sizes were typically 5 m. Three key test areas were selected for investigation of XBeach 2D performance. These included: (a) a large dune blowout region approximately 1 km north of Formby Point (Figs. 12); (b) a region of steep, un-vegetated dunes at Formby Point (Figs. 13); and (c) a region of lower, vegetated dunes approximately 2 km south of Formby point (Figure 7.14). In case (a) dune erosion by aeolian processes has made the dune frontage susceptible to overwashing and possible breaching, and thus an interesting area to examine the impacts of an extreme event. However, the consequences of coastal flooding at this location are localised and only affect non-residential holiday caravans. The dunes at location (b) are steep, deeply dissected by footpath access routes to the beach and undercut in places by previous storm events. The footpaths provide a possible flood route towards some residential housing and high grade agricultural land. The lower dunes at location (c) front residential properties where breaching of the dune defences and subsequent flooding could have serious economic and human costs.

The 2D XBeach model runs used the same forcing conditions (i.e. the 31 March 2010 storm event, Figure 7.8) and parameter settings (Appendix K) as in the 1D runs. Figure 7.12a shows inundation and subsequent drainage of the dune blowout region (a). The spatial distribution of erosion (negative values) and accretion (positive values) at the end of this simulation is shown in Figure 7.12b. Typically these simulations indicate losses and gains of sediment in the range 1m to 4m and 3m to 4m, respectively, with higher values at certain locations to balance the local budget. At the highest tidal level, long waves are able to penetrate far enough through the blowout to result in some localised flooding. However, the inundation during this particular storm was insufficient to threaten the caravan park. Figure 7.12b shows that the bulk of the erosion occurs at the foot of the dunes either side of the blowout (c. 3 m recession). Accretion is concentrated immediately in front of the dune toe, and over the slope of the blowout. These results are consistent with observed post-storm erosion and accretion distributions (SMBC, *Pers. Comm.*).

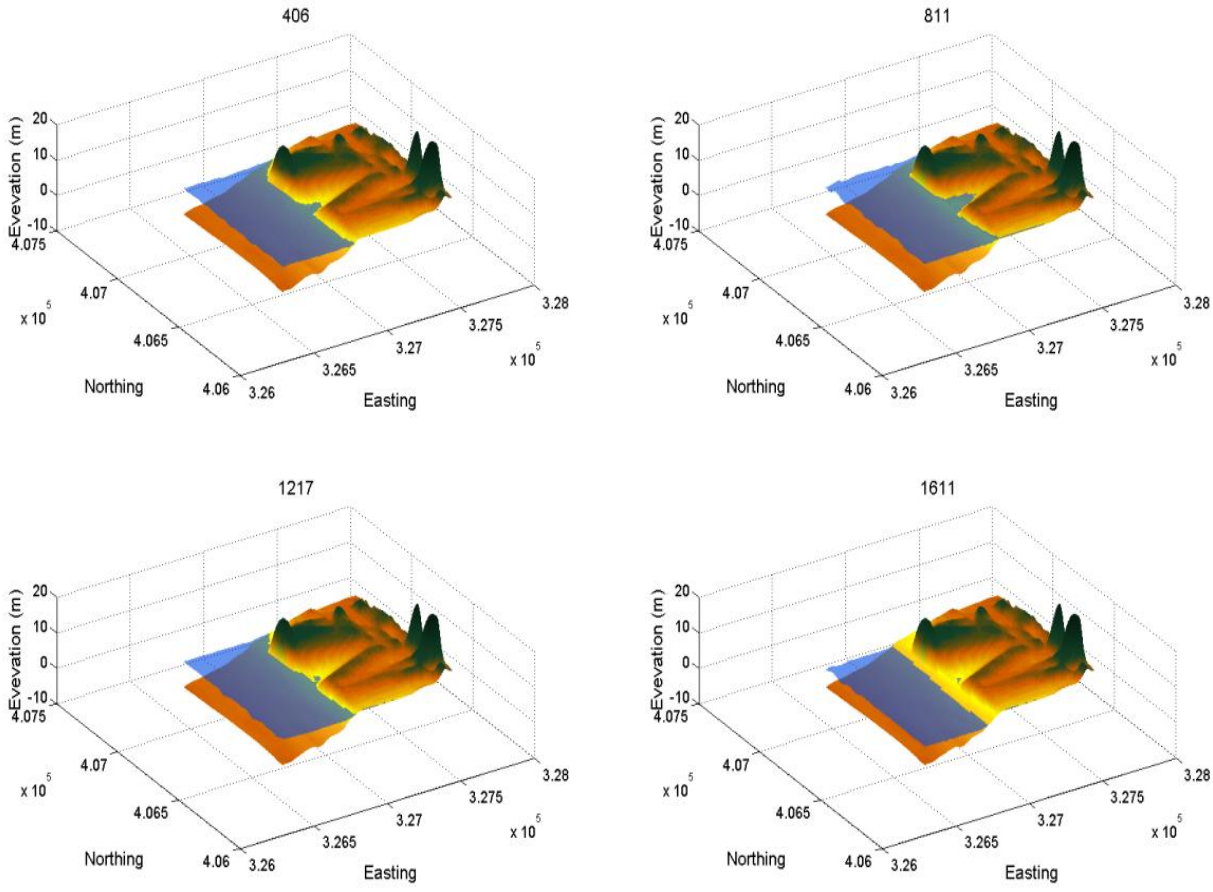

Figure 7.12 Extreme event simulation in 2D (with enhancements) around P17 (Figure 7.8) showing inundation of a dune blowout region. The numbers above each plot indicate elapsed time from the start of the model run (s).

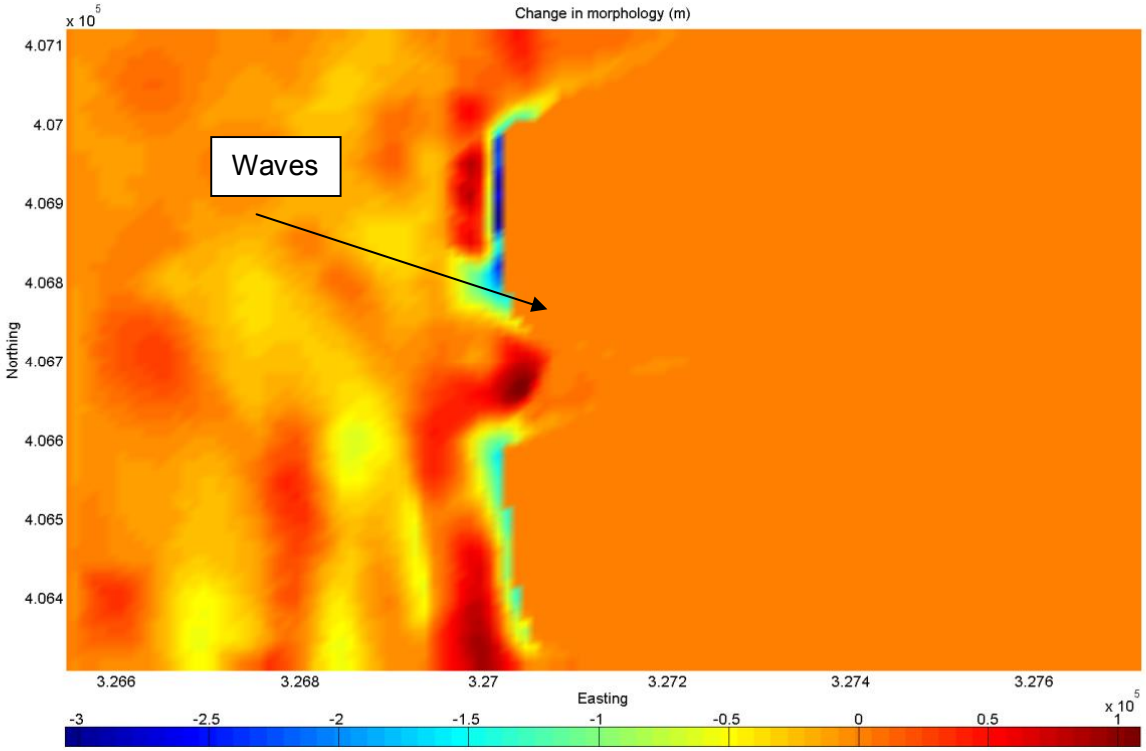

Figure 7.12b. The spatial distribution of erosion (negative values) and accretion (positive values) resulting from the extreme event simulation in 2D (with enhancements) around P17 (Figure 7.10).

Figure 7.13 shows four stages in the 2D simulation of region (b). The resulting erosion and accretion at this location was not very significant and is therefore not illustrated here. In this case, the time when waves were able to reach the foot of the dunes at high water was limited to less than 30 minutes and thus there was insufficient time for dune soaking and associated undercutting. The XBeach model was able to simulate some slumping of the dunes, but accurate reproduction of this phenomenon was not possible owing the absence of a phreatic surface in the model. The deeply dissected footpath access points through the dunes provided a conduit for flood water to spread inland. However, the length of time water levels exceeded the threshold for inundation was very restricted, and thus prevented from spreading far inland. The small erosion impact predicted at this site is attributable both to the size of the dune frontage, the vegetation cover and the limited time the dunes were exposed to soaking and wave action.

An example of the mechanism leading to the erosion of the dune frontage during three successive spring tides in November 2008 is shown in Figure 7.13b. It shows that wave undercutting (combined with soaking of the dune toe) results in slumping and the deposition of sediment directly onto the beach face in front of the dunes. This material is then moved cross-shore and (mainly) alongshore by wave action during the next high water event. In spring, summer and early autumn months, some of the sediment can dry sufficiently to allow aeolian transport to move it rapidly alongshore, and in some circumstances back into the dune area. At present the detailed physical processes giving rise to these changes in coastal morphology and not well simulated in XBeach. A further complicating factor at some sites along the Sefton coast concerns the nicotine waste deposits previously dumped by industry in the last century, and now exposed at the coastline by subsequent shoreline retreat.

These form dark, resistant layers in the dune sediments (Figure 7.13b) that act to slow down erosion until undercutting results in sufficient instability for slope failure to occur. Although an attempt was made in XBeach to simulate this using a multiple sediment fractions approach, the simulations failed to reproduce effects like those shown in Figure 7.13b and are thus not illustrated here. However, it is believed that the present XBeach model may not have been correctly parameterised and further work to investigate this is ongoing.

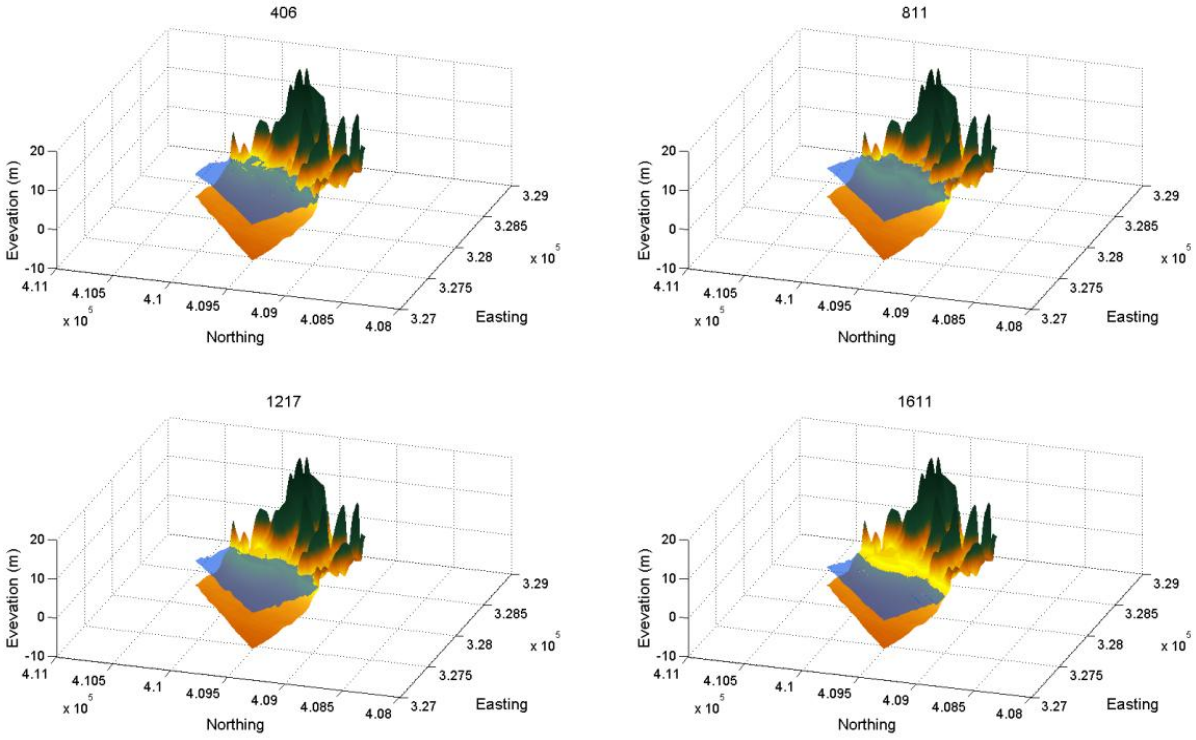

Figure 7.13a Extreme event simulation in 2D (with enhancements) around P14 (Figure 7.10) showing dune inundation and erosion. The numbers above each plot indicate elapsed time from the start of the model run (s).

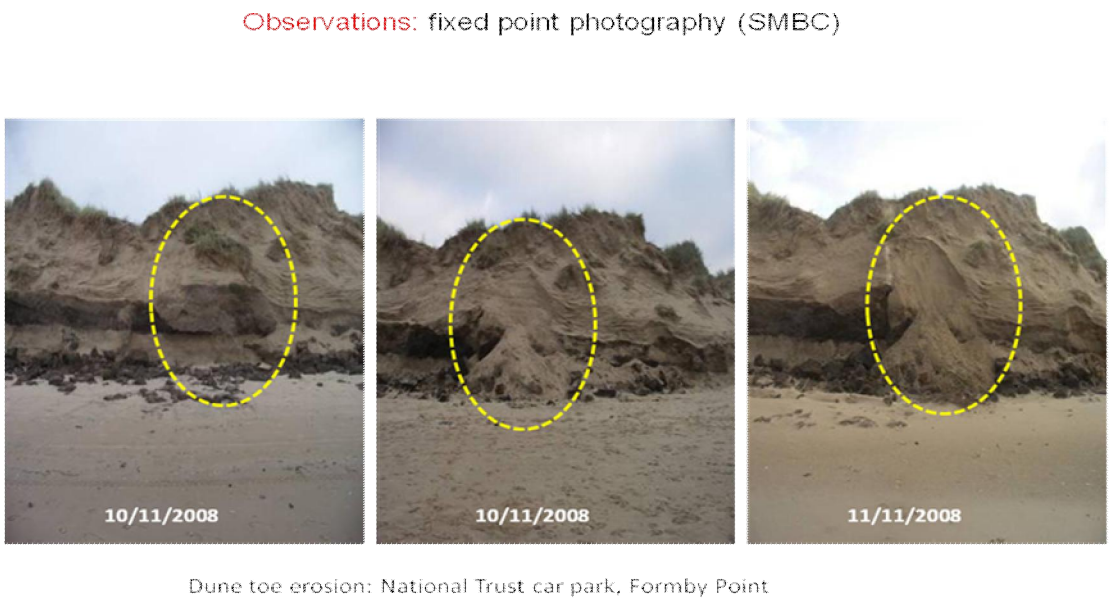

Figure 7.13b. Examples of dune front erosion during three successive spring tides in November 2008.

Four stages in the 2D simulation of site (c) are shown in Figure 7.14a and the resulting erosion and accretion distribution is shown in Figure 7.14b. In this case the results indicate that the present dune frontage has sufficient height and width to withstand a storm impact of this magnitude with only some local inundation behind some of the lower frontal dunes (Figure 7.14a). However, the simulations indicated dune recessions O(4m) at many locations, leaving some areas vulnerable to future storm damage, and perhaps an elevation in flooding risk to locations behind the dunes should they breach.

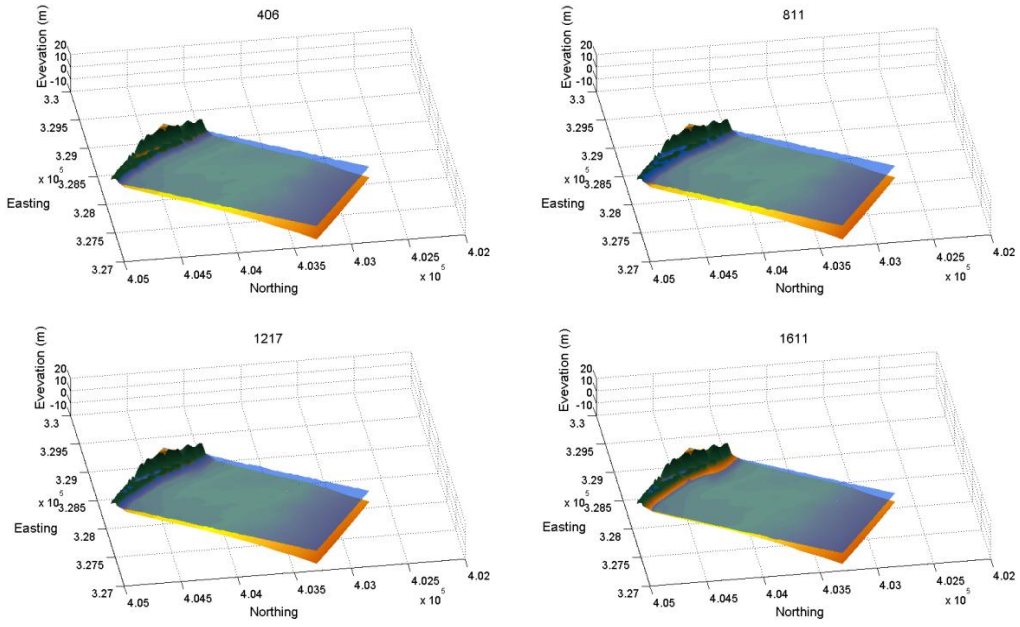

Figure 7.14a. 2D Extreme event simulation to the south of Formby Point showing inundation of regions behind the dunes and erosion. The numbers above each plot indicate elapsed time from the start of the model run (s).

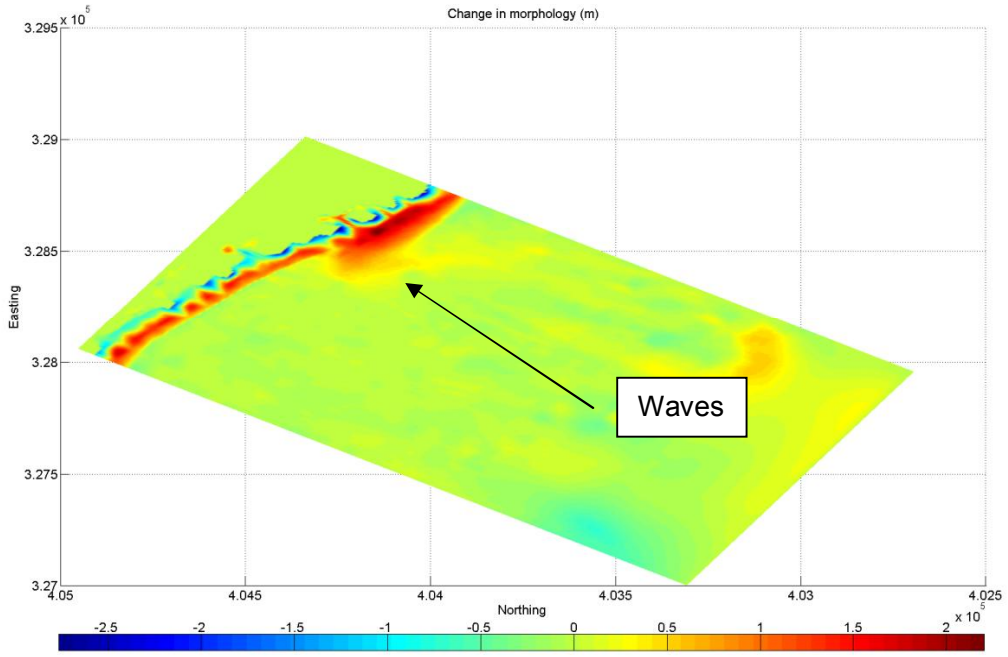

Figure 7.14b. The spatial distribution of erosion (negative values) and accretion (positive values) resulting from 2D extreme event simulation to the south of Formby Point (Figure 7.16).

As a general comment on the spatial distribution of erosion and accretion predicted by XBeach in these 2D simulations it is clear that on the basis of field observations, the simulated deposition of eroded dune sediments on the shoreface is unrealistic. It is observed that normally the dunes are undercut by wave action during the peak water level, and the majority of erosion is due to slumping processes. Although sediment released in to the littoral system by this mechanism is distributed across the upper beach profile by subsequent wave and tidal flows, there is a lag, and longshore transport processes play a key role in removing the eroded sediment. This has been investigated through the utilisation of longer model runs (> 10 tidal cycles). These show that although eroded sediment is slowly distributed across the model domain in a manner that approximates to reality, the time taken to achieve this is too long and requires further investigation.

7.3.3 2D wide area modelling

In order to examine the performance of XBeach for longer stretches of coastline, runs were performed on the coastline from approximately 1.5 km south of Formby point to approximately 4 km north from Formby Point. Following sensitivity tests, a variable grid mash was employed in these simulations with highest resolution of *c.* 2 m at the dune frontage, and a resolution of *c.* 8 m offshore. It is recognised from the outset that the curved nature of the shoreline in the model domain present problems for XBeach, and thus the results presented here must be treated with some caution.

To be consistent with the simulations described above, these model runs again used data from the March 2010 storm. The pre-storm bathymetry and topography (from lidar) used in the 2D wide-area simulation of the Sefton coastline is shown in Figure 7.15a. Figure 7.15b shows in the left panel a typical snapshot showing water depth and selected current vectors at t+6 hours.

Predicted post-storm erosion and accretion are shown in the right panel of this figure. This shows that total erosion and accretion varies alongshore in the range ± 1.5 m. The pattern of erosion generally follows the pre-storm topographic variation, with the largest losses associated with topographically lower areas. The bulk of the eroded sediment is dumped c. 50 m to 100 m offshore from the dune frontage. XBeach model runs examining the longer-term fate of this material (not illustrated) indicate that it some is moved further offshore with the bulk transported alongshore to the north. This result, although not quantifiable, reflects the observed post-storm behaviour of eroded beach sediments.

Although XBeach beach profile simulations describe above were able to reproduce the March 2010 storm response at the selected locations with some skill, the presence of an unusual accretion feature was measured approximately 100 m from the Formby Point region during the beach topography survey on 5/4/2010 (Figure 7.16, upper panel). This sediment is thought to originate from erosion of the dune front at Formby Point and remained on the beach for a few subsequent tides before being removed. In model tests with XBeach, it was not possible to reproduce this feature. Examining changes in beach volume during the March 2010 storm during the storm period (Figure 7.16, lower panel) generally good agreement is found at all alongshore locations between measured and predicted values. Thus, although the accretion feature was not reproduced accurately, the total losses and gains in beach volume predicted by XBeach agree well with the measured values.

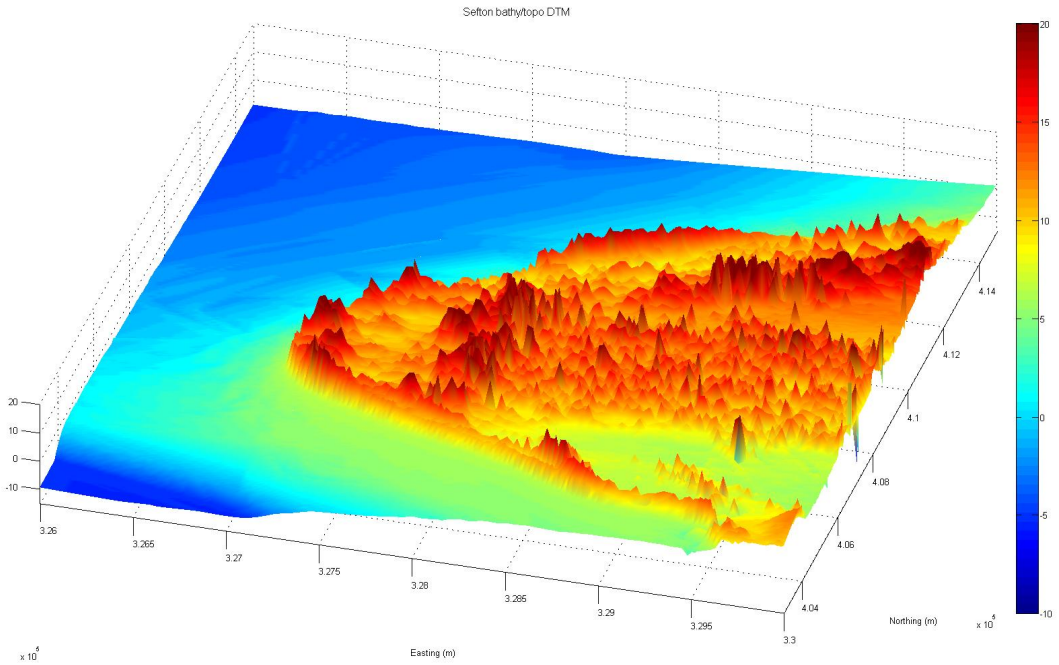

Figure 7.15a Pre-storm bathymetry and topography (from lidar) used in the 2D wide-area simulation of the Sefton coastline for the March 2010 storm.

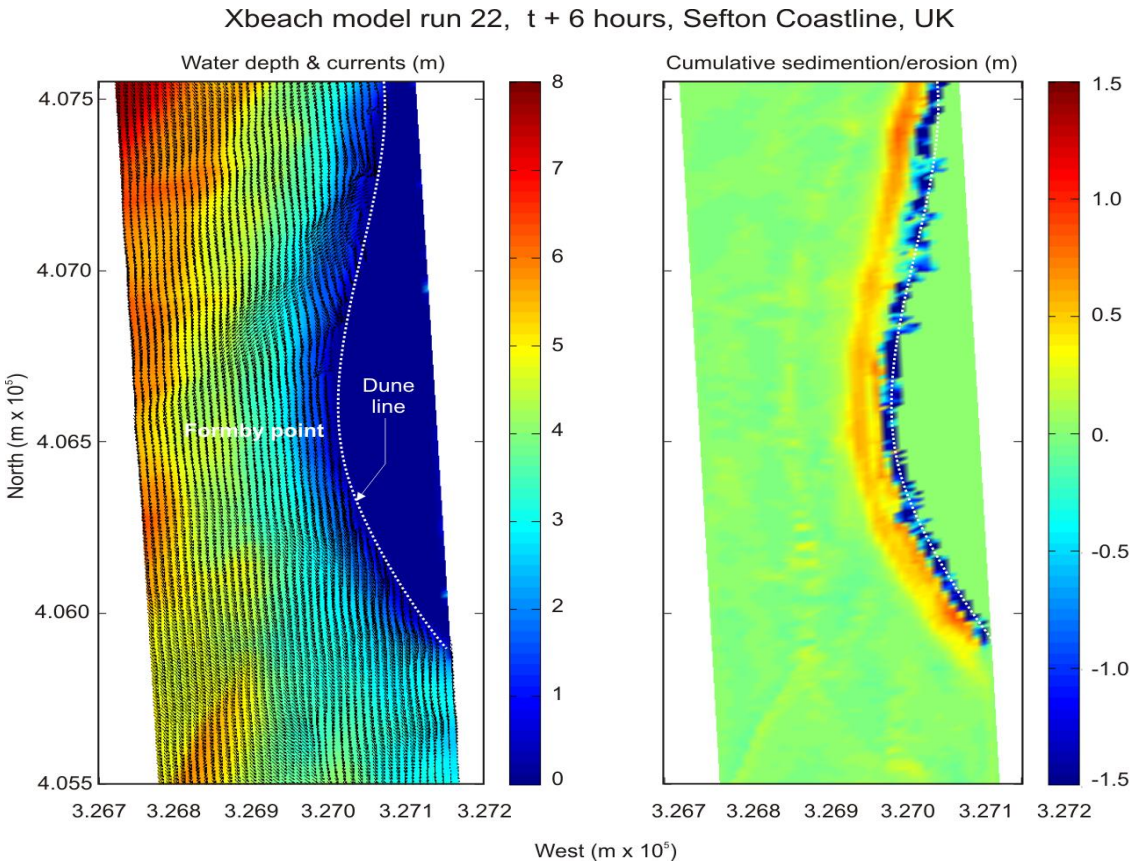

Figure 15b. 2D wide-area simulation of the Sefton coastline for the March 2010 storm. a) Typical snapshot showing water depth and current vectors at t+6 hours. b) Predicted post-storm erosion and accretion.

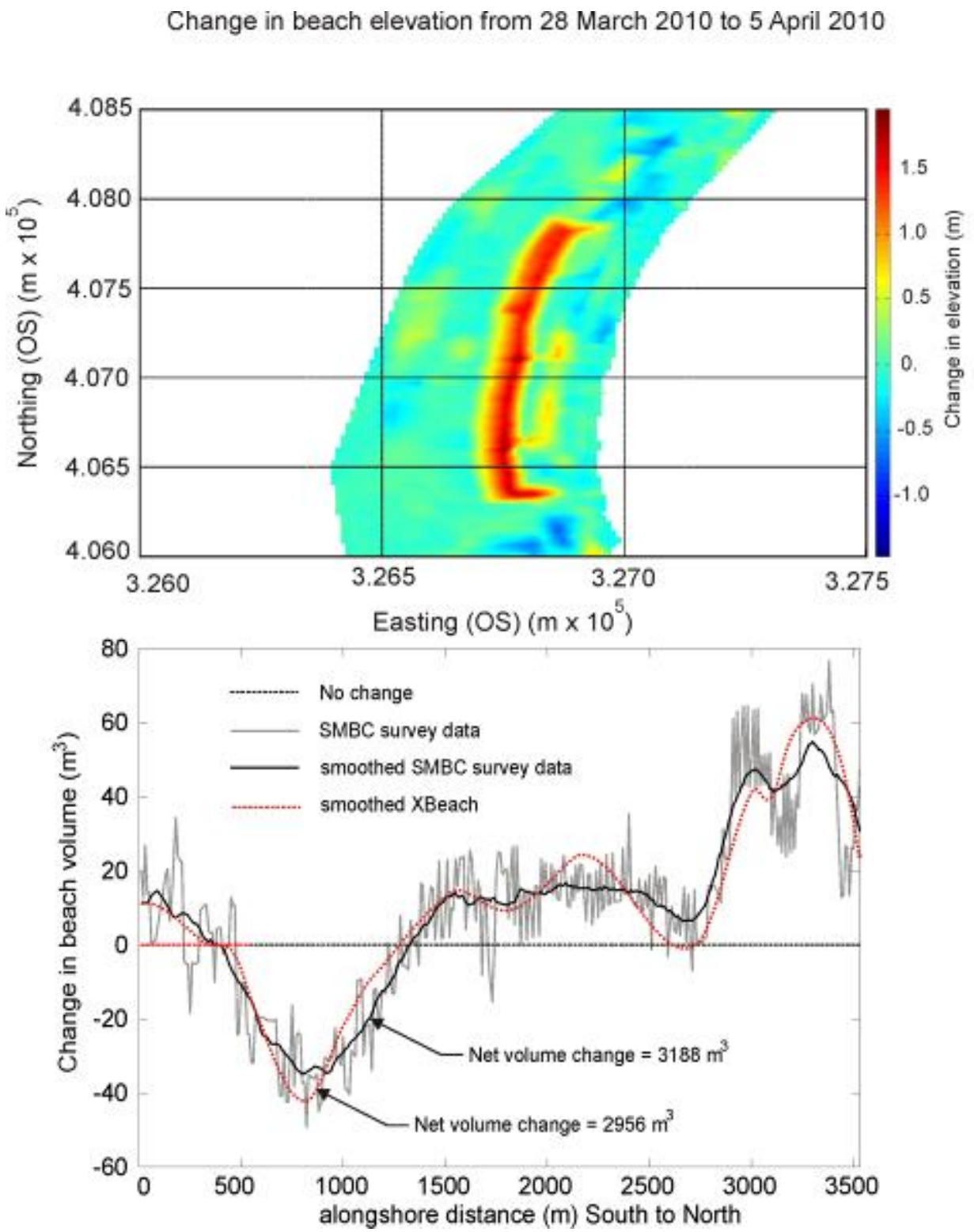

Figure 7.16 Measured changes in beach topography between 28/3/2010 and 5/4/2010 showing the unusual accretion feature close to Formby Point (upper panel) and measured and predicted (XBeach) alongshore changes in beach volume during the same period (lower panel).

7.3.4 Coastal flooding model

The lower reach of the River Alt, just north of Hightown was identified early in the study as an area especially susceptible to flooding by a combination of extreme tidal levels and fluvial discharge (Figure 7.17). The lower reaches of the river have flood defence embankments, and a series of flow control measures to reduce the flood threat to adjacent residential areas. As the shoreline is fronted by relatively high dunes with good integrity, it is considered that the principal flooding threat arises from a combination of a spring tide and surge > 1.5 m propagating up the river channel and interacting with a typical river discharge > 14 cumecs following heavy rainfall. In addition, low frequency waves are thought likely to propagate into the river at high water adding further to the instantaneous water levels.

Figure 7.17 Oblique aerial photograph of the River Alt north of Hightown at low water (left panel); and GoogleEarth image of the River Alt showing the extent of the XBeach flooding model and the course of the river. Note the proximity of light industry and residential areas.

The coastal flooding model was setup using a combination of lidar data and bathymetric surveys to define the bathymetry and topography. Although the lidar was able to measure the height of the river surface at the time of the overflight, nothing was known about the depth of the channel. Further, flow regulation structures spanning the river caused data loss in some places. The available topography and bathymetry were gridded at 3 m resolution for the model area shown in Figure 7.17, and edited to remove structures and to define the river channel and flood defences. In this process, a constant gradient was imposed on the river channel from the northern point where the river discharge enters the model to the southern end where the river discharge enters the sea. The value of this gradient was established through calibration tests. These aimed to establish a mean river flow velocity of 0.75 m/s measured for a discharge of 14 cumecs (a typical value for a flood in this river). At the resolution of the model, the details of the river flood defences could not be captured. Thus, the river channel was flanked on either side by fixed elevation levees 2.5 m above the bank. These are therefore representative of the situation in the field. A number of model runs were undertaken to establish the threshold for flooding and to determine the speed and extent of the flood waters.

Four stages in a typical flood simulation for the River Alt are shown in Figure 7.18a. In this simulation the river discharge was 14 cumecs, the Spring tide elevation ranged between 7.5 m to 10 m CD with an imposed additional surge level of 1.5 m, and waves with Hs = 1.75 m, Tp = 8 s and θ = 270 degrees.

In the simulation, river water flowed down the channel and discharged at the coast. A period of 1 hour was allowed for this to reach equilibrium in the model before imposing the tide, surge and waves at the seaward boundary of the model. As the tidal level increased, water levels in the river increased and extended inland. At a critical level the river defences were overtopped and a large area of residential land was flooded. The flood depth reached 3 m in places, and maximum flood water flow rates exceeded 1 m/s. Flood waters remained after the river level fell as there is no provision for flood water drainage in the model. In reality, the River Alt defences also include a number of pumping stations designed to lower river levels in extreme situations and thus reduce the likelihood and/or flood impact. Nevertheless, the model has highlighted some potentially damaging consequences of flooding at this location.

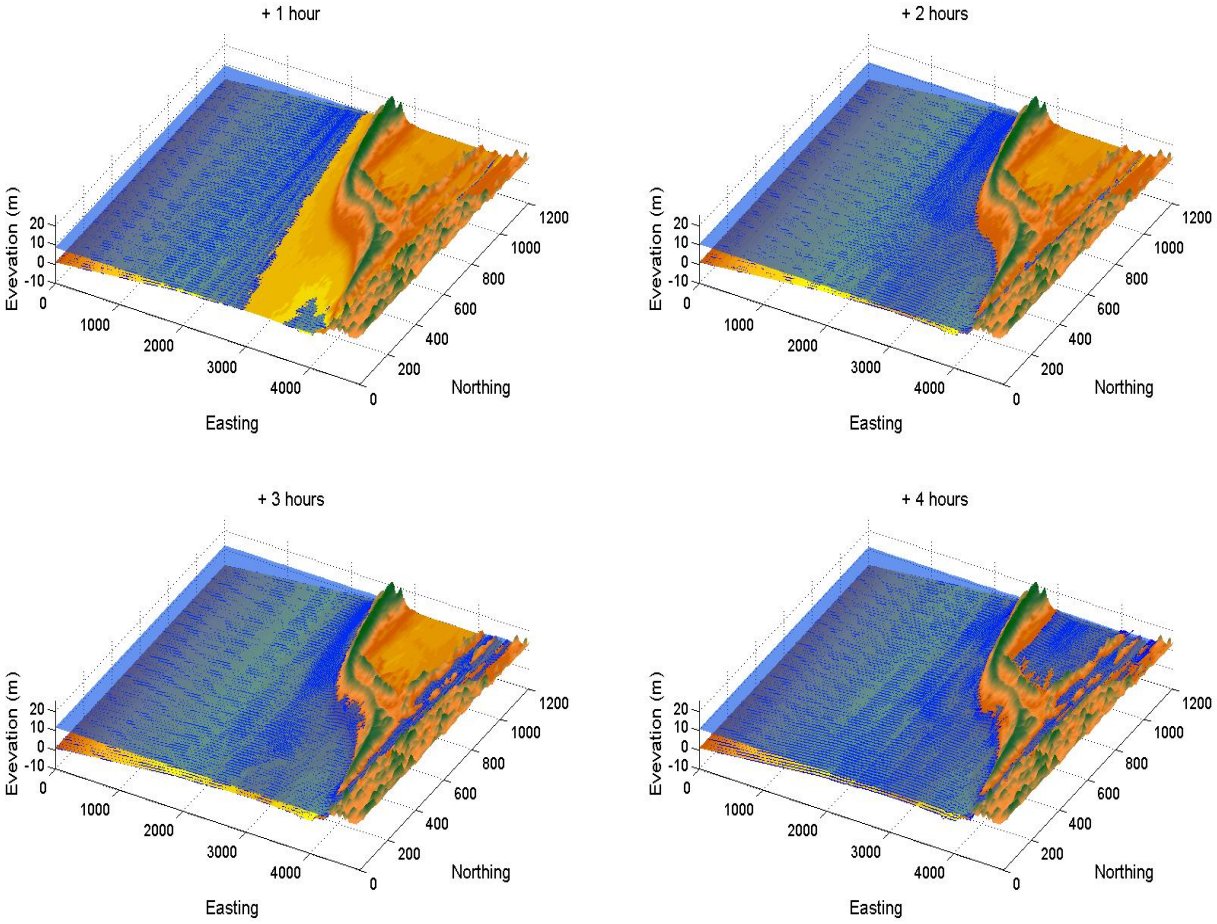

Figure 7.18a. 2D simulation of an enhanced storm impact on the River Alt, north from Hightown showing stages in coastal flooding attributable to high tidal levels and flood fluvial discharge. The numbers above each plot indicate elapsed time from the start of the model run (hours).

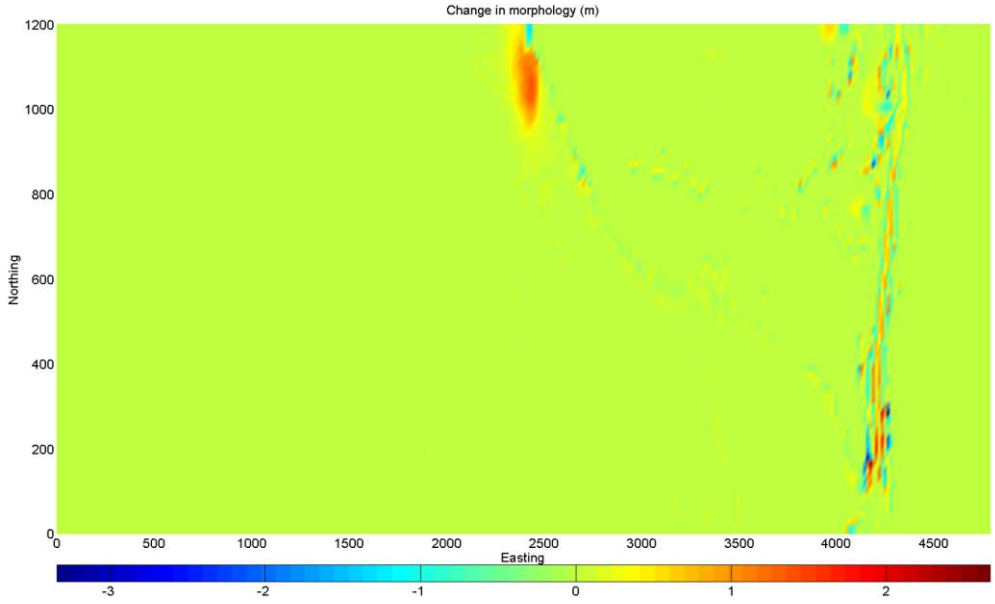

Figure 7.18b. 2D simulation of an enhanced storm impact on the River Alt, north from Hightown showing predicted morphological impacts

Figure 7.18b shows the resulting patterns of erosion and accretion. With the exception of some damage to the coastal dunes in the north, the bulk of the impact occurs to the flood defences. This is an unrealistic result since the construction of the levees would prevent such damage in reality. On reflection it would might have been more realistic to define the flood defences as hard structures in the model, in reality, these embankments are composed principally of clay, and are therefore susceptible to failure if exposed to high water pressures for extended periods.

7.4 Summary and conclusions

The 31 March 2010 storm allowed the UK team to calibrate the site specific XBeach model and XBeach simulations of the storm have been judged successful. Post-storm morphology, quantified using the dune toe survey data to define the dune recession, indicates that XBeach predictions of erosion are approximately correct. It is now considered that the XBeach model setup for the UK site is completed and provides a good and reliable indication of storm impact on the dune frontage.

In the majority of the modelling reported here, the temptation to ‘tune’ the XBeach parameter setting to obtain the closest match between observed and predicted morphological change has been resisted as far as possible, and ‘factory’ settings recommended by the development team at Deltares have been used.

In studies to identify through sensitivity analyses which XBeach parameters exert the greatest influence on simulation outcomes it was found that no single parameter exerted a strong influence on a given model providing the value chosen did not fall outside the recommended guidelines. Further, the results indicated that any changes made to multiple parameter settings must be carried out in a systematic way, and remain physically realistic.

Test were undertaken to assess if multiple 1D or a single 2D XBeach model is required to accurately describe the observed spatial differences in coastal responses to a storm. With the recent addition of a modelling option to add oblique wave to 1D models, the alongshore current is simulated, resulting in more effective removal of eroded sediment in the alongshore direction. In the simulations reported here, this gave better agreement between measured and predicted post-storm profiles (increase in Brier skills score of c. 10%). Results also matched more closely those obtained using the 2D version of the model. 1D model runs are quicker to perform making multiple test practicable and allowing sensitivity analyses of model outcomes to be undertaken.

Using the optimised XBeach model it has been possible to simulate beach profile responses to a number of historical storms in the period 2002 to 2008, where field data is available to quantify the gross morphological impact of a storm for model validation purposes, but the hydrodynamic data needed to drive the model is more restricted. Using model results from POLCOMS-WAM-GOTM, 6 storms were examined and in all case XBeach was able to reproduce with moderate skill the recession of the dune frontage and the major changes to beach topography. This work was extended further to examine the coastal response to an as yet unobserved extreme event and to elevated mean sea level in line with IPCC predictions. Although it is of course not possible to validate the predictions made by XBeach for the scenarios tested, the results indicated that the present coastline of Sefton is robust, and with the exception of some weaker areas where coastal flood routes may develop, it remains resilient to severe storm impacts. It is considered that these results demonstrate that XBeach has a good ability to assess the impact of storms in the future and may even have utility when predicting how a given coastline may respond to elevated sea levels and more severe storms.

In the present simulations a lack of data on the beach and dune groundwater profile, or on dune sediment moisture content above the water table prevented the inclusion of groundwater effects in the XBeach model. It is suggested that one of the reason XBeach tended to overestimate dune erosion is related to an underestimation of the intrinsic soil strength in the model and to complex groundwater interactions around the time of high water. This aspect of XBeach modelling has been examined for gravel barrier beaches (Williams et al., 2009; 2010) where the inclusion of a dynamic phreatic surface in the XBeach model gave results that matched more closely those observed in the laboratory and in the field. It is planned in the future to obtain the necessary field data to include groundwater in the XBeach model and thus enable a better physical description of the beach/dune system. Similar comments also apply to the present rather poor description of the physical properties of beach and dune sediments in the models, especially spatial variations (horizontal and vertical) in grain size. Although XBeach offers some facilities to incorporate this information it was not possible with present resources to take advantage of this using field data. It is noted, however, that in another modelling study undertaken to examine the recent severe erosion of Dawlish Warren in the southwest UK, the inclusion of better sediment information improved Brier skill scores by around 30% compared with runs using a single grain size descriptor. It is therefore recommended that efforts should be made to acquire as much field information about sediment properties as possible in future studies.

The River Alt study presents a situation that is not uncommon in the UK, and one that provides an efficient flood route for salt water intrusions into inland areas. In cases where coastal dunes are less well-developed than for the case examined here, storm damage and breaching could greatly enhance inundation of similar fluvial systems by the sea, and lead to unexpected flooding to inland areas. It is believed that although other flood models with flexible mesh gridding systems provide a better means of simulating situations like the River Alt (e.g. MIKE), they are unable to reproduce well coastal processes that might act to compromise defences. In this respect the use of XBeach may provide an early warning of such events and thus provide an opportunity to devise suitable mitigation.

When considering which parameters setting to use in XBeach one should not lose sight of the inherent inaccuracies and uncertainties in the field data used to define bathymetry/topography, tidal/surge water levels, waves and beach sediments. Although great care is taken to acquire and assemble the most accurate field data, there remains significant uncertainty in a number of areas. For example, a need to adjust of XBeach model parameters to optimise agreement between measured and predicted beach profile responses might arise because the offshore wave conditions are subject to error, or the mobility of the sediment might be modified by the presence of fine sediment or biological activity not accounted for in the model. Although flume experiments (even at prototype scale) can assist calibration of the XBeach model and indicate appropriate parameter settings, these are not always directly transferable to the field. The present 'community-wide' effort to apply XBeach to many different beach environments and hydrodynamic regimes, and to share results with the model developers is an excellent way to advance future model performance, highlighting as it does model deficiencies.

As a final comment it is clear that the unusual beach accretion feature discussed above (Figure 7.16, upper panel) provides a reality check on the performance of XBeach. Up to this point XBeach has apparently performed well and showed moderate or good skill in simulating gross morphological changes along the Sefton shoreline attributable to storms. This field measurement asks questions of the model performance, and challenges our understanding of storm impacts on this coastline. Much work is still required before it is possible to state with some confidence that a forecast storm will have an impact closely similar to that predicted by a numerical model. That said, it has been demonstrated that the main features of morphological change along the Sefton shoreline during March 2010 storm have been reproduced by XBeach, and thus the model can be viewed as a means of reducing uncertainty when trying to predict the impact of storms. In terms of providing an 'early warning' of threats to life, property and infrastructure the present work has demonstrated that XBeach can be a useful tool for coastal managers tasked with providing guidance to citizens, businesses, transport networks, emergency services and utilities.

8 Dziwnow Spit, Poland

Natalia Brzezowska, Joanna Dudzińska-Nowak and Kazimierz Furmańczyk, U. Szczecin, Poland

8.1 Objectives

The modeller's objective is the prediction of short-term coast changes caused by storm events. The XBeach model can be used to show weak spots on the part of Polish coast and to calculate volume changes in the profiles.

8.2 Site and climatology

8.2.1 Description of area

The Polish study site is the 14 km long Dziwnow Spit of barrier type built of Holocene deposits (mainly sands) with dunes 3.5 to 10 meters high. Behind the spit there is a relatively wide lowland of glacial or glaciofluvial origin, which is in most cases filled with peat. The surface is 1 to 3 m a.s.l. (above sea level). In lowland there is Kaminski Lagoon, the depth of which is rather small (maximum 2-3 m). At the middle of the spit there is a connection between lagoon and sea (Dziwna). The mean beach width calculated for the pilot area is 33 m. General view of the area is presented in Figure 8.1.

Figure 8.1 Dziwnow Spit from the air.

There is an underwater longshore bar system (2-3 bars) along the whole case study area. Irregularities in the shape of the underwater longshore bars are connected with the location of circulation systems. At the case study area there are nearshore rip currents about every 120 m along the coast (Furmańczyk et al., 2001). Irregularities on the 2nd and 3rd longshore bars indicate even larger circulation systems. Cross-shore output "gates" in the coastal zone were also identified (Furmańczyk et al., 2002). They are visible as a very wide (up to 3 km) system of channels with great water mass movement towards the open sea. These "gates" together

with river mouths create the most extended circulation system in the coastal zone. Beach and bottom sediments in the pilot area are of siliciclastic origin (sand, gravel) and have a light (white) colour (Musielak et al., 2005).

The sand grain size is very fine, fine, medium to gravely sand, changing along the beaches and the outline. At 12th November 2009 the granulometric characteristics of the beach were measured in two profiles located in the middle of the control areas no.1 and no.2 (Figure 8.10). Results are presented in Table 8.1.

Table 8.1 Cross-shore granulometric characteristic of the beach (sample 1 - dune foot, sample 6 – near water line).

Area	Sample	D50	D90
no.1	1	0.29	0.22
	2	0.25	0.19
	3	0.25	0.19
	4	0.25	0.19
	5	0.25	0.19
	6	0.25	0.19
no.2	1	0.28	0.22
	2	0.33	0.23
	3	0.35	0.25
	4	0.23	0.17
	5	0.35	0.23

The mean annual wind speed over the open sea exceeds 6 ms^{-1}.The frequency of stormy weather (above 8 Bft) can vary from 2 to 5%, depending on the month. With its NNW exposure, the pilot area coast section has the most violent and most frequent storm surges. However, the maximum wave parameters are not so high as along other sections of the Polish coast.

The average tide range in the Baltic is small (estimated less then 10 cm). This is because of the small area of the Baltic, its geographical situation and the construction of the Danish Straits, which prevent propagation of North Sea tides into the Baltic. Thus, surface waves (wind waves and swell) are the most important factor of the Baltic coastal zone hydrodynamics.

In 1870 the village of Dziwnow had 171 inhabitants. In 1939 the population of Dziwnow achieved 832 inhabitants. The main factor of demographic growth were health (salt springs and bromine-iodine springs) and sea-side recreation. In 2003 Dziwnow village received a city rights. Now it has 2983 of local residents (Sypion et al., 2005).
The total area of the whole community amounts 3791 ha, and the total resident population of the community Dziwnow is 4150 (07.2008). The population density is 109 persons per sq. km. The seasonal population (in summer) achieves 22 thousands of tourists.

Since the beginning of 20th century, when a connection between lagoon and the sea was constructed as an artificial channel (1892-1900) increasing erosion was observed. Since then different kind of protection measures were done. The most important of which were: groins construction in years 1918-1923, seawall in 1924, seawall in 1959/60 and beach nourishment. The last measure was applied four times between 1988-1996. The value of deposited material was 122 thousand $m^{3.}$.

At the beginning of 21th century beach nourishments were made twice, in 2000 and 2004. Historical development of the protection is presented on Figure 8.2.

.

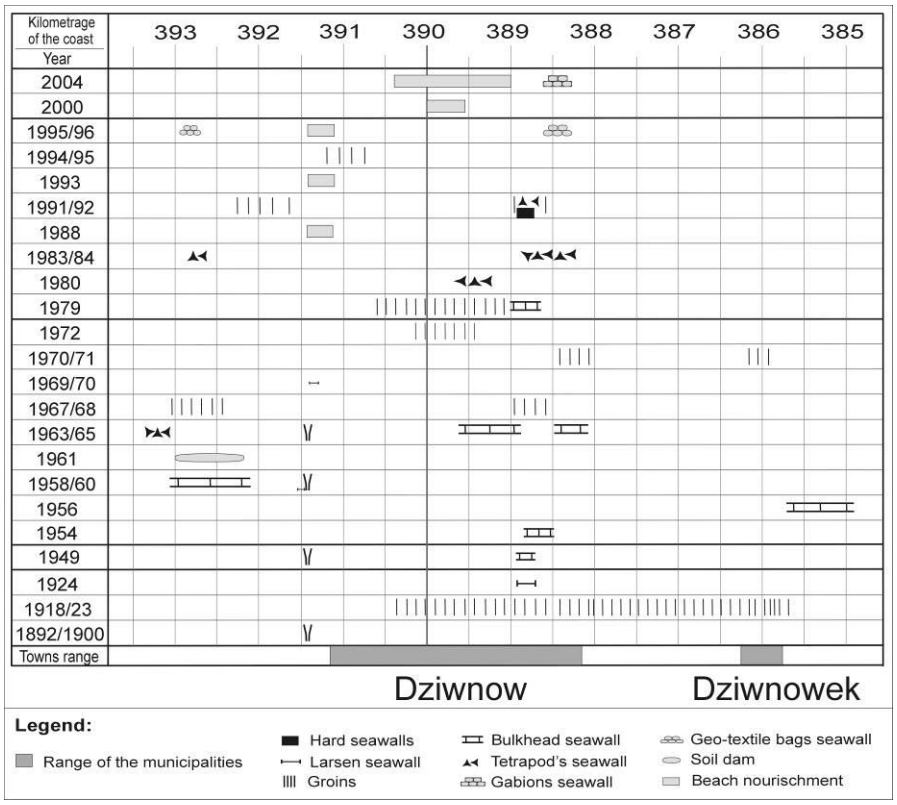

Figure 8.2 Diagram of the coastal protections methods development (Dudzińska-Nowak, 2006).

Value of the coastal changes was measured by Dudzińska-Nowak (2006) in a period between1938 and 1996 on a base of air photographs (Figure 8.3). In some places the erosion rate excides 1 m/y and in others there small accumulation of about 0,3 m/y is observed. An average value of shore line change was determined in this area of -0,10 m/y, and the average rate of erosion was -0,4 m/y (Dudzińska-Nowak, 2006).

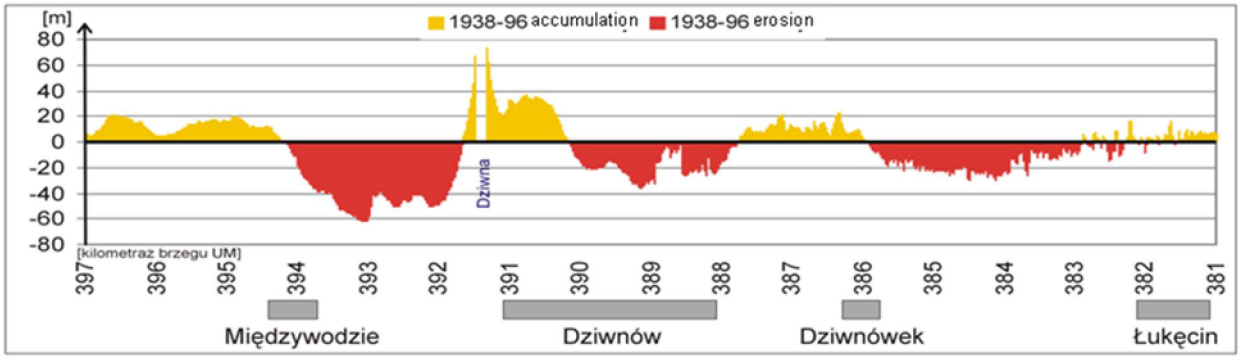

Figure 8.3 Coast line changes on the investigated area in time period 1938-1996 on a base air photographs (red areas – erosion, yellow areas - accumulation) (Dudzińska-Nowak, 2006).

Prediction of the coastal changes in the area for the next 25 years was done by Furmańczyk and Dudzińska-Nowak (2008) taking into account changeable character of the coast line development (Figure 8.4 and Figure 8.5).

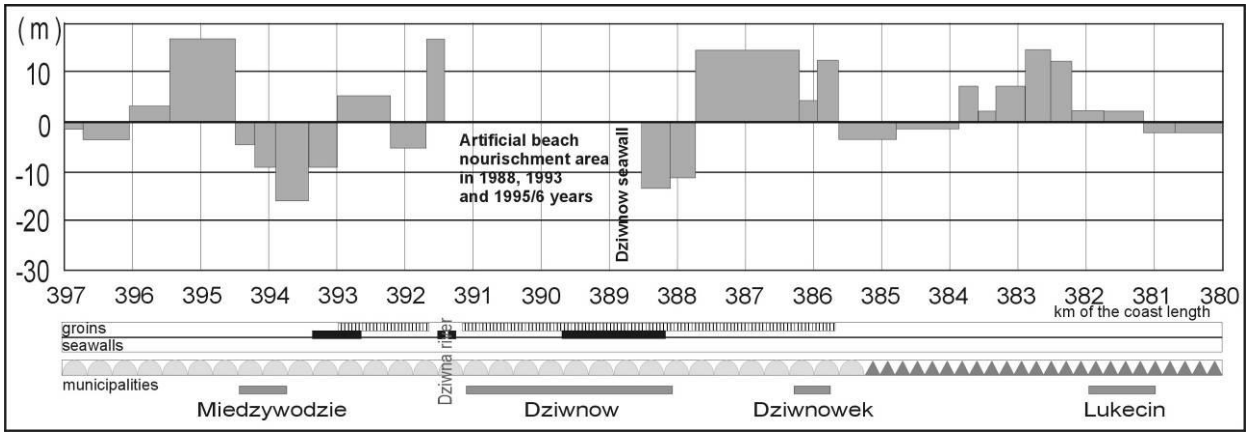

Figure 8.4 Diagram of the 25 years coastal changes prediction – optimistic scenario (Furmańczyk, Dudzińska-Nowak, 2008).

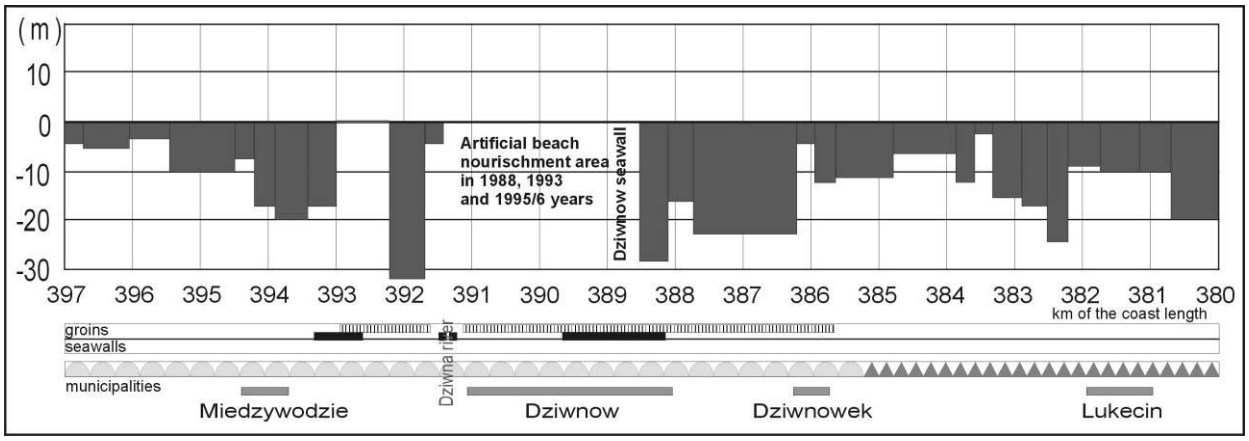

Figure 8.5 Diagram of the 25 years coastal changes prediction – pessimistic scenario (Furmańczyk, Dudzińska-Nowak, 2008).

Winds of the Southern Baltic are caused by the atmospheric circulation moderate latitudes, modified by the pseudo-monsoon exchange of air masses with those from the Atlantic Ocean and the European continent. The superposition brings about the predominance from SW and W directions, throughout the year and in most months, with the exception of spring. As to wind speed, one can distinguish tree zones: open sea, shore and land. The mean annual wind speed over the open sea exceeds 6 ms-1, but falls down near the shore and over land. The percentage of situations with wind speeds above 6 Beaufort is highest in the period from October to March, and exceeds 15-20% in particular months.

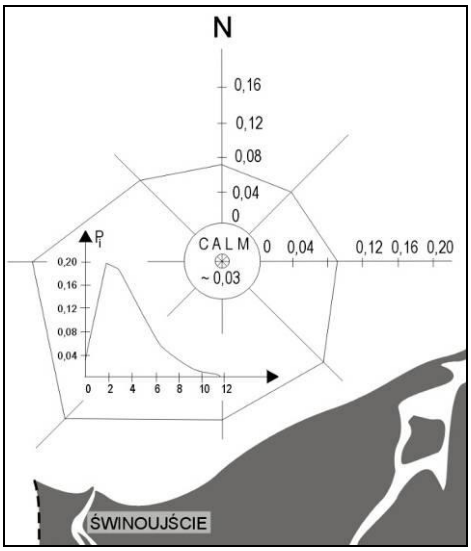

Figure 8.6 Wind rose for the Pomeranian Bay coast (Zeidler et al. 1995).

In the coastal zone, the highest mean monthly wind speeds (5-7 ms-1) are characteristic for the autumn-winter months, whereas the lowest are recorded from May to August (2,5-3,5 ms-1), when the Baltic Sea basin is characterised by low pressure gradients. The autumn-winter season contains the greatest number of days with strong winds (more western intensive cyclonic circulation, westerly on the Polish coast). In the coastal waters, the cases of stronger winds are more frequent than on land and reach -25%. The frequency of stormy weather (above 8 Bft) can vary from 2% to 5%, depending on the month and area. A wind rose for the Pomeranian Bay coast is depicted in Figure 8.6.

The wave climate in Poland is highly diversified because of the wealth of fetches and wind speeds occurring throughout the year. An illustration can be provided by the chart of waves in four classes of wave height and eight classes of wave direction (Figure 8.7). The waves have been hindcasted by the spectral method of Krylov and are arranged in the classes following from the wind statistics. At all ten regions identified along the Polish coast (distinguished by climatic, orographic, topographic and other criteria in an earlier study by Zeidler et al., 1995), the figures given on the chart refer to waves at the 20-m water depth and are generated using mean annual wind conditions (depicted by wind roses).

In the design for coastal protection and management and other maritime activities as well, one should take into account exceptional conditions causing extraordinary damage to coast or structures, that is a certain probability of extreme storm within which one can later take waves of a given frequency of occurrence (such as significant wave, %1-wave etc.). The definition of such a ‘design wave’ for Poland suffer from both theoretical and empirical shortcomings, in part due to the unresolved problem of joint probability distributions for waves and water level. Although no clear-cut standards in Poland are enforced to outline the first aspect (probability of extreme storm) one can assume the 100-yr return period for less populated areas and 1 000 years for heavily populated lowlands. Yet, in wave forecast for such design conditions, it remains unknown weather waves and water levels are correlated or uncorrelated. In addition, one should not overlook the fact that the wave height in the coastal zone is very sensitive towards depth, which makes the issue of water level quite important.

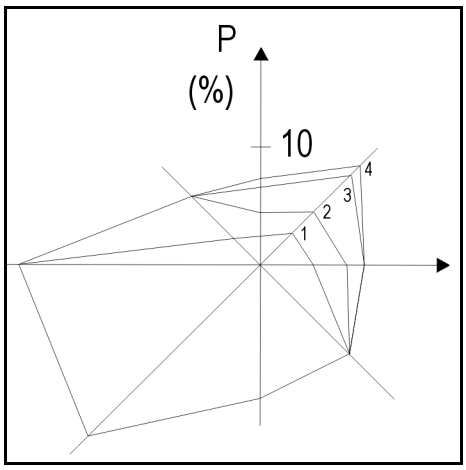

Figure 8.7 Wave rose for the Pomeranian Bay coast: (1) 0<H<25cm; (2) 26<H<50cm; (3) 51<H<100cm, (4) H>101 cm (Zeidler et al. 1995).

8.2.2 Storms considered

Since 1 June 2008, i.e. from the beginning of observations taken within the MICORE project, 1 extreme storm (12.10.2009) was noticed, which caused significant morphological shore changes (the sea level registration in this period is presented in Figure 8.8). The storm return period was about 4 years (RP>4) and the storm duration lasted for almost 4 days (93 hours)..The storm of 12.10.2009 was considered for the calibration of the XBeach model.

The highest sea level observed on tide gauge located in the Dziwna (Dziwnow Port Authority area) during the storm was 0,76 m. above mean sea level (0 m N.N. - Normal Null). The maximum significant wave height (Hs) reached 3.2 m with a spectral peak period (Tp) of 11.17 sec. A summary of the hydrodynamic conditions during this event is presented in Figure 8.9.

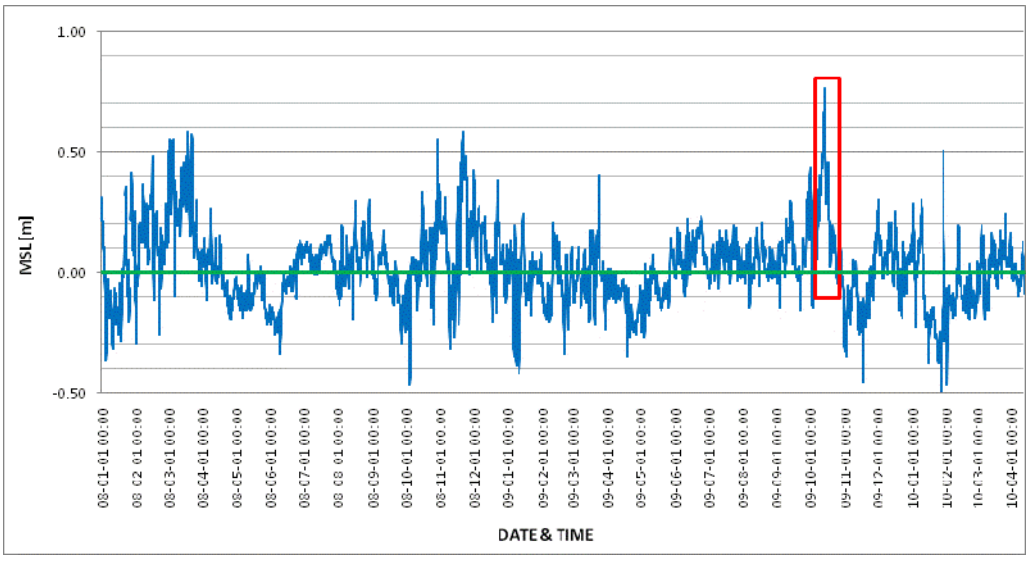

Figure 8.8 Time-series of mean sea level since 1st January 2008 to 1st April 2010. Green line show mean sea level in the Polish coast; red rectangle show storm surge during selected storm (data from MO tide gauge).

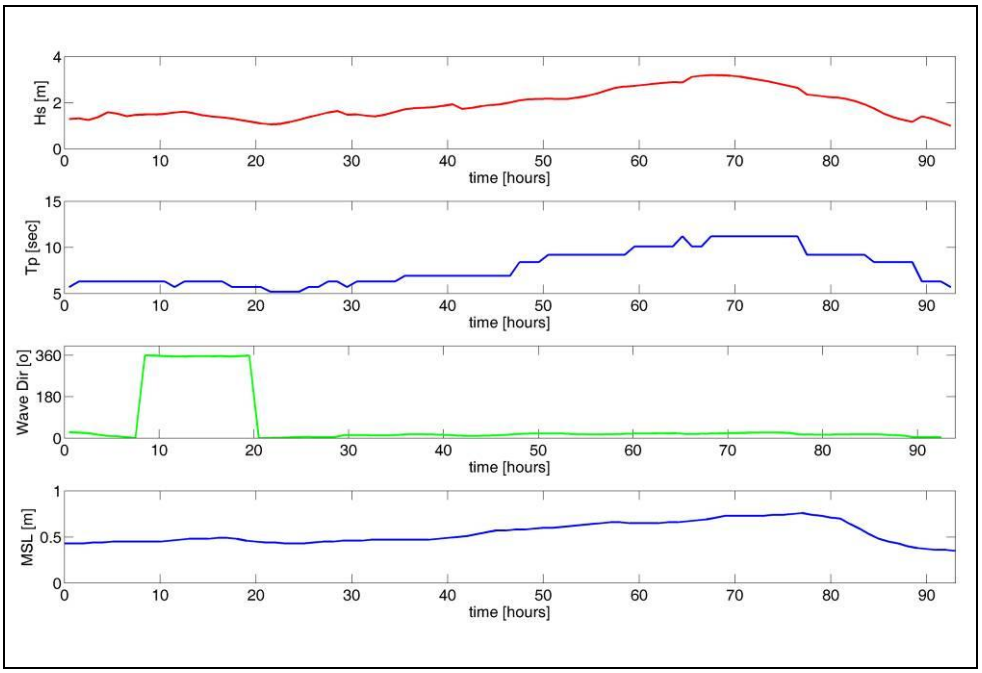

Figure 8.9 Time-series of significant wave height (Hs), wave period (Tp), wave direction (Wave Dir) and mean sea level (MSL) during extreme storm (data from WAM model and MO tide gauge)..

8.2.3 Measurements

From the 15 km long Dziwnow Spit, two control areas were established. First one (no.1) 500 m long eastwards from Dziwna mouth. Second one (no.2), 500 m long, is located at the eastern end of the study area (Figure 8.10).

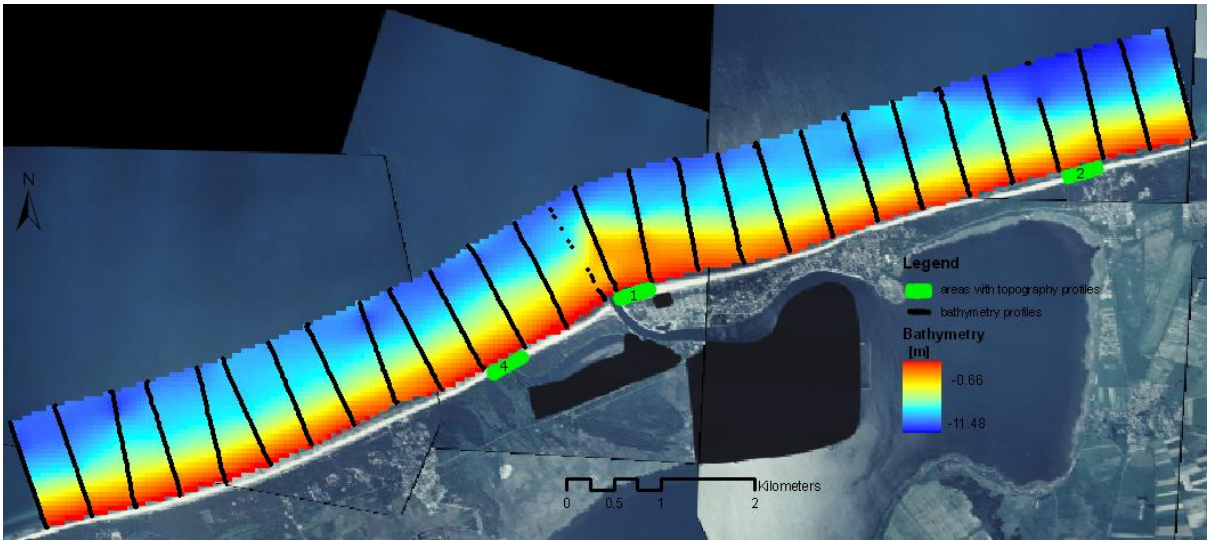

Figure 8.10 Localization of measurements and control areas.

Measurement type and period which have been collected till the end of 2009 and which were used to calibrate the model are presented in Figure 8.11.

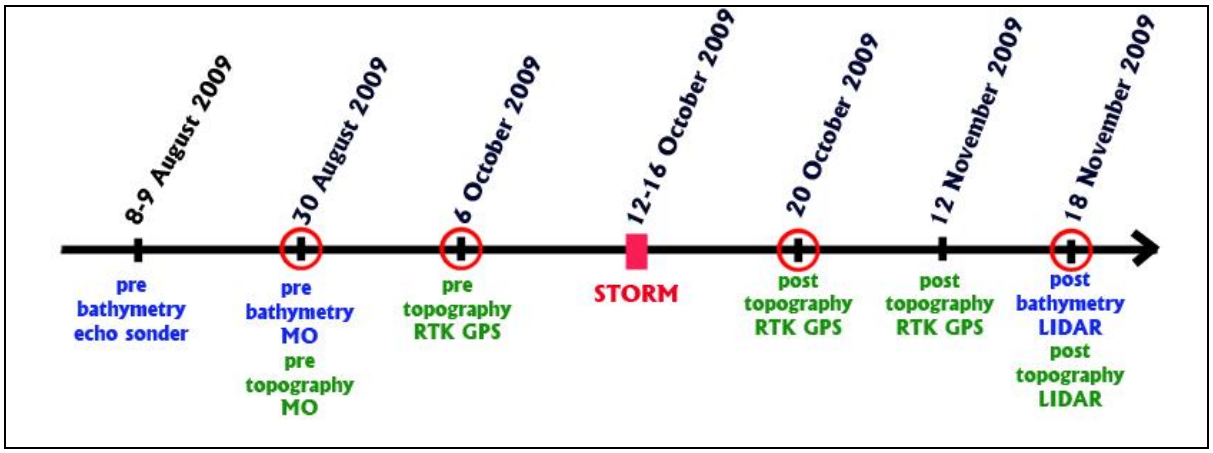

Figure 8.11 Dates of pre- and post-storm measurements carried out between August and November 2009 used to model calibration.

8.2.3.1 Topography

Pre-storm surveys were carried out on 6th October 2009 at both sites. Topographical measurements using RTK GPS were performed on subjected areas. From the survey, a sequence of profiles, with 25 m interval alongshore and a 5 m resolution between points in the cross-shore profiles was created.

Post-storm measurements were made on 20th October 2009 and on 12th November 2009 and included the same range of surveying methods. Pre- and post-storm surveying (RTK GPS) for both areas no.1 and no.2 were used to create a 3D model, which are presented in one diagram for comparison (Figure 8.12 and Figure 8.13).

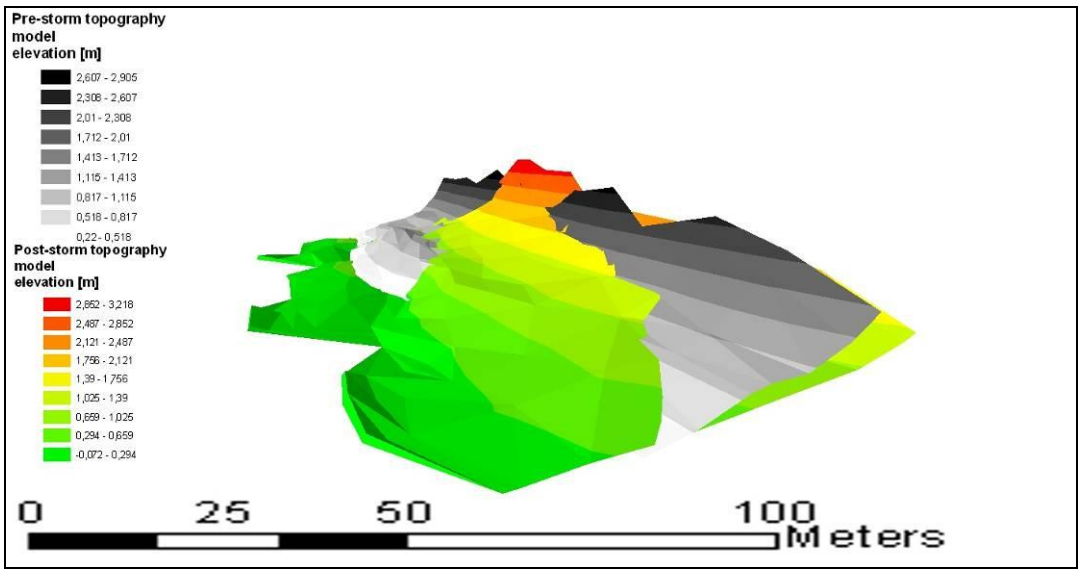

Figure 8.12 3D models comparison created on the base of pre- and post-storm RTK GPS measurements (area no.1).

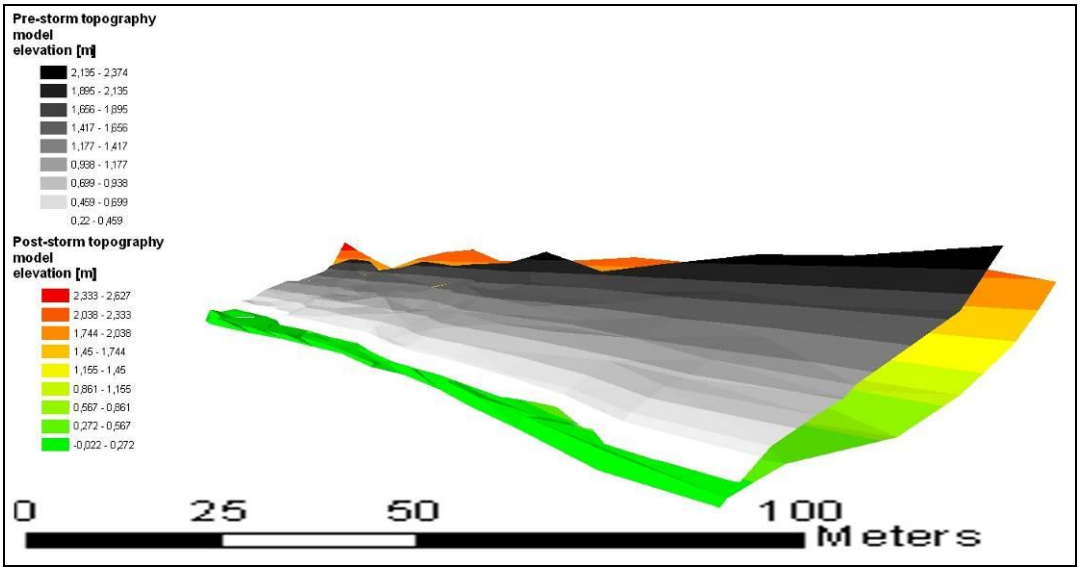

Figure 8.13 3D models comparison created on the base of pre- and post-storm RTK GPS measurements (area no.2).

8.2.3.2 Bathymetry

Pre-storm bathymetry was measured on 8-9th August 2009 making use of an echo sounder. This survey was carried out at both sides of Dziwna estuary and covered the whole research area. Unfortunately, due to bad weather conditions post-storm bathymetry surveys couldn't be obtained.

As a post-storm bathymetry use is made of measurements from an aerial laser scanner on 18th November 2009 with application of HawkEyell scanner (green LIDAR). Performed registration is characterized by measurement density of 1 pt / 4 m^2 which gives an accuracy x, y > 3m and z > 0.5 m. During the registration there were technical problems with the laser scanner which caused some areas without any registered points (which is visible as a white place on Figure 8.14). Unfortunately it occurs exactly in place where 386 and 386.5 profiles used to model calibration are located. In the 386 profile there is no data on the distance 250-380 m from the offshore end of profile (Fig. 8.18). In the profile 386.5 from 0-240 m and 420-520 m from the offshore end of profile there is no data (Fig.8.17). Bathymetry of white places visible at Figure 8.14 were calculated on a base of interpolation automatically. In this case they should not be taken for calculation, but they did.

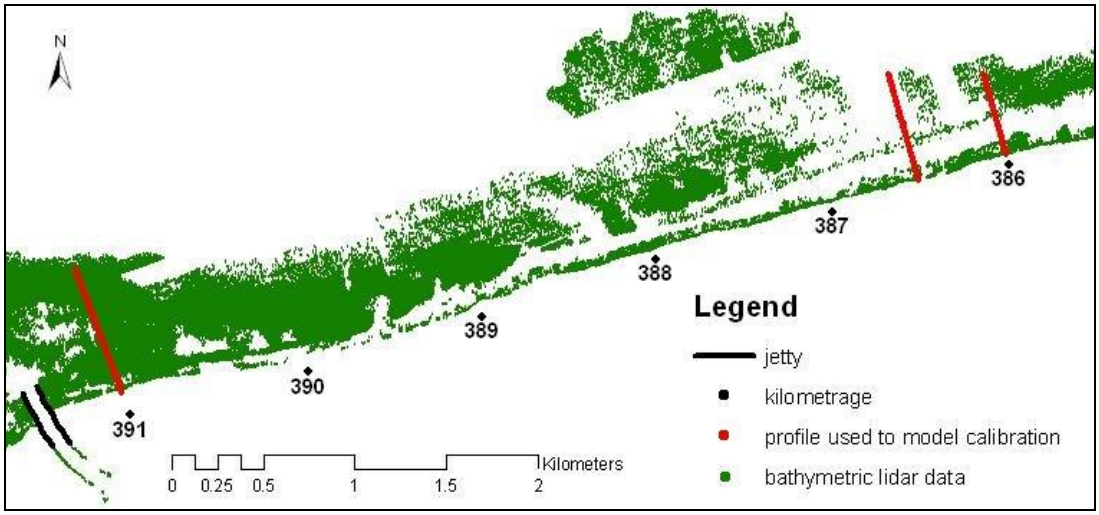

Figure 8.14 Points location of bathymetric lidar registration

8.2.3.3 Topography and Bathymetry

Additionally we received from the Maritime Office in Szczecin (MO) profiles bathymetry and topography, which are taken in 30th August 2009 every 500 m. Three of them (391, 386.5, 386) were taken for XBeach model calibration. Their location is presented on Figure 8.10.

8.2.3.4 Additional events and activities from month December 2009 - March 2010

From study area one more control area was selected (no.4). It is located on the west side of Dziwnow Spit at Martwa Dziwna lagoon. The selected area represents area with almost no protection systems. Three surveys using GPS RTK were carried out at this time.

In this period of time the weather conditions were very bad. Beach was covered by snow and ice. Field measurements were performed just before snow covered the beach at the areas no.1 and no.4 (15th December 2009) and just after ice melting at area no.1 (1st March 2010). Moreover measurements were repeated at both areas on 19th April 2010.

Figure 8.15 Ice conditions in the Dziwnow Spit beach.

8.2.3.5 Waves

Wave and wind parameters were taken from 44-year hindcast of wave field WAM model over the Baltic Sea performed within HIPOCAS project done by Oceanographic Institute of University of Gdańsk. Basic characteristics of WAM model of Baltic Sea are shown in Table 8.2. The bathymetry data for the Baltic Sea were provided by the Institut für Osteseeforschung in Warnemünde (IOW) (Seifert and Kayser, 1995). The meteorological data, were 1-hourly gridded wind velocity fields provided by GKSS. The wind velocity data were performed also in GKSS from the atmospheric REMO model (REgional MOdel; Jacob and Podzun, 1997; Von Storch et al., 2000; Feser et al., 2001) forced with NCEP (National Centres for Environmental Prediction) reanalysis (Kalnay et al., 1996). The REMO modelling area covers Europe and NE Atlantic with 0.5°×0.5° resolution. For the modelling of currents and waves over the Baltic Sea, a subset of gridded REMO data were extracted. The measurements of free-surface elevation were conducted in the southern part of the Baltic Sea at three buoy stations located in the vicinity of Niechorze (Pomeranian Bay), in Lubiatowo and in the Puck Bay (Table 8.3, Figure 8.16) (Cieślikiewicz and Paplińska-Swerpel, 2008).

Table 8.2 Basic characteristic of WAM model applied over the Baltic Sea (Cieślikiewicz, Paplińska-Swerpel, 2008).

	WAM model setup parameters
Grid step	5′×5′ (~5 Nm)
Direction resolution	15°
Frequency resolution $f=\sigma/2\pi$	$f_1=0.050545$ Hz, $f_n=1.1\ f_{n-1}$; $n=2,\ldots,25$
Time step (propagation)	300 s
Time step (source)	300 s

Table 8.3 Locations of directional waverider buoy stations and periods of measurements (Cieślikiewicz, Paplińska-Swerpel, 2008).

	Location	Geographical coordinates	Water depth(m)	Distance off-shore (km)	Period of measurements
1	Niechorze	54°09′ N, 15°03′ E	18	6	18 Apr 97–9 May 97
					05 Sep 97–14 Jan 98
2	Lubiatowo	54°51′ N, 17°48′ E	20	5	01 Nov 96–31 Jan 97
		54°53′ N, 17°51′ E	20	5	15 Jan 98–31Aug 99
		54°50′ N, 17°48′ E	20	5	10 Oct 00–21 Oct 01
3	Puck Bay	54°26′ N, 18°43′ E	15	6	22 Aug 95–4 Jan 96

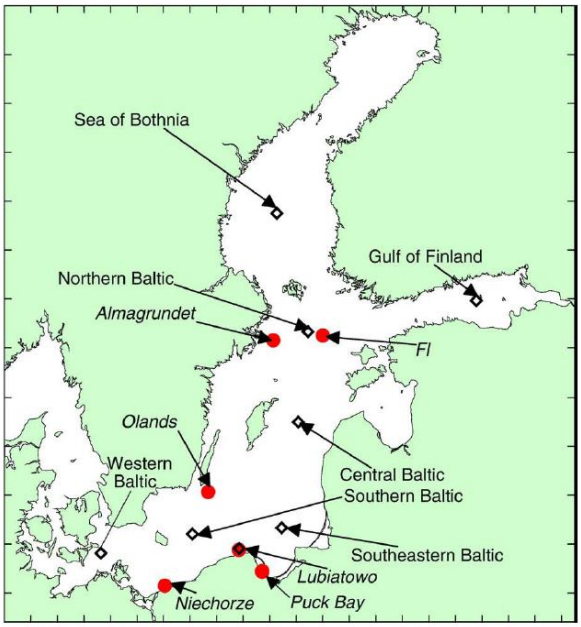

Figure 8.16 Locations of wave measuring buoys in the Baltic Sea.

8.2.3.6 Tides

Hydrodynamical data were taken from a tide gauge (Maritime Office property) located on Dziwna river (Dziwnow Port Authority area). These data are recorded constantly every 4 hours.

8.3 Model results

8.3.1 Simulation results with XBeach model

Three cross-shore profiles were used for model calibration. One is located at the eastern edge of control area no.1 (profile 391) and the other two are located at the edges of control area no. 2. (profiles 386.5 and 386) (Figure 8.10). Due to difference in time between echo sounder measurements of bathymetry by US and MO, it was decided to apply the MO data in the model because they were taken more close to the storm date.

The profiles used for XBeach calibration were taken as a combinations of MO profiles (bathymetry and dune sections) and US surveys of beach profiles (RTK GPS).

Due to some different location of US- beach profiles according to MO-bathy and dune profiles, US-profiles had to be adjusted to MO-profiles. Data do not create one profile which can be used as input to the model. Therefore it was necessary to change the local coordinate system to the model coordinate system and to rotate and project data on the shore normal which means on a line perpendicular to the shore. This processes allowed to create correct input data to the XBeach model.

The XBeach model was run for 3 profiles in 1D mode. The profiles were interpolated to a cross-shore varying grid with a minimum cell size of 3 m. Offshore wave data were input to the model considering a Jonswap spectrum, setting instat=41 and using time series from WAM model. Wave direction values were changed to 270^{o} which means that waves come perpendicular to shore. Surge data were used as a hourly mean sea level values.

Simulations were performed for each profile using slightly different parameter settings primarily for morfac (morphological factor) 5 and 10 and then for other parameters like water depth for return flow (hmin), longwave stirring (lws), asymmetry transport (facua) and critical avalanching slope under water (wetslp). Not all parameter combinations were tested but already some correlations can be observed. Table 8.4. show applied parameters in each case. The value of Brier Skill Score were given for part of profiles within -6 m (depth on which changes in depth profiles before and after the storm are smaller than the threshold value of accuracy of lidar 0.5 m) and maximum wave run up.

Table 8.4 Values of parameters used for model simulations.

Parameter/ simulation no.	**1**	**2**	**3**	**7**	**8**	**9**	**10**	**11**	**12**	**13**	**14**	**15**
hmin	0.05	0.1	0.2	0.2	0.2	0.2	0.2	0.2	0.05	0.2	0.05	0.05
morfac	10	10	10	10	10	10	10	10	10	10	10	10
lws	1	1	1	0	0	0	0	0	0	1	0	1
facua	0.2	0.2	0.2	0.2	0	0.1	0.3	0.2	0.1	0	0.2	0.1
wetslp	0.3	0.3	0.3	0.3	0.3	0.3	0.3	0.2	0.3	0.2	0.2	0.3

All BSS values for each simulation are shown in Table 8.5 and Table 8.6. The BSS values for all tested cases range from -0.32 to 0.39. The morfac parameter does not significantly affect model performance (compare Table 8.5 and Table 8.6). The essential difference occurs for the transition from lws=1 to lws=0. Keeping other parameters in the simulations the same, lws has the greatest impact on the model performance (e.g. case 12 and 15 for 386.5 profile as well as 1 and 14 for all profiles, see Table 8.5 and Table 8.6). Next, the parameter hmin has no great importance in simulations where lws=0 (12 and 14 compared to 7 to 11 in all profiles), whereas for lws=1, the BSS value is increasing (e.g. 1-3 simulation in 386 and 386.5 profiles). The facua parameter is quite sensitive. By increasing this parameter from 0 to 0.3 (at constant hmin=0.2 and lws=0) each profile responded in a different way. In profile 386.5 and 391 the BSS increases until facua=0.2 and thereafter decreases. In profile 386 this value decreases with subsequent simulations (cases 7 to 10). However, the worst result are achieved if lws=1 and facua=0. The same situation with facua=0.2 yields more reliable results (e.g. 3 compared to 13 in all profiles). Last investigated parameter – is wetslp, which seems to be insignificant as can be observed comparing simulation 7 to 11.

Table 8.5. Values of Brier Skill Score calculated for each simulation with morfac=10 (in yellow marked the highest BSS for each profile).

Profile/ Simulation no.	1	2	3	7	8	9	10	11	12	13	14	15
386.5	0.14	0.15	0.31	0.32	0.38	0.39	0.16	0.32	0.33	-0.19	0.31	-0.32
386	-0.03	-0.02	0.01	0.12	0.2	0.17	0.05	0.1	0.17	-0.19	0.09	-0.13
391	-0.04	-0.03	-0.03	0.02	-0.13	-0.04	-0.01	0.02	-0.04	-0.24	0.02	-0.15

Table 8.6. Values of Brier Skill Score calculated for each simulation with morfac=5 (in yellow marked the highest BSS for each profile).

Profile/ Simulation no.	1	2	3	7	8	9	10	11	12	13	14	15
386.5	0.22	0.31	0.33	0.28	0.37	0.33	0.19	0.32	0.32	-0.11	0.31	0.13
386	-0.11	-0.09	-0.02	0.11	0.19	0.17	0.02	0.1	0.16	-0.51	0.1	-0.29
391	-0.11	-0.11	-0.08	0.01	-0.13	-0.03	-0.02	0.02	-0.04	-0.29	0.01	-0.21

The best results (highest BSS values) are shown in Figure 8.17, 8.18 and 8.19 respectively for profile 386.5 (simulation 9), 386 (simulation 8) and 391 (simulation 11). Examinations have proven that disabling long wave stirring generally provides better results. The facua parameter seems to be a deciding factor in this situation. In the 386.5 profile, dune erosion is predicted properly, although beach erosion tends to be too large. XBeach completely eroded the first bar, while the second one had not been eroded enough. Next profile, 386, presented on Figure 8.18 shows excessive erosion of dune and beach in combination with smoothened underwater part of profile. Last 391 profile provides satisfying forecast of beach erosion. Only the first bar was definitely omitted by XBeach.

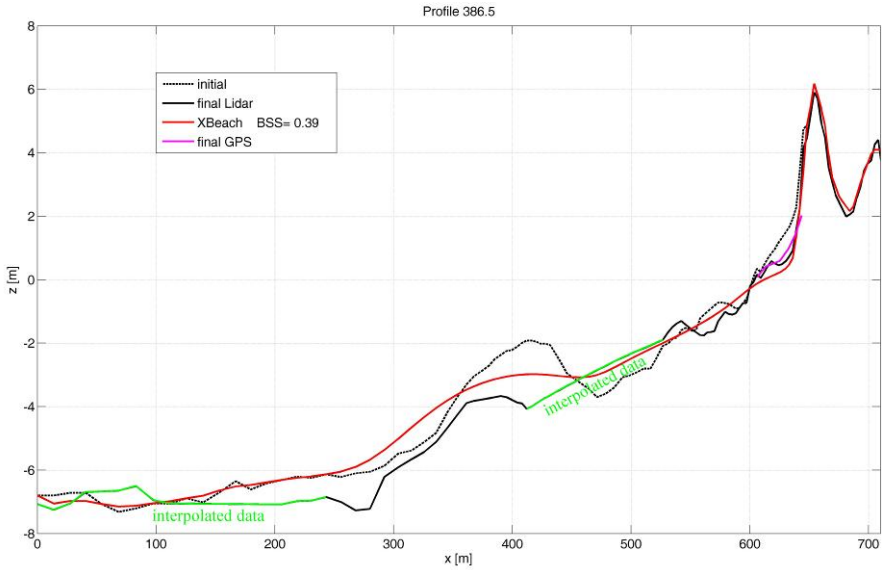

Figure 8.17 XBeach model results for profile 386.5 with the highest BSS value.

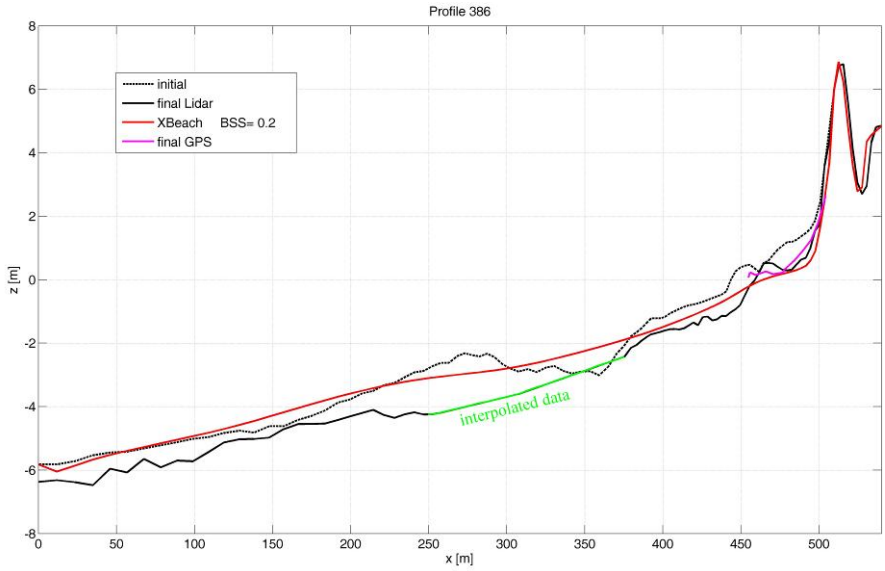

Figure 8.18 XBeach model results for profile 386 with the highest BSS value

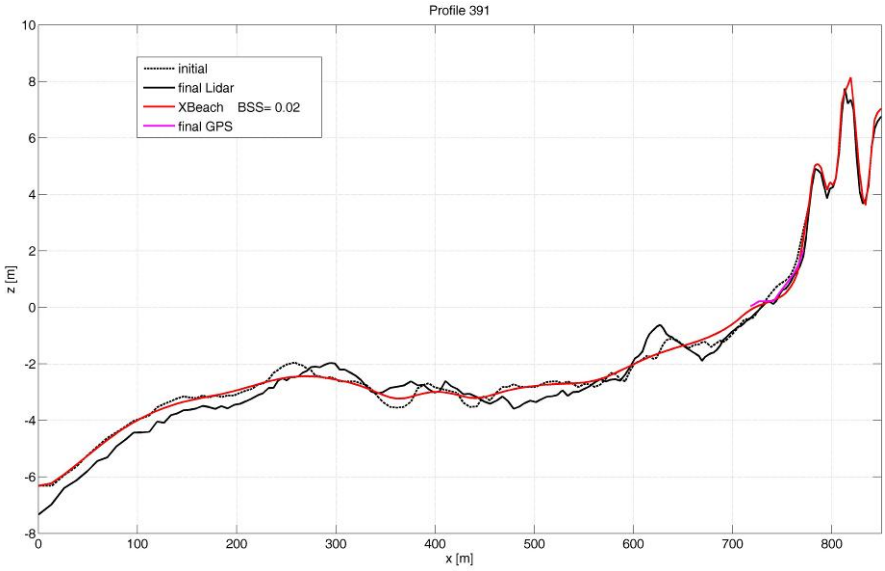

Figure 8.19 XBeach model results for profile 391 with the highest BSS value

Despite the highest BSS values, other simulations seem to better reflect expectations of the profile response, particularly in the nearshore area. Profile 386.5, simulation 7 with lower BSS presents more accurately the beach erosion (Figure 8.20). Profile 386 reveals conformity with simulation 9, again because of more adequate beach erosion (Figure 8.21). Profile 391 in turn is the most appropriate if the highest BSS value is applied (Figure 8.19).

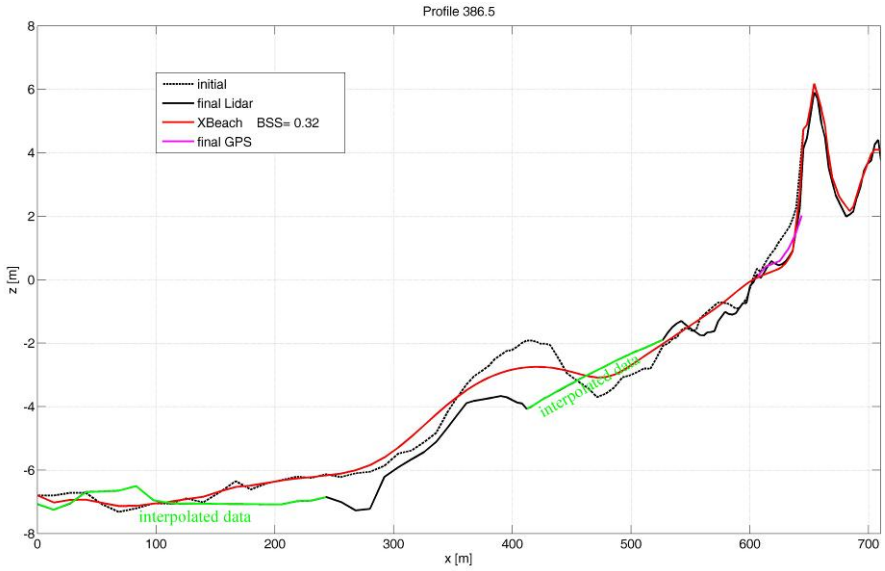

Figure 8.20. Xbeach model results for profile 386.5 where BSS value is not the highest, but Xbeach profile are more conform to final Lidar profil at beach and dune section.

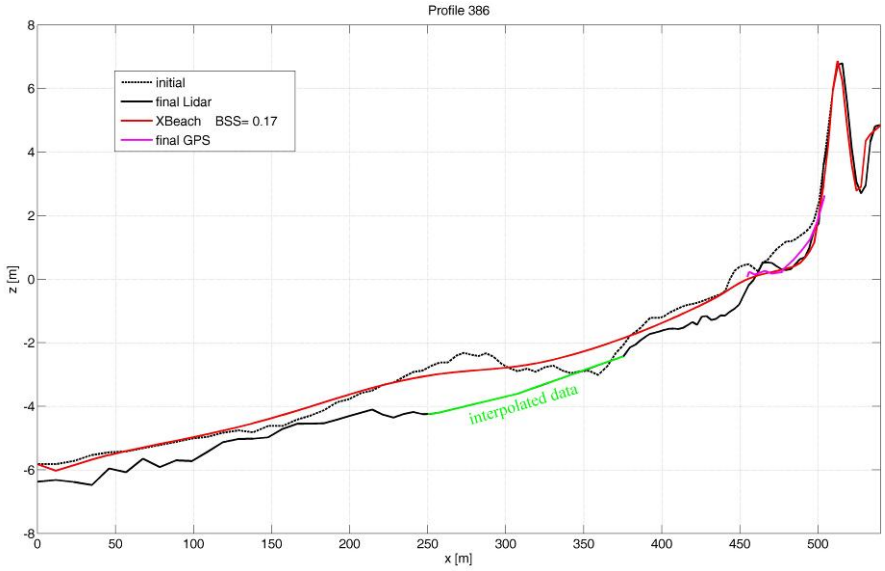

Figure 8.21 Xbeach model results for profile 386 where BSS value is not the highest, but Xbeach profile are more conform to final Lidar profile at beach and dune section.

8.4 Synthesis

Profiles used in the XBeach calibration are located at different locations in the investigated area. Furthermore, their initial shapes also vary. Profiles 386 and 386.5 are situated next to the groins (their length is equal to 65 and 40 m) at 20 m and 10 m distance respectively. Both profiles are characterized by an existing well-developed bar system (two bars in 386.5 and one in 386 profile) and beach step.

Changes caused by storm event are quite large and as a result higher BSS values are obtained for these profiles. Profile 391 has only one small bar. This profile is located close to the jetty and it seems obvious that this hard structure has a strong influence on the processes, which makes the situation more complex. On the other hand, changes caused by mentioned storm events become insignificant, which results in not so high BSS values.

8.5 Conclusions

Three profiles located in the investigated area Dziwnow Spit were used to test the XBeach model. Pre-storm and post-storm measurements of bathymetry and topography and hydrodynamic data (available from a WAM model and a tide gauge) served as input data. Simulation results for profiles located in an area where natural process are not disturbed by the presence of structures (profile 386.5 and 386) showed higher BSS values than profile 391 which is situated close to the jetty. XBeach modelling in its present stage has not yield a satisfying BSS value close to 1. The highest value of 0.39 was obtained for profile 386.5 with the following parameter settings: morfac=10, hmin=0.2, lws=0, facua=0.1 and wetslp=0.3. Primary observations revealed that the morfac parameter has no significant impact on the BSS values. For the lws parameter all simulations turned out to gain higher BSS values with lws=0. Three other parameters were found to have important impact on the BSS values. In our case the best BSS value and the best fit in the beach and dune section (in all profiles) occurs with hmin= 0.2 and wetslp=0.3. The optimal value for the facua parameter significantly differentiates for profiles 386.5 and 386 (facua=0 or 0.1) and profile 391 (facua=0.2), which is located close to the jetty. Our test show good reproduction of beach and dune erosion while the underwater part of the profiles, especially where a bar system is present, are too smooth.

9 Kamchia Shkorpilovtsi Beach, Bulgaria

Ekaterina Trifonova, Petya Eftimova and Nikolay Valchev, IO-BAS.

9.1 Objectives

The overall objective of modelling effort is to evaluate the storm-induced morphological changes for the study site Kamchia-Shkorpilovtsi. This will be done both in operational (near-real time) mode for a given wave forecast and in scenario mode to determine storm impact for several scenarios with different return periods.

To achieve this goal the following tasks are carried out:

1. selection of models – XBeach and IO-BAS morphodynamical model,
2. Preparation of the necessary data out of dataset gathered during site monitoring,
3. model calibration and validation.

9.2 Site and climatology

9.2.1 Description of area

The study area Kamchia-Shkorpilovtsi is located within the western Black Sea coast, and starches from cape Paletsa to cape Cherni Nos (Figure 9.1), which are to be found at a distance of 25 km and 40 km south from the town of Varna, respectively. It comprises the longest and the largest sandy beach along the Bulgarian Black Sea coast, with well-developed dunes and two rivers mouths, those of the river Kamchia and the river Fandakliyska. In the central sector of the site, near the mouth of the river Fandakliyska there is a scientific pier built perpendicularly to the shoreline. It is a 250m-long permeable construction that reaches about 4.5 m water depth.

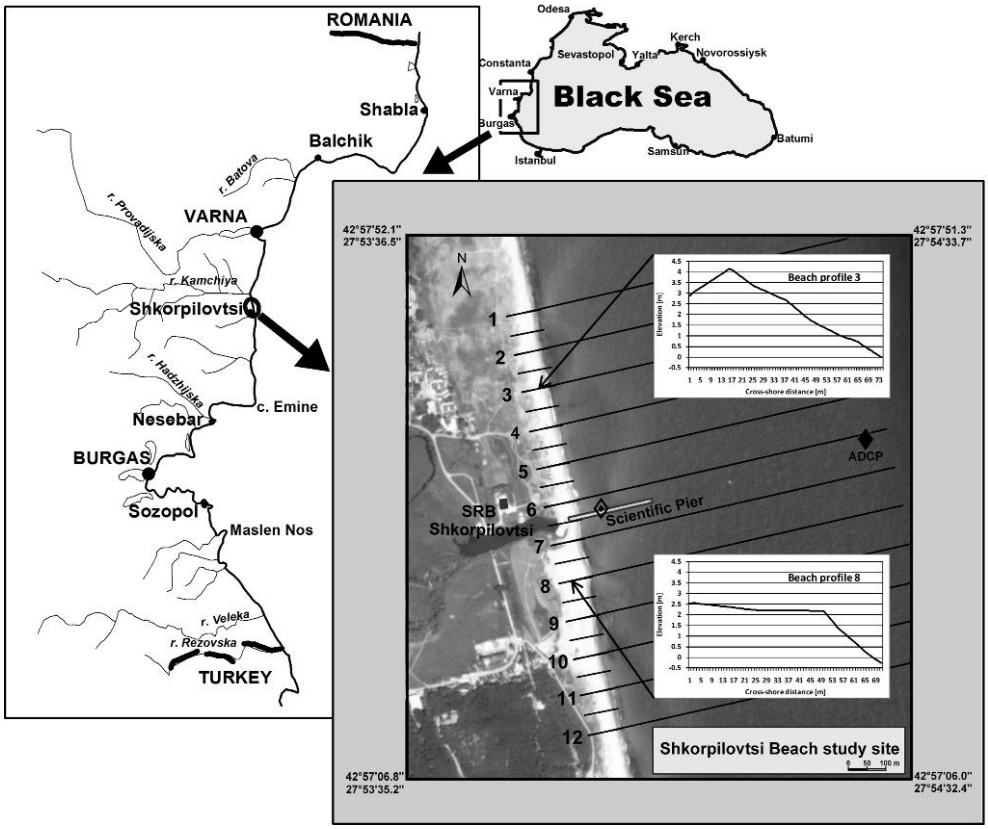

Figure 9.1 Study site location. Deployment of measuring equipment is indicated as follows: ◊ - position of meteorological station and radar sea level gauge; ♦ - location of the ADCP. Topo-bathymetric profiles are drawn with straight black lines. Typical cross-shore beach profiles are shown: Profile 3 in the north part is uni-sloped with dune crest at 4.0m and Profile 8 in the south part is bi-sloped.

The beach is formed as a result of accumulation of erosive and fluvial sediments. The main morphological feature of the study area is its rectilinear shoreline with almost parallel isobaths. Another typical feature is submerged bar at depths of about 4 m, located at the seaward part of the pier. The bottom slant is covered with sand of different size. In its upper part down to 2.5 m depth, over 95 % of bottom sediments consist of coarse and medium sand fractions (0.30 ÷ 0.76mm). As the depth grows the content of these fractions decreases and at 8-10 m over 90 % of the sediment grain size is less than 0.25 mm. The medium and coarse sand contain mostly quartz. The beach is open to waves of the eastern half. Beach and dune morphology within the study area is presented by two types of cross-shore beach profiles – northern type with dunes and average beach slope 8/100 and southern type – dune-less with bi-slope profile at slopes 1/100 in its near-land end and 10/100 in the near-sea end (Figure 9.1).

The large seasonal variability is the most remarkable feature of wind and wave climate in the western Black Sea. In general, wind regime in the region corresponds to a particular atmospheric pressure field over East Europe. During the storm season the most relevant configuration is determined by the mutual position, displacement and resulting interactions between East European (Siberian) anticyclone and Mediterranean cyclones (Sorkina, 1974). Thus, the most intense and frequent winds directed onshore are those from NE, E and SE. Having the largest fetch, they trigger the severest storms. Winds from NE prevail in the northern and middle sections of the shelf zone, while the impact of eastern winds increases southward.

Ordinarily, southeast winds are less significant in terms of storm intensity but are still of importance for the northern shelf in particular (Valchev et al., 2008). Following the wind patterns waves propagate most frequently from E, NE and SE. The waves from other directions are less important in terms of both probability of occurrence and wave height. Although, usually storm season extends from October to March (Reference …, 1982), it is not uncommon that energetic wave events take place also in April and September and even in August.

Tide in the Western part of the Black sea ranges between 6 and 8 cm (Rogev, 1975) and in the other parts of the sea does not exceed 10 cm (Mishev et al., 1978). Black Sea is therefore tideless, and as such the non-tidal fluctuations as surges are more significant for the local near-shore hydrodynamics. Maximum surge along the Bulgarian Black Sea coast (1.4 m) was registered in February 1979 during severe storm (Belberov et al., 1982).

9.2.2 Storms considered

Field measurements were carried out during two storm seasons 2008-2009 and 2009-2010. A summary of different types of measurements used in WP4 for model calibration is presented in Figure 9.2. The first season was moderate with respect to the weather conditions and registered storms hardly reached 1 year return period. Two storms were initially taken into consideration for the modelling purposes – February 2009 and April 2009. Storms during the second storm season were a bit more energetic: three important events were observed – in November and December 2009, and in March 2010. However, only the last one was intensive enough to be considered storm (it exceeded the threshold established within WP1). Its return period was about 5 years.

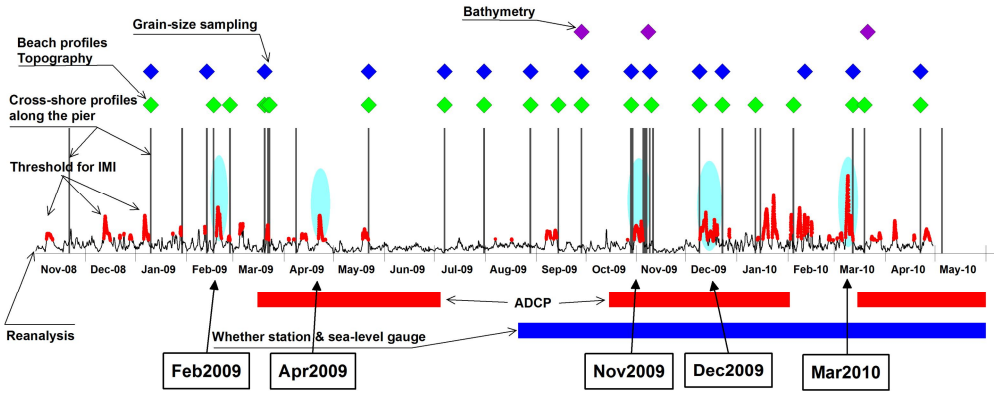

Figure 9.2 Summary of all types of measurements performed and wave history during two measuring seasons.

During field measurements a TRDI WH 600kHz ADCP was deployed to provide hydrodynamic forcing at the site external boundary. The deployment location at depth of about 19 m is in the zone of weak wave transformation and absence of seabed changes (Figure 9.1). The following wave data were used: significant wave height; peak wave period, and directional wave spectra. An ADCP was deployed during 16.03- 04.07.2009, 15.10 - 02.02.2010, and 15.03 - 20.07.2010.

Detailed information about morphological changes in terms of maxima of shoreline retreat and thickness of the eroded layer caused by five examined storms are presented in Table 9.1.

Table 9.1 Overview of morphological changes caused by the examined storms

Storm	Maximum shoreline retreat	Maximum thickness of eroded layer	
		Submerged beach	Subaerial beach
	[m]	[m]	[m]
February 2009	7	1.11	0.96
April 2009	11	0.98	0.99
November 2009	12	0.68	1.08
December 2009	6	1.05	1.42
March 2010	13.4	0.92	2.14

9.2.2.1 February 2009

During the period 18.02.2009 - 20.02.2009 a moderate storm occurred in the western Black Sea. The event lasted 92 hours. During the growth phase wind speed increased up to 18.3 m/s, wave heights – up to 2.48 m, mean wave periods were about 5.6 s, as the wind and wave direction gradually turned NE to E (Figure 9.3, Table 9.2) . The second phase (about one day long) is characterized with stable wave condition (Hs ≈ 2 m and Tm ≈ 5 s), as the wind and wave direction remained in the E quarter. During the decay phase the wind and wave directions turned SE.

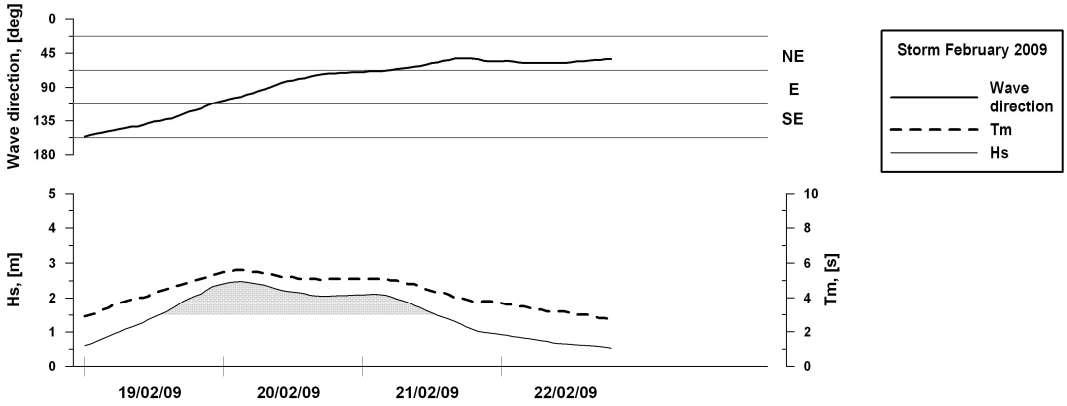

Figure 9.3 Time series of significant wave height Hs, mean wave period Tm, and mean wave direction for the storm February 2009.

Table 9.2 Statistics for the storm February 2009

Wave	Duration, [h]	Hs ave, [m]	Hs min, [m]	Hs max, [m]	Tm ave, [s]	Tm min, [s]	Tm max, [s]	Theta ave, [deg]	Theta min, [deg]	Theta max, [deg]
Reanalisys	92	1.52	0.53	2.48	4.3	2.7	5.6	85	52	156

The field campaign covering the storm duration included pre-storm (on 17.02.2009) and post-storm (on 27.02.2009) measurements. The initial profile is characterized by a well-exposed terrace at 0.7 m depth and slightly exposed bar at 3.6 m depth located 170 m from the shoreline. The average slope inclination is about 1.9/100. As a result of the wave action the shoreline retreats with 9 m, as the beach face is eroded. The average thickness of the eroded layer is 0.4 m, and maximal – 1.2 m near the shoreline. Part of the eroded material is deposited at depth from 1.3 to 2.3 m, causing a shift of the terrace offshore. The new terrace is extended mainly shoreward, and its inclination is increased up to 2.3/100. The average thickness of the accreted layer is 0.25 m.

As a result of this storm sandy bar, located at 160–170 m, was washed out, and the material was probably deposited farther seaward (Figure 9.4).

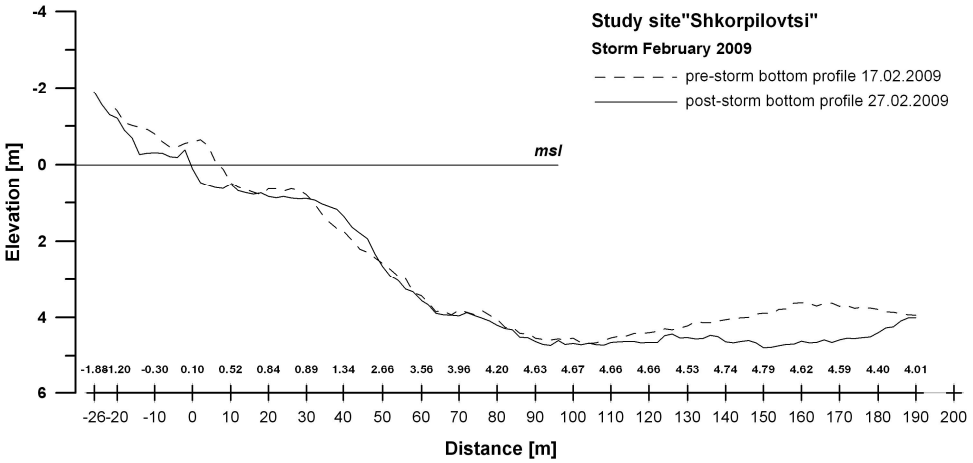

Figure 9.4 Pre-storm and post-storm profiles along the scientific pier for storm February 2009

9.2.2.2 April 2009

In April 2009, a short storm with duration of two days occurred in the western Black Sea. The phase of decay took place very soon after the storm developed. During the first phase wind speed increased up to 14.9 m/s, significant wave heights - up to 3.01 m, and peak wave periods were about 9.9 s, as the wind and wave direction remained almost constant in E quarter. During the decay phase the wind and wave directions turned to ENE (Figure 9.5, Table 9.3).

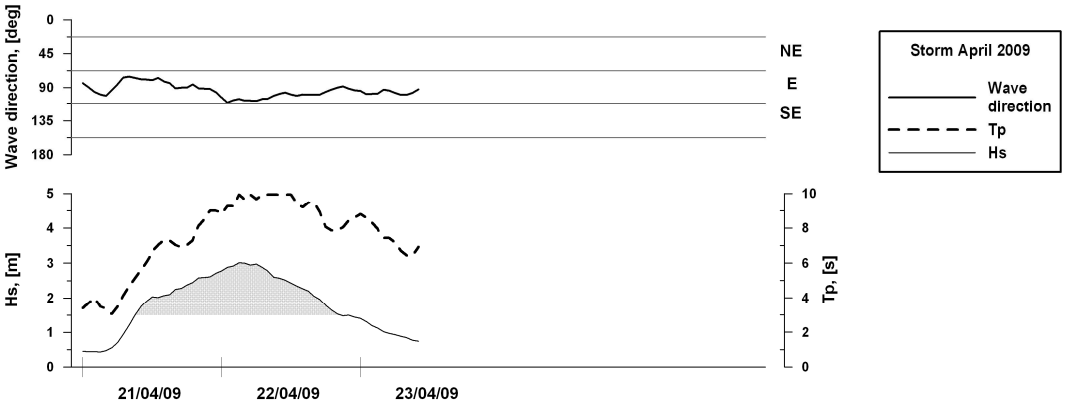

Figure 9.5 Time series of significant wave height Hs, mean wave period Tm, and mean wave direction for the storm April 2009.

Table 9.3 Statistics for the storm April 2009

Wave	Duration, [h]	Hs ave, [m]	Hs min, [m]	Hs max, [m]	Tp ave, [s]	Tp min, [s]	Tp max, [s]	Theta ave, [deg]	Theta min, [deg]	Theta max, [deg]
ADCP	59	1.81	0.43	3.01	7.5	3.1	9.9	94	75	111

The field campaign covering the storm duration included pre-storm (on 08.04.2009) and post-storm (on 22.05.2009) measurements. Initial profile was almost flat down to 4m depth with slope 5.1/100. As a result of wave action the shoreline retreat is insignificant, but the submerged beach between shoreline and 3 m depth was considerably eroded. The average thickness of the eroded layer is 0.29 m, and maximum – 1.14 m 30 m off shoreline.

Near the shoreline a scarp is formed (21.2/100). During this storm sandy bar at 190 m was not affected (Figure 9.6).

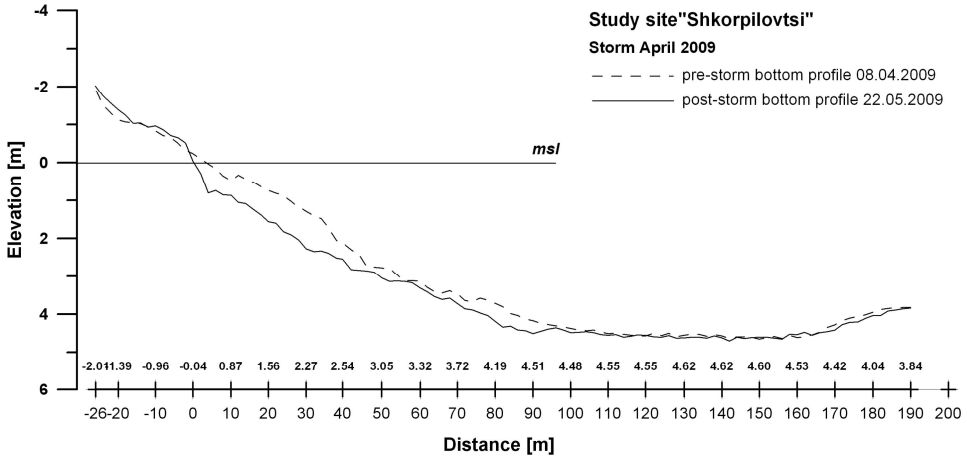

Figure 9.6 Pre-storm and post-storm profiles along the scientific pier for storm April 2009

9.2.2.3 November 2009

In the end of October weak but long (124 hours) storm occurred. Wave heights varied in the range 0.81 - 1.95, as maximum Hs 1.95 m occurred on 03.11.2009. Direction of wave approach was instable but as a whole it remained in E quarter (Figure 9.7, Table 9.4).

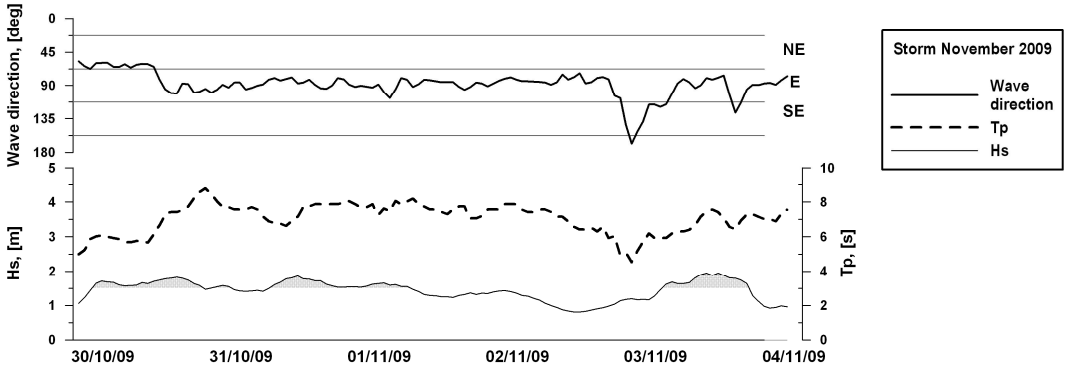

Figure 9.7 Time series of significant wave height Hs, peak wave period Tp, and mean wave direction for the storm November 2009

Table 9.4 Statistics for the storm November 2009

Wave	Duration, [h]	Hs ave, [m]	Hs min, [m]	Hs max, [m]	Tp ave, [s]	Tp min, [s]	Tp max, [s]	Theta ave, [deg]	Theta min, [deg]	Theta max, [deg]
ADCP	124	1.44	0.81	1.95	7.0	4.5	8.8	88	57	169

The field campaign covering the storm duration included pre-storm (on 29.10.2009) and post-storm (on 05.11.2009) measurements. The initial profile is characterized by a well exposed terrace at 1.7 m depth and slightly exposed bar located 50 m off the shoreline. As a result of wave action the shoreline retreat is insignificant, but the beach face of subaerial beach was considerably eroded – the maximum thickness of eroded layer is 0.8 m, while the average was 0.36 m. During this storm the sandy bar at 170 m was slightly affected, as the thickness of eroded layer on the bar reached 0.20 m. (Figure 9.8)

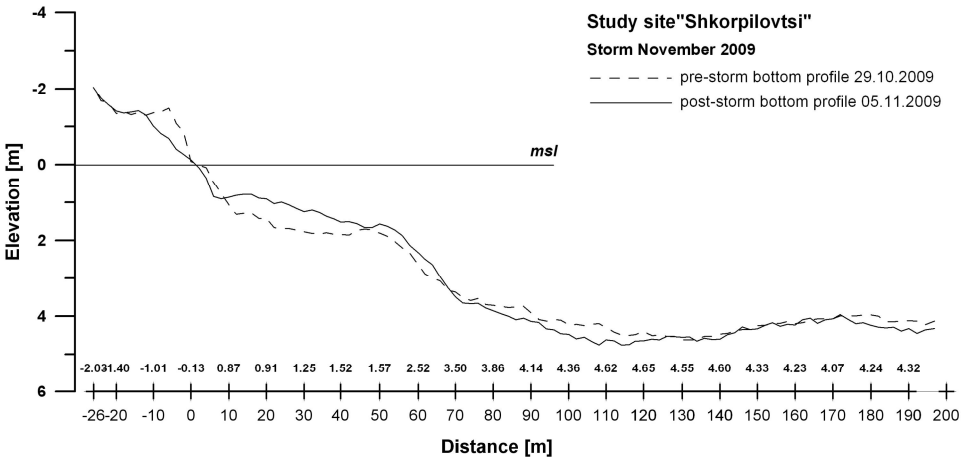

Figure 9.8 Pre-storm and post-storm profiles along the scientific pier for storm November 2009

9.2.2.4 December 2009

A similar situation was observed in the middle of December. Storm with duration of 120 hours distinguished with instable and varying wind and wave direction from eastern quarter. The total energy of this event was somewhat higher than the previous. The average Hs was 1.42 m, and the maximum Hs reached 2.43 m on 12.12.2009 (Figure 9.9, Table 9.5).

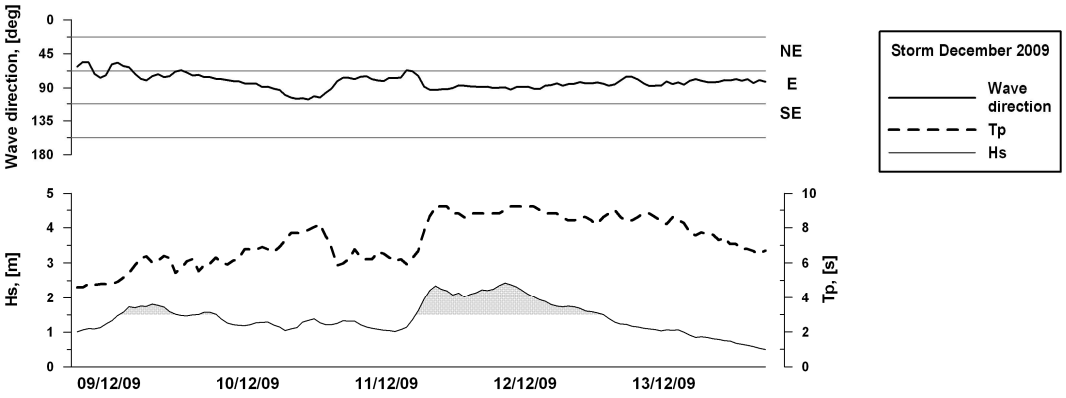

Figure 9.9 Time series of significant wave height Hs, peak wave period Tp, and mean wave direction for the storm December 2009

Table 9.5 Statistics for the storm December 2009

Wave	Duration, [h]	Hs ave, [m]	Hs min, [m]	Hs max, [m]	Tp ave, [s]	Tp min, [s]	Tp max, [s]	Theta ave, [deg]	Theta min, [deg]	Theta max, [deg]
ADCP	120	1.42	0.50	2.43	7.3	4.6	9.2	82	56	105

A field campaign covering the storm duration included pre-storm (on 19.12.2009) and post-storm (on 23.12.2009) measurements. The initial profile is characterized by a weak exposed terrace at 1.4 m depth without bar at the off-shore side of the terrace. As a result of wave action the beach face is eroded and the thickness of eroded layer here reached 0.9 m. Eroded sand was deposited between shoreline and depths of about 1.5 m. The largest erosion is observed in the next section between 1.5 m and 4 m depth – the averaged thickness of eroded layer is 0.6 m, and maximal – 1.1 m. During this storm sandy bar at 170 m was weakly affected - thickness of eroded layer on the bar was about 0.22 m (Figure 9.10).

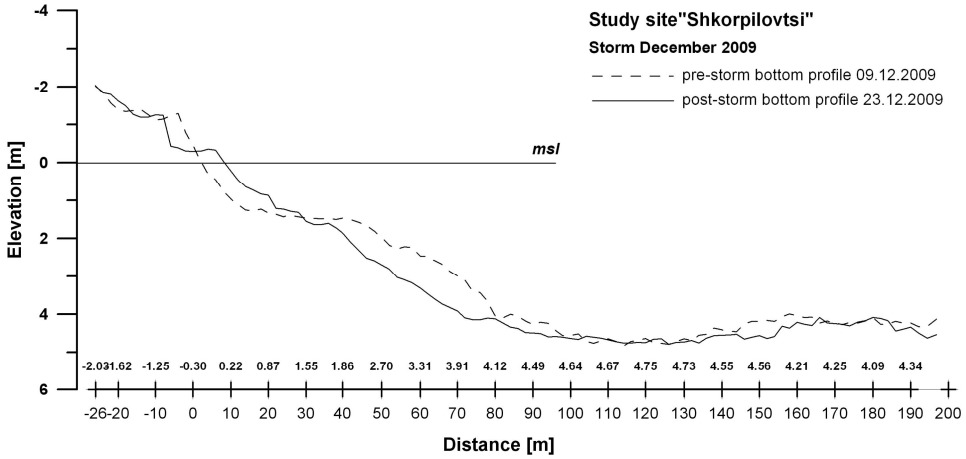

Figure 9.10 Pre-storm and post-storm profiles along the scientific pier for storm December 2009

9.2.2.5 March 2010

In the beginning of March a short but very intense storm occurred in the western Black sea. This event was distinguished with all features of the severe storms known from the historical overview – well defined phases – growth took place on 08.03, peak - 09.03 and decay - 09.03 – 10.03. Wind and wave direction were quite stable turning from ESE to ENE. Maximum Hs reached almost 4.20 m (Figure 9.11, Table 9.6).

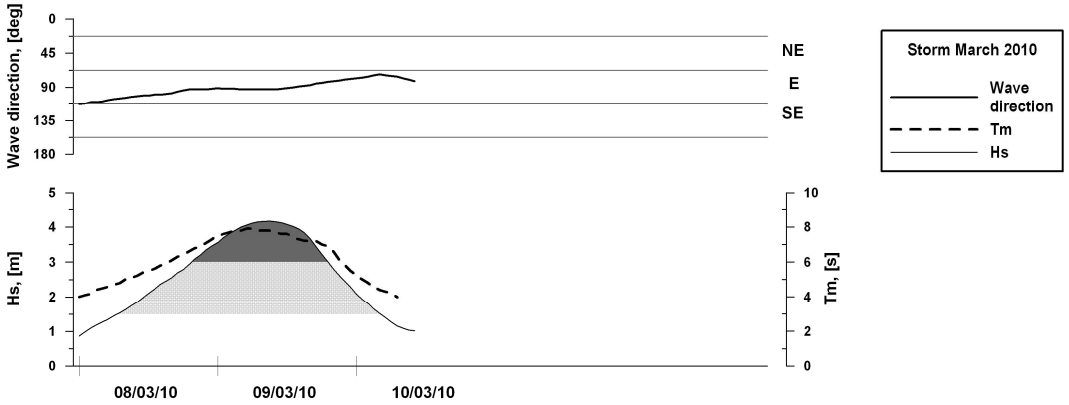

Figure 9.11 Time series of significant wave height Hs, peak wave period Tp, and mean wave direction for the storm March 2010

Table 9.6 Statistics for the storm March 2010

Wave	Duration, [h]	Hs ave, [m]	Hs min, [m]	Hs max, [m]	Tm ave, [s]	Tm min, [s]	Tm max, [s]	Theta ave, [deg]	Theta min, [deg]	Theta max, [deg]
Reanalisys	59	2.60	0.86	4.17	6.0	3.4	7.9	92	73	113

The field campaign covering the storm duration included pre-storm (on 04.02.2009) and post-storm (on 12.03.2009) measurements. The upper part of the initial profile was of convex type with inclination 3.5/100 between the landward point of the profile and depth 1.2 m, and 8.7/100 between depth 1.2 m and depth 3.9 m. As a result of wave action this convex shape is eroded – averaged thickness of eroded layer 0.42 m, and maximal – 0.92 m. During this storm sandy bar at 140–170 m was washed out – the averaged thickness of eroded layer was 0.45 m, while the maximal – 0.91 m (Figure 9.12).

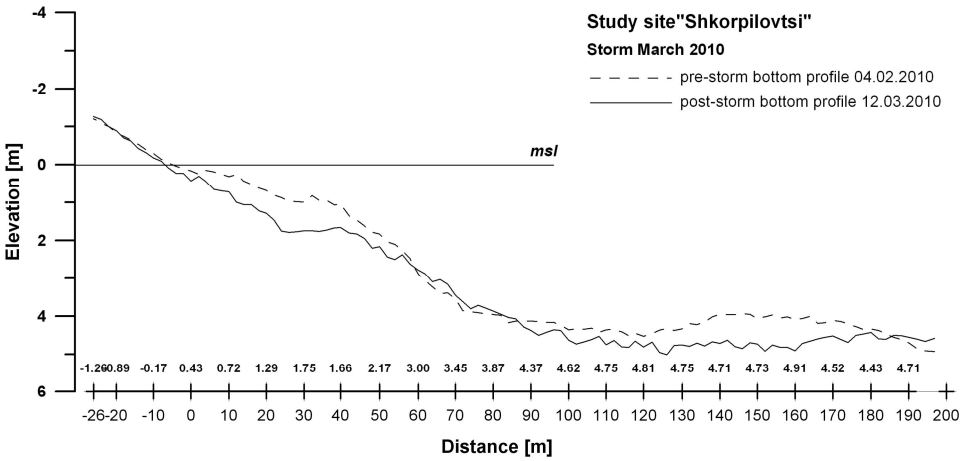

Figure 9.12 Pre-storm and post-storm profiles along the scientific pier for storm March 2010

During the described storms the offshore forcing was energetic enough to cause intense sediment transport (sheet flow regime). However, examining the duration and integral wave energy of events we concluded that 4 out of 5 events (in February, April, November and December 2009) are not relevant for model calibration. Their return period hardly reached the 1 year return period level. Only the storm of March 2010 was clearly more severe in comparison to others: The significant wave height Hs reached 4.17 m as it did not drop below 3 m for a day. The surge level increased up to 0.7 m.

The morphological response of the barred sandy cross-shore profile to a storm impact supposes not only erosion of the subaerial beach but also of the submerged bar. It can be also expected that the eroded sand would be deposited deeper than the pre-storm bar position. Such pattern was observed only after two storms - December 2009 и March 2010. Although not very energetic, only the storm of March 2010 showed typical pattern of extreme event. Therefore, exactly this storm was considered for calibration of selected models.

9.2.3 Measurements

9.2.3.1 Offshore forcing

Time series of measuring complex, installed in the middle of the scientific pier, were used for the model calibration. Among them storm surge data, measured with radar sea level gauge VEGAPULS61, were the most important input. The sea level peak (0.7 m) coincided with the maximum of Hs and occurred in a time span when wind was directed from ENE, i.e. normally to the shore (Figure 9.13). However, continuous unfavorable weather conditions in February prevented ADCP deployment. Therefore, wave conditions during the storm were estimated using the reanalysis forcing.

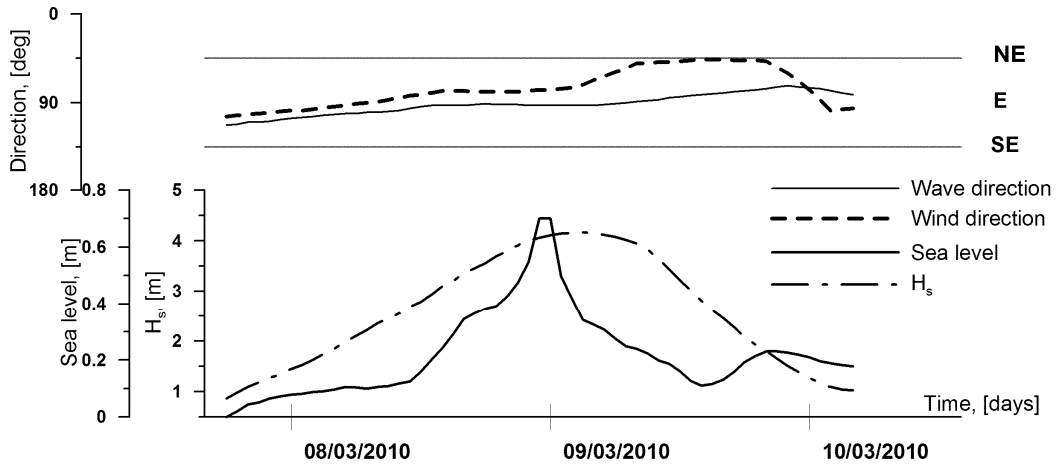

Figure 9.13 Sea level measured at Shkorpilovtsi study site combined with wave and wind parameters during the storm in March 2010

9.2.3.2 Topography and bathymetry

Detailed pre-storm and post-storm topography and bathymetry grids of the study site were generated for the purpose of 2D modelling. The pre-storm grid (Figure 9.14) was compiled from bathymetry data measured on 08.11.2009 and topographic survey carried out on 04.02.2010 (beach face), 11.01.2010 (beach area), and dune and inland area measured later on. The grid incorporates as well cross-shore profile data measured at every 2m along the pier up to 5 m depth.

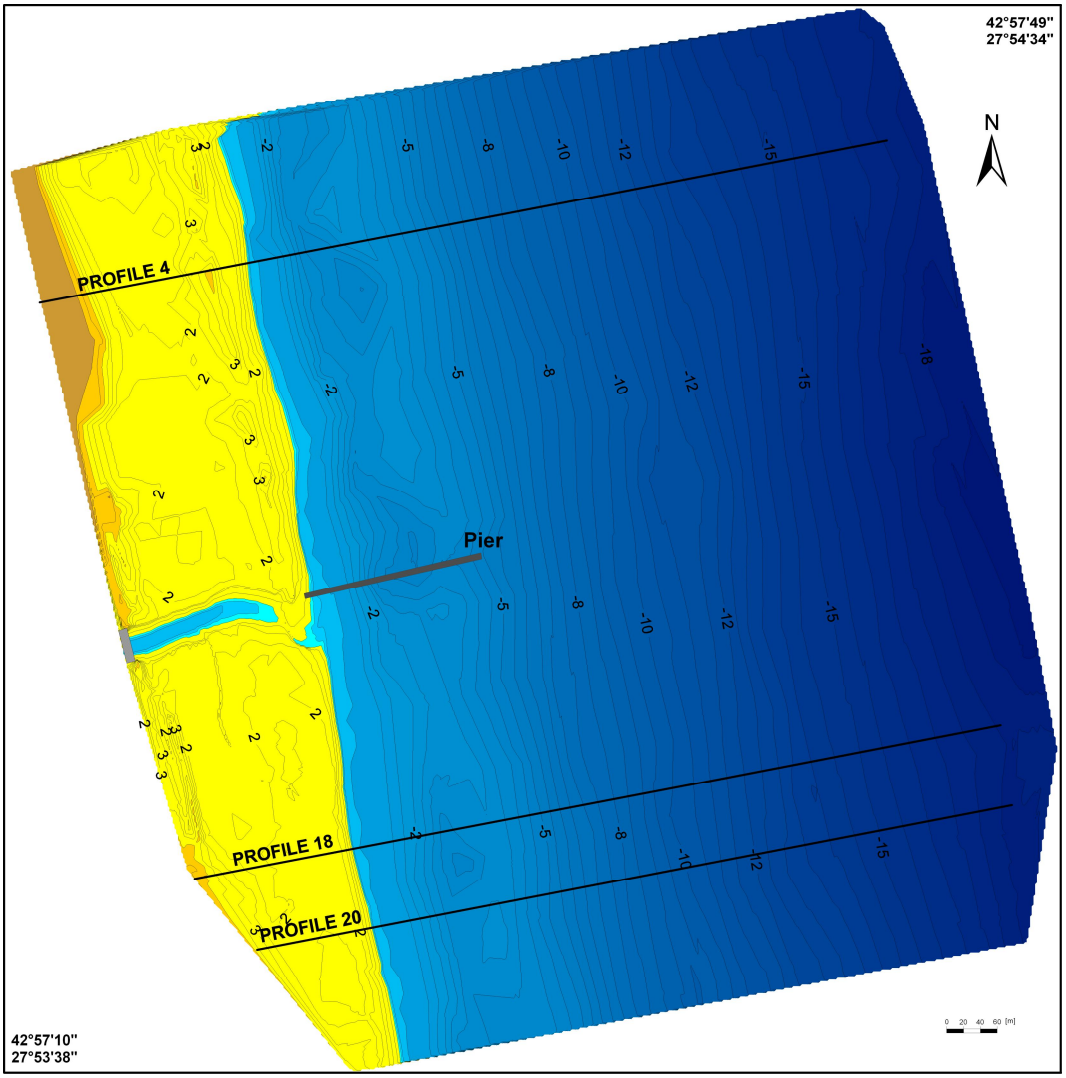

Figure 9.14 Map of pre-storm bathymetry for 2D modelling and location of transects used for 1D modelling.

The post-storm grid (Figure 9.15) comprises bathymetry measured on 21.03.2010, subaerial beach and cross-shore profile along the pier measured immediately after the storm – on 12.03.2010. The dune and inland data coincides with the pre-storm bed.

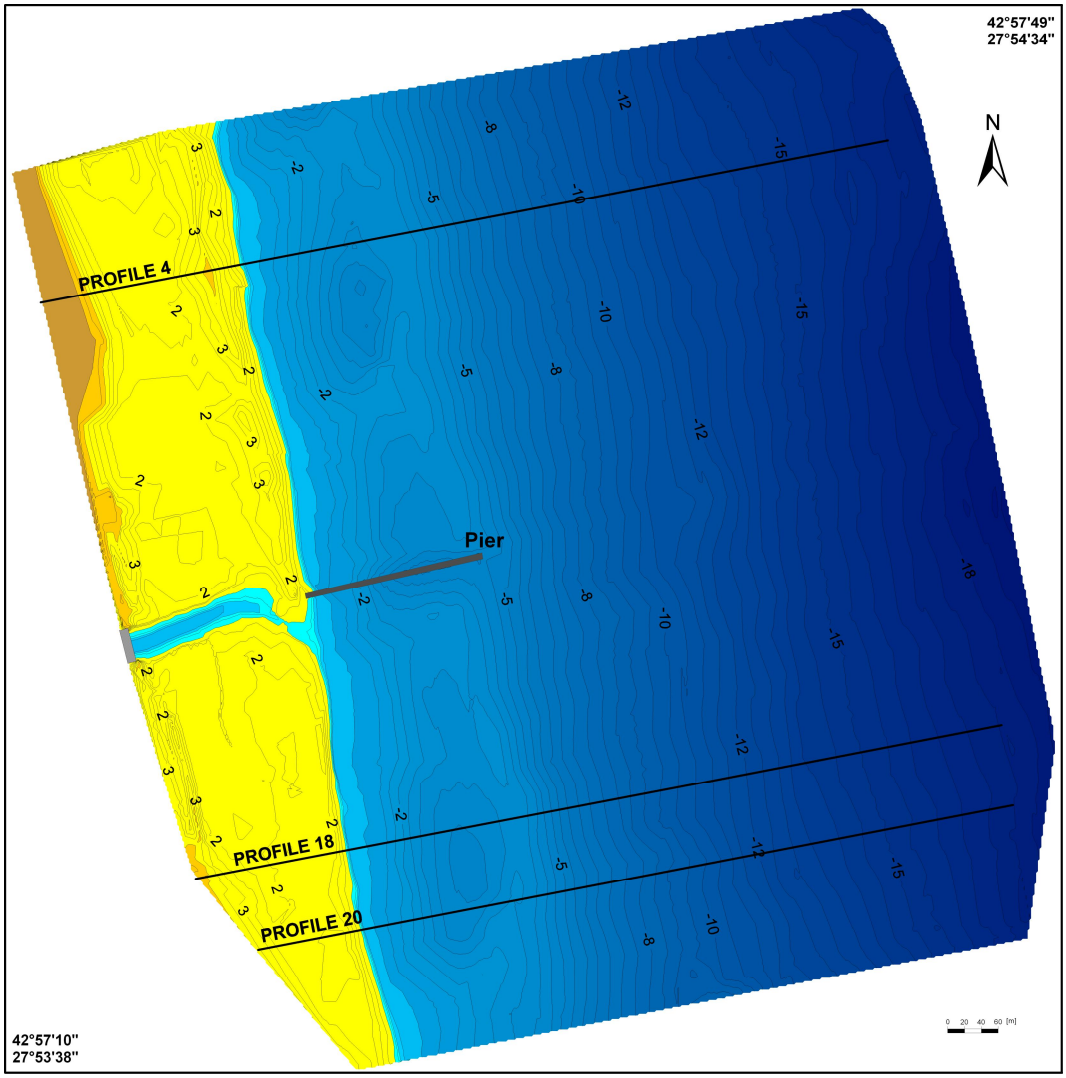

Figure 9.15 Map of post-storm bathymetry for 2D modelling and location of transects used for 1D modelling

As already described, the submerged sandy bar located at about 4 m depth is an important morphological feature. However, it is beyond the pier end. Therefore, data gathered through regular pier profile gauging are not enough to describe the storm impact comprehensively. Hence, three other profiles were selected for model calibration (Figure 9.14, Figure 9.15).

In the northern part of the site the foredune elevation at Profile 4 is about 4 m. There, the pre-storm beach berm width was about 30 m with well defined beach-face with elevation above MSL of 2.1 m (Figure 9.16). Usually, the beach berm in the north part of the site is flooded during storms with a 1-year return period. Due to the storm impact the convex shaped profile was eroded as sand was re-deposited in the trough. The bar is eroded as well and sand is re-deposited offshore of the bar.

In contrast, in the south part of the site the beach berm width varies extensively as before the storm in the area of selected profiles 18 and 20 it was about 80 m and 55 m, respectively (Figure 9.17 and Figure 9.18). During storms with a1-year return period flooding never extends to the road that is regarded as beach rear-line. Here, the beach berm height is from 2.1 m to 2.6 m.

The pre-storm profile had following features: it was of a convex type (i.e. similar to the pier profile) between the shoreline and trough before the bar; submerged bar height over the trough varied from 0.2 m to 1.0 m for the selected profiles. As a result of wave action beach berm eroded and shoreline retreated. The maximum thickness of eroded layer reached 1.6 m at Profile 20. Submerged profile portion was eroded everywhere between the shoreline and bar and sand re-deposited offshore of the bar.

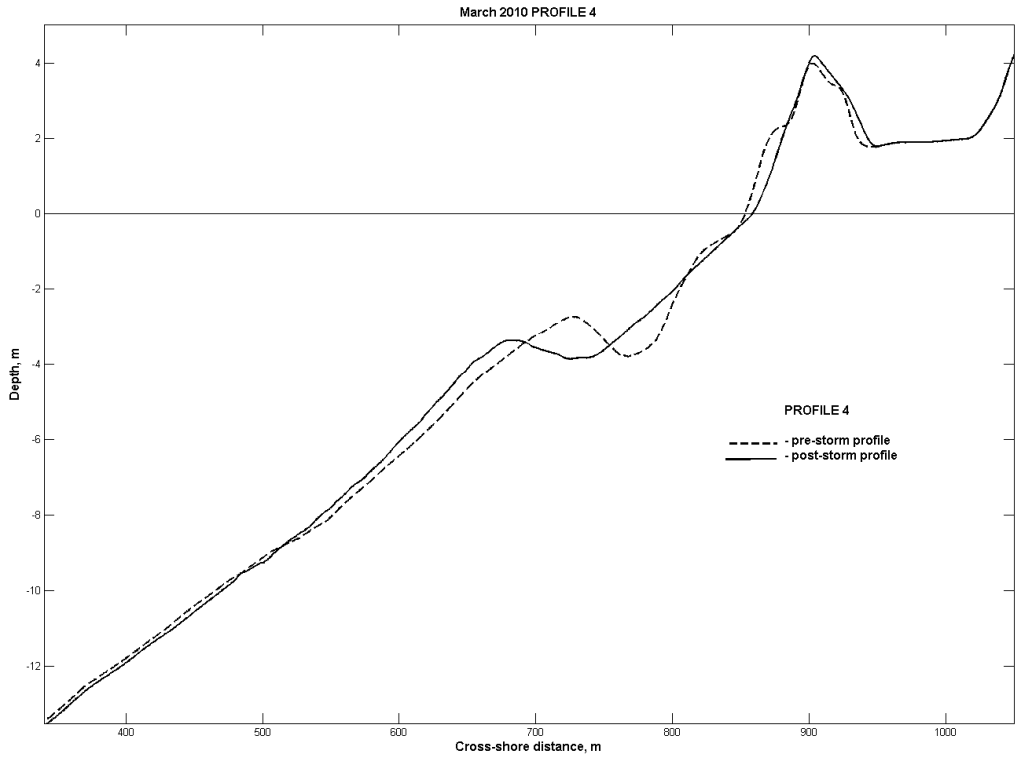

Figure 9.16 Pre-storm and post-storm profiles along the Profile 4, shown in Figure 9.14 and Figure 9.15 for storm March 2010

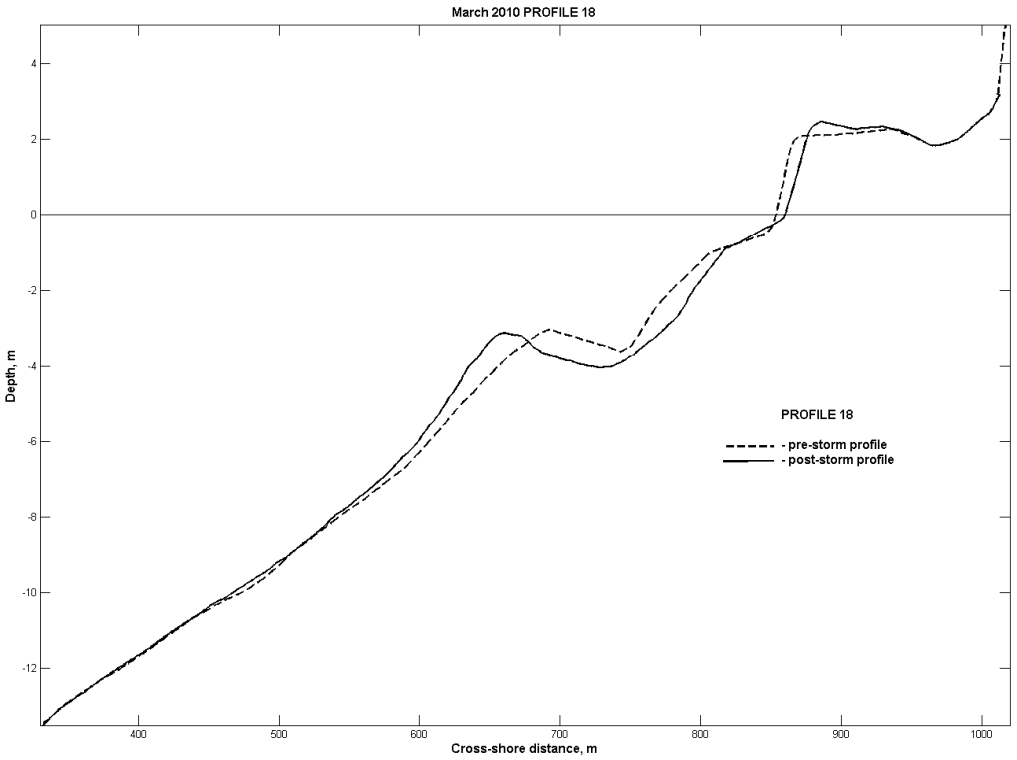

Figure 9.17 Pre-storm and post-storm profiles along the Profile 18, shown in Figures 14 and 15 for storm March 2010

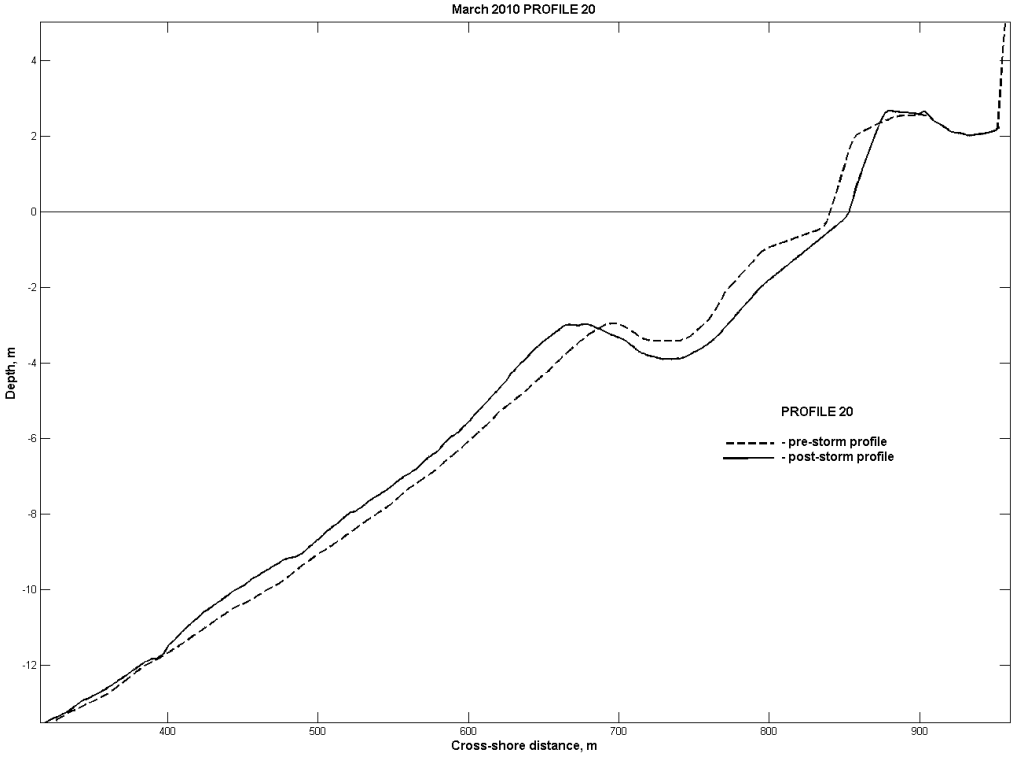

Figure 9.18 Pre-storm and post-storm profiles along the Profile 20, shown in Figure 9.14 and Figure 9.15 for storm March 2010

9.3 Model results

Model efforts were focused on 1D and 2D modelling. 1D implementation of two selected models was carried out and models were calibrated with field data. XBeach was used for the 2DH modelling.

9.3.1 Simulation results with off-the-shelf model

The IO-BAS morphodynamical model (Trifonova, 2007) was used as the off-the-shelf model. The IO-BASMM was calibrated considering grain size pattern along the cross-shore profile. The model was run for three selected profiles with grain size distribution being: uniform (D50=0.3mm; D50=0.4mm) and variable along the profile in accordance with measurements at the study site (D50 varies from 0.40 at the subaerial beach to 0.13 mm at 18 m depth).

Berm erosion is predicted only for Profile 18 for the case of variable sediments, while in other two cases IO-BASMM does not predict it (Figure 9.19, Figure 9.20, Figure 9.21). Furthermore, the model predicts erosion of the convex profile portion between shoreline and bar and re-deposition of sand in the trough for all profiles which in reality happens only at Profile 4. Hence, the model does not predict the erosion pattern in the upper portion of the submerged profile for 18 and 20. Erosion of submerged bar is predicted for all three profiles, but the model locates the offshore sand re-deposition at depths of 10-12 m, while actually this happened at 4 – 8 m. Brier skill score for tests with IO-BASMM are presented in Table 9.7. Positive BSS are calculated only for Profile 04, while for profiles 18 and 20 for all test cases BSS are negative.

Table 9.7 Brier skill score for IO-BASMM

Profile No	Variable grain size	Uniform grain size	
		D50=0.3mm	D50=0.4mm
Profile 04	0.36	0.46	0.43
Profile 18	-0.13	-0.14	-0.08
Profile 20	-0.12	-0.08	-0.05

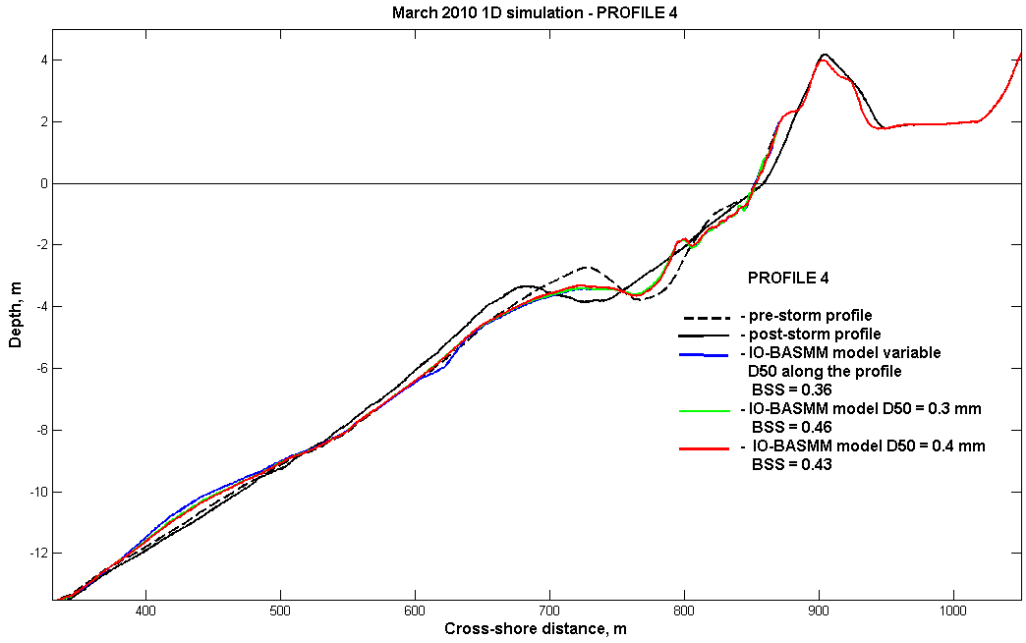

Figure 9.19 Model results of IO-BASMM for the Profile 4

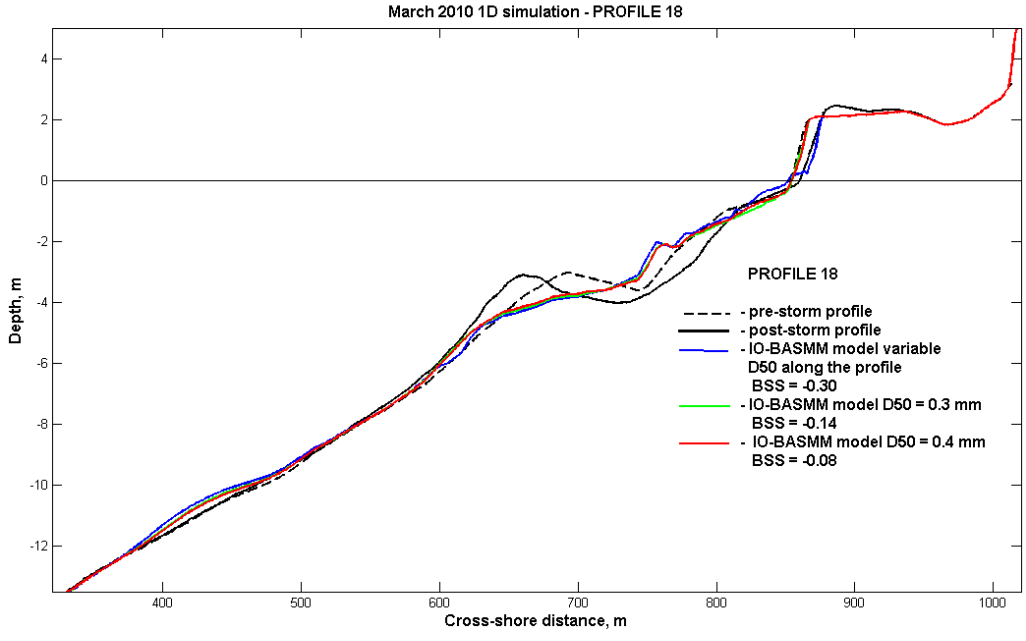

Figure 9.20 Model results of IO-BASMM for the Profile 18

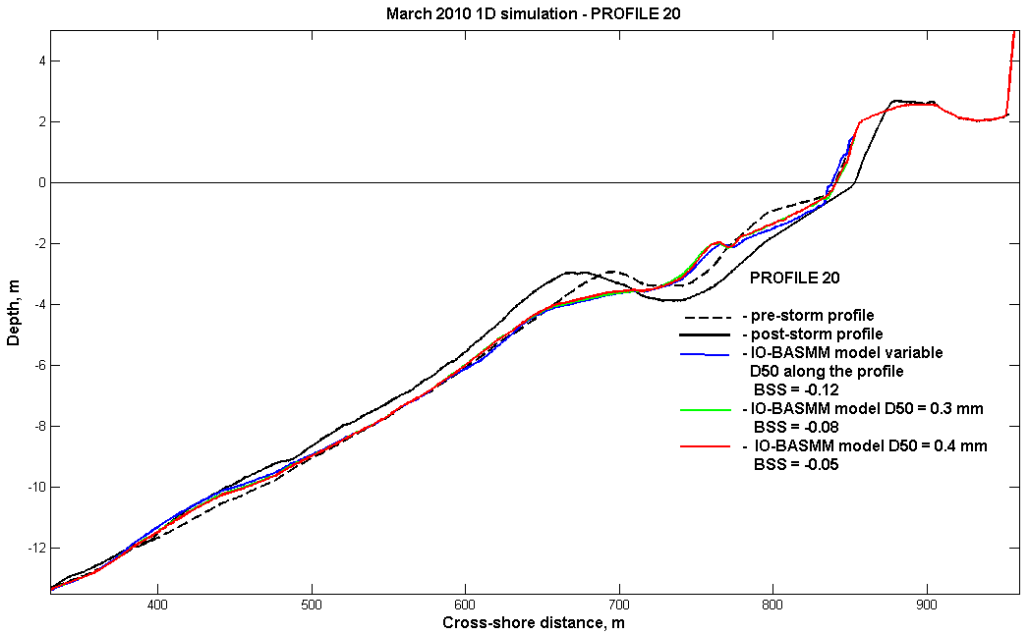

Figure 9.21 Model results of IO-BASMM for the Profile 20

9.3.2 Simulation results with XBeach model

XBeach 2DH model was used for 1D and 2D simulations of March 2010 storm. 1D simulations were performed with Revision Range 1440 of XBeach, while Revision 1629M was used for 2D simulations. The duration of simulation was 59 hours and hydrodynamic conditions at the offshore boundary were refreshed at every hour. The wave input was introduced through instat = 41 (i.e. a table of sea states). Surge input was applied uniformly along the offshore boundary. The parameter morfac was set to 10 for all simulations, while a directional spreading coefficient of 1000 used for 1D cases. A variable grid was used for all simulations. The grid dimensions of the profiles used for 1D modelling are as follows: Profile 4 is 1100 m long, with depths between -18 and 10 m (nx=218), Profile 18 – 1026 m long with depths between -18 and 5 m (nx=190), and Profile 20 is 966 m long with depths between -18 and 5 m (nx=163). The dimensions of the 2D grid are 1200 m in cross-shore direction and 1175 m in long-shore direction (nx=145, ny=108). Different parameters were considered, as the most influential for 1D tests appeared to be the parameter facua (controlling onshore transport) and sediment grain size distribution. Herein, only selected results are shown. XBeach was run in 1D mode on the three selected profiles (Figure 9.22, Figure 9.23, and Figure 9.24). Profile 18 (Figure 9.23) was selected for testing of four different facua values (-0.5; -0.2; 0.0; 0.2). In addition, tests were performed with two different types of sediment distribution on Profile 4 (Figure 9.24). The first case was with uniform sediments distribution (D50 = 0.3 mm), and the second one was with four sediment fractions varying in off-shore direction from 0.4 mm to 0.15 mm.

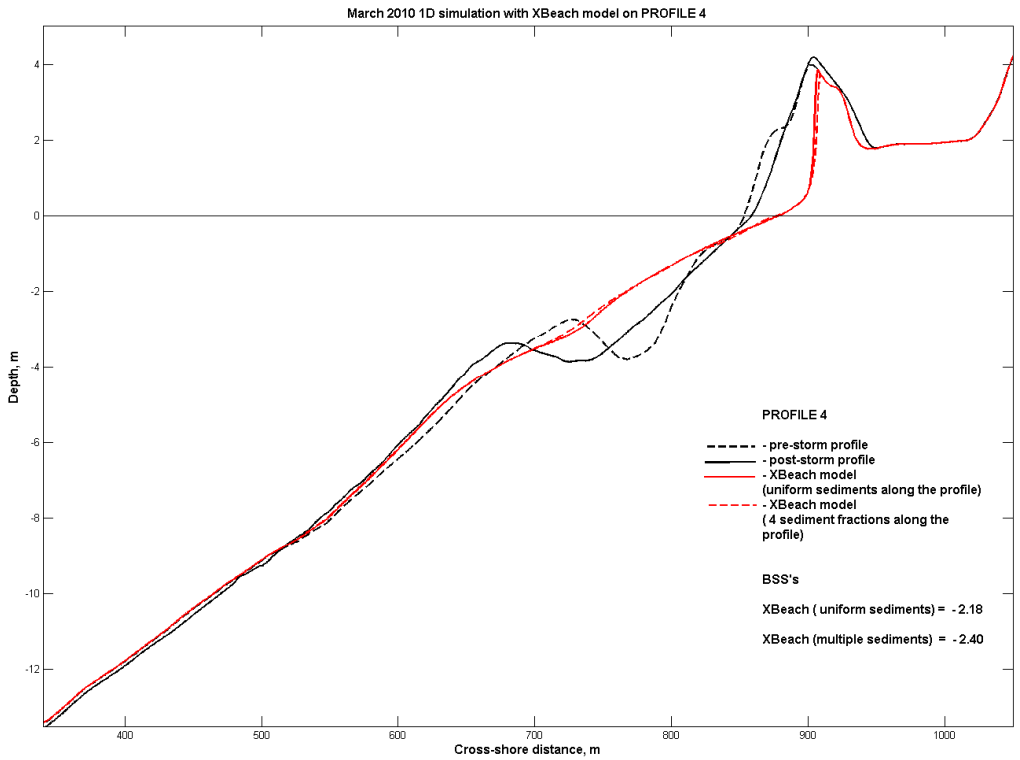

Figure 9.22 Model results of XBeach for the Profile 4

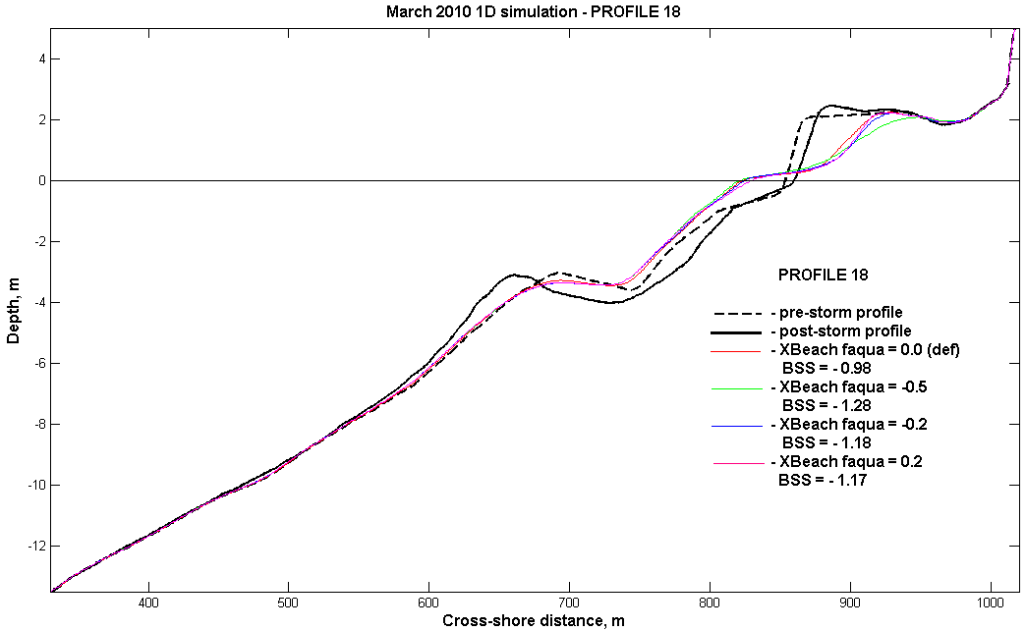

Figure 9.23 Model results of XBeach for the Profile 18

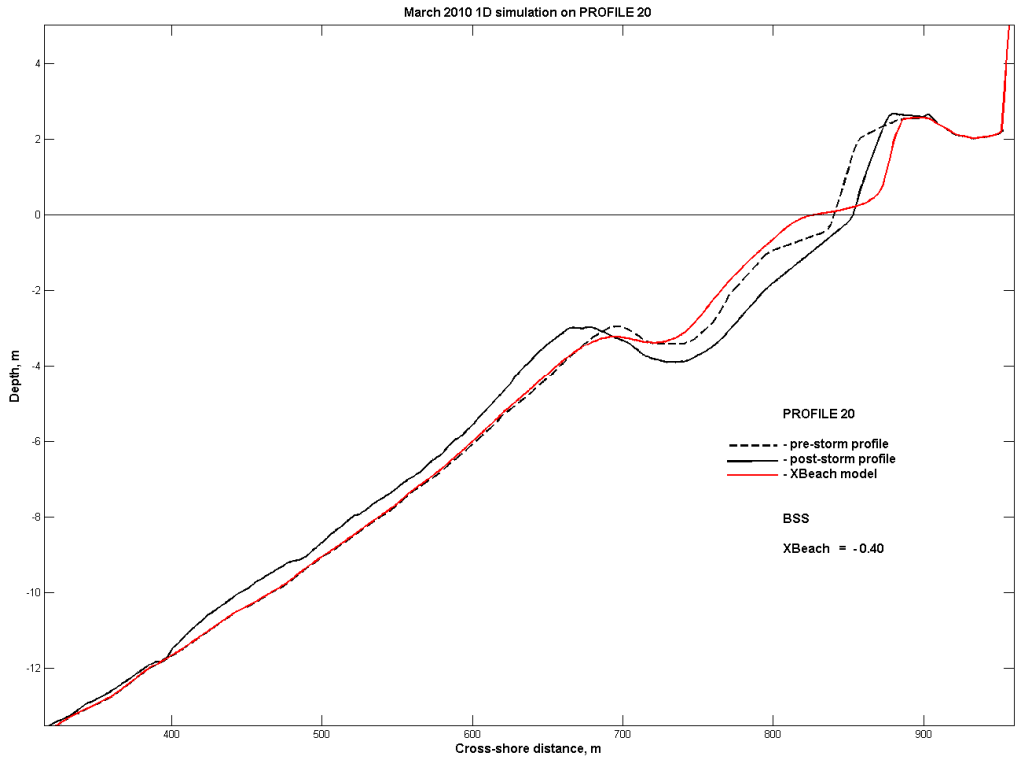

Figure 9.24 Model results of XBeach for the Profile 20

XBeach over-predicts the berm erosion causing re-deposition of the sand in the vicinity of the shoreline (Figure 9.22, Figure 9.23, and Figure 9.24). XBeach predicts re-deposition of the sand between the shoreline and the bar for all profiles, while there is erosion observed all over at this location for profiles 18 and 20. Erosion of submerged bar and re-deposition of sand offshore the bar is predicted for all three profiles, but the observed off-shore bar migration is not reproduced.

Brier skill score for 1D tests with XBeach are presented in Table 9.8. 1D XBeach does not produce positive BSS for any of the selected profiles.

Table 9.8 Brier skill score for 1D XBeach

Profile No	**Default settings /red line/**	**Additional tests**	
		Variable parameter	BSS
Profile 04	-2.18	Multiple sediments	-2.40
Profile 18	-0.98	faqua=-0.5 faqua=-0.2 faqua= 0.2	-1.28 -1.18 -1.17
Profile 20	-0.40	-	-

The 2D XBeach results reflect overall erosion-accretion pattern resulting from the March 2010 storm impact: berm erosion, sand deposition in the trough between shoreline and bar, bar erosion and accretion behind the bar (Figure 9.25 – right panel). It could be seen that strong berm erosion occurred along the whole beach area (Figure 9.25 left panel), as the maximum erosion of 1.6 m was registered in the southern part (Profile 20). The sandy spit blocking the river mouth was washed away during the storm as well.

Three notable patches of accumulation can be observed between the shoreline and the submerged bar. The sand of the upper part of the submerged bar was eroded and displaced offshore causing bar migration.

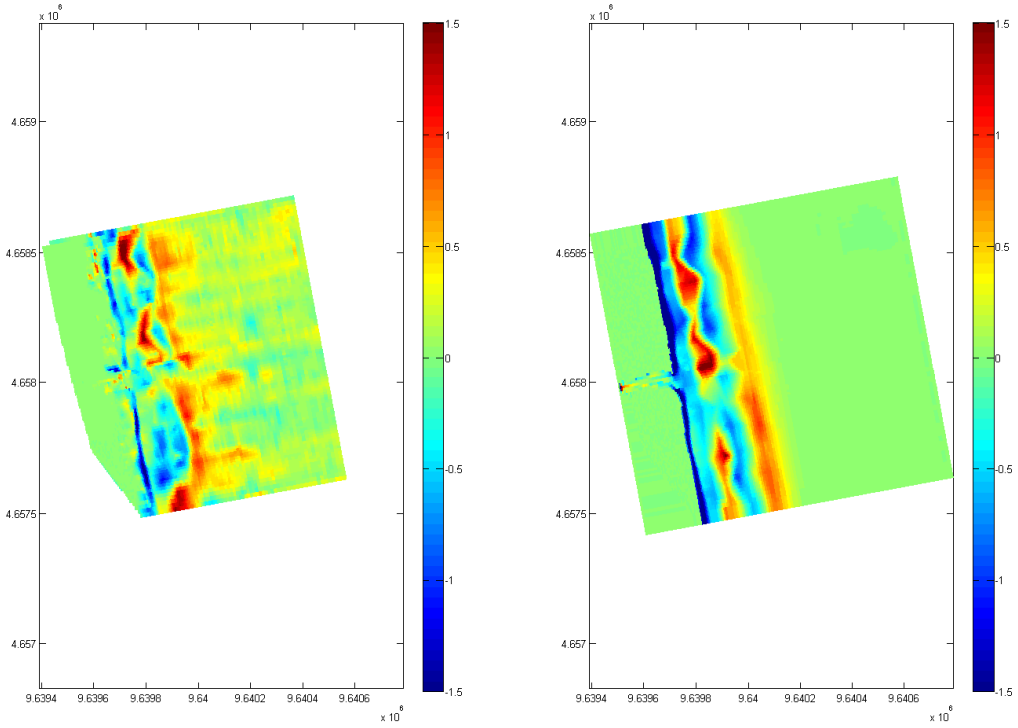

Figure 9.25 Measured deformations (left panel), calculated deformations (right panel)

In order to compare 2D and 1D model performance, three transects of the 2D pre-storm, post-storm and calculated grids were extracted coinciding with the Profiles 4, 18, and 20 used for 1D modelling (Figures 9.26-9.28). In comparison with the 1D XBeach results (Figures 9.22-, 9.24, replotted in Figures 9.26-9.28 as the red dashed lines) here the berm erosion is considerably less at all profiles. Erosion spreads not only over the sub-aerial beach but is predicted also down to depths of about 2 m. However, profile shape at deeper profile portion (at depths between 0.5 and 5 m) is predicted as a uni-sloped surface, i.e. the trough and bar are not present. It should be noted that XBeach is not intended as a bar-migration model.

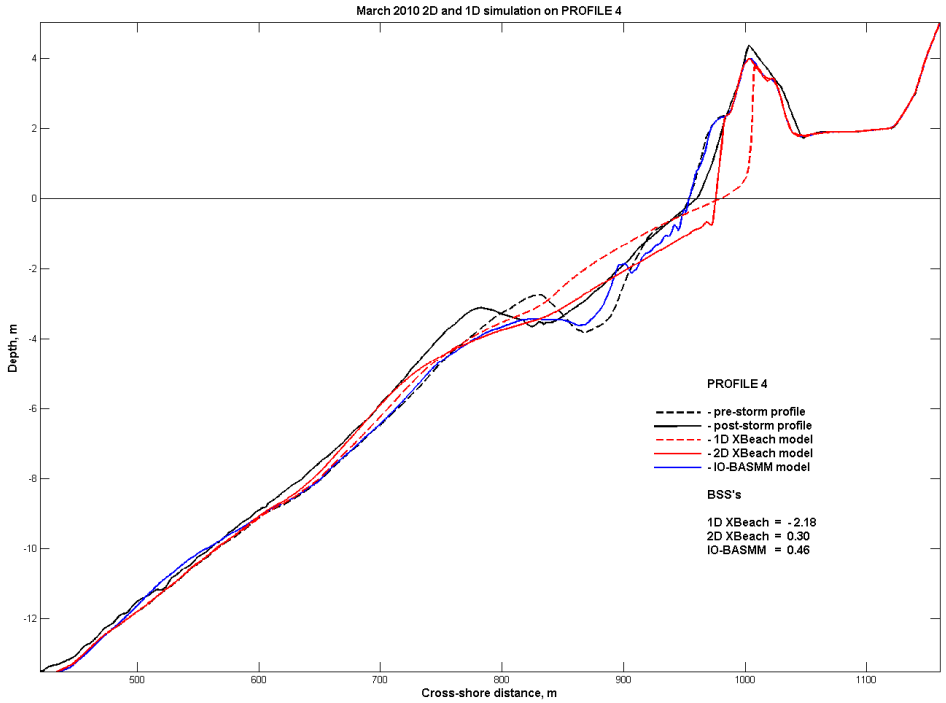

Figure 9.26 Model results of 2D XBeach simulation sliced at Profile 4

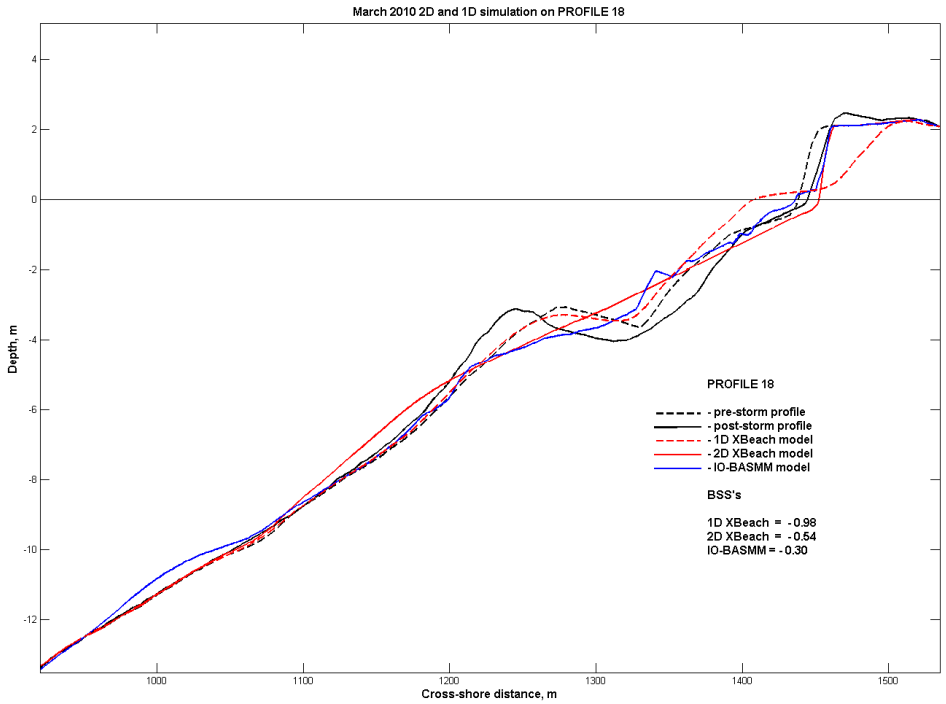

Figure 9.27 Model results of 2D XBeach simulation sliced at Profile 18

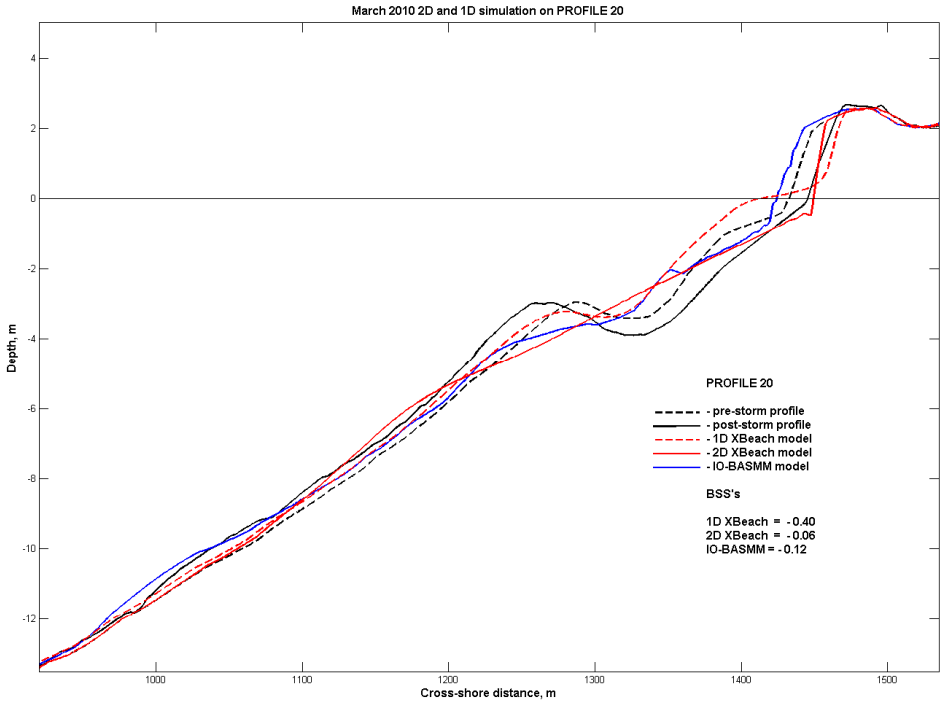

Figure 9.28 Model results of 2D XBeach simulation sliced at Profile 20

Brier skill score for tests with 2D XBeach are presented in Table 9.8. Positive BSS are only for Profile 04, while for profiles 18 and 20 BSS are negative.

Table 9.9 Brier skill score for 2D XBeach

Profile No	BSS
Profile 04	0.30
Profile 18	-0.54
Profile 20	-0.06

9.4 Synthesis

Comparison of results obtained by means of two models (IO-BASMM and 1D XBeach) shows that neither of them give satisfactory results at the sub-aerial beach. XBeach overestimates berm erosion in all cases, while IO-BASMM does the contrary except for the simulation over Profile 18 (Figure 9.20). Variable parameter facua has an effect mostly on berm erosion, as maximum erosion rate is predicted using facua=-0.5. Introduction of multiple sediment fractions does not improve the predicted erosion pattern but slightly increase berm erosion.

In the profile portion between shoreline and trough, where erosion takes place during storm, IO-BASMM predicts small erosion (i.e. underestimates erosion), while XBeach predicts deposition. Submerged bar erosion is underestimated by XBeach, and deposition is not reflected in two model outputs (Profiles 18 and 20 – Figure 9.23 and Figure 9.24). IO-BASMM reproduces bar erosion, but both quantity and location of sand deposit off-shore is not

predicted correctly. Described model performance results in either negative or very low BSS values for both models (Tables 9.7, Table 9.8)

2D XBeach implementation shows considerably better prediction of berm erosion, although the case is not the same with respect to the bar. Moreover, calculated maximum run-up represents very well observed post-storm state of the sub-aerial beach and almost coincides with measured impact (Figure 9.29).

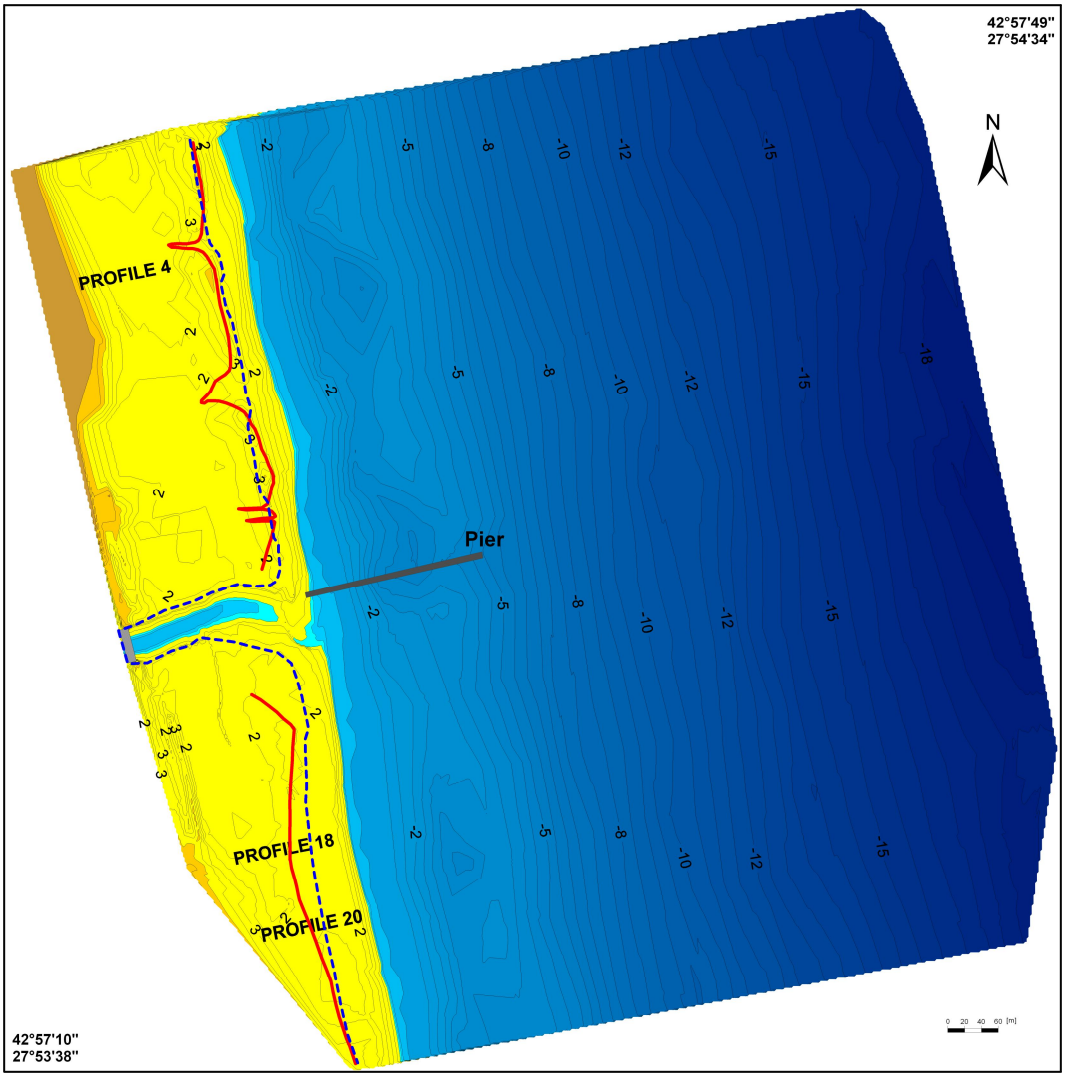

Figure 9.29. Maximum wave run-up position: observed (red line) and calculated (dashed blue line)

9.5 Conclusions

Two morphodynamical models were calibrated and their performance was assessed against field measurements. In order to evaluate the model capability to reproduce storm impact on the study site it should be pointed out that model output will be used to sustain a warning system. Having in mind that all storm impact indicators are related to changes at the sub-aerial beach it can be concluded that 2D XBeach is the most appropriate modelling option. This is corroborated by the reliable prediction of beach berm erosion and maximum run-up.

10 Testbed, the Netherlands

10.1 Objectives

The field data available form the MICORE project are a valuable source for the development, calibration and validation of models such as XBeach. Especially since the data covers a wide range of situations with several storm impact regimes (dune erosion, overwash and breaching), different type of hydrodynamic boundary conditions (relative importance waves, tide and surge) and a range of geotechnical properties (grain size distribution and associated beach steepness, the presence of hard elements).

A shortcoming of the MICORE dataset (and of field data in general) is that the measured storm conditions do not correspond to normative storm conditions for which the Dutch design our water defenses and which have a small probability of occurrence (1/10000 per year). In addition the real world is usually so complex and the availability of measurements in detail is limited that it is difficult to associate the measured response to physical processes in detail. This is desirable if we want to extend the description of physical processes in the model.

Therefore, in addition to the field data from MICORE, other data sources (especially from the laboratory but also normative field measurements) are used to develop, calibrate and validate the XBeach model. This data is stored (like the MICORE cases) in an automated testbed environment that weekly produces a report describing the (quantified) performance of the latest model version.

In the MICORE project the automated testbed environment appeared to be a useful tool in the development of the XBeach code (which was required to asses the various sites) and in the understanding of measured storm response in the field campaigns. Therefore the testbed report is attached as an additional WP4 product and is presented in Appendix L.

11 References

Akouango, E., 1997. Morphodynamique et dynamique sédimentaire dans le Golfe du Lion. Contribution à l'étude de la zone côtière dans l'actuel et le Quaternaire récent. Unpublished Thesis, Univ. de Perpignan, 200 p.

Andrews, D.G. and McIntyre, M.E., 1978. An exact theory of nonlinear waves on a Lagrangian-mean flow. Journal of Fluid Mechanics, 89(4): 609-646.

AWK, 1998. Kustlijnkaarten, evolutie tot mei 1998. Deel 1 : Franse Grens tot Oostende (in Dutch)

AWK, 1999. Kustlijnkaarten, evolutie tot mei 1999. Deel 1 : Franse Grens tot Oostende (in Dutch)

Bailard J.A. 1981. An energetics total load sediment transport model for a plane sloping beach. *J. of Geophys. Res.* V.86. № C 11. 10938–10954.

Battjes, J.A., and J.P.F.M. Janssen (1978) Energy Loss and Set-Up due to Breaking of Random Waves. Proc. of the 16th Int. Conf. On Coastal Eng. pp. 569-587, Hamburg, 569-587.

BCEOM. Étude générale pour la protection et l'aménagement durable du Lido de Sète à Marseillan, Volet Érosion. Montpellier, BCEOM, juin 2000. 110p (in French).

Belberov, Z., Zahariev, V., Krylov, Y., Kostichkova, D., Manyarova, R., Polyakov, Y., 1982. Analysis of the catastrophic storm in February 1979 near the Bulgarian Black sea coast, Oceanology, Sofia, 9, 3-12 (in Bulgarian).

Blott, S. J. & Pye, K., 2003. Sefton coast, intertidal sediment survey in 2003 - results summary and interpretative report, external investigation, Report ER502, Kenneth Pye Associates Ltd.

Booij, N., R.C. Ris and L.H. Holthuijsen (1999). A third generation wave model for coastal regions, Part I, Model description and validation. J. Geophys. Res., 104, C4, 7649-7666.

Broker Hedegaard, I., Deigaard, R. and Fredsoe, J., 1991. Onshore/Offshore sediment transport and morphological modelling of coastal profiles. In: Coastal Sediments '91, ASCE, Seattle, WA, Vol. 1, pp. 643-657.

Caplin, R. E., 1991. A comparison of past and present foreshore profiles along a section of the Sefton coast to assist coastal management. Liverpool Polytechnic.

Carrasco, A.R., Ferreira, Ó., Davidson, M., Matias, A., Dias, J.A., 2008. An evolutionary categorisation model for backbarrier environments. Marine Geology, 251, 156-166.

Cieślikiewicz, W., Paplińska-Swerpel, B., 2008. A 44-yearhindcast of wind wave Fields over Baltic Sea. Coast.Engng. 55, 894-905. Seifert, T., Kayser, B., 1995. A High Resolution Spherical Grid Topography of the Baltic Sea. Meereswissenschaftliche Berichte, vol. 9. Institut für Ostseeforschung,Warnemünde, pp. 72–88.

Correia, F., Dias, J., Boski, T., Ferreira, Ó., 1996. The retreat of the eastern Quarteira cliffed coast and its possible causes. In: Jones, P., Healy, M., Williams, A. (eds.), Studies in European Coastal Management. Samara Publishing Limited, Cardigan, pp. 129-136.

Devoy, R. J. N. (2000). Climate warming and the links to the coast. ICE (Joint Ireland-Wales EU Interreg Project) Newsletter, March 2000.

DHI, 2009. LITPROF, http://www.dhigroup.com/Software/Marine/LITPACK/...

Details/LITPROFModule.aspx

Dias, J.A., 1986. Observações sobre a origem das areias das ilhas barreira da Ria Formosa. Proceedings of IV Congresso do Algarve, RACAL Clube, 579-587 (in Portuguese).

Dias, J.A., 1988. Aspectos geológicos do Litoral Algarvio. Geonovas, 10, 113-128 (in Portuguese).

Dodet, G., Bertin, X. and Taborda, R., 2010. Wave climate variability in the North-East Atlantic Ocean over the last six decades. Ocean Modelling, 31(3-4): 120-131.

Dolbeth, M., Ferreira, Ó., Teixeira, H., Marques, J.C., Dias, J.A., Pardal, M.A., 2007. Beach morphodynamic impact on a macrobenthic community along a subtidal depth gradient. Marine Ecology Progress Series, 352, 113-124.

Draper, L. (1992). Wave Climate Atlas of the British Isles. HMSO, London.

Draper, L., Carter, D. J. T., 1982. Waves at Morcambe Bay light vessel in 1957. Summary and interpretation report, IOS Report, UK.

Dudzińska-Nowak J., 2006 Coastline Long-term Changes of the Selected Area of the Pomeranian Bay, Coastal Dynamic, Geomorphology and Protection, A.Tubielewicz (red.), EUROCOAST – LITTORAL 2006, Gdańsk, pp.163-170.

Elfrink, B., Brøker, I. and Deigaard, R. (2000) Beach profile evolution due to oblique wave attack. Proc. 27th Int. Conf. on Coastal Engineering, ASCE, Sydney.

Engelund, F. and Fredsøe, J. (1976) A sediment transport model for straight alluvial channels, Nordic Hydrology, 7, pp. 296-306.

Esteves, L.S., Williams, J.J., Nock, A., Lymbery, G., 2009. Quantifying shoreline changes along the Sefton Coast (UK) and the implications for research-informed coastal management. Journal of Coastal Research SI 56, 602-606.

Esteves, L.S., Brown, J.M., Williams, J.J., and Lymbery, G. 2010. Quantifying thresholds for significant dune erosion along the Sefton Coast, northwest England. Geomorphology (submitted).

Ferreira, Ó. 2005. Storm groups versus extreme single storms: Predicted erosion and management consequences. *Journal of Coastal Research* 42:155-161.

Ferreira, Ó., Garcia, T., Matias, A., Taborda, R., Dias, J.A., 2006. An integrated method for the determination of set-back lines for coastal erosion hazards on sandy shores. Continental Shelf Research, 26, 1030-1044.

Ferreira, Ó., Vousdoukas, M.V., and Ciavola, P. 2009. MICORE Review of Climate Change Impacts on Storm Occurrence (Open access, Deliverable WP1.4). https://micore.eu/area.php?idarea=28.

Feser, F., Weisse, R., von Storch, H., 2001. Multi-decadal atmospheric modelling for Europe yields multi-purpose data. Eos 82 (28) (July 10).

Folk, R.L. 1980. *Petrology of the Sedimentary Rocks*. Austin, Texas, U.S.A: Hemphill Publishing Company.

Fredsøe, J., Andersen, O.H., and Silberg, S. (1985) Distribution of Suspended Sediment in Large Waves. Journal of Waterway, Port, Coastal and Ocean Engineering, ASCE, Vol. III, No. 6, pp. 1041-1059.

Furmańczyk, K., Dudzińska, j., 2001. Krajobraz morskiej strefy brzegowej Zatoki Pomorskiej (odcinek Świnoujście – Pogorzelca), Ogólnopolska Konferencja XV – lecia Wydziału Nauk Przyrodniczych, Szczecin – Łukęcin, 15 – 17.11.2001r. Człowiek I Środowisko Przyrodnicze Pomorza Zachodniego, 2001,s.33-34.

Furmańczyk, K., Musielak, S., 2002 Importan Features of Coastline Dynamics in Poland "Nodal Points" nad "Gates" in Baltic coastal Ecosystems – Structure, Function and coastal zone management. CEEDES – Series, Springer, Berlin 2002 p.141-147.

Furmańczyk, K., Dudzińska-Nowak, J., 2008 Prediction of the coastal erosion on a base of remote sensing method – selected example of the South Baltic. LITTORAL 2008. Proceedings. 8pp (CD) .

Galappatti, R. and Vreugdenhil, C.B. (1985), A depth integrated model for suspended transport, Journal of Hydraulic Research, 23(4), 359-377.

Gama, C., Dias, J.A., Ferreira, Ó., Taborda, R., 1994. Analysis of storm surge in Portugal, between June 1986 and May 1988. Proceedings of the Second International Symposium on Coastal Zone Research-Management and Planning, EUROCOAST, (Lisbon, Portugal), pp. 381-387.

Gresswell, R. K., 1937. The geomorphology of the south-west Lancashire coastline. The Geographical Journal 90, 335-348.

Gresswell, R. K., 1953. Sandy Shores in South Lancashire. Liverpool University Press, Liverpool, 181pp.

Halcrow, 2009. North West England and North Wales Shoreline Management Plan 2 (consultation draft, revision 1 Oct. 2009), Appendix C: Baseline Processes, 40p. Available online from http://mycoastline.org/documents/AppendixC-C.4F_Seftoncoast.pdf (accessed on 23 Feb. 2010).

Halliwell, A. R., 1973. Residual drift near the sea bed in Liverpool Bay; an observational study. Geophys. J. Roy. Astronom. Soc., 32, 439-458.

Holt, J.T., James, D.J., 2001. An s coordinate density evolving model of the northwest European continental shelf: 1. Model description and density structure. Journal of Geophysical Research 106, 14015–14034.

Houthuys R., 2008. Studie naar de erosietrends langsheen de Belgische kust, study carried out for AWK.

HRS, 1977. Sand winning at Southport. Hydraulics Research Station Rept., EX 708, Wallingford, UK.

IMDC, 2004. Veiligheid Vlaamse Kust, report I/RA/11226/04.001/ktr (in Dutch)

IMDC, 2005. Hydraulisch Randvoorwaardenboek Vlaamse Kust (I/RA/11226/03.041/KTR) (in Dutch)

IMDC, 2010. Analyserapport metingen in het kader van Micore, in opmaak. (cfr.NO10130) (in Dutch).

Jacob, D. and R. Podzun, 1997. Sensitivity studies with the regional climate model REMO. Meteorol. Atmos. Phys. 63, 119–129.

Jay, H. 1998. Beach–Dune Sediment Exchange and Morphodynamic Responses: Implications for Shoreline Management, The Sefton Coast, NW England. PhD Thesis, University of Reading, 353p.

Jones, J. E. and A. M. Davies (1997). "Storm surge computations for the eastern Irish Sea including wave-current interaction." Annales Geophysicae, 15, Supplement II: p.C379.

Jones, J. E. and A. M. Davies (1998). "Storm surge computations for the Irish Sea using a three-dimensional numerical model including wave-current interaction." Continental Shelf Research, 18: 201-251.

Kalnay, E., Kanamitsu, M., Cistler, R., Collins,W., Deaven, D., Gandin, L., Iredell, M., Saha, S., White, G.,Woollen, J., Zhu, Y., Chelliah, M., Ebisuzaki,W., Higgins,W., Janowiak, J., Mo, K.C., Ropelewski, C.,Wang, J., Leetma, A., Reynolds, R., Jenne, R., Joseph, D.,1996. The NCEP/NCAR 40-year reanalysis project. Bull. Am. Meteorol. Soc. 77, 437–471.

Kustatlas, 2008. www.kustatlas.be, viewed 1-15/07/2008 (in Dutch).

Lanckneus J., V. Van Lancker, G. Moerkerke, , D. Van Den Eynde, M. Fettweis, M. De Batist, P. Jacobs, 2002. Investigation of the natural sand transport on the Belgian continental shelf BUDGET: final report Brussels : OSTC, 2002 (SP1075)

Larson, M. and Kraus, N.C. (1989) SBEACH: Numerical modelling for simulating storm-induced beach change – Report 5: empirical foundation and model development. Technical report, CERC-89-9, U.S. Army Engineer Waterways Experiment Station, Coastal Engineering Research Center, Vicksburg, Mississippi.

Larson, M., Kraus, N. and Byrnes, M.R., 1990. SBEACH: Numerical model for simulating storm-induced beach change, Report 2: Numerical formulation and model tests, Technical Report. CERC-89-9. US Army Engineer Waterways Experiment Station, Vicksburg, MS.

Larson, M., Wise, R.A. and Kraus, N., 2004. Modelling dune response by overwash transport. In: J. Mckee Smith (Editor), Coastal Engineering 29th International Conference. World Scientific, Lisabon, Portugal, pp. 2133-2145.

Larson, M., Erikson, L., Hanson, H., 2004. An analytical model to predict dune erosion due to wave impact. Coastal Engineering 51, 675-696.

Martins, J.T., Ferreira, Ó., Ciavola, P., Dias, J.A., 1996. Monitoring of profile changes at Praia de Faro, Algarve: a tool to predict and solve problems. IN: Taussik, J., Mitchell, J. (Eds.), Partnership in Coastal Zone Management. Samara Publishing, pp. 615-622.

Mishev, K., Popov, V., Dimitrov, V., Valkanov, A., Rozhdestvenski, A. 1978. Physical and geographical features. In: Valkanov A., Marinov H., Danov H, Vladev P (Eds.), Black Sea – collection. Publ. House “G.Bakalov”, Varna, pp. 35-86.

Morton, R.A. and Sallenger, A.H., 2003. Morphological impacts of extreme storms on sandy beaches and barriers. Journal of Coastal Research, 19(3): 560-573.

Musielak S., Furmańczyk K., Dutkowski M., 2005: Plaża czy brzeg – co chronić? ZZOP w Polsce – Stan obecny i perspektywy, Problemy Erozji Brzegu, Szczecin Oficyna in Plus, str. 61-96.

Parker, W.R., 1969. A report on research conducted into aspects of the marine environment affecting coast erosion between Ainsdale and Hightown, Lancashire. Lancashire County Council (June 1969), 99p.

Parker, W. R., 1975. Sediment mobility and erosion on a multi-barred foreshore (southwest Lancashire, UK). In Hails, J. R. And Carr, A. P., (eds,), Nearshore Sediment Dynamics and Sedimentation, Wiley, London, pp. 151-177

Pye, K., Neal, A., 1994. Coastal dune erosion at Formby Point, north Merseyside, England: causes and mechanisms. Marine Geology 119, 39-56.

Pye, K., 2003. Sefton coast, comparison of intertidal sediment survey in 1996 and 2003, Report IR002. Kenneth Pye Associates Ltd.

Pye, K., Blott, S.J., Short, B. and Witton, S.J., 2006a. Preliminary Investigation of Sea Bed Sediment Characteristics in Liverpool Bay. Kenneth Pye Associates Ltd., External Research Report ER602, 169 pp.

Pye, K., Blott, S.J., Short, B. and Witton, S.J., 2006b. Sediment Properties and Sediment Transport in Liverpool Bay, Northwest England. Kenneth Pye Associates Ltd., Internal Research Report IR601.

Pye, K., Blott, S.J., 2008. Decadal-scale variation in dune erosion and accretion rates: an investigation of the significance of changing storm tide frequency and magnitude on the Sefton Coast, UK. Geomorphology 102, 652-666.

Reference book of climate of PR Bulgaria – Wind., 1982, Publ. House 'Nauka iizkustvo', Sofia, IV, 383 (in Bulgarian).

Roelvink, D., Reniers, A., Van Dongeren, A., Van Thiel de Vries, J., McCall, R., and Lescinski, J. 2009. Modelling storm impacts on beaches, dunes and barrier islands. *Coastal Engineering* 56 (11-12):1133-1152.

Rogev, B., 1975. Sea level fluctuations in front of Burgas and Varna. Proc. of State Geogr. Inst. Sofia.

Seifert, T., Kayser, B., 1995. A High Resolution Spherical Grid Topography of the Baltic Sea. Meereswissenschaftliche Berichte, vol. 9. Institut für Ostseeforschung,Warnemünde, pp. 72–88.

SMBC (Technical Services Department), 1981. LiverpooL Bay bed movement of sediment and longshore drift. Metropolitan Borough of Sefton (Technical Services Department)

Sorkina, A.I. (Ed.), 1974. Climatic Handbook of the Black Sea. M., Gidrometeoizdat, p. 406 (in Russian).

Soulsby, R. L. (1997), Dynamics of Marine Sands, Thomas Telford, London.

Steetzel, H.J., 1993; Cross-shore Transport during Storm Surges, Technical Advisory Committee for the Flood Defences, TAW report No. C1-93.05, Delft, The Netherlands, 291 pp.

Steetzel, H.J., 1993. Cross-shore transport during storm surges. Ph.D. Thesis Delft University of Technology, ISBN 9090063455.

Stockdon, H.F., Holman, R.A., Howd, P.A. and Sallenger, A.H., 2006. Empirical parameterization of setup, swash, and runup. Coastal Engineering, 53(7): 573-588.

Sypion, N., Furmańczyk K., Dudzińska-Nowak J., Łęcka A. 2005 Socjoekonomiczna charakterystyka odcinka Niechorze Międzyzdroje. ZZOP w Polsce – stan obecny i perspektywy. Problemy erozji brzegu. Praca zbiorowa pod red. K.Furmańczyka. Oficyna In Plus 2005, Szczecin, Str. 84-95.

Trifonova, E. 2007. Modelling of Cross Shore Profile Changes under Combination of Extreme Storm Events. Proceedings of the 4th International Conference Port Development and Coastal Environment PDCE 2007. 25-27 September 2007. Varna, Bulgaria. 301-311.

U. Cantabria, 2009. http://www.smc.unican.es/en/

UK Department of Energy, 1990. 'Metocean Parameters - Wave Parameters', Supporting Document to (49), London, HMSO.

Valchev, N., Davidan, I., Belberov, Z., Palazov, A., Valcheva, N., 2008. Estimation of wind wave climate of the Western Black Sea during the last 50 years, Proc. 9th Int. Conf. 'Marine Sciences and Technologies – Black Sea', Varna, Bulgaria, 231-239.

van Rijn, L.C., Walstra, D.J.R., Grasmeijer, B., Sutherland, J., Pan, S., Sierra, J.P., 2003. The predictability of cross-shore bed evolution of sandy beaches at the time scale of storms and seasons using process-based profile models. Coastal Eng., 47(3), 295–327.

Versluys, T., 2007. Golfmetingen binnenhaven Oostende: Storm 8-9 november 2007, Eerste verslag, GBO172/087, UGent, Faculteit Ingenieurswetenschappen – Vakgroep Civiele Techniek – IR15.

Von Storch, H., Langenberg, H., Feser, F., 2000. A spectral nudging technique for dynamical downscaling purposes. Mon. Weather Rev. 128, 3664–3673.

Vousdoukas, M.I., Almeida, L.P., and Ferreira, Ó. 2010 submitted. The morphodynamic response of a mesotidal reflective beach to consequent storms and variations in water level. *Marine Geology*.

Williams, J.J., Masselink, G., Buscombe, D., Turner, I.L., Matias, A., Ferreira, A. Metje, N., Coates, L., Chapman, D., Bradbury, A., Albers, A. & Pan, S., 2009. BARDEX (Barrier Dynamics Experiment): taking the beach into the laboratory. Journal of Coastal Research, SI 56, 158-162.

Williams, J. J., Ruiz de Alegría-Arzaburu, A., McCall, R. T., Van Dongeren, A., 2010. Modelling gravel barrier profile response to combined waves and tidal Forcing using XBeach. Coastal Engineering SI (submitted)

Woodworth, P.L., Blackman, D. L. 2002. Changes in extreme high waters at Liverpool since 1768. International Journal of Climatology 22, 697-714.

Wright, L.D. and Short, A.D. (1984) Morphodynamic variability of surf zones and beaches: A synthesis, Marine Geology, 56, 93-118.

Zeidler, R.B., Wróblewski, A., Miętus, M., Dziadziuszko, Z., Cyberski, J., 1995. Wind, wave and storm surge regime at the Polish Baltic Coast. In: Polish Coast- Past, Present and Future. Ed. Rotnicki K. Sp. Is. Journal of Coastal Research, p. 33- 56.

A SWAN

A.1 Originator

TU Delft

A.2 Website/reference

www.swan.tudelft.nl

A.3 Description

SWAN (Booij et al. 1999) is a third-generation wave model designed to overcome traditional difficulties of applying wave models in coastal regions. The SWAN model was developed for shallow waters at Delft University of Technology (TU Delft), with support from the Office of Naval Research (USA) and the Ministry of Transport, Public Works and Water Management (The Netherlands).

The primary “traditional difficulty” of applying such models in nearshore regions is that such applications must be computed at high geographic resolution, e.g., with a computational grid finer than 100 m. If a conditionally stable geographic propagation scheme is employed at such resolution, then a high temporal resolution must be used also, which makes computations very demanding. SWAN solves this problem by using an unconditionally stable geographic propagation scheme.

Some advantages of using this model are related to the following functionalities:

- wave propagation through geographic space;
- wave refraction due to spatial variations in bottom and current;
- wave shoaling due to spatial variations in bottom and current;
- wave blocking and reflections by opposing currents;
- wave transmission through, blockage by or reflection against obstacles;
- wave generation by wind;
- wave dissipation by whitecapping;
- wave dissipation by depth-induced wave breaking;
- wave dissipation by bottom friction;
- wave-wave interactions (quadruplets and triads);
- nesting with other wave models (i.e., WAM, WAVEWATCH III) and SWAN itself.

A.4 Governing equations

According to Rogers et al. (2003) the governing equation of SWAN and other third-generation wave action models is the action balance equation:

$$\frac{\partial N}{\partial t}+\frac{\partial C_{g,x}N}{\partial x}+\frac{\partial C_{g,y}N}{\partial y}+\frac{\partial C_{g,\sigma}N}{\partial \sigma}+\frac{\partial C_{g,\theta}N}{\partial \theta}=\frac{S}{\sigma}$$

where σ is the relative (intrinsic) frequency (the wave frequency measured from a frame of reference moving with a current, if currents are provided); N is wave action density, equal to energy density divided by relative frequency (N = E/σ); θ is wave direction; Cg is the wave action propagation speed in (x, y, σ, θ) space; and S is the total of source/sink terms expressed as wave energy density. In deep water, the right-hand side of the above equation is dominated by three terms, S ≈ Sin + Snl + Sds (input by wind, four-wave nonlinear interactions, and dissipation, respectively). Source term formulations used in wave models are by no means universal, but the default formulations used in SWAN are a fair representation of the mainstream. A discussion of the three source terms follows.

A.4.1 Wind input

Wind input in SWAN is expressed as the sum of linear and exponential wave growth:

$$S_{in}(\sigma,\theta)=A+BE(\sigma,\theta)$$

Exponential wave growth (B) is typically larger than linear wave growth (A) by one or more orders of magnitude. For the term B, a SWAN user has the option of using the formulation of WAM cycle 3 or the formulation of WAM cycle 4. The default is the WAM cycle 3 formulation,

$$B=\max\left\{0,\ 0.25\frac{\rho_a}{\rho_w}\left[28\frac{U_*}{c}\cos\left(\theta_{wave}-\theta_{wind}\right)-1\right]\right\}\sigma$$

where ρ_a and ρ_w are the densities of air and water, U* is the wind friction velocity, c is the wave phase speed, θ_{wind} is the mean wind direction, and θwave is the mean wave direction.

A.4.2 Four-wave interactions

Four-wave interactions have the effect of transferring energy from the spectral peak to lower and higher frequencies. The energy transfer to lower frequencies leads to lowering of the spectral peak frequency (sometimes referred to as “downshifting”), and the transfer to higher frequencies leads to increased dissipation by breaking.

In SWAN, the Discrete Interaction Approximation (DIA) is used. To some degree, the DIA sacrifices accuracy for the sake of computational expediency. Using the DIA in a wave model tends to result in broader spectra than would result using more rigorous methods.

A.4.3 Whitecapping

Whitecapping is probably the less understood deep water source/sink mechanism. This dissipation is not easily measured, so prevailing theories provide only vague guidance and the formulas used in wave models tend to be quite empirical. The expression for the dissipation sink term that can be written as

$$S_{ds}(\delta,\theta) = C_{ds}\left(\frac{s}{s_{PM}}\right)^{m} \sigma\left(\frac{\sigma}{\sigma_m}\right)^{2n-1} E(\sigma,\theta)$$

where C_{ds} is an empirical coefficient of proportionality, s is the overall wave steepness

$$s = k_m\sqrt{E_{tot}}$$

the subscript m denotes mean, k is wave number, and subscript PM (Pierson–Moskowitz) denotes the fully developed sea state for which s is assumed to be a constant. For arbitrary depths,

$$S_{ds}(\sigma,\theta) = C_{ds}\left(\frac{s}{s_{PM}}\right)^{m} \sigma_m\left(\frac{k}{k_m}\right)^{n} E(\sigma,\theta)$$

where n is a free parameter.

The tuning of the whitecapping source term used by SWAN was performed conducing numerical experiments with different whitecapping term coefficients C_{ds} and 2n to close the energy balance in deep water and (at the model's duration-unlimited, fetch-unlimited asymptote) match the bulk parameters of the Pierson–Moskowitz spectrum, which was thought to be representative of a limiting spectrum.

SWAN uses the following expression (Ris et al. 1999; Booij et al. 1999):

$$S_{ds}(\sigma,\theta) = \Gamma\sigma_m\left(\frac{k}{k_m}\right)E(\sigma,\theta)$$

Here, the steepness parameter Γ is defined as

$$\Gamma = C_{ds}\left[(1-\delta)+\delta\left(\frac{k}{k_m}\right)\right]\left(\frac{s}{s_{PM}}\right)^{m}$$

C_{ds} and δ are tunable coefficients and s is the overall wave steepness.

SWAN with WAM cycle 3 (WAMDI Group 1988) formulation has m=4, C_{ds}=2.36 x 10-5, and δ=0. This is the default formulation in SWAN. The value for C_{ds} is equivalent to that given in WAMDI Group (1988), modified because different definitions for mean wavenumber and mean frequency are used. Thus, SWAN's default deep-water source term formulation (represented as the sum of three individual source terms) is tuned to match bulk quantities (total energy and peak frequency) of the (fully developed) Pierson–Moskowitz spectrum via the parameters Cds and n, using m=4.

B STWAVE

B.1 Originator

Coastal and Hydraulics Laboratory; Engineer Research and Development Center

B.2 References / Websites

http://chl.erdc.usace.army.mil/chl.aspx?p=s&a=Software;9

B.3 Short Description:

STWAVE (STeady State spectral WAVE) is an easy-to-apply, flexible, robust, half-plane model for nearshore wind-wave growth and propagation. STWAVE simulates depth-induced wave refraction and shoaling, current-induced refraction and shoaling, depth- and steepness-induced wave breaking, diffraction, parametric wave growth because of wind input, and wave-wave interaction and white capping that redistribute and dissipate energy in a growing wave field.

C LITPROF

C.1 Originator

DHI Water & Environment

C.2 References / Websites

http://www.dhigroup.com/Software/Marine/LITPACK.aspx

C.3 Short Description:

Wave energy balance based on the deterministic approx of Battjes and Janssen (1978) for irregular waves; depth-averaged momentum equation for the longshore current; mass flux balance, including wave drift and surface roller; assumed velocity profile; sediment transport based on the intra-wave period approach; Engelund and Fredsøe (1976) model for bed load transport; Suspended sediment concentrations are calculated from the diffusion equation for suspended sediment, Fredsøe et al. (1985).

Hydrodynamic processes considered: shoaling, refraction, directional spreading, breaking.

Influent processes in sediment transport: skewness, lagrangian drift, streaming, undertow, surface roller.

Inputs (wind, boundary conditions, bathymetry, etc.) – wave climate at beach profile entrance, morphology and sedimentology of beach profile.

D TRANSED

D.1 Originator

FFCUL

D.2 References / Websites

http://www.aslo.org/phd/dialog/200004-2.html

D.3 Short Description:

The Model TRANSED is a 1DV sediment transport model based on the determination of the mean sediment transport rate on the intra-wave period and depends on the forcing mechanisms wave and current, the bottom type (with bed forms or flat) and the sediment particle characteristics. The model allows applying the most used methods in the description of the combined wave and current bottom boundary layer and bed forms and in the computation of the parameters: reference concentration, suspended concentration and bed-load and suspended-load transport. It expected that a web page about this model will be available soon.

E XBeach

E.1 Originator

Consortium of Unesco-IHE, Deltares, TU Delft (all The Netherlands) and U. Miami (USA) with input from a worldwide community

E.2 Website

http://XBeach.org

E.3 Description

The model solves coupled 2D horizontal equations for wave propagation, flow, sediment transport and bottom changes, for varying (spectral) wave and flow boundary conditions. Because the model takes into account the variation in wave height in time (long known to surfers) it resolves the special long wave motions created by this variation. This so-called 'surf beat' is responsible for most of the swash waves that actually hit the dune front or overtop it. Because of this innovation the XBeach model is better able to model the development of the dune erosion profile, to predict when a dune or barrier island will start overwashing and breaching and to model the developments throughout these phases.

The model has been tested against a variation of cases, including laboratory (Deltaflume, Oregon State flume) and field cases (Duck NC, Santa Rosa Island Florida, sand dike breach in 'T Zwin, Netherlands).

F SMC-model

F.1 Originator

University of Cantabria and the Spanish Ministry of Environment

F.2 Website

http://www.smc.unican.es/en/

F.3 Short Description

The SMC model is developed by the University of Cantabria and the Spanish Ministry of Environment. UCA will apply this “off-the-shelf” model as users (not developers). Further references to the model can be found at: http://www.smc.unican.es/en/.

The model includes general, low-resolution bathymetries of the Spanish coast and historical wave data. As input the user can include specific bathymetry information and wave data in order to apply the model for a specific local area.

SMC is a software package including a set of programs and numerical models, structured according to different spatial and temporal scales, which are aimed at predicting beach morphodynamic behaviour. It is composed of different applications integrated into the whole SMC package, which can also be used independently. The main software applications are the following:

ATLAS: It provides of mean and extreme regimes of tidal levels and flooding heights for open beaches along the Spanish coast on a regional scale.

ODIN: It provides of wave-related information at any Spanish coastal zone, namely: visual mean directional wave regime (wave height and period) both in deep water and at given depths; wave characteristics related to mean energy flux; and mean annual wave conditions.

BACO: This software includes bathymetric data coupled to the models, obtained from nautical charts from the whole Spanish coast.

MOPLA: It allows the simulation of wave propagation from deep water to the shoreline. Currents in the breaker zone are calculated on the basis of these waves, and finally beach morphodynamic evolution is simulated.

It includes the following models:

Oluca: parabolic model of wave propagation (monochromatic and spectral); it performs refraction, diffraction (Laplace equation) and refraction-diffraction from mild-slope models and parabolic approach.

Copla: model of beach currents induced by the breaking of spectral waves; it does not include cross-shore transport.

Eros: model of erosion-sedimentation and bathymetric evolution of beaches due to spectral waves on a planform.

Based on these models, MOPLA allows the calculation of long-term beach planform evolution with approaches similar to those by Hsu and Evans (1989).

PETRA: The model Petra is the numerical module of SMC that solves to a beach profile, equations of sediment transport within the surf zone and changes in the bathymetry associated with spatial variations in sediment transport. The magnitude of transport is based on the environmental characteristics such as, water, sediment and bathymetry and the hydrodynamic conditions of waves and wave induced currents. Petra was developed to predict the morphological evolution of a beach profile under the action of certain conditions of waves on a time scale of events. Therefore, this type of model is useful for simulating the behavior of a beach (sand volume eroded, receding shoreline) under the action of a storm.

Petra is based on modelling of physical processes that affect the beach profile, wave propagation, undertow currents, sediment transport and bathymetry change. In general accepts stationary hydrodynamic conditions for a specified time, giving lead to a variation of the profile. With the new profile is recalculating the hydrodynamic conditions and computes a new transport stream.

F.3.1 Hydrodynamic Model

In terms of hydrodynamics Petra uses a phase-average formulation for the calculation of the wave field over the profile. Simultaneously, the variations of the radiation stresses are evaluated and thus the alteration of the average water level due to the presence of waves are calculated, using linear wave theory.

F.3.2 Wave Dissipation Model

In terms of modelling the wave dissipation rate within the surf zone Petra has implemented four different models: Battjes and Janssen (1978), Thornton and Guza (1983), Rattanapitikon and Shibayama (1998) and Larson (1995). The first two are based in a hydraulic jump type dissipation models and the others in the hypothesis proposed by Dally et al. (1985).

It is important to consider the simplifications that have been adopted in the description of the sea state. The model uses to characterize the sea state the wave period (Tp) and direction (theta) with mean values, leaving randomness of the waves only to the wave height. Therefore, the hypothesis that is accepted is that the energy spectrum is narrow in frequency and directions. An important consideration in the models used is the link between the conservation equation of energy flow and average later level variation equation. Thus, the models of Battjes and Janssen (1978), Thornton and Guza (1983) and Larson (1996) solve two equations simultaneous (for the dissipation rate using the depth total local ($d = h + \eta$)). However, the model Rattanapitikon and Shibayama (1998) used as a depth only h, thus the calculation of the mean water level is made after calculating the evolution of wave height. The values of the default parameters used by each model are presented in Table F.1 .

Table F.1 Default values for the parameters of the different dissipation models

Dissipation Model	Parameters			
Battjes and Janssen (1978)	γ based on offshore wave steepness			-
Thornton and Guza (1983)	γ = 0.6	B=O(1) depending on the type of breaking		
Rattanapitikon and Shibayama (1998)	-	K_5= 0.10	K_6= 1.60	K_7= 0.10
Larson (1995)	γ = 0.78	-	-	-

F.3.3 Return Current Model

The formulation that is used to determine net flows on the bed takes into account the vertical structure of the average current (undertow) and the boundary layer drag (Stokes drag). The solution by DeVriend and Stive (1987) for stationary net current is based on a 3 layer model. In the model Petra to use the simplified expression for the return current is used as presented by Ranasinghe et al. (1999). The turbulent closure model adopted is based on DeVriend and Stive (1987) that includes enhancement of vertical eddy viscosity due to orbital motion and wave dissipation. Model uses the for the empirical constants of eddy viscosity due to orbital motion (K) and wave dissipation (M) the values recommended by Southgate and Nairn (1983) i.e. K=0.083 and M=0.025.

F.3.4 Sediment Transport Model

The transport module determines the sediment transport based on the fields of wave fields and net bottom currents. A modification of Bailards (1981) energetic approach is being used in Petra. This formula computes the total transport, by summing the suspended transport and the bedload transport. This formulation has undergone modifications by different authors in order to model more adequately the processes affecting the physical transport. The Petra is using the Ranasinghe et al. (1999) modification that is adding to the formulation the effect of proportion of broken waves at each point of the profile.

F.3.5 Transport in the swash zone

One of the main mechanisms that change the beach profile is sediment transport over the of the swash zone. So in order to model a proper retreat of the coastline in a event time-scale a formulation adequate to represent the sediment transport over this area must be implemented. The net transport on the swash-slope is primarily a function of local slope, the sediment characteristics and properties of the water level amounting over the slope. In the Petra model the formulation of Wise et al. (1996) is utilized, where the sediment transport over the swash zone is been computed as a function of a reference sediment transport at a point with depth of 0.3-0.5Hrms.

The length of the run-up, the distance of the actual point from the reference point, the local slope and the average slope of the swash zone are used to parameterise the sediment transport over the area.

After the calculation of the sediment transport the sediment conservation equation is solved and the new profile is calculated. In addition a stability criterion based on physical stability of the slope is applied. If the slope at some point exceeds the angle of repose the sediment produced an avalanche of material until an equilibrium it reached.

F.3.6 References

Battjes, J.A. and Janssen, J.P.F.M., (1978). “Energy loss and set-up due to breaking of random waves”. Proc. 16th Int. Conf. Coastal Eng., Houston, TX. ASCE, New York. Vol. 1, pp. 569-589.

Dally, W.R., (1992). “Random breaking waves: Field verification of a wave-by-wave algorithm for engineering application”. Coastal Eng. Vol 16(4), pp. 369-397.

De Vriend, H.J. and Stive, M.J.F., (1987). “Quasi-3D modelling of nearshore currents”. Coastal Eng. Vol. 11(5/6), pp. 565-601.

Larson, M., (1995). “Model for decay of random waves in the surf zone”. J. Waterway, Port, Coast., and Ocean Eng. Vol. 121(1), pp. 1-12.

Ranasinghe, R., Pattiaratchi, C. and Masselink, G., (1999). “A morphodynamic model to simulate the seasonal closure of tidal inlets”. Coastal Engineering. Vol.37, pp. 1-36.

Rattanapitikon, W., and Shibayama, T., (1998). “Energy dissipation model for regular and irregular breaking waves”. Coastal Engineering, Vol. 40, nº4, pp.327-346University of Cantabria and the Spanish Ministry of Environment

G SBEACH

G.1 Originator

CHL-CERC, USA and U. of Lund, Sweden.

G.2 Website

http://chl.erdc.usace.army.mil/chl.aspx?p=s&a=SOFTWARE;31

G.3 Short description

SBEACH calculates dune and beach erosion produced by storm waves and water levels; bar formation and movement produced by breaking waves are also simulated. The model is empirically based and was originally developed from a large data set of net cross-shore sand transport rates and beach profile change observed in large tanks. The empirical formulation, model sensitivity tests, and a field validation case are described in various reports.

SBEACH is a 1DV semi-empirical time-dependent dune erosion model on the basis of time-averaged process descriptions of wave transformation and sediment transports, i.e. the hydrodynamics are stationary and the morphodynamics are instationary. Every morphological time step the wave transformation is calculated on the basis of conservation of energy flux:

$$\frac{d}{dx}(F\cos\theta) = \frac{k}{d}(F - F_s)$$

Where F is the energy flux and F_s the energy flux of a stable (not yet breaking) wave. θ is the angle of incoming waves, k is an empirical wave decay coefficient, and d is the water depth including storm surge and wave set up.

From the wave transformation the sediment transports and the bed level changes are computed. The sediment transport is calculated on the basis of the empirical formulations:

$$Q_s = K\left[D - D_{eq} + \frac{\varepsilon}{K}\frac{dh}{dx}\right] \qquad (7.1)$$

where D is the instantaneous wave energy dissipation, D_{eq} is the wave energy dissipation for the equilibrium profile, K is a transport coëfficiënt,ξ is an empirical coefficient and dh/dx is the local bottom slope.

The supply of sediment from the dry dune is based on a linear relation between wave impact and the weight of the sand which is eroding (Overton en Fisher, 1988).

H MARS

H.1 Originator

MARS2D (Model for Applications at Regional Scale) coastal hydrodynamic model is developed by IFREMER (Lazure and Dumas, 2007; Lazure *et al.*, 2009).

H.2 Website

http://www.ifremer.fr/delao/francais/hydrodynamique/outils/sigmodele/mars/index.htm (in French)

H.3 Short description

MARS2D simulates the oceanic circulation from shoreline to few hundreds of kilometres offshore. The 2D version of the code is based on the Saint – Venant equations. Interested readers should refer to Lazure and Dumas, 2008 or Lazure *et al.*, 2009 for details. The numerical scheme is based on finite difference; a regular grid is used.

$$\frac{\partial u}{\partial t}+u\frac{\partial u}{\partial x}+v\frac{\partial u}{\partial y}+g\frac{\partial \zeta}{\partial x}-fv-\varepsilon\left(\frac{\partial^2 u}{\partial x^2}+\frac{\partial^2 u}{\partial y^2}\right)+g\frac{u\sqrt{u^2+v^2}}{k^2H^{4/3}}+\frac{\partial Pa}{\partial x}+\frac{\tau_x}{\rho H}=0$$

Where u and v are the horizontal velocity components, ζ is the free surface level, f is the Coriolis term and H is the water depth.

MARSD provides information concerning marine currents and sea level in a plane and quasi-horizontal liquid flow. The main parameters calculated by MARS2D are the horizontal current,

the Eulerian residuals, the water depth, the mean level and the tidal harmonics.

Other functionalities are offered by MARS:

- The effect of meteorological forcings such as wind or atmospheric pressure can be modelled.
- The structure of the code enables the use of nested grids (*cf.* figure above).
- A 3D version of the code is available (Lazure and Dumas, 2007; Lazure *et al.*, 2009).
- The diluted tracer transport modelling (salinity or pollutant for example) is including. It is based on an advection-diffusion equation.
- The calculation can be performed with complex bathymetries (dry areas in the computational domain: intertidal flats and flood plains).

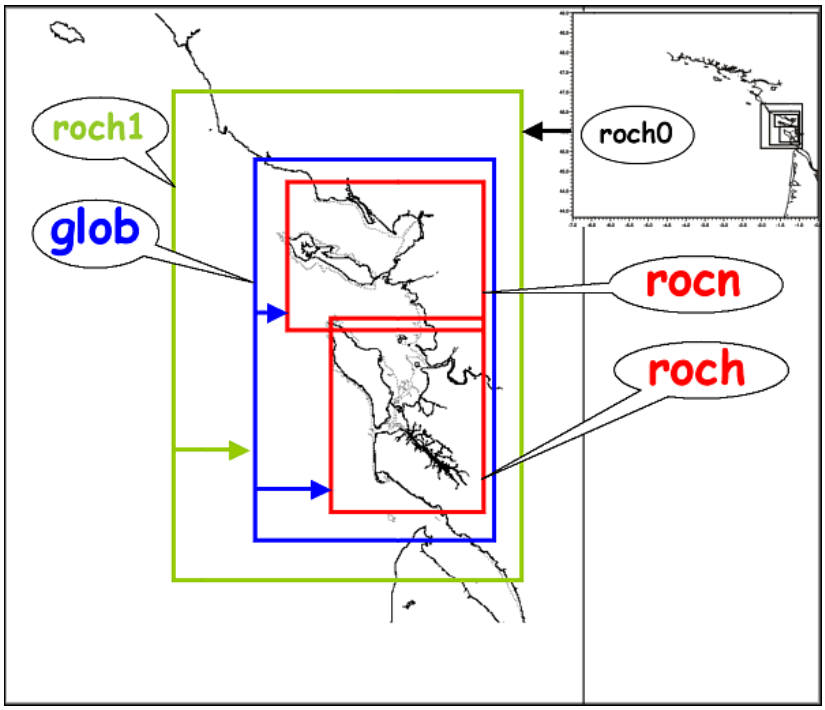

Figure H.1 Illustration of the use of nested grids. Calculation domain used for the "Pertuis Charentais" area (France).

H.4 References:

Lazure P. and Dumas F. (2007) An external–internal mode coupling for a 3D hydrodynamical model for applications at regional scale (MARS), Advances in Water Resources 31. 233–250

Lazure P., Garnier V., Dumas F., Herry C. and Chifflet M. (2009) Development of a hydrodynamic model of the Bay of Biscay. Validation of hydrology. Continental shelf research. doi: 10.1016/j.csr.2008.12.017

I Durosta

I.1 Originator

Dr. H.J. Steetzel (formerly Delft Hydraulics, presently Alkyon Consultancy and Research).

I.2 Website

-

I.3 Short description

DUROSTA is a two-dimensional, time-dependent cross-shore transport model that computes the dynamic adjustment of an arbitrary coastal profile to arbitrarily changing water level and wave conditions during a storm surge. The model can be applied to check the safety, or for the design of a coastal profile. An option of the program is that a fixed structure, for example a revetment, can be defined in the coastal profile. In this way the development of scour hole in front of the revetment or the amount of local erosion due to wave run-up above the revetment can be assessed.

J Storms along the Sefton Coast

J.1 Introduction.

The Sefton coastline, NW England (Figure J.1), comprising natural sand dunes (16km long) and seawalls to protect urban areas is vulnerable to erosion and flooding during storm events. In common with other coastal areas there is not always a clear boundary between those areas at risk from flooding and those at risk from coastal erosion. In a number of locations coastal erosion will lead directly to tidal flooding and urban flooding can result from failure of a protection structure or by wave overtopping. Storm impacts on the sand dune system can cause landward realignment. This will be most significant immediately after the storm event and will be reduced when the dunes have recovered through slumping and windblown sand accretion. The extent of erosion for an isolated storm event will depend on the initial state of the dunes system, e.g. whether a previous high tide has eroded or destabilised the dune face. In cases where the sand dune system is breached there are a number of areas that could be exposed to tidal flooding. Given the large tidal range here, a very important factor controlling the impact severity of a given storm is the phasing between Spring tides and the storm.

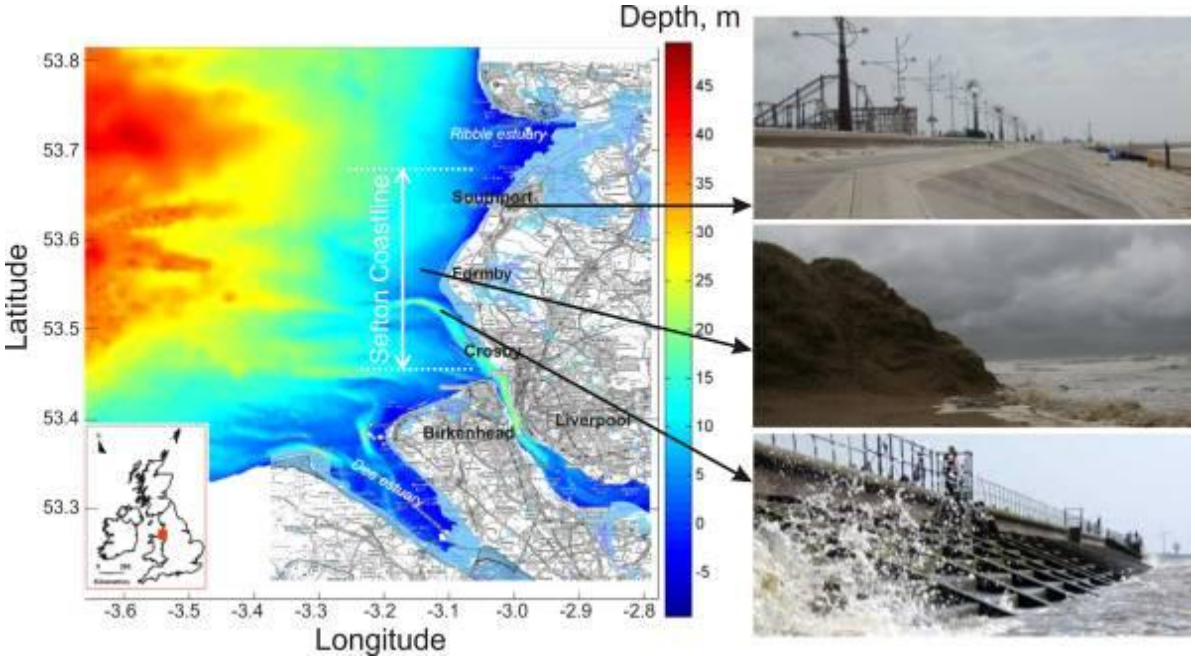

Figure J.1: Liverpool Bay situated in NW England and the Sefton coastline with natural and hard defences.

Together wind waves and elevated water levels can cause flooding and extensive erosion in low-lying coastal areas. The water level at the coast may be a combination of mean sea level, tides, surges and wave-setup. Often surges and waves are generated by the same storm event. In areas with a wide continental shelf, a travelling external surge may combine with the locally generated surge and waves. Significant interaction between the propagation of the tide and surge can also occur. Since wave height at the coast is controlled largely by water depth, the effect of tides and surges on waves must be considered. Similarly, consideration must be given to waves which also contribute to the total water level by means of wave setup through

radiation stress. Provided good bathymetry and wind forcing data are available, these processes are well understood and accurately predicted by models such a POLCOMS-WAM used in the present study. Other interactions between surges and waves include the processes of surface wind stress and bottom friction as well as depth and current refraction of waves by water levels and currents. The full details of these processes are still not well understood and are not accounted for in existing models. In order to determine the characteristics of extreme offshore storm events along the Sefton coast using the best available models, a validated, coupled, wave-tide-surge model hindcast been used to simulate the hydrodynamic effects of storm action at the coastline (Brown et al. 2010a).

J.2 Extreme conditions

Sand dunes not react only to storm events but also to a wide range of high tidal levels (>9.5m CD). Here the offshore conditions which could lead to a significant shoreline response are examined. Extreme storm events have been identified from an 11-year data set (1996 – 2007) of model hindcasts and observations (Brown et al, 2010b). Here we examine the characteristics of the storm event occurring on the 27th October 2002 to demonstrate the sequence of events that lead to extreme erosive conditions along the Sefton Coast. This event generated some of the most extreme storm conditions in recent years with a surge level of 2.26m measured in Liverpool and offshore wave heights reached 4.09m within Liverpool Bay.

J.2.1 Wave conditions

In Liverpool Bay the waves are locally generated within the eastern Irish Sea (Figure J.2). The most extreme wave heights offshore in Liverpool Bay are in the range 4.0 to 5.6m and are typically generated when the winds blow from the west through to northwest. These directions provide the longest fetches (~200km) to the Sefton Coast (Pye & Neal, 1994). The eastern Irish Sea is sheltered from external swell due to the surrounding coastline and the shallow depths throughout the Irish Sea.

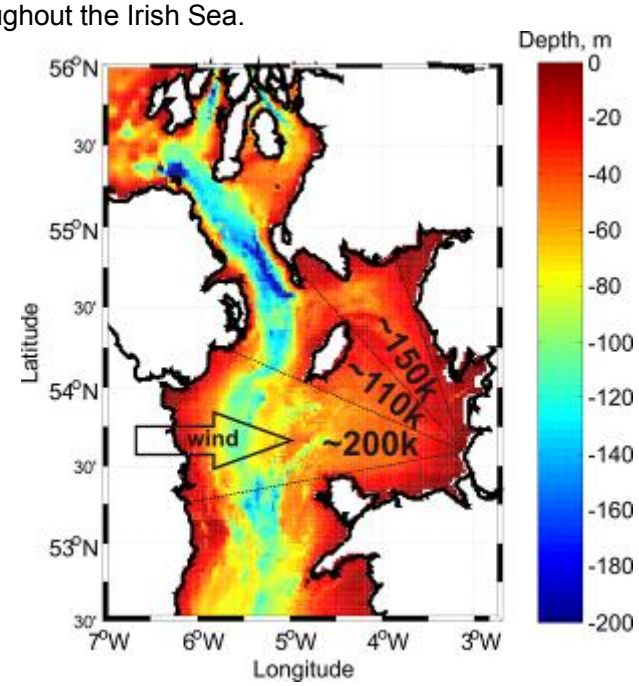

Figure J.2: Fetch regions for local wave generation along the Sefton coast, the region for extreme waves is marked with an arrow.

J.2.2 Surge conditions

The surge generated externally to the eastern Irish Sea is at least as important as the locally generated surge within the eastern Irish Sea (Olbert & Hartnett, 2010). The external surge depends on both wind and pressure forcing, while the wind contribution becomes increasingly important within Liverpool Bay. The most extreme surge conditions result from winds blowing over the longest (south-westerly) fetches, to the offshore boundary of the eastern Irish Sea (Figure J.3). This wind direction results in an extreme external surge condition and moderate local surge generation. However, if the wind veers to the west from southwest an extreme local surge is generated, which contributes to, and interacts with, the extreme external surge creating the most severe surge elevations for the Sefton coast and Liverpool Bay. Within Liverpool Bay the most extreme surge conditions range between 1.0 m to 2.5 m.

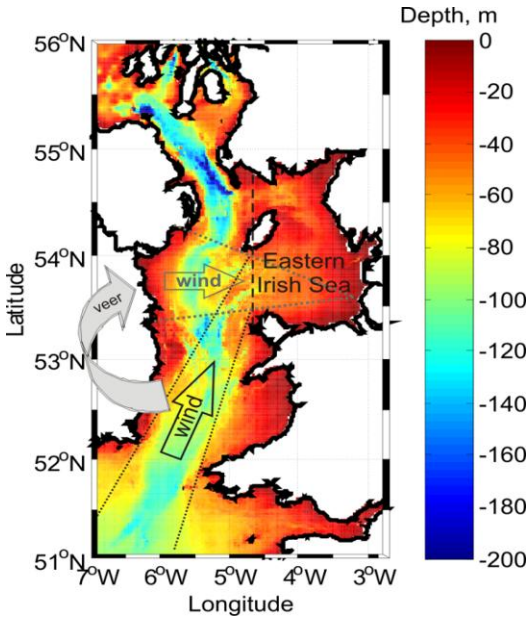

Figure J.3: Fetches for extreme external (black region) and local (grey region) surge generation leading to extreme surge levels along the Sefton coast.

J.2.3 Tidal conditions

Liverpool Bay is a macro tidal region, with a mean spring and neap tidal range of 8.22m and 4.28m, respectively, at Liverpool (NTSLF, http://www.pol.ac.uk/ntslf/). The highest mean high water spring is 9.32m CD, while the highest astronomical tide is 10.29m CD. Significant impacts on the dune system, and elevated flood risks, are most likely to occur when storm events are coincident with high tidal levels. Extreme tidal levels are mainly associated with spring tides combined with surge and wave set-up. Due to tide-surge interaction in Liverpool Bay the peak of the surge event often occurs on the rising tide and not at high water (Woodworth and Blackman, 2002). Consequently, it is the increase in observed high water compared with the predicted tidal high water level that is more important than the peak surge level (Figure J.4). This additional water level is known as the skew surge (de Vries et al., 1995). For Liverpool Bay the most extreme skew surge levels are 0.8m to 1.8m, in response to winds from the southwest through to west. Thus for modelling purposes it is essential that the tide-surge interactions are correctly simulated.

J.2.4 Tidal conditions

The most severe storm conditions result from the westerly passage of Atlantic depressions which generate south-westerly winds in the range 17-30m/s. This facilitates the generation of a large external surge, which propagates into the eastern Irish Sea. If the wind veers westerly, the locally generated wave and surge conditions become extreme. At the peak of the tide hard defences are at risk from wave overtopping and breaching from extreme water levels, while the dunes are exposed to wave attack (Figure J.5). During spring tide conditions the threat of coastal flooding is at its greatest. The most extreme storm conditions are likely to occur when a low pressure system travels from the west towards the northwest across the Irish Sea and just to the north of Liverpool Bay following a track which lies in the region shown in Figure J.6.

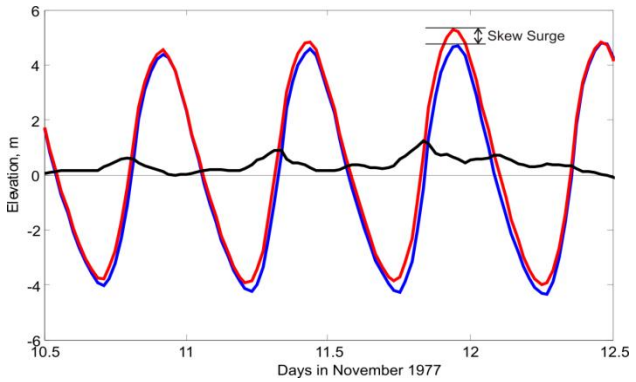

Figure J.4: The November 1977 storm event shows the peaks in the surge (black line) occurring on the rising tide (blue line) and the resultant water level (red line). The peak in the skew surge occurs on the 12th November as a result of tide-surge interaction.

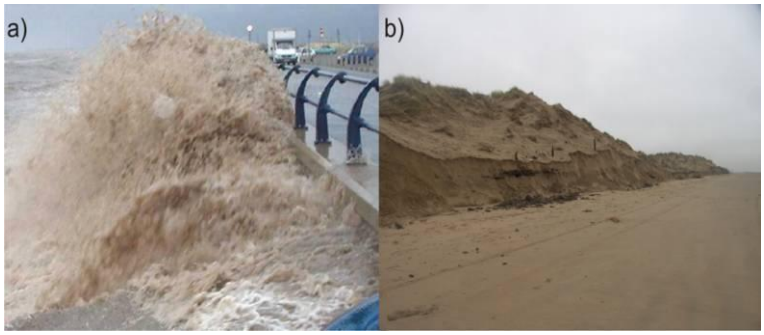

Figure J.5: a) Waves impacting the sea wall constructed in 2002 at Southport and b) sand dune undercutting due to high tidal levels in February 2010.

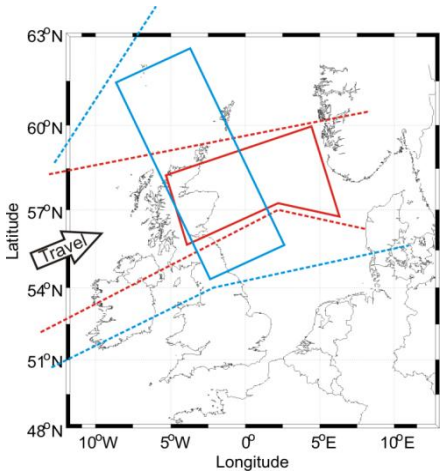

Figure J.6: Storm track regions generating extreme surge (blue) and waves (red) along the Sefton coast. The boxes indicate the location of the depressions centre at the time of peak surge (blue) or peak wave (red) conditions. The arrow represents the general direction of travel of the storm across the region.

The time of peak waves and peak surge may or may not coincide. This will depend on the sequence of wind veering and the tide-surge interactions. Extreme surge generation depends on a strong south-westerly wind component, but tide surge-interaction will be most active when the peak in surge occurs, by which time the wind may have veered. Being dependent on a strong westerly wind component, the maximum wave heights can be coincident with the time of peak surge, or occur at a different time when the storm track has moved to a location generating a strong westerly wind component. Often the location of the pressure system at the time of the peak in the wave conditions occurs after that for peak surge conditions, as the pressure system moves from the blue region into the red region (Figure J.6). This is due to the local generation of the waves requiring westerly wind conditions, and the surge requiring veering wind conditions dominated by an initial southwest direction. On 27th October 2002 the peak in waves occurred an hour after the peak in surge as the low pressure system moved further northeast and the winds veered from a south-westerly to a westerly direction. The storm tracks across the Irish Sea of the two dispersions, which occurred in the period 25th -29th October 2002, are shown in Figure J.7. The first (blue track, Figure J.7) had a central low pressure of 968 – 976mb and the second (red track, Figure J.7) had a central low pressure of 972 – 980mb. Each storm generated a peak in the storm conditions. The sequence of events at Formby point is presented in Figure J.8. As the depressions tracked over the UK and into the North Sea, veering south-westerly to westerly winds, reaching speeds of 16-18m/s locally, were generated in the eastern Irish Sea (Figure J.8a). The time series of the modelled wind speed, wind direction, significant wave height, surge elevation, tidal elevation and total elevation are given at Formby point in Figure J.8.

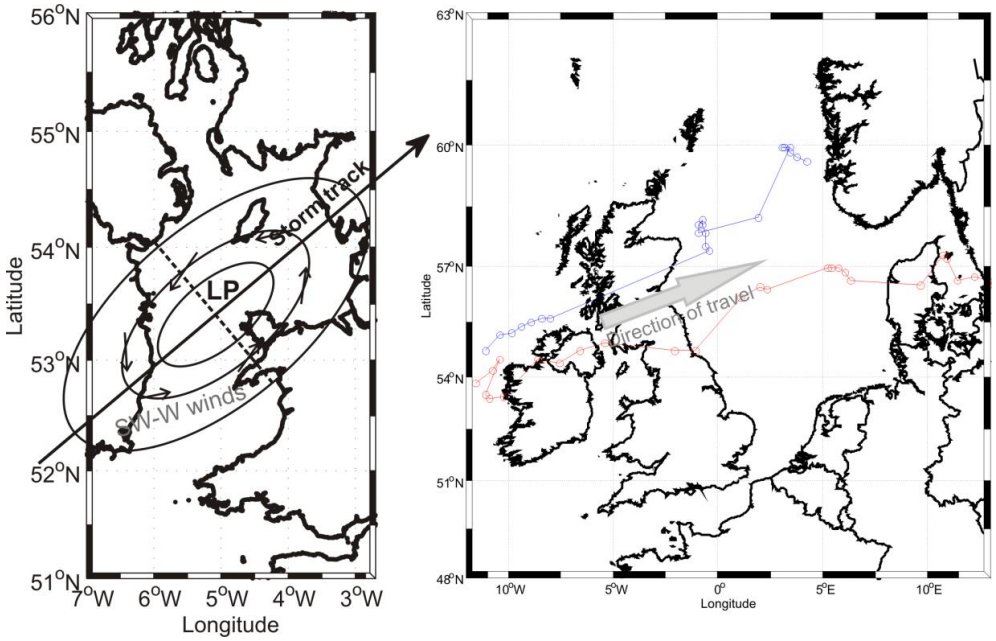

Figure J.7: The storm tracks of the centre of the low pressure system generating storm conditions on the 26th October 2002 (blue track) and 27th October 2002 (red track). A schematic of a low pressure system and its corresponding winds is also given.

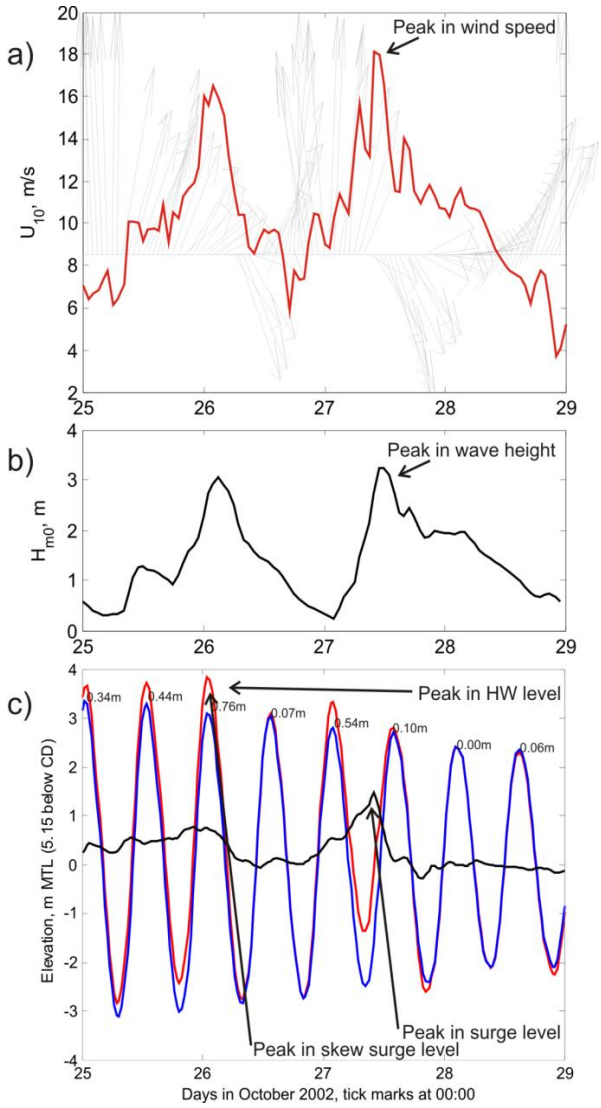

Figure J.8: The modelled wind speed with direction at 10m (a), the significant wave height (b) and the surge elevation with tidal elevation and total (tide + surge) elevation (c) at for Formby point. The numbers in (c) indicate the skew surge value during each tide.

The time series in events for the storm in October 2002 shows how the tidal range in relation to the peak in the storm is important. At Formby point there are two peaks in the wind speeds. Both occur as winds veer from south west to west leading to extreme hydrodynamic and wave conditions. The most extreme winds occurred on the 27th generating the most extreme waves and surge during this period. However, on the 26th a larger tidal range causes a greater flood risk due to the skew surge. Although the surge during the 26th is not extreme (<1m) the skew surge (additional water level at HW) is slightly larger than that during the 27th. Combined with the larger tidal range on the 26th the skew surge leads to the highest total water level generating an extreme storm tide. The slightly weaker wind speeds at this time produce slightly reduced but still extreme wave heights (>3m) on top of the raised water levels. This combined effect leads to the greatest risk of coastal erosion and flooding on the 26th, while the wind wave and surge conditions are most extreme on the 27th.

The failure of hard coastal defences will depend principally on the instantaneous wave conditions; conversely, the dune stability is much more complex. An initial set of high tidal levels or storm tides with or without waves may destabilised the due system, but not lead to (significant) breaching or realignment. While a second set of less extreme tides combined with waves or in isolation may cause a significant impact on the system in response to a weakened dune toe.

Dune toe surveys of Formby point around this storm period were carried out by the Sefton Council on the 24th September 2002 and again on the 26th November 2002 (Figure J.9). The surveys show a significant retreat of 2.5m to 5m around the point between these surveys. The retreat could be due to a combination of high tides during October to November and/or as a consequence of the isolated extreme storm during 25th to 27th October 2002.

Figure J.9: The dune toe position surveyed on the 24th September 2002. The arrows indicate the dune retreat which occurred following this survey and 26th November 2002.

J.3 Historical events

Historically extreme events can be associated with westerly-weather types generating storm conditions similar to the sequence that occurred in October 2002, presented above. One example is the 11th November 1977 storm.

The veering winds across the Irish Sea (Figure J.10) generated wide spread coastal flooding and damage along the NW English coast (Figure J.5) as a result of a ~1.5m surge and ~3.5m waves coinciding with spring high tide.

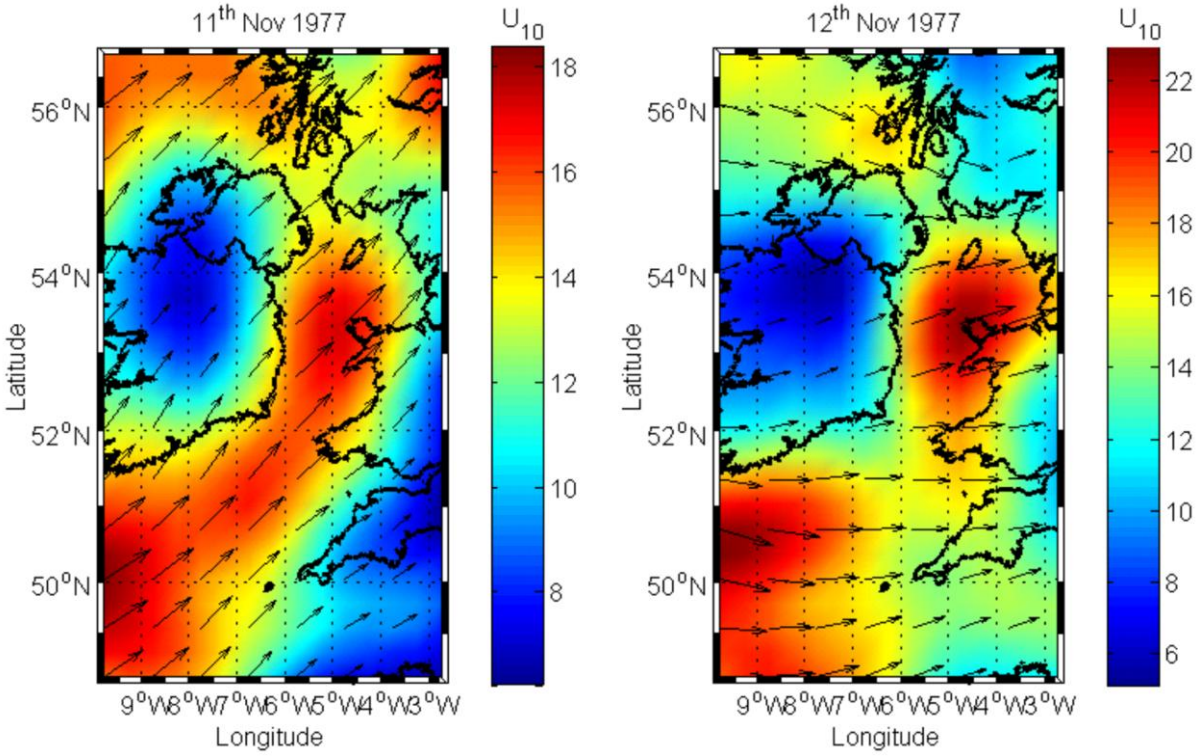

Figure J.10: The 10m wind, U_{10}, over the Irish Sea at 12:00 on the 11th November 1977 and 00:00 12th November 1977.

In the past damaging storm events to the Sefton coast have been reported to have occurred in October 1961, January 1965, February 1967, April 1968, January 1975, January 1976, November 1977, January 1983, February 1990, February 1997, February 2002, March 2004, February 2008 (Pye & Neal, 1994; Pye & Blott, 2008). Many of these events are associated with times of extreme tidal levels elevated by surge. Extreme high waters in the past have also been observed at Liverpool in 1905, 1976, 1977, 1990 and 1997 (Woodworth and Blackman, 2002). However, as demonstrated above, there is a complex interplay between the meteorological conditions, the tidal modulation of water levels, antecedent conditions and the coastal system making predictions of impacts difficult to predict with confidence.

J.4 References

Brown, J. M., Souza, A. J., & Wolf, J. (2010a) An 11-year validation of wave-surge modelling in the Irish Sea, using a nested POLCOMS-WAM modelling system. *Ocean Modelling*, 33(1-2): 118-128, doi: 10.1016/j.ocemod.2009.12.006

Brown, J. M., Souza, A. J., & Wolf, J. (2010b) An investigation of recent decadal-scale storm events in the eastern Irish Sea. Journal of Geophysical Research (Oceans). 115(C05018):12pp, doi:10.1029/2009JC005662

De Vries, H., M., Breton, T., De Mulder, Y., Krestenitis, J., Ozer, R., Proctor, K., Ruddick, J. C., Salomon, and A., Voorrips (1995), A comparison of 2D storm surge models applied to three shallow European seas. *Environmental Software*, 10(1), 23–42.

Olbert, A.I., Hartnett, M., 2010, Storms and surges in Irish coastal waters, *Ocean Modelling*, 34(in press), 13pp.

Pye, K., and S. J., Blott (2008), Decadal-scale variation in dune erosion and accretion rates: An investigation of the significance of changing storm tide frequency and magnitude on Sefton coast, UK. *Geomorphology*, 102(3−4), 652−666.

Pye, K., Neal, A., 1994. Coastal dune erosion at Formby Point, north Merseyside, England: Causes and mechanisms. Marine Geology, 119(1–2), 39–56.Woodworth, P. L., Blackman, D. L., 2002. Changes in extreme high waters at Liverpool since 1768. International Journal of Climatology, 22(6), 697–714.

K The Liverpool Bay Model

The National Oceanographic Centre in Liverpool has developed a 'pre-operational' simulation suite of models to run alongside the Irish Sea Observatory. These models provide daily forecasts of shelf sea variables on two scales: 12 km (Atlantic Margin) and Irish Sea 1.8 km (High Resolution). While the 1.8km Irish Sea domain is state-of-the-art in terms of resolution of shelf scale models, it is not adequate the resolve the geographic (topography and coastline) and dynamic (drying of tidal flat, strain-induced periodic stratification etc) features of near-coastal regions. Hence, a 180m resolution model of Liverpool Bay, including the Dee, Mersey and Ribble estuaries (High Resolution Liverpool Bay Model) has been developed recently to address this. At the heart of this modelling system is the hydrodynamic model POLCOMS (Proudman Oceanographic Laboratory Coastal Ocean Modelling System). With meteorology and river flows as inputs, the model is able to predict currents, temperature, salinity and sediment transport.

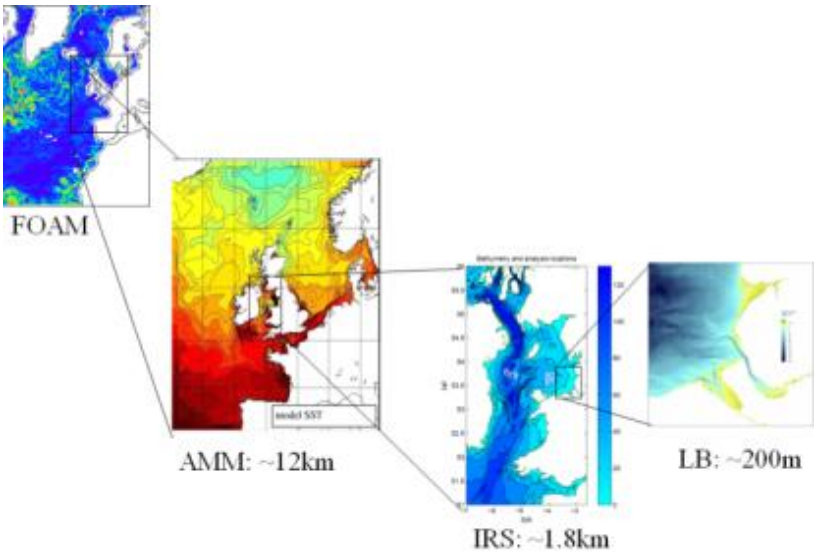

Figure K.1. The suite of pre-operational models: Atlantic Margin and Irish Sea. Information from the Met Office's FOAM model feeds into the Atlantic Margin model; results from one model are used as boundary conditions in the next model. These POLCOMS models forecast sea temperature, salinity, tidal elevations and currents. Additional modules are also available for waves, suspended sediments, light levels, nutrients and biology.

Prior to implementation of Liverpool bay model in the suit of Irish Sea Observatory models, basic validation is provided here as a guide to using these models to inform process studies . The objective is to routinely compare real-time and survey data with model outputs, specifically vertical profiles and horizontal gradients. Results will inform planning of future surveys and coastal management, as well as improve model performance.

K.1 Model description

POLCOMS is a 3-D baroclinic B-grid model developed by Holt and James (2001), which incorporates refinements such as a 'Piece-wise Parabolic Method' (PPM) advection scheme,

turbulence closure (using the General Ocean Turbulence Model) and, more recently, a 'Total Variation Diminishing' (TVD) wetting-drying scheme. This model is well suited to high performance (large area and/or high resolution) applications being high optimised for massively parallel computers. Figure K.1 summarises the suite of POLCOMS models that produces forecasts to supplement the near real-time measurements in the Coastal Observatory (Howarth et al., 2008; http://coastobs.pol.ac.uk/polcoms).

K.1.1 Wetting and drying using TVD volume fluxes

In POLCOMS wetting and drying is achieved by calculating volume fluxes using a TVD (Total Variation Diminishing) scheme (Sweby 1984). The single layer barotropic shallow water equations are as follows:

$$\frac{\partial u}{\partial t} = fv - g\frac{\partial \zeta}{\partial x} - u\frac{\partial u}{\partial x} - v\frac{\partial u}{\partial y} \tag{K.1}$$

$$\frac{\partial v}{\partial t} = -fu - g\frac{\partial \zeta}{\partial y} - u\frac{\partial v}{\partial x} - v\frac{\partial v}{\partial y} \tag{K.2}$$

$$\frac{\partial \zeta}{\partial t} = -\frac{\partial (Hu)}{\partial x} - \frac{\partial (Hv)}{\partial y} \tag{K.3}$$

These equations are solved in the barotropic part of the three-dimensional POLCOMS model. This is a finite-difference model based on the Arakawa B-grid using forward time stepping with a splitting between external and internal time steps. A PPM scheme (Piecewise Parabolic Method; Colella and Woodward 1984, see also James 1996) is used for momentum advection (the last two terms in Equations 1 and 2) but a TVD scheme is used for calculating the volume fluxes in Equation A2.3. This scheme has the property of positivity, so it ensures that the total depth H never becomes negative. For this reason, it handles wetting and drying in a straightforward manner. It also reduces grid scale noise, which can be a problem on the B grid, so reducing the need for a filter. It is possible for depths to become very small using this method, but the addition of bottom friction to the above equations is effective in reducing the velocity in such very shallow water. It is advantageous to add also the condition that if the sea bed at one point is higher than the sea level at a neighbouring point, the elevation gradient is calculated after subtracting this difference from the level at the higher point, so the elevation difference is replaced by the water depth at the higher point. This means that the height of a dry box is ignored while the effective height of a semi-wet box is reduced.

The TVD calculation of volume flux Hu is based on a combination of first-order upwind and Lax-Wendroff schemes, as described for scalar and momentum fluxes in James (1996). If (in one dimension) suffix i denotes elevation points and i + ½ denotes velocity points, the upwind flux into elevation point i + 1 from the lower numbered side is

$$F^{UP} = u_{i+\frac{1}{2}}(H_i + H_{i+1})/2 + \left|u_{i+\frac{1}{2}}\right|(H_i - H_{i+1})/2 \tag{K.4}$$

while the Lax-Wendroff flux

$$F^{LW} = u_{i+½}\{(H_i + H_{i+1})/2 + u_{i+½}\Delta t(H_i - H_{i+1})/2\Delta x\}, \quad \text{(K.5)}$$

where Δt and Δx are the time and space steps.

The total TVD flux

$$F = F^{UP} + \varphi(r)(F^{LW} - F^{UP}), \quad \text{(K.6)}$$

where φ(r) is a limiter function, defined as follows. Let $r = F^{LMU}_{i+½-s} / F^{LMU}_{i+½}$, where FLMU = FLW - FUP and $s = \text{sign}(u_{i+½})$. Several limiter functions are available. The one used here is Superbee:

$$\varphi(r) = \max(0, \min(2r,1), \min(r,2)). \quad \text{(K.7)}$$

The TVD and PPM methods used in POLCOMS are based on one-dimensional schemes with directional splitting.

K.1.2 Bathymetry and boundary conditions

Bathymetry data used in the model are from LIDAR and echo sounding surveys for the Dee, Mersey and Ribble estuaries conducted by the UK Environment Agency and these are given with respect to Ordnance Datum Newlyn (ODN). The estuaries bathymetry data are accurate to a few centimetres and originally at 2-m horizontal resolution on British National Grid coordinates; they are first mapped on to longitude/latitude. At Liverpool Gladstone Lock and Hilbre Island at the mouth of the Dee, local CD is 4.93 m below ODN, therefore an offset of −4.93 m was added to the Dee and Mersey estuary depths to convert them to CD. Similarly the offset for the Ribble is −4.90 m. Water depths for the remaining parts of Liverpool Bay, from Admiralty Charts, are below the local Chart Datum (CD), which corresponds approximately to the Lowest Astronomical Tide (LAT) level. Admiralty Chart depths are to the nearest 0.1 m nearshore, and to the nearest meter offshore on a WGS84 longitude/latitude coordinate system.

Differences between how depths are referenced should be resolved through the use of a Vertical Offshore Reference Frame (www.cege.ucl.ac.uk/research/geomatics/vorf). A simpler approach is to reduce all datasets (in local CD) together on to a 1/400° long × 1/600° lat (approximately 180-m) rectangular grid, using gridding software (e.g., Kriging method in 'Surfer'). However, this does not account for increasing mean level with distance upstream in estuaries.

K.1.3 Model open boundary conditions

For tide-only model runs, amplitudes and phases of elevations and currents for each of 15 tidal constituents (diurnal: Q1, O1, P1, S1, K1; semi-diurnal: 2N2, Mu2, N2, Nu2, M2, L2, T2, S2, K2; quarter-diurnal: M4) were obtained from the Irish Sea 1.8 km model. Alternatively, times-series of observed elevations and currents can be used. These are interpolated onto the open boundary locations, to drive the Liverpool Bay model. POLCOMS uses Flather type flux/radiation barotropic boundary conditions (Holt and James, 2001).

K.1.4 Model bathymetry

Models require bathymetry with respect to Mean Tide Level (MTL). Jones (1994, pp43–45) outlines a method for determining differences between MTL and LAT (Lowest Astronomical Tide), linked to the amplitude of the M2 tidal elevations. An amplitude factor is calculated

$$A_{FACT} = \frac{\text{MTL} - \text{LAT}}{\text{MTL} - \tfrac{1}{2}(\text{MLWS} - \text{MLWN})} \tag{K.8}$$

where MLWS and MLWN are Mean Low Water Springs and Mean Low Water Neaps, respectively. Values for these can be found in Admiralty Tide Tables (ATT). Table 3.1 in Jones (1994) lists values for European shelf seas, in which the mean value of AFACT is 1.71. This is the factor by which the M2 elevation amplitude is multiplied to obtain the LAT to MTL offset.

The initial bathymetry has 5.15 m added to it to give the appropriate MTL at Liverpool. At this stage the water depths become deeper than their 'correct' values towards the western side of the model area; on the north-western part they are approximately 0.8 m too deep. The Liverpool Bay model was run to obtain timeseries of elevations from which the M2 elevation amplitude at each model grid-point ζˆM2(x, y), and then with the adjusted bathymetry and with the same open boundary conditions. After the second iteration, differences are less than 0.05 m.

K.2 Comparisons with observations

Table K.1 lists some results from the Liverpool Bay model (run for a spring-neap cycle) of four main constituents at three locations. Also listed are corresponding values from the UK National Tide Gauge Network (part of the National Tidal and Sea Level Facility, www.pol.ac.uk/ntslf) and Admiralty Tide Tables. While the model phases of M2 and S2 are similar, the amplitudes are generally a few centimeters larger than those observed. For K1 and O1, amplitudes are similar, and model phases lead slightly. Results are expected to improve for longer model runs.

Table K.1. Amplitudes and phases of four tidal constituents from the Liverpool Bay model, and corresponding values from the UK Tide Gauge Network and Admiralty Tide Tables (2000, Vol. 1, Part III).

Location	Mean tide level	M_2		S_2		K_1		O_1	
Liverpool Bay model	**(above CD)**	**ampl.**	**phase**	**ampl.**	**phase**	**ampl.**	**phase**	**ampl.**	**phase**
Liverpool Gladstone	5.15 m	3.11 m	324°	1.08 m	015°	0.12 m	185°	0.10 m	033°
Hilbre Island	5.09 m	3.04 m	317°	1.06 m	008°	0.12 m	182°	0.10 m	029°
Llandudno	*4.59* m	2.78 m	310°	0.99 m	358°	0.12 m	174°	0.10 m	022°
UK Tide Gauge Network									
Liverpool Gl, 1992–2000	5.20 m	3.03 m	321°	0.97 m	005°	0.12 m	191°	0.11 m	041°
Hilbre Island, 1964	5.14 m	2.92 m	318°	0.95 m	000°	0.11 m	189°	0.11 m	039°
Llandudno, 1994–2000	4.07 m	2.68 m	310°	0.86 m	351°	0.12 m	185°	0.11 m	036°
Admiralty Tide Tables									
Liverpool Gladstone	5.15 m	3.08 m	322°	1.00 m	007°	0.12 m	190°	0.11 m	042°
Hilbre Island	5.15 m	2.94 m	318°	0.96 m	001°	0.14 m	186°	0.12 m	041°
Llandudno	4.10 m	2.61 m	312°	0.82 m	355°	0.14 m	186°	0.12 m	036°

K.2.1 Sea surface currents

Two HF radar stations (at Formby Point and Llanddulas) each record radial components of sea surface currents for the Coastal Observatory (see http://cobs.pol.ac.uk/wera/). The M2 tidal constituents from a harmonic analysis of surface currents (combined vectors) recorded in 2007 are shown in Figure K.2 (red). These overlay surface currents from the Liverpool Bay model (shown in blue).

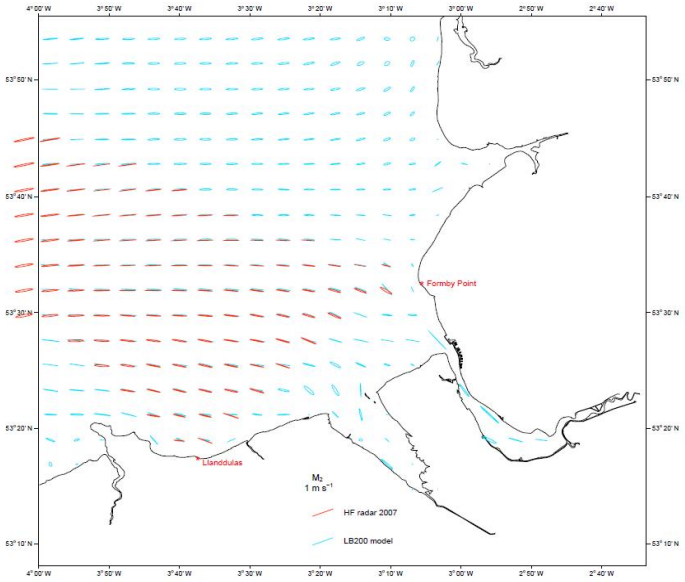

Figure K.2. Comparison of M2 surface current ellipses: HF radar during 2007 (red), and 180-m Liverpool Bay model (approximately one out of every 25 points is shown, in blue).

Offshore currents are mostly east-west and nearly rectilinear, becoming elliptical nearer the deeper northern part of the model area. Model currents are almost orientated in line with the HF radar currents, except nearshore. However, the model major axis amplitudes are smaller than radar amplitudes by a few percent, and there are also subtle differences in the eccentricities.

K.2.2 Stratification

Comparison between observed and measured stratification are shown in Figure K.3, Here we show data collected in the permanent mooring of the Coastal observatory during February 2003 and a model simulation, including tidal and riverine input only. It is clear that the model does a good job reproducing the amplitude and phase of the stratification showed as the near-bed-near-bottom density difference. The differences are mainly due to wind effects and to the three-dimensionality of the process near the mouth of the Mersey. This is shown in Figure K.4 where we see the potential energy anomaly at different stages of the tide.

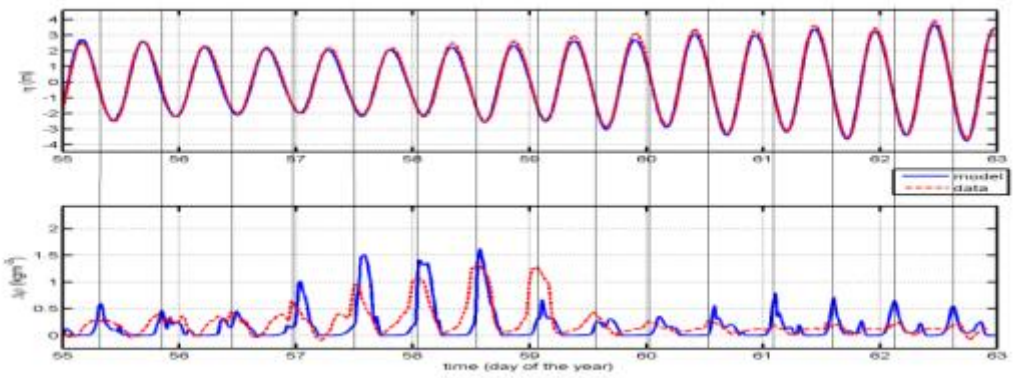

Figure K.3. Surface elevation (top panel); and Bottom-surface density difference, at the main mooring in the Irish Sea Observatory (bottom panel). Blue model red data.

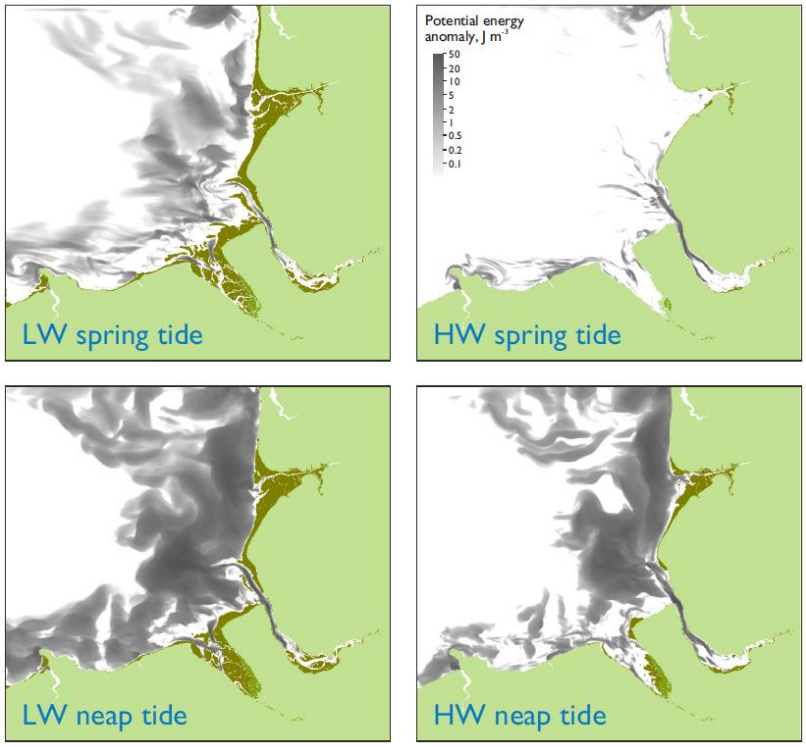

Figure K.4. Stratification in Liverpool Bay at different stages of the tidal cycle, represented using the potential energy anomaly.

K.2.3 Surge modelling

Surge results from the POLCOMS-WAM-GOTM model are compared with observations at the Hibre Island tide gauge during two storm-surge periods: Novmber 1977 and January 2007. Both show a promising comparison with peak surge values being well modelled both in terms of timing and amplitude.

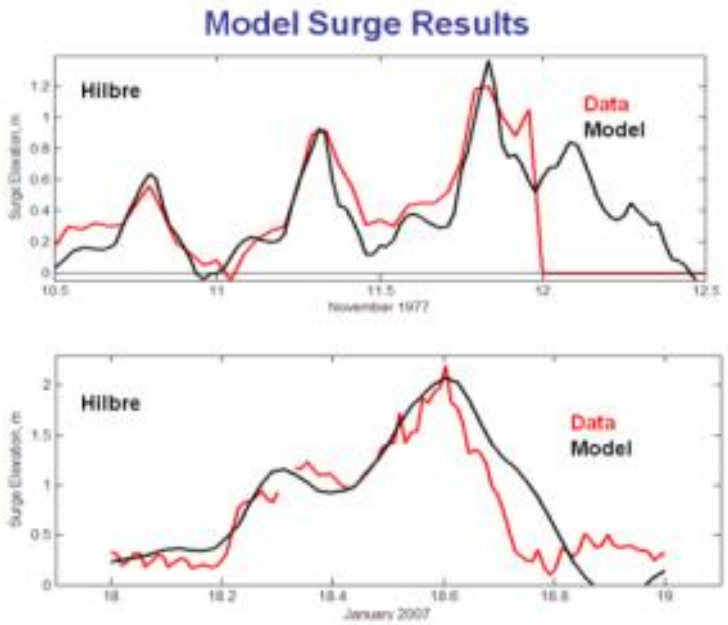

Figure K.5 Liverpool Bay Model surge results at Hibre Island for January 2007 and November 1977

K.3 References

Admiralty Tide Tables (Published annually, in four volumes), Vol. 1: *United Kingdom and Ireland. United Kingdom Hydrographic Office*, Taunton.

Coastal Observatory Irish Sea: POLCOMS Models (http://cobs.pol.ac.uk/polcoms), and The POL High Frequency (HF) Radar web site (http://cobs.pol.ac.uk/wera/).

Department of Civil, Environmental and Geomatic Engineering, University College London, Vertical Offshore Reference Frames project (www.cege.ucl.ac.uk/research/geomatics/vorf).

Holt, J.T., James, I.D. (2001), An s coordinate density evolving model of the northwest European continental shelf: 1, Model description and density structure, *Journal of Geophysical Research*, 106(C7), 14015–14034.

Howarth, M.J., Proctor, R., Balfour, C., Knight, P.J., Palmer, M., Player, R.J. (2008), The Liverpool Bay Coastal Observatory. In: PECS 2008: *Physics of Estuaries and Coastal Seas*, Liverpool, UK, 25th - 29th August 2008. Liverpool, 411-414.

Jones, J.E. (1994), *Numerical modelling of tides, surges, residual circulation and salinity in shelf seas*. Ph.D. Thesis, University of Liverpool. 300pp.

Colella, P., Woodward, P.R., 1984. The piecewise parabolic method (PPM) for gas-dynamical simulations. *Journal of Computational Physics,* 54, 174-201.

James, I.D., 1996. Advection schemes for shelf sea models. *Journal of Marine Systems,* 8, 237-254.

Sweby, P.K., 1984. High resolution schemes using flux limiters for hyperbolic conservation laws. *SIAM Journal of Numerical Analysis*, 21, 995-1011.

L Testbed report

The pdf of the testbed report is attached.

XBeach testbed report

status update None (02/16/11 13:41:32)

Revision: None

February 16, 2011

XBeach testbed report

Published and printed by:

Deltares
Rotterdamseweg 185
p.o. box 177
2600 MH Delft
The Netherlands

telephone: +31 88 335 85 85
fax: +31 88 335 85 82
e-mail: info@deltares.nl
www: http://www.deltares.nl

For support contact:

telephone: +31 88 335 85 55
fax: +31 88 335 81 11
e-mail: xbeach.support@deltares.nl
www: http://www.xbeach.org/

Contents

1 Introduction **1**

1.1 Introduction to the XBeach model 1

1.2 Model approach and innovations 2

1.3 XBeach testbed 3

2 Release information **5**

2.1 Release notes 5

2.2 Change log 5

3 Overview **7**

4 Test results **11**

4.1 Carrier and Greenspan 11

4.2 Long wave propagation 12

4.3 Boers 1C 13

4.4 Zelt case 1 15

4.5 Delilah 19

4.6 Deltaflume M1263 part III test 1 21

4.6.1 Introduction 21

4.6.2 Conditions 22

4.6.3 Results 22

4.6.4 References 23

4.7 Deltaflume M1263 part III test 2 23

4.7.1 Introduction 23

4.7.2 Conditions 23

4.7.3 Results 24

4.7.4 References 24

4.8 Deltaflume M1263 part III test 3 24
4.8.1 Introduction 25
4.8.2 Conditions 25
4.8.3 Results 25
4.8.4 References 26
4.9 Deltaflume M1263 part III test 4 26
4.9.1 Introduction 27
4.9.2 Conditions 27
4.9.3 Results 27
4.9.4 References 28
4.10 Deltaflume M1263 part III test 5 28
4.10.1 Introduction 29
4.10.2 Conditions 29
4.10.3 Results 29
4.10.4 References 29
4.11 DeltaflumeH298 T1 30
4.11.1 Results 30
4.12 DeltaflumeH298 T3 31
4.12.1 Results 32
4.13 Deltaflume LIP 11D 2E 33
4.14 Deltaflume 2006 T01 36
4.14.1 Results 36
4.15 T01 Zebra 46
4.15.1 MPI 49
4.16 Deltaflume 2006 T04 51
4.17 1953 storm surge 55
4.18 Zwin T01 57
4.18.1 Results 58
4.18.2 MPI 59
4.19 River Outflow 61
4.19.1 MPI 62
4.20 MICORE Cadiz 62
4.21 MICORE Dziwnow Spit 63
4.22 MICORE Lido de Sete 64

4.23 Assateague Island 66
4.24 NetCDF output 68
4.25 MICORE Mariakerke 68
4.26 MICORE Lido di Dante 70
4.27 MICORE Praia de Faro 71
4.28 MICORE Kamchia Shkorpilovtsi Beach 73

5 Default settings **75**
5.1 Carrier and Greenspan 75
5.2 Long wave propagation 76
5.3 Boers 1C 76
5.4 Zelt case 1 77
5.5 Delilah 78
5.6 Deltaflume M1263 part III test 1 79
5.7 Deltaflume M1263 part III test 2 80
5.8 Deltaflume M1263 part III test 3 81
5.9 Deltaflume M1263 part III test 4 81
5.10 Deltaflume M1263 part III test 5 82
5.11 DeltaflumeH298 T1 83
5.11.1 Results 83
5.12 DeltaflumeH298 T3 84
5.12.1 Results 84
5.13 Deltaflume LIP 11D 2E 85
5.14 Deltaflume 2006 T01 87
5.14.1 Results 87
5.15 T01 Zebra 93
5.16 Deltaflume 2006 T04 94
5.17 1953 storm surge 96
5.18 Zwin T01 97
5.18.1 Results 97
5.19 River Outflow 98
5.20 MICORE Cadiz 98
5.21 MICORE Dziwnow Spit 98
5.22 MICORE Lido de Sete 99

5.23 Assateague Island 99
5.24 MICORE Mariakerke 100
5.25 MICORE Lido di Dante 100
5.26 MICORE Praia de Faro 101
5.27 MICORE Kamchia Shkorpilovtsi Beach 101

Chapter 1

Introduction

1.1 Introduction to the XBeach model

The devastating effects of hurricanes on low-lying sandy coasts, especially during the 2004 and 2005 seasons have pointed at an urgent need to be able to assess the vulnerability of coastal areas and (re-)design coastal protection for future events, and also to evaluate the performance of existing coastal protection projects compared to do-nothing scenarios. In view of this the Morphos-3D project was initiated by USACE-ERDC, bringing together models, modelers and data on hurricane winds, storm surges, wave generation and nearshore processes. As part of this initiative an open-source program, XBeach for eXtreme Beach behaviour, has been developed to model the nearshore response to hurricane impacts. The model includes wave breaking, surf and swash zone processes, dune erosion, overwashing and breaching.

Existing tools to assess dune erosion under extreme storm conditions assume alongshore uniform conditions and have been applied successfully along relatively undisturbed coasts (Vellinga, 1986, Steetzel, 1993, Nishi and Kraus, 1996, Larson et al., 2004), but are inadequate to assess the more complex situation where the coast has significant alongshore variability. This variability may result from anthropogenic causes, such as the presence of artificial inlets, sea walls, and revetments, but also from natural causes, such as the variation in dune height along the coast or the presence of rip channels and shoals on the shoreface (Thornton et al., 2007). A particularly complex situation is found when barrier islands protect storm impact on the main land coast. In that case the elevation, width and length of the barrier island, as well as the hydrodynamic conditions (surge level) of the back bay should be taken into account to assess the coastal response. Therefore, the assessment of storm impact in these more complex situations requires a two-dimensional process-based prediction tool, which contains the essential physics of dune erosion and overwash, avalanching, swash motions, infragravity waves and wave groups.

With regard to dune erosion, the development of a scarp andepisodic slumping after undercutting is a dominant process (van Gent et al., 2008). This supplies sand to the swash and surf zone that is transported seaward by the backwash motion and by the undertow; without it the upper beach scours down and the dune erosion process slows down considerably. One-dimensional (cross-shore) models such as DUROSTA (Steetzel, 1993) focus on the underwater offshore transport and obtain the supply of sand by extrapolating these transports to the dry dune. Overton and Fisher (1988), Nishi and Kraus (1996) focus on the supply of sand by the dune based on the concept of wave impact. Both approaches rely on heuristic estimates of the runup and are well suited for 1D application but difficult to apply in a horizontally 2D

setting. Hence, a more comprehensive modelling of the swash motions is called for.

Swash motions are up to a large degree a result from wave-group forcing of infragravity waves (Tucker, 1954). Depending on the beach configuration and directional properties of the incident wave spectrum both leaky and trapped infragravity waves contribute to the swash spectrum (Huntley et al., 1981). Raubenheimer and Guza (1996) show that incident band swash is saturated, infragravity swash is not, therefore infragravity swash is dominant in storm conditions. Models range from empirical formulations (e.g. Stockdon et al., 2006) through analytical approaches (Schaeffer, 1994, Erikson et al., 2005) to numerical models in 1D (e.g. List, 1992, Roelvink, 1993b) and 2DH (e.g. van Dongeren et al., 2003, Reniers et al., 2004a, 2006). 2DH wavegroup resolving models are well capable of describing low-frequency motions. However, for such a model to be applied for swash, a robust drying/flooding formulation is required.

1.2 Model approach and innovations

Our aim is to model processes in different regimes as described by Sallenger (2000). He defines an Impact Level to denote different regimes of impact on barrier islands by hurricanes, which are the 1) swash regime, 2) collision regime, 3) overwash regime and 4) inundation regime. The approach we follow to model the processes in these regimes is described below.

To resolve the swash dynamics the model employs a novel 2DH description of the wave groups and accompanying infragravity waves over an arbitrary bathymetry (thus including bound, free and refractively trapped infragravity waves). The wave-group forcing is derived from the time-varying wave-action balance e.g. Phillips (1977) with a dissipation model for use in combination with wave groups (Roelvink, 1993a). A roller model (Svendsen, 1984; Nairn et al., 1990; Stive and de Vriend, 1994) is used to represent momentum stored in surface rollers which leads to a shoreward shift in wave forcing.

The wave-group forcing drives infragravity motions and both longshore and cross-shore currents. Wave-current interaction within the wave boundary layer results in an increased wave-averaged bed shear stress acting on the infragravity waves and currents (e.g. Soulsby et al., 1993 and references therein). To account for the randomness of the incident waves the description by Feddersen et al. (2000) is applied which showed good skill for longshore current predictions using a constant drag coefficient (Ruessink et al., 2001).

During the swash and collision regime the mass flux carried by the waves and rollers returns offshore as a return flow or a rip-current. These offshore directed flows keep the erosion process going by removing sand from the slumping dune face. Various models have been proposed for the vertical profile of these currents (see Reniers et al., 2004b for a review). However, the vertical variation is not very strong during extreme conditions and has been neglected for the moment.

Surf and swash zone sediment transport processes are very complex, with sediment stirring by a combination of short-wave and long-wave orbital motion, currents and breaker-induced turbulence. However, intra-wave sediment transports due to wave asymmetry and wave skewness are expected to be relatively minor compared to long-wave and mean current contributions (van Thiel de Vries et al., 2008). This allows for a relatively simple and transparent formulation according to SoulsbyVan Rijn (Soulsby, 1997) in a shortwave averaged but wave-group resolving model of surf zone processes. This formulation has been applied successfully in describing the generation of rip channels (Damgaard et al., 2002 Reniers et al., 2004a) and barrier breaching (Roelvink et al., 2003).

In the collision regime, the transport of sediment from the dry dune face to the wet swash, i.e. slumping or avalanching, is modeled with an avalanching model accounting for the fact that saturated sand moves more easily than dry sand, by introducing both a critical wet slope and dry slope. As a result slumping is predominantly triggered by a combination of infragravity swash runup on the previously dry dune face and the (smaller) critical wet slope.

During the overwash regime the flow is dominated by lowfrequency motions on the time scale of wave groups, carrying water over the dunes. This onshore flux of water is an important landward transport process where dune sand is being deposited on the island and within the shallow inshore bay as overwash fans (e.g. Leatherman et al., 1977; Wang and Horwitz, 2007). To account for this landward transport some heuristic approaches exist in 1D, e.g. in the SBeach overwash module (Larson et al., 2004) which cannot be readily applied in 2D. Here, the overwash morphodynamics are taken into account with the wave-group forcing of low-frequency motions in combination with a robust momentum-conserving drying/flooding formulation (Stelling and Duinmeijer, 2003) and concurrent sediment transport and bed-elevation changes.

Breaching of barrier islands occurs during the inundation regime, where a new channel is formed cutting through the island. Visser (1998) presents a semi-empirical approach for breach evolution based on a schematic uniform cross-section. Here a generic description is used where the evolution of the channel is calculated from the sediment transports induced by the dynamic channel flow in combination with avalanche-triggered bank erosion.

1.3 XBeach testbed

The XBeach code and related functionalities develop fast. As a result there is a need from modelers and code developers to develop a tool that gives insight in the effect of code developments on model performnace. The XBeach testbed tries to fulfill this need by running a range of tests including analytical solutions, laboratory tests and practical field cases every week with the latest code.

Chapter 2

Release information

2.1 Release notes

We have been working on a lot of cool stuff that still needs to be described in more detail:

- hard structures
- multiple sediment fractions
- bed load and suspended load
- output options
- wave schemes
- non-hydrostatic model
- wave shap parameterization
- drifters
- river outflow
- boundary condition stuff
- ...

2.2 Change log

REVISION: 1713 AUTHOR: mccall DATE: 02/15/11 16:48:23
MESSAGE: par%bedfricfile: try bed friction varying in space
FILES: /trunk/initialize.F90 M
/trunk/params.F90 M

REVISION: 1696 AUTHOR: mccall DATE: 02/10/11 10:46:09
MESSAGE: mpi runup gauge on slocal

FILES: /trunk/varoutput.F90 M

REVISION: 1691 AUTHOR: mccall DATE: 02/09/11 16:58:22
MESSAGE: iomsg is Fortran 2003, doesn't work for older compilers

FILES: /trunk/filefunctions.F90 M

Chapter 3

Overview

In the table below the statuses of all tests found in the testbed are summarized. In case a test is ignored or has failed, the corresponding message is given in the column "Message". Please note that success or failure of the test runs are given in column "Run status", while the success or failure of the Matlab analyses are given in column "Matlab status". The last columns provide an overview of the main characteristics of each test.

Tests can be run multiple times using different settings. Different runs are identified by a run name, which follows after the test name and a dot sign. If a test is run once only, it is common use to name the run *default*.

Table 3.1: Status overview testbed tests

Test	Run	Analysis	Default run	Default analysis	Configuration	Waves*	Water levels**	Fractions	Morphology	Hard layers	Groundwater flow
CarrierGreenspan.default	✓	✓	✓	✓	1D	ST	C	1			
CarrierGreenspan.mpi	✓	–	–	–	1D	ST	C	1			
long_wave_propagation.default	✓	✓	✓	✓	1D	ST	C	1			
long_wave_propagation.mpi	✓	–	–	–	1D	ST	C	1			
Boers_1C.default	✓	✓	✓	✓	1D	WG	C	1			
Boers_1C.mpi	✓	–	–	–	1D	WG	C	1			
Zelt_Case1.default	✓	✓	✓	✓	2D	WG	C	1			
Zelt_Case1.mpi	✓	✓	–	–	2D	WG	C	1			
Delilah_199010131000.default	✓	✓	✓	✓	2D	WG	C	1			
Delilah_199010131000.mpi	✓	–	–	–	2D	WG	C	1			
Delilah_199010131000.meanvars	✓	–	✓	–	2D	WG	C	1			
Deltaflume_M1263-3_Test-1.default	✓	✓	✓	✓	1D	WG	C	1	✓		
Deltaflume_M1263-3_Test-1.mpi	✓	–	–	–	1D	WG	C	1	✓		
Deltaflume_M1263-3_Test-2.default	✓	✓	✓	✓	1D	WG	C	1	✓		
Deltaflume_M1263-3_Test-2.mpi	✓	–	–	–	1D	WG	C	1	✓		
Deltaflume_M1263-3_Test-3.mpi	✓	–	–	–	1D	WG	V	1	✓		
Deltaflume_M1263-3_Test-3.default	✓	✓	✓	✓	1D	WG	V	1	✓		
Deltaflume_M1263-3_Test-4.mpi	✓	–	–	–	1D	WG	V	1	✓		

Table 3.1: Status overview testbed tests

Test	Run	Analysis	Default run	Default analysis	Configuration	Waves*	Water levels**	Fractions	Morphology	Hard layers	Groundwater flow
Deltaflume_M1263-3_Test-4.default	✓	✓	✓	✓	1D	WG	V	1	✓		
Deltaflume_M1263-3_Test-5.default	✓	✓	✓	✓	1D	WG	C	1	✓		
Deltaflume_M1263-3_Test-5.mpi	✓	–	–	–	1D	WG	C	1	✓		
DeltaflumeH298_T1.mpi	✓	–	–	–	1D	WG	C	1	✓	✓	
DeltaflumeH298_T1.default	✓	✓	✓	✓	1D	WG	C	1	✓	✓	
DeltaflumeH298_T3.default	✓	✓	✓	✓	1D	WG	C	1	✓	✓	
DeltaflumeH298_T3.mpi	✓	–	–	–	1D	WG	C	1	✓	✓	
DeltaflumeLIP11D_1B	–	–	–	–	1D	WG	C	1	✓		
DeltaflumeLIP11D_2E.mpi	✓	–	–	–	1D	WG	C	1	✓		
DeltaflumeLIP11D_2E.default	✓	✓	✓	✓	1D	WG	C	1	✓		
Deltaflume2006_T01.default	✓	✓	✓	✓	1D	WG	C	1	✓		
Deltaflume2006_T01.mpi	✓	–	–	–	1D	WG	C	1	✓		
Deltaflume2006_T01_zebra.mpi	✓	✓	–	–	1D	WG	C	2	✓		
Deltaflume2006_T01_zebra.default	✓	✓	✓	✓	1D	WG	C	2	✓		
Deltaflume2006_T02	–	–	–	–	1D	WG	C	1	✓		
Deltaflume2006_T04.default	✓	✓	✓	✓	1D	WG	C	1	✓		
Deltaflume2006_T04.mpi	✓	–	–	–	1D	WG	C	1	✓		
Deltaflume2006_DP01	–	–	–	–	1D	WG	C	1	✓		
1953_storm_surge.default	✓	✓	✓	✓	1D	WG	V	1	✓		
1953_storm_surge.mpi	✓	–	–	–	1D	WG	V	1	✓		
Zwin_T01.default	✓	✓	✓	✓	2D	ST	V	1	✓		
Zwin_T01.mpi	✓	✓	–	–	2D	ST	V	1	✓		
River_Outflow.default	✓	✓	✓	✓	2D	ST	C	1	✓		
River_Outflow.mpi	✓	✓	–	–	2D	ST	C	1	✓		
MICORE_Kamchia_Shkorpilovtsi_Beach.default	✓	✓	✓	✓	1D	WG	V	2	✓		✓
MICORE_Praia_de_Faro.mpi	–	–	–	–	1D	WG	V	1	✓		
MICORE_Mariakerke.default	✓	✓	✓	✓	1D	WG	V	1	✓	✓	
Curvi_MV2	–	–	–	–	2D	WG	C	1			
Netcdf.mpi	–	–	–	–	1D	ST	C	1			
Netcdf.default	✓	✓	–	–	1D	ST	C	1			
Assateague_Island.profB2	✓	–	✓	–	1D	ST	C	1	✓		
MICORE_Lido_di_Dante.default	✓	✓	✓	✓	1D	WG	V	1	✓		
MICORE_Lido_di_Dante.mpi	–	–	–	–	1D	WG	V	1	✓		
Curvi_Island	–	–	–	–	2D	WG	C	1			
Assateague_Island.profC	✓	–	✓	–	1D	ST	C	1	✓		
Assateague_Island.profA	✓	✓	✓	✓	1D	ST	C	1	✓		
Assateague_Island.profB1_mpi	✓	–	–	–	1D	ST	C	1	✓		
MICORE_Kamchia_Shkorpilovtsi_Beach.mpi	–	–	–	–	1D	WG	V	2	✓		✓
MICORE_Dziwnow_Spit.default	✓	✓	✓	✓	1D	WG	V	1	✓		
Assateague_Island.profB1	✓	–	✓	–	1D	ST	C	1	✓		
MICORE_Lido_de_Sete.mpi	–	–	–	–	1D	WG	V	1	✓		
MICORE_Cadiz.mpi	–	–	–	–	1D	WG	V	1	✓		

Table 3.1: Status overview testbed tests

Test	Run	Analysis	Default run	Default analysis	Configuration	Waves*	Water levels**	Fractions	Morphology	Hard layers	Groundwater flow
MICORE_Lido_de_Sete.default	✓	✓	✓	✓	1D	WG	V	1	✓		
MICORE_Cadiz.default	✗	✓	✗	✓	1D	WG	V	1	✓		
MICORE_Praia_de_Faro.default	✓	✓	✓	✓	1D	WG	V	1	✓		
MICORE_Mariakerke.mpi	–	–	–	–	1D	WG	V	1	✓	✓	
MICORE_Dziwnow_Spit.mpi	–	–	–	–	1D	WG	V	1	✓		

* ST = stationary, WG = wave groups, NH = non-hydrostatic
** C = constant, V = varying

Chapter 4

Test results

4.1 Carrier and Greenspan

Contact: Bas Hoonhout <bas.hoonhout@deltares.nl>

The purpose of this test is to check the ability of the model to represent runup and rundown of non-breaking long waves. To this end, a comparison was made with the analytical solution of the NSWE by Carrier and Greenspan (1958), which describes the motion of harmonic, non-breaking long waves on a plane sloping beach without friction.

A free long wave with a wave period of 32 seconds and wave amplitude of half the wave breaking amplitude ($a_{in} = 0.5 \cdot a_{br}$) propagates over a beach with constant slope equal to $1/25$. The wave breaking amplitude is computed as $a_{br} = {}^{1}/_{\sqrt{128}\cdot\pi^3} \cdot s^{2.5} \cdot T^{2.5} \cdot g^{1.25} \cdot h_0^{-0.25} = 0.0307 meter$, where s is the beach slope, T is the wave period and h_0 is the still water depth at the seaward boundary. The grid is non uniform and consists of 160 grid points. The grid size dx is decreasing in shoreward direction and is proportional to the (free) long wave celerity ($\sqrt{g \cdot h}$).The minimum grid size in shallow water was set at $dx = 0.1 meter$.

To compare XBeach output to the analytical solution of Carrier and Greenspan, the first are non-dimensionalized with the beach slope s, the acceleration of gravity g, the wave period T, a horizontal length scale L_x and the vertical excursion of the swash motion A. The horizontal length scale L_x is related to the wave period via $T = \sqrt{{}^{L_x}/_{g\cdot s}}$ and the vertical excursion of the swash motion A is expressed as: $A = a_{in} \cdot {}^{\pi}/_{\sqrt{0.125\cdot s\cdot T\cdot\sqrt{{}^{g}/_{h_0}}}}$

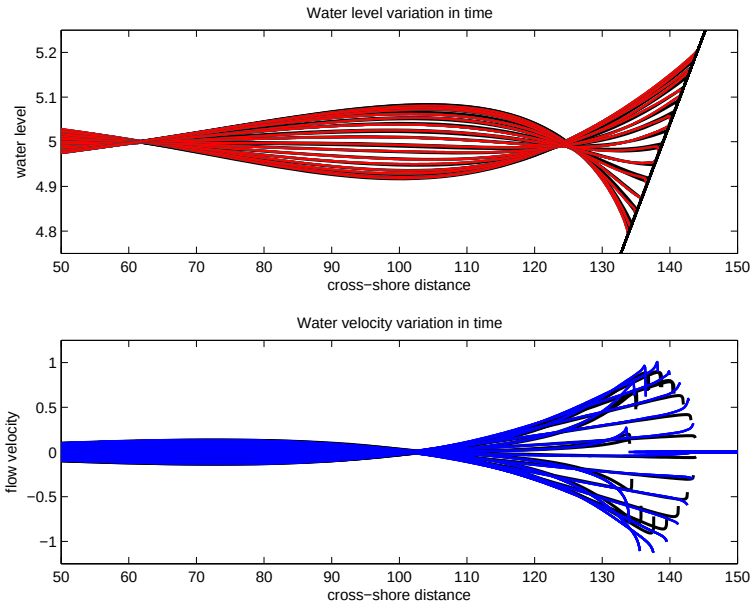

Figure 4.1

The two panels in Figure 4.1 compare the XBeach results with the analytical solution. The agreement should be reasonably well, though there are small deviations in the water level near the water line and the flow velocities seem to lag slightly on the analytical solution during the second part of the run down. Since the analytical solution is stationary, numerical output over multiple waves is shown in Figure 4.1, verifying that also the numerical solution is reasonably stationary.

Carrier, G.F., and Greenspan, H.P., *Water waves of finite amplitude on a sloping beach.* Journal of Fluid Mechanics, 1958, vol. 4, 97 - 109

4.2 Long wave propagation

Contact: Bas Hoonhout <bas.hoonhout@deltares.nl>

The purpose of the this test is to check if the NSWE numerical scheme is not too dissipative and that it does not create large errors in propagation speed.

A long wave with a small amplitude of $0.01m$ and period of $80s$ was sent into a domain of $5m$ depth, grid size of $5m$ and a length of $1km$. At the end, a fully reflecting wall is imposed. The wave length in this case should be $\sqrt{9.81 \cdot 5} \cdot 80 = 560m$. The velocity amplitude should be $\sqrt{g/h} \cdot A = \sqrt{9.81/5} \cdot 0.01 = 0.014m$. After the wave has reached the wall, a standing wave with double amplitude should be created.

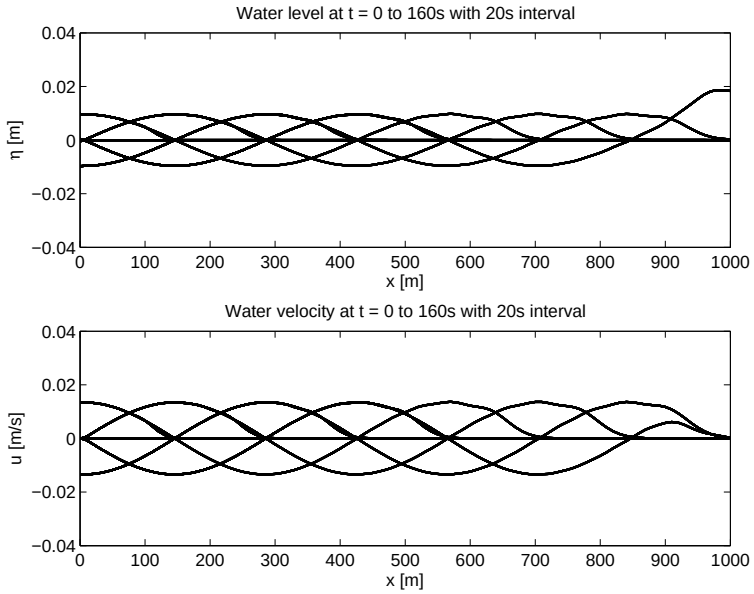

Figure 4.2

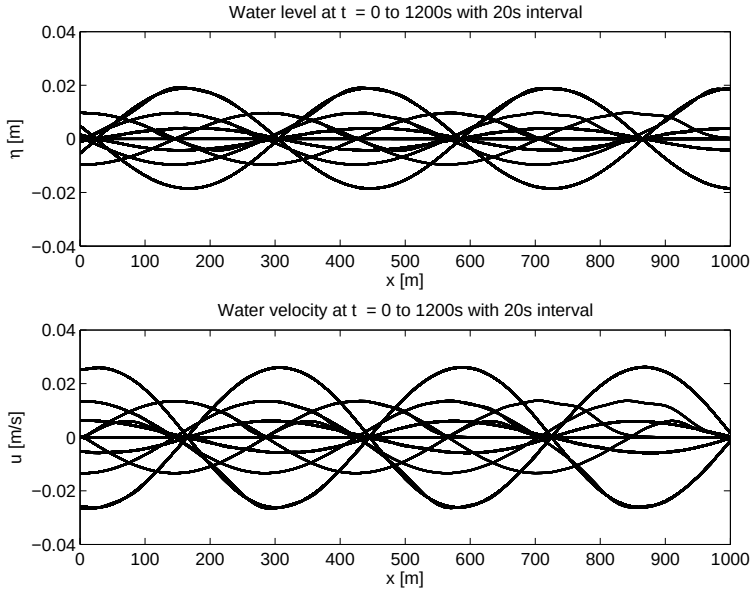

Figure 4.3

As Figure 4.2 and Figure 4.3 should show, the model accurately represents this situation. There is hardly any dissipation, the wave length is very close to what it should be and there is no reflection off the seaward boundary.

4.3 Boers 1C

Contact: Ap van Dongeren <ap.vandongeren@deltares.nl>

Boers (1996) performed experiments with irregular waves in the physical wave flume at Delft University of Technology with a length of 40 meters and a width of 0.8 m. The flume is

equipped with a hydraulically driven, piston type wave generator with second-order wave generation and Active Reflection Compensation. Boers ran waves over a concrete bar-trough beach, which was modelled after the Delta Flume experiments. He ran three different irregular wave conditions, but in this report we will focus on case 1C, a Jonswap spectrum with $H_{m,0} = 0.1 mand T_p = 3.3$s. The surface elevation was measured in 70 locations shown in Figure 4.4.

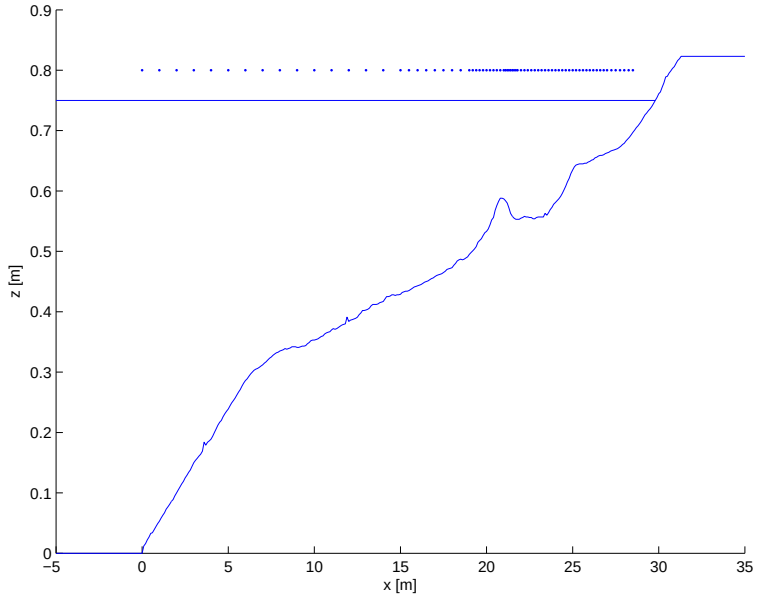

Figure 4.4

The comparison between the model and the data for the wave height transformation of the short waves and the long waves (defined as waves with a frequency greater than $f_p/2$ and less than $f_p/2$, respectively) is shown in Figure 4.5.

The top dark blue line indicates the short wave height transformation, which should compare well with the measurements, except for details around the breakpoint. The green line and stars indicate the mean (steady) set-up which should be well-predicted, except in the trough region (x=21-25 m). The red lines and stars indicate the total (incoming and reflected) low frequency wave, which is slightly overpredicted in the shoaling zone (up to the breakpoint) and stays too large after that.

The observational data is separated into incoming and reflected long wave components using an array of wave gauges (Bakkenes, 2002) and the numerical data has been separated into two components using co-located surface elevation and velocity information. The incoming long wave (cyan line) follows the observations (cyan stars) with a notable overprediction seaward of the breaking zone. The reflected long waves (black lines) match the observations (black stars) quite well.

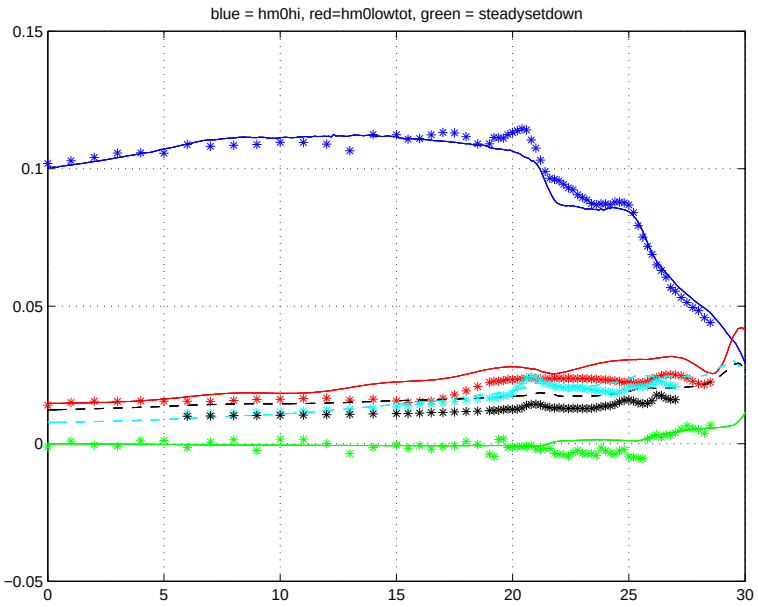

Figure 4.5

The model should perform reasonably well against the data for this well-measured but complex case.

Bakkenes, H.J., 2002. *Observation and seperation of bound and free low-frequency waves in the nearshore zone.* MSc Thesis, Delft University of Technology, Delft, The Netherlands.

Boers, M. (1996), *Simulation of a Surf Zone with a Barred Beach, Part 1: Wave heights and Wave breaking*, Communications on Hydraulic and Geotechnical Eng., Delft University of Technology, Civil Engineering, Report No. 96-5, 116 p.

4.4 Zelt case 1

Contact: Ap van Dongeren <ap.vandongeren@deltares.nl>

The verification cases so far considered solely the cross-shore dimension and assumed a longshore uniform coast. In the following cases the potential of the model to predict coastal and dune erosion in situations that include the two horizontal dimensions is further examined. A first step towards a 2DH response is to verify that the 2DH forcing by surge run-up and rundown is accurately modelled by testing not against Zelt (1986), but actually Özkan-Haller & Kirby (1997). The reason is that Zelt modeled the NSW equations including some dispersive and dissipative terms, which the present model does not have. For that reason, we also compared our model to the results of Özkan-Haller & Kirby (1997) who modeled the NSW equations using a Fourier-Chebyshev Collocation method, which does not have any numerical dissipation or dispersion errors. They use a moving, adapting grid with a fixed Δy (which is equal to the present model's Δy in this comparison) but with a spatially and temporally varying Δx so that the grid spacing in x near the shoreline is very small. In the present model Δx is set equal to Δy, which means that we can expect to have less resolution at the shoreline than Özkan-Haller & Kirby (1997).

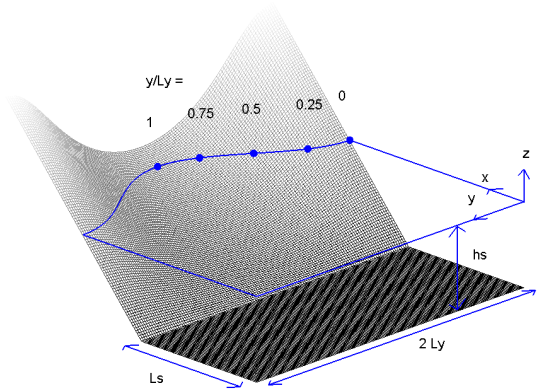

Figure 4.6

Figure 4.6 shows the definition sketch of the concave beach bathymetry in the present coordinate system, converted from the original system by Zelt (1986). The bathymetry consists of a flat bottom part and a beach part with a sinusoidally varying slope. For Zelt (1986)'s fixed parameter choice of $\sqrt{\beta} = \frac{h_s}{L_y} = \frac{4}{10\pi}$, the bathymetry is given by

$$h = \begin{cases} h_s & , \quad x \leq L_s \\ h_s - \frac{0.4\,(x - L_s)}{3 - \cos\left(\frac{\pi y}{L_y}\right)} & , \quad x > L_s \end{cases} \tag{4.1}$$

where h_s is the shelf depth, L_s is the length of the shelf in the modeled domain and L_y is the length scale of the longshore variation of the beach. This results in a beach slope of $h_x = \frac{1}{10}$ in the center of the bay and of $h_x = \frac{1}{5}$ normal to the "headlands". In the following we chose $L_y = 8\,m$, which determines $h_s = 1.0182\,m$. We set $L_s = L_y$. Different values for L_s only cause phase shifts in the results, but no qualitative difference, so this parameter is not important in this problem. Also indicated in the figure are the five stations where the vertical run-up (the surface elevation at the shoreline) will be measured.

At the offshore ($x = 0$) boundary we specify an incoming solitary wave, which in dimensional form reads

$$\zeta_i\,(t) \;=\; \alpha\; h_s \operatorname{sech}^2 \left(\sqrt{\frac{3\,g}{4\,h_s}\,\alpha\,(1+\alpha)} \quad (t \;-\; t_o) \right) \tag{4.2}$$

which is similar to Zelt (1986)'s Eq. (5.3.7). The phase shift t_o is chosen such that the surface elevation of the solitary wave at $t = 0$ is 1% of the maximum amplitude. The only parameter yet to be chosen is α. We will compare our model to Zelt's case of $\alpha = \frac{H}{h_s} = 0.02$, where H is the offshore wave height. Zelt found that the wave broke for a value of $\alpha = 0.03$, so the present test should involve no breaking, but has a large enough nonlinearity to exhibit a pronounced two-dimensional run-up.

Any outgoing waves will be absorbed at the offshore boundary by the absorbing-generating boundary condition. At the lateral boundaries $y = 0$ and $y = 2\,L_y$ we specify a no-flux (wall) boundary condition following Zelt. The model equations used in this test are the nonlinear shallow water equations without forcing or friction. The numerical parameters are $\Delta x = \Delta y = \frac{1}{8}\,m$ with a Courant number $\nu = 0.7$.

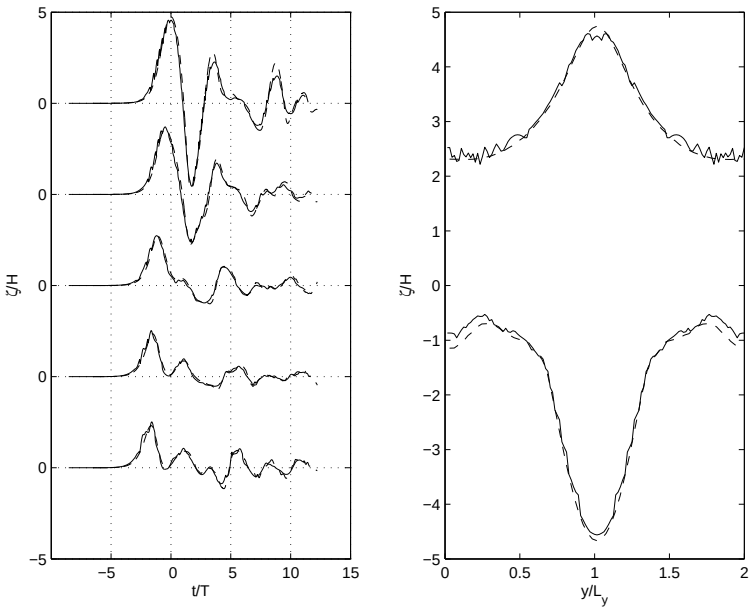

Figure 4.7

The first panel in Figure 4.7 shows the vertical runup normalized with the offshore wave height H as a function of time, which is normalized by $\sqrt{g\,h_s}/L_y$ at the 5 cross-sections indicated in Figure 4.6. The solid lines represent the present model results, while the dashed lines denotes Ozkan & Kirby (1997)'s numerical results. We should see that the agreement is generally good, except that the present model does not capture the second peak in the time series at $y/Ly = 1$ very well. This secondary peak or "ringing" is due to the wave energy that is trapped along the coast and propagates towards the midpoint of the bay (Zelt, 1986). It is suspected that this focusing mechanism is not properly captured, because the present method approximates the shoreline as a staircase pattern, which in effect lengthens the shoreline. Also, the spatial derivatives are not evaluated parallel and perpendicular to the actual shoreline but in the fixed x and y directions. The agreement at the locations $y/Ly = 0.25$, $y/Ly = 0.5$ and $y/Ly = 0.75$ is generally good despite the large gradient of the local shoreline relative to our grid.

The second panel in Figure 4.7 shows the maximum vertical run-up and run-down, normalized by H, versus the alongshore coordinate y. The maximum runup should agree well with Ozkan & Kirby (1997), but that the maximum rundown is not represented well in the center of the domain. The wiggles in the solid line are evidence of the staircasing of the shoreline: since the shoreline is not treated as a continuous but rather as a discrete function, so is the runup in the individual nodes.

Table 4.1: Error statistics Zelt Case 1

	R^2	Sci	Rel. bias	BSS
Timeseries (min)	0.07	0.16	-0.15	-5.11
Timeseries (max)	0.98	2.25	0.03	0.97
Max. runup	0.98	0.03	0.02	0.99

In conclusion, the shoreline boundary condition agrees well with the analytical solutions for the longshore uniform case but shows some discrepancies for the case of a concave beach, which can be attributed to the "staircase" discretization of the shoreline. The above results are consistent with the results obtained with the SHORECIRC model which is based on similar hydrodynamic equations, see Van Dongeren and Svendsen (1997), and show that also the current model is capable of representing run-up and run-down.

Özkan-Haller, H.T. and J.T. Kirby (1997). *A Fourier-Chebyshev collocation method for the shallow water equations including shoreline runup.* Applied Ocean Research, 19, pp. 21-34.

Zelt, J.A. (1986). *Tsunamis: the response of harbours with sloping boundaries to long wave excitation.* Doctoral dissertation, Rep. No. KH-R-47, W.M. Keck Laboratory of Hydraulics and Water Resources, Division of Engineering and Applied Science, California Institute of Technology, Pasadena, CA, 318 p.

In this section the results for the Zelt test are shown using an MPI-enabled version of XBeach.

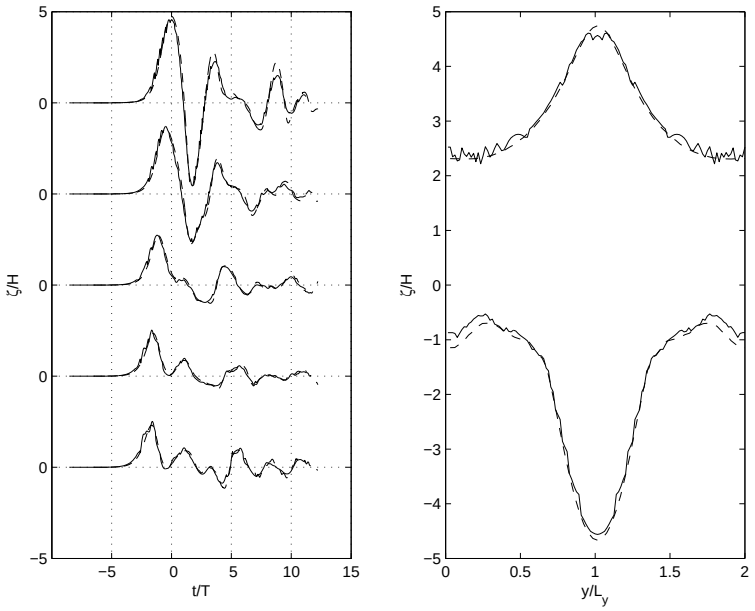

Figure 4.8

Table 4.2: Error statistics Zelt Case 1

	R^2	Sci	Rel. bias	BSS
Timeseries (min)	0.08	0.16	-0.15	-5.11
Timeseries (max)	0.98	2.25	0.03	0.97
Max. runup	0.98	0.03	0.02	0.99

4.5 Delilah

Contact: Robert McCall <robert.mccall@deltares.nl>

In order to verify the 2DH hydrodynamics of XBeach when forced by directionally-spread short waves, a simulation is set up to compare model results to field measurements. In this case the DELILAH field experiment at Duck, North Carolina is selected as a suitable test location. The period that is modeled is October 13th 1990, which was a stormy day, between 16:00 and 17:00 hours. The significant wave height at 8 m water depth was 1.81 m, with a peak period of 10.8 s and a mean angle of incidence of -16 relative to the shoreward normal. This period is selected because the wave conditions are energetic enough to generate a significant infragravity wave component and the incident wave spectrum is sufficiently narrow-banded to justify the assumptions in the model boundary conditions. The model is forced with the wave spectrum measured at 8 m water depth (Birkemeier et al., 1997). A measured tidal signal is imposed on the model boundaries of which the mean level is 0.69 m above datum. The slope of the wave front in the roller model is set to 0.05, which is found to be a slight improvement over the value of 0.10 used in the previous sections. A constant grid size of 5 m in cross shore and 10 m in longshore direction is used. The resolution of the wave model in directional space is 15. The model is set to generate output at the location of the primary cross shore measurement array, gauge numbers 10, 20, 30, 40, 50, 60, 70, 80 and 90 (Figure 4.9).

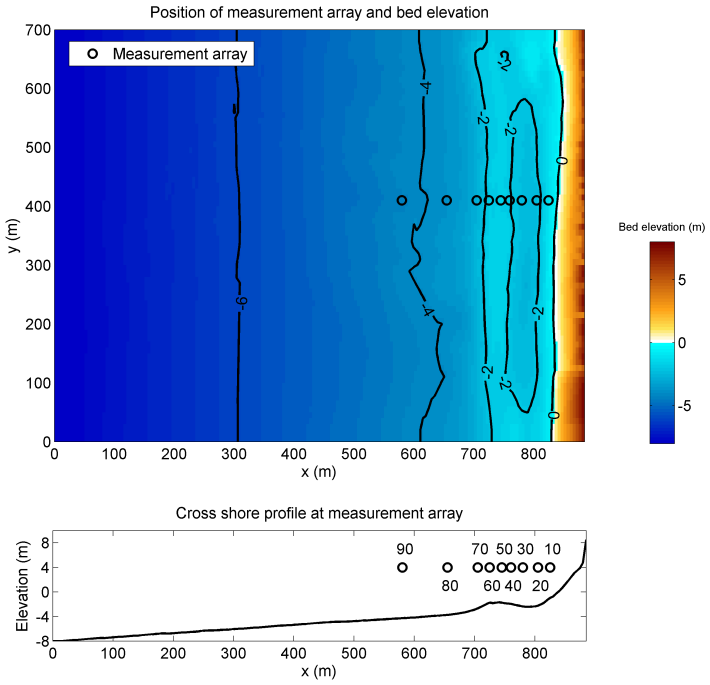

Figure 4.9: DELILAH field experiment 1990. Top panel: Plan view of the model location and measurement gauge array (circles). Bottom panel: Cross shore profile at the location of the measurement gauge array (circles) and measurement gauge names.

The modeled time-averaged wave heights of the short waves are compared to the time-averaged wave heights measured at the gauges. These results are shown in the first panel of Figure 4.10. Unfortunately, no data exist for gauge number 60.

The infragravity wave height is calculated as follows (van Dongeren et al., 2003):

$H_{rms,low} = \sqrt{8 \int_{0.005Hz}^{0.05Hz} Sdf}$

The second panel of Figure 4.10 should show that the XBeach model overestimates the infragravity wave height, but does follow the measured cross shore trend well.

The measured and modelled time-averaged longshore current are shown in the third panel of Figure 4.10. It can be seen that the model strongly under predicts the longshore current in the trench between measurement gauge 60 and the shore. Further calibration of the short wave and roller parameters is required in order to improve the simulated longshore current in this trough. The correlation coefficient, scatter index, relative bias and Brier Skill Score for the simulation are shown in Table 4.3.

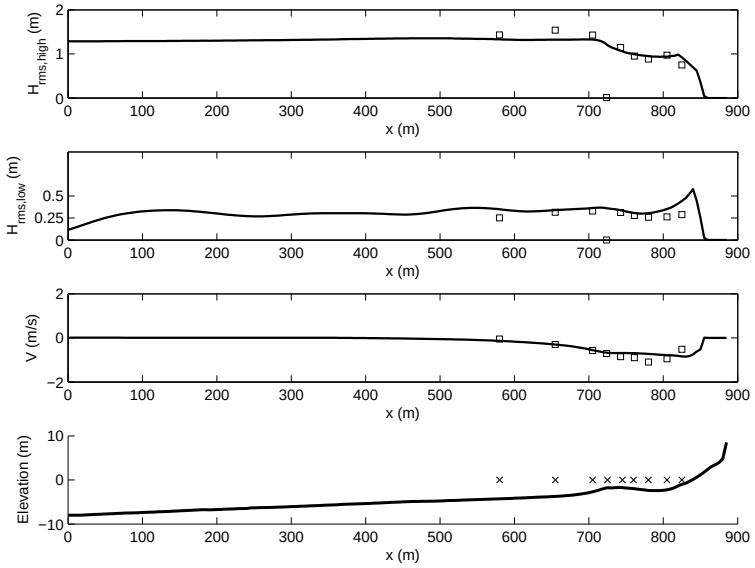

Figure 4.10: DELILAH field experiment 1990. First panel: Time-averaged measured (squares) and modelled (line) RMS-wave height of the short waves. Second panel: Time-averaged measured (squares) and modeled (line) RMS-wave height of the infragravity waves. Third panel: Time-averaged measured (squares) and modeled (line) longshore velocity. Fourth panel: Cross shore profile at the location of the measurement gauge array with the positions of the gauges (crosses).

Table 4.3: Error statistics Delilah

	R^2	Sci	Rel. bias	BSS
$H_{rms,HI}$	0.85	0.10	-0.03	0.83
$H_{rms,LO}$	0.17	0.26	0.22	-1.57
v	0.56	0.26	0.10	0.41

The modeled and measured sea surface elevation spectra at all nine gauge locations are shown in Figure 4.11. Note that the modeled surface elevation spectra only contain low frequency components associated with wave groups. The figure shows a migration of energy from high to low frequencies in shoreward direction in the measured spectra. The simulated spectra reproduce well the trend of increasing energy in the low frequency band in shoreward direction, but the amount of energy in the simulated low frequency band is less than in the measurements. In conclusion it can be stated that the model reproduces to a high degree of accuracy the short wave transformation in the shoaling and breaker zone. The transfer of energy from high to low frequencies in the model has qualitative skill. The longshore velocity

in the nearshore requires additional calibration of the short wave and roller parameters.

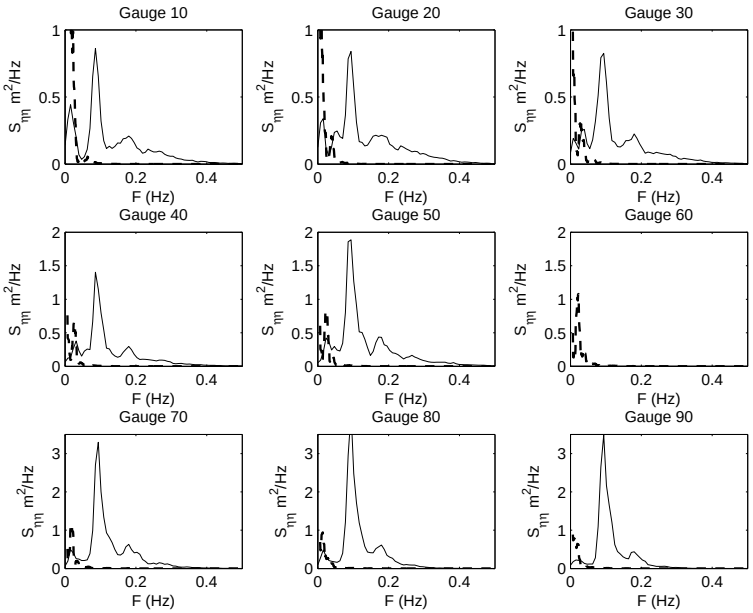

Figure 4.11: DELILAH field experiment 1990: Measured (solid line) and modelled (dashed line) surface elevation spectra for nine locations in the primary cross shore array. Gauge 90 is the most seaward.

Birkemeier, W.A., C. Donoghue, C. E. Long, K. K. Hathaway, and C. F. Baron (1997) *1990 DELILAH Nearshore Experiment: Summary report*, Tech. Rep. CHL-97-4-24, Field Res. Facil., U.S. Army Corps of Eng., Waterways Exper. Stn., Vicksburg., Miss.

Van Dongeren, A., A. Reniers, J. Battjes, and I. Svendsen (2003), *Numerical modeling of infragravity wave response during DELILAH*, J. Geophys. Res., 108(C9), 3288, doi:10.1029/2002JC001332.

4.6 Deltaflume M1263 part III test 1

Contact: Kees den Heijer <Kees.denHeijer@Deltares.nl>

4.6.1 Introduction

The M1263 dune erosion experiments were carried out in the large wave flume of Delft Hydraulics (now Deltares).

The dimensions of the so-called Deltaflume are as follows:

length	233 m
depth	7 m (locally 9 m)
width	5 m

The facility is equipped with a flap-type programmable wave generator,

maximum wave height random waves:	$H_s = 2$ m
maximum wave height periodic waves:	$H = 3$ m
wave period range:	$T = 2$ s to $T = 10$ s.

This experiment was carried out to verify the scale relations as developed by Vellinga (1986). Within the XBeach testbed, this test gives insight in the performance of the model with respect to one of the major experiments where DUROS (Vellinga, 1986) is based on.

4.6.2 Conditions

The cross-shore profile is based on a simplified profile which is considered as more or less representative for most of the Dutch coast. This profile is often referred to as *reference profile*. It has been scaled according to:

$n_d = 5$

$n_l = n_d(n_d/n_w^2)^{0.28} = 5(5/1)^{0.28} = 5^{1.28} = 7.85$

Sand from prototype with $D_{50} = 225$ μm was used as a bed material.

This experiment was carried out with constant hydraulic conditions:

wave height	1.5 m
wave period	5.4 s

4.6.3 Results

Figure 4.12 shows the profile development in time, simulated compared to measured. Table 4.4 shows the Brier Skill Scores at the moments in time which are comparable to profile measurements.

Table 4.4: Brier skill scores (time)

t [s]	BSS
360	0.67
1080	0.87
3600	0.86
10800	0.82
21600	0.88
36000	0.90

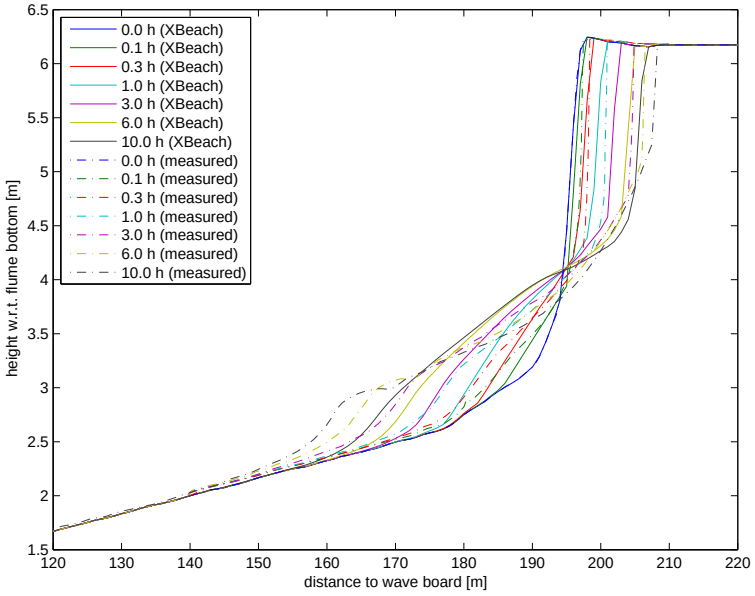

Figure 4.12: Comparison between measured and modelled profiles

4.6.4 References

Vellinga, P. (1986). Beach and Dune Erosion during Storm Surges. PhD thesis, Delft University of Technology. Also published as: Delft Hydraulics communications, no. 372, 1986.

4.7 Deltaflume M1263 part III test 2

Contact: Kees den Heijer <Kees.denHeijer@Deltares.nl>

4.7.1 Introduction

Similar to the previous one, this experiment was carried out to verify the scale relations as developed by Vellinga (1986). Within the XBeach testbed, this test gives again insight in the performance of the model with respect to one of the major experiments where DUROS (Vellinga, 1986) is based on.

4.7.2 Conditions

In this experiment, the same cross-shore profile as in Test 1 (subsection 4.6.2).

Sand from prototype with $D_{50} = 225$ μm was used as a bed material.

This experiment was carried out with constant hydraulic conditions:

wave height	1.5 m
wave period	5.4 s

4.7.3 Results

Figure 4.13 shows the profile development in time, simulated compared to measured. Table 4.5 shows the Brier Skill Scores at the moments in time which are comparable to profile measurements.

Table 4.5: Brier skill scores (time)

t [s]	BSS
360	0.79
1080	0.85
3600	0.87
10800	0.88
21600	0.90
36000	0.92

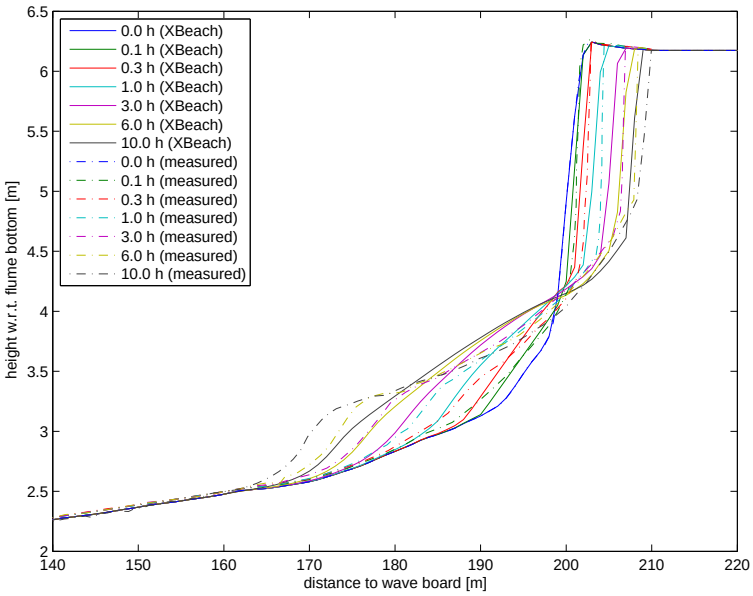

Figure 4.13: Comparison between measured and modelled profiles

4.7.4 References

Vellinga, P. (1986). Beach and Dune Erosion during Storm Surges. PhD thesis, Delft University of Technology. Also published as: Delft Hydraulics communications, no. 372, 1986.

4.8 Deltaflume M1263 part III test 3

Contact: Kees den Heijer <Kees.denHeijer@Deltares.nl>

4.8.1 Introduction

The aim of this experiment was to get more insight in the so far applied schematisation concerning the hydraulic conditions (WL | Delft Hydraulics, 1984). In this test the conditions are varying in time, whereas most other tests have constant conditions at the maximum level (storm surge level = NAP + 5m) with a shorter duration. Constant conditions were applied since the time scale of the dune erosion process was not yet known. It was more or less assumed that the erosion after 5 hours of constant conditions at the maximum storm surge level was comparable to a full storm surge with varying conditions.

Within the XBeach testbed, this test focusses on dune erosion under time varying conditions, which are very important for real cases.

4.8.2 Conditions

In this experiment, the same cross-shore profile as in Test 1 and 2 (subsection 4.6.2).

Sand from prototype with $D_{50} = 225$ μm was used as a bed material.

This experiment was carried out with time varying hydraulic conditions (Figure 4.16), of which the maximum values were:

wave height	1.5 m
wave period	5.4 s

4.8.3 Results

Figure 4.15 shows the profile development in time, simulated compared to measured. Table 4.6 shows the Brier Skill Scores at the moments in time which are comparable to profile measurements.

Table 4.6: Brier skill scores (time)

t [s]	BSS
6480	0.92
14400	0.92
69480	0.39

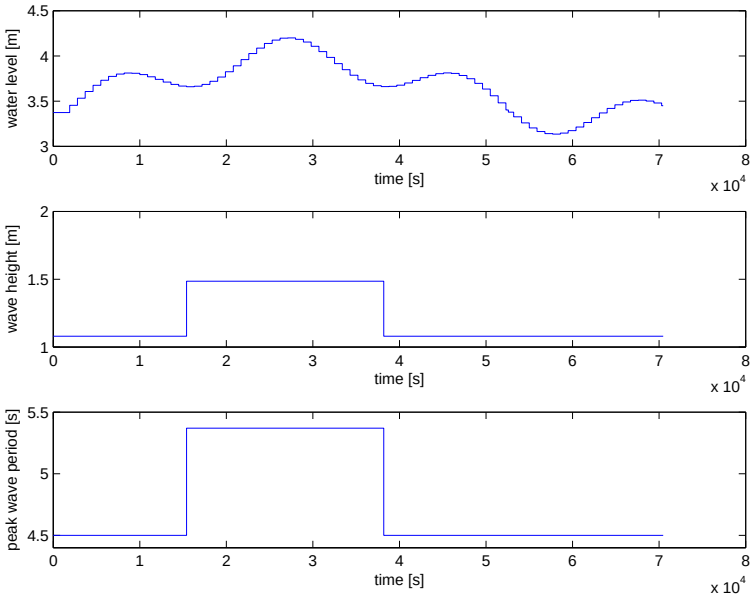

Figure 4.14: Hydraulic boundary conditions as function of time

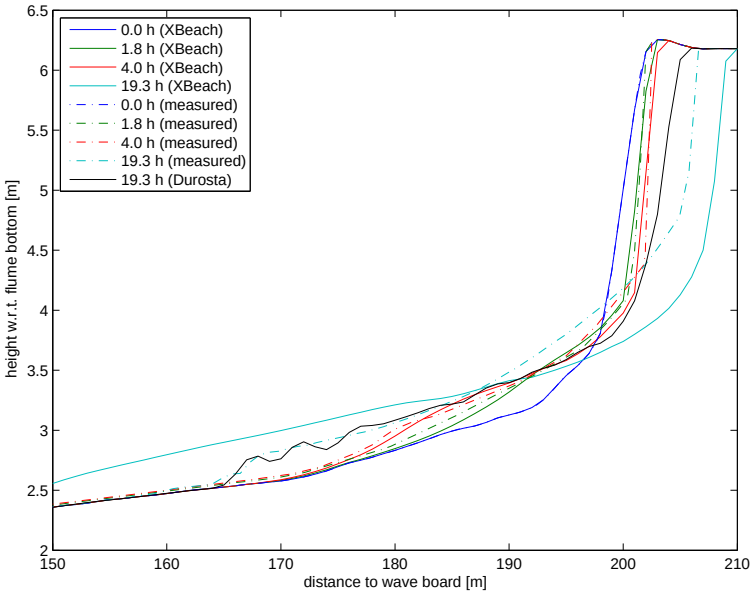

Figure 4.15: Comparison between measured and modelled profiles

4.8.4 References

Vellinga, P. (1986). Beach and Dune Erosion during Storm Surges. PhD thesis, Delft University of Technology. Also published as: Delft Hydraulics communications, no. 372, 1986.

4.9 Deltaflume M1263 part III test 4

Contact: Kees den Heijer <Kees.denHeijer@Deltares.nl>

4.9.1 Introduction

This experiment was meant as a large scale reproduction of the 1953 storm for a profile at the Delfland coast (The Netherlands). This also includes time varying conditions.

4.9.2 Conditions

The cross-shore profile in this experiment is a representation of a profile at the Delfland coast. It has been scaled according to:

$n_d = n_H = n_L = {n_T}^2 = 3.27$

$n_l = (3.27)^{1.28} = 4.56$

$n_t = (n_d)^{0.5} = (3.27)^{0.5} = 1.81$

Sand from prototype with $D_{50} = 225$ μm was used as a bed material.

This experiment was carried out with time varying hydraulic conditions (Figure 4.16), of which the maximum values were:

wave height	1.85 m
wave period	5.0 s

4.9.3 Results

Figure 4.17 shows the profile development in time, simulated compared to measured.

Table 4.7 shows the Brier Skill Scores at the moments in time which are comparable to profile measurements.

Table 4.7: Brier skill scores (time)

t [s]	BSS
18360	0.63
61200	0.72

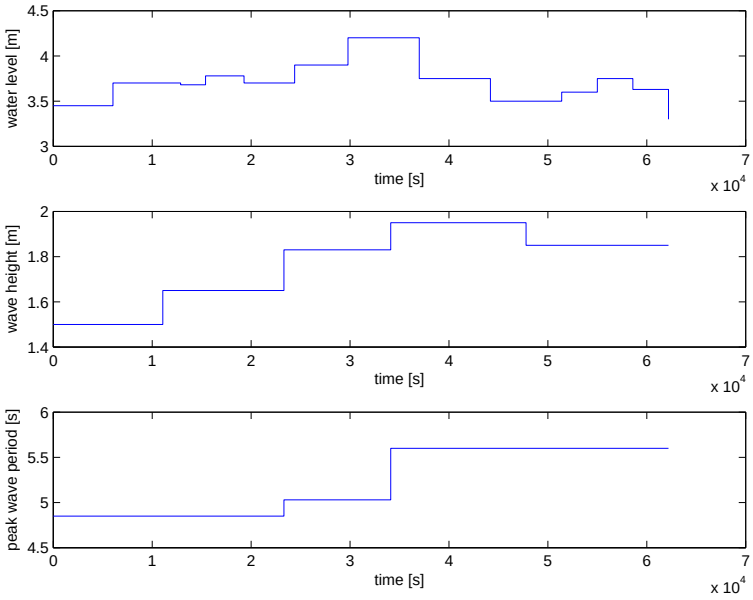

Figure 4.16: Hydraulic boundary conditions as function of time

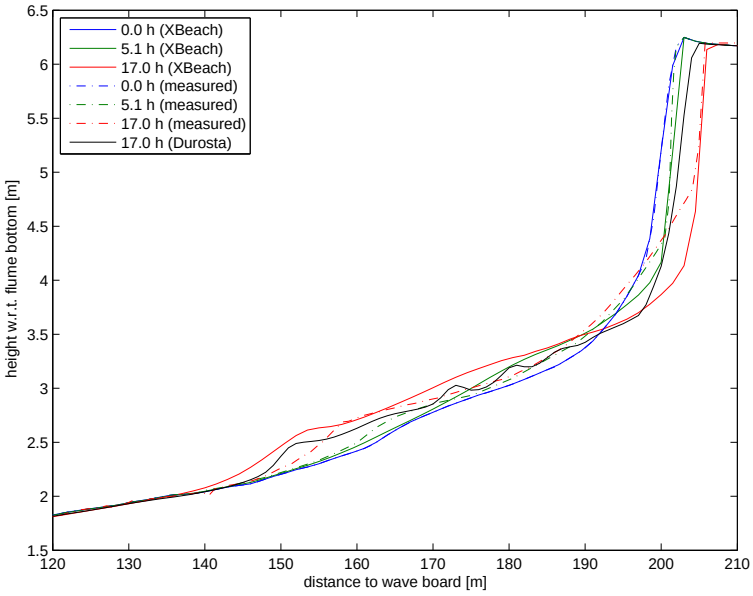

Figure 4.17: Comparison between measured and modelled profiles

4.9.4 References

Vellinga, P. (1986). Beach and Dune Erosion during Storm Surges. PhD thesis, Delft University of Technology. Also published as: Delft Hydraulics communications, no. 372, 1986.

4.10 Deltaflume M1263 part III test 5

Contact: Kees den Heijer <Kees.denHeijer@Deltares.nl>

4.10.1 Introduction

This experiment was set up as a full scale replica of a moderate storm surge in nature. Albeit that the conditions were constant.

4.10.2 Conditions

The cross-shore profile in this experiment was derived from the reference profile (subsection 4.6.2).

4.10.3 Results

Figure 4.18 shows the profile development in time, simulated compared to measured. Table 4.8 shows the Brier Skill Scores at the moments in time which are comparable to profile measurements.

Table 4.8: Brier skill scores (time)

t [s]	BSS
10800	0.87
21600	0.98

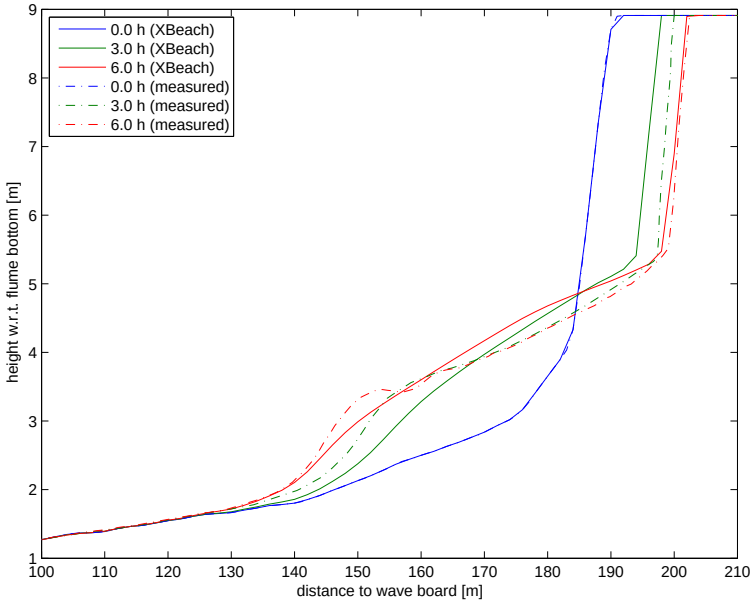

Figure 4.18: Comparison between measured and modelled profiles

4.10.4 References

Vellinga, P. (1986). Beach and Dune Erosion during Storm Surges. PhD thesis, Delft University of Technology. Also published as: Delft Hydraulics communications, no. 372, 1986.

4.11 DeltaflumeH298 T1

Contact: Jaap van Thiel de Vries <jaap.vanthieldevries@deltares.nl>

In test T1 of the Deltflume H298 series (Steetzel,1987) scour hole development in front of a dune revetment is ivestigated. The test was carried out at a depth scale nd = 5 (Vellinga, 1986) and the initial profile in the flume correponds to the reference profile for the Dutch Holland coast. At the dune foot (located at x = 193 m from the wave board and z = 3.80 m above the flumes floor) a concrete revetment is applied that covers almost the whole dune face (slope of 1:1.8). The lower end of the revetment is located at z = 2.5 m and the top end at z = 6.2 m. The test was conducted with a constant water level (set at z = 4.2 m) and wave conditions that correpsond to a Pierson Moskowitz spectrum with Hm0 = 1.52 m and Tp = 5.37s. The sand applied in the test has a median grain diameter (D_{50}) of approximately 210 um.

4.11.1 Results

Simulated and measured profile development are compared in (Figure 4.19). In the physical experiment the scour hole devlops till a depth of z = 2.59 m above after seven hours simulation (is 1.21 meter below the dune foot). Computed bedlevel changes for sources and sinks (sourcesink=1) versus sediment transport gradients (sourcesink=0) are comparable. Without any relevant model improvements it is concluded that XBeach underestimates the erosion depth at the toe of the revetment. It seems an explaination may be found in simulated sediment suspensions in the proximity of the revtment, which are underestimated with a factor two (Figure 4.20). The simulated mean flow is supposed to be in reasonable agreement with measurements.

Steetzel, H.J., 1987. Systematic reserach on the effectiveness of dune toe revetments, Large scale model investigation (in Dutch), Report H298-I, Delft Hydraulics, Delft, The Netherlands.

Table 4.9

	R^2	SCI	Rel. Bias	BSS
sedero	0.6409	0.8598	0.0338	0.2544

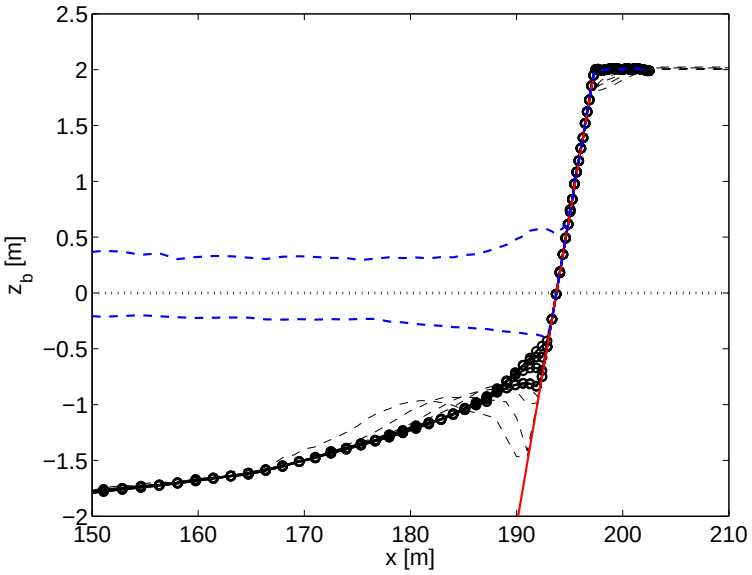

Figure 4.19

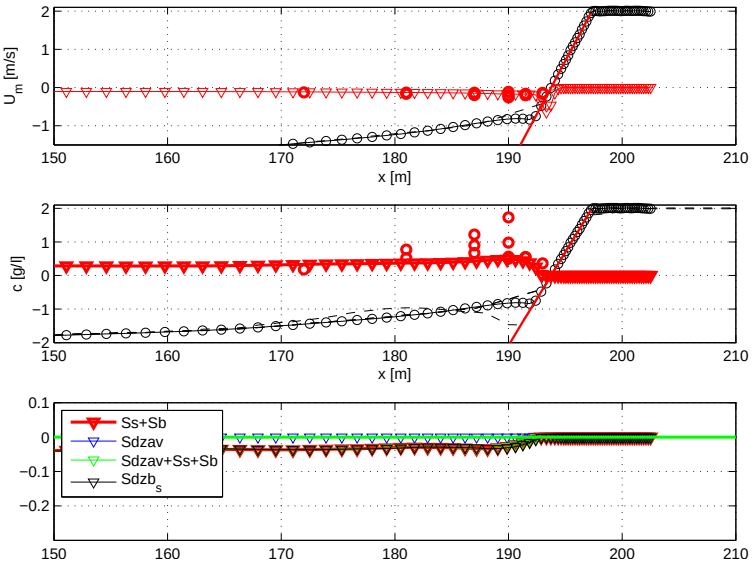

Figure 4.20

4.12 DeltaflumeH298 T3

Contact: Jaap van Thiel de Vries <jaap.vanthieldevries@deltares.nl>

In test T3 of the Deltflume H298 series (Steetzel,1987) erosion above medium height dune revetment is ivestigated. The test was carried out at a depth scale nd = 5 (Vellinga, 1986) and the initial profile in the flume correponds to the reference profile for the Dutch Holland coast. At the dune foot (located at x = 193 m from the wave board and z = 3.80 m above the flumes floor) a concrete revetment is applied that partly covers the dune face (slope of 1:1.8). The lower end of the revetment is located at z = 2.5 m and the top end at z = 4.8 m. The test was conducted with a constant water level (set at z = 4.2 m) and wave conditions that correpsond to a Pierson Moskowitz spectrum with Hm0 = 1.52 m and Tp = 5.37s. The

sand applied in the test has a median grain diameter (D_{50}) of approximately 210 um.

4.12.1 Results

Simulated and measured profile development are compared in (Figure 4.21). In the physical experiment the eroded volume above the revetment is $10.37m^3$ and at the toe of the revtment a scour hole devlops till a depth of z = 0.92 m above after seven hours simulation (is 1.21 meter below the dune foot). Without any relevant model improvements it is concluded that XBeach underestimates the erosion volume above the revetment and the erosion depth at the toe of the revetment. Considering the limited erosion volume above the revetment it is hypothesized that in addition to long wave run-up also short wave runup should be included in the avalanching algorithm (which is the main mechanism to release sand from the dunes). As mentioned before in test T1 a reasonable explaination for the underestimation of the scour depth at the toe of the revetment may be found in simulated sediment suspensions in the proximity of the revtment, which are underestimated with a factor two ((Figure 4.22)). The simulated mean flow is supposed to be in reasonable agreement with measurements.

Steetzel, H.J., 1987. Systematic reserach on the effectiveness of dune toe revetments, Large scale model investigation (in Dutch), Report H298-I, Delft Hydraulics, Delft, The Netherlands.

Table 4.10

	R^2	SCI	Rel. Bias	BSS
sedero	0.1889	0.9913	0.0487	0.0168

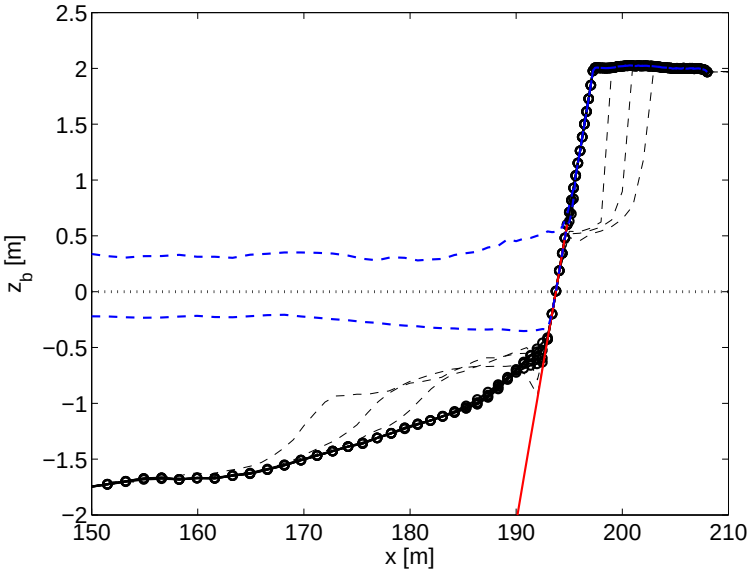

Figure 4.21

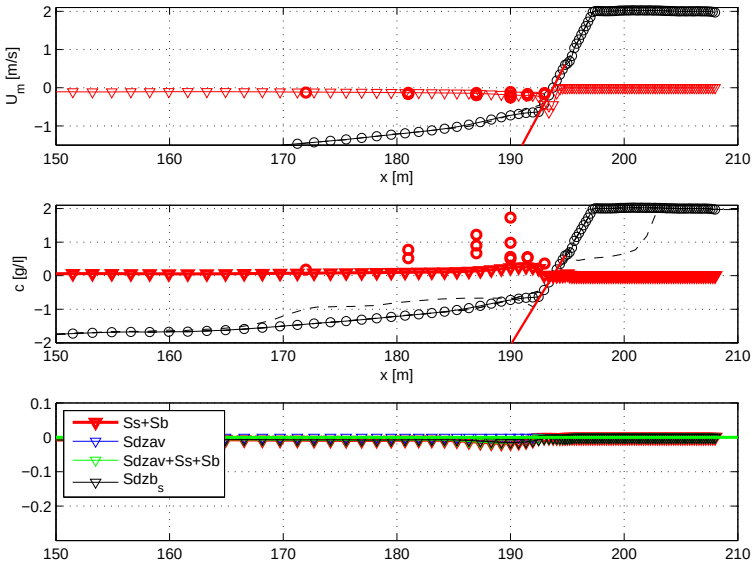

Figure 4.22

4.13 Deltaflume LIP 11D 2E

Contact: Bas Hoonhout <bas.hoonhout@deltares.nl>

This model test, described in Arcilla et al. (1994), concerns extreme conditions with a raised water level at 4.58 m above the flume bottom, a significant wave height, H_{m0}, of 1.4 m and peak period, T_p, of 5 s. Bed material consisted of sand with a D_{50} of approximately 0.2 mm. During the test substantial dune erosion took place.

Based on the integral wave parameters H_{m0} and T_p and a standard Jonswap spectral shape, time series of wave energy were generated and imposed as boundary condition. Since the flume tests were carried out with first-order wave generation (no imposed super-harmonics and sub-harmonics), the hindcast runs were carried out with the incoming bound long waves set to zero ('first order wave generation'). Active wave reflection compensation was applied in the physical model, which has a result similar to the weakly reflective boundary condition in XBeach, namely to prevent re-reflecting of outgoing waves at the wave paddle (offshore boundary).

A grid resolution of 1 m was applied and the sediment transport settings were set at default values. For the morphodynamic testing the model was run for 0.8 hours of hydrodynamic time with a morphological factor of 10, effectively representing a morphological simulation time of 8 hours.

Test results are given for the root mean square wave height, H_{rms}, and the root mean square orbital velocity, U_{rms}, separated in high-frequency (frequencies above $f_p/2$ corresponding to incident waves) and low-frequency parts (corresponding to infragravity waves). In XBeach model terms, these parameters are defined as follows:

$$H_{rms,HI} = \sqrt{< H^2 >} \tag{4.3}$$

$$u_{rms,HI} = \sqrt{< u_{rms}^2 >} \quad , \quad u_{rms} = \frac{1}{\sqrt{2}} \frac{\pi H}{T_p sinh(kh)} \tag{4.4}$$

$$H_{rms,LO} = \sqrt{8 < (\eta - < \eta >)^2 >} \tag{4.5}$$

$$u_{rms,LO} = \sqrt{< (u^L - < u^L >)^2 >} \tag{4.6}$$

$$\tag{4.7}$$

In Figure 4.23 the results are shown for first order wave generation (as in the flume tests). The model is clearly capable of capturing both the HF and LF wave heights and orbital velocities. For this test, the agreement is better if incoming bound long waves are omitted from the flow boundary condition (as they were in the laboratory test).

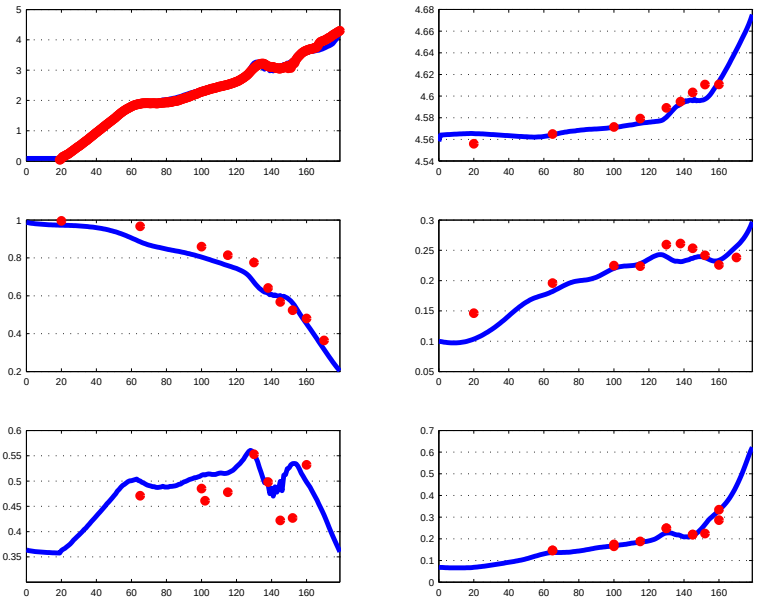

Figure 4.23: Computed and observed hydrodynamic parameters for test 2E of the LIP11D experiment. Top left: bed level and mean water level. Top right: measured (dots) and computed mean water level with first-order steering (drawn line) as function of the cross-shore distance. Middle left: same for HF wave height; middle right: same for LF wave height; bottom left: same for HF orbital velocity; bottom right: same for LF orbital velocity.

In Figure 4.24 the horizontal distribution of sedimentation and erosion after 8 hours is shown, and the evolution in time of the erosion volume and the dune retreat. We see a good agreement for all three parameters. Noteworthy is the episodic behaviour of the dune erosion, both in measurements and model, although the almost exact (deterministic) reproduction of the (stochastic) dune retreat must be a coincidence. An important conclusion for physical model tests is that for dune erosion it does make a difference whether first-order or second-order wave steering is applied.

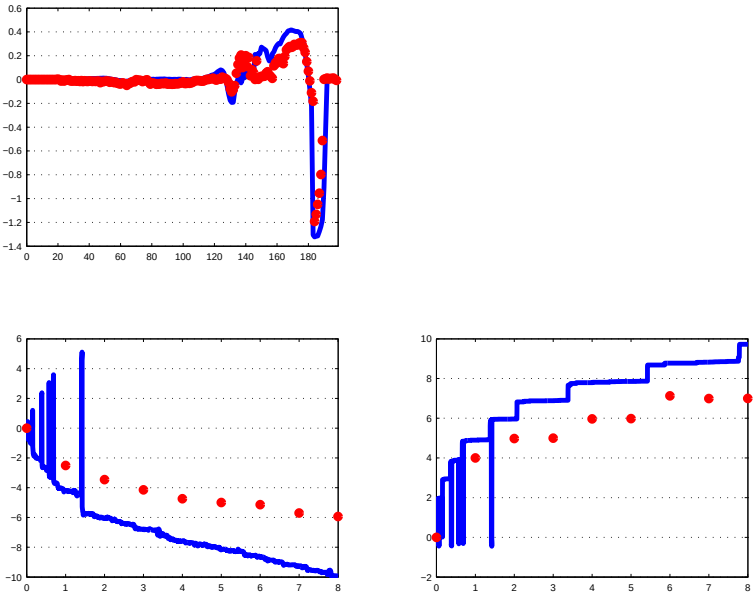

Figure 4.24: Computed and observed sedimentation and erosion after 8 hrs (top panel); erosion volume as function of time (bottom left) and dune retreat (bottom right) as function of time for test 2E of the LIP11D experiment, (Arcilla et al, 1993). All results with first-order steering.

A key element in the modelling is the avalanching algorithm; even though surfbeat waves running up and down the upper beach are fully resolved by the model, without a mechanism to transport sand from the dry dune face to the beach the dune face erosion rate is substantially underestimated. The relatively simple avalanching algorithm described above, whereby an underwater critical slope of 0.3 and a critical slope above water of 1.0 are applied, proves to be quite successful in representing the retreat of the upper beach and dune face. In Figure 4.25 the measured and modelled bed evolution are shown, which looks quite good in the upper region.

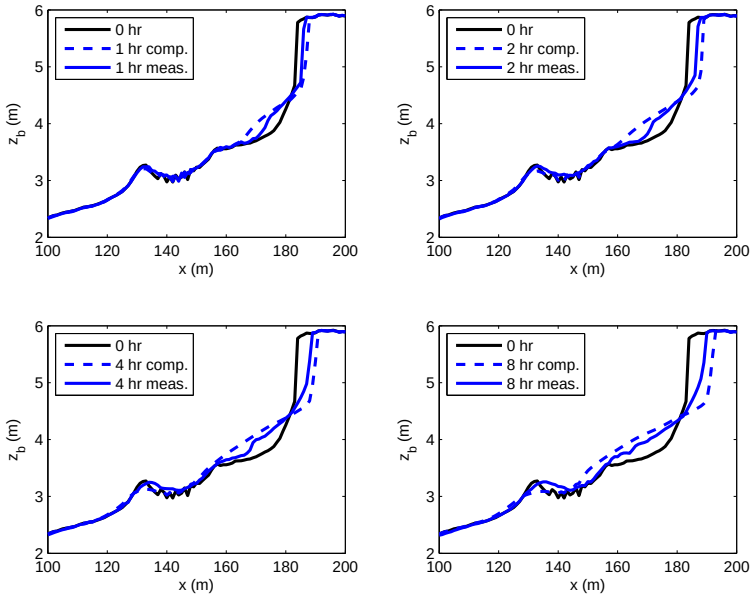

Figure 4.25: Measured and modelled bed level after 1, 2, 4 and 8 hours of wave action, for a water level of 4.56 m above the flume bottom.

Error statistics for the standard run are collected in Table 4.11, and generally show a scatter index and relative bias of less than 10% for the hydrodynamic parameters and overall erosion volumes and dune retreat. An exception is the mean velocity, for which the higher scatter and bias can be attributed to the (neglected) 3D structure of this parameter. The horizontal distribution of the sedimentation and erosion at the end of the test shows a higher scatter, determined in part by the areas with small changes; the Brier Skill Score shows a value of 0.72, which for morphodynamic models is considered good (Van Rijn et al., 2003).

Table 4.11: Error statistics Deltaflume LIP 11D 2E

	R^2	Sci	Rel. bias	BSS
$SEDERO$	0.91	0.61	-0.11	0.64
ETA	0.84	0.00	-0.00	0.89
VOL	0.87	0.66	-0.64	0.60
R	0.85	0.30	0.29	0.75
$URMS$	0.21	0.11	0.07	0.01
$URMS_{LO}$	0.87	0.09	0.00	0.86

Arcilla, A. S., J. A. Roelvink, B. A. OConnor, A. Reniers, and J. A.Jimenez (1994), *The Delta flume 93 experiment*, in Coastal Dynamics '94, edited by A. S. Arcilla, N. C. Kraus, and S. J. F. Marcel, pp. 488-502, Am. Soc. of Civ. Eng., Reston, Va.

Van Rijn, L.C., D. J. R. Walstra, B. Grasmeijer, J. Sutherland, S. Pan, J. P. Sierra, *The predictability of cross-shore bed evolution of sandy beaches at the time scale of storms and seasons using process-based Profile models*, Coastal Engineering, Volume 47, Issue 3, January 2003, Pages 295-327, ISSN 0378-3839, DOI: 10.1016/S0378-3839(02)00120-5.

4.14 Deltaflume 2006 T01

Contact: Jaap van Thiel de Vries <jaap.vanthieldevries@deltares.nl>

The aim of this test is to make a detailed comparison between simulated physics over an evolving bathymetry and the measurements obtained during the Deltaflume experiment in 2006 (Van Gent et al, 2008). For brevity this comparison is performed only for test T01 (this test corresponds best to the Dutch normative conditions). The simulation is performed on a regular grid with dx = 1 m and input to the model are time series of short wave varying energy (low pass filtered on the wave group time scale) and incoming (bound) long waves. The time series are constructed from pressure and flow measurements at x = 41 m from the wave board. The short wave group velocity (associated with advection of wave action) is based on the Tm-1,0 wave period. Other model settings can be found in Van Thiel de Vries (2009)

4.14.1 Results

Wave height transformation and wave setup (Figure 4.26) are favourably reproduced with the model. The long wave height is slightly underestimated whereas the wave setup is slightly overestimated. The correlation between measured short wave variance and long wave water surface elevations (Figure 4.27) corresponds reasonably well with the measurements. Towards the shoreline this correlation increases (Abdelrahman and Thornton, 1987; Roelvink and

Stive, 1989) meaning the highest short waves travel on top of long waves, which likely causes that more short wave energy gets closer to the dune face.

Short wave skewness and asymmetry are reasonably predicted with the extended Rienecker Fenton model (Figure 4.28). However, in the inner surf zone both wave skewness and asymmetry are overestimated. Possible explanations are wave breaking, which limits the steepness and height of waves and the presence of free harmonics in the flume. Both these effects are not included in the wave shape model but indeed are present in the flume test (see Van Thiel de Vries, 2009). From simulated skewness and asymmetry it follows that the total nonlinearity of a short wave is overestimated close to the dune face (Figure 4.29). The phase Beta is favourably simulated with the model but is underestimated further offshore.

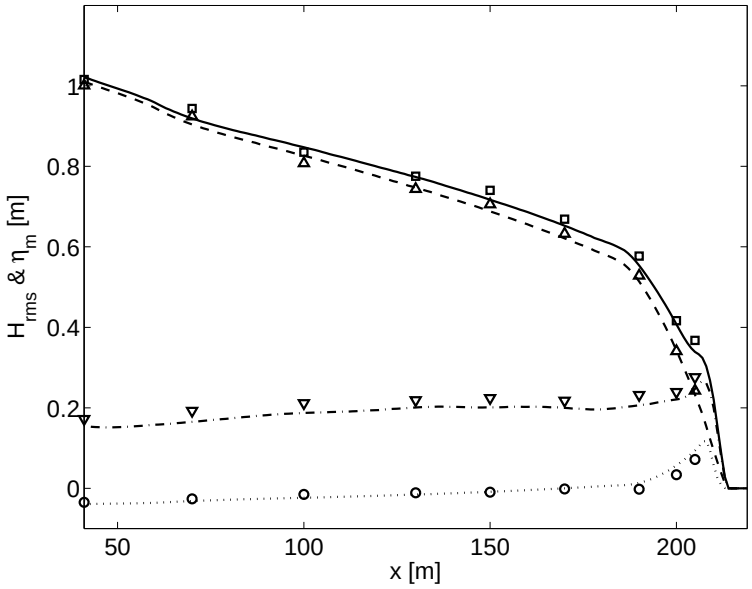

Figure 4.26: Simulated wave setup (dotted line) and transformation of the total (solid line), short (dashed line) and long (dashed-dotted line) wave height compared with measurements of the wave setup (circles) and the total (squares), short (upward triangles) and long (downward triangles) wave height.

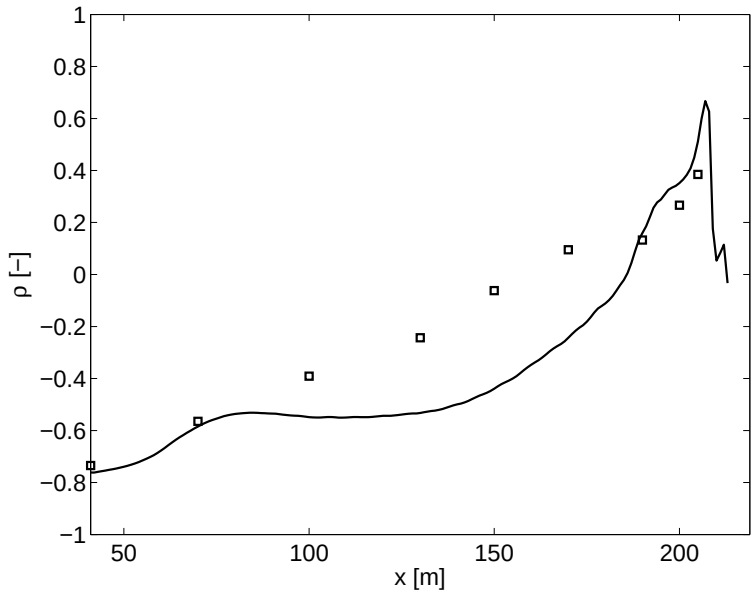

Figure 4.27: Simulated correlation ρ between the short wave variance and long wave water surface elevations (solid line) compared with the measured correlation (squares) as function of cross-shore position.

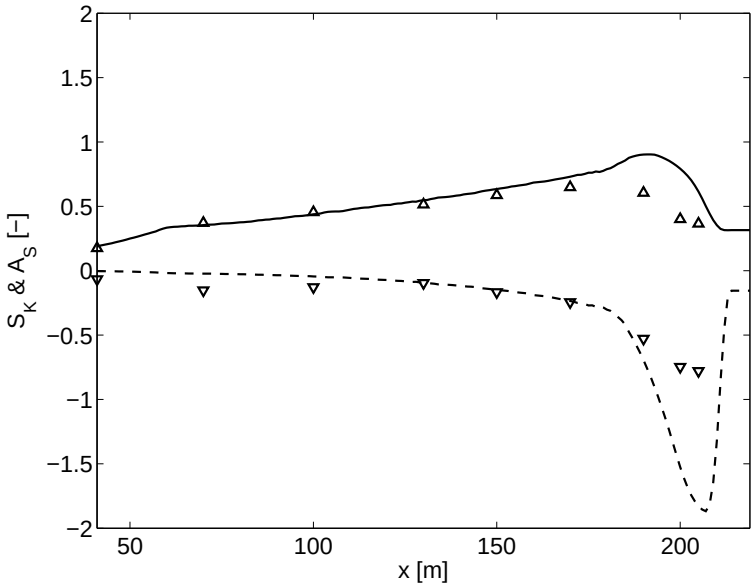

Figure 4.28: Simulated wave skewness S_K (solid line) and asymmetry A_S (dashed line) compared with measured skewness (upward triangles) and asymmetry (downward triangles) as function of cross-shore position.

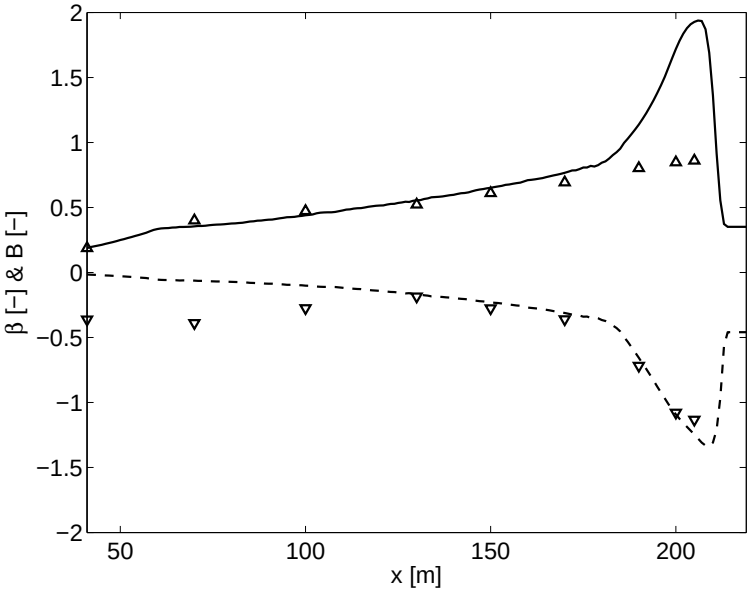

Figure 4.29: Simulated wave nonlinearity B (solid line) and phase β (dashed line) compared with measured nonlinearity (upward triangles) and phase (down-ward triangles) as function of cross-shore position.

The simulated test and depth averaged flow velocity shows the same trend as in the measurements and increases towards the shoreline (Figure 4.30). However, in the simulation the cross-shore range with a higher offshore mean flow is smaller and extends less far seaward than in the measurements. This is possibly explained by differences in measured and simulated profile development (Figure 4.36) or inaccurate measurements. In addition, another explanation may be found in the incorrect modelling of the roller energy dissipation. Simulations (not shown) with a smaller roller dissipation rate revealed that roller energy in the inner surf increases, leading to higher return flow over a broader cross-shore range.

Long waves contribute to the time and depth averaged flow close to the shoreline. The contribution of long waves to the mean flow is explained by on average larger water depths during the interval associated with shoreward flow velocities in relation to the interval with offshore flow velocities. Considering continuity and a uniform vertical structure of the long wave flow this means a time and depth averaged offshore directed flow should be present.

Nonlinear waves may cause onshore sediment transport presuming non-uniform sediment stirring over the wave cycle and a positive correlation between sediment suspension and the intra wave flow. In order to include the wave averaged effect of nonlinear waves on the sediment transport a mean flow u_A is computed, which is added to the mean (Eulerian) flow U_m (see Van Thiel de Vries et al., 2009 for more details). The simulated time averaged flow associated with nonlinear waves shows a comparable evolution as in the measurements but is overestimated especially closer to the dune face. Near the shoreline the wave skewness related sediment transport vanishes (Figure 4.28) since waves develop towards fully saw tooth shaped bores that have negligible skewness.

The orbital flow velocity (Figure 4.31) is favourably predicted by the model. The short wave orbital flow velocity is slightly overestimated whereas the long wave orbital flow is underestimated. The underestimation of the simulated long wave orbital flow corresponds well to the slight underestimation of the observed long wave water surface variance.

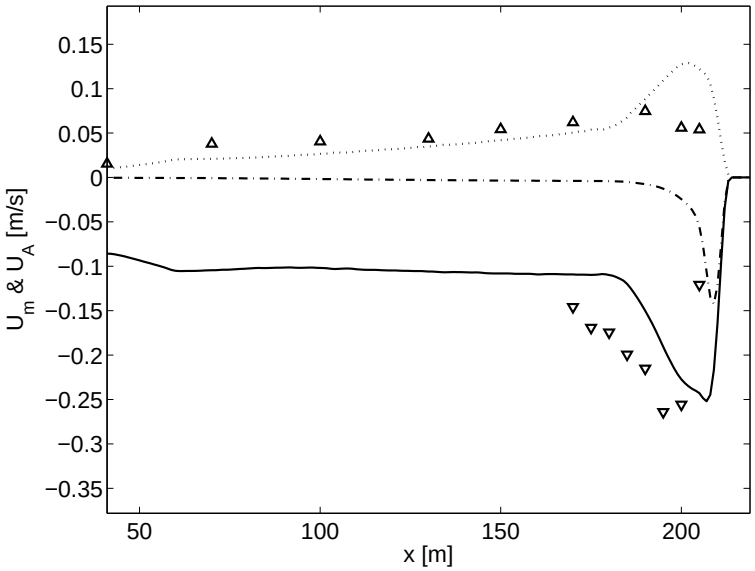

Figure 4.30: Simulated test and depth averaged flow Um due to short and long waves (solid line) and long waves only (dashed line) as function of the cross-shore position. The dotted line corresponds to the wave averaged sediment advection velocity u_A due to nonlinear short waves. Markers correspond to measured undertow flow velocities due to short and long waves (downward triangles) and the sediment advection velocity due to nonlinear waves (upward triangles).

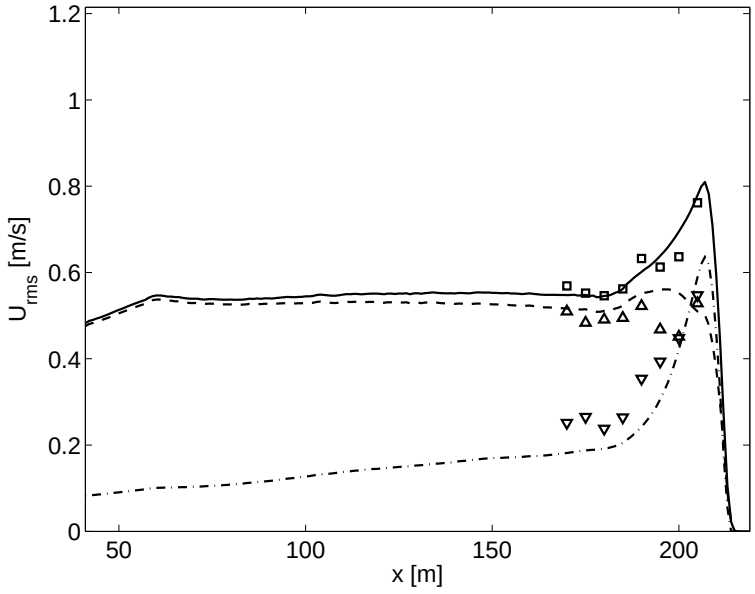

Figure 4.31: Transformation of the simulated total (solid line), short (dashed line) and long (dashed-dotted line) wave orbital flow compared with the meas-ured total (squares), short (upward triangles) and long (downward triangles) wave orbital flow as function of cross-shore position.

The simulated test and depth averaged sediment concentration increases towards the shoreline but is underestimated, especially in deeper water where the modelled sediment concentration is smaller (Figure 4.32 and Figure 4.33). In the proximity of the dune face the simulated mean sediment concentration is within a factor two with the measurements. Further offshore the discrepancy between simulations and measurements is larger. The sharp rise in the near dune

sediment concentration compares well with the bore averaged near-bed turbulence intensity (Figure 4.34) that also increases towards the shoreline. This increase in turbulence intensity through the inner surf is explained by more intensive wave breaking (turbulence production at the water surface increases) and by decreasing water depth (generated turbulence at the water surface is more effective in reaching the bed).

The simulated time averaged sediment transport compares well with the measured sediment transport computed from profile changes (Figure 4.35). Sediment is eroded from the dune face via avalanching and as a result the sediment transport associated with avalanching is dominant over the dune face and in the swash zone. From the swash zone seaward, the flow based sediment transport becomes more important. At 205 m from the wave board, in a water depth that varies between 0.1 m and 0.2 m, the flow related sediment transport is dominant.

The simulated flow related sediment transport is separated in sediment transports associated with nonlinear waves (SW), long waves (SL) and the short wave driven under-tow (SR) (Figure 4.36):

$S_W = u_A ch$

$S_L = u^L ch$

$S_R = (u^E - u^L) ch$

The offshore sediment transport results from the short wave and roller driven under-tow (SR) combined with the transport associated with the long waves (SL). The transport that follows from the short wave undertow is dominant in the present simu-lation but the long wave related sediment transport cannot be neglected (about 30

Profile evolution and dune erosion volumes are favourably predicted with the model during test T01 (Figure 4.37 and Figure 4.38). Between t = 2.04 and 6.0 hours (interval E) the dune erosion rate is slightly underestimated. At the offshore edge of the developing foreshore, the model seems not capable to reproduce the steep transition from the original (unaffected) profile towards the newly developed foreshore. A bar type feature is observed at this transition that is hypothesized to be related to (partly) plunging breakers that generate a water jet, which penetrates in the water column and causes additional sediment stirring when it reaches the bed. Though the effect of wave breaking induced turbulence on sediment suspension is included in the simulation, the applied model only considers spilling breakers, which are expected to be less efficient than plunging breakers in stirring up sand.

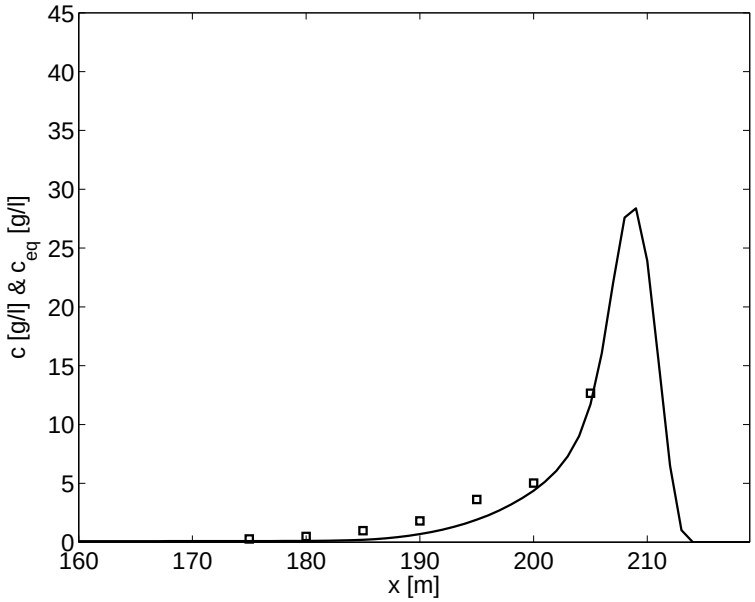

Figure 4.32: Simulated test and depth averaged sediment concentration (solid line) compared with the sediment concentrations obtained from suction tubes (squares).

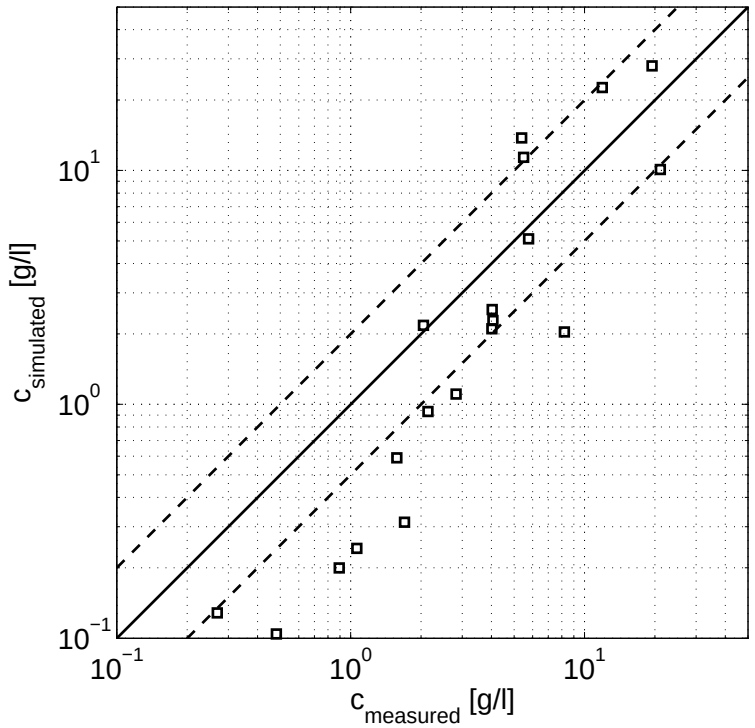

Figure 4.33: Scatter plot of simulated time and depth averaged sediment concentrations compared with vertically integrated suction tube measurements. The solid line corresponds to a perfect match between measurements and simulations whereas simulation results between the dashed lines are within a factor two with the measurements.

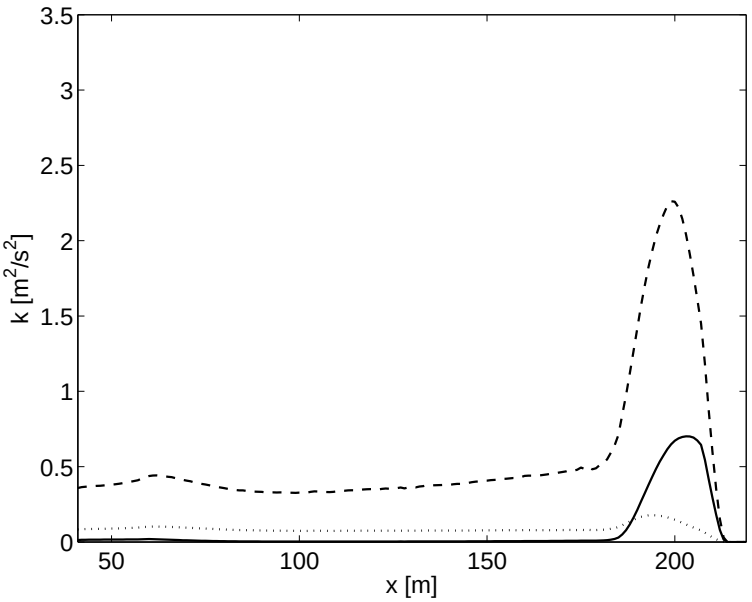

Figure 4.34: Simulated wave averaged turbulence energy (dotted line), bore averaged turbulence energy (dashed line) and near-bed bore averaged turbulence energy (solid line) as function of cross-shore position.

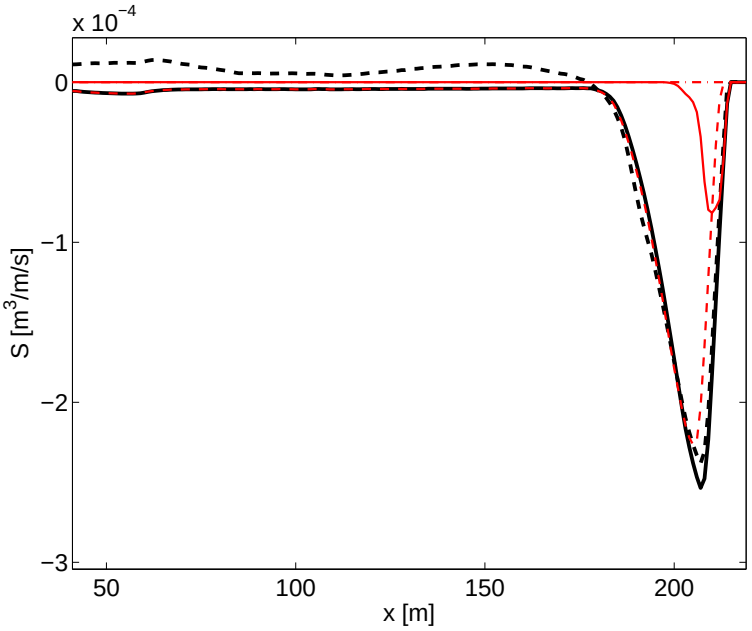

Figure 4.35: Measured (thick dashed line) and simulated (thick solid line) test av-eraged sediment transport from bed level changes. The simulated transport is separated in a transport due to avalanching (dashed-dotted line) and a transport related to the hydrodynamics (dotted line).

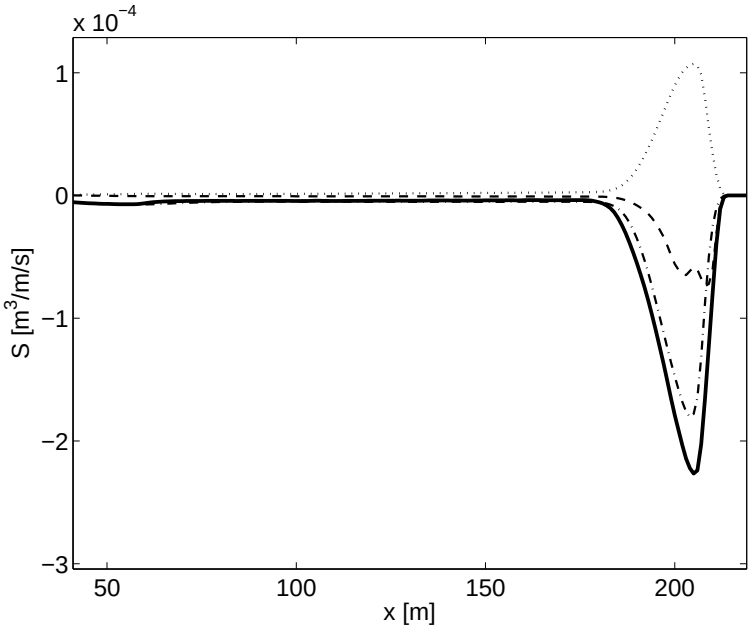

Figure 4.36: Simulated test averaged sediment transport related to the hydrodynamics (solid line) divided into wave asymmetry related sediment transport (dotted line), long wave related sediment transport (dashed line) and sediment transport associated with the short wave undertow (dashed-dotted line).

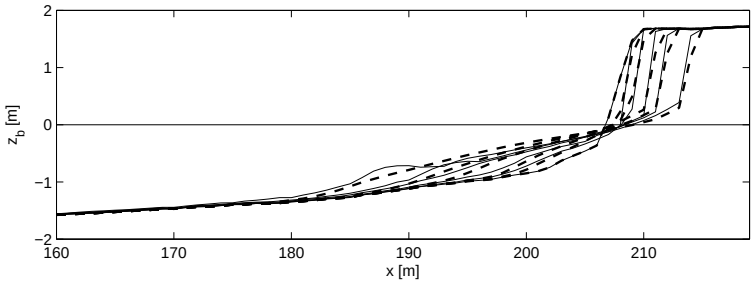

Figure 4.37: Simulated profile evolution (dashed lines) compared with measured profile evolu-tion (solid lines) after t = 0.0, 0.1, 0.3, 1.0, 2.04 and 6.0 hours.

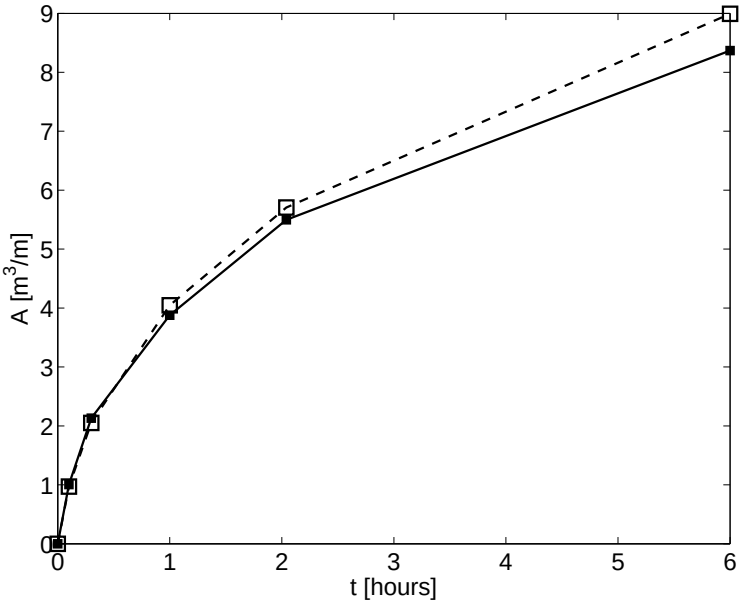

Figure 4.38: Simulated dune erosion volume above still water level (dashed line with open squares) compared with the measured dune erosion volume (solid lines with closed squares) as function of time.

It is concluded that profile evolution and dune erosion during test T01 are favourably simulated. Also simulated wave heights, flows, sediment concentrations and sediment transports compare reasonably well with measurements. However, looking at the results in more detail some discrepancies are found:

1. The long wave height and especially associated long wave orbital flows are underestimated.

2. The test and depth averaged flow between x = 170 m and x = 200 m is underestimated. Close to the shoreline no reliable measurements are available to verify the model results.

3. The simulated sediment concentration compares well with measurements close to the dune face. However, for smaller sediment concentrations in deeper water the simulated concentration is underestimated.

4. The offshore sediment transport is mainly driven by the short wave and roller induced undertow whereas the offshore directed long wave related sediment transport cancels out with the onshore sediment transport due to nonlinear short waves.

It is remarked that shoreward of the maximum offshore sediment transport, the importance of the long wave related transport increases and eventually becomes dominant in relation to the transport associated with short wave and roller driven undertow. Considering the mainly long wave associated sediment transport in proximity of the dune face and the importance of long wave run-up for avalanching it is expected that long waves are mainly responsible for the swash zone sediment transport.

Abdelrahman, S.M. and Thornton, E.B., 1987. Changes in the short wave amplitude and wavenumber due to presence of infragravity waves, Proceedings of Specialty Conference on Coastal Hydrodynamics, pp. 458-478.

Roelvink, J.A. and Stive, M.J.F., 1989. Bar-generating cross-shore flow mechanisms on a beach. Journal of Geophysical Research, 94(C4): 4785-4800.

Van Gent, M.R.A., Van Thiel de Vries, J.S.M., Coeveld, E.M., De Vroeg, J.H. and Van de Graaff, J., 2008. Large-scale dune erosion tests to study the influence of wave periods. Coastal Engineering, 55(12): 1041-1051.

Van Thiel de Vries, J.S.M., 2009. Dune erosion during storm surges. PhD Thesis, Delft University of Technology, Delft, The Netherlands.

Table 4.12

	R^2	SCI	Rel. Bias	BSS
$H_{rms,hf}$	0.9987	0.0190	-0.0066	0.9973
$H_{rms,lf}$	0.9890	0.1028	-0.1010	0.9764
ρ	0.9145	0.5439	-0.2817	0.7582
S_k	0.7380	0.3901	0.2503	-0.0445
A_s	0.9757	1.0544	-0.4466	-1.2395
β	0.9595	0.2797	0.1574	0.8145
B	0.8951	0.7444	0.4090	-2.4322
$U_{rms,hf}$	-0.4830	0.1064	0.0733	-1.3922
$U_{rms,lf}$	0.9686	0.1934	-0.1510	0.8254
U_m	0.2272	0.3589	0.1791	-0.7106
C_m	0.9961	0.9997	-0.7562	0.0008
sedero	0.9904	0.1503	-0.0187	0.9778
A	0.9997	0.0623	0.0361	0.9907

4.15 T01 Zebra

Contact: Robert McCall <robert.mccall@deltares.nl>

The purpose of this simulation is to ensure the multiple sediment fractions model in XBeach performs as expected. In this test, the Deltaflume 2006 T01 test is recreated with two types of sand with different colours, red and blue. The sand is initially placed in a zebra-stripe pattern in the profile. The properties of both types of sand such as the grain size and mobility are the same as the sand used in the Deltaflume experiment. For the test to be successful, the following conditions should be met:

- The simulated final profile should be the same as the final profile in the original Deltaflume 2006 T01 test.

- The two sediment types should mix and form layers over each other.

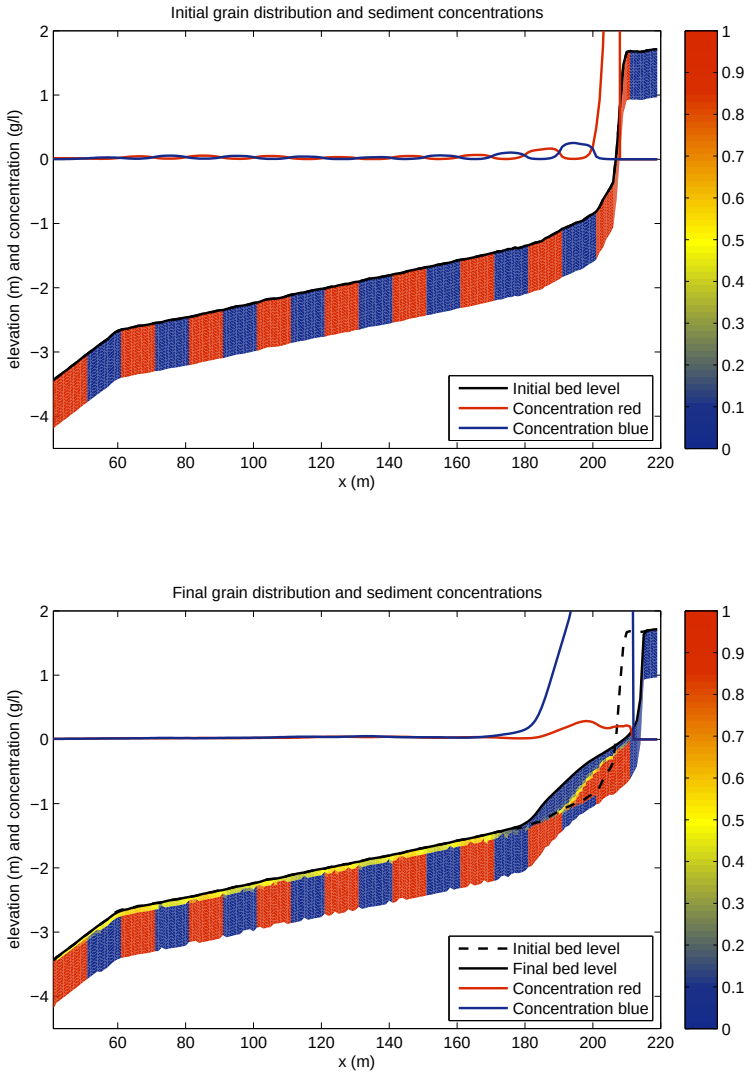
Initial grain distribution and sediment concentrations
elevation (m) and concentration (g/l)
x (m)
Initial bed level
Concentration red
Concentration blue
Final grain distribution and sediment concentrations
elevation (m) and concentration (g/l)
x (m)
Initial bed level
Final bed level
Concentration red
Concentration blue

Figure 4.39

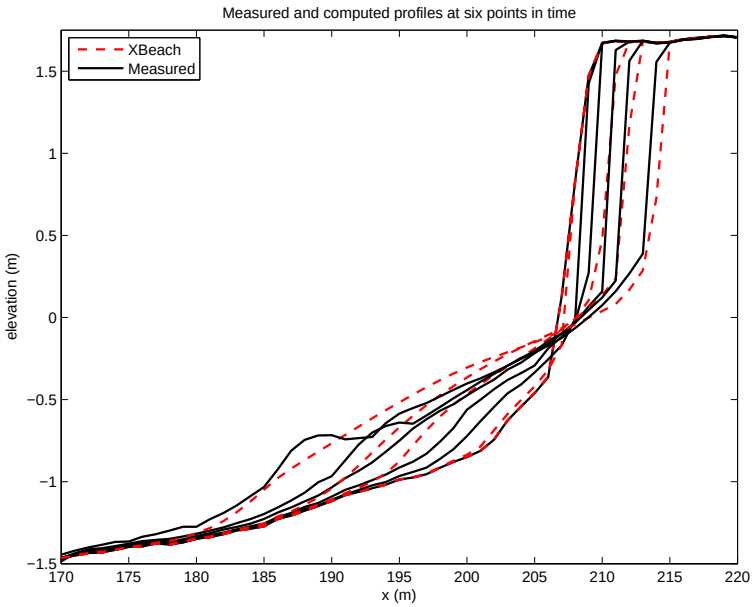

Figure 4.40

The two panels in Figure 4.39 show the initial and final distribution of red and blue sediment in the profile near the dune face. The red and blue lines in the same figure show the sediment concentration of each sediment type in the water column. If the simulation is successful, the red and blue sediment will be well mixed on the foreshore and fresh blue sediment will be deposited over the red sediment at the dune foot as the dune face retreats. The concentration of blue sediment in the water column should be higher than the concentration of red sediment in the water in areas where only blue sediment is available in the top layer of the bed.

The red lines in Figure 4.40 show the predicted dune face retreat and bed level change in the XBeach multiple-sediment model. The black lines in the same figure are the corresponding measured profiles. If the simulation has been successful, the red and black lines will align reasonably well. The results of this simulation should be compared to the Deltaflume 2006 T01 test described earlier in this report.

Table 4.13

	R	SCI	Rel. Bias	BSS (S)	BSS (ME)	α	β	γ
$t = 360s$	0.9973	0.0751	-0.0255	0.9943	0.9944	0.9945	0.0003	0.0007
$t = 1080s$	0.9781	0.2101	-0.0332	0.9503	0.9557	0.9567	0.0064	0.0012
$t = 3600s$	0.9968	0.0799	-0.0244	0.9931	0.9936	0.9937	0.0005	0.0007
$t = 7344s$	0.9944	0.0976	-0.0216	0.9888	0.9904	0.9889	0.0000	0.0006
$t = 21600s$	0.9705	0.2061	-0.0165	0.9393	0.9571	0.9419	0.0026	0.0004

Table 4.13 shows the error statistics of the predicted bed level of the multiple-sediment model of the Deltaflume 2006 T01 test. These statistics should be compared quantitatively with the error statistics of the original Deltaflume 2006 T01 model, described earlier in this report (Table 4.12).

The figure below shows the development of the mean BSS (S) score for the profile position as a function of XBeach revision numbers.

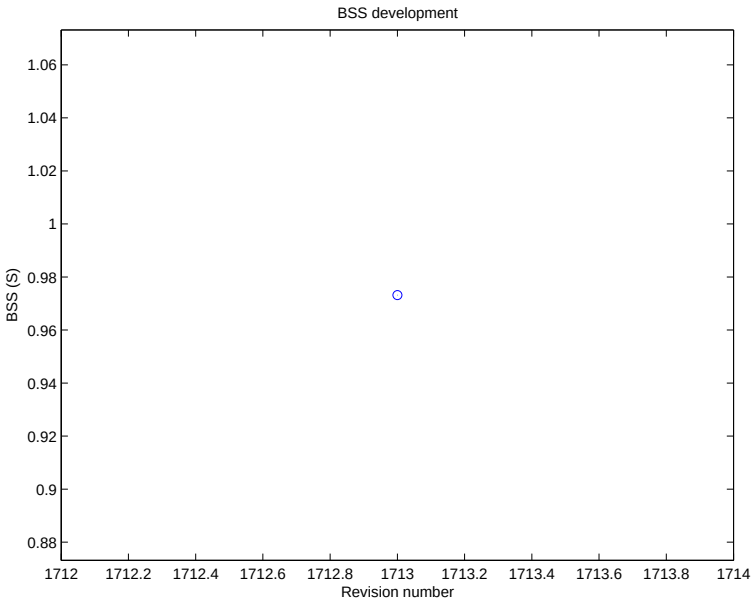

Figure 4.41

4.15.1 MPI

Two processes are used in the MPI-version of this simulation. The results of this simulation should compare well with the results of the serial version. If the simulation is successful, Figure 4.42 will be similar to Figure 4.39, and Figure 4.43 will be similar to Figure 4.40.

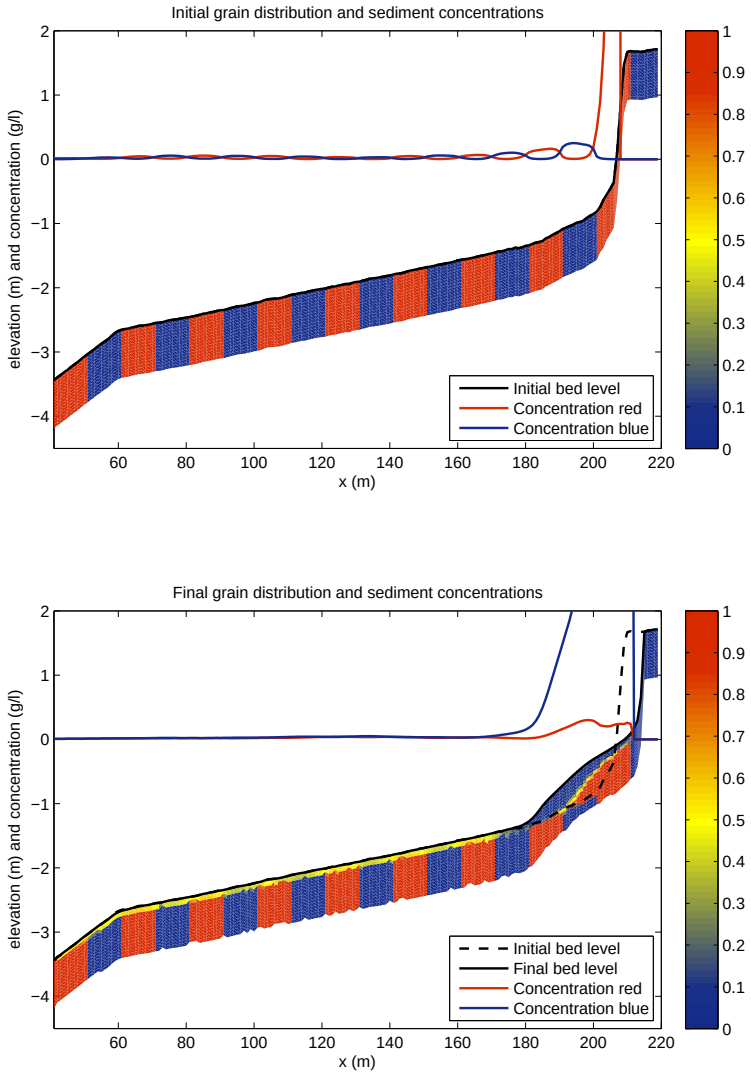
Initial grain distribution and sediment concentrations
elevation (m) and concentration (g/l)
x (m)
Initial bed level
Concentration red
Concentration blue
Final grain distribution and sediment concentrations
elevation (m) and concentration (g/l)
x (m)
Initial bed level
Final bed level
Concentration red
Concentration blue

Figure 4.42

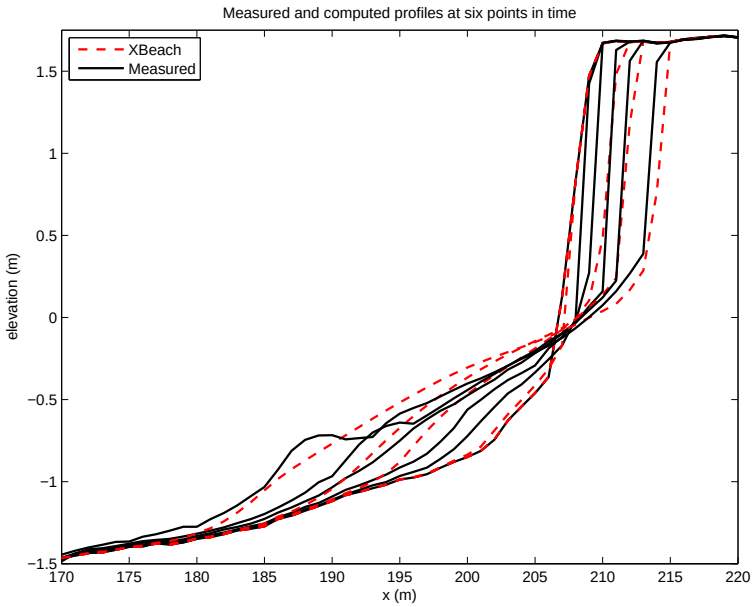

Figure 4.43

4.16 Deltaflume 2006 T04

Contact: Bas Hoonhout <bas.hoonhout@deltares.nl>

We continue with a more recent test of a more complex profile (van Gent et al., 2008, test T4) in which a small dune in front of a large volume dune is breached (Figure 4.44). This test is the best controlled case with dune overwash known to us. The test duration is six hours and profile measurements were obtained after 0.l, 0.3, 1.0, 2.0 and 6.0 hours. Also detailed measurements of wave transformation, near dune flows and sediment concentrations are available for comparing with model results. In the physical model test the still water level was set at 4.5 m above the flumes floor and imposed wave conditions correpsond to a Pierson-Moskowitz spectrum with $H_{m0} = 1.5$ m and $T_p = 4.90$ s. The wave paddle was operated with active wave reflection and second order steering. Further details may be found in Van Gent et al., 2008 and Van Thiel de Vries et al., 2008.

The simulation is performed for 6 hours on a uniform grid in which the grid size δ x is set at 1 m. In order to make a detailed comparison between measured and simulated hydrodynamics over the developing profile, the simulation is carried out with a morphological factor of 1. The offshore model boundary is located at 41 m from the wave board and we use measured water surface elevations and flow velocities at this location to obtain time series of the incident wave energy and the incoming bound long wave water surface elevations. Other model settings are the same as for test 2E of the LIP11D experiment and are listed in Appendix I.

Figure 4.44 compares the modelled and observed profile evolution. Both model and data first show a scarping of the profile, a brief period of overwashing followed by a smoothing out of the remainder of the berm and a renewed attack on the actual dune face, which is slow as most of the wave energy dissipates on the shallow upper profile left by the berm. The modelled profile evolution appears to be slightly slower than observed and also at the end of the test the modelled upper profile is slightly too low, which could be due to lack of onshore sediment transports.

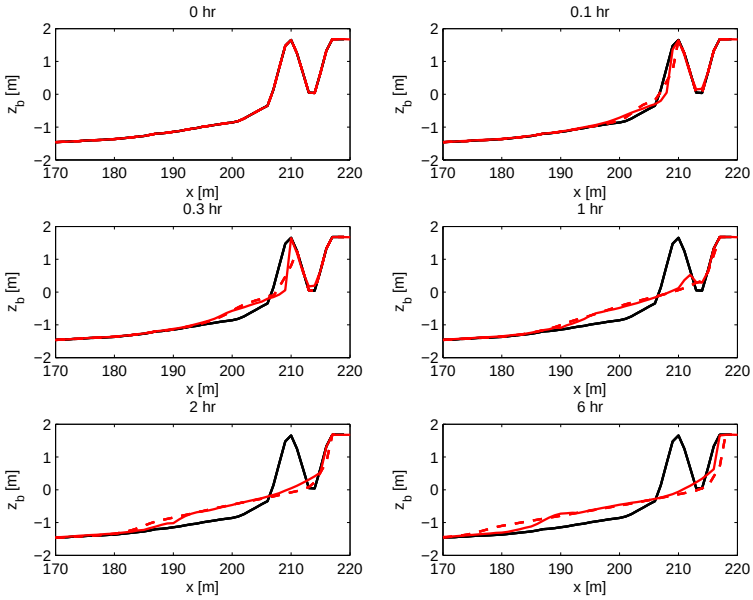

Figure 4.44: Deltaflume 2006 test T04. Measured (drawn lines) and modelled (dashed lines) profile after 0, 0.1, 0.3, 1, 2 and 6 hours of wave action.

Test averaged hydrodynamic parameters are compared in Figure 4.45 and reveal a good agreement between measured and simulated wave height transformation for both incident and long waves (upper left panel), the wave orbital flows for both incident and long waves (upper right panel) and the time and depth averaged return flow (lower right panel). It is remarked that the measured time and depth averaged flows just in front of the dune (at x = 205 m) should be interpreted with care since in the physical model only limited observation points over depth are available (Van Thiel de Vries et al., 2008).

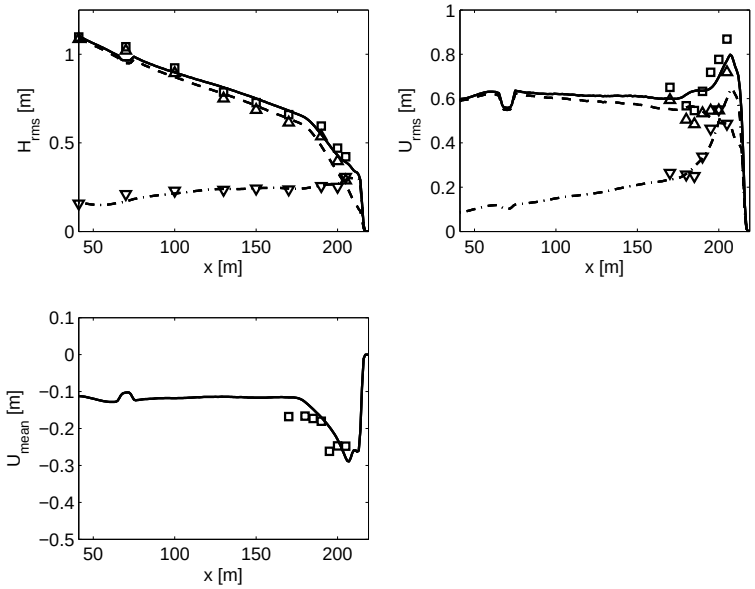

Figure 4.45: Deltaflume 2006 test T04. Upper left panel: Measured (markers) and simulated (lines) LF (downward triangles / dashed-dotted line), HF (upward triangles / dashed line) and total (squares / solid line) wave height. Upper right panel: Measured (markers) and simulated (lines) orbital flow velocity. Lower left panel: Measured (squares) and simulated (solid line) time and depth averaged flow velocity.

A more detailed analysis of the hydrodynamics is given in Figure 4.46 and Figure 4.47 which compare measured and simulated wave spectra and water surface elevation time series respectively. It is remarked that the measured wave spectra and water surface elevations include both the incident waves and long waves whereas the simulation results are associated with (wave group generated) long waves only. Considering the wave spectra first, it is seen that the measured wave spectra show a shift in variance towards lower frequencies as the waves propagate to the dune face. At the offshore model boundary most of the measured wave variance is associated with incident waves and the simulated long wave spectrum explains a marginal part of the measured wave spectrum. However, getting close to the dune face the incident wave variance reduces due to depth induced breaking whereas the long wave variance increases due to shoaling (Battjes, 2004). At the most shoreward pressure sensor (about 10 meter from the dune face) most of the measured wave variance is associated with long waves and is favorably simulated with the surfbeat model. The same phenomenon can be observed in Figure 4.47, which shows a reasonably good correlation ($R^2 = 0.32$) between measured and simulated water surface elevations close to the dune face (lower right panel). Also the time series show steep long wave fronts indicating breaking as was shown in the bichromatic wave case by Van Dongeren et al. (2007).

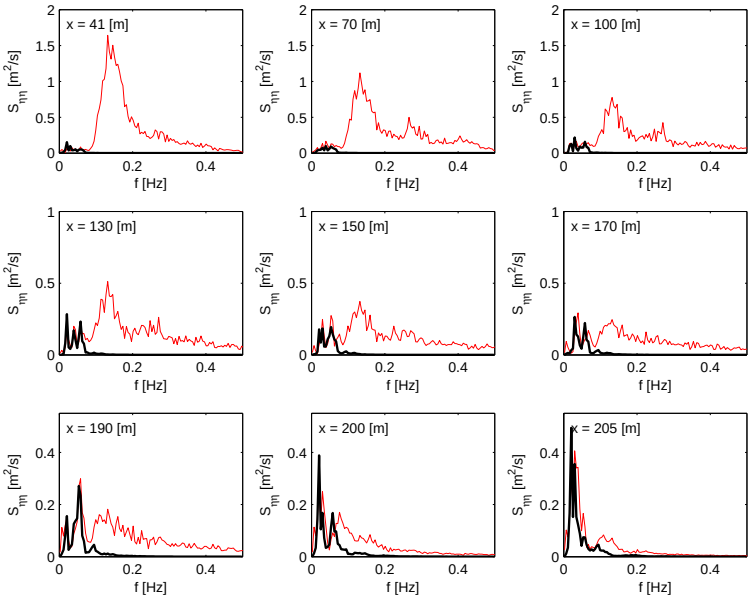

Figure 4.46: Measured wave spectra including both incident waves and long waves (thin line) compared with simulated long wave spectra (thick line) at different cross-shore positions (see upper left corner of sub-panels). Measured and simulated spectra are computed over the whole test duration.

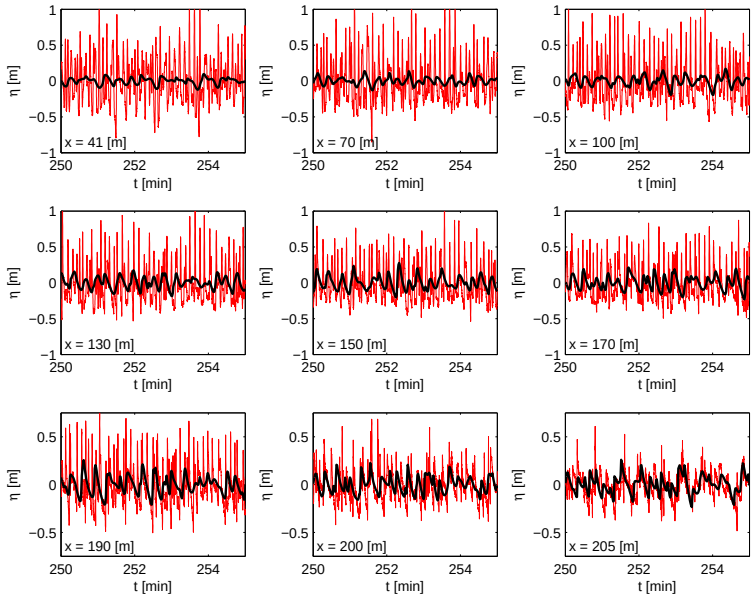

Figure 4.47: Measured water surface elevations including both incident and long waves (thin line) compared with simulated long wave water surface elevations (thick line) at different cross shore positions (see lower left corner of sub-panels) after 4.17 wave hours.

A comparison is given between the observed and modelled sediment concentrations and sediment transports (Figure 4.48) shows that the model clearly underestimates the concentration near the dune face, whereas the sediment transport is somewhat overestimated. The explanation for this could be found in an overestimation of the near dune time and depth averaged undertow which compensates for underestimating the near dune sediment concentrations. Throughout the flume, the sediment transport is too much seaward, as no onshore processes are included yet; work to improve this is currently underway but beyond the scope of this paper.

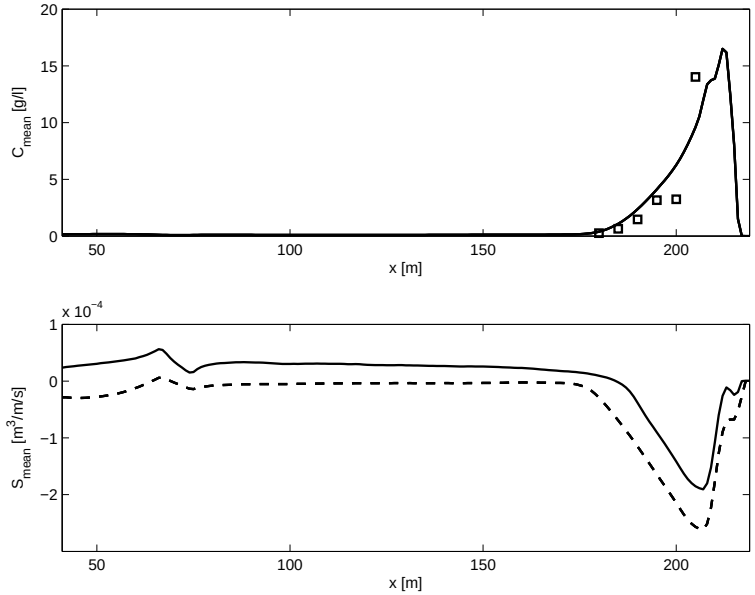

Figure 4.48: Deltaflume 2006. Test T04. Top panel: observed depth-averaged concentrations (squares) vs. model result. Bottom panel: total sediment transport observed from profile evolution (drawn line) vs. model result (dashed line).

Error statistics are collected in Table 4.14, and generally show a scatter index and relative bias of less than 10% for the hydrodynamic parameters and overall erosion volumes and dune retreat. An exception is the mean velocity, for which the higher scatter and bias can be attributed to the (neglected) 3D structure of this parameter. The horizontal distribution of the sedimentation and erosion at the end of the test shows a bit higher scatter, determined in part by the areas with small changes; the Brier Skill Score shows a value of 0.98.

Table 4.14: Error statistics Deltaflume 2006 T04

	R^2	Sci	Rel. bias	BSS
H_{rms}	0.88	0.05	-0.02	0.98
$H_{rms,HI}$	0.88	0.05	-0.02	0.98
$H_{rms,LO}$	0.81	0.07	-0.02	0.81
U_{rms}	0.75	0.10	-0.03	0.63
$U_{rms,HI}$	-0.56	0.18	-0.05	-0.71
$U_{rms,LO}$	0.76	0.15	-0.00	0.75
U_m	0.73	0.18	0.12	0.47
Sed/Ero	0.96	0.24	-0.07	0.95

Battjes, J.A., H.J. Bakkenes, T.T. Janssen and A.R. Van Dongeren (2004). *Shoaling of subharmonic gravity waves.* J. Geoph. Res. , 109, C2, C02009, 10.1029/2003JC001863.

Van Dongeren, A., J. Battjes, T. Janssen, J van Noorloos, K. Steenhauer, G. Steenbergen, and A. Reniers (2007), *Shoaling and shoreline dissipation of low-frequency waves*, J. Geophys. Res., 112, C02011, doi:10.1029/2006JC003701.

Van Gent, M.R.A., Van Thiel de Vries, J.S.M., Coeveld, E.M., De Vroeg, J.H. and Van de Graaff, J., 2008. *Large scale dune erosion tests to study the influence of the wave periods.* Coastal Engineering, 55(12): 1041-1051.

Van Thiel de Vries, J.S.M., M.R.A. van Gent, D.J.R. Walstra and A.J.H.M. Reniers, 2008. *Analysis of dune erosion processes in large-scale flume experiments*, Coastal Eng., 55(12).

4.17 1953 storm surge

Contact: Jaap van Thiel de Vries <jaap.vanthieldevries@deltares.nl>

In order to test the model performance in prototype conditions, this test studies the impact of the 1953 storm surge on the Dutch coast at Delfland. The initial profile for the simulation is obtained from test T4 of the M1263-III experiment conducted in the Deltaflume (Vellinga, 1984) and is scaled-up to prototype. The profile is representative for the coast at Delfland. The applied grid is uniform with dx = 4.56 m and the applied hydrodynamic conditions vary over the storm (see Figure 4.49). Simulation settings are default except for the maximum erosion rate dzmax, which is scaled-up to 0.17 m3/ms applying the scale relation for the erosion volume (Vellinga, 1988).

Simulated profile evolution is shown in Figure 4.50. The erosion volume above maximum storm surge level is about 100 m3/m. This is in reasonable agreement with the measured erosion volumes (above storm surge level) after the 1953 storm surge which had a mean value of 90 m3/m and a standard deviation of 26 m3/m. At the end of the storm surge the dune foot is located approximately 1 m above the maximum storm surge level.

Evolution of the simulated dune erosion volume is shown in Figure 4.51. It is concluded the simulated erosion volumes are in reasonable agreement with the observed erosion volumes at delfland after the 1953 storm surge. In addition the evolution of the simulated dune erosion volume reveals that most dune erosion occurs in a relatively short time interval between t = 10 hours and t = 15 hours when the mean water level is increasing towards the maximum storm surge level. After the peak of the storm surge the erosion rates are relatively small. At the end of the storm surge the dune foot in the simulations is located approximately 1 m above the maximum storm surge level.

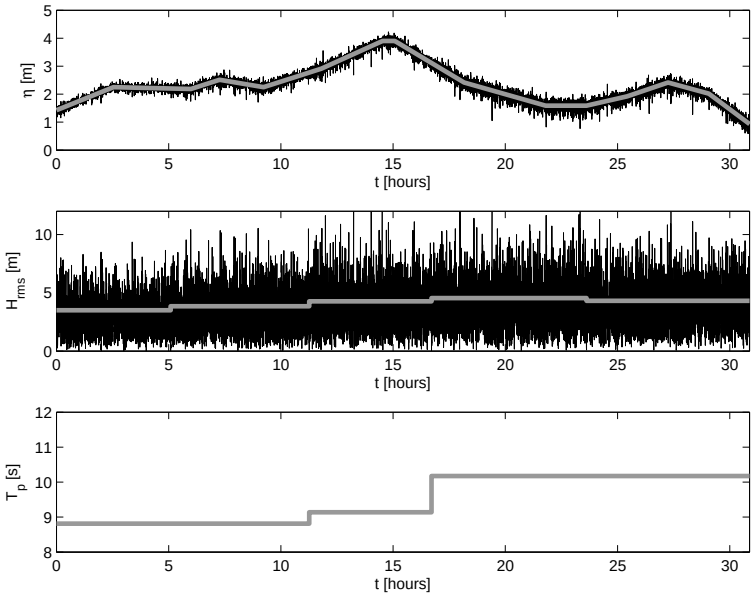

Figure 4.49: Imposed (thick line) and simulated (black line) hydrodynamic conditions at the offshore model boundary. Upper panel: Surge level above mean sea level as function of time. The simulated surge time series include water surface fluctuations due to long waves. Middle panel: Short wave height as function of time. Simulated wave height time series include fluc-tuations on the wave group time scale. Lower panel: Short wave peak period as function of time.

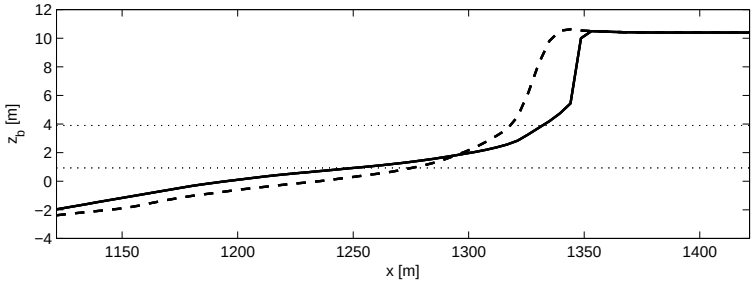

Figure 4.50: Simulated profile evolution during the 1953 storm surge (dashed line is initial profile and solid line is post surge profile). The minimum and maximum surge levels are indi-cated by the dotted lines.

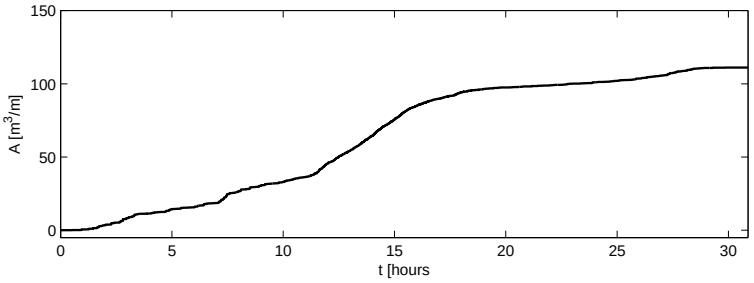

Figure 4.51: Upper panel: Imposed storm surge level as function of time. Lower panel: Simu-lated dune erosion volume above the maximum storm surge level during the 1953 storm surge as function of time

4.18 Zwin T01

Contact: Dano Roelvink <d.roelvink@unesco-ihe.org>

Having examined two-dimensional hydrodynamics, we move to 2D morphodynamics. The next test carried out is that on the Zwin breach growth experiment, as reported by Visser (1998). In the mouth of the Zwin, a tidal inlet located at the border between the Netherlands and Belgium, an artificial dam was constructed with a crest height of 3.3 m +N.A.P. (Dutch datum, approx. MSL), crest width 8 m, inner slope 1:3 outer slope 1:1.6 and length 250 m. An initial depression of 0.8 m was made in the middle of the dam having a width of 1 m and a side slope of 1:1.6 to ensure that the breach initiated at this location. The level of the surrounding sea bed was about 0.7 m + N.A.P. The mean tidal prism of the Zwin is about 350,000 m3. The polder area A_p as a function of the water level behind the dam is given by:

$A_p = (170.000m)z_s - 100.000m^2, 0.6m < zs < 2.3m + NAP$

$A_p = (2.100.000m)z_s - 4.540.000m^2, zs > 2.3m + NAP$

At t = 0, about 10 minutes prior to high water, the water level at the seaside was NAP + 2.72 m. At t = 10 minutes a water level of 2.75 m + N.A.P. was reached. For the remainder of the test, which had a total duration of 1 hour, the water level marginally decreased. After 1 the breach growth became nil, as the water level of the polder area behind the breached equaled the sea level. The wave height near the dam was negligible during the experiment. The wind speed was about 2 m/s.

Until t = 6.5 minutes the breach depth grew whereas the breach width remained constant. At t = 6.5 minutes the original dike structure had nearly completely disappeared over the initial depression width of 1 m. Near t = 6.5 minutes the onset of lateral breach growth was observed. The scour hole developed further down to a depth of 1.6 m -N.A.P. (4.9 m below the original dam crest level). The rate of lateral breach growth was about 2 cm/s. After approximately 40 minutes the process slowed down considerably and after approximately one hour the water levels at both sides were equal.

A schematized representation of the Zwin test was created in XBeach, with at the sea side a uniform bed level at 0.7 m +NAP, and inside the basin a prismatic profile with the deepest point at 0.7 m + NAP and sloping sides, such that the polder area as a function of the water level was in accordance with the equations above. The grid is non-equidistant with grid sizes gradually varying from 0.5 m near the breach to approx. 50 m far away from it. The median grain diameter D50 of the bed material was set to 0.3 mm in accordance with the prototype test conditions for the artificial dam. The applied critical slopes for avalanching are the same

as in other tests and standard settings were applied for the transport formulations. Waves were negligible in the test and were set to zero. The model was run with a CFL of 0.5 and remained smooth and stable despite the steep slopes and supercritical flows.

4.18.1 Results

In Figure 4.52 a sequence of 3D images is shown depicting the various stages in the breaching process: the initial overflowing, the cutting back of the breach, the deepening and finally the widening of the breach. Qualitatively and quantitatively the results are in agreement with the experiment by Visser (1998), although details may be different due to the schematized initial bathymetry.

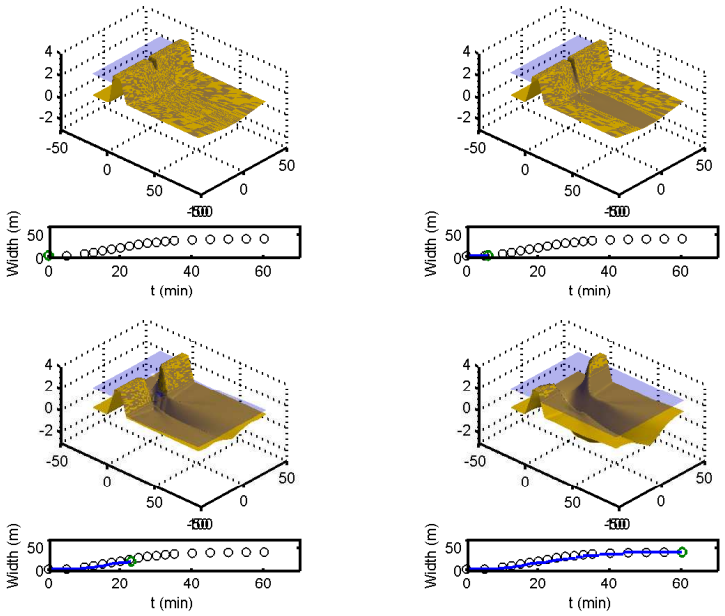

Figure 4.52: Sequence of 3D visualizations of the breach during the Zwin test (Visser, 1998). Bed level, water level and development of breach width (dots: observation, line: model).

In Figure 4.53 a comparison is given between measured and simulated water levels, flow velocities and development of the breach width in time. Observation point MS2 is 30 m upstream of the centre point of the breach and MS4 is 30 m downstream of it. In MS4 there was some ambiguity in the measured initial water level, which explains the initial discrepancy between measurements and simulations. The slight reduction in water level at the end of the measurement in MS2 is due to a rather narrow channel that was present in reality but not in the model, which causes higher velocities than in our model and a reduction of the mean water surface. In spite of these differences, the overall agreement for the development of the velocity in MS4 and for the breach widening is quite satisfactory. Measured and simulated flow velocities compare reasonably well in MS4.

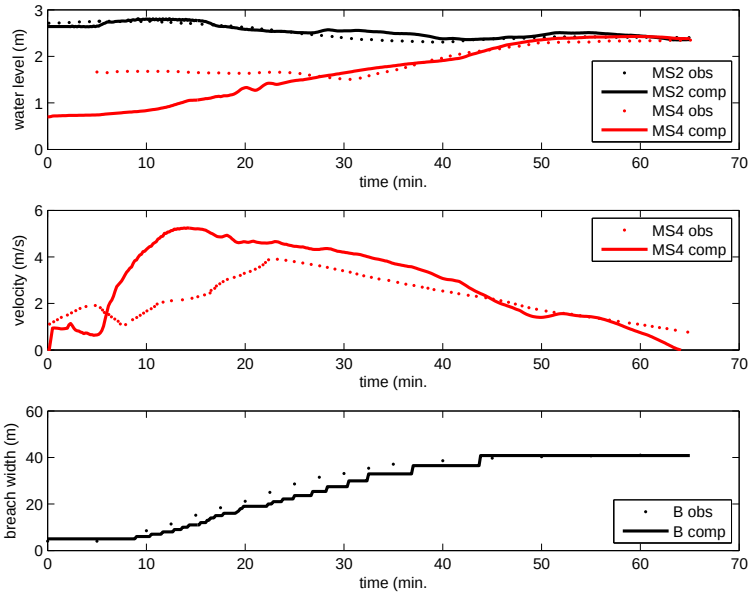

Figure 4.53: Zwin test (Visser, 1998). Observed (drawn lines) and modelled (dashed lines) time series of water level (top panel and velocity (middle panel). Bottom panel: development of breach width, observations (dots) vs. model (drawn line).

Visser, P.J. 1998. *Breach growth in sand dikes.* Ph.D.-thesis Delft University of Technology, the Netherlands.

4.18.2 MPI

In Figure 4.54 a sequence of 3D images is shown depicting the various stages in the breaching process: the initial overflowing, the cutting back of the breach, the deepening and finally the widening of the breach. Qualitatively and quantitatively the results are in agreement with the experiment by Visser (1998), although details may be different due to the schematized initial bathymetry.

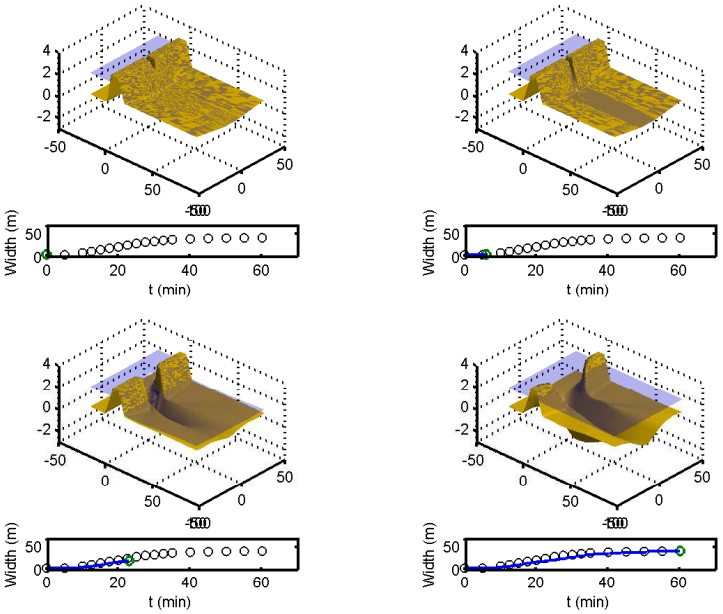

Figure 4.54

In Figure 4.55 a comparison is given between measured and simulated water levels, flow velocities and development of the breach width in time. Observation point MS2 is 30 m upstream of the centre point of the breach and MS4 is 30 m downstream of it. In MS4 there was some ambiguity in the measured initial water level, which explains the initial discrepancy between measurements and simulations. The slight reduction in water level at the end of the measurement in MS2 is due to a rather narrow channel that was present in reality but not in the model, which causes higher velocities than in our model and a reduction of the mean water surface. In spite of these differences, the overall agreement for the development of the velocity in MS4 and for the breach widening is quite satisfactory. Measured and simulated flow velocities compare reasonably well in MS4.

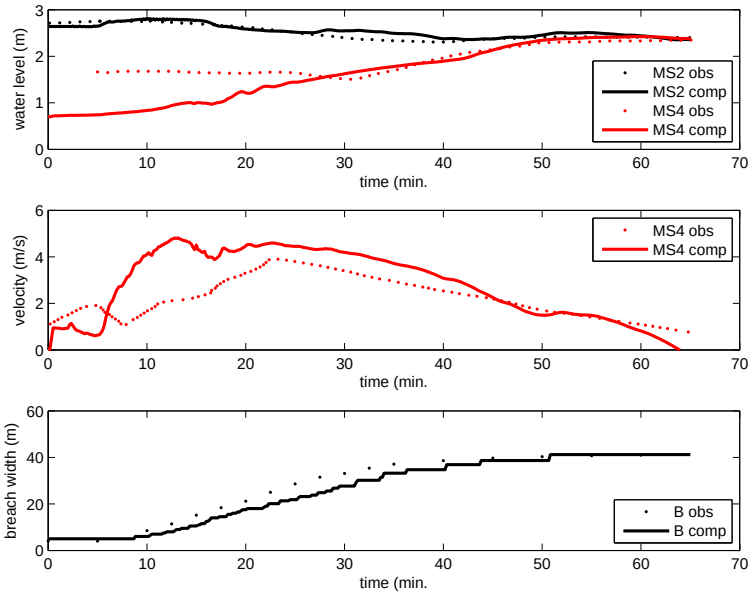

Figure 4.55

Visser, P.J. 1998. *Breach growth in sand dikes.* Ph.D.-thesis Delft University of Technology, the Netherlands.

4.19 River Outflow

Contact: Dano Roelvink <d.roelvink@unesco-ihe.org>

The river outflow case is meant to test the models for the combined effects of a river outflow and a steady wave-driven longshore current on the sediment transport and the morphological evolution. Though purely hypothetical, this case contains many salient features of real-life applications, such as longshore currents through open side-boundaries and exchange of water and sand through a gap in a closed boundary. Thus, the formulation of open boundary conditions is also tested here.

The initial topography consists of a plane beach (slope 1: 50), which is interrupted by a 75 m wide river mouth with a water outflow of 150 m3/s. The bottom contours are straight and parallel to the shoreline, except for a shallow submerged channel in line with the river.

The computational grid is rectangular, with 56 nodes in the x-direction (cross-shore) and 111 nodes in the y-direction (longshore), with a uniform grid spacing of 15 m. The waves are irregular and long-crested, with a root-mean-square height of 2m at a water depth of 13.5 m. The direction of wave incidence is 30 with respect to the shore-normal. The peak wave period is 8 s. The bed material is uniform sand of 250 am, with a settling velocity of 0.031 m/s.

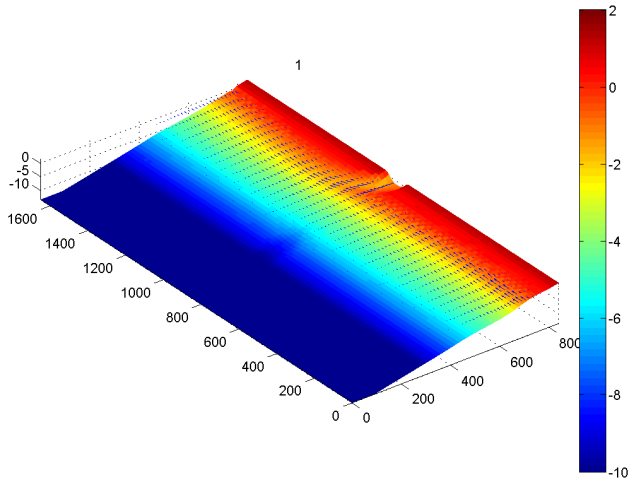

Figure 4.56

In this figure the bathymetry is shown after approx. 4 days; arrows indicate the sediment transport vectors. plotted for every cross-shore cell and every third longshore cell. When functioning correctly, we see a channel that has turned towards the north and striasght contour lines downstream of the channel.

4.19.1 MPI

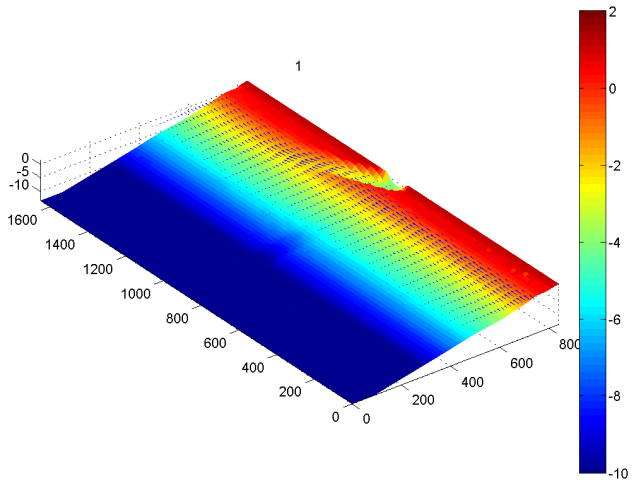

Figure 4.57

In this figure the bathymetry is shown after approx. 4 days; arrows indicate the sediment transport vectors. plotted for every cross-shore cell and every third longshore cell. When functioning correctly, we see a channel that has turned towards the north and striasght contour lines downstream of the channel.

4.20 MICORE Cadiz

Contact: Theocharis Plomaritis <haris.plomaritis@uca.es>

The field site is located around Cadiz town, in south-western Spain, facing the Atlantic Ocean. It is constituted by two different beaches extending along 10 km, providing the opportunity for studying the effects of storms on different types of coastal environments.

The study area is a mesotidal coast with a mean tidal range of 3.2 m and 1.1 m during springs and neaps tides, respectively. Dominant winds blow from ESE (19.6% of annual occurrence) and WNW (12.8%), which together with coastline orientation makes sea and swell waves approach generally from the third and fourth quadrants. According to this, prevailing longshore drift is directed south-eastwards. Significant wave height is usually lower than 1 m, with waves over 4 m high being uncommon and occurring only during the most important storms, which usually take place between November and March and approach from the third quadrant. In fact, waves greater than 1.5 m are considered storm waves, so the area can be classified as a low-energy one.

The storm event that was selected is a moderate storm event with a return period of about 1 year. The maximum significant wave (Hs) height during the peak of the event was 3.7m with a spectral period (Tp) of 8.7sec. The total duration of the storm was 46 hours (light grey shaded area). The tidal conditions over that period were from springs to neaps with an average tidal range of 2.27m.

Both the Xbeach model and the off-the-shelf model Petra were used to predict the morpho-

logical changes of the storm described above. Despite the fact that applied models simulate different physical processes, both produce a relative good final profile (Figure 4.58). Nevertheless some discrepancies with the measured profile are present. XBEACH better predicts the near berm erosion and beach slope and PETRA performs better in the intermediate and low intertidal area.

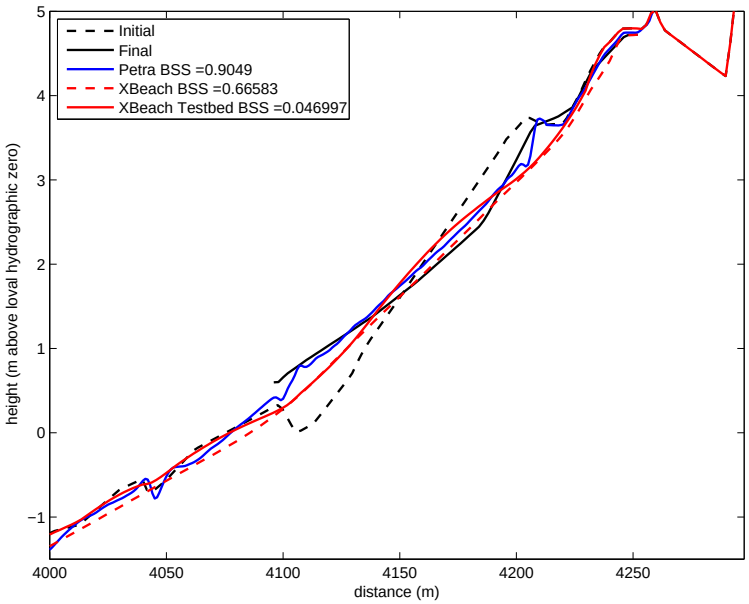

Figure 4.58

4.21 MICORE Dziwnow Spit

Contact: Natalia Brzezowska <nataliabrzezowska@gmail.com>

The Polish study site is the 14 km long Dziwnow Spit of barrier type built of Holocene deposits (mainly sands) with dunes 3.5 to 10 meters high. Behind the spit there are relatively wide lowlands of glacial or glaciofluvial origin, in most cases filled with peat. Their surface is 1 to 3 m above sea level. In the lowlands alos the Kaminski Lagoon is found with a rather small depth (maximum 2-3 m). At the middle of the spit there is a connection between the lagoon and sea (Dziwna). The mean beach width calculated for the pilot area is 33 m.

The average tide range in the Baltic is very small and is less then 10 cm. This is due to the small area of the Baltic, its geographical situation and the presence of the Danish Straits, which prevent propagation of North Sea tides into the Baltic. Thus, surface waves (wind waves and swell) are the most important factor of the Baltic coastal zone hydrodynamics. The wave climate in Poland is highly diversified because of the wealth of fetches and wind speeds occurring throughout the year.

Since 1 June 2008, (from the beginning of observations taken within MICORE project) 1 extreme storm (12.10.2009) was noticed which caused significant morphological changes at the shore. The storm return period was about 4 years and was simulated with the XBeach model.

The storm occurred on 12.10.2009 and lasted for almost 4 days (93hours). The highest sea level observed on tide gauge located in the Dziwna (Dziwnow Port Authority area) was 0,76 m. above mean sea level. The maximum significant wave height (Hs) reached 3.2 m and teh

maximum peak period (Tp) was 11.17 sec.

The XBeach model was run for profile 386 in 1D mode. The profile was interpolated to a cross-shore varying grid with a minimum cell size of 3 m. Offshore wave data timeseries from the WAM model were inputted to XBeach using a Jonswap spectrum and setting instat=41. Wave direction values were changed to 270 degrees, which means that incoming waves are shore normal. Surge input data were taken as the hourly mean sea level.

It is visible from the simulation (see Figure 4.59), that at this stage the amount of dune erosion is avoerestimated by XBeach according to post-storm data.

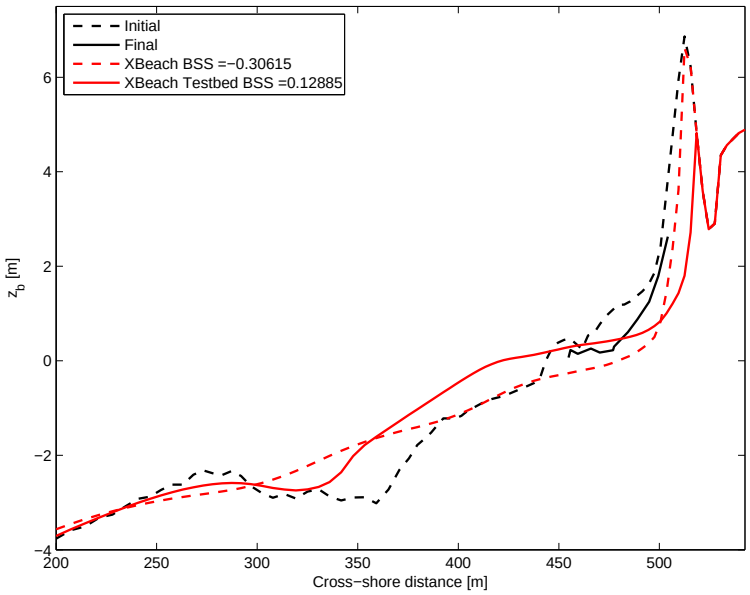

Figure 4.59

4.22 MICORE Lido de Sete

Contact: Balouin Yann <y.balouin@brgm.fr>

The Lido of Sete is a typical Mediterranean sedimentary coastal system trapped between the rocky coast of the Mont Saint Clair at Sete, and the volcanic cliffs of the Cap dAgde.

Both the beach system and dune system are very narrow, covered by wooden stacks. The dune system was built artificially during the retreat of the national road that was initially fronting the beach. The nearshore zone is characterized by the presence of a set of longshore bars. Crescentic patterns with different wavelengths are observed. In the studied area, two nearshore bars are present.

Exchanges with the adjacent sandy coastlines are very low and the study area can be considered as an independent coastal sedimentary cell. Coastal dynamics in this sedimentary cell is governed by two main factors: the wave action and the wind.

The most important wind directions are NNW, Tramontane winds (36%). NE and SE winds blow 15% of the time. The mean eolian transport in the site of Ste (BCEOM, 2000) is about 250m3/m/yr. This estimation is based upon observations made between 1978 and 1983. Thus, the morphological behavior of these systems is based upon two dynamic factors: the south-eastern storms and the land winds. The first pushes the sediments hold in the

submerged system onto the backshore (or conversely, depending on the capacity of energy absorption of the beach), and the second returns the sediments to the beach, hence restoring the shoreline.

The Mediterranean Sea is a micro-tidal system with tidal amplitude of 0.10m during neap tide and 0.46 m during the highest spring tide. The data from tide gauges and satellite observations show that the mean sea level raised 15 cm since the beginning of the 20th century, at a mean speed of 1.5 mm/yr. Wave climate is of low energy with a mean significant wave height of 0.8 m. 80% of waves significant heights are less than 1 m. However, storm events can have a significant impact on the coastline. Those events are associated with SE waves having a significant heights that sometimes reaches 8 m. Energetic SE events (Hs 4m) usually occur during the period from November to March. Storm surge can easily reach 1 m, and when Hs is over 4 m, the beach is usually submerged.

The beach is eroding with a shoreline retreat that was around 1 m/y during the last 50 years. However, during storms, shoreline retreat can reach more than 10 m. The main storm impacts that can be observed are beach erosion, dune erosion, dune overtopping.

Measurements within the MICORE project are available for the period November 2008 to March 2009. The strongest wave height occured at December 26th 2008, with a significant wave height reaching 4 m offshore the lido of Sete. The mean water level (observed in the port of Sete) was around 40 cm/MSL, and the storm surge was around 25 cm. The results presented here are obtained for a computation starting the 22/12/2008 and ending the 06/01/2009, and are for the South Area.

With the present parameters, the model does not reproduce properly the beach evolution (Figure 4.60). Indeed the model 1) under-overestimates the offshore migration of the bar, 2) over-estimates the erosion of the upper part of the beach, 3) gives an accretion of the bottom part of the beach, which does not occur in the observation and 4) Slight erosion of the inner bar.

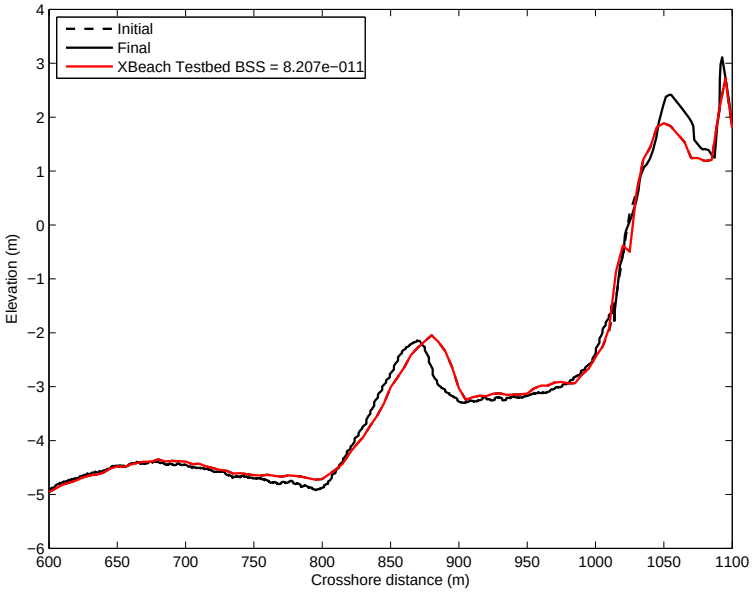

Figure 4.60

4.23 Assateague Island

Contact: Bas Hoonhout <bas.hoonhout@deltares.nl>

Besides well-controlled laboratory cases, the model is also applied to the field. The first example concerns the morphodynamic response of sandy dunes to extreme storm impacts at Assateague Island, Maryland, USA, which was analyzed before by Jimnez et al (2006). Two consecutive northeasters attacked the barrier island during late January and early February, 1998. The bathymetry was measured using LIDAR in September 1997 and again February 9th and 10th, 1998 after the two storms had subsided.

Three types of dunes were identified by Jimnez et al (2006), shown in Figure 4.61. Profile A (upper left panel) is initially characterized by a steep faced dune, where the maximum run-up exceeded the dune crest height and the mildly sloped back of the dune. The morphological response is characterised by profile lowering, decrease of the beach face slope and landward barrier displacement, while retaining barrier width.

Profile type B is a double-peaked dune profile and has two different shapes. Profile B1 (upper right panel) is initially characterized by a primary and secondary dune, both of which are lower than the maximum run-up height and which are separated by a valley. Profile B2 (bottom left panel) initially has two peaks of which the seaward one is lower. The backside of the barrier of either type is therefore either characterized by a secondary dune line (profile B1) or a taller crest of the dune (profile B2) which prevents the eroded sand from being transported to the backside of the dune. The main morphological response for these profile types is a decrease of the beach face slope, outer shoreline retreat and narrowing of the barrier.

The height of the dune crest of profile C (lower right panel) exceeds the maximum run-up height and so little overwash is observed. The morphological response of this type of profile is crest lowering due to slumping, decrease of the beach face slope and retreat of the outer shoreline. The width of the barrier is seen to decrease.

The storm impact of the two North Easters on Assateague Island were modelled with XBeach for the four profiles described by Jimnez et al. (2006). The profiles were extended with a shallow foreshore and a 1:100 slope in seaward direction till a water depth of 9 m below NAVD88. As XBeach has not been shown to accurately simulate morphological change during very long storm durations, the simulations were run for a total of 20 hours. The measured wave and surge conditions were parameterized for each storm by a constant surge level and a constant wave spectrum (Pierson-Moskowitz) (see Table 4.15). This approach assumes that two 72 hour storms with varying surge and wave conditions can be approximated by two 10 hour simulations with constant maximum surge and wave conditions following a similar approach as Vellinga (1986). This approach also facilitates further sensitivity studies into the effect of varying hydraulic forcing conditions. The calculation grid size varies from 18 m at the offshore boundary to 2 m on the islands. A morphological acceleration factor of 5 is applied. The final simulated bed profiles are shown in Figure 4.61.

Table 4.15: Hydrodynamic boundary conditions XBeach simulations

	Storm 1	Storm 2
Surge level [m +NAVD]	0.8	1.0
H_s [m]	4.1	3.9
T_p [s]	8.5	8.5

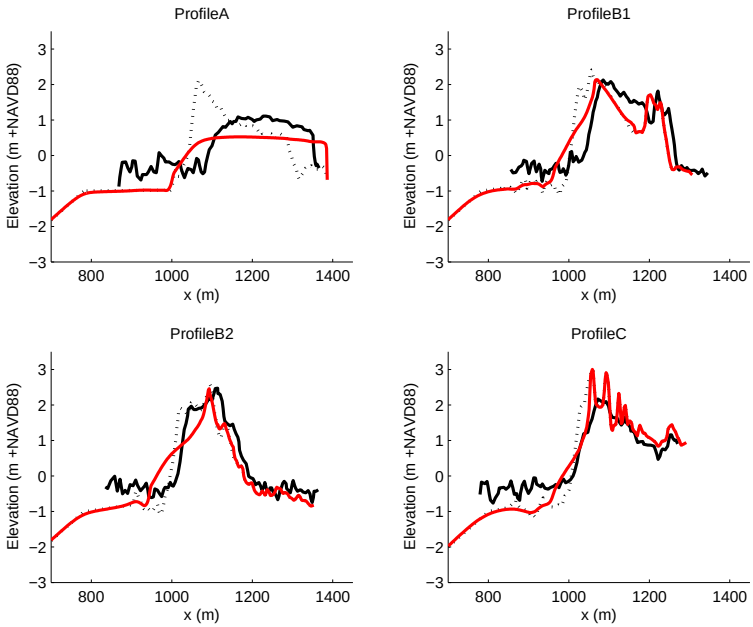

Figure 4.61: Pre-storm profiles (black dotted line), measured post-storm profiles (black solid line) and modelled post-storm profiles (red solid line). Upper left panel: profile A. Upper right panel: profile B1. Lower left panel: profile B2. Lower right panel: profile C. The seaward side is on the left in all panels. Note that the measured post-storm profiles contain only the sea surface and emerged topography and no submerged topography.

The profile changes calculated by XBeach are largely consistent with the description of dune evolution given by Jimnez et al (2006). Jimnez et al observed that profile A became flatter, with large quantities of eroded sediment deposited on the back side of the barrier island, due to the consistent wave over-topping. The model replicates this behaviour, except that the island is lowered more than in the measurements and that the seaward face of the island does not roll back as it does in the measurements.

The observed response of profile B1 was dune face retreat, overwash deposition in the dune valley between the primary and secondary dunes and narrowing of the island, Jimnez et al (2006) also noted decrease of the beach face slope. It can be seen in Figure 4.61 that the morphological development of the island is well represented by the model. The simulated dune crest retreat corresponds closely to the measured retreat. Overwash takes place in the model and sediment is deposited in the valley between the primary and secondary dunes, although the magnitude of deposition is less than in the measurements.

The XBeach model of profile B2 shows a slope reduction on the seaward side and lowering of the seaward dune. The second dune crest retains its crest level as described in the work of Jimnez et al (2006). The beach slope decrease in the XBeach model is in line with the description given by Jimnez et al (2006), but differs from their measured profile. It is unclear why the measured profile shows almost no erosion of the beach face.

Jimenez et al. (2006) observed, in general, profile C to lower in height, the seaward dune slope to become smaller, and seaside retreat of the shoreline resulting in barrier narrowing. The XBeach model shows retreat of the upper dune face and a reduction of the seaward dune slope. The model over predicts the sedimentation at the base of the dune and under predicts the crest lowering.

Jimnez, J.A., Sallenger, A.H. and Fauver, L., 2006. *Sediment transport and barrier island*

changes during massive overwash events, ICCE 2006, San Diego.

Vellinga, P., 1986. *Beach and dune erosion during storm surges.* PhD Thesis, Delft University of Technology.

4.24 NetCDF output

Contact: Bas Hoonhout <bas.hoonhout@deltares.nl>

The purpose of this test is to check the ability of the model to provide the output in NetCDF format. This test is a copy of the Carrier and Greenspan test presented in this report as well. The output of this test is provided in both the binary and the NetCDF format. The two formats are compared in the graph presented in Figure 4.62.

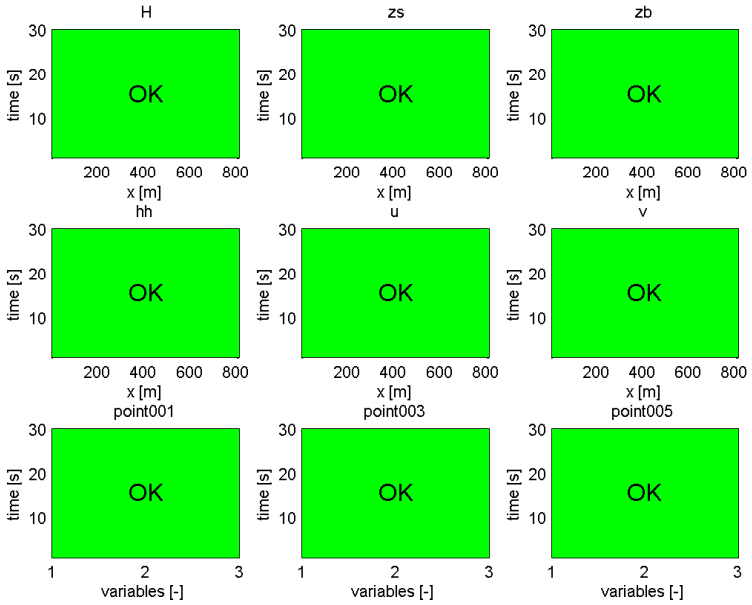

Figure 4.62: Comparison between Fortran and NetCDF output in dimensions x and time. Green dots represent a match, while red dots represent a mismatch.

4.25 MICORE Mariakerke

Contact: Annelies Bolle <annelies.bolle@imdc.be>

The Ostend beach (adjacent to Mariakerke), located almost in the middle of the Belgian coast, is a dissipative beach, characterised by a low beach gradient, a surf zone with the presence of numerous spilling lines of breakers and by fine to medium sandy sediments (D50=0.214 mm). The study area is densely populated with apartment buildings on the dyke and a promenade protected by a seawall without naturally-developed dunes. The coastal defence is designed for to give protection for a T100 storm event (return period of 100 years).

The Belgian coast has a bi-diurnal tide with a small asymmetry and an average tidal range of 4m. The tidal wave moves along the coast from west to east. The tidal range decreases in the same direction by 0.5 m. Spring tides occur twice a month when the tidal variation has reached its maximum (5 m), while for neap tides occur the tidal range reaches its minimum,

i.e. 3 m. The tidal curve has an asymmetric shape because the low tide lasts half an hour longer than the high tide. Meteorological circumstances can significantly influence the curve as well. Long-lasting intense winds may influence the water level, resulting in extremely low or high water levels. This important tidal range is linked to quite significant tidal currents, which exceeds generally 1.5 knots in the near shore areas. Because of the shallow seas and the short fetch, waves are typically short crested at the Belgian coast.

The wave climate along the coast is mainly determined by meteorological circumstances, predominantly westerly winds, and by the shallow depth of the North Sea. Under normal circumstances the wave along the coast is lower than 1 meter. During (heavy) storms wave heights of over 5 meters can occur. The wave period is 3 to 4 seconds under calm weather conditions, but during storms it can reach 10 to 15 seconds (IMDC, 2005).

Between 08/11/2007 0000Z and 1800Z an active depression moves from just southeast of Iceland towards Norway and settles afterwards in south Scandinavia. On the back of this depression, strong northerly wind fields develop and spread over the Norwegian Sea and the North Sea. This situation causes high water levels and waves along the North Sea Coasts (Versluys, 2007).

Currently, beach and dune erosion at the Belgian coast is estimated with Durosta. For the storm of November 2007, calculations have been performed with Durosta for Ostend beach and compared with the measurements. Durosta has been run with default settings. Several profiles (1D) have been modelled on a grid that varies from 6m offshore to 1m near the seawall. The seawall has been included as a non-erodible element.

To compare the performance of XBeach with Durosta, the same 1D-profiles haven been modelled for Ostend beach. The grid in XBeach has been chosen identical to that of Durosta and varies from 6m offshore to 1m near the seawall. The performance of XBeach will be compared with Durosta. Since Durosta is a 1D model, also XBeach has been applied in 1D mode.

In Figure 4.63 the model results from XBeach and Durosta are compared with the measurements for the November 2007 storm at Ostend beach. Additionally the Brier Skill Score has been determined between the dyke and -500m.

Both XBeach and Durosta give a more uniform beach profile than is observed in the measurements. Small bars in the profile are hardly predicted with both models. For the presented results XBeach obtains a better score than Durosta.

Comparing both models it is concluded that XBeach delivers (also for most other cases presented in the WP4 report) a slightly better result than Durosta. Especially the prediction of the beach erosion front seems a bit more accurate in XBeach.

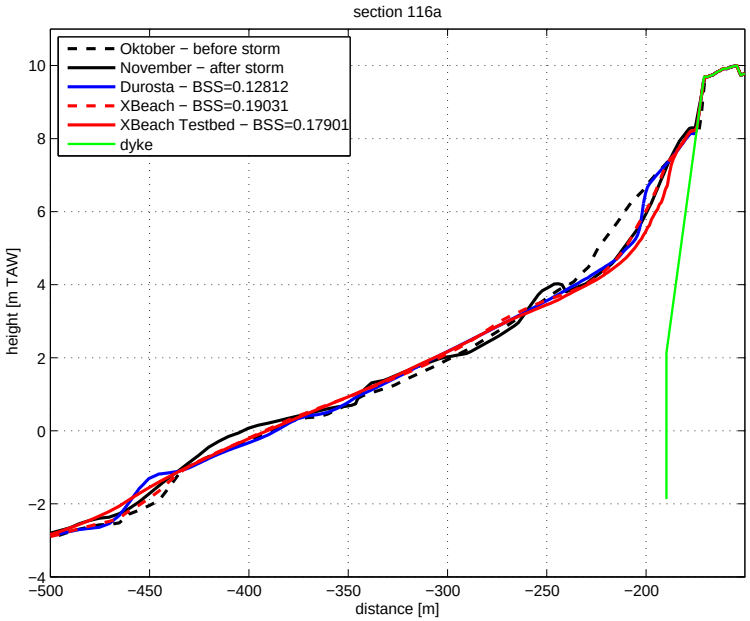

Figure 4.63

4.26 MICORE Lido di Dante

Contact: Mitchell Harley <mitchell.harley@unife.it>

The study site is the Lido di Dante-Lido di Classe area, an 8 km stretch of sandy beaches along the Emilia-Romagna coastline in northern Italy on the Adriatic Sea. The site is a mixture of urbanised (approximately 40% of the total area) and relatively pristine (approximately 60%) coastal environments. The seaside towns of Lido di Dante and Lido di Classe are located at the sites northern and southern boundaries respectively. In these regions the beaches are protected by offshore breakwaters and groins and backed by moderate coastal development in the form of beach huts, holiday accommodation and paved roads. Between these two towns is a natural park consisting of natural vegetated dunes and no coastal protection. Three river mouths are located at the site: one at Lido di Dante (Fiumi Uniti); one at Lido di Classe (Fiume Savio); and one in the centre of the natural park (Torrente Bevano).

The submerged beach is generally composed of fine sand, while the beachface is made up of fine to medium sands (D50 = 0.03 mm). The intertidal beach slope varies significantly along the 8 kms of coastline, from mild (2.5%) to steep (14%). Steep values are representative of areas adjacent to coastal defence structures (i.e. groins) while the area inside the natural park is characterised by lower gradients. The mean submerged beach slope is 3%. According to the morphodynamic classification of Wright and Short (1984), the beaches are considered as having intermediate beach states. Low tide terraces are often observed both in the protected and natural areas. Submerged longshore bars meanwhile are only present in the areas outside of the offshore structures.

The wave climate of this region is generally small, with 91% of significant wave heights below 1.25 m. The prevalent wave direction is from the east, while the most intense storms are from the ENE (known as the "Bora wind"). The Bora wind is a strong, cold, gusty wind that blows intermittently but mainly during the winter months. It not only has a strong influence on the wave climate of this region, but of the general circulation patterns of the entire Adriatic

Sea. South-easterly waves meanwhile are much less significant, since SE winds are sheltered to some degree by the Conero Headland approximately 120 km south of the site.

In regards to water level variations, the area is microtidal with a mean neap tidal range of 30-40 cm and a mean spring tidal range of 80-90 cm. The tidal signal has both diurnal and semidiurnal components. Tidal anomalies of up to double the maximum tidal elevation can occur as a result of surge. This is particularly the case during SE wind conditions, where, considering the SE-NE orientation of the Adriatic Sea, there is the greatest fetch for wind-driven surge.

Within the 2008-2010 MICORE monitoring period, three storms were selected for calibration of the off-the-shelf and XBeach models. Each storm has distinct properties that encompass the range of storm conditions typical for the Emilia-Romagna region. Here the modelling is restricted to profile MN15 for the 1-3 December 2008 storm.

At this stage XBeach substantially overestimates erosion (see Figure 4.64). Whereas measurements indicate only moderate frontal dune erosion, (excluding MS17 for the 1-3 December 2008 storm) the dune is overtopped and completely destroyed in the simulations. The results even indicate erosion into the artificially-generated 3m dune placed at the back of the profile.

Because of the large disparity between the XBeach model and measurements for Italy, quantitative analysis of the results has not been conducted at this stage.

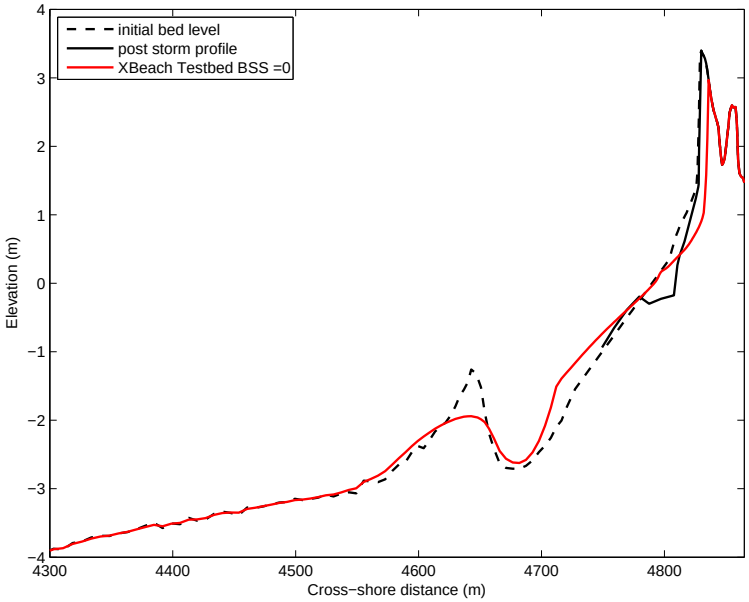

Figure 4.64

4.27 MICORE Praia de Faro

Contact: Michalis Vousdoukas <vousdoukas@gmail.com>

The study area is Anco Peninsula constituting the westernmost barrier of the Ria Formosa barrier island system. It is a NW-SE oriented sandy barrier that is attached to mainland by its western terminus.

The area is mesotidal, with an average tidal range of about 2 m that can reach up to 3.5 m during spring tides. Analysis of two years of records from a tidal gauge on the Algarve Coast

showed a maximum observed storm surge level of +0.75 m (Gama et al., 1994). The return period of a sea level 2.23 m above Mean Sea Level (MSL) is 10 years (Gama et al., 1994).

The offshore wave climate is dominated by west-southwest waves (71% of occurrences). SE waves that consist of short period waves generated by regional winds (locally called Levante) are also frequent (about 23%). Wave energy is moderate with an average annual significant offshore wave height of 1.0 m and average peak period of 8.2 s (Costa et al., 2001).

Storm events in the region are considered when the significant offshore wave height exceeds 3 m (Pessanha and Pires, 1981) and typically correspond to less than 1% of the offshore wave climate (Costa et al., 2001). A 5.0 m significant wave height for a SE storm has a return period of 50 years, whilst a 5.7 m SW storm is expected every 5 years (Pires, 1998). Due to its northwest-southeast orientation it is directly exposed to west-southwesterly waves, and is relatively protected from SE waves.

Several storm events have been recorded during the MICORE campaign among which the two most important are discussed in the MICORE report. Here a group of several individual WSW storms is simulated that took place at Faro beach from 18/12/2009 until 5/1/2010. The significant wave height reached 4 m and the peak period up to 20 sec, while given the long duration intense wave conditions coincided with both spring and neap tides. The event had a significant impact on the coast, as overtopping and dune erosion occurred at several sections.

The obtained simulation results with XBeach were in general not satisfactory as they result in negative BSS values. Apart from the unrealistic berm erosion, another significant difference between the measured and simulated profiles is that upper profile change in Faro beach appeared to decelerate during the storm period (see Figure 4.65), a behavior which the model did not appear to follow. After the morphological change of the first storms, the beach appeared to reach a new equilibrium state, which was affected only when storm conditions coincided with exceptionally high tidal levels. On the other hand, current XBeach modelling efforts resulted in erosion even in these equilibrium conditions.

Another deviation from the field observations, apart from the increased berm erosion and scarping, is a narrower profile section with morphological change, compared to the one shown by the data.

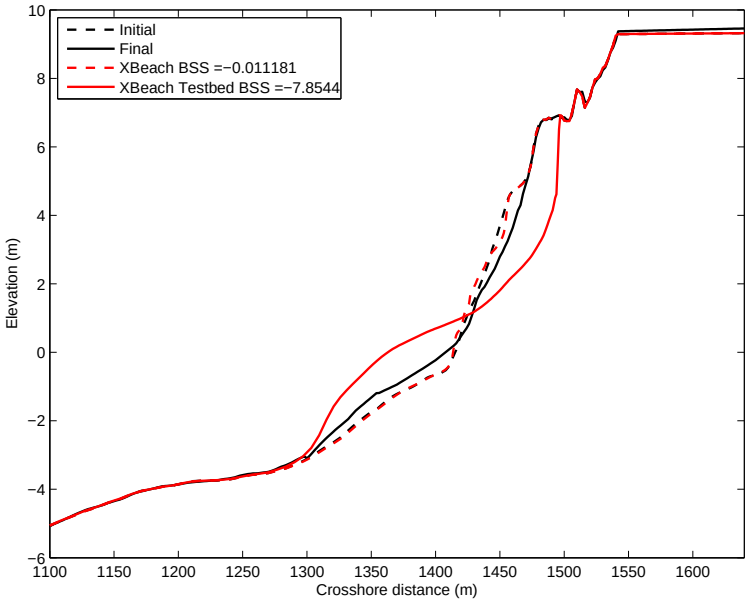

Figure 4.65

4.28 MICORE Kamchia Shkorpilovtsi Beach

Contact: Petia Eftimova <eftimova@io-bas.bg>

The study area, called Kamchia-Shkorpilovtsi, is situated in the western Black Sea, and spreads from cape Paletsa to cape Cherni Nos (Figure 9.1), located 25 and 40 km to the south of Varna city, respectively. It comprises the longest and the largest sandy beach along the Bulgarian Black Sea coast, with well-developed dunes and the two rivers mouths, these of the Kamchia River and the Fundakliiska River. In the middle of the site, near the mouth of the Fundakliiska River a scientific pier is built perpendicularly to the shoreline, reaching 4.5 m water depth. The beach is formed as a result of accumulation of erosive and fluvial sediments. The main morphological feature of the study area is its rectilinear shoreline with almost parallel isobaths. The bottom slope is covered with sands of different size. In its upper part down to 2.5 m depth, over 95

The beach is open to waves of the eastern half. In the case of severe storms the wind speed magnitude can reach 35-40 m/s and 9 m height of maximum significance wave at depths of about 1000 m. The large seasonal variability is one of the most marked features of the wave climate. The winter storms are much more frequent than the summer ones. In the western Black Sea the most frequent are the winds from northeast and east, which trigger the most severe storms.

In the beginning of March a short but very intense storm occurred in the western Black sea. This event was distinguished with all features of the severe storms known from the historical overview well defined phases growth took place on 08.03, peak 09.03 and decay 09.03 - 10.03. Wind and wave direction were quite stable turning from ESE to ENE. Maximum SWH reached almost 4.20 m.

Model results for this storm are shown in Figure 4.66. Both models predict washing out of the upper part of the profile, but XBeach overestimates it significantly. Both models predict re-deposition of eroded material downward the profile, while in reality such accretion was

not observed. Both models predict washing out of the permanent bar, and both of them underestimate the erosion rate.

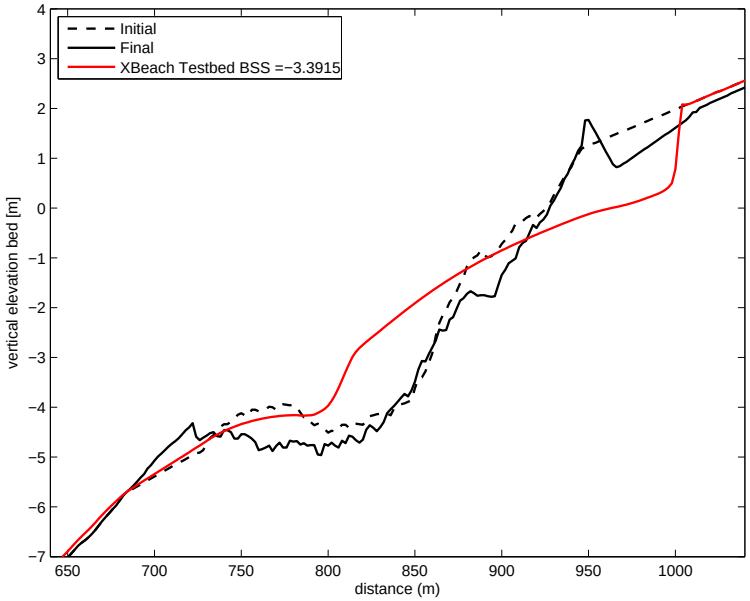

Figure 4.66

Chapter 5

Default settings

This chapter contains a comparison of most of the figures and tables that can also be found in the previous chapter with the figures and tables that are based on the model results obtained when using the default settings of the XBeach model. These results give an indication for what kind of cases the default settings of the XBeach model are sufficient and for what kind of cases adjustments of the default settings are needed. The figures and tables resulting from the default settings are shown on the left side while the original figures and tables are shown on the right side.

5.1 Carrier and Greenspan

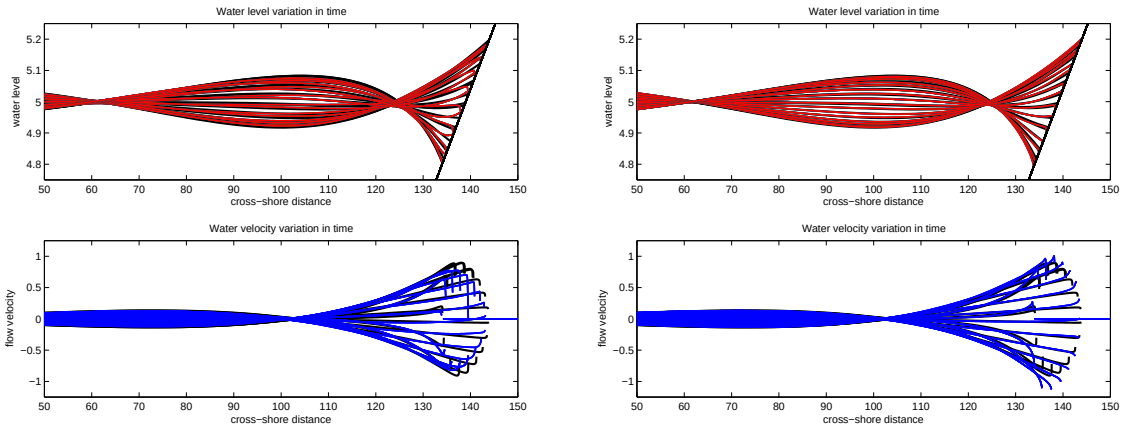

Figure 5.1

5.2 Long wave propagation

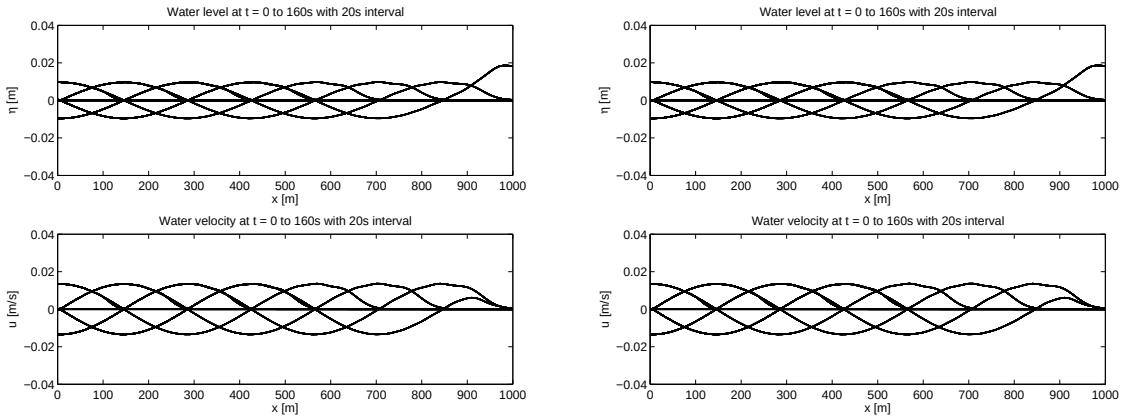

Figure 5.2

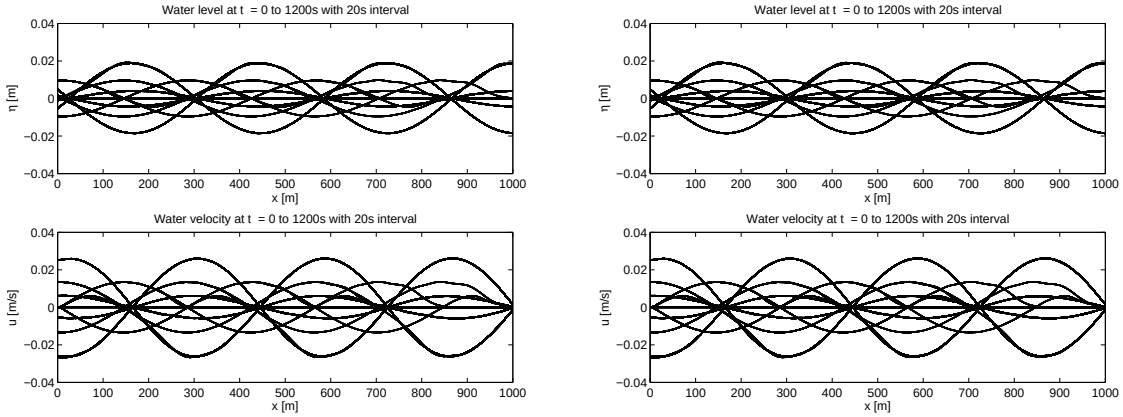

Figure 5.3

5.3 Boers 1C

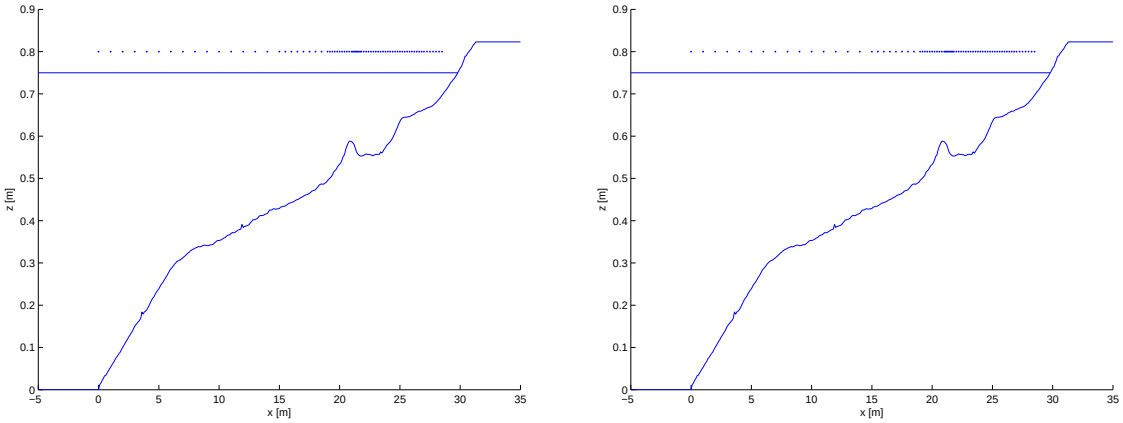

Figure 5.4

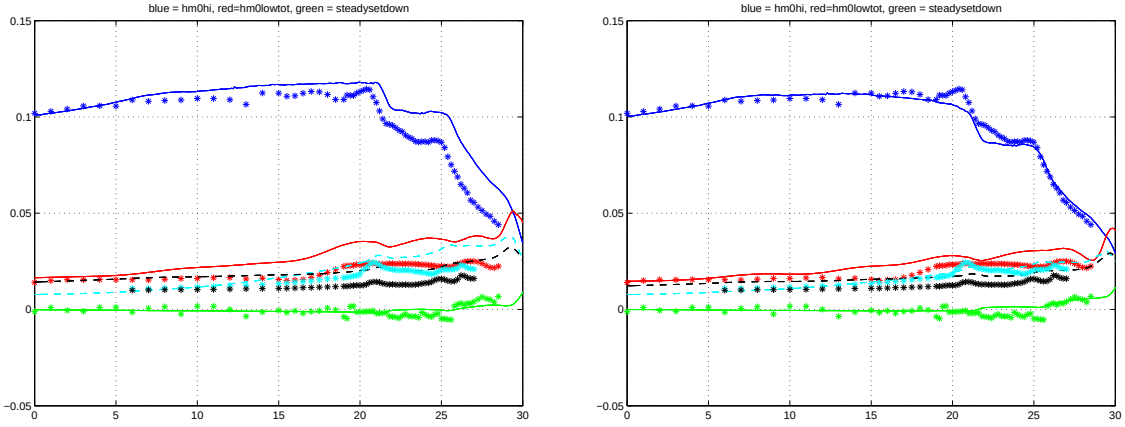

Figure 5.5

5.4 Zelt case 1

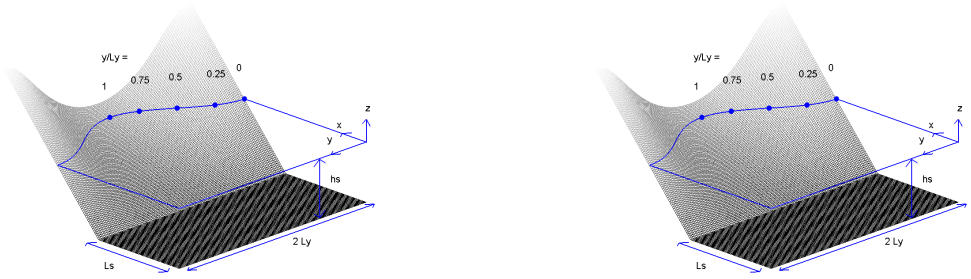

Figure 5.6

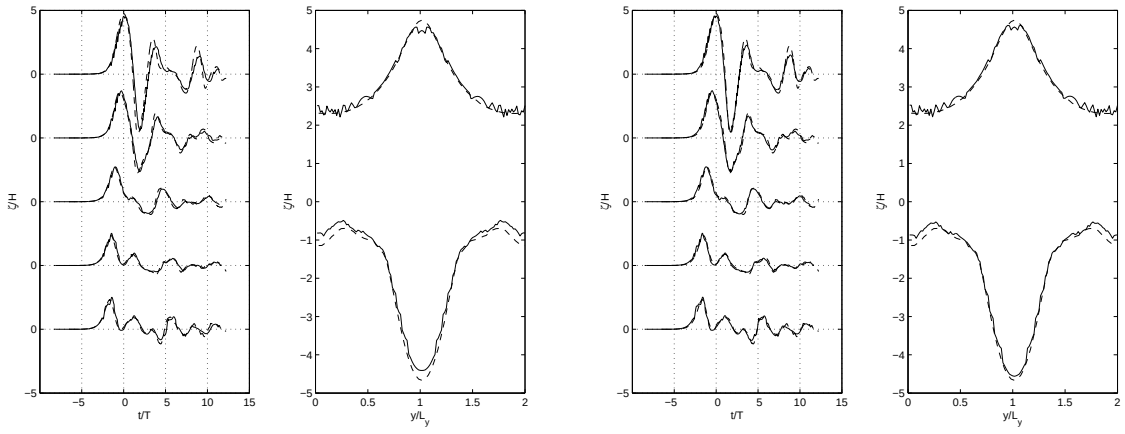

Figure 5.7

Table 5.1: Error statistics Zelt Case 1

	R^2	Sci	Rel. bias	BSS	R^2	Sci	Rel. bias	BSS
Timeseries (min)	0.04	0.17	-0.14	-5.11	0.07	0.16	-0.15	-5.11
Timeseries (max)	0.98	2.23	0.03	0.97	0.98	2.25	0.03	0.97
Max. runup	0.98	0.03	0.01	0.99	0.98	0.03	0.02	0.99

5.5 Delilah

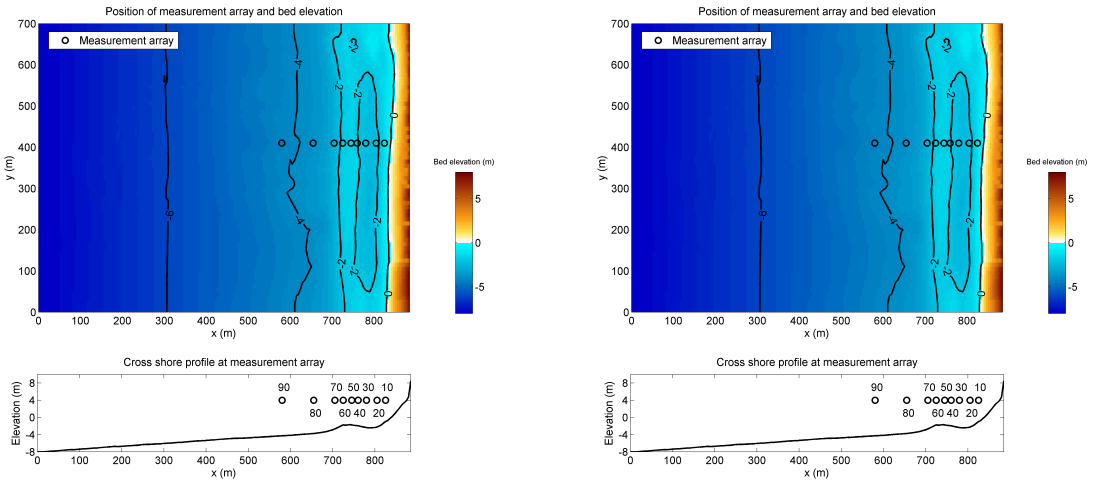

Figure 5.8: DELILAH field experiment 1990. Top panel: Plan view of the model location and measurement gauge array (circles). Bottom panel: Cross shore profile at the location of the measurement gauge array (circles) and measurement gauge names.

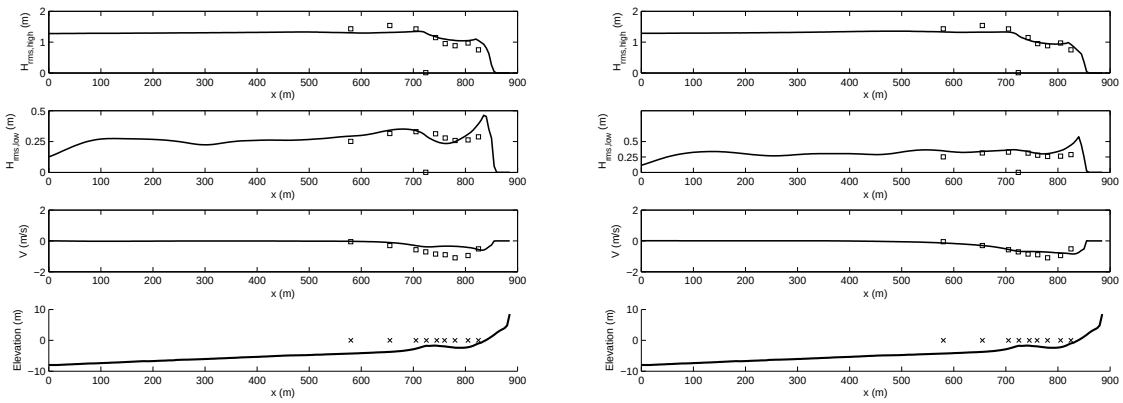

Figure 5.9: DELILAH field experiment 1990. First panel: Time-averaged measured (squares) and modelled (line) RMS-wave height of the short waves. Second panel: Time-averaged measured (squares) and modeled (line) RMS-wave height of the infragravity waves. Third panel: Time-averaged measured (squares) and modeled (line) longshore velocity. Fourth panel: Cross shore profile at the location of the measurement gauge array with the positions of the gauges (crosses).

Table 5.2: Error statistics Delilah

	R^2	Sci	Rel. bias	BSS
$H_{rms,HI}$	0.84	0.14	0.03	0.65
$H_{rms,LO}$	0.28	0.18	0.05	-2.22
v	0.31	0.57	0.49	0.11

	R^2	Sci	Rel. bias	BSS
$H_{rms,HI}$	0.85	0.10	-0.03	0.83
$H_{rms,LO}$	0.17	0.26	0.22	-1.57
v	0.56	0.26	0.10	0.41

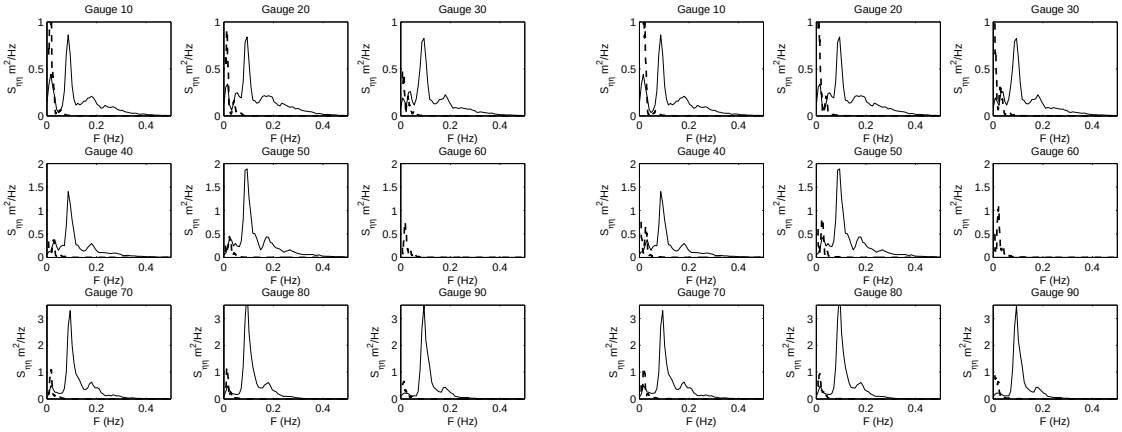

Figure 5.10: DELILAH field experiment 1990: Measured (solid line) and modelled (dashed line) surface elevation spectra for nine locations in the primary cross shore array. Gauge 90 is the most seaward.

5.6 Deltaflume M1263 part III test 1

Table 5.3: Brier skill scores (time)

t [s]	BSS
360	0.65
1080	0.70
3600	0.92
10800	0.99
21600	0.96
36000	0.93

t [s]	BSS
360	0.67
1080	0.87
3600	0.86
10800	0.82
21600	0.88
36000	0.90

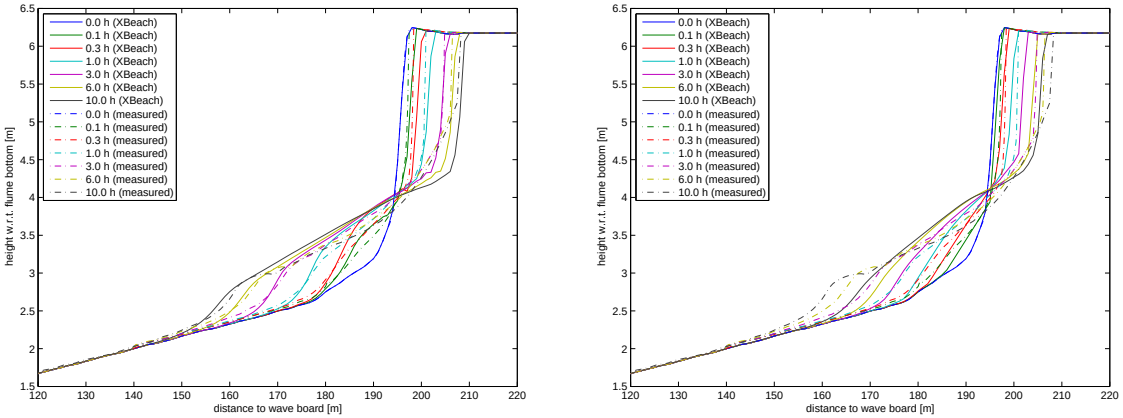

Figure 5.11: Comparison between measured and modelled profiles

5.7 Deltaflume M1263 part III test 2

Table 5.4: Brier skill scores (time)

t [s]	BSS
360	0.52
1080	0.90
3600	0.94
10800	0.96
21600	0.93
36000	0.83

t [s]	BSS
360	0.79
1080	0.85
3600	0.87
10800	0.88
21600	0.90
36000	0.92

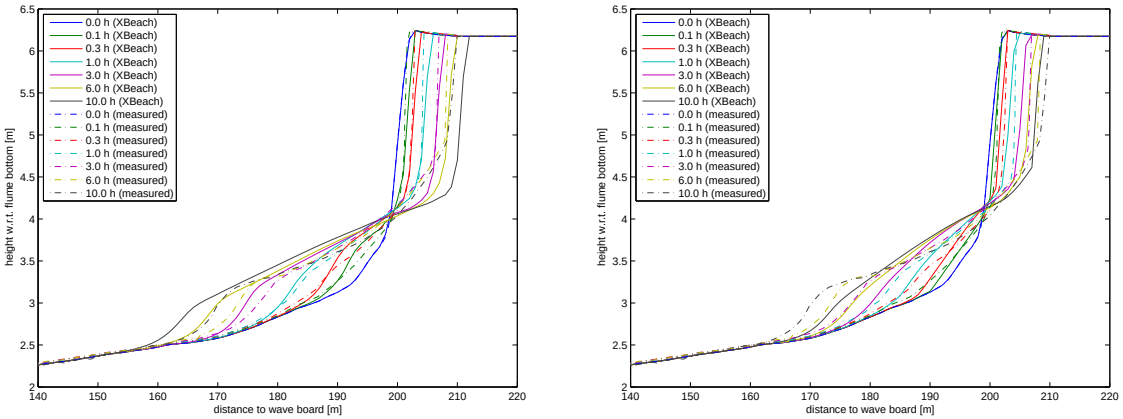

Figure 5.12: Comparison between measured and modelled profiles

5.8 Deltaflume M1263 part III test 3

Table 5.5: Brier skill scores (time)

t [s]	BSS
6480	0.92
14400	0.83
69480	-0.48

t [s]	BSS
6480	0.92
14400	0.92
69480	0.39

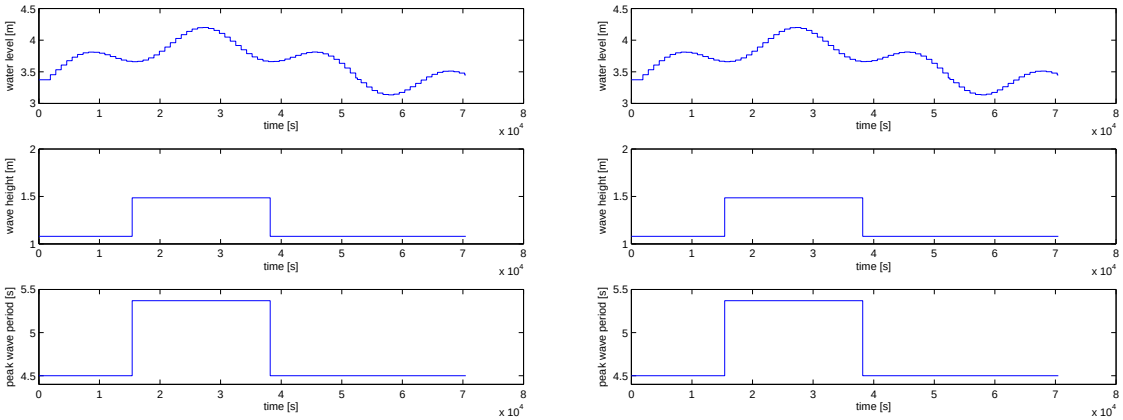

Figure 5.13: Hydraulic boundary conditions as function of time

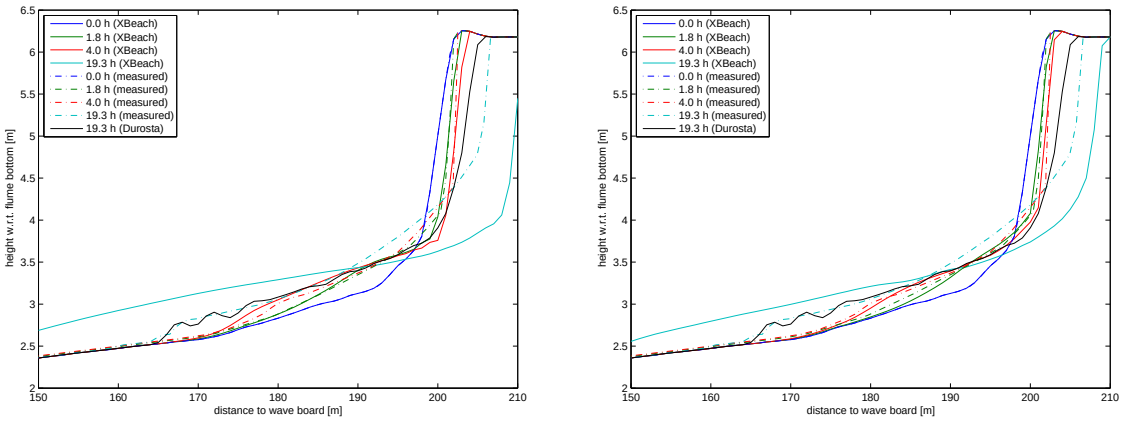

Figure 5.14: Comparison between measured and modelled profiles

5.9 Deltaflume M1263 part III test 4

Table 5.6: Brier skill scores (time)

t [s]	BSS
18360	-0.01
61200	0.04

t [s]	BSS
18360	0.63
61200	0.72

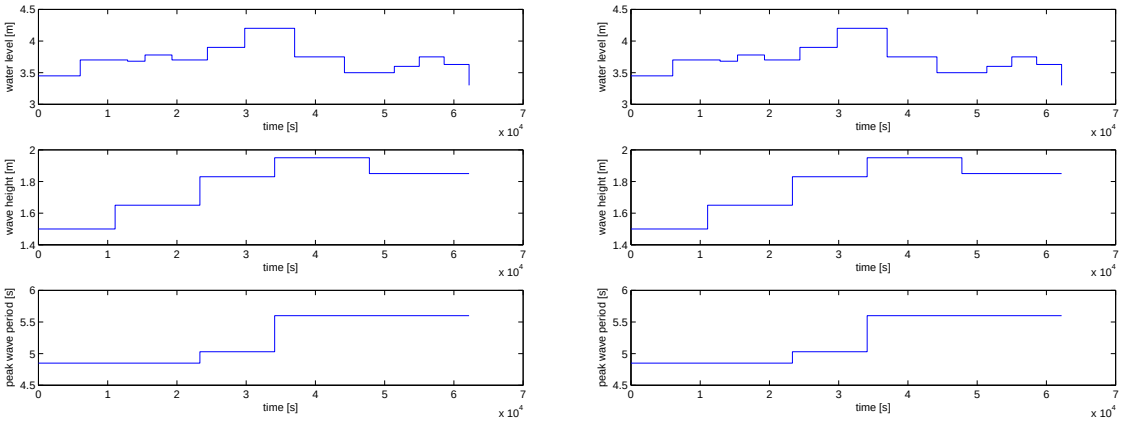

Figure 5.15: Hydraulic boundary conditions as function of time

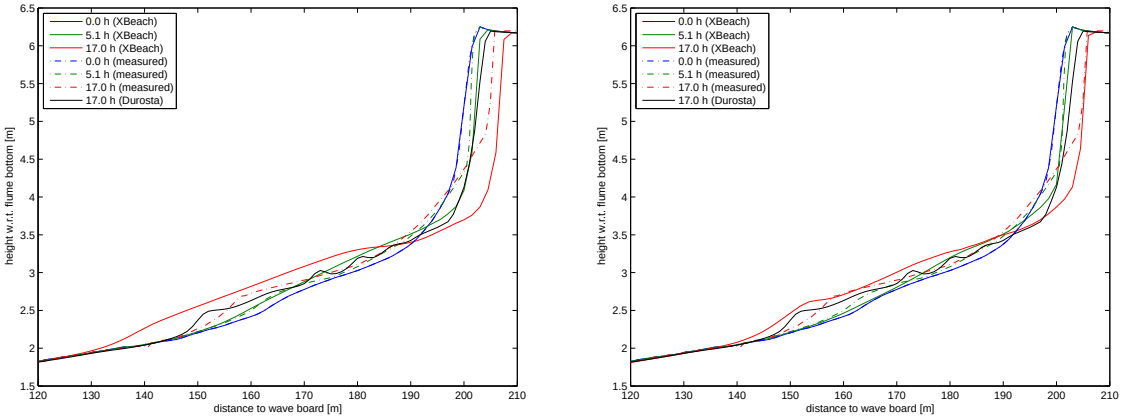

Figure 5.16: Comparison between measured and modelled profiles

5.10 Deltaflume M1263 part III test 5

Table 5.7: Brier skill scores (time)

t [s]	BSS
10800	0.72
21600	0.54

t [s]	BSS
10800	0.87
21600	0.98

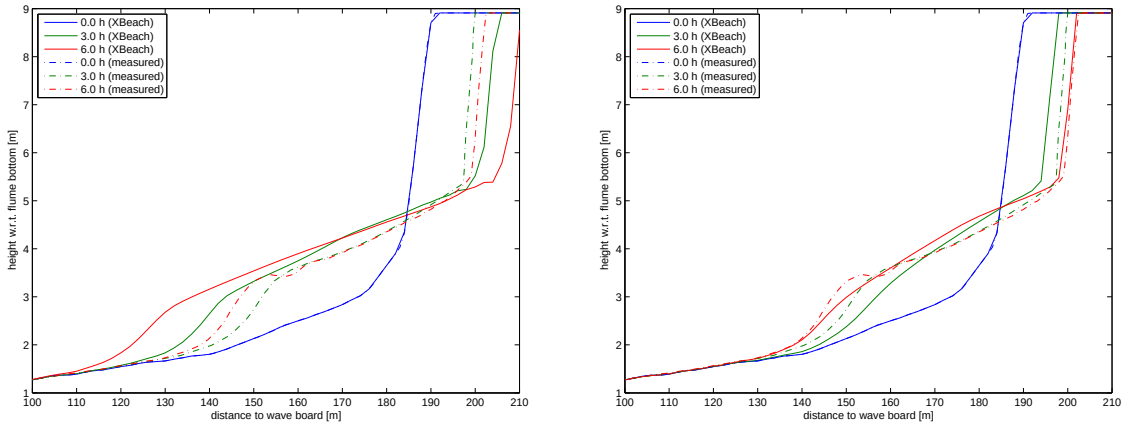

Figure 5.17: Comparison between measured and modelled profiles

5.11 DeltaflumeH298 T1

5.11.1 Results

Table 5.8

	R^2	SCI	Rel. Bias	BSS		R^2	SCI	Rel. Bias	BSS
sedero	0.9080	0.6265	0.0494	0.6059	sedero	0.6409	0.8598	0.0338	0.2544

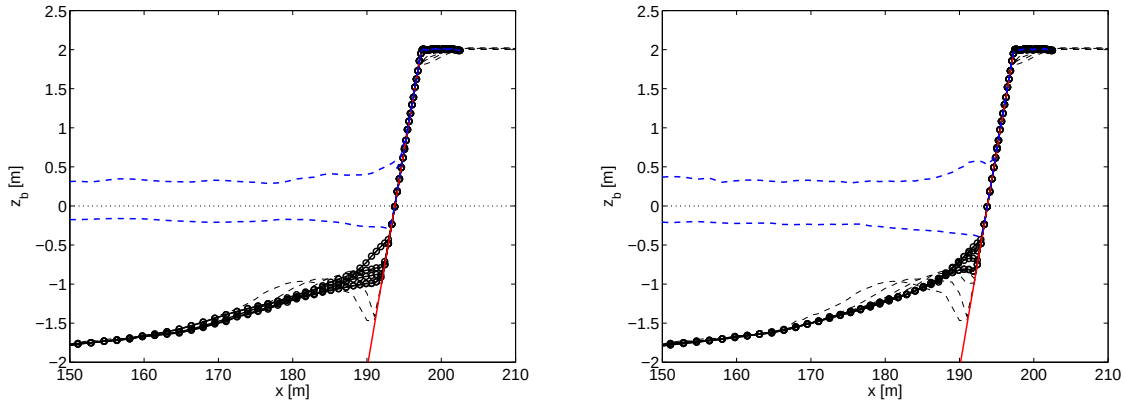

Figure 5.18

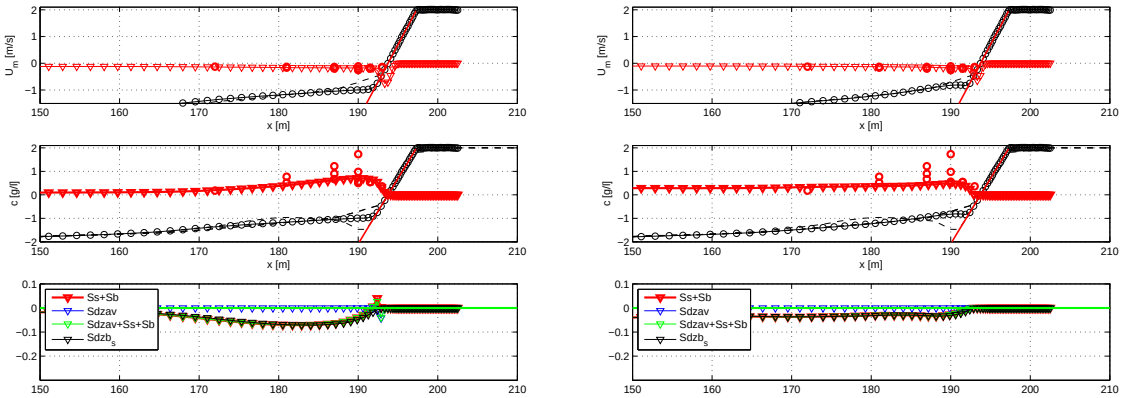

Figure 5.19

5.12 DeltaflumeH298 T3

5.12.1 Results

Table 5.9

	R^2	SCI	Rel. Bias	BSS		R^2	SCI	Rel. Bias	BSS
sedero	0.4781	0.9054	0.0334	0.1790	sedero	0.1889	0.9913	0.0487	0.0168

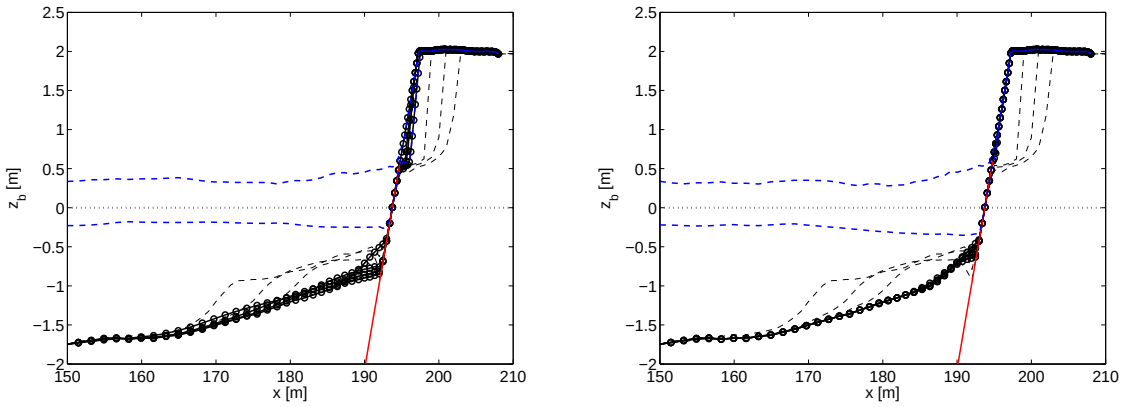

Figure 5.20

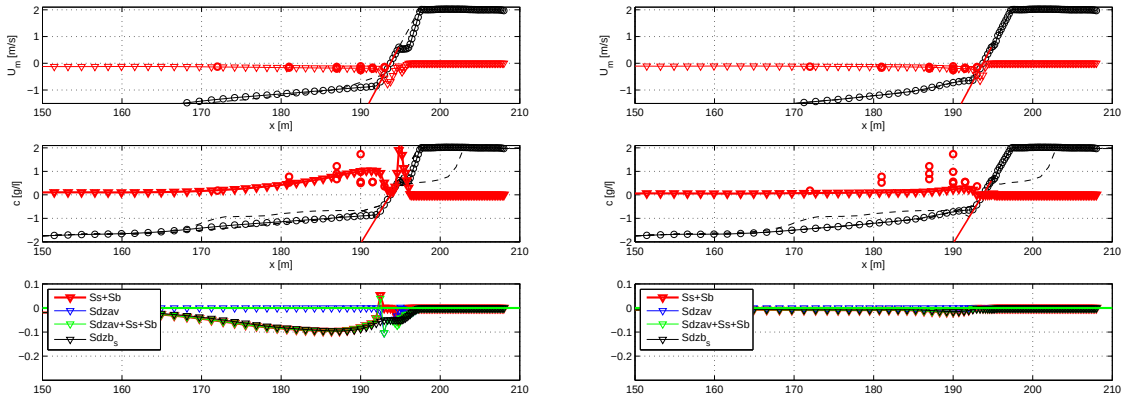

Figure 5.21

5.13 Deltaflume LIP 11D 2E

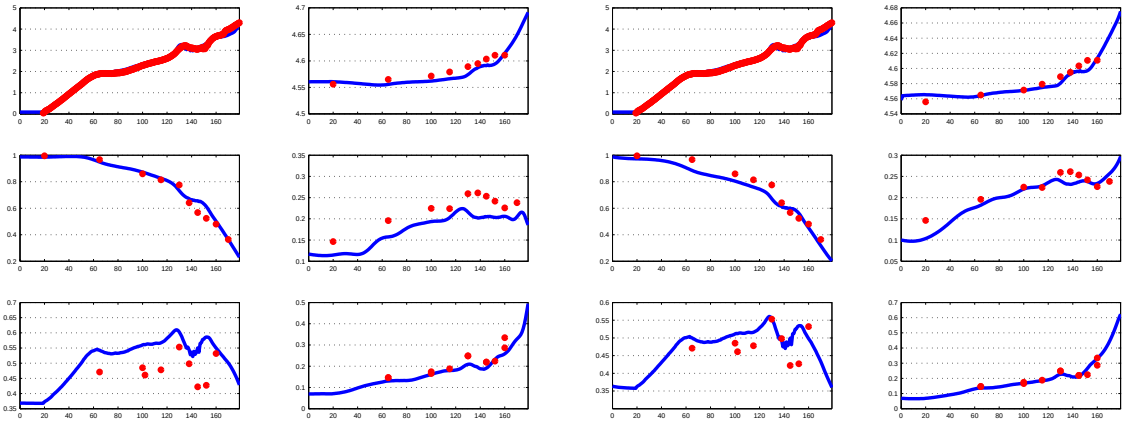

Figure 5.22: Computed and observed hydrodynamic parameters for test 2E of the LIP11D experiment. Top left: bed level and mean water level. Top right: measured (dots) and computed mean water level with first-order steering (drawn line) as function of the cross-shore distance. Middle left: same for HF wave height; middle right: same for LF wave height; bottom left: same for HF orbital velocity; bottom right: same for LF orbital velocity.

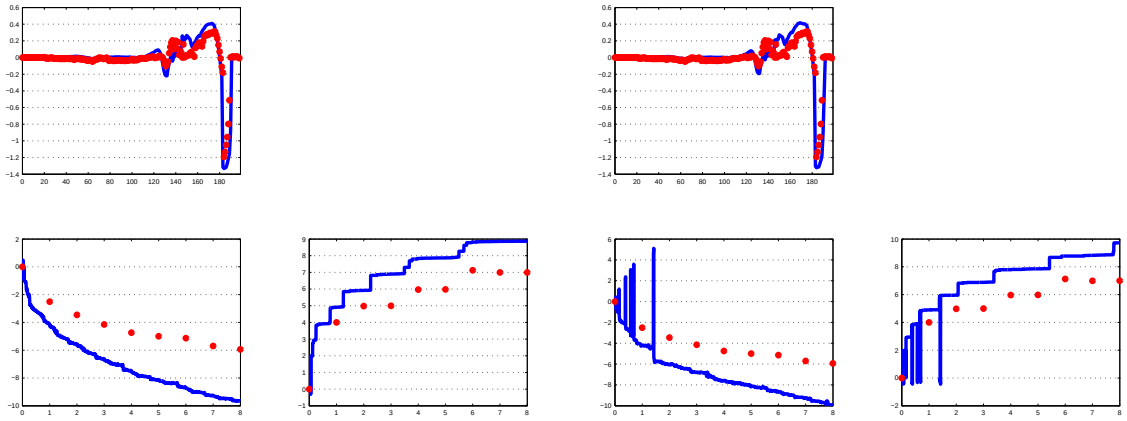

Figure 5.23: Computed and observed sedimentation and erosion after 8 hrs (top panel); erosion volume as function of time (bottom left) and dune retreat (bottom right) as function of time for test 2E of the LIP11D experiment, (Arcilla et al, 1993). All results with first-order steering.

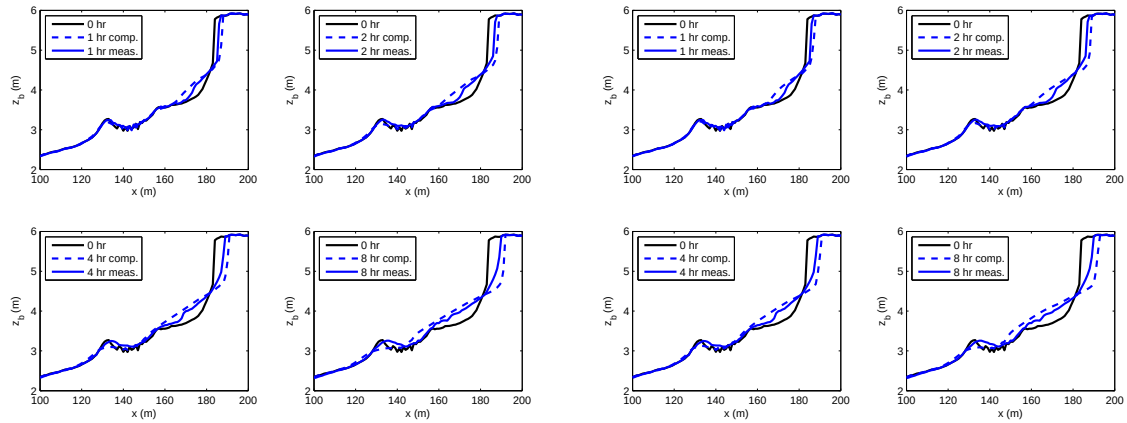

Figure 5.24: Measured and modelled bed level after 1, 2, 4 and 8 hours of wave action, for a water level of 4.56 m above the flume bottom.

Table 5.10: Error statistics Deltaflume LIP 11D 2E

	R^2	Sci	Rel. bias	BSS
$SEDERO$	0.91	0.60	-0.14	0.66
ETA	0.82	0.00	-0.00	0.86
VOL	0.87	0.63	-0.61	0.59
R	0.85	0.28	0.27	0.86
$URMS$	0.20	0.19	0.17	-0.01
$URMS_{LO}$	0.86	0.14	-0.11	0.85

	R^2	Sci	Rel. bias	BSS
$SEDERO$	0.91	0.61	-0.11	0.64
ETA	0.84	0.00	-0.00	0.89
VOL	0.87	0.66	-0.64	0.60
R	0.85	0.30	0.29	0.75
$URMS$	0.21	0.11	0.07	0.01
$URMS_{LO}$	0.87	0.09	0.00	0.86

5.14 Deltaflume 2006 T01

5.14.1 Results

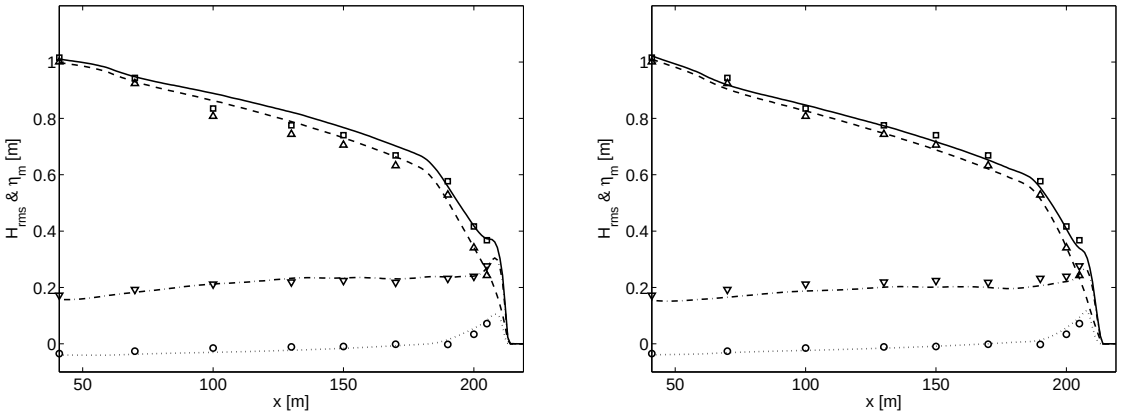

Figure 5.25: Simulated wave setup (dotted line) and transformation of the total (solid line), short (dashed line) and long (dashed-dotted line) wave height compared with measurements of the wave setup (circles) and the total (squares), short (upward triangles) and long (downward triangles) wave height.

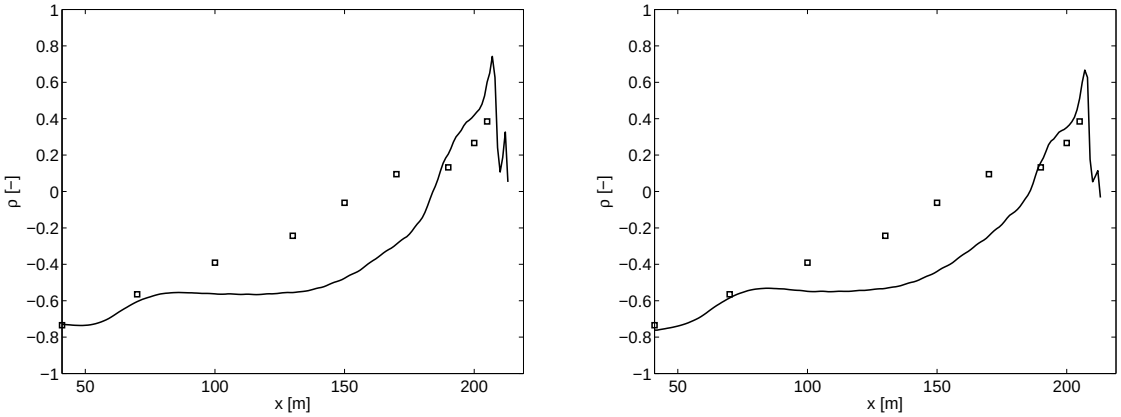

Figure 5.26: Simulated correlation ρ between the short wave variance and long wave water surface elevations (solid line) compared with the measured correlation (squares) as function of cross-shore position.

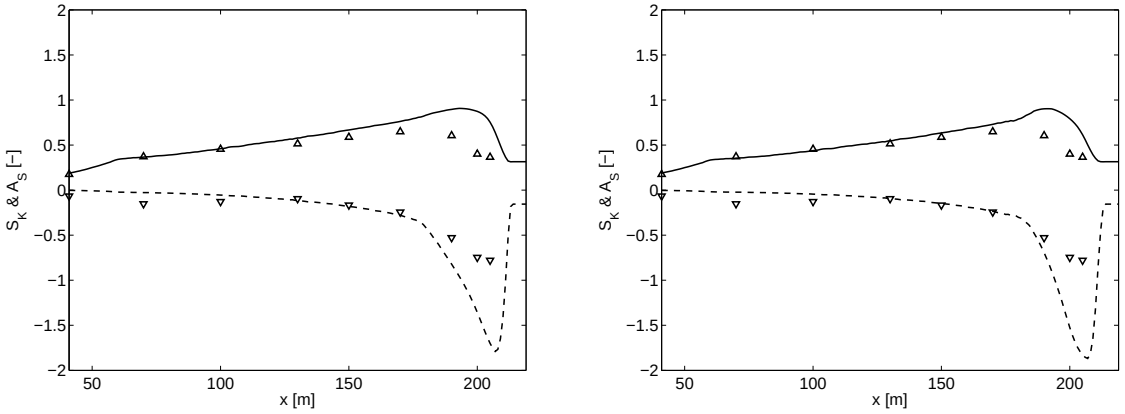

Figure 5.27: Simulated wave skewness S_K (solid line) and asymmetry A_S (dashed line) compared with measured skewness (upward triangles) and asymmetry (downward triangles) as function of cross-shore position.

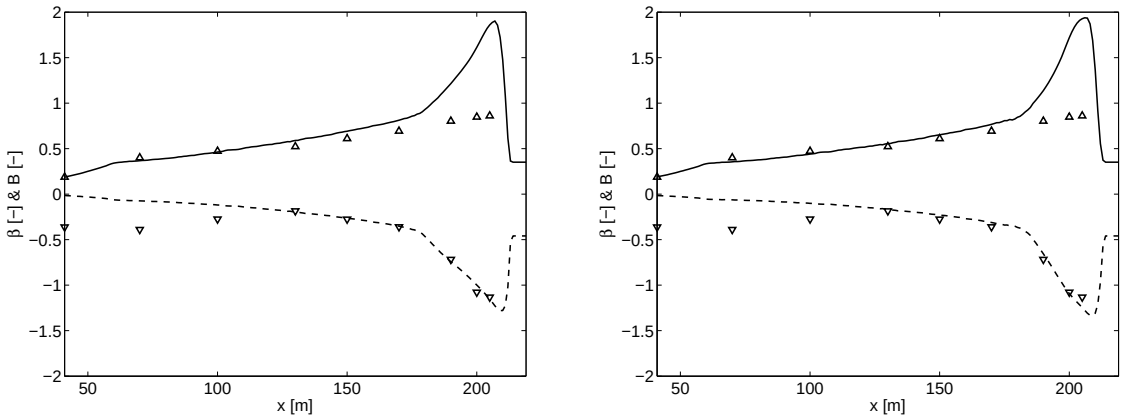

Figure 5.28: Simulated wave nonlinearity B (solid line) and phase β (dashed line) compared with measured nonlinearity (upward triangles) and phase (down-ward triangles) as function of cross-shore position.

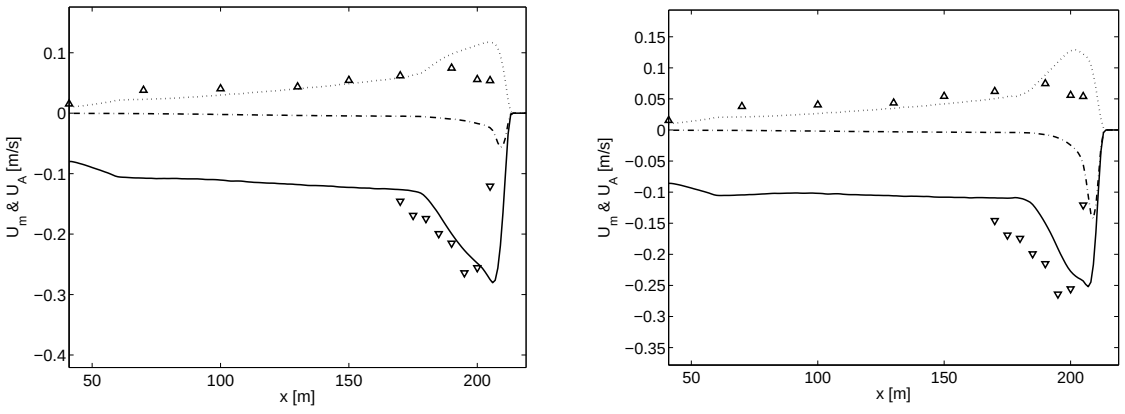

Figure 5.29: Simulated test and depth averaged flow Um due to short and long waves (solid line) and long waves only (dashed line) as function of the cross-shore position. The dotted line corresponds to the wave averaged sediment advection velocity u_A due to nonlinear short waves. Markers correspond to measured undertow flow velocities due to short and long waves (downward triangles) and the sediment advection velocity due to nonlinear waves (upward triangles).

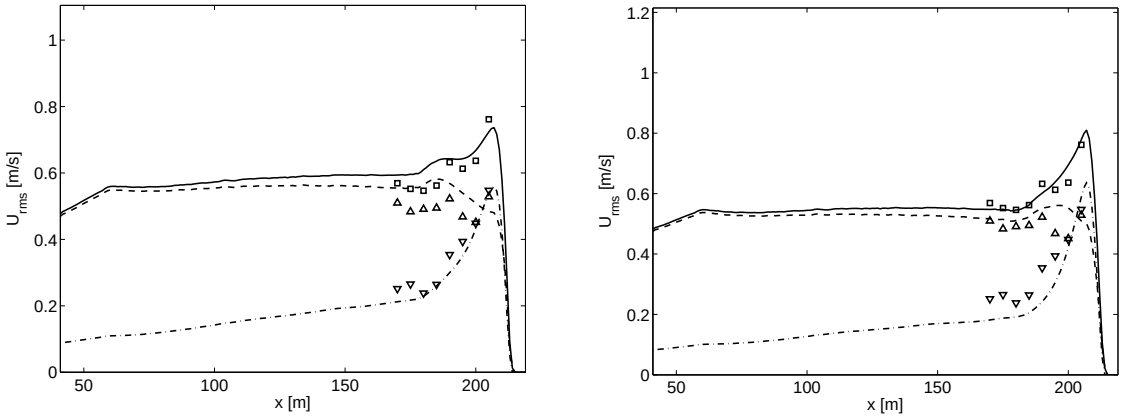

Figure 5.30: Transformation of the simulated total (solid line), short (dashed line) and long (dashed-dotted line) wave orbital flow compared with the meas-ured total (squares), short (upward triangles) and long (downward triangles) wave orbital flow as function of cross-shore position.

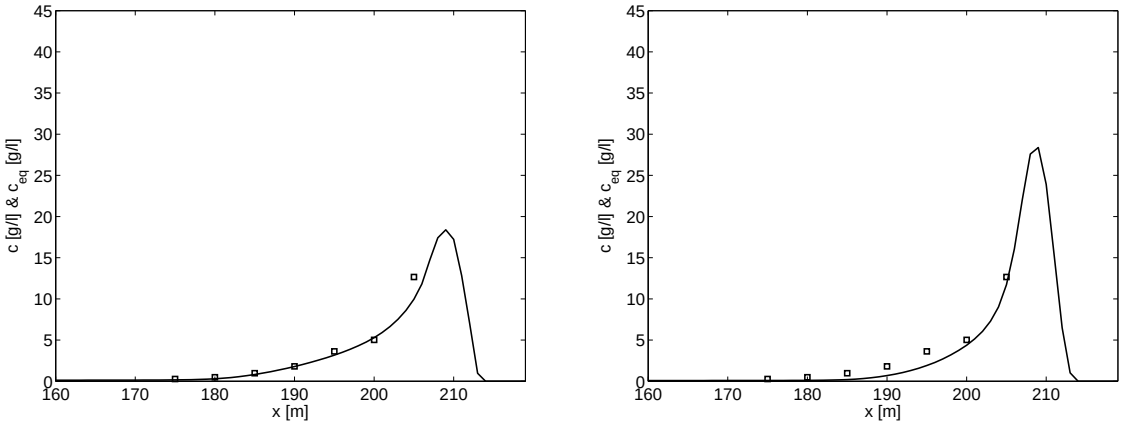

Figure 5.31: Simulated test and depth averaged sediment concentration (solid line) compared with the sediment concentrations obtained from suction tubes (squares).

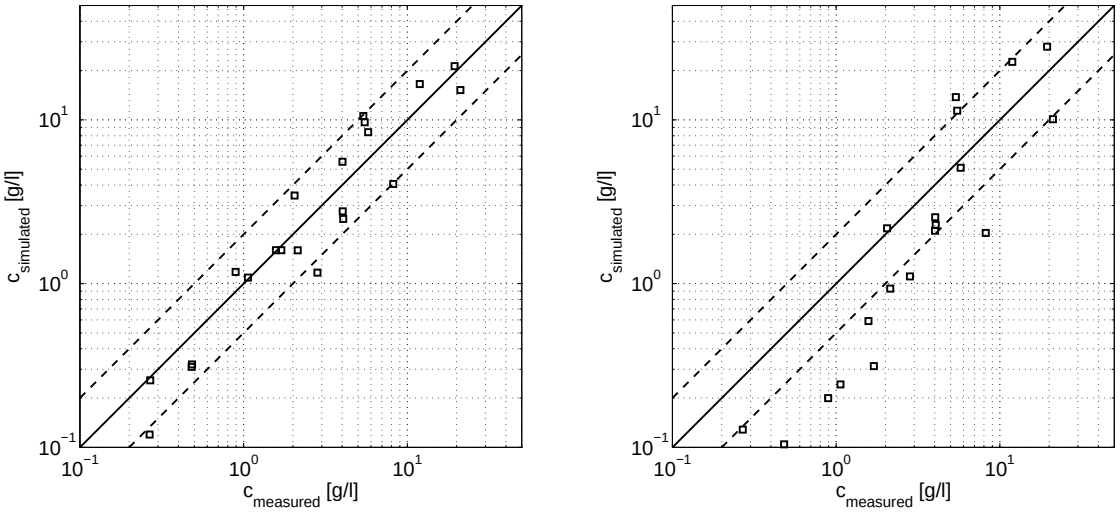

Figure 5.32: Scatter plot of simulated time and depth averaged sediment concentrations compared with vertically integrated suction tube measurements. The solid line corresponds to a perfect match between measurements and simulations whereas simulation results between the dashed lines are within a factor two with the measurements.

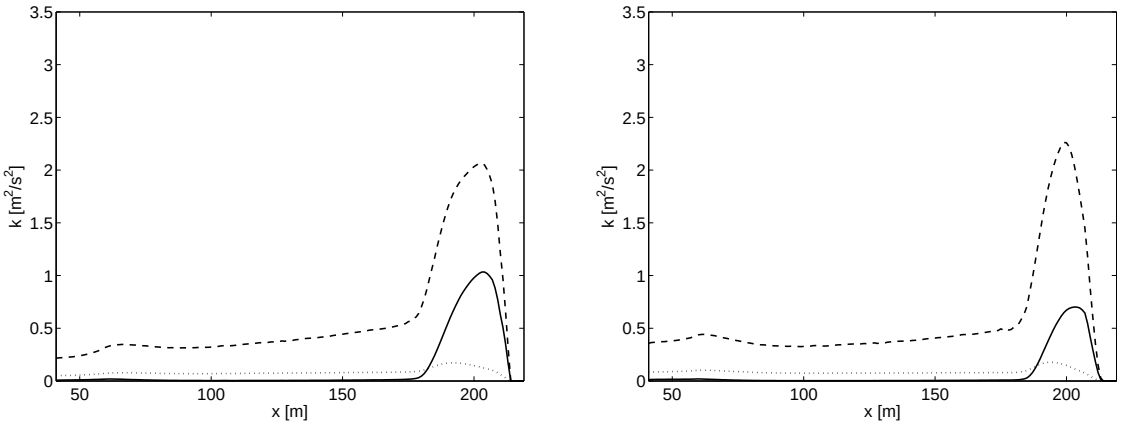

Figure 5.33: Simulated wave averaged turbulence energy (dotted line), bore averaged turbulence energy (dashed line) and near-bed bore averaged turbulence energy (solid line) as function of cross-shore position.

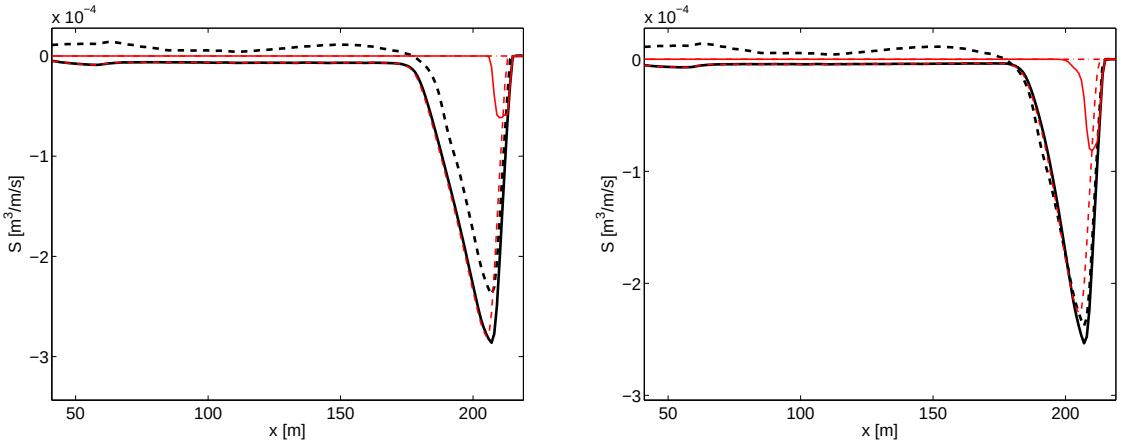

Figure 5.34: Measured (thick dashed line) and simulated (thick solid line) test av-eraged sediment transport from bed level changes. The simulated transport is separated in a transport due to avalanching (dashed-dotted line) and a transport related to the hydrodynamics (dotted line).

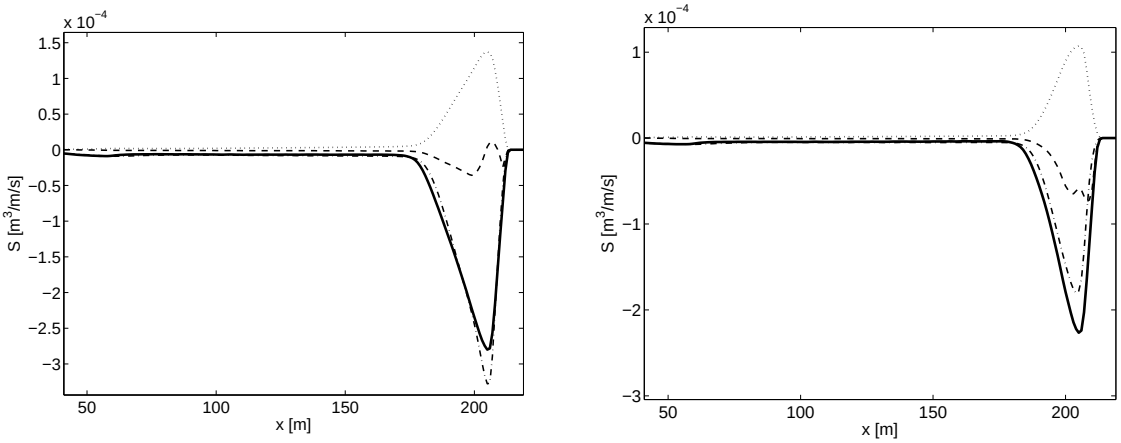

Figure 5.35: Simulated test averaged sediment transport related to the hydrodynamics (solid line) divided into wave asymmetry related sediment transport (dotted line), long wave related sediment transport (dashed line) and sediment transport associated with the short wave undertow (dashed-dotted line).

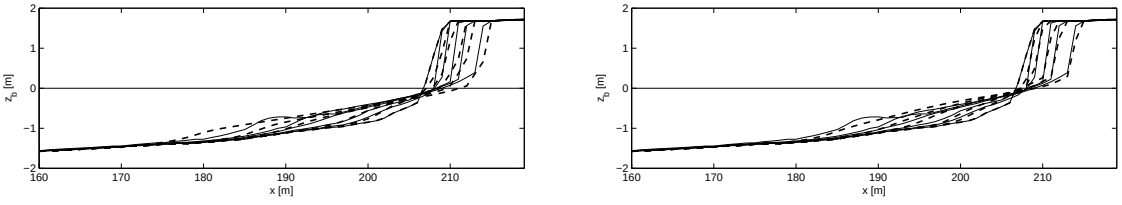

Figure 5.36: Simulated profile evolution (dashed lines) compared with measured profile evolu-tion (solid lines) after t = 0.0, 0.1, 0.3, 1.0, 2.04 and 6.0 hours.

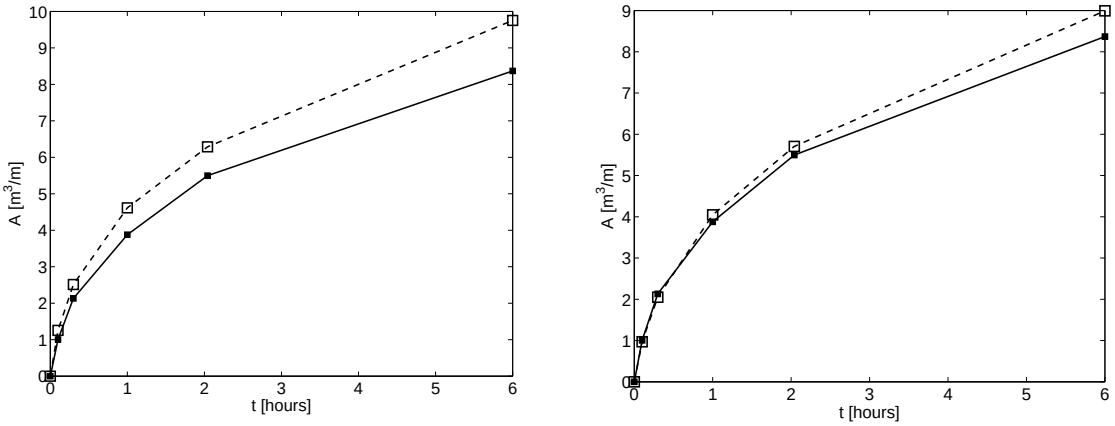

Figure 5.37: Simulated dune erosion volume above still water level (dashed line with open squares) compared with the measured dune erosion volume (solid lines with closed squares) as function of time.

Table 5.11

	R^2	SCI	Rel. Bias	BSS	R^2	SCI	Rel. Bias	BSS
$H_{rms,hf}$	0.9955	0.0412	0.0241	0.9903 $H_{rms,hf}$	0.9987	0.0190	-0.0066	0.9973
$H_{rms,lf}$	0.9580	0.0434	0.0064	0.8794 $H_{rms,lf}$	0.9890	0.1028	-0.1010	0.9764
ρ	0.8894	0.6301	-0.2543	0.6288 ρ	0.9145	0.5439	-0.2817	0.7582
S_k	0.6653	0.4831	0.3292	-0.4582 S_k	0.7380	0.3901	0.2503	-0.0445
A_s	0.9858	0.9173	-0.4322	-0.6073 A_s	0.9757	1.0544	-0.4466	-1.2395
β	0.9436	0.2660	0.1517	0.8342 β	0.9595	0.2797	0.1574	0.8145
B	0.9201	0.6986	0.4185	-1.7760 B	0.8951	0.7444	0.4090	-2.4322
$U_{rms,hf}$	0.0352	0.1290	0.1027	-1.4465 $U_{rms,hf}$	-0.4830	0.1064	0.0733	-1.3922
$U_{rms,lf}$	0.9853	0.0935	-0.0773	0.9669 $U_{rms,lf}$	0.9686	0.1934	-0.1510	0.8254
U_m	0.2746	0.3073	0.0213	-0.6628 U_m	0.2272	0.3589	0.1791	-0.7106
C_m	0.9891	0.9997	-0.7561	0.0006 C_m	0.9961	0.9997	-0.7562	0.0008
sedero	0.9733	0.2732	-0.0456	0.9274 sedero	0.9904	0.1503	-0.0187	0.9778
A	0.9997	0.1652	0.1442	0.9767 A	0.9997	0.0623	0.0361	0.9907

5.15 T01 Zebra

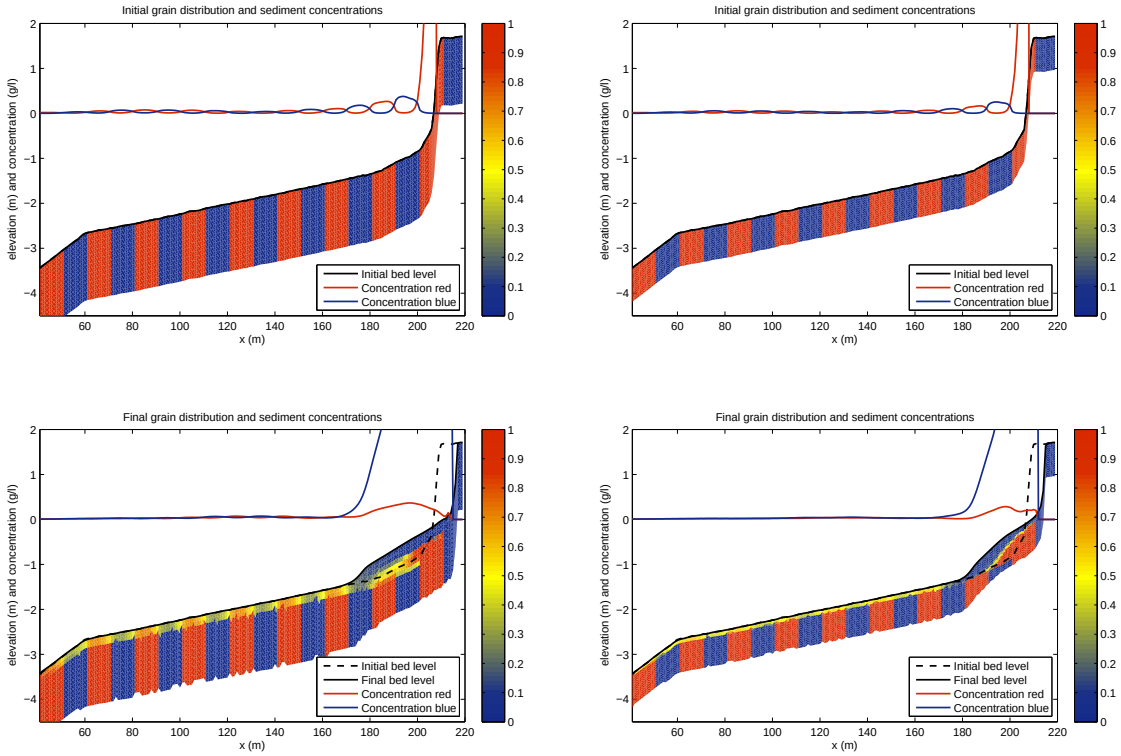

Figure 5.38

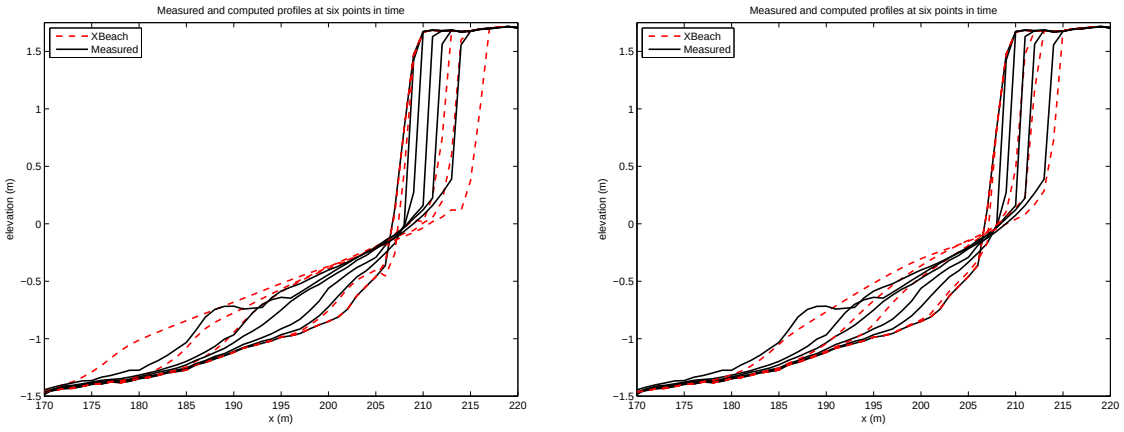

Figure 5.39

Table 5.12

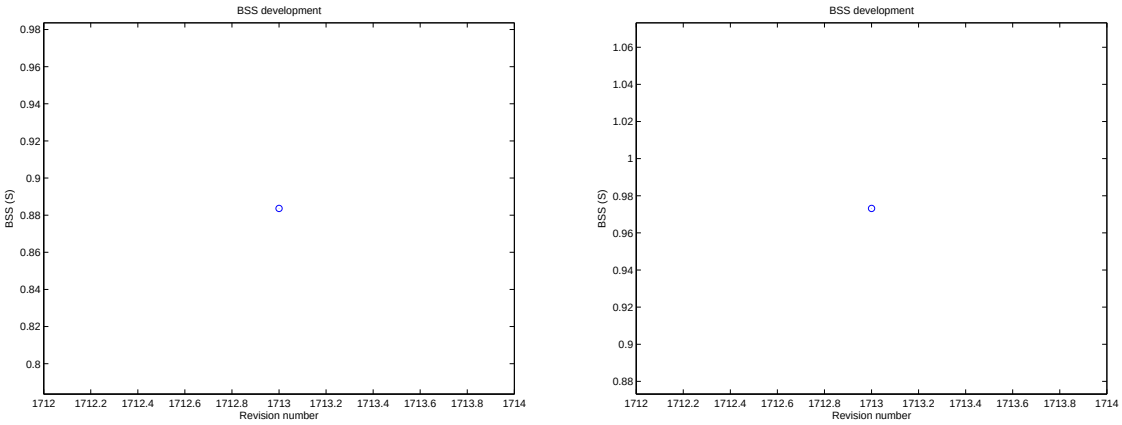

Figure 5.40

5.16 Deltaflume 2006 T04

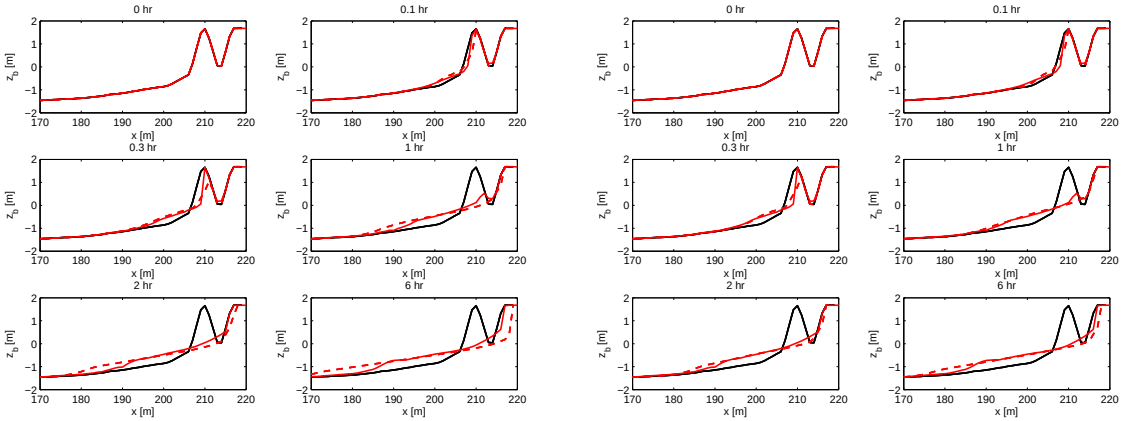

Figure 5.41: Deltaflume 2006 test T04. Measured (drawn lines) and modelled (dashed lines) profile after 0, 0.1, 0.3, 1, 2 and 6 hours of wave action.

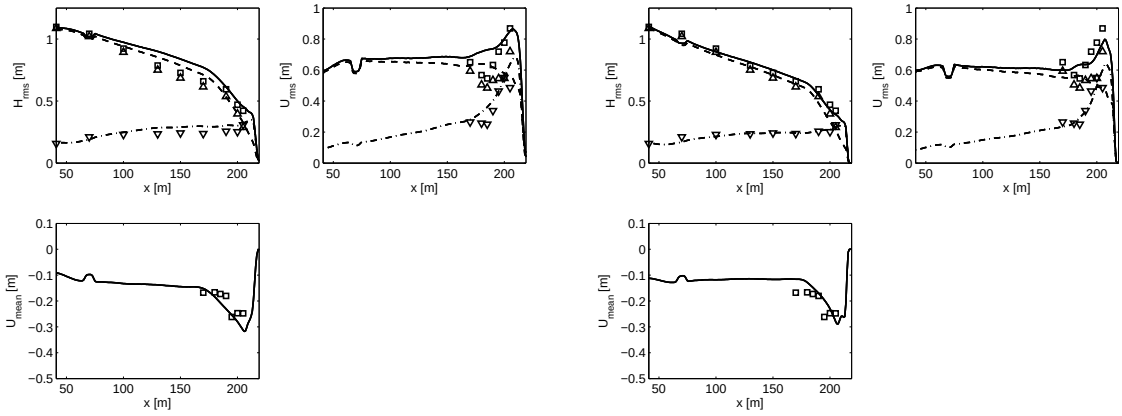

Figure 5.42: Deltaflume 2006 test T04. Upper left panel: Measured (markers) and simulated (lines) LF (downward triangles / dashed-dotted line), HF (upward triangles / dashed line) and total (squares / solid line) wave height. Upper right panel: Measured (markers) and simulated (lines) orbital flow velocity. Lower left panel: Measured (squares) and simulated (solid line) time and depth averaged flow velocity.

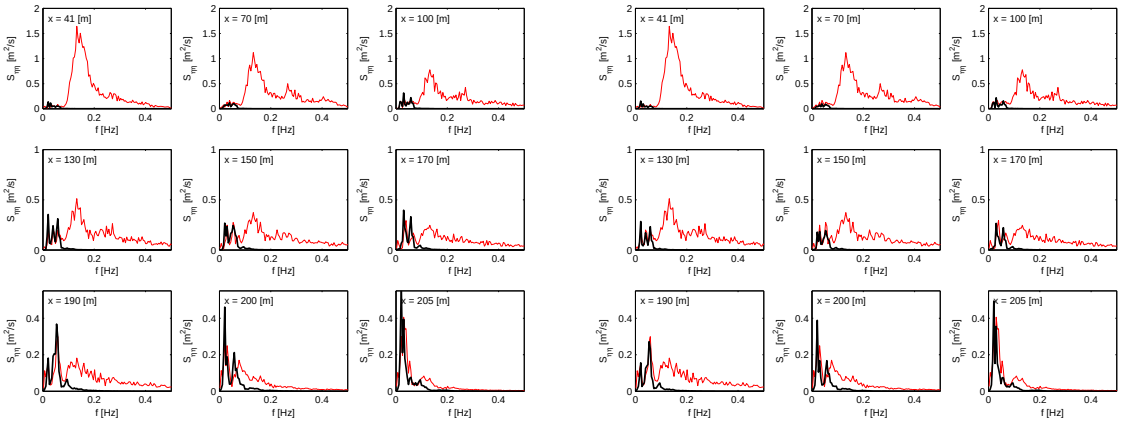

Figure 5.43: Measured wave spectra including both incident waves and long waves (thin line) compared with simulated long wave spectra (thick line) at different cross-shore positions (see upper left corner of sub-panels). Measured and simulated spectra are computed over the whole test duration.

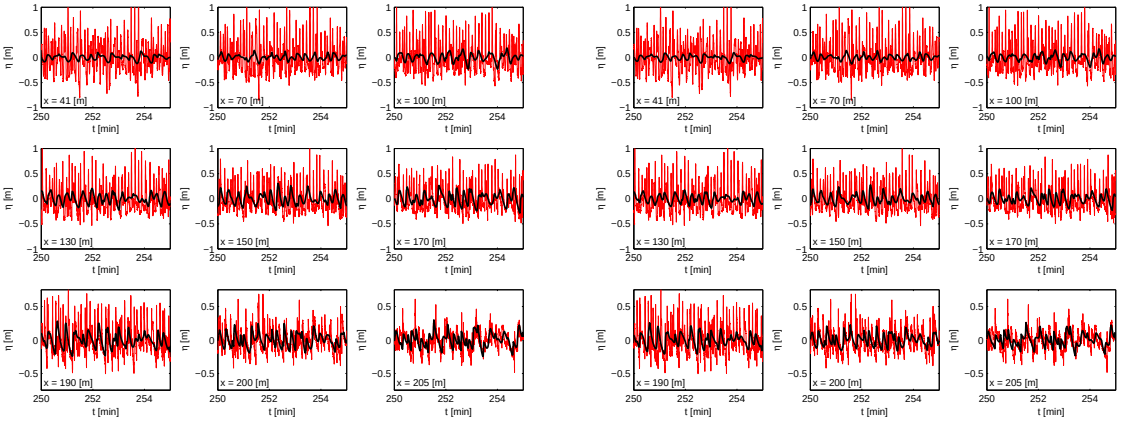

Figure 5.44: Measured water surface elevations including both incident and long waves (thin line) compared with simulated long wave water surface elevations (thick line) at different cross shore positions (see lower left corner of sub-panels) after 4.17 wave hours.

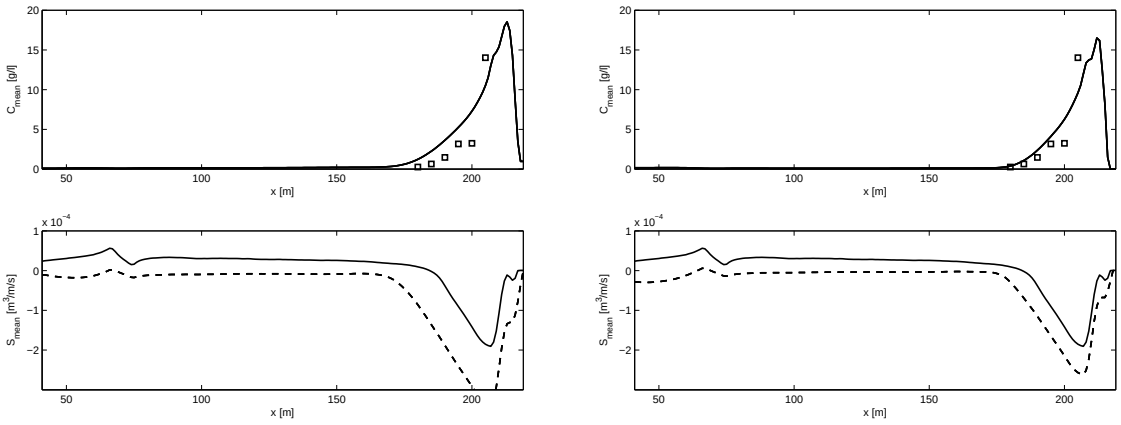

Figure 5.45: Deltaflume 2006. Test T04. Top panel: observed depth-averaged concentrations (squares) vs. model result. Bottom panel: total sediment transport observed from profile evolution (drawn line) vs. model result (dashed line).

Table 5.13: Error statistics Deltaflume 2006 T04

	R^2	Sci	Rel. bias	BSS
H_{rms}	0.87	0.09	0.06	0.95
$H_{rms,HI}$	0.87	0.08	0.05	0.97
$H_{rms,LO}$	0.78	0.16	0.12	0.55
U_{rms}	0.74	0.15	0.11	0.59
$U_{rms,HI}$	-0.63	0.19	0.08	-0.70
$U_{rms,LO}$	0.77	0.20	0.15	0.79
U_m	0.73	0.18	-0.12	0.55
Sed/Ero	0.94	0.32	-0.08	0.90

	R^2	Sci	Rel. bias	BSS
H_{rms}	0.88	0.05	-0.02	0.98
$H_{rms,HI}$	0.88	0.05	-0.02	0.98
$H_{rms,LO}$	0.81	0.07	-0.02	0.81
U_{rms}	0.75	0.10	-0.03	0.63
$U_{rms,HI}$	-0.56	0.18	-0.05	-0.71
$U_{rms,LO}$	0.76	0.15	-0.00	0.75
U_m	0.73	0.18	0.12	0.47
Sed/Ero	0.96	0.24	-0.07	0.95

5.17 1953 storm surge

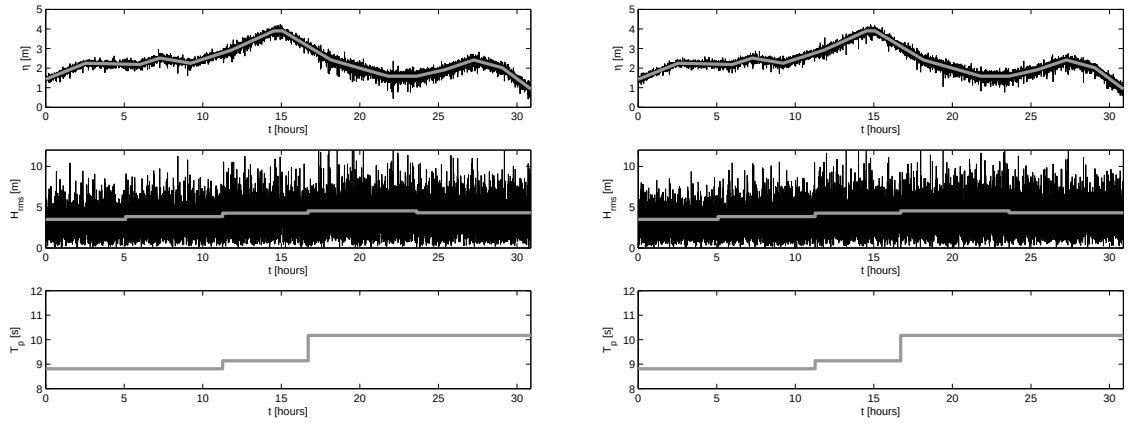

Figure 5.46: Imposed (thick line) and simulated (black line) hydrodynamic conditions at the offshore model boundary. Upper panel: Surge level above mean sea level as function of time. The simulated surge time series include water surface fluctuations due to long waves. Middle panel: Short wave height as function of time. Simulated wave height time series include fluc-tuations on the wave group time scale. Lower panel: Short wave peak period as function of time.

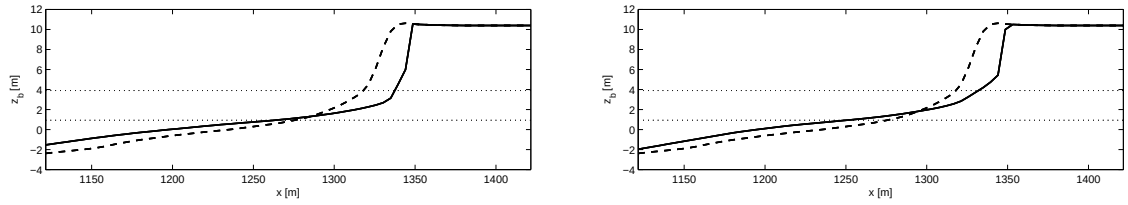

Figure 5.47: Simulated profile evolution during the 1953 storm surge (dashed line is initial profile and solid line is post surge profile). The minimum and maximum surge levels are indi-cated by the dotted lines.

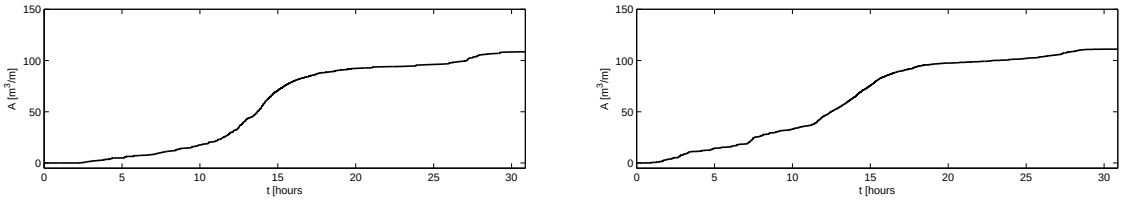

Figure 5.48: Upper panel: Imposed storm surge level as function of time. Lower panel: Simu-lated dune erosion volume above the maximum storm surge level during the 1953 storm surge as function of time

5.18 Zwin T01

5.18.1 Results

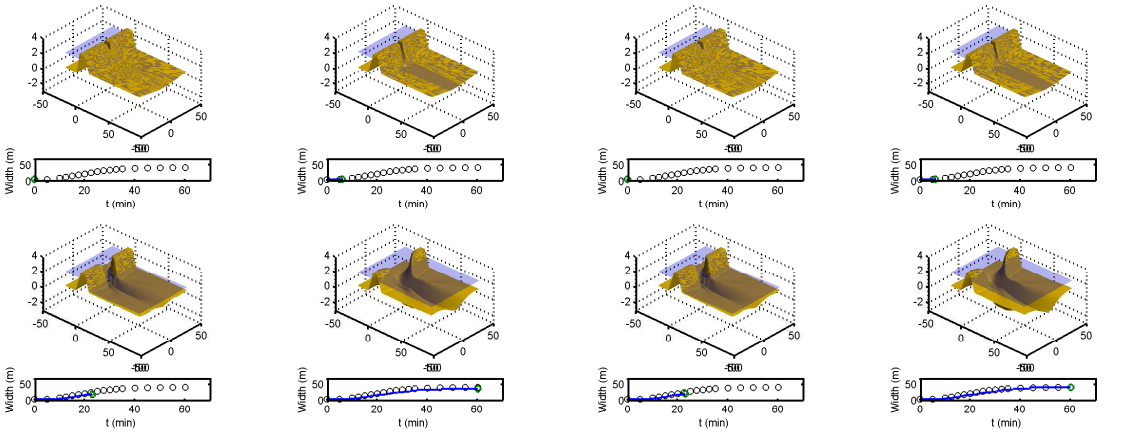

Figure 5.49: Sequence of 3D visualizations of the breach during the Zwin test (Visser, 1998). Bed level, water level and development of breach width (dots: observation, line: model).

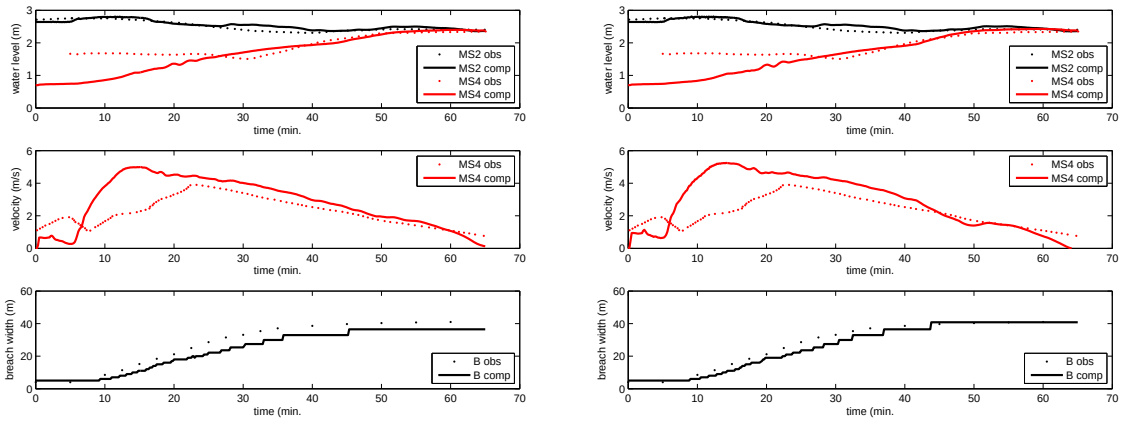

Figure 5.50: Zwin test (Visser, 1998). Observed (drawn lines) and modelled (dashed lines) time series of water level (top panel and velocity (middle panel). Bottom panel: development of breach width, observations (dots) vs. model (drawn line).

5.19 River Outflow

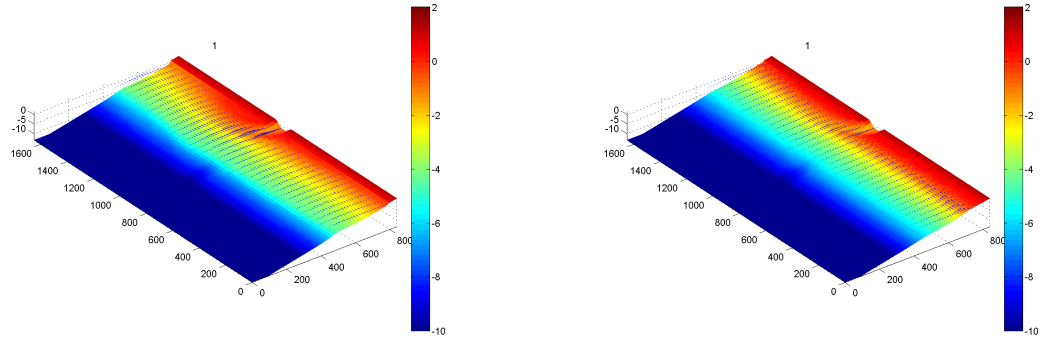

Figure 5.51

5.20 MICORE Cadiz

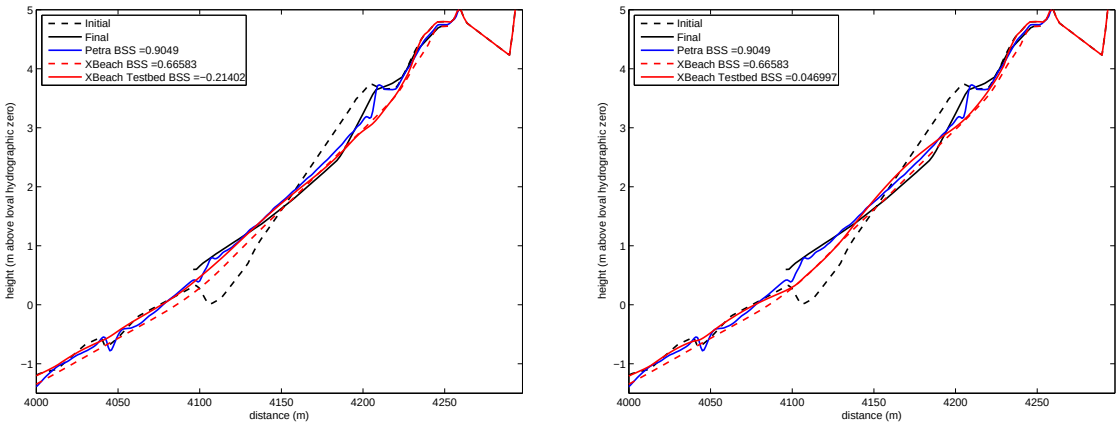

Figure 5.52

5.21 MICORE Dziwnow Spit

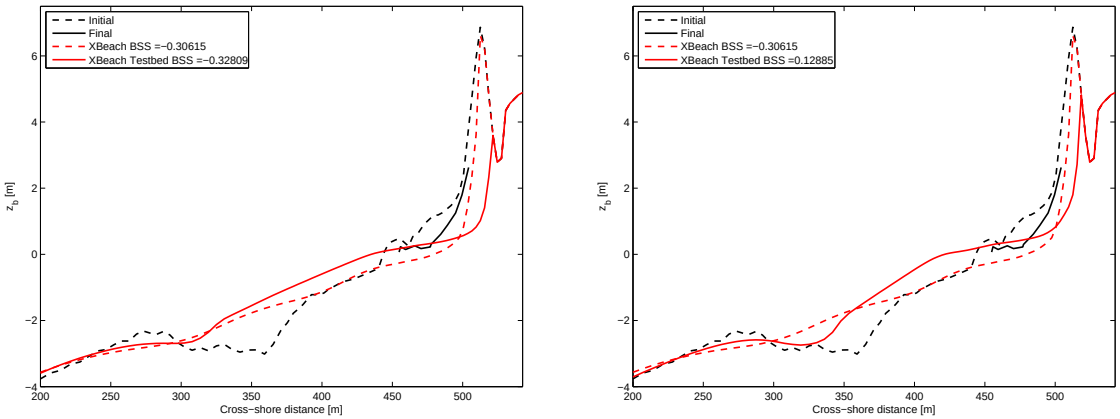

Figure 5.53

5.22 MICORE Lido de Sete

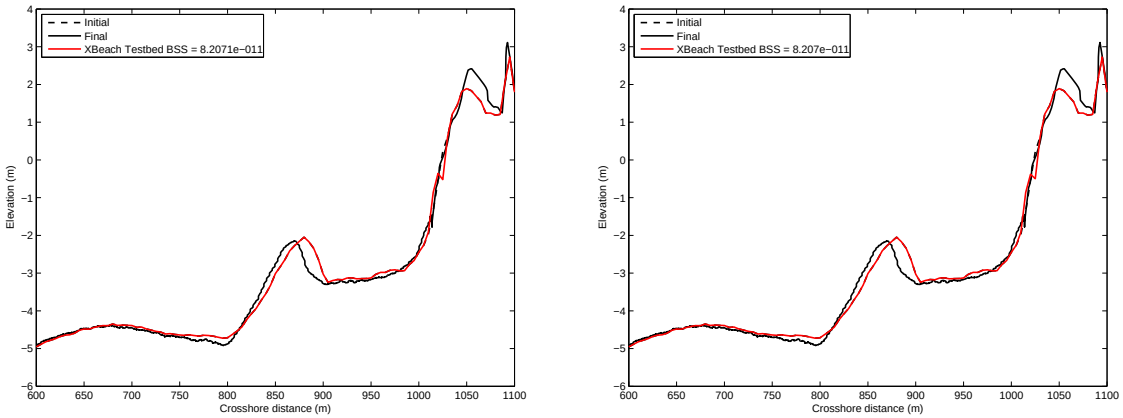

Figure 5.54

5.23 Assateague Island

Table 5.14: Hydrodynamic boundary conditions XBeach simulations

	Storm 1	Storm 2		Storm 1	Storm 2
Surge level [m +NAVD]	0.8	1.0	Surge level [m +NAVD]	0.8	1.0
H_s [m]	4.1	3.9	H_s [m]	4.1	3.9
T_p [s]	8.5	8.5	T_p [s]	8.5	8.5

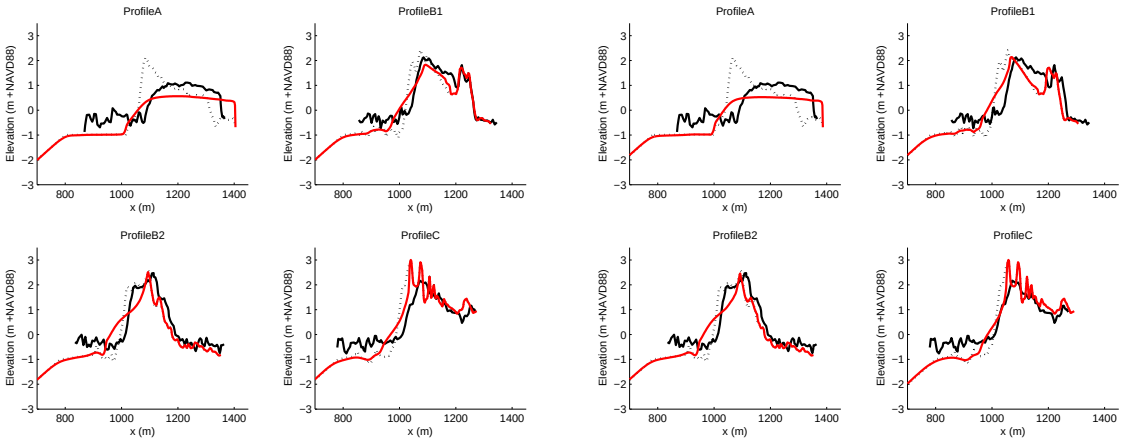

Figure 5.55: Pre-storm profiles (black dotted line), measured post-storm profiles (black solid line) and modelled post-storm profiles (red solid line). Upper left panel: profile A. Upper right panel: profile B1. Lower left panel: profile B2. Lower right panel: profile C. The seaward side is on the left in all panels. Note that the measured post-storm profiles contain only the sea surface and emerged topography and no submerged topography.

5.24 MICORE Mariakerke

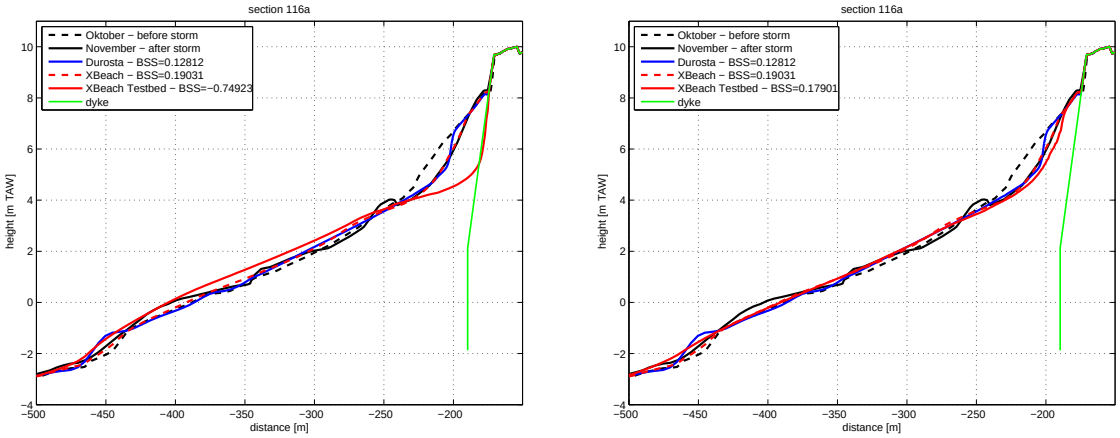

Figure 5.56

5.25 MICORE Lido di Dante

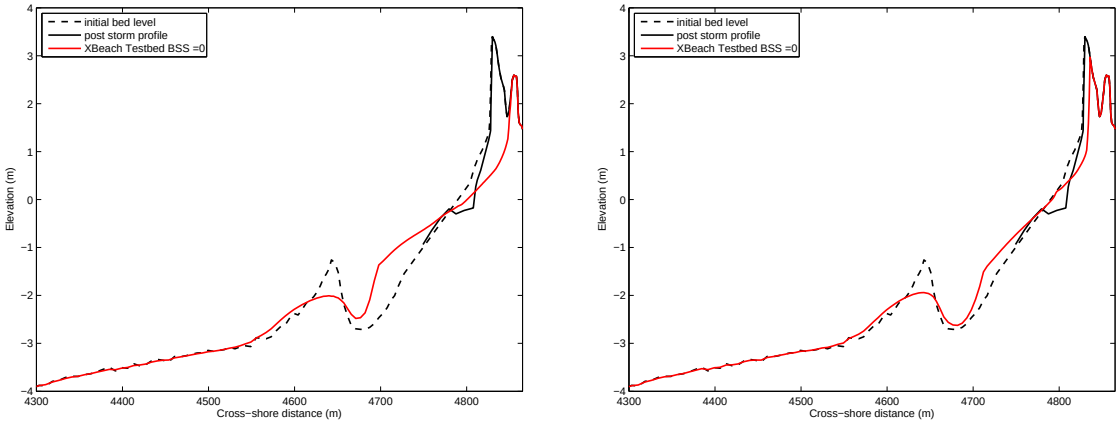

Figure 5.57

5.26 MICORE Praia de Faro

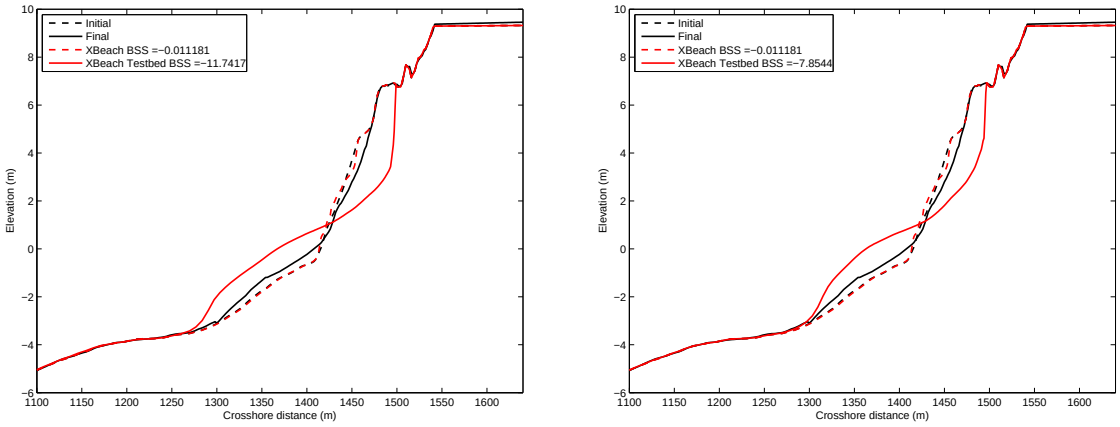

Figure 5.58

5.27 MICORE Kamchia Shkorpilovtsi Beach

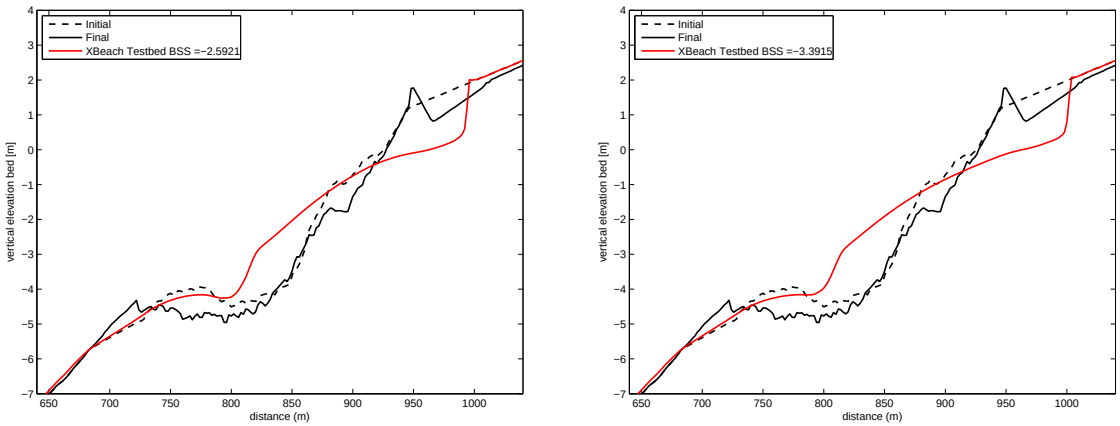

Figure 5.59